EMERGING INFECTIOUS DISEASES®

CDC
Centers for Disease Control and Prevention

Congenital Syphilis

October 2023

Edvard Munch (1863–1944), *Inheritance*, 1897–1899. Oil on canvas, 55.5 in × 47.25 in/141 cm × 120 cm. Munch Museum, Oslo, Norway. Photo credit: Erich Lessing. Digital image from Art Resource, New York, New York, USA.

EMERGING INFECTIOUS DISEASES®

Emerging Infectious Diseases is published monthly by the Centers for Disease Control and Prevention, 1600 Clifton Rd NE, Mailstop H16-2, Atlanta, GA 30329-4027, USA. Telephone 404-639-1960; email, eideditor@cdc.gov

EMERGING INFECTIOUS DISEASES®

Congenital Syphilis **October 2023**

On the Cover

Edvard Munch (1863–1944), *Inheritance*, 1897–1899. Oil on canvas, 55.5 in × 47.25 in/141 cm × 120 cm. Munch Museum, Oslo, Norway. Photo credit: Erich Lessing. Digital image from Art Resource, New York, New York, USA

About the Cover p. 2184

Synopses

Medscape EDUCATION ACTIVITY

Medscape EDUCATION ACTIVITY

Research

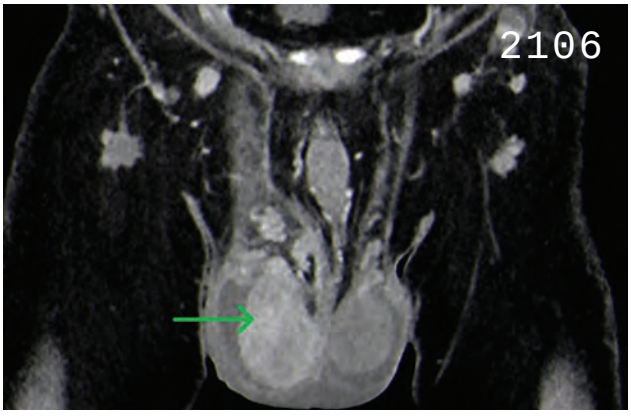

EMERGING INFECTIOUS DISEASES®
October 2023

Policy Review

Dispatches

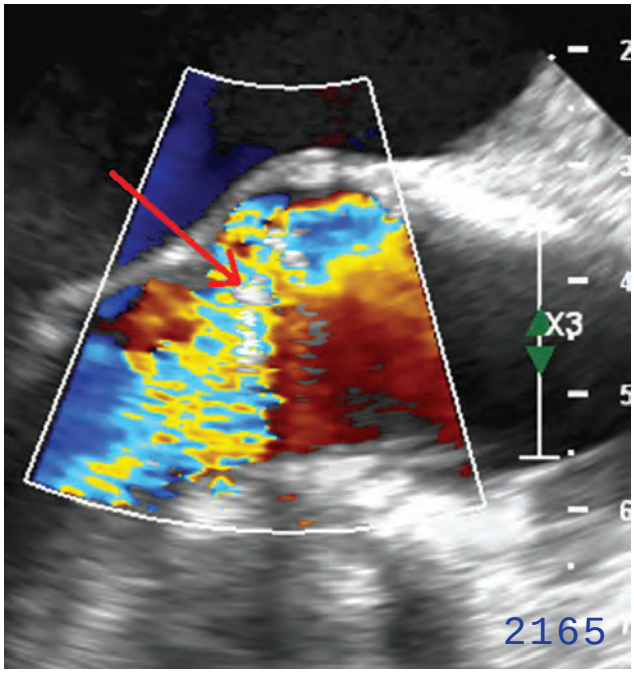

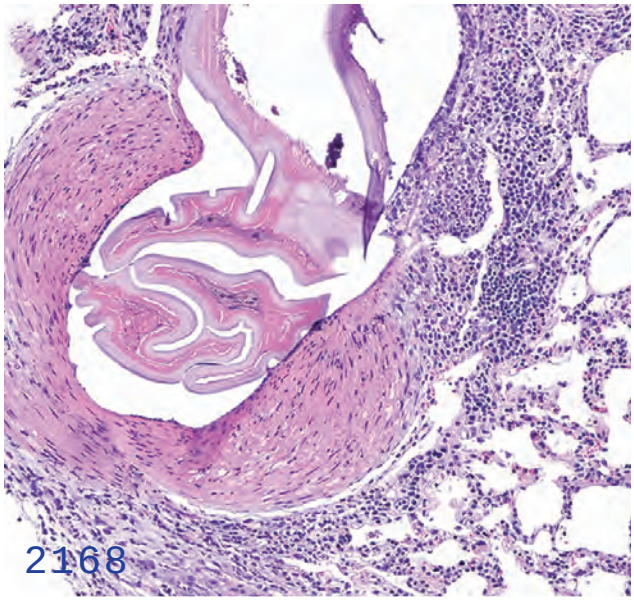

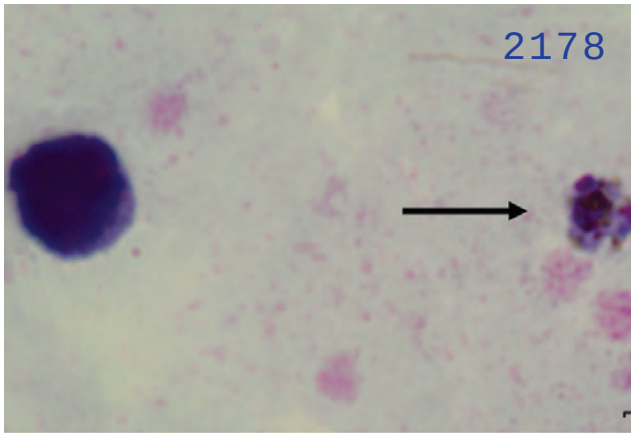

EMERGING INFECTIOUS DISEASES®
October 2023

Research Letters

Books and Media

About the Cover

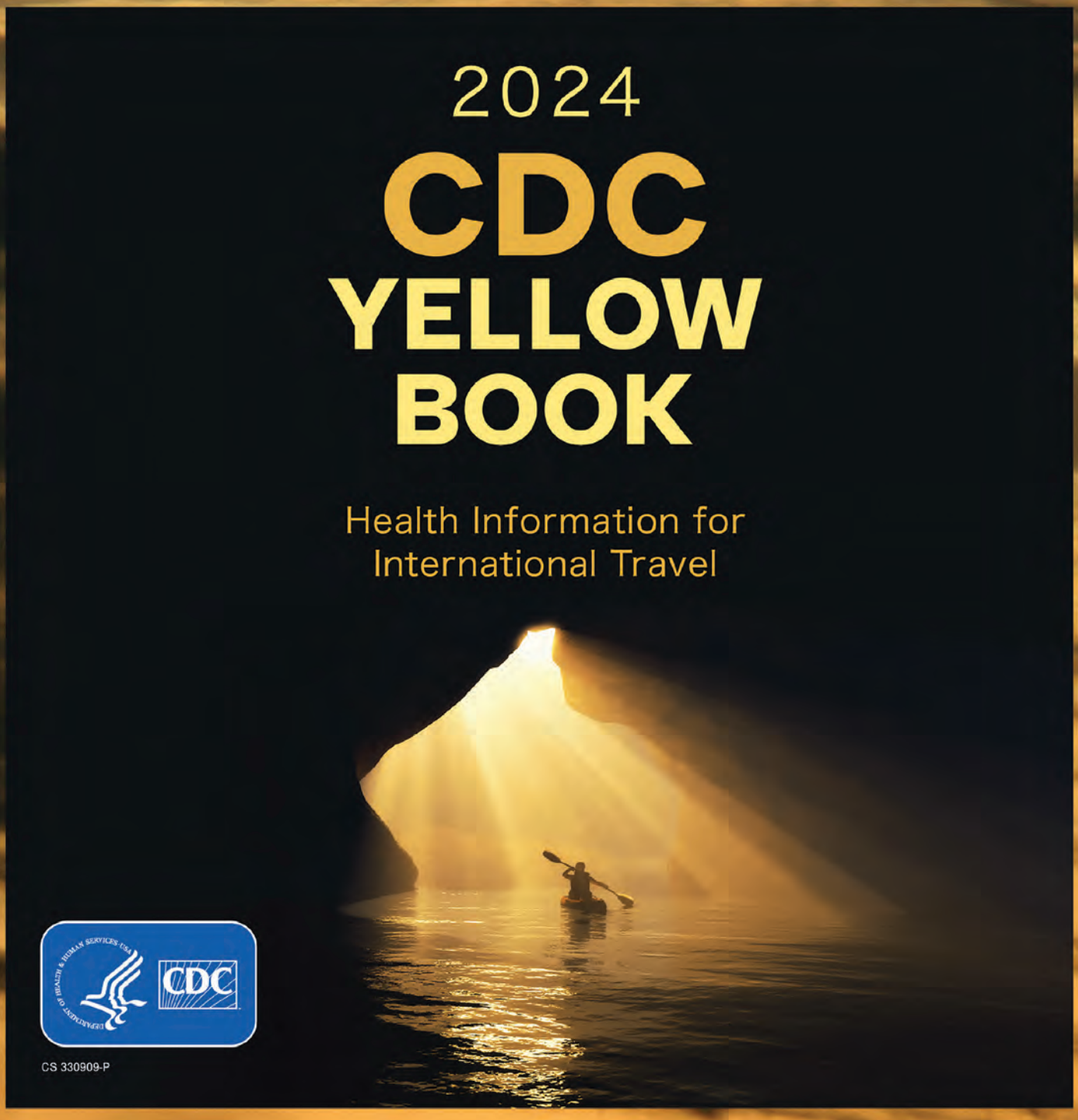

Launch of CDC Yellow Book 2024 – A Trusted Travel Medicine Resource

CDC is pleased to announce the launch of the CDC Yellow Book 2024. The CDC Yellow Book is a source of the U.S. Government's recommendations on travel medicine and has been a trusted resource among the travel medicine community for over 50 years. Healthcare professionals can use the print and digital versions to find the most up-to-date travel medicine information to better serve their patients' healthcare needs.

The CDC Yellow Book is available in print through Oxford University Press and online at www.cdc.gov/yellowbook.

Serotype Distribution and Disease Severity in Adults Hospitalized with *Streptococcus pneumoniae* Infection, Bristol and Bath, UK, 2006–2022

Catherine Hyams,[1] Robert Challen,[1] David Hettle, Zahin Amin-Chowdhury, Charli Grimes, Gabriella Ruffino, Rauri Conway, Robyn Heath, Paul North, Adam Malin, Nick A. Maskell, Philip Williams, O. Martin Williams, Shamez N. Ladhani, Leon Danon, Adam Finn

In support of improving patient care, this activity has been planned and implemented by Medscape, LLC and Emerging Infectious Diseases. Medscape, LLC is jointly accredited with commendation by the Accreditation Council for Continuing Medical Education (ACCME), the Accreditation Council for Pharmacy Education (ACPE), and the American Nurses Credentialing Center (ANCC), to provide continuing education for the healthcare team.

Medscape, LLC designates this Journal-based CME activity for a maximum of 1.00 ***AMA PRA Category 1 Credit(s)™***. Physicians should claim only the credit commensurate with the extent of their participation in the activity.

Successful completion of this CME activity, which includes participation in the evaluation component, enables the participant to earn up to 1.0 MOC points in the American Board of Internal Medicine's (ABIM) Maintenance of Certification (MOC) program. Participants will earn MOC points equivalent to the amount of CME credits claimed for the activity. It is the CME activity provider's responsibility to submit participant completion information to ACCME for the purpose of granting ABIM MOC credit.

All other clinicians completing this activity will be issued a certificate of participation. To participate in this journal CME activity: (1) review the learning objectives and author disclosures; (2) study the education content; (3) take the post-test with a 75% minimum passing score and complete the evaluation at http://www.medscape.org/journal/eid; and (4) view/print certificate. For CME questions, see page 2187.

NOTE: It is Medscape's policy to avoid the use of Brand names in accredited activities. However, in an effort to be as clear as possible, the use of brand names should not be viewed as a promotion of any brand or as an endorsement by Medscape of specific products.

Release date: September 14, 2023; Expiration date: September 14, 2024

Learning Objectives

Upon completion of this activity, participants will be able to:

- Assess long-term trends in the epidemiology of pneumococcal disease
- Analyze how the COVID-19 pandemic affected the epidemiology of pneumococcal disease
- Distinguish how the introduction of the conjugate pneumococcal vaccines affected circulating pneumococcal serotypes
- Identify common serotypes of pneumococcal illness after the emergence of SARS-CoV-2
- Assess clinical trends related to patients hospitalized with pneumococcal disease

CME Editor

Thomas J. Gryczan, MS, Technical Writer/Editor, Emerging Infectious Diseases. *Disclosure: Thomas J. Gryczan, MS, has no relevant financial relationships.*

CME Author

Charles P. Vega, MD, Health Sciences Clinical Professor of Family Medicine, University of California, Irvine School of Medicine, Irvine, California. *Disclosure: Charles P. Vega, MD, has the following relevant financial relationships: served as a consultant or advisor for Boehringer Ingelheim; GlaxoSmithKline; Johnson & Johnson.*

Authors

Catherine Hyams, MBPhD; Robert Challen, PhD; David Hettle, MBChB; Zahin Amin-Chowdhury, MSc; Charli Grimes, MSc; Gabriella Ruffino, MBChB; Rauri Conway, MBChB; Robyn Heath, BSc; Paul North, BsC; Adam Malin, PhD; Nick A. Maskell, MD; Philip Williams, PhD; O. Martin Williams, PhD; Shamez N. Ladhani, PhD; Leon Danon, PhD; Adam Finn, PhD.

Author affiliations: University of Bristol, Bristol, UK (C. Hyams, R. Challen, R. Heath, L. Danon, A. Finn); Southmead Hospital, Bristol (C. Hyams, C. Grimes, G. Ruffino, R. Conway, N.A. Maskell, A. Finn); Bristol Royal Infirmary, Bristol (D. Hettle, P. North, P. Williams, O.M. Williams); UK Health Security Agency, London, UK (Z. Amin-Chowdhury, S.N. Ladhani); The Royal United Hospital, Bath, UK (A. Malin)

DOI: https://doi.org/10.3201/eid2910.230519

[1]These authors contributed equally to this article.

Ongoing surveillance after pneumococcal conjugate vaccination (PCV) deployment is essential to inform policy decisions and monitor serotype replacement. We report serotype and disease severity trends in 3,719 adults hospitalized for pneumococcal disease in Bristol and Bath, United Kingdom, during 2006–2022. Of those cases, 1,686 were invasive pneumococcal disease (IPD); 1,501 (89.0%) had a known serotype. IPD decreased during the early COVID-19 pandemic but during 2022 gradually returned to prepandemic levels. Disease severity changed throughout this period: CURB65 severity scores and inpatient deaths decreased and ICU admissions increased. PCV7 and PCV13 serotype IPD decreased from 2006–2009 to 2021–2022. However, residual PCV13 serotype IPD remained, representing 21.7% of 2021–2022 cases, indicating that major adult PCV serotype disease still occurs despite 17 years of pediatric PCV use. Percentages of serotype 3 and 8 IPD increased, and 19F and 19A reemerged. In 2020–2022, a total of 68.2% IPD cases were potentially covered by PCV20.

Streptococcus pneumoniae remains the leading bacterial cause of community-acquired pneumonia, despite widespread use of effective pneumococcal vaccines with >100 recognized pneumococcal serotypes. In the United Kingdom, unconjugated 23-valent pneumococcal polysaccharide vaccine (PPV23) is offered to all adults ≥65 years of age and persons ≥2 years of age who are at increased risk for pneumococcal disease. In September 2006, a 7-valent pneumococcal conjugate vaccine (PCV7) was implemented into the national childhood immunization program, then replaced with a 13-valent PCV (PCV13) in April 2010. The PCVs were given at a 2 + 1 schedule but replaced with a 1 + 1 schedule in April 2020 (*1*). Because PCVs prevent carriage acquisition in addition to protection against disease, both PCVs had a large and major direct and indirect (herd) effect on pneumococcal disease caused by the respective serotypes (*2*–*4*).

By 2016–2017, PCV7 pneumococcal serotype disease had virtually disappeared in children and decreased to a large degree in adults. Invasive pneumococcal disease (IPD) caused by PCV13 serotypes has also decreased substantially but subsequently plateaued, with a residual incidence of 8 IPD cases/100,000 population in England (*5*–*7*). At the same time, pneumococcal cases caused by non-PCV13 serotypes increased across all age groups, especially in older adults, resulting in no net reduction in total IPD cases in older adults in 2016–2017 compared with the pre-PCV13 period, a phenomenon known as serotype replacement (*5*–*7*). Monitoring those effects nationally is vital for planning of healthcare use and developing new preventive strategies, including use of higher-valent pneumococcal vaccines (*8*,*9*).

The effect of serotype replacement has not been reported in the United States; data suggest that the incidence on nonvaccine serotype disease has remained stable, in both children and older adults (*10*). Clarification of the reasons for differences seen in studies from the United States and United Kingdom is needed because serotype replacement is a threat to the effectiveness of current vaccine programs, and PCV scheduling remains a policy decision area. It remains unclear why such differences occur; however, several factors might be involved, such as methods differences in surveillance approaches, exposure to pneumococcal transmission, risk factor profiles between patient populations, and serotype interactions (*11*). Small differences in carriage prevalence and clonal lineages might result in greatly different rates of IPD because serotype-specific invasiveness varies by orders of magnitude.

In England, the UK Health Security Agency conducts national IPD surveillance, which includes limited data on noninvasive pneumococcal disease, clinical phenotype, and disease severity (*5*–*7*). Evidence from a large pneumococcal pneumonia cohort in Nottingham, UK, suggests there are relatively few differences between patients with PCV13 and non-PCV13 serotype respiratory infections (*12*). Nevertheless, changing serotype distribution could result in changes in pneumococcal disease phenotypes, which might have implications for use of available polyvalent serotype-specific pneumococcal vaccines. Furthermore, the COVID-19 pandemic has disrupted the epidemiology of multiple respiratory infections (*13*,*14*) and provided new insights into virus–bacteria–host interactions. Many countries, including the United Kingdom, implemented measures such as social distancing and school closures that were intended to decrease SARS-CoV-2 transmission and alleviate pressure on healthcare services (*15*). Those measures reduced the transmission of other respiratory pathogens (*14*), but it is unclear to what extent they disrupted pneumococcal transmission (*16*,*17*). The measures might also have caused changes in serotype distribution of pneumococcal infection and disease.

In this retrospective cohort study conducted at 3 large National Health Service (NHS) hospitals, which represent all secondary care provision within a defined geographic area, we examined trends in pneumococcal serotype distribution in adults after PCV7 and PCV13 implementation into the childhood immunization program and the effect of the COVID-19 pandemic over the first 3 years. We report confirmed

pneumococcal disease incidence during 2006–2022, both overall and by vaccine serotypes, and assess trends in severity of pneumococcal disease in hospitalized adults.

Materials and Methods

Study Design

This study was approved by the UK Health Research Authority (IRAS 265437). We conducted a retrospective cohort study including all patients ≥16 years of age who were admitted to any of three large UK NHS hospitals in southwest England: University Hospitals Bristol and Weston, North Bristol, and The Royal United Hospital (Bath) NHS Trusts. The study covered the period January 1, 2006–December 31, 2022, and included patients who had a confirmed microbiologic diagnosis of pneumococcal infection. Those hospitals provide all secondary care within a defined geographic area with 100,000 unplanned adult admissions annually, including the regional cardiothoracic, pleural, respiratory specialist, and general medical and respiratory services.

We identified eligible cases retrospectively by searching the Laboratory Information Management System database (Clinisys WinPath Enterprise). We confirmed identification of *S. pneumoniae* by using culture or PCR from a sterile site at a central laboratory by using standard microbiologic techniques. Culture was confirmed by using API-20 Strep (bioMérieux) or matrix-assisted laser desorption/ionization time-of-flight) mass spectrometry (Bruker). A positive result on pneumococcal urinary antigen test (UAT) (Binax) was also considered confirmation of pneumococcal infection. Patients were included if they tested positive on any or all tests.

We linked confirmed cases with the UK Health Security Agency (UKHSA) national reference laboratory database to obtain serotype data, which we collected at the end of the study to avoid risk for bias in clinical data collection. We reviewed clinical records at each hospital and recorded data in a standardized manner, including laboratory and radiologic investigations. We recorded patient observations within 24 hours of when care was sought for a pneumococcal infection, and established vaccination status by using electronically linked general practitioner records. We calculated the CURB65 severity score (confusion, blood urea nitrogen, respiratory rate, blood pressure, and age ≥65 years) (https://www.mdcalc.com/calc/324/curb-65-score-pneumonia-severity) at admission for each clinical episode and recorded clinical outcomes, including length of hospitalization and intensive care unit (ICU) admission. We determined inpatient death (i.e., patient death before discharge) through review of the medical records and used it as a marker of case-fatality. All adult patients were managed at the discretion of the admitting clinical team.

Case Definitions

Total pneumococcal disease included all positive cases, whether identified by sterile site culture/PCR or positive UAT result with clinical confirmation of sterile site infection (i.e., IPD) or noninvasive pneumococcal disease (positive UAT result only). Total cases where the serotype was identified are referred to as serotype-known disease: pneumococcal serotypes were further grouped by vaccine serotypes: PCV7, PCV13–7 (PCV 13 minus PCV7 serotypes, PCV15–13, PCV20–15, PCV20–13, and serotypes not contained in a PCV (non-PCV) (Appendix, https://wwwnc.cdc.gov/EID/article/29/10/23-0519-App1.pdf). The primary infection site was derived from the managing clinician's diagnosis. Respiratory infection included both consolidative infection (i.e., pneumonia) according to British Thoracic Society/National Institute for Health and Care Excellence (BTS/NICE) guidelines (*18*) and nonpneumonic lower respiratory tract infection.

Statistical Analysis

Data are reported as medians and interquartile ranges for continuous variables or means and SDs where the distributions were confirmed to be normal by using the Anderson Darling normality test. Categorical variables are presented as counts and percentages. We calculated multinomial CIs by using the Wilson score interval method for binomial percentages (*19*), which we tested on simulated data and found to be well calibrated for this problem. We compared baseline characteristics by using the Fisher exact test for categorical variables, the 2-sample Kolmogorov-Smirnov test for nonparametric continuous variables, the Wilcoxon rank-sum test for score variables, or the 2-sided Student t-test for parametric continuous variables. There were minimal missing data, and only for categorical variables. When these data were present, they were included as a separate category before statistical testing.

We performed multinomial time series analysis by fitting a single-hidden-layer neural network and using the nnet package (*20*) in R (The R Foundation for Statistical Research) with a time-varying natural spline term for class probabilities and a knot point for each class every 2 years. We performed binomial time series analysis by using a maximum-likelihood

approach with local polynomial regression and a logistic link function assuming that the count of positive and negative results are a quasi-binomially distributed quantity in the R package locfit according to the methods of Loader (*21*) with a bandwidth equivalent to 2 years' worth of data and a polynomial of degree 2.

We obtained yearly estimates for the ≥16 years of age population of clinical commissioning groups of NHS Bath and North East Somerset and NHS Bristol, North Somerset, and South Gloucestershire regions from NHS Digital. We interpolated yearly point estimates to daily estimates by using a local polynomial regression and estimated pneumococcal disease incidence as the rate of monthly admission counts by using a local polynomial regression assuming a quasi-Poisson distribution, logarithmic link function, and the methods of Loader (*21*). We expressed admission rates as disease cases per 1,000 person-years by using interpolated population estimates. We performed all analyses by using R version 4.2.

Results

During 2006–2022, we identified 3,719 adults (median age 66.1 years, interquartile range 50.2–78.9 years) who had pneumococcal disease. Of those persons, 1,840 (49.5%) were male, 1,879 (50.5%) were female, 1,621 (43.6%) had positive blood cultures, 2,379 (64.0%) were UAT positive, and 15 (0.4%) were PCR positive. Among the cases, 1,686 (45.3%) were IPD and 2,033 (54.7%) were non-IPD. Respiratory infection accounted for 92.3% (3,436/3,719) of all cases of pneumococcal disease, 84.2% of IPD, and 99.2% of noninvasive pneumococcal disease (Table 1). Pneumococcal serotype was available for 1,501 (40%) cases. The demographics and clinical characteristics of patients with known-serotype pneumococcal disease were similar to those with unknown serotype infection (Appendix).

The incidence of IPD among hospitalized adults showed a slight upward trend during 2006–late 2019 (Figure 1, panel A). During the early part of the COVID-19 pandemic in 2020, pneumococcal disease incidence suddenly decreased. However, during

Table 1. Characteristics of patients hospitalized with confirmed pneumococcal infection, Bristol, UK, 2006–2022*

Characteristic	Invasive disease, n = 1,686	Noninvasive disease, n = 2,033	p value
Age, y, median (IQR)	65.9 (50.8–79)	66.3 (50–78.8)	0.74
Sex			
M	847 (50.2)	993 (48.8)	0.41
F	839 (49.8)	1,040 (51.2)	
Serotype status			
Serotype identified	1,501 (89.0)	0	<0.001
No serotype	185 (11.0)	2,033 (100.0)	
Smoker			
Nonsmoker	495 (29.4)	597 (29.4)	0.95
Ex-smoker	680 (40.3)	829 (40.8)	
Current smoker	511 (30.3)	607 (29.9)	
Charlson Comorbidity Index, median (IQR)	4 (1–6)	4 (1–6)	0.31
Test type			
Blood culture only	1,325 (78.6)	0 (0)	<0.001
UAT only	51 (3.0)	2,033 (100.0)	
Blood culture and UAT	295 (17.5)	0	
CSF PCR	8 (0.5)	0	
Blood PCR	7 (0.4)	0	
Infection site			
Lung	1,419 (84.2)	2,017 (99.2)	<0.001
Meningitis	172 (10.2)	0	
Septic arthritis	36 (2.1)	0	
ENT	15 (0.9)	2 (0.1)	
Other	44 (2.6)	14 (0.7)	
PPV23 vaccination, time before illness			
None	967 (57.4)	1,171 (57.6)	0.99
<6 mo	60 (3.6)	72 (3.5)	
≥6 mo	659 (39.1)	789 (38.8)	
Missing	0	1 (0)	
Noninvasive ventilation	39 (2.3)	103 (5.1)	<0.001
Intubation	236 (14.0)	234 (11.5)	0.026
Inpatient death†	255 (15.1)	253 (12.4)	0.019

*Values are no. (%) except as indicated. Significance was determined by using the Fisher exact test for categorical variables, the 2-sample Kolmogorov-Smirnov test (continuous variables), and the 2-sample Wilcoxon rank-sum test (continuous variables). Normality of distributions determined by using the Anderson-Darling normality test. CSF, cerebrospinal fluid; ENT, ear, nose, and throat; IQR, interquartile range; PPV23, 23-valent pneumococcal polysaccharide vaccine; UAT, urine antigen test.
†Determined though review of medical records (i.e., death before discharge from hospital).

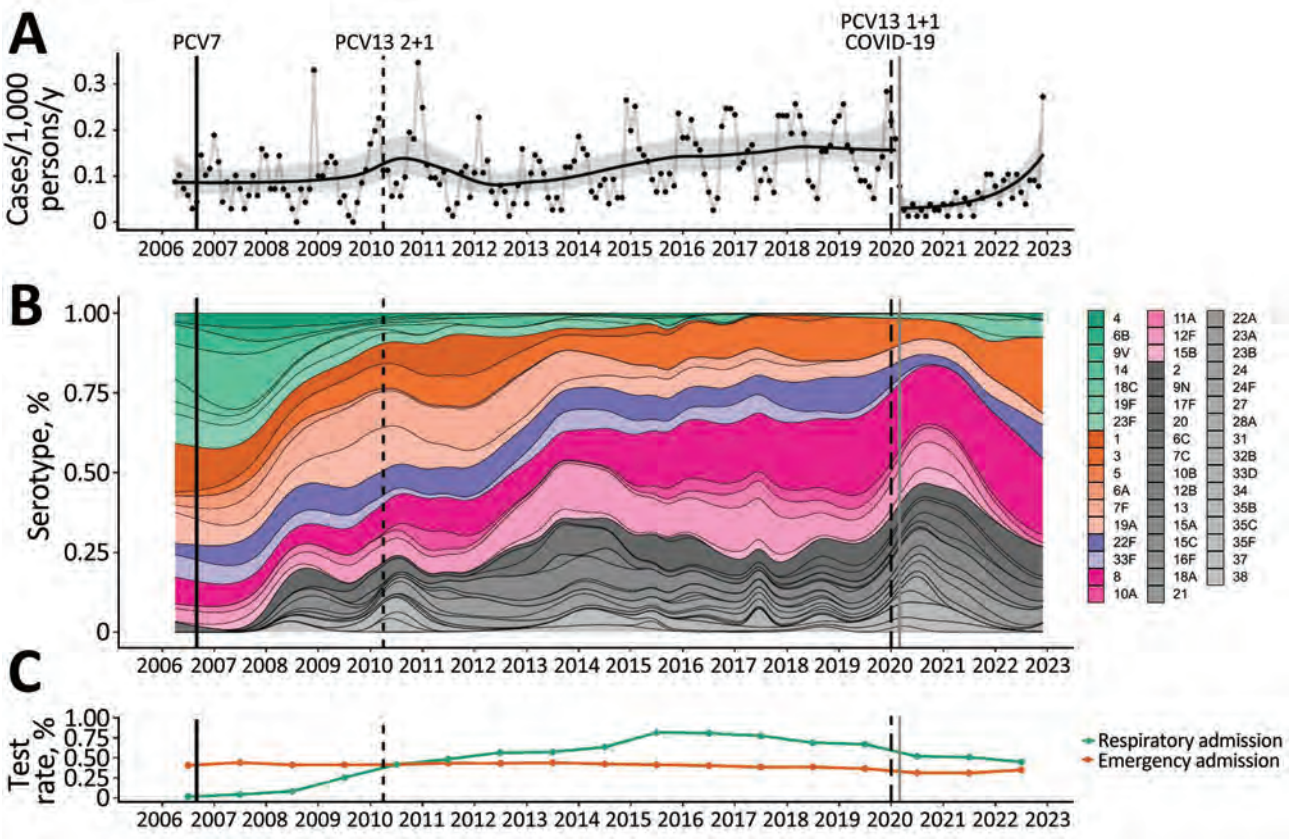

Figure 1. Distribution of pneumococcal serotypes in hospitalized patients, Bristol and Bath, UK, 2006–2022. A) Incidence of blood culture–positive pneumococcal disease. Data shown include only invasive disease; for comparison with noninvasive disease, see the Appendix (https://wwwnc.cdc.gov/EID/article/29/10/23-0519-App1.pdf). Black dots indicate monthly observations, black line indicates a binomial time series model, and gray shading indicate 95% CIs. Population estimates are provided in the Appendix. B) Multinomial percentage of pneumococcal serotypes in the invasive pneumococcal disease population with known serotype. Green bars indicate 7-valent PCV (PCV7) serotypes; orange, PCV13–7 (PCV13 minus PCV7 serotypes); purple, PCV15–13; pink, PCV20–15; gray, serotypes not contained in PCV vaccines. Individual serotypes are shown in the legend on the panel. C) Testing rates for blood cultures with respect to acute admissions and BinaxNOW (https://www.abbott.com) tests with respect to acute respiratory admissions. Estimates are presented at the midyear time point, relative to the data they represent. For all panels, vertical lines indicate introduction of PCV7 (solid black), PCV13 (2 + 1 schedule) (thin black dashed line), PCV13 (1 + 1 schedule) (thick black dashed line) into the UK childhood vaccination program and the beginning of large hospital admissions in Bristol caused by SARS-CoV-2 (solid gray). PCV, pneumococcal conjugate vaccine.

2022, incidence gradually increased so that by December 2022 it had returned to a level similar to that observed before the COVID-19 pandemic (Figure 1, panel A). Noninvasive pneumococcal disease showed a broadly similar pattern but is harder to interpret because of changing BinaxNOW testing patterns over the study period (Figure 1, panel C; Appendix Figures 3, 4). PCV7 serotype disease decreased from 29.4% (95% CI 24.1%–35.4%) in 2006–2009 to 7.0% (95% CI 3.7%–12.7%) of serotype-known disease in 2021–2022, and PCV7-serotypes caused minimal disease from mid-2017 until their re-emergence during the COVID-19 pandemic. PCV13–7 disease represented 34.3% (95% CI 28.6%–40.4%) of serotype-known disease in 2006–2009, decreased slightly to 29.3% (95% CI 25.6%–33.3%) by 2010–2015, and continued to decrease to 21.7% (95% CI 15.5%–29.6%) in 2021–2022, with serotypes 1, 3, and 19A persisting. In contrast, the percentage of PCV20–13 and non-PCV serotype disease increased during this period (Figure 1, panel B).

Although blood culture testing rates remained stable over time, there were changes in UAT testing rates. The decreased pneumococcal disease incidence observed during the COVID-19 pandemic occurred without an equivalent decrease in BinaxNOW and blood culture testing over the same time period (Figure 1, panel C). After SARS-CoV-2 emergence, the most commonly identified serotypes were 3, 8, 9N, 19F, 19A and 22F (Figure 2, panels A, B). In 2022, 6.2% (95% CI 3.2%–11.8%) of disease was attributable to PCV15–13, 33.3% (95% CI 25.8%–

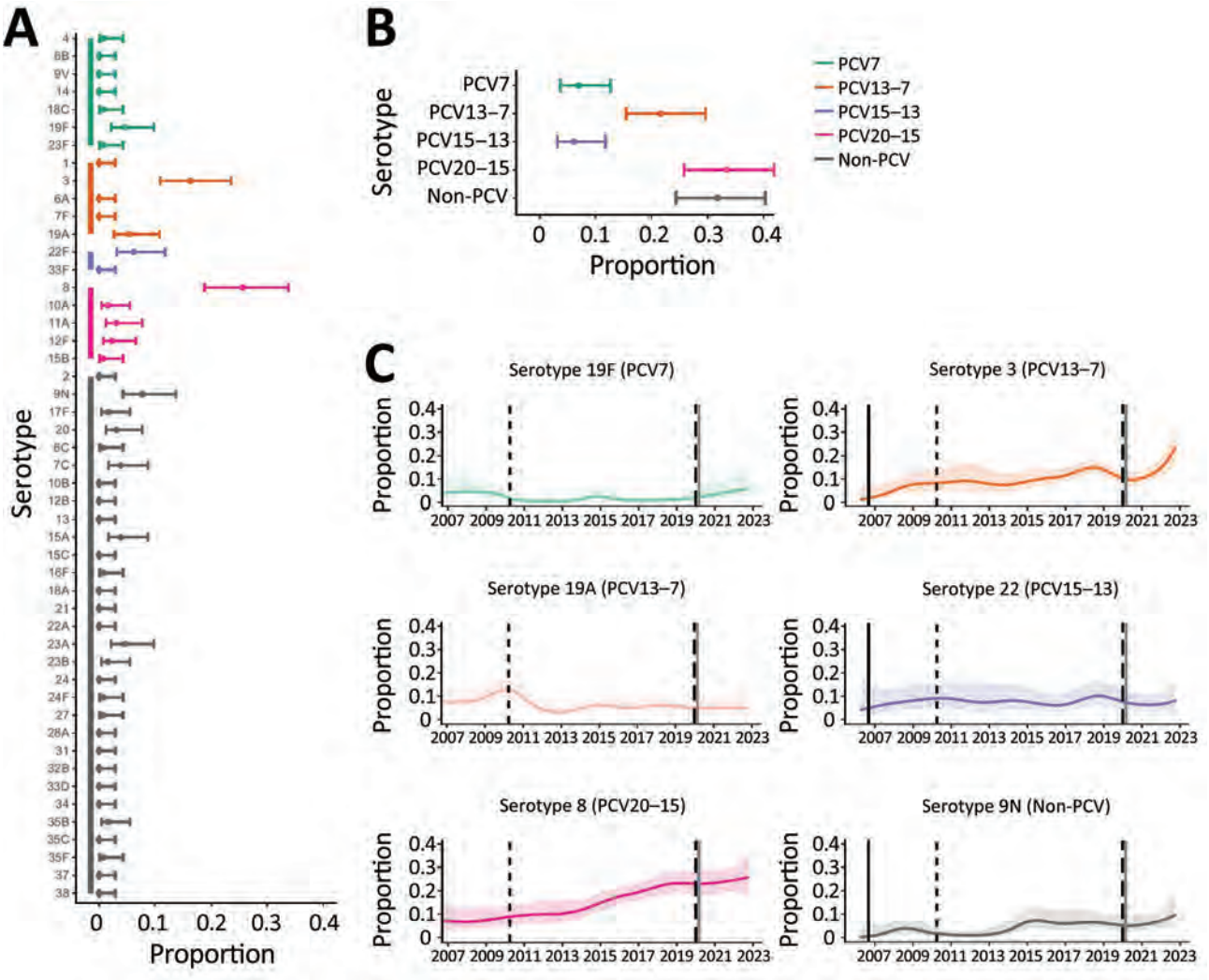

Figure 2. Distribution of pneumococcal serotypes in hospitalized patients after emergence of SARS-CoV-2. A, B) Proportion of pneumococcal disease attributable to each serotype (A) and PCV vaccine group (B) from 129 case-patients in Bristol, UK, hospitalized during January 1, 2021–December 31, 2022. C) Binomial (one versus others) time series models showing the percentage of disease during January 2006–December 2022 attributable to each of the 6 most common pneumococcal serotypes. Solid lines indicate smoothed point estimates; error bars/shaded areas indicate 95% CIs. The 95% CIs in panels A and B do not coincide exactly with those in panel C because they represent different length time periods and use different models. Additional data and time points are available in Table 2 (https://wwwnc.cdc.gov/EID/article/29/10/23-0519-T2.htm). PCV, pneumococcal conjugate vaccine.

41.8%) to PCV20–15, and 31.8% (95% CI 24.4%–40.2%) to non-PCV serotypes; a major percentage of disease arose from serotypes in current PCVs (Figure 2). Among known-serotype cases, PCV7 serotypes represented 7.0% (95% CI 3.7%–12.7%) and PCV13–7 serotypes 21.7% (95% CI 15.5%–29.6%) of cases (Table 2, https://wwwnc.cdc.gov/EID/article/29/10/23-0519-T2.htm). Overall, the percentage of disease caused by 19F, 19A, and 22F remained relatively stable throughout the study, and an expansion of serotypes 3 and 8 disease occurred, along with a slight increase in serotype 9N (Figure 2, panel C).

Before the emergence of SARS-CoV-2, the age of patients admitted with IPD increased over time (Figure 3, panel A) and disease severity decreased, as shown by the average CURB65 severity scores at admission (Figure 3, panel B). ICU admission rates increased in earlier years and then plateaued, inpatient deaths decreased, and length of hospital admission remained broadly stable (Figure 3, panels C–E). Those trends were disrupted during the early stages of the SARS-CoV-2 pandemic and largely reverted to their previous trajectories in 2021–2022. The percentage of patients 45–55 years of age trended upwards compared with the prepandemic period, and

the percentage of IPD case-patients requiring ICU admission also increased, but those trends were based on small numbers. We could not account for the increase in ICU admissions seen after SARS-CoV-2 emergence through change in bed availability or clinical care pathways.

Discussion

This study examining hospitalized adults with pneumococcal disease in Bristol and Bath, UK, encompasses 17 years of PCV implementation into the UK childhood vaccination program and includes 3 years of the COVID-19 pandemic. Although the percentage of

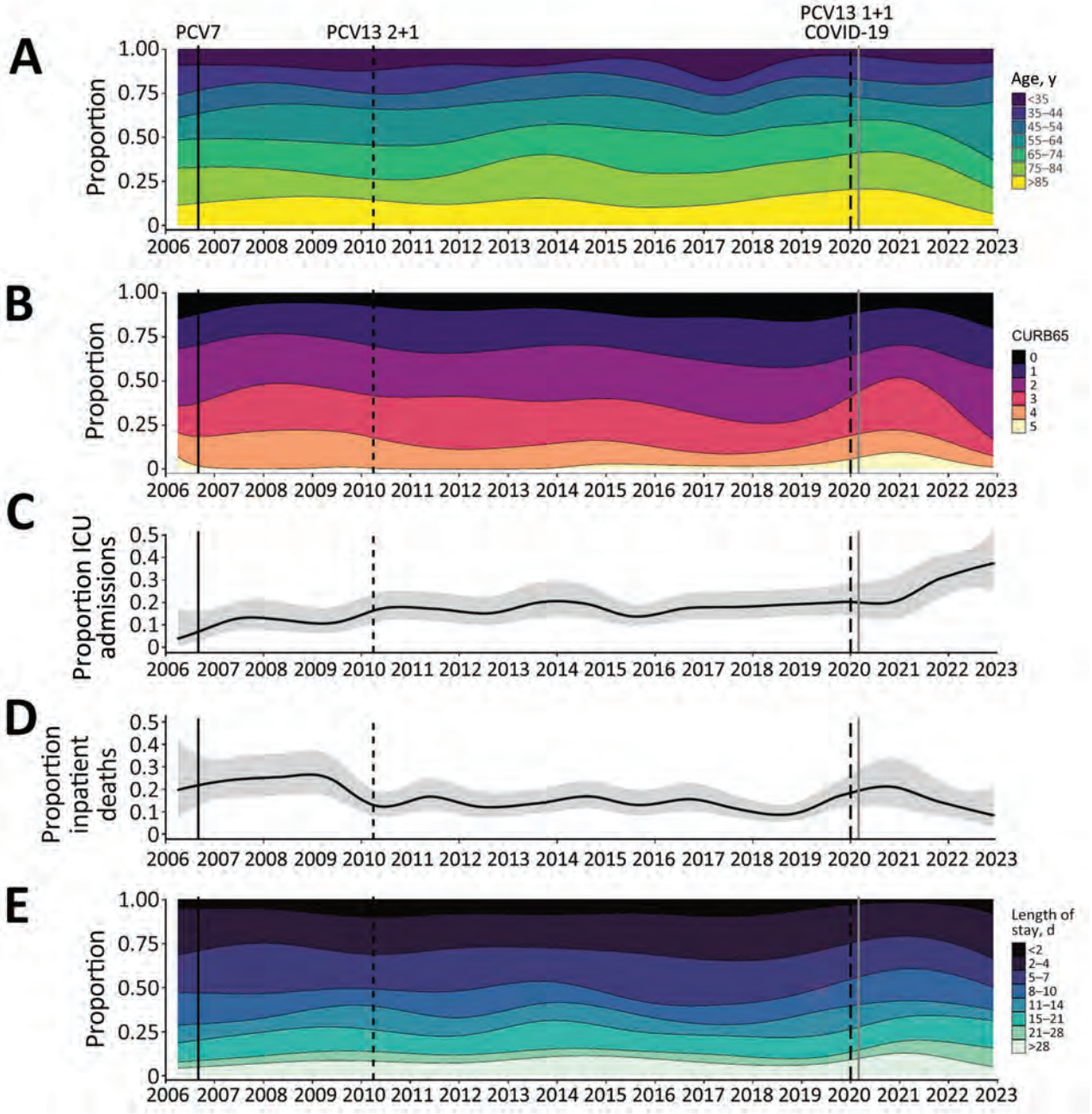

Figure 3. Severity of manifestations and outcome of invasive pneumococcal disease in hospitalized adults over time, Bristol, UK. A) Age categories; B) CURB65 scores; C) ICU admissions; D) inpatient deaths; E) length of stay in a hospital. For panels A, B, and E, categories are shown in the legend adjacent to each panel. The solid line in the multinomial time series models shown in panels C and D indicates binomial time series models; gray areas indicate 95% CIs. Across all panels, vertical lines indicate dates of 7-valent PCV (PCV7) (solid black) and PCV13 2 + 1 (thin black dashed line) and 1 + 1 (thick dash blacked line) schedule vaccine introduction and SARS-CoV-2 emergence (solid gray). Results for noninvasive pneumococcal disease are shown in the Appendix (https://wwwnc.cdc.gov/EID/article/29/10/23-0519-App1.pdf). ICU, intensive care unit; PCV, pneumococcal conjugate vaccine.

IPD caused by PCV serotypes has decreased across all age groups, a major fraction of adult pneumococcal disease is still caused by PCV7 (7.0% [95% CI 3.7%–12.7%]) and PCV13–7 (21.7% [95% CI 15.5%–29.6%]) serotypes (*5*,*22*). In addition, the percentage of adult disease caused by those serotypes has increased since COVID-19 pandemic restrictions began in March 2020, which also coincided with a change in the UK childhood immunization schedule from 3 doses to 2 doses of PCV13 since April 2020. The persistence of PCV13 serotype and PCV7 serotype disease in adults in this study occurred in the context of a longstanding, high-coverage national childhood vaccination program. This persistence suggests that, although giving PCVs to most children has had some indirect effects, those effects do not completely protect adults from PCV serotype disease.

The persistence of some PCV13 serotypes is concerning because they are associated with more severe disease and deaths in adults. In addition, we have observed large increases in the percentage of non-PCV13 serotype disease since PCV13 implementation, consistent with national surveillance throughout the UK and Europe (*5*–*7*,*12*,*22*). During 2016–2019, non-PCV13 serotypes caused 78.8% (95% CI 75.2%–82.1%) of cases among persons who had identified serotypes; during 2021–2022 that percentage was 71.3% (95% CI 63.0%–78.4%). During 2021–2022, PCV20–13 serotypes accounted for 39.5% (95% CI 31.5%–48.2%) of adult disease with identified serotypes.

Despite indirect effects operating to some degree, PCV serotypes continue to cause adult disease that is severe enough to require hospital admission. Although PCV7 serotypes remain rare causes of adult pneumococcal disease, serotype 19F has reemerged. We found that most residual PCV serotype disease is caused by PCV13–7 serotypes, especially serotypes 3 and 19A, observations that are consistent with other reports (*5*,*7*,*12*,*22*). The continued circulation of serotype 3, especially after the pandemic restrictions were lifted, is critical because this serotype is associated with more severe disease, especially in older adults. Ongoing circulation might, in part, be caused by clade II expansion after a clade distribution shift (*23*). Serotype 19A is also of concern because it has previously been associated with high antimicrobial drug resistance rates in some countries (*24*).

Indirect effects of PCVs are believed to occur by reduction in nasopharyngeal carriage and density of vaccine serotypes in vaccinated children, which interrupts transmission to both vaccinated and unvaccinated contacts (*2*–*4*). Generally, sustained high PCV coverage in children is assumed to result in reliable indirect effects in adults: the UK 1 + 1 PCV13 childhood immunization schedule relies, to a degree, on those indirect effects to protect infants who only receive 1 priming PCV dose before their 1-year booster (*25*). However, we cannot explain the recent percentage increase in PCV13 serotype disease we observed by decreasing pediatric PCV vaccination rates. In the United Kingdom, vaccination is offered free of charge and is associated with high uptake; PCV uptake was >90% for the first dose by 12 months of age and >94% for the second dose by 24 months of age in southwestern England in 2021–2022 (*26*).

A concerning finding is the high percentage of cases that are not vaccine preventable: during 2016–19, PCV20–13 and non-PCV serotypes represented 53.0% (95% CI 48.8%–57.2%) and 25.8% (95% CI 22.3%–29.7%) of cases, respectively; in 2021–2022, those percentages of 39.5% (95% CI 31.5%–48.2%) and 31.8% (95% CI 24.4%–40.2%). In 2021–22, PCV15 serotypes represented 34.9% (95% CI 27.2%–43.4%) of IPD cases, PCV20 serotypes 68.2% (95% CI 59.8%–75.6%) and non-PCV serotypes 31.8% (95% CI 24.4%–40.2%). Although serotype replacement has been observed in Europe and serotype distribution change in the United States (*5*–*7*,*21*,*27*,*28*), reports from the United States describe consistently stable rates of non-PCV13 serotype IPD after childhood PCV13 introduction (*29*). Serotype replacement might occur through expansion of non-PCV strains or capsular switching of previously vaccine-preventable strains, in which recombination at the capsular gene locus results in serotype change (*30*). In concordance with other studies, we found serotype 8 disease increasing, along with 23A and 9N (*5*,*7*,*12*).

We observed a disproportionate decrease in pneumococcal disease incidence early in the COVID-19 pandemic, without a concomitant decrease in BinaxNOW and blood culture testing rates. This finding might have been caused by reduced circulation and transmission of many respiratory pathogens, including pneumococcus, because of social distancing policies (*13*,*14*,*16*) breaking transmission chains and affecting host–pathogen–pathogen interactions, so that severe pneumococcal infection became less common. Preceding viral infection is a major risk factor for pneumonia, and the relationships between influenza and respiratory syncytial virus and pneumococcus are well described (*31*,*32*). Pneumococcus might also modulate host immune responses to SARS-CoV-2 (*33*). Prospective surveillance found that Europe experienced major and sustained reductions in invasive disease caused by pneumococcus, *Haemophilus influenzae*, and *Neisseria meningitidis* in early

2020 (*34*). Our study confirms that reduced testing practices in hospitals do not explain such reductions.

However, changes in healthcare use might explain the incidence decreases that occurred. For example, susceptible patients had fewer admissions to secondary care during the pandemic (*35*). An increased admission threshold or avoidance of secondary care would increase community-level management of cases and reduce case-patients who have pneumococcal disease seeking treatment and consequently being diagnosed in hospitals. Because fewer investigations are performed in community-level care, such cases would be missed by surveillance that is reliant on microbiologic testing.

By combining microbiologic results with clinical data, we are able to report on both disease epidemiology and severity over time. We found some evidence of more severe disease, especially after SARS-CoV-2 emergence. The observed disruption to the broadly stable previous trends in disease severity during the early part of the SARS-CoV-2 pandemic might be a result of observation bias, a consequence of the pandemic, or both. Although ICU admission rates increased for pneumococcal disease, admission CURB65 severity scores were lower, consistent with the 2018 BTS national pneumonia audit, which also reported decreased admission CURB65 scores (*36*). This apparent discrepancy might be explained by changes in patients or their treatment (e.g., older patients with more severe disease might be less likely to receive ICU care than younger patients because of clinical prognostic decision making). Other recent changes in treatment, such as increased availability of positive pressure support or earlier antimicrobial drug administration, might also have changed patient courses and outcomes, including severity and death. Major changes in pneumococcal infection severity have occurred since 2020, including an increased percentage of adults 45–55 years of age who required hospital treatment. The recent increase in cases is probably related to relaxation of COVID-19 restrictions. Recent studies highlight the critical role of respiratory viruses (e.g., respiratory syncytial virus, human metapneumovirus, influenza virus) in contributing to pneumococcal disease (*17*). Large, out-of-season viral outbreaks that occurred after easing of COVID-19 restrictions (*37*) are therefore likely to have contributed to the increasing pneumococcal disease rates we report in this study, which will need careful surveillance in future years. Independent of changes in clinical practice, serotype distribution changes might affect patient outcomes and healthcare use as invasive potential varies by serotype.

By combining microbiologic results with clinical data, we are able to report on both disease epidemiology and severity over time. We found some evidence of more severe disease especially after SARS-CoV-2 emergence. The observed disruption to the broadly stable previous trends in disease severity during the early part of the SARS-CoV-2 pandemic might be a result of observation bias, a consequence of the pandemic, or both. Although ICU admission rates increased for pneumococcal disease, we observed a reduction in admission CURB65 severity scores, consistent with the 2018 BTS national pneumonia audit, which also reported decreased admission CURB65 scores (*36*). This apparent discrepancy might be explained by changes in patients or their treatment (e.g., older patients with more severe disease might be less likely to receive ICU care than younger patients because of clinical prognostic decision making). Other recent changes in treatment, such as increased availability of positive pressure support or earlier antimicrobial drug administration, might also have changed patient courses and outcomes, including severity and death. Major changes in pneumococcal infection severity have occurred since 2020, including an increased percentage of adults 45–55 years of age who required hospital treatment. The recent increase in cases is probably related to relaxation of COVID-19 restrictions. Recent studies highlight the critical role of respiratory viruses (e.g., respiratory syncytial virus, human metapneumovirus, influenza virus) in contributing to pneumococcal disease (*17*). Large, out-of-season viral outbreaks that occurred after easing of COVID-19 restrictions (*37*) are therefore likely to have contributed to the increasing pneumococcal disease we report in this study, which will need careful surveillance in future years. Independent of changes in clinical practice, serotype distribution changes might affect patient outcomes and healthcare use as invasive potential varies by serotype.

One strength of this study was that we identified patients who had with pneumococcal infections in a population of ≈1 million adults and report disease over a 17-year period with epidemiologic data supported by detailed clinical information at an individualized patient level. Data on admission numbers and testing practices enabled us to interpret incidence considering these factors, which might otherwise bias the estimates obtained. In addition, linkage with the UKHSA national reference laboratory enabled us to report serotype data whenever available. Our study also reports pneumococcal disease confirmed by UAT; this result was not detected by national surveillance and enabled us to

estimate pneumococcal disease incidence and burden more accurately.

One limitation of this study was that UAT does not identify serotype; we were thus unable to report serotype data in 60% of our cohort. However, patients with known and unknown serotype disease had broadly similar demographic and clinical characteristics and outcomes. UAT has a sensitivity of 65%, so test results might remain positive for some time after pneumococcal disease has been treated (*38*). Although the data are concordant with national UKHSA epidemiologic and BTS pneumonia audit data (*36*), providing major reassurance, this regional study might not be representative of other regions or populations. As a retrospective observational study, only information as documented in medical records could be included. Patient treatment decisions might have varied over time and by treating physicians, and systemic changes in patient treatment, healthcare provision, or admission threshold and microbiologic testing practices might have occurred. Those factors might have affected the trends reported in this analysis. Finally, the serotype trends reported in 2020–2022 were based on substantially lower case numbers than those seen before the emergence of SARS-CoV-2. Ongoing monitoring of trends will be useful as disease incidence adjusts after the COVID-19 pandemic.

In conclusion, this study provides evidence that PCV13 serotypes continue to cause pneumococcal disease in adults, suggesting that indirect effects of the childhood PCV program might not lead to additional reductions in the residual burden of those serotypes in adults. After the COVID-19 pandemic, serotype distribution changes have resulted in an increase in adult pneumococcal disease attributable to PCV serotypes, and a major burden of current disease could be directly prevented by introducing PCV20, which has recently been licensed for adults. Ongoing surveillance of adult pneumococcal disease is vital to evaluate vaccine effect and monitor replacement disease. The extent of indirect effects of PCVs should continue to be carefully evaluated and considered in formulating future public health policy recommendations.

Acknowledgments

We thank the research teams at The Royal United, North Bristol, and University Hospitals of Bristol and Weston National Health Service Trusts for participating in the study. Data used in this study are sensitive and cannot be made publicly available without breaching patient confidentiality rules. Therefore, individual participant data and a data dictionary are not available to other researchers.

C.H. is principal investigator of the AvonCAP study, which is an investigator-led University of Bristol study supported by Pfizer. A.F. is a member of the Joint Committee on Vaccination and Immunization and was, until December 2022, chair of the World Health Organization European Technical Advisory Group of Experts on Immunization committee. In addition to receiving support from Pfizer as chief investigator of the AvonCAP study, he leads another project investigating transmission of respiratory bacteria in families jointly supported by Pfizer and the Gates Foundation. The other authors have no relevant conflicts of interest to declare.

Contributions: C.H., R.C., O.M.W., S.L., and A.F. generated research questions and the analysis plan; C.H., R.H., D.H., G.F., R.C., P.N., P.W., and Z.A.C. collected data; C.H., R.H., and D.H. verified data; C.H., R.C., L.D., and A.F. analyzed data; and A.F., O.M.W., and A.M. provided oversight of the research. All authors contributed to preparation of the manuscript and its revision for publication and had responsibility for the decision to publish.

About the Author

Dr. Hyams is a postdoctoral research fellow at the University of Bristol, Bristol, UK. Her primary research interests are respiratory infections, such as pneumococcus, respiratory syncytial virus, and COVID-19, and vaccine effectiveness.

References

1. UK Health Security Agency. Pneumococcal: the green book. Chapter 25. 2022 [cited 2023 Mar 10]. https://www.gov.uk/government/publications/pneumococcal-the-green-book-chapter-25
2. Chan J, Nguyen CD, Dunne EM, Kim Mulholland E, Mungun T, Pomat WS, et al. Using pneumococcal carriage studies to monitor vaccine impact in low- and middle-income countries. Vaccine. 2019;37:6299–309. https://doi.org/10.1016/j.vaccine.2019.08.073
3. Loughlin AM, Hsu K, Silverio AL, Marchant CD, Pelton SI. Direct and indirect effects of PCV13 on nasopharyngeal carriage of PCV13 unique pneumococcal serotypes in Massachusetts' children. Pediatr Infect Dis J. 2014;33:504–10. https://doi.org/10.1097/INF.0000000000000279
4. Simell B, Auranen K, Käyhty H, Goldblatt D, Dagan R, O'Brien KL; Pneumococcal Carriage Group. The fundamental link between pneumococcal carriage and disease. Expert Rev Vaccines. 2012;11:841–55. https://doi.org/10.1586/erv.12.53
5. Ladhani SN, Collins S, Djennad A, Sheppard CL, Borrow R, Fry NK, et al. Rapid increase in non-vaccine serotypes causing invasive pneumococcal disease in England and Wales, 2000–17: a prospective national observational cohort study. Lancet Infect Dis. 2018;18:441–51. https://doi.org/10.1016/S1473-3099(18)30052-5
6. Miller E, Andrews NJ, Waight PA, Slack MP, George RC. Herd immunity and serotype replacement 4 years

after seven-valent pneumococcal conjugate vaccination in England and Wales: an observational cohort study. Lancet Infect Dis. 2011;11:760–8. https://doi.org/10.1016/S1473-3099(11)70090-1
7. Waight PA, Andrews NJ, Ladhani SN, Sheppard CL, Slack MP, Miller E. Effect of the 13-valent pneumococcal conjugate vaccine on invasive pneumococcal disease in England and Wales 4 years after its introduction: an observational cohort study. Lancet Infect Dis. 2015;15:535–43. https://doi.org/10.1016/S1473-3099(15)70044-7
8. Holubar M, Stavroulakis MC, Maldonado Y, Ioannidis JP, Contopoulos-Ioannidis D. Impact of vaccine herd-protection effects in cost-effectiveness analyses of childhood vaccinations. A quantitative comparative analysis. PLoS One. 2017;12:e0172414. https://doi.org/10.1371/journal.pone.0172414
9. Temple B, Toan NT, Uyen DY, Balloch A, Bright K, Cheung YB, et al. Evaluation of different infant vaccination schedules incorporating pneumococcal vaccination (The Vietnam Pneumococcal Project): protocol of a randomised controlled trial. BMJ Open. 2018;8:e019795. https://doi.org/10.1136/bmjopen-2017-019795
10. Centers for Disease Control and Prevention. Pneumococcal disease: surveillance and reporting 2023 [cited 2023 Jun 13]. https://www.cdc.gov/pneumococcal/surveillance.html
11. Lewnard JA, Hanage WP. Making sense of differences in pneumococcal serotype replacement. Lancet Infect Dis. 2019;19:e213–20. https://doi.org/10.1016/S1473-3099(18)30660-1
12. Pick H, Daniel P, Rodrigo C, Bewick T, Ashton D, Lawrence H, et al. Pneumococcal serotype trends, surveillance and risk factors in UK adult pneumonia, 2013–18. Thorax. 2020;75:38–49. https://doi.org/10.1136/thoraxjnl-2019-213725
13. Amin-Chowdhury Z, Aiano F, Mensah A, Sheppard CL, Litt D, Fry NK, et al. Impact of the coronavirus disease 2019 (COVID-19) pandemic on invasive pneumococcal disease and risk of pneumococcal coinfection with severe acute respiratory syndrome coronavirus 2 (SARS-CoV-2): prospective national cohort study, England. Clin Infect Dis. 2021;72:e65–75. https://doi.org/10.1093/cid/ciaa1728
14. Chow EJ, Uyeki TM, Chu HY. The effects of the COVID-19 pandemic on community respiratory virus activity. Nat Rev Microbiol. 2023;21:195–210. https://doi.org/10.1038/s41579-022-00807-9
15. Her Majesty's Government. Social distancing review. 2021 [cited 2023 Mar 10]. https://assets.publishing.service.gov.uk/government/uploads/system/uploads/attachment_data/file/999413/Social-Distancing-Review-Report.pdf
16. Choi YH, Miller E. Impact of COVID-19 social distancing measures on future incidence of invasive pneumococcal disease in England and Wales: a mathematical modelling study. BMJ Open. 2021;11:e045380. https://doi.org/10.1136/bmjopen-2020-045380
17. Dagan R, van der Beek BA, Ben-Shimol S, Greenberg D, Shemer-Avni Y, Weinberger DM, et al. The COVID-19 pandemic as an opportunity for unravelling the causative association between respiratory viruses and pneumococcus-associated disease in young children: a prospective study. EBioMedicine. 2023;90:104493. https://doi.org/10.1016/j.ebiom.2023.104493
18. Lim WS, Baudouin SV, George RC, Hill AT, Jamieson C, Le Jeune I, et al.; Pneumonia Guidelines Committee of the BTS Standards of Care Committee. BTS guidelines for the management of community acquired pneumonia in adults: update 2009. Thorax. 2009;64(Suppl 3):iii1–55. https://doi.org/10.1136/thx.2009.121434
19. Brown LD, Cai TT, DasGupta A. Interval estimation for a binomial proportion. Stat Sci. 2001;16:101–33. https://doi.org/10.1214/ss/1009213286
20. Ripley BD. Pattern recognition and neural networks. Cambridge: Cambridge University Press; 1996. https://doi.org/10.1017/CBO9780511812651
21. Loader C. Local regression and likelihood. New York: Springer-Verlag; 1999. https://doi.org/10.1007/b98858
22. Hanquet G, Krizova P, Dalby T, Ladhani SN, Nuorti JP, Danis K, et al.; SpIDnet group1. Serotype replacement after introduction of 10-valent and 13-valent pneumococcal conjugate vaccines in 10 countries, Europe. Emerg Infect Dis. 2022;28:137–8. https://doi.org/10.3201/eid2801.210734
23. Groves N, Sheppard CL, Litt D, Rose S, Silva A, Njoku N, et al. Evolution of *Streptococcus pneumoniae* Serotype 3 in England and Wales: a major vaccine evader. Genes (Basel). 2019;10:845. https://doi.org/10.3390/genes10110845
24. Cassiolato AP, Almeida SCG, Andrade AL, Minamisava R, Brandileone MCC. Expansion of the multidrug-resistant clonal complex 320 among invasive *Streptococcus pneumoniae* serotype 19A after the introduction of a ten-valent pneumococcal conjugate vaccine in Brazil. PLoS One. 2018;13:e0208211. https://doi.org/10.1371/journal.pone.0208211
25. Flasche S, Van Hoek AJ, Goldblatt D, Edmunds WJ, O'Brien KL, Scott JA, et al. The potential for reducing the number of pneumococcal conjugate vaccine doses while sustaining herd immunity in high-income countries. PLoS Med. 2015;12:e1001839. https://doi.org/10.1371/journal.pmed.1001839
26. NHS Digital. Childhood vaccination coverage statistics, England. 2021–22 [cited 2023 Mar 13]. https://digital.nhs.uk/data-and-information/publications/statistical/nhs-immunisation-statistics/2021-22
27. van der Linden M, Falkenhorst G, Perniciaro S, Imöhl M. Effects of infant pneumococcal conjugate vaccination on serotype distribution in invasive pneumococcal disease among children and adults in Germany. PLoS One. 2015;10:e0131494. https://doi.org/10.1371/journal.pone.0131494
28. Løchen A, Croucher NJ, Anderson RM. Divergent serotype replacement trends and increasing diversity in pneumococcal disease in high income settings reduce the benefit of expanding vaccine valency. Sci Rep. 2020;10:18977. https://doi.org/10.1038/s41598-020-75691-5
29. Ahmed SS, Pondo T, Xing W, McGee L, Farley M, Schaffner W, et al. Early impact of 13-valent pneumococcal conjugate vaccine use on invasive pneumococcal disease among adults with and without underlying medical conditions, United States. Clin Infect Dis. 2020;70:2484–92. https://doi.org/10.1093/cid/ciz739
30. Lewnard JA, Hanage WP. Making sense of differences in pneumococcal serotype replacement. Lancet Infect Dis. 2019;19:e213–20. https://doi.org/10.1016/S1473-3099(18)30660-1
31. Sender V, Hentrich K, Henriques-Normark B. Virus-induced changes of the respiratory tract environment promote secondary infections with *Streptococcus pneumoniae*. Front Cell Infect Microbiol. 2021;11:643326. https://doi.org/10.3389/fcimb.2021.643326
32. Weinberger DM, Klugman KP, Steiner CA, Simonsen L, Viboud C. Association between respiratory syncytial virus activity and pneumococcal disease in infants: a time series analysis of US hospitalization data. PLoS Med. 2015;12:e1001776. https://doi.org/10.1371/journal.pmed.1001776
33. Mitsi E, Reiné J, Urban BC, Solórzano C, Nikolaou E, Hyder-Wright AD, et al. *Streptococcus pneumoniae* colonization

associates with impaired adaptive immune responses against SARS-CoV-2. J Clin Invest. 2022;132:e157124. https://doi.org/10.1172/JCI157124
34. Brueggemann AB, Jansen van Rensburg MJ, Shaw D, McCarthy ND, Jolley KA, Maiden MCJ, et al. Changes in the incidence of invasive disease due to *Streptococcus pneumoniae*, *Haemophilus influenzae*, and *Neisseria meningitidis* during the COVID-19 pandemic in 26 countries and territories in the invasive respiratory infection surveillance initiative: a prospective analysis of surveillance data. Lancet Digit Health. 2021;3:e360–70. https://doi.org/10.1016/S2589-7500(21)00077-7
35. Alqahtani JS, Oyelade T, Aldhahir AM, Mendes RG, Alghamdi SM, Miravitlles M, et al. Reduction in hospitalised COPD exacerbations during COVID-19: a systematic review and meta-analysis. PLoS One. 2021;16:e0255659. https://doi.org/10.1371/journal.pone.0255659
36. British Thoracic Society. National adult community acquired pneumonia audit. 2018/19.| Better lung health for all [cited 2023 Mar 10]. https://www.brit-thoracic.org.uk/quality-improvement/clinical-audit/national-adult-community-acquired-pneumonia-audit-201819/
37. UK Health Security Agency. Surveillance of influenza and other seasonal respiratory viruses in winter 2021 to 2022. September 30, 2022 [cited 2023 Mar 27]
38. Hyams C, Williams OM, Williams P. Urinary antigen testing for pneumococcal pneumonia: is there evidence to make its use uncommon in clinical practice? ERJ Open Res. 2020;6:00223–02019. https://doi.org/10.1183/23120541.00223-2019

Address for correspondence: Catherine Hyams, Bristol Vaccine Centre, 39-41 St. Michael's Hill, University of Bristol, Bristol BS8 1QU, UK; email: catherine.hyams@bristol.ac.uk

Spike in Congenital Syphilis, Mississippi, USA, 2016–2022

Manuela Staneva, Charlotte V. Hobbs, Thomas Dobbs

In support of improving patient care, this activity has been planned and implemented by Medscape, LLC and Emerging Infectious Diseases. Medscape, LLC is jointly accredited with commendation by the Accreditation Council for Continuing Medical Education (ACCME), the Accreditation Council for Pharmacy Education (ACPE), and the American Nurses Credentialing Center (ANCC), to provide continuing education for the healthcare team.

Medscape, LLC designates this Journal-based CME activity for a maximum of 1.00 ***AMA PRA Category 1 Credit(s)™***. Physicians should claim only the credit commensurate with the extent of their participation in the activity.

Successful completion of this CME activity, which includes participation in the evaluation component, enables the participant to earn up to 1.0 MOC points in the American Board of Internal Medicine's (ABIM) Maintenance of Certification (MOC) program. Participants will earn MOC points equivalent to the amount of CME credits claimed for the activity. It is the CME activity provider's responsibility to submit participant completion information to ACCME for the purpose of granting ABIM MOC credit.

All other clinicians completing this activity will be issued a certificate of participation. To participate in this journal CME activity: (1) review the learning objectives and author disclosures; (2) study the education content; (3) take the post-test with a 75% minimum passing score and complete the evaluation at http://www.medscape.org/journal/eid; and (4) view/print certificate. For CME questions, see page 2188.

NOTE: It is Medscape's policy to avoid the use of Brand names in accredited activities. However, in an effort to be as clear as possible, the use of brand names should not be viewed as a promotion of any brand or as an endorsement by Medscape of specific products.

Release date: September 20, 2023; Expiration date: September 20, 2024

Learning Objectives

Upon completion of this activity, participants will be able to:

- Distinguish characteristics of infants with congenital syphilis
- Analyze changes in the incidence of congenital syphilis
- Evaluate risk factors for congenital syphilis
- Assess clinical outcomes of infants with congenital syphilis

CME Editor

Tony Pearson-Clarke, MS, Technical Writer/Editor, Emerging Infectious Diseases. *Disclosure: Tony Pearson-Clarke, MS, has no relevant financial relationships.*

CME Author

Charles P. Vega, MD, Health Sciences Clinical Professor of Family Medicine, University of California, Irvine School of Medicine, Irvine, California. *Disclosure: Charles P. Vega, MD, has the following relevant financial relationships: served as a consultant or advisor for Boehringer Ingelheim; GlaxoSmithKline; Johnson & Johnson.*

Authors

Manuela Staneva, MD, MPH; Charlotte V. Hobbs, MD; Thomas Dobbs, MD, MPH.

Author affiliations: Mississippi State Department of Health, Jackson, Mississippi, USA (M. Staneva); University of Mississippi Medical Center, Jackson (C.V. Hobbs, T. Dobbs)

DOI: https://doi.org/10.3201/eid2910.230421

In Mississippi, USA, infant hospitalization with congenital syphilis (CS) spiked by 1,000%, from 10 in 2016 to 110 in 2022. To determine the causes of this alarming development, we analyzed Mississippi hospital discharge data to evaluate trends, demographics, outcomes, and risk factors for infants diagnosed with CS hospitalized during 2016–2022. Of the 367 infants hospitalized with a CS diagnosis, 97.6% were newborn, 92.6% were covered by Medicaid, 71.1% were African American, and 58.0% were nonurban residents. Newborns with CS had higher odds of being affected by maternal illicit drug use, being born prematurely (<37 weeks), and having very low birthweight (<1,500 g) than those without CS. Mean length of hospital stay (14.5 days vs. 3.8 days) and mean charges ($56,802 vs. $13,945) were also higher for infants with CS than for those without. To address escalation of CS, Mississippi should invest in comprehensive prenatal care and early treatment of vulnerable populations.

Congenital syphilis (CS), caused by infection with the bacterium *Treponema pallidum*, is a severe disease with potential for immediate and long-term health complications. Infection in pregnant mothers can lead to serious neonatal conditions, such as deformities, hepatosplenomegaly, anemia, jaundice, and failure to thrive (*1*). Even though syphilis can be asymptomatic in infants at birth, later sequalae, such as neurologic disorders, occur in ≈40% of untreated children (*2*). In addition, syphilis has been associated with severe pregnancy outcomes, including spontaneous abortion, preterm delivery, stillbirth, and infant death (*3*).

According to Centers for Disease Control and Prevention surveillance data, the nationwide rate of CS increased by 30.5% in 1 year, from 59.7/100,000 live births in 2020 to 77.9/100,000 live births in 2021 (*4*). In some states, CS rates increased even more dramatically. In Mississippi, for example, CS incidence rose from 104.3/100,000 live births in 2020 to 182.0/100,000 live births in 2021, a 74.5% jump in a single year. For this study, we examined trends, demographics, risk factors, coexisting conditions, and outcomes among infants in Mississippi hospitalized with a CS diagnosis. We aimed to better understand this emerging public health crisis in a state that continues to experience deep social and health inequities.

Methods

Data

For this retrospective cross-sectional study, we analyzed hospital discharge data from Mississippi for 2016–2022. The Mississippi State Department of Health, in collaboration with the Mississippi Hospital Association, collects those data and shares them with the Agency for Healthcare Research and Quality Healthcare Cost and Utilization Project as part of the organization's national hospital care database (*5*). The rich population-level data contain demographic, clinical, and financial information derived from billing claims submitted by all nonfederal acute-care hospitals in Mississippi.

Case Definition

For this study, we included infants ≤1 year of age living in Mississippi. To meet the goals of our investigation, we created 2 study groups. The first comprised all infants hospitalized with CS, including those diagnosed at delivery hospitalization and those who were admitted after delivery (postdelivery subcohort). We used data from this more inclusive group to study prevalence, trends, and demographics among infants hospitalized with CS. The second group (delivery subcohort) included only infants either delivered in the hospital or delivered outside of the hospital but admitted with a delivery code from the International Classification of Diseases, 10th Revision, Clinical Modification (ICD-10-CM). We needed data from the delivery subcohort because we were interested in pregnancy outcomes associated with syphilis, including preterm and low-birthweight deliveries. To identify the delivery subcohort, we developed an algorithm that incorporated infant age and ICD-10-CM code Z38, the neonatal diagnostic code for birth. In hospital discharge data, neonatal patient age was based on date of admission. In our delivery subcohort, we included all infants whose ages were recorded as 0–3 days with day 0 being the day of birth.

Data Variables

We used ICD-10-CM code A50 to identify diagnoses of infant hospitalizations with CS. We referenced related ICD-10-CM codes to study newborns affected by maternal use of illicit substances: opiates (P04.14), amphetamines (P04.16), cocaine (P04.41), hallucinogens (P04.42), cannabis (P04.81), unspecified drugs of addiction (P04.40, P04.49), and neonatal abstinence syndrome (P9.61; i.e., severe withdrawal symptoms). For preterm deliveries, we referenced codes P0.72 for extreme newborn immaturity (≤27 completed weeks of gestation) and P0.73 for premature births (≤36 completed weeks of gestation). We referenced ICD-10-CM code P22 to screen the data for newborn respiratory distress, which were of special interest for this study because this condition is a major cause of neonatal illness and death (*6*). To evaluate birthweight, we used the variable for birthweight in the dataset.

Likewise, we detected deaths of infants with diagnosed CS based on the dataset variable for discharge status, which includes in-hospital deaths. Finally, we used neonatal ICD-10-CM code P95 to identify stillbirths and screened those records for CS diagnoses.

For our research, we collected key demographic characteristics, such as urbanicity, race, and socioeconomic status, for each individual CS patient. We defined urban versus nonurban status on the basis of the CDC National Centers for Health Statistics urban–rural classification scheme (7), in which counties with ≥50,000 inhabitants are classified urban and counties with <50,000 nonurban (10,000–49,999, micropolitan; <10,000, rural). We categorized data on race into 3 groups: African American, White, and others (because few infants with CS in the study were not either African American or White). The following racial categories are included in the hospital discharge dataset: White, African American/Black, American Indian/Alaska Native, Asian, Native Hawaiian/other Pacific Islander, multiracial, declined, and race unavailable/unknown. We were unable to examine ethnicity because few infants of Hispanic origin were included in the CS cohort. We used Medicaid insurance coverage as a proxy for low socioeconomic status.

Statistical Analyses

We used data from individual patients as units of analysis. To select individual patients, we used unique identifying numbers and flagged the first hospitalization for each patient. We included only data from first admissions, not transfers or readmissions. Our analyses included descriptive and inferential statistics. We compared demographic and clinical characteristics between patients with and without CS using independent t-tests for continuous variables and χ^2 tests for categorical variables. To evaluate the strength of association between different demographic and clinical factors and CS, we performed multivariable regression and obtained adjusted odds ratios (aORs) (*8*). We conducted all analyses using SAS 9.2 statistical software (*9*).

Results

During the 2016–2022 study period, 367 infants were hospitalized in Mississippi with diagnosed CS. Of those infants, 97.6% were newborn (≤28 days), 92.6% covered by Medicaid, 71.1% African American, and 58.0% residents of nonurban counties; 50.7% were male and 49.3% female. Most infants with CS (340; 92.6%) were identified as delivery hospitalizations and included in the delivery subcohort. The remaining 27 infants were postdelivery admissions. Among the postdelivery admissions, 18 were newborn and 9 were >28 days of age, meaning ≈7% of the infants with CS received the diagnosis during postdelivery hospitalization.

Trend Analyses

The number of infants hospitalized with CS spiked by 1,000% over the study period, rising sharply from 10 infants in 2016 to 110 in 2022 (Figure 1, panel A). The rate of hospitalization of infants with CS increased from 2.0/10,000 total infant hospitalizations in 2016 to 24.8/10,000 total infant hospitalizations in 2022, representing a 1,140% increase (Figure 1, panel B). Additional analyses revealed 2 notable trends. First, the rate increase in the number of infants hospitalized with CS varied by race. Although infants with CS were overwhelmingly African American, the magnitude of increase was higher among White infants. Among African American infants, CS hospitalizations increased by 1,029%, rising from 7 infants in 2016 to 79 in 2022. Over the same time period, the admissions

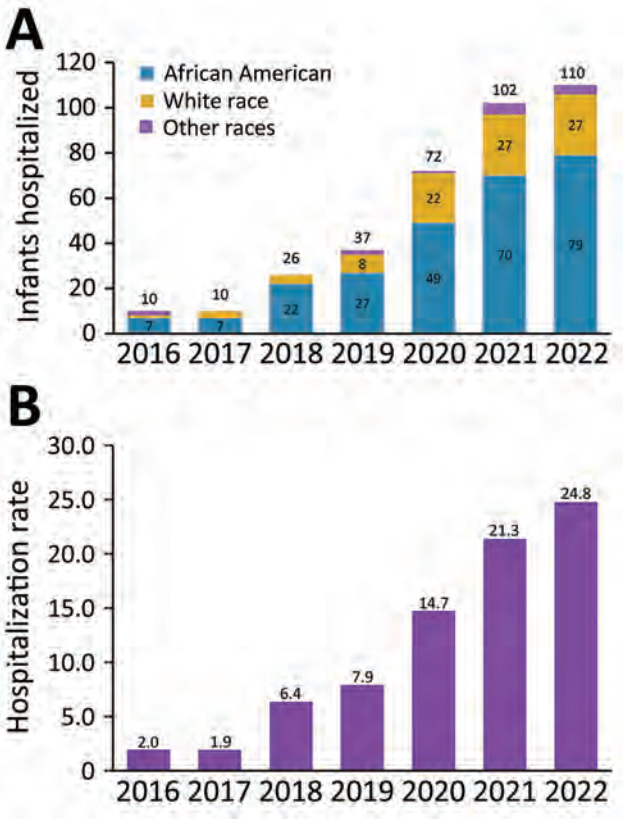

Figure 1. Infants hospitalized with congenital syphilis, Mississippi, USA, 2016–2022. A) Number of infants hospitalized by year and race. B) Hospitalization rates for congenital syphilis per 10,000 delivery hospitalizations. Numbers above bars are rates for each year. We obtained the rates by dividing the number of infants hospitalized with congenital syphilis by the total number of delivery hospitalizations per year.

among White infants jumped by 2,600%, from 1 infant in 2016 to 27 in 2022. Second, hospitalization for infants with CS started to increase in 2018, before the onset of the COVID-19 crisis; the pandemic, however, accelerated this uptrend.

Demographic Risk Factors

Bivariate analyses of associations between CS and different demographic characteristics revealed that infants with CS were more likely than those without to be African American (71.1% vs. 43.3%; p<0.001), covered by Medicaid (92.6% vs. 63.9%; p<0.001), and >3 days of age (7.4% vs. 2.0%; p<0.001). After adjusting for covariates, Medicaid insurance coverage (aOR, 5.24, 95% CI, 3.58–8.00) was the strongest independent demographic risk factor; however, infants >3 days of age (aOR, 3.82, 95% CI, 2.52–5.55) and African American race (aOR, 2.26, 95% CI, 1.37–4.06) also retained associations with congenital syphilis risk (Table 1).

Clinical Characteristics of the Delivery Cohort

We compared findings on clinical characteristics from this analysis between infants with and without CS (Table 2). In the bivariate analysis, newborns with CS were significantly more likely than those without CS (21.5% vs. 2.4%; p<0.001) to have a maternal illicit drug use ICD-10-CM code on record. Among newborns with CS, 73 were affected by maternal substance use; however, only 36/73 (49.3%) records for those newborns included a substance-specific diagnostic code. Among those 36 infants, maternal use of cannabis was recorded for 69.4%, cocaine 27.8%, amphetamines 25.0%, and opioids 2.8%. Drug-use categories were not mutually exclusive, and 7/36 CS-infected newborns with recorded substance-specific diagnostic codes were exposed to >1 substance in utero. Neonatal abstinence syndrome was present in 8 cases.

In the multivariable analysis of clinical characteristics, the variable with the strongest association with CS was maternal substance use. Even after controlling for demographic risk factors, the CS cohort had almost 10 times higher odds of being affected by maternal illicit drug use than the cohort without CS (aOR, 9.39, 95% CI 7.16–12.16). Aside from minor variations, the proportion of maternal illicit drug use among the CS cohort remained high throughout the study period. In 2016, the year with the highest proportion of substance-exposed infants, 25% of all newborns with CS also had a diagnostic code indicating maternal use of illicit drugs. During the last 3 years of the study period, there was a gradual but steady increase in the proportion of newborns hospitalized with CS and exposed to illicit substances in utero: 17.7% in 2020, 22.7% in 2021, and 23.8% in 2022 (Figure 2).

Infants in the CS cohort were also more likely to suffer from severe complications, including prematurity and low birthweight, than infants in the cohort without CS. Among newborns with CS, 92 (27.1%) were premature, compared with 43 (12.7%) for newborns without CS. Among premature infants with CS, 8/92 were extremely premature (i.e., born before completing 28 weeks of gestation). Newborns with CS had >2 times higher odds of being born prematurely than did newborns without CS (aOR 2.26, 95% CI 1.77–2.86) after controlling for demographic risk factors. Among 87 newborns with CS who had birthweights <2,500 g, 59 had low birthweight (LBW) of 1,500–2,499 g and 28 had very low birthweight (VLBW) of <1,500 g. Compared with the cohort without CS, infants in the CS cohort were

Table 1. Demographic characteristics of infants hospitalized with and without congenital syphilis diagnosis, Mississippi, USA, 2016–2022

Patient characteristics	Congenital syphilis, no. (%)	No congenital syphilis, no. (%)	p value	Crude odds ratio (95% CI)	Adjusted odds ratio (95% CI)
Total	367	238,227			
Age group, d					
0–3	340 (92.6)	233,528 (98.0)	<0.001	Referent	Referent
4–365	27 (7.4)	4,699 (2.0)		3.947 (2.60–5.73)	3.82 (2.52–5.55)
Sex				Referent	Referent
F	179 (49.0)	116,615 (49.0)	0.981	1.003 (0.82–1.23)	1.01 (0.82–1.24)
M	186 (51.0)	121,483 (51.0)		Referent	Referent
Race					
African American	261 (71.1)	103,102 (43.3)	<0.001	2.83 (1.72–5.07)	2.26 (1.37–4.06)
White	92 (25.1)	119,502 (50.2)		0.86 (0.51–1.58)	1.01 (0.60–1.86)
Other	14 (3.8)	15,623 (6.5)		Referent	Referent
Residence					
Nonurban	213 (58.0)	133,829 (56.2)	0.472	1.08 (0.88–1.33)	1.02 (0.83–1.26)
Urban	154 (42.0)	104,398 (43.8)		Referent	Referent
Primary expected payer					
Medicaid	340 (92.6)	152,221 (63.9)	<0.001	7.11 (4.91–10.78)	5.24 (3.58–8.00)
Private/other	27 (7.4)	86,006 (36.1)		Referent	Referent

Table 2. Delivery subcohort: clinical characteristic for infants with and without congenital syphilis, Mississippi, USA, 2016–2022

Infant characteristics	Congenital syphilis, no. (%)	No congenital syphilis, no. (%)	p value	Crude odds ratio (95% CI)	Adjusted odds ratio (95% CI)*
Maternal substance use	340	233,529	<0.001		
Y	73 (21.5)	5,597 (2.4)		11.14 (8.53–14.36)	9.39 (7.16–12.16)
N	267 (78.5)	227,932 (97.6)		Referent	Referent
Birthweight†					
Very low birthweight	28 (8.5)	4,430 (1.9)	<0.001	5.38 (3.55–7.81)	4.05 (2.67–5.90)
Low birthweight	59 (17.9)	22,556 (9.7)		2.23 (1.66–2.94)	1.81 (1.35–2.40)
Normal birthweight	242 (73.6)	205,901 (88.3)		Referent	Referent
Preterm					
Y	92 (27.1)	29,544 (12.7)	<0.001	2.56 (2.01–3.24)	2.26 (1.77–2.86)
N	248 (72.9)	203,985 (87.3)		Referent	Referent
Newborn respiratory distress					
Y	72 (21.2)	21,204 (9.1)	<0.001	2.69 (2.06–3.47)	2.54 (1.94–3.28)
N	268 (78.8)	212,325 (90.9)		Referent	Referent

*Each of the models was adjusted for demographic characteristics, including race, sex, residence, and payer. We excluded newborns of undetermined/unknown sex from this analysis.
†Not all newborn records had recorded birthweight; therefore, we excluded newborns with unknown birthweight from this analysis (11 records for the congenital syphilis cohort and 642 records for the cohort without congenital syphilis). Very low birthweight, <1,500 g; low birthweight, 1,500-2,500 g; normal birthweight, >2,500 g.

more likely to be LBW (17.9% vs. 9.7%; p<0.001) and VLBW (8.5% vs. 1.9%; p<0.001). Alarmingly, odds for newborns with CS to be LBW were nearly 2 times higher (aOR 1.81, 95% CI 1.35–2.40) and to be VLBW >4 times higher (aOR 4.05, 95% CI 2.67–5.90) than for newborns without CS. On average, newborns with CS weighed 349 g less (mean birthweight 2,788 g) than newborns without CS (3,137 g; p<0.001) (Figure 3). Newborn respiratory distress was also more common among the CS cohort (21.2%) than for the cohort without CS (9.1%; p<0.001). Given the well-established connection between prematurity and respiratory distress in newborns, it is unsurprising that 1 in 5 premature newborns with CS in our study was also diagnosed with respiratory distress. Among the 72 newborns with diagnoses for CS and respiratory distress, 48 (66.7%) also had a diagnostic code for preterm delivery.

Use of Resources

In terms of resource use, infants with CS had a longer mean hospital stay (14.5 days vs. 3.8 days; p<0.001) and mean hospital charges ($56,802 vs. $13,945; p<0.001) than did infants without CS. During 2016–2022, hospital charges for the CS cohort totaled $20,846,196; Medicaid-insured infants accounted for $19,444,608 (93.3%) of those charges.

Mortality

During the last 4 years of the study period (2019–2022), 6 infants with CS died in hospital, half of those during the last year of the study period (2022). Among the infants with CS who died, 83.3% had extremely low birthweight (<1,500 g), and 66.7% were extremely premature. Among our study population, no records indicated both stillbirth and CS.

Discussion

From 2016 through 2022, CS hospitalization rates in Mississippi increased more than 10-fold. Although the upward trend was consistent with national-level surveillance data for CS, the upturn in Mississippi was even steeper (*10*). This spike is troubling because decades of research have demonstrated the dire health consequences of CS, including prematurity, low birthweight, and death (*11*).

As CS rates in Mississippi rose steeply in recent years, associated harmful health outcomes contributed to the already high state infant illness and death burden. In our study, the percentage of premature infants among the CS cohort (27.1%) was >2 times higher than for the cohort without CS (12.7%). Likewise, the CS cohort had a higher proportion of newborns with VLBW. We acknowledge that other associated risk factors more commonly seen in the CS cohort, such as maternal substance abuse, might also have contributed to this difference. Still, those differences require urgent action because preterm birth

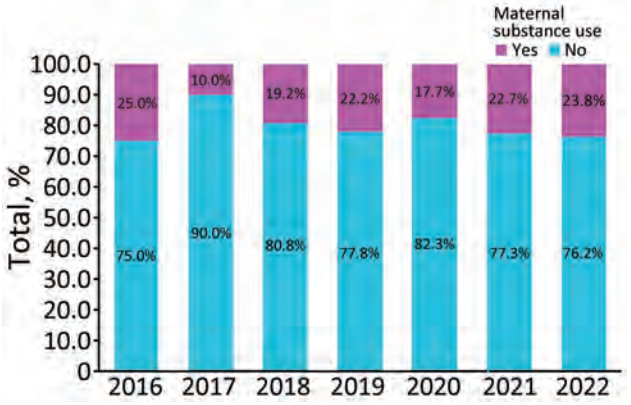

Figure 2. Maternal illicit drug use among newborns with congenital syphilis, Mississippi, USA, 2016–2022.

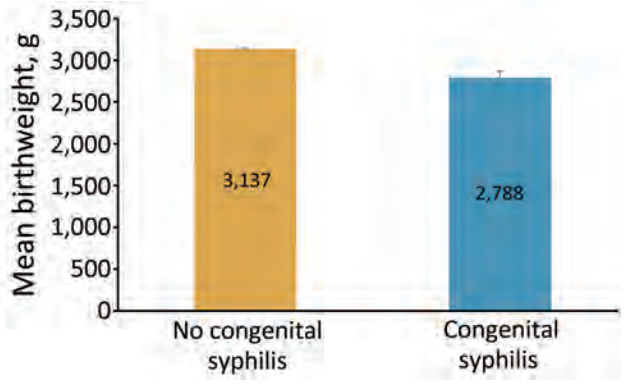

Figure 3. Mean birthweight for newborns with and without congenital syphilis, Mississippi, USA, 2016–2022. Error bars indicate 95% CIs.

and VLBW are leading causes of infant death in Mississippi, a state that already has the highest preterm birth and infant mortality rates in the nation (*12*).

Our study provides evidence that the spike in CS is already elevating the high number of infant deaths in the state. Our research identified 6 infant deaths associated with a CS diagnosis during the study period. Half those deaths occurred in 2022, underlying the current nature of this rapidly escalating reemergent public health menace and urgent need for public health interventions. Infant deaths associated with CS are preventable; Mississippi could reduce infant illness and death by promptly diagnosing and treating pregnant patients with syphilis (*13*).

In addition to harmful health sequalae, CS was associated with significant healthcare expenditure as measured by the mean length of stay and hospital charges. The mean length of stay was nearly 4 times higher among the CS cohort than for the cohort without CS. Furthermore, total charges for this preventable condition reached >$20 million during the 7-year study period. This result further underlines the pressing need to prevent CS to reduce its physical and economic toll in Mississippi.

To combat this emerging crisis, however, it is critical to understand the different behavioral, social, and economic factors driving up maternal syphilis rates (*14*–*16*). In Mississippi, for example, the rise in the CS rate paralleled another concerning trend: rapid increase in newborn hospitalization associated with maternal substance use (*17*). In our study, nearly 1 in 4 infants with CS was born to a mother with a substance use disorder. This finding reveals the entanglement between the ongoing drug epidemic and the resurgence of maternal and congenital syphilis and suggests the need for holistic approaches that treat illicit drug use as one way to curtail CS rates (*18*).

We further uncovered substantial economic and racial disparities among families of infants diagnosed with CS, consistent with previous research (*19*). In our study, >70% of infants hospitalized with CS were African American, and nearly all (91%) infants with this diagnosis were insured by Medicaid. Our demographic analysis demonstrates the intertwined nature of social, economic, and racial disparities with health outcomes and highlights the roles of poverty and institutional racism in fueling transmission of severe but preventable infections, such as syphilis (*20*).

In addition to behavioral and socioeconomic risk factors, insufficient prenatal screening has been implicated in rapidly rising CS rates (*21*,*22*). Until March 2023, Mississippi was one of only a few states not mandating syphilis screening for prospective mothers (*23*,*24*). By contributing to underscreening, this policy omission led to missed opportunities to detect and treat maternal syphilis before the birth of infants. Despite being a resource-constrained state with a history of profound health disparities, Mississippi has neither expanded Medicaid nor adopted presumptive eligibility for uninsured pregnant persons. Failure to pursue such policies created more structural barriers for early and effective prenatal care that enabled the syphilis problem to persist and grow. Redirected public health efforts and disrupted medical care because of the COVID-19 pandemic also played roles in ratcheting up CS incidence by impeding prevention efforts and consequentially precipitating increased syphilis transmission (*25*,*26*). Those and other obstacles to timely prenatal testing and care have delayed diagnosis and treatment of syphilis case-patients during pregnancy.

To address the evolving CS crisis in Mississippi effectively, comprehensive public health and health policy approaches must be implemented. State agencies and political leaders should be encouraged to adopt all available tools to support early comprehensive prenatal care. At the front line of this battle, public health structures should receive adequate resources to diagnose and treat the most vulnerable populations, including underserved and uninsured/underinsured infected mothers, in a timely and effective manner. In addition, healthcare providers and systems should align their processes to prioritize and ensure early diagnosis and treatment of syphilis in pregnancy. Enhancing sexual health literacy, including providing comprehensive sex education for youth, would further empower Mississippi residents to prevent or seek treatment for reemerging syphilis infection.

Our investigation shows that the rapid rise of CS hospitalizations in Mississippi is a serious public health concern because of its grave social and health-related consequences. By analyzing hospital discharge records from Mississippi, we performed an in-depth epidemiologic evaluation of infants hospitalized with CS. Although limited by lack of data on prenatal care, perinatal syphilis treatment, and laboratory diagnostic tests, the database provided population-level data that enabled us to explore statewide trends, study comorbidities and costs, and make robust inferences specific to the population of Mississippi. Study findings suggest the benefits of obtaining more granular data, improving public health surveillance, and enhancing education for physicians and providers to diagnose and treat syphilis.

Congenital syphilis is a disease with dire health, social, and financial consequences that can be prevented. Providing comprehensive prenatal care, effective screening, and early treatment for pregnant women in Mississippi constitute not only sound public health policy in general but also smart strategies to improve pregnancy outcomes, reduce infant illness and death, curtail medical costs, and promote greater health equity.

About the Author

Dr. Staneva is an epidemiologist with the Mississippi State Department of Health. Her research work is devoted to the use of population-level healthcare data for building robust public health surveillance systems. Dr. Dobbs is an infectious disease physician, a former Mississippi State Health Officer, and current dean of the John D. Bower School of Population Health at the University of Mississippi Medical Center. His primary research interest is the intersection between preventable diseases, health disparities, and health policies.

References

1. Centers for Disease Control and Prevention. Congenital syphilis: main clinical manifestations in infants [cited 2023 Feb 2]. https://www.cdc.gov/ncbddd/birthdefects/surveillancemanual/quick-reference-handbook/congenital-syphilis.html
2. De Santis M, De Luca C, Mappa I, Spagnuolo T, Licameli A, Straface G, et al. Syphilis infection during pregnancy: fetal risks and clinical management. Infect Dis Obstet Gynecol. 2012;2012:430585. https://doi.org/10.1155/2012/430585
3. Cooper JM, Sánchez PJ. Congenital syphilis. Semin Perinatol. 2018;42:176–84. https://doi.org/10.1053/j.semperi.2018.02.005
4. Centers for Disease Control and Prevention. Sexually transmitted disease surveillance 2021 [cited 2023 Feb 2]. https://www.cdc.gov/std/statistics/2021/default.htm
5. Agency for Healthcare Research and Quality. Healthcare Costs and Utilization Project (HCUP). Databases information. Rockville, MD. 2022 [cited 2023 June 25]. https://www.ahrq.gov/data/hcup/index.html
6. Ekhaguere OA, Okonkwo IR, Batra M, Hedstrom AB. Respiratory distress syndrome management in resource limited settings—current evidence and opportunities in 2022. Front Pediatr. 2022;10:961509. https://doi.org/10.3389/fped.2022.961509
7. Centers for Disease Control and Prevention. National Center for Health Statistics. NCHS urban-rural classification scheme for counties [cited 2023 June 25]. https://www.cdc.gov/nchs/data_access/urban_rural.htm
8. Cummings P. The relative merits of risk ratios and odds ratios. Arch Pediatr Adolesc Med. 2009;163:438–45. https://doi.org/10.1001/archpediatrics.2009.31
9. SAS Institute Inc. SAS/ACCESS 9.4 interface to ADABAS: reference. Cary (NC): SAS Institute; 2013.
10. Centers for Disease Control and Prevention. Sexually transmitted disease surveillance 2021 [cited 2023 Feb 2]. https://www.cdc.gov/std/statistics/2021/default.htm
11. Newman L, Kamb M, Hawkes S, Gomez G, Say L, Seuc A, et al. Global estimates of syphilis in pregnancy and associated adverse outcomes: analysis of multinational antenatal surveillance data. PLoS Med. 2013;10:e1001396. https://doi.org/10.1371/journal.pmed.1001396
12. Centers for Disease Control and Prevention. Infant mortality [cited 2023 Feb 2]. https://www.cdc.gov/reproductivehealth/maternalinfanthealth/infantmortality.htm
13. Pascoal LB, Carellos EVM, Tarabai BHM, Vieira CC, Rezende LG, Salgado BSF, et al. Maternal and perinatal risk factors associated with congenital syphilis. Trop Med Int Health. 2023;28:442–53. https://doi.org/10.1111/tmi.13881
14. Biswas HH, Chew Ng RA, Murray EL, Chow JM, Stoltey JE, Watt JP, et al. Characteristics associated with delivery of an infant with congenital syphilis and missed opportunities for prevention—California, 2012 to 2014. Sex Transm Dis. 2018;45:435–41. https://doi.org/10.1097/OLQ.0000000000000782
15. Schmidt R, Carson PJ, Jansen RJ. Resurgence of syphilis in the United States: an assessment of contributing factors. Infect Dis (Auckl). 2019;12:1178633719883282. https://doi.org/10.1177/1178633719883282
16. Thornton C, Chaisson LH, Bleasdale SC. Characteristics of pregnant women with syphilis and factors associated with congenital syphilis at a Chicago hospital. Open Forum Infect Dis. 2022;9:ofac169.
17. Mississippi State Department of Health. COVID-19 and neonatal hospitalizations related to maternal substance use in Mississippi: an escalating crisis. Jackson (MS). 2022 [cited 2023 Feb 2]. https://msdh.ms.gov/page/resources/19423.pdf
18. Centers for Disease Control and Prevention (CDC). Integrated prevention services for HIV infection, viral hepatitis, sexually transmitted diseases, and tuberculosis for persons who use drugs illicitly: summary guidance from CDC and the U.S. Department of Health and Human Services. MMWR Recomm Rep. 2012;61(RR-5):1–40.
19. Umapathi KK, Thavamani A, Chotikanatis K. Incidence trends, risk factors, mortality and healthcare utilization in congenital syphilis-related hospitalizations in the United States: a nationwide population analysis. Pediatr Infect Dis J. 2019;38:1126–30. https://doi.org/10.1097/INF.0000000000002445
20. Boutrin MC, Williams DR. What racism has to do with it: understanding and reducing sexually transmitted diseases in youth of color. Healthcare (Basel). 2021;9:673. https://doi.org/10.3390/healthcare9060673

21. Fang J, Silva RM, Tancredi DJ, Pinkerton KE, Sankaran D. Examining associations in congenital syphilis infection and socioeconomic factors between California's small-to-medium and large metro counties. J Perinatol. 2022;42:1434–9. https://doi.org/10.1038/s41372-022-01445-y
22. Kimball A, Torrone E, Miele K, Bachmann L, Thorpe P, Weinstock H, et al. Missed opportunities for prevention of congenital syphilis—United States, 2018. MMWR Morb Mortal Wkly Rep. 2020;69:661–5. https://doi.org/10.15585/mmwr.mm6922a1
23. Warren HP, Cramer R, Kidd S, Leichliter JS. State requirements for prenatal syphilis screening in the United States, 2016. Matern Child Health J. 2018;22:1227–32. https://doi.org/10.1007/s10995-018-2592-0
24. Mississippi State Department of Health. Emergency addition of syphilis infection during pregnancy as a reportable disease and requirement of syphilis testing during pregnancy [cited 2023 Feb 2]. https://msdh.ms.gov/page/resources/19717.pdf
25. Javaid S, Barringer S, Compton SD, Kaselitz E, Muzik M, Moyer CA. The impact of COVID-19 on prenatal care in the United States: qualitative analysis from a survey of 2519 pregnant women. Midwifery. 2021;98:102991. https://doi.org/10.1016/j.midw.2021.102991
26. Stanford KA, Almirol E, Schneider J, Hazra A. Rising syphilis rates during the COVID-19 pandemic. Sex Transm Dis. 2021;48:e81–3. https://doi.org/10.1097/OLQ.0000000000001431

Address for correspondence: Thomas Dobbs, John D. Bower School of Population Health, 2500 N State St, Jackson, MS 39216, USA; email: tdobbs@umc.edu

Carbapenem-Resistant *Klebsiella pneumoniae* in Large Public Acute-Care Healthcare System, New York, New York, USA, 2016–2022

Jennifer Lee, Subin Sunny, Elizabeth Nazarian, Mary Fornek, Marie Abdallah, Briana Episcopia, Marie-Claire Rowlinson, John Quale

Controlling the spread of carbapenem-resistant Enterobacterales is a global priority. Using National Healthcare Safety Network data, we characterized the changing epidemiology of carbapenem-resistant *Klebsiella pneumoniae* (CRKP) in a large public health system in New York, New York, USA. During 2016–2020, CRKP cases declined; however, during 2021–June 2022, a notable increase occurred. Of 509 cases, 262 (51%) were considered community-onset, including 149 in patients who were living at home. Of 182 isolates with proven or presumptive (ceftazidime/avibactam susceptible) enzymes, 143 were serine carbapenemases; most confirmed cases were *K. pneumoniae* carbapenemase. The remaining 39 cases were proven or presumptive metallo-β-lactamases; all confirmed cases were New Delhi metallo-β-lactamases. After 2020, a marked increase occurred in the percentage of isolates possessing metallo-β-lactamases. Most patients with metallo-β-lactamases originated from long-term care facilities. An aggressive and universal program involving surveillance and isolation will be needed to control the spread of CRKP in the city of New York.

Carbapenems have long served as tools in our arsenal against infections caused by multidrug resistant gram-negative bacteria; as such, the spread of carbapenem-resistant Enterobacterales (CRE) represents a serious public health threat. Because CRE infections are associated with poorer clinical outcomes and have limited treatment options, the Centers for Disease Control and Prevention has labeled CRE as an urgent threat (*1*,*2*).

Since its identification in 2001, *Klebsiella pneumoniae* carbapenemase (KPC) has been the predominant carbapenemase in CRE in medical centers across the United States (*3*,*4*). This carbapenemase has been also problematic in long-term care facilities throughout the United States (*5*,*6*). Although isolates with class B carbapenemases, particularly the New Delhi metallo-β-lactamase (NDM), are endemic in several regions of the world, they have been somewhat unusual in the United States, accounting for only ≈10% of identified carbapenemases (*4*,*7*). Given their greater resistance to β-lactam antibiotics (e.g., β-lactam/β-lactamase–inhibitor antibiotics, including ceftazidime/avibactam), the spread of isolates harboring metallo-β-lactamases is particularly worrisome (*8*).

For more than a decade, KPC has been the predominant carbapenemase found in the New York, New York, USA (New York City), region (*9*,*10*). However, in 2018, sporadic instances of residents of long-term care facilities in New York harboring NDM-possessing *K. pneumoniae* were reported (*10*,*11*). In this article, we document the changing epidemiology of carbapenem-resistant *K. pneumoniae* in hospitals across a large public health system in New York City.

Methods

The New York City Health and Hospitals Enterprise consists of 11 acute care medical centers, of which 5 are level I trauma centers, 1 is a level II trauma center, and 1 is a level II pediatric trauma center. New York City Health and Hospitals serves >1.2 million patients annually. In 2022, >164,000 inpatient visits and 1 million emergency department visits occurred. All of the hospitals are public hospitals that serve patients primarily of low socioeconomic status; health equity

Author affiliations: New York City Health and Hospitals/Kings County, New York, New York, USA (J. Lee, S. Sunny, M. Abdallah, B. Episcopia, J. Quale); New York City Health and Hospitals/Central Office, New York (M. Fornek); Wadsworth Center, New York State Department of Health, Albany, New York, USA (E. Nazarian, M.-C. Rowlinson)

DOI: https://doi.org/10.3201/eid2910.230153

barriers involving pregnancy, asthma, hypertension, diabetes, aging and frailty, substance use disorder, mental health, and violence are well-recognized in this population. Throughout the system, all patients with CRE are placed on strict contact precautions; completing a rigorous protocol is required to discontinue those precautions.

For this study, we obtained listings of patients with laboratory-identified carbapenem-resistant *K. pneumoniae* from the Centers for Disease Control and Prevention National Healthcare Safety Network database. Only 1 patient isolate per calendar year was included in the study. Following National Healthcare Safety Network definitions, we considered cases community-onset if the isolate was recovered in the outpatient setting or during the first 3 days of admission and healthcare facility–onset if recovered after 3 days of admission. We considered cases to be community-onset healthcare facility–associated if the patient had been discharged from an inpatient facility within 90 days (*12*,*13*) or if the patient had dialysis-dependent end-stage renal disease. We retrospectively reviewed medical records, including taking note of whether the patient was admitted from home, from a long-term care facility, or from another acute-care hospital. In addition, we documented the results of carbapenemase testing and ceftazidime/avibactam susceptibility testing performed by the clinical laboratory, if available. We also included results of carbapenemase testing of isolates submitted to the New York State Department of Health. We considered isolates in which KPC or OXA-48 were detected as proven serine carbapenemase producers and isolates susceptible to ceftazidime/avibactam to be presumptive serine carbapenemase producers (*14*). Similarly, we considered isolates with NDM detected proven metallo-β-lactamase producers and isolates that were resistant to ceftazidime/avibactam presumptive metallo-β-lactamase producers (*14*).

We used the Student t-test to compare continuous values and χ^2 analysis to compare categorical values. This study was approved by the SUNY Downstate Medical Center Institutional Review Board and the Health and Hospitals System to Track and Approve Research program.

Results

During January 1, 2016–June 30, 2022, a total of 509 patients with carbapenem-resistant *K. pneumoniae* were identified. Of the 509 patients, 306 (60.1%) were men and 203 (39.9%) women; 193 (38%) were Black, 114 (22%) were Hispanic, 106 (21%) were White, and 50 (10%) were Asian. Major sources of positive cultures were genitourinary tract (52%), respiratory tract (21%), bloodstream (12%), and skin or soft tissue (11%). Of the 509 patients, 262 were considered to have community-onset positive cultures; sources were genitourinary tract (65%), respiratory tract (11%, of which 38% were transtracheal aspirates), bloodstream (11%), and skin or soft tissue (7%). The remaining 247 patients were considered to have hospital-onset cultures; sources were genitourinary tract (38%), respiratory tract (30%, of which 40% were transtracheal aspirates), bloodstream (13%), and skin or soft tissue (38%). Of note, only 4 of the 29 transtracheal isolates in the hospital-onset group occurred after March 2020, suggesting that the COVID-19 pandemic did not influence the results.

Of the 262 patients with community-onset cultures, 149 lived at home and 108 in a long-term care facility; 5 were transfers from another acute-care hospital. Of the 149 patients that resided at home, 68 were considered to have community-onset healthcare facility–associated positive cultures (61 patients had been discharged as an inpatient within 90 days and 7 were on maintenance hemodialysis). Of the 247 patients with hospital-onset cultures, 133 lived at home, 103 lived in a long-term care facility, and 11 were transfers from another acute-care facility.

Cases declined steadily during 2016–2020, but this trend was reversed during the latter part of 2021 and early 2022, when a noticeable increase in the number of cases occurred (Figure 1). The rates of hospital-onset cases followed a similar trend (Figure 1). Correlated with this increase was a marked change in patients' place of residence before the culture. During 2016–2020, a total of 143 (36.3%) of 394 patients with carbapenem-resistant *K. pneumoniae* originated from long-term care facilities. During the next 18 months, however, 68 (59.1%) of 115 patients originated from long-term care facilities ($p<0.0001$).

Carbapenemase identification or ceftazidime/avibactam susceptibility testing was performed in 182 cases. A total of 143 patients had serine carbapenemases (proven KPC in 43 and OXA-48 in 3 patients; 97 patients with susceptibility to ceftazidime/avibactam). There were 39 patients with metallo-β-lactamases (proven NDM in 15 and resistance to ceftazidime/avibactam in 24). Concomitant with the trends we have noted, a marked shift in the type of carbapenemases also occurred during the study period (Figure 2). During 2016–2020, only 12 (11.8%) of 102 patients were found to have metallo-β-lactamases. During January 2021–June 2022, however, 27 (33.8%) of 80 patients had metallo-β-lactamases ($p = 0.0007$ compared with 2016–2020). In all, 67 patients with

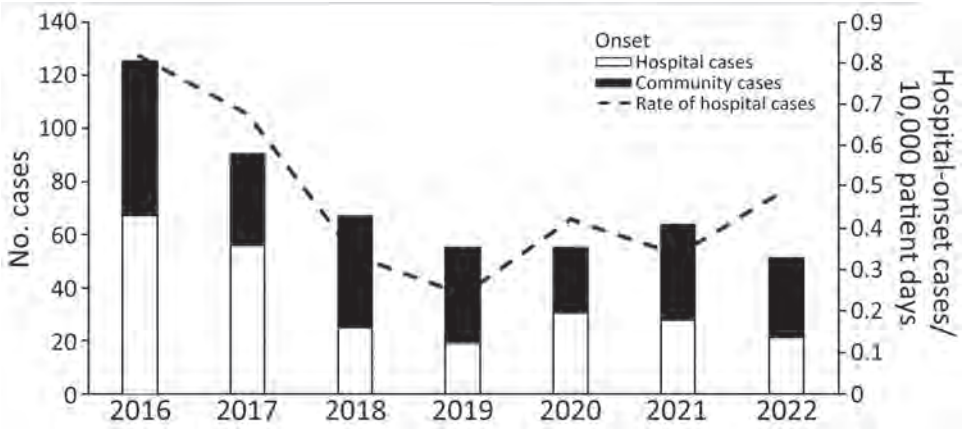

Figure 1. Number of community-onset cases versus hospital-onset cases and rate of hospital-onset infections with carbapenem-resistant *Klebsiella pneumoniae*, New York, New York, USA, 2016–2022.

serine carbapenemases originated from long-term care facilities; they resided in 30 different facilities before the culture. Twenty of the patients with metallo-β-lactamases originated from long-term care facilities, and they resided in 13 different facilities.

Discussion

This retrospective review of patients with carbapenem-resistant *K. pneumoniae* revealed several notable observations. First, it is disconcerting that approximately half of the patients had community-onset cultures; 31% of patients with community-onset isolates lived at home, were not on hemodialysis, and had not been recently hospitalized. Previous studies have indicated cases of community-onset CRE are rather unusual, accounting for ≈10% of cases (*15*,*16*).

The reason for the high percentage of community-onset CRE seen in our study might be multifactorial. The New York City Health and Hospitals acute care hospitals serve predominantly urban communities of low socioeconomic status. High rates of community-associated methicillin-resistant *Staphylococcus aureus* and *Clostridioides difficile* infections have been reported in communities of low socioeconomic status and have been attributed to poverty and overcrowding (*17*,*18*). Increasing rates of community-onset isolates possessing extended-spectrum β-lactamases have been well documented (*19*). Healthcare exposure might be a key factor, but studies in Europe have also documented overcrowding, low socioeconomic status, and environmental and agricultural factors in the spread of extended-spectrum β-lactamase–possessing isolates in the community (*20*,*21*). Similar factors might promote the spread of carbapenemase-producing pathogens in the community. Previous studies have documented contamination of the areas surrounding hospitals, including in New York City, with carbapenemase-producing pathogens (*22*,*23*). Colonization of animals, including companion animals, might also be a potential source for spread of carbapenemase-producing bacteria in the community (*24*–*26*). Further study is needed to assess the contribution

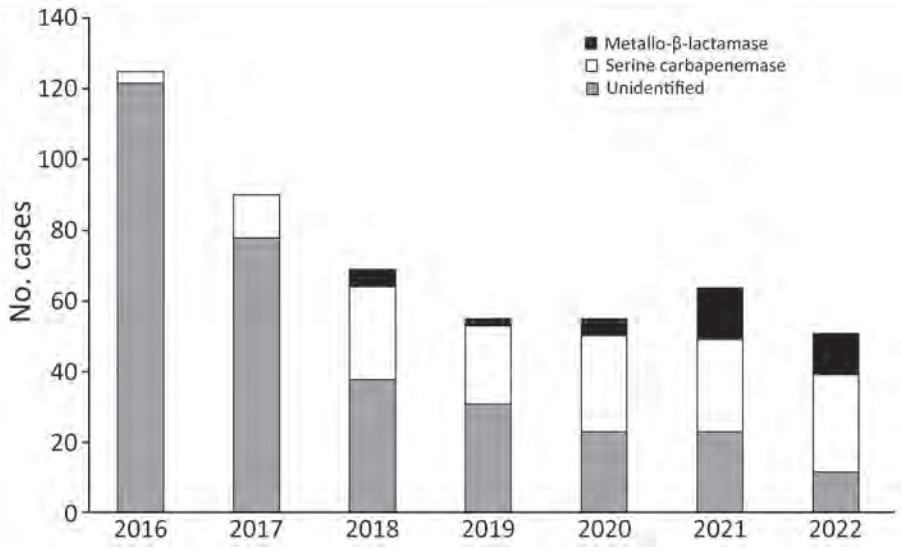

Figure 2. Number of proven and presumptive serine and metallo-β-lactamases identified from carbapenem-resistant *Klebsiella pneumoniae*, New York, New York, USA, January 2016–June 2022.

of healthcare-related factors, socioeconomic factors, and environmental factors in the community spread of carbapenem-resistant *K. pneumoniae* in the New York City region.

Second, we observed an increasing number of patients with carbapenem-resistant *K. pneumoniae* after the onset of the COVID-19 pandemic. This increase parallels the increase in methicillin-resistant *S. aureus*, *C. difficile*, and other hospital-acquired infections seen during the pandemic (*27*–*29*). Again, this finding is likely multifactorial. Increased antibiotic use, particularly of cephalosporins, early in the pandemic has been documented and was likely a contributing factor (*28*,*30*). Isolation of CRE has been associated with prolonged hospitalization; during the pandemic, carbapenem resistance among Enterobacterales was recovered in 4.2% of patients who had been hospitalized for 15–28 days but increased to 19% for stays beyond 28 days (*31*). During the pandemic, the emphasis on respiratory precautions might have overshadowed the need for contact precautions; issues regarding hand hygiene compliance and shortages of personal protective equipment might have been contributing factors.

Third, we observed a marked increase in metallo-β-lactamases since 2021 in this region. Before 2018, it was distinctly unusual for a carbapenemase other than KPC to be recovered in New York City (*10*). However, in 2018, reports of a small number of patients possessing the metallo-β-lactamases NDM, all residing in long-term care facilities in the region, emerged (*10*,*11*). Since then, carbapenem-resistant *K. pneumoniae* with NDM (or resistant to ceftazidime-avibactam) have spread, now accounting for one third of all isolates. Most patients in our study with presumptive or proven NDM-possessing isolates originated from long-term care facilities, indicating establishment in these centers as well. Our data provide an accurate glimpse of the status of carbapenemase producers in long-term care facilities in New York City. Of the existing 158 long-term facilities in the Bronx, Brooklyn, Manhattan, and Queens, we included patients from 67 sites in this study. Finally, reliance on the new β-lactam/β-lactamase inhibitors to treat CRE in our region can no longer be assumed, and carbapenemase identification or susceptibility testing is now essential.

The first limit of this retrospective study is that the number of cases of community-onset CRE might be underestimated, because recognition of the isolate in cases classified as hospital-onset simply might have been delayed. Also, detailed characterization of the patients with community-onset isolates is needed to determine the extent of healthcare exposure before the identification of CRE. We did not conduct statistical evaluation of the changing rates. Finally, the carbapenemase was identified in only a small percentage of isolates. We relied on ceftazidime/avibactam susceptibility to distinguish between serine and metallo-enzymes. Although unusual, mutations in the carbapenemase KPC might lead to resistance to ceftazidime/avibactam; however, these mutations often restore carbapenem susceptibility (*32*).

In conclusion, the number of community-onset cases, the increasing overall numbers, and the emergence of NDM-possessing carbapenem-resistant *K. pneumoniae* identified in this study are concerning. Aggressive and universal surveillance and isolation measures involving both acute-care and long-term care facilities, such as those implemented in Israel (*33*), will likely be needed to control further spread of these pathogens.

About the Author

Dr. Lee is an infectious diseases physician at NYC Health and Hospitals/Kings County. Her primary research interests include epidemiologic studies of healthcare-associated infections and social determinants of outcomes in HIV and hepatitis care.

References

1. Tamma PD, Goodman KE, Harris AD, Tekle T, Roberts A, Taiwo A, et al. Comparing the outcomes of patients with carbapenemase-producing and non-carbapenemase producing carbapenem-resistant Enterobacteriaceae bacteremia. Clin Infect Dis. 2017;64:257–64. https://doi.org/10.1093/cid/ciw741
2. Centers for Disease Control and Prevention. Antibiotic resistance threats in the United States, 2019 [cited 2022 Dec 28]. https://www.cdc.gov/drugresistance/Biggest-Threats.html
3. Yigit H, Queenan AM, Anderson GJ, Domenech-Sanchez A, Biddle JW, Steward CD, et al. Novel carbapenem-hydrolyzing β-lactamase, KPC-1, from a carbapenem-resistant strain of *Klebsiella pneumoniae.* Antimicrob Agents Chemother. 2001;45:1151–61. https://doi.org/10.1128/AAC.45.4.1151-1161.2001
4. Brown AC, Malik S, Huang J, Bhatnagar A, Balbuena R, Reese N, et al. Metallo-β-lactamase-positive carbapenem-resistant Enterobacteriaceae and *Pseudomonas aeruginosa* in the Antibiotic Resistance Laboratory Network, 2017–2018. [Abstract 484]. Open Forum Infect Dis. 2019;6(Suppl 2):S237. https://doi.org/10.1093/ofid/ofz360.557
5. Chen H-Y, Jean S-S, Lee Y-L, Lu M-C, Ko W-C, Liu PY, et al. Carbapenem-resistant Enterobacterales in long-term care facilities: a global and narrative review. Front Cell Infect Microbiol. 2021;11:601968. https://doi.org/10.3389/fcimb.2021.601968
6. Lin MY, Lyles-Banks RD, Lolans K, Hines DW, Spear JB, Petrak R, et al.; Centers for Disease Control and Prevention Epicenters Program. The importance of long-term acute care

hospitals in the regional epidemiology of *Klebsiella pneumoniae* carbapenemase-producing Enterobacteriaceae. Clin Infect Dis. 2013;57:1246–52. https://doi.org/10.1093/cid/cit500
7. Logan LK, Weinstein RA. The epidemiology of carbapenem-resistant Enterobacteriaceae: the impact and evolution of a global menace. J Infect Dis. 2017;215(suppl_1):S28–36. https://doi.org/10.1093/infdis/jiw282
8. Tamma PD, Aitken SL, Bonomo RA, Mathers AJ, van Duin D, Clancy CJ. Infectious Diseases Society of America antimicrobial-resistant treatment guidance: gram-negative bacterial infections, version 1.1 [cited 2022 Dec 28]. https://www.idsociety.org/practice-guideline/amr-guidance
9. Landman D, Bratu S, Kochar S, Panwar M, Trehan M, Doymaz M, et al. Evolution of antimicrobial resistance among *Pseudomonas aeruginosa*, *Acinetobacter baumannii* and *Klebsiella pneumoniae* in Brooklyn, NY. J Antimicrob Chemother. 2007;60:78–82. https://doi.org/10.1093/jac/dkm129
10. Iregui A, Ha K, Meleney K, Landman D, Quale J. Carbapenemases in New York City: the continued decline of KPC-producing *Klebsiella pneumoniae*, but a new threat emerges. J Antimicrob Chemother. 2018;73:2997–3000. https://doi.org/10.1093/jac/dky322
11. Ostrowsky B, Snavely E, Kogut S, Giardina R, Adams E, Nazarian E, et al. Working together: A tale of carbapenemase-producing organism investigations in three New York City nursing homes. [Abstract 491]. Open Forum Infect Dis. 2019;6(Suppl 2):S239. https://doi.org/10.1093/ofid/ofz360.2510
12. Brennan BM, Coyle JR, Marchaim D, Pogue JM, Boehme M, Finks J, et al. Statewide surveillance of carbapenem-resistant enterobacteriaceae in Michigan. Infect Control Hosp Epidemiol. 2014;35:342–9. https://doi.org/10.1086/675611
13. Gijón D, Curiao T, Baquero F, Coque TM, Cantón R. Fecal carriage of carbapenemase-producing Enterobacteriaceae: a hidden reservoir in hospitalized and nonhospitalized patients. J Clin Microbiol. 2012;50:1558–63. https://doi.org/10.1128/JCM.00020-12
14. Spiliopoulou I, Kazmierczak K, Stone GG. *In vitro* activity of ceftazidime/avibactam against isolates of carbapenem-non-susceptible Enterobacteriaceae collected during the INFORM global surveillance programme (2015–17). J Antimicrob Chemother. 2020;75:384–91. https://doi.org/10.1093/jac/dkz456
15. Bulens SN, Reses HE, Ansari UA, Grass JE, Carmon C, Albrecht V, et al. Carbapenem-resistant Enterobacterales in individuals with and without health care risk factors—Emerging Infections Program, United States, 2012–2015. Am J Infect Control. 2023;51:70–7. https://doi.org/10.1016/j.ajic.2022.04.003 PMID: 35909003
16. Kelly AM, Mathema B, Larson EL. Carbapenem-resistant Enterobacteriaceae in the community: a scoping review. Int J Antimicrob Agents. 2017;50:127–34. https://doi.org/10.1016/j.ijantimicag.2017.03.012
17. See I, Wesson P, Gualandi N, Dumyati G, Harrison LH, Lesher L, et al. Socioeconomic factors explain racial disparities in invasive community-associated methicillin-resistant *Staphylococcus aureus* disease rates. Clin Infect Dis. 2017;64:597–604. https://doi.org/10.1093/cid/ciw808
18. Skrobarcek KA, Mu Y, Ahern J, Basiliere E, Beldavs ZG, Brousseau G, et al. Association between socioeconomic status and incidence of community-associated *Clostridioides difficile* infection—United States, 2014–2015. Clin Infect Dis. 2021;73:722–5. https://doi.org/10.1093/cid/ciab042
19. Doi Y, Park YS, Rivera JI, Adams-Haduch JM, Hingwe A, Sordillo EM, et al. Community-associated extended-spectrum β-lactamase-producing *Escherichia coli* infection in the United States. Clin Infect Dis. 2013;56:641–8. https://doi.org/10.1093/cid/cis942
20. Paumier A, Asquier-Khati A, Thibaut S, Coeffic T, Lemenand O, Larramendy S, et al.; French Clinical Laboratories Nationwide Network. Assessment of factors associated with community-acquired extended-spectrum β-lactamase-producing *Escherichia coli* urinary tract infections in France. JAMA Netw Open. 2022;5:e2232679. https://doi.org/10.1001/jamanetworkopen.2022.32679
21. Mughini-Gras L, Dorado-García A, van Duijkeren E, van den Bunt G, Dierikx CM, Bonten MJM, et al.; ESBL Attribution Consortium. Attributable sources of community-acquired carriage of *Escherichia coli* containing β-lactam antibiotic resistance genes: a population-based modelling study. Lancet Planet Health. 2019;3:e357–69. https://doi.org/10.1016/S2542-5196(19)30130-5
22. Islam MA, Islam M, Hasan R, Hossain MI, Nabi A, Rahman M, et al. Environmental spread of New Delhi metallo-β-lactamase-1-producing multidrug-resistant bacteria in Dhaka, Bangladesh. Appl Environ Microbiol. 2017;83:e00793–17. https://doi.org/10.1128/AEM.00793-17
23. Rose M, Landman D, Quale J. Are community environmental surfaces near hospitals reservoirs for gram-negative nosocomial pathogens? Am J Infect Control. 2014;42:346–8. https://doi.org/10.1016/j.ajic.2013.12.025
24. Cole SD, Peak L, Tyson GH, Reimschuessel R, Ceric O, Rankin SC. New Delhi metallo-β-lactamase-5–producing *Escherichia coli* in companion animals, United States. Emerg Infect Dis. 2020;26:381–3. https://doi.org/10.3201/eid2602.191221
25. Köck R, Daniels-Haardt I, Becker K, Mellmann A, Friedrich AW, Mevius D, et al. Carbapenem-resistant *Enterobacteriaceae* in wildlife, food-producing, and companion animals: a systematic review. Clin Microbiol Infect. 2018;24:1241–50. https://doi.org/10.1016/j.cmi.2018.04.004
26. Endimiani A, Brilhante M, Bernasconi OJ, Perreten V, Schmidt JS, Dazio V, et al. Employees of Swiss veterinary clinics colonized with epidemic clones of carbapenemase-producing *Escherichia coli*. J Antimicrob Chemother. 2020;75:766–8. https://doi.org/10.1093/jac/dkz470
27. Aslam S, Asrat H, Liang R, Qiu W, Sunny S, Maro A, et al. Methicillin-resistant *Staphylococcus aureus* bacteremia during the coronavirus disease 2019 (COVID-19) pandemic: trends and distinguishing characteristics among patients in a healthcare system in New York City. Infect Control Hosp Epidemiol. 2022 Sep 9 [Epub ahead of print]. https://doi.org/10.1017/ice.2022.238 PMID 36082528
28. Maro A, Asrat H, Qiu W, Liang R, Sunny S, Aslam S, et al. Trends in Clostridioides difficile infection across a public health hospital system in New York City 2019–2021: a cautionary note. Am J Infect Control. 2022;50:1389–91. https://doi.org/10.1016/j.ajic.2022.04.015
29. Weiner-Lastinger LM, Pattabiraman V, Konnor RY, Patel PR, Wong E, Xu SY, et al. The impact of coronavirus disease 2019 (COVID-19) on healthcare-associated infections in 2020: a summary of data reported to the National Healthcare Safety Network. Infect Control Hosp Epidemiol. 2022;43:12–25. https://doi.org/10.1017/ice.2021.362
30. Rose AN, Baggs J, Wolford H, Neuhauser MM, Srinivasan A, Gundlapalli AV, et al. Trends in antibiotic use in United States hospitals during the coronavirus disease

2019 pandemic. Open Forum Infect Dis. 2021;8:b236. https://doi.org/10.1093/ofid/ofab236
31. Kubin CJ, McConville TH, Dietz D, Zucker J, May M, Nelson B, et al. Characterization of bacterial and fungal infections in hospitalized patients with coronavirus disease 2019 and factors associated with health care-associated infections. Open Forum Infect Dis. 2021;8:b201. 10.1093/ofid/ofab201 https://doi.org/10.1093/ofid/ofab201
32. Findlay J, Poirel L, Juhas M, Nordmann P. KPC-mediated resistance to ceftazidime-avibactam and collateral effects in *Klebsiella pneumoniae.* Antimicrob Agents Chemother. 2021;65:e0089021. https://doi.org/10.1128/AAC.00890-21
33. Schwaber MJ, Lev B, Israeli A, Solter E, Smollan G, Rubinovitch B, et al.; Israel Carbapenem-Resistant Enterobacteriaceae Working Group. Containment of a country-wide outbreak of carbapenem-resistant Klebsiella pneumoniae in Israeli hospitals via a nationally implemented intervention. Clin Infect Dis. 2011;52:848–55. https://doi.org/10.1093/cid/cir025

Address for correspondence: John Quale, NYC Health and Hospitals/Kings County, 451 Clarkson Ave, Brooklyn, NY, 11203, USA; email: john.quale@nychhc.org

Posttransfusion Sepsis Attributable to Bacterial Contamination in Platelet Collection Set Manufacturing Facility, United States

Ian Kracalik, Alyssa G. Kent, Carlos H. Villa, Paige Gable, Pallavi Annambhotla, Gillian McAllister, Deborah Yokoe, Charles R. Langelier, Kelly Oakeson, Judith Noble-Wang, Orieji Illoh, Alison Laufer Halpin, Anne F. Eder, Sridhar V. Basavaraju

During May 2018–December 2022, we reviewed transfusion-transmitted sepsis cases in the United States attributable to polymicrobial contaminated apheresis platelet components, including *Acinetobacter calcoaceticus–baumannii* complex or *Staphylococcus saprophyticus* isolated from patients and components. Transfused platelet components underwent bacterial risk control strategies (primary culture, pathogen reduction or primary culture, and secondary rapid test) before transfusion. Environmental samples were collected from a platelet collection set manufacturing facility. Seven sepsis cases from 6 platelet donations from 6 different donors were identified in patients from 6 states; 3 patients died. Cultures identified *Acinetobacter calcoaceticus–baumannii* complex in 6 patients and 6 transfused platelets, *S. saprophyticus* in 4 patients and 4 transfused platelets. Whole-genome sequencing showed environmental isolates from the manufacturer were closely related genetically to patient and platelet isolates, indicating the manufacturer was the most probable source of recurrent polymicrobial contamination. Clinicians should maintain awareness of possible transfusion-transmitted sepsis even when using bacterial risk control strategies.

In the United States, bacterial contamination of platelet blood components is well documented and largely a consequence of room temperature storage during their 5–7-day shelf life (*1*–*3*). Approximately 2.2 million platelet components are transfused annually in the United States, of which ≈2 million (96%) are collected by using apheresis methods (*4*). Published data from active and passive surveillance indicate bacterial contamination of platelet components (1:2,500–1:5,000) is more frequent than transfusion-transmitted sepsis (1:10,000–1:100,000) (*5*). Bacterial contamination of platelet components most commonly occurs during blood collection and typically involves either a single identified species of gram-positive bacteria associated with normal skin microflora or, less commonly, gram-negative bacteria from asymptomatic donor bacteremia. However, multiple episodes of polymicrobial contamination with identical bacterial species in platelet components across different states is exceedingly rare, suggesting a possible common source of contamination. One platelet donation can yield up to 3 platelet components, and each component might cause septic reactions in different patients (*2*,*6*,*7*). Signs and symptoms of transfusion-transmitted sepsis typically occur within minutes to hours after transfusion and include fever, chills, and hypotension; such reactions might be severe or fatal, although many recipients of bacterially contaminated platelets remain asymptomatic (*3*).

Strategies to mitigate sepsis risk caused by bacterial contamination of platelets include bacterial cultures incubated before release for transfusion,

Author affiliations: Centers for Disease Control and Prevention, Atlanta, Georgia, USA (I. Kracalik, A.G. Kent, P. Gable, P. Annambhotla, G. McAllister, J. Noble-Wang, A.L. Halpin, S.V. Basavaraju); Food and Drug Administration, Silver Spring, Maryland, USA (C.H. Villa, O. Illoh, A.F. Eder); University of California San Francisco School of Medicine, San Francisco, California, USA (D. Yokoe, C.R. Langelier); Utah Department of Health, Salt Lake City, Utah, USA (K. Oakeson)

DOI: https://doi.org/10.3201/eid2910.230869

secondary rapid testing after bacterial culture with a bacterial detection device, and pathogen reduction after platelet collection (*8*). In the United States, a pathogen-reduction device for platelets that uses synthetic psoralen and ultraviolet light to inactivate microorganisms was approved by the US Food and Drug Administration (FDA) in 2014 and adopted voluntarily by some blood establishments. In response to ongoing reports of transfusion-transmitted sepsis, FDA established regulations and recommendations in guidance during September 2019 to implement certain bacterial risk control strategies for platelets collected before October 1, 2021, including pathogen reduction, bacterial culture methods, and secondary rapid testing (*8*).

We report on a multistate investigation in the United States of transfusion-transmitted sepsis involving 2 uncommon contaminants of platelet blood components, *Acinetobacter calcoaceticus-baumannii* complex (ACBC) or *Staphylococcus saprophyticus*, and other species (e.g., *Leclercia adecarboxylata*) seen in combination among recipients of apheresis platelet components (not pathogen reduced) and pathogen-reduced apheresis platelet components. We describe the epidemiologic and laboratory efforts to identify the source of platelet contamination.

Methods

Overview of the Investigation

During May–October 2018, the Centers for Disease Control and Prevention (CDC) and FDA received 4 reports of transfusion-transmitted sepsis attributable to platelet components collected by 1 blood establishment from 3 donors at separate collection facilities in 3 states. Implicated platelet components underwent bacterial risk mitigation strategies before transfusion, including primary bacterial culture, pathogen reduction or a combination of primary culture, and secondary rapid testing (Table). Preliminary whole-genome sequencing (WGS) showed that respective species isolates were closely related genetically, suggesting a common source of contamination. CDC issued 2 calls for cases through the Epidemic Information Exchange (Figure 1).

On April 16, 2019, FDA issued a safety communication, updated on December 2, 2021 and December 22, 2022, encouraging blood establishments and healthcare facilities to report platelets contaminated with ACBC or *S. saprophyticus* by submitting a MedWatch report or by directly contacting FDA Center for Biologics Evaluation and Research (*10,11*). As the investigation progressed, additional reports identified *L. adecarboxylata* as a

Table. Characteristic of confirmed and probable transfusion-transmitted sepsis associated with bacterially contaminated platelet products for 7 patients, United States, 2018–2021*

Characteristic	Patient A	Patient B	Patient C	Patient D	Patient E	Patient F	Patient G
Sex	M	M	M	M	M	F	F
State	CA	UT	CT	CT	NC	OH	VA
Year	2018	2018	2018	2018	2020	2021	2021
Posttransfusion clinical status	Alive	Deceased	Alive	Alive	Deceased	Deceased	Alive
Platelet collection system	Amicus	Amicus	Amicus	Amicus	Amicus	Amicus	Amicus
Platelet storage media	PA	PAS	PAS	PAS	PAS	PAS	PAS
Bacterial control strategy	PR	PC	PC, RT	PC, RT	PR	PR	PR
Platelet age, d	5	5	4	4	5	5	4
Platelet co-component transfused	No	No	Yes	Yes	Yes	Yes	Yes
Posttransfusion cultures							
Patient blood							
ACBC	Yes	Yes	Yes	Yes	Yes	Yes	No
Staphylococcus saprophyticus	No	No	Yes	Yes	Yes	Yes	No
Leclercia adecarboxylata	No	No	No	No	Yes	No	No
Enterobacter spp.	No	No	No	No	No	No	Yes
Transfused platelet product							
ACBC	Yes	Yes	Yes	Yes	Yes	Yes	No
S. saprophyticus	Yes	No	Yes	Yes	Yes	Yes	Yes
L. adecarboxylata	No	No	No	No	Yes	Yes	Yes
Enterobacter spp.	No	No	No	No	No	No	Yes
Bacillus spp.	No	No	No	No	No	Yes	No
Signs and symptoms							
Fever	Yes	Yes	Yes	Yes	Yes	No	Yes
Hypotension	Yes	Yes	Yes	Yes	Yes	Yes	Yes
Chills	Yes	Yes	Yes	Yes	No	No	Yes
Tachycardia or bradycardia	Yes	Yes	No	No	Yes	Yes	Yes

*Platelets were stored in a combination of platelet additive solution and plasma. Patients C and D received platelet components from the same platelet collection. Amicus platelet collection sets and associated solutions (saline and anticoagulant) are manufactured by Fenwal International, Inc., a Fresenius Kabi Company (https://www.fresenius-kabi.com). ACBC, *Acinetobacter calcoaceticus–baumannii* complex; PAS, platelet additive solution; PC, primary culture; PR, pathogen reduction; RT, secondary rapid test.

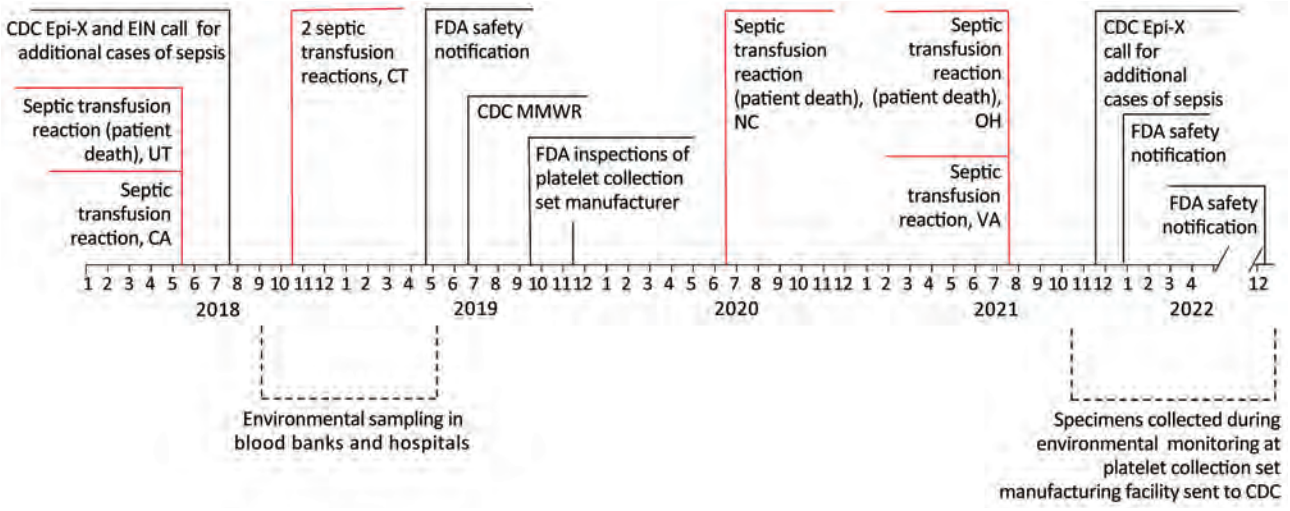

Figure 1. Investigation timeline of transfusion-transmitted sepsis cases and key events for bacterial contamination in platelet collection set manufacturing facilities, United States, 2018–2022. CDC, Centers for Disease Control and Prevention; EIN, Emerging Infections Network; Epi-X, Epidemic Information Exchange; FDA, Food and Drug Administration; MMWR, report published in Morbidity and Mortality Weekly Report (*9*).

platelet contaminant in combination with ACBC or *S. saprophyticus*. Beginning in May 2021, isolates identified during routine environmental sampling by a platelet collection set manufacturer were sent to CDC for testing.

This activity was determined to meet the requirements of public health surveillance as defined in Title 45 of the Code of Federal Regulations, part 46.102(l) (2). No institutional review board approval was needed.

Identification of Transfusion-Transmitted Sepsis Cases

We identified cases of transfusion-transmitted sepsis through mandatory reporting of transfusion-related deaths to the FDA under 21 CFR 606.170(b) or voluntary reports to the CDC or FDA by US blood establishments, health departments, or healthcare facilities. We reviewed reports of transfusion-transmitted sepsis for case definition and imputability criteria contained within the National Healthcare Safety Network Hemovigilance Module protocol (Appendix, https://wwwnc.cdc.gov/EID/article/29/10/23-0869-App1.pdf). We included cases if identical bacterial species were isolated from a transfused patient and a transfused platelet component, and an implicated strain (ACBC or *S. saprophyticus*) was isolated from either a transfused patient or transfused platelet component.

Contaminated Platelets

Blood establishments or healthcare facilities voluntarily reported, to the FDA or CDC, platelets contaminated with ACBC or *S. saprophyticus* identified by primary bacterial culture screening before distribution; contaminated units were not released for transfusion. As required under 21 CFR 606.171, information collected on patients and contaminated platelet components included the blood collection establishment, date and location of donation, collection method and platform, collection kit manufacturer, use of additive solution, and bacterial risk control strategy.

Environmental Sampling

We reviewed focused environmental surface sampling (Appendix) conducted by CDC and local and state health departments in blood establishments and healthcare facilities in 5 US states (California, Connecticut, Massachusetts, North Carolina, and Utah) from which platelet components were collected, or in hospitals in which cases of transfusion-transmitted sepsis were reported. We used epidemiologic data collected during the investigation to identify potential reservoirs, and sampling locations, such as equipment used to store platelet components.

As part of routine environmental monitoring procedures, the manufacturer (Fenwal International, Inc., a Fresenius Kabi Company, https://www.fresenius-kabi.com) of Amicus platelet collection sets and associated solutions (saline and anticoagulant) collected environmental isolates in 2 of their platelet collection set manufacturing facilities located in Puerto Rico and the Dominican Republic. A subset of the manufacturer's environmental isolates were sent to CDC for species verification and WGS.

Microbiologic Investigation

Microbiologic characterization included isolates from patients, implicated transfused platelet components, contaminated platelet products identified before transfusion, and environmental sampling. We performed species identification by using matrix-assisted laser desorption ionization–time-of-flight mass spectrometry (Appendix). Polymicrobial contamination was defined as identification of >1 species from a platelet component or patient.

WGS and Analysis

CDC or state health departments performed WGS. At CDC, we used Maxwell 16 MDx System (Promega, https://www.promega.com) to extract genomic DNA. We created DNA libraries by using the NuGEN Ovation Ultralow V2 System (Agilent, https://www.agilent.com). We performed DNA sequencing on the Illumina MiSeq Sequencing platform (https://www.illumina.com). We performed quality control, preliminary analyses, and high-quality single-nucleotide variant (hqSNV) analysis by using the QuAISAR-H Pipeline (https://github.com/DHQP/QuAISAR_singularity) and SNVPhyl (https://snvphyl.readthedocs.io) (Appendix) (*12*).

We queried the National Center for Biotechnology Information (NCBI) RefSeq database (https://www.ncbi.nlm.nih.gov/refseq), which yielded 7,921 ACBC and 160 *S. saprophyticus* genomes. We compared NCBI data with isolates implicated in cases of sepsis by using a maximum-likelihood phylogenetic method based on core genes (Appendix).

One ACBC isolate cultured from the environment in a platelet collection set manufacturing facility underwent multilocus sequence typing at an outside laboratory. Results were sent to CDC for additional analysis, but the isolate was not available for WGS.

Results

Transfusion-Transmitted Bacterial Sepsis Cases

During May 2018–November 2022, a total of 7 cases of platelet transfusion-transmitted sepsis were identified in patients from 6 states (California, Utah, Connecticut, North Carolina, Ohio, and Virginia) (Table). Some of those cases have been previously reported but are included here for completeness and context in the larger investigation (*9*,*13*–*15*). Of the cases, 3 were identified through reports to FDA of transfusion-related fatalities under 21CFR 606.170(b); others were voluntarily reported by state health departments or blood establishments. Other than receipt of platelet transfusion, no commonalities were observed among persons who died.

Blood establishments collected platelets implicated in transfusion-transmitted sepsis by using apheresis on the Amicus platform (Fenwal International, Inc.) and suspended these platelets in 65% platelet additive solution (InterSol Solution/Platelet Additive Solution 3 [PAS-C]; Fenwal International, Inc.) and 35% plasma. Platelets were collected from 6 different donors in 6 states, all by 1 blood establishment. Two of the implicated platelet units were from the same collection procedure. FDA traced lot numbers of all materials used in the collections, including collection sets, anticoagulant solutions, saline, additive solutions, and sampling devices, to identify potential common elements. Platelet collection sets were from a single manufacturer consisting of multiple lot numbers of collection sets, saline, anti-coagulant solution, and PAS-C manufactured during 2018–2020. Blood establishments performed various measures (e.g., terminal cleaning) to reduce the risk for bacterial contamination of all platelet components.

Of the 7 platelet components implicated in sepsis, 4 (57%) were pathogen reduced and 3 (43%) underwent primary bacterial culture at least 24 hours after collection and were negative; of those 3 components, 2 (67%) also underwent secondary rapid testing at day 4 and were negative (Table). Polymicrobial contamination was identified in 6/7 (86%) cases; in 1 case, only ACBC was isolated. Posttransfusion blood cultures identified ACBC in 6/7 (86%) patients, *S. saprophyticus* in 4/7 (57%) patients, *L. adecarboxylata* in 1/7 (14%) patients, and *Enterobacter* spp. in 1/7 (14%) patients. Cultures from implicated platelet components identified ACBC in 6/7 (86%) cultures, *S. saprophyticus* in 6/7 (86%) cultures, *L. adecarboxylata* in 3/7 (43%) cultures, *Enterobacter* spp. in 1/7 (14%) cultures, and *Bacillus* spp. in 1/7 (14%) cultures (Table).

Disposition of co-components from the 7 cases of transfusion-transmitted sepsis included 3/7 (43%) platelet co-components transfused into 3 other patients without incident, as reported by blood establishments or transfusion services; 2/7 (14%) sequestered co-components that were culture negative; and 2/7 (14%) co-components that caused septic reactions were part of this investigation (patients C and D) (Table). Blood establishments or transfusion services did not report additional details of their investigation into the co-component transfusions. In patients in whom septic reactions were observed, onset of symptoms ranged from 30 minutes to 3 hours after start of transfusion and most frequently included hypotension (7/7, 100%) and fever (6/7, 86%).

Bacterially Contaminated Platelet Components

During February 2019–November 2022, primary bacterial culture identified, before transfusion, 38 isolates from 35 nonpathogen-reduced apheresis platelet components contaminated with *Acinetobacter* spp. or *S. saprophyticus* collected in 12 states (Arizona, California, Connecticut, Massachusetts, Maryland, Missouri, New York, North Carolina, Ohio, Pennsylvania, Texas, and Wisconsin). Of those samples, 21/35 (60%) were contaminated with *S. saprophyticus*, 11/35 (31%) with *Acinetobacter* spp., 2/35 (6%) each with 2 different strains of *S. saprophyticus*, and 1/35 (3%) with both *S. saprophyticus* and *Acinetobacter* spp. (Figure 2).

Contaminated platelet components had been suspended in 100% plasma (20/35, 57%) or 65% PAS-C/35% plasma (15/35, 43%). A total of 29/35 (83%) contaminated platelet components interdicted before transfusion were collected by using the Amicus Platform by 1 blood establishment; 6/35 (17%) were collected on the Trima Accel Platform (Terumo BCT, https://www.terumobct.com) by a second blood establishment. One additional platelet component collected on the Trima Platform was transfused into a patient, and *A. radioresistens* was cultured from the remaining platelet component, which underwent WGS. However, that case did not meet the transfusion-transmitted sepsis case definition and imputability criteria (Appendix), and the isolate did not cluster with other strains implicated in cases of sepsis. No commonalities (e.g., solutions or storage containers) between contaminated components from different blood establishments or collection set manufacturers were identified.

Environmental Sampling

A total of 90 environmental samples were collected from blood establishment and healthcare facilities in 5 states (California, Connecticut, Massachusetts, North Carolina, and Utah) during May, June, and November 2018; February and May 2019; and July 2020. Of the 90 samples cultured, 29 (32%) yielded 34 implicated strain isolates. Recovery of isolates was primarily associated with samples taken from equipment used to store (e.g., platelet agitators) and transport platelet components (e.g., quality control cart) (Appendix Table 1). Of the 34 isolates, 19 (56%) were ACBC, 11 (32%) were *S. saprophyticus*, and 4 (12%) were *L. adecarboxylata*.

Because cases of transfusion-transmitted sepsis all involved collection sets and solutions (i.e., anticoagulant solution, saline, PAS-C) from the same manufacturer, FDA inspected the manufacturing facilities in Puerto Rico and the Dominican Republic to assess the risk for a common source of contamination. As part of those activities, during October 2021–October 2022, additional culture and sequencing was performed on 74 environmental samples collected at the 2 manufacturing facilities (Appendix Table 2), yielding 84 isolates: 35 *Acinetobacter* spp. and 49 *S. saprophyticus*. FDA inspections of the manufacturing facilities identified deficiencies related to environmental controls and the assurance of platelet collection set sterility (*16*).

WGS and Analysis

A total of 191 isolates obtained over 4 years underwent WGS: 118 environmental isolates from healthcare facilities, blood establishments and 2 platelet collection set manufacturing facilities; 56 from contaminated platelet components; and 17 from

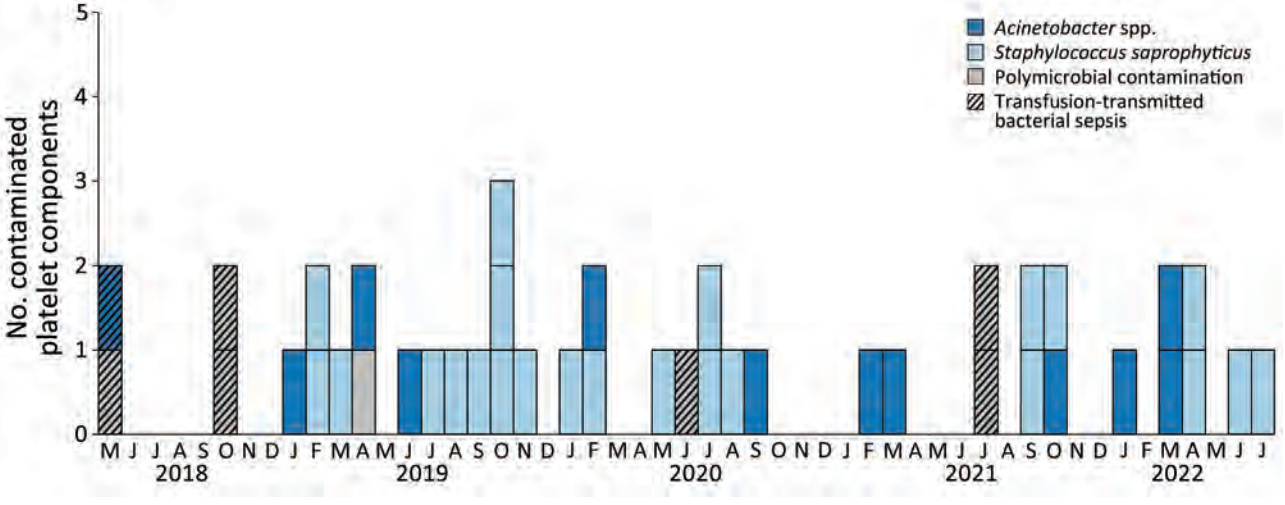

Figure 2. Platelet components contaminated with *Acinetobacter* spp. or *Staphylococcus saprophyticus* identified from cases of transfusion-transmitted bacterial sepsis or routine bacterial testing before transfusion, United States, 2018–2022.

posttransfusion patient blood (Figure 3). Sequencing and analysis showed that respective isolates of ACBC, *S. saprophyticus*, and *L. adecarboxylata* from different sources were closely related genetically and formed several closely related, respective outbreak clusters. Isolates from posttransfusion patient blood, platelet components, and a platelet collection set manufacturing facility formed 3 distinct *S. saprophyticus* outbreak clusters: cluster A (20 isolates, differing by 1–38 pairwise hqSNVs, across 97.9% of the reference isolate core genome), cluster B (39 isolates, 0–48 hqSNVs, 98.9% core genome) and cluster C (3 isolates, 0–32 hqSNVs, 99.0% core genome).

Isolates from patient blood, platelet components, and the hospital/blood establishment environment were distributed across 2 distinct ACBC outbreak clusters: cluster 1, a potentially novel species (closest average nucleotide identity to *A. seifertii* at 90.8%) within ACBC (19 isolates, varied by 0–79 hqSNVs, 94.9% core genome) and cluster 2, *A. seifertii* (15 isolates, 5–129 hqSNVs, 95.2% core genome). For the *L. adecarboxylata* isolates, sequencing and analysis showed 1 outbreak cluster (5 isolates, 1–32 hqSNVs, 97.2% core genome).

Of the 7 cases of transfusion-transmitted sepsis, all were collected on the Amicus platform and had at least 1 implicated bacterial isolate in the investigation cluster. Of the primary culture positive units (not clinical cases), most units collected on the Amicus platform were in the investigation clusters (20/29 components; 69%), but only 2/6 units (33%) collected on the Trima platform were in the investigation clusters. Furthermore, these 2 Trima isolates were collected in the same location (Appendix Figure).

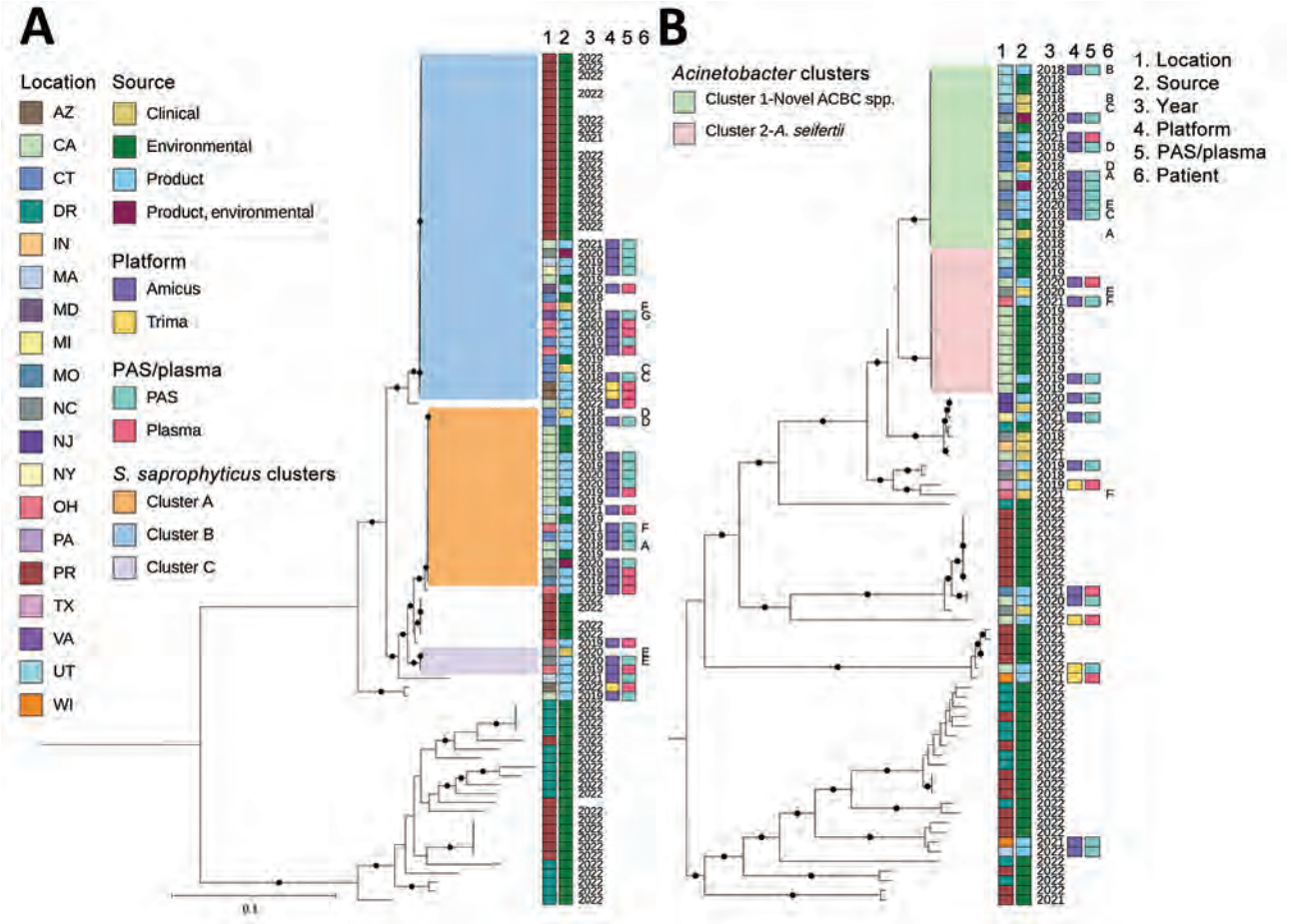

Figure 3. Whole-genome sequencing of *Staphylococcus saprophyticus* (A) and ACBC (B) isolates implicated in the bacterial contamination of platelet blood products, United States, 2018–2022. Maximum-likelihood phylogenies based on core genes were generated by using Roary (https://github.com/sanger-pathogens/Roary) and RaxML (https://cme.h-its.org); phylogenetic trees were midpoint rooted. Clusters were identified based on SNVPhyl (https://snvphyl.readthedocs.io) and highlighted if they included isolates linked to a sepsis transfusion case. *Acinetobacter* spp. isolates not falling in the ACBC were also included. Black circles on branches indicate 100% support for the branch of 100 bootstraps. US states are identified by 2-letter postal codes. Scale bars indicate nucleotide substitutions per site. ACBC, *Acinetobacter calcoaceticus–baumannii* complex; DR, Dominican Republic; PAS, platelet additive solution; PR, Puerto Rico.

One ACBC isolate obtained in July 2022 from a platelet collection set manufacturer was the same potentially novel ACBC species in outbreak cluster 1 and was closely related by multilocus sequence typing, but was not available for WGS and analysis at CDC. In the NCBI, ACBC isolates from cluster 1, which included this potentially novel species, grouped distinctly from all other ACBC with available data (Figure 4). All outbreak clusters in ACBC and *S. saprophyticus* clustered apart from publicly available NCBI genomes (Figures 4, 5).

Discussion

In this investigation, we found that a platelet collection set manufacturer was the most probable source of multiple episodes of polymicrobial contamination of platelet components. Previous, large, multiyear studies of platelet collections and transfusions did not show polymicrobial contamination (*7*,*17*,*18*). During the investigation, primary culture of some platelet collections by blood establishments, before transfusion, identified bacterial contamination with implicated strains, thus averting possible septic reactions. However, despite the use of bacterial risk control strategies, including primary culture, secondary rapid testing, or pathogen reduction, 7 cases of transfusion-transmitted sepsis were attributed to bacterial contamination of platelet components and resulted in 3 deaths. The manufacturer of the secondary rapid test has since updated the device to improve detection of ACBC (*19*). Using pathogen reduction or other detection-based bacterial risk control strategies cannot eliminate the risk for transfusion-transmitted sepsis; however, the risk is expected to be reduced by those measures and remains low (*2*,*5*,*20*,*21*). Of the ≈2.1 million apheresis platelet units transfused in 2021, ≈843,000 were pathogen reduced, and ≈1.2 million underwent various bacterial testing methods (*4*), suggesting the cases described in our study were rare events.

FDA continues to conduct inspections of the manufacturer to ensure control of the manufacturing process and maintain sterility of platelet collection sets and solutions. FDA has communicated that strategies to ensure the bacterial safety of platelet components recommended in FDA guidance remain acceptable at this time (*8*,*10*,*11*). Because some platelet donations in this investigation were tested before the implementation date of the December 2020 guidance on bacterial risk control strategies, bacterial culture methods consistent with the guidance might not have been implemented by blood establishments.

Identifying the source of platelet contamination was challenging. We initially hypothesized the contamination was an isolated event resulting from donor infection or colonization. Only 1 previously reported cluster of transfusion-transmitted sepsis has been attributed to bacterial contamination from a common source and implicated blood collection sets (*22*). Our investigation then focused on environmental contamination in hospitals and blood establishments; however, identification of genetically related implicated strains, temporally and geographically dispersed, shifted our attention to a common source contamination at the level of materials used in manufacturing of platelet components. Another challenge was the complex chain of blood donation and product manufacturing, including collection kit (e.g., platelet collection bags and additive solutions) manufacturers and kit assembly facilities across 3 locations. Traceback efforts initiated in 2018 did not identify a putative contamination source. Not until 2021 were environmental isolates identified at a platelet collection set manufacturing facility and subsequently sequenced in 2022 to identify isolates situated within the *S. saprophyticus* outbreak-related clusters.

Before this investigation, there were no confirmed reports of sepsis attributable to bacterial contamination of pathogen-reduced platelets (*23*). Published studies hypothesized that cases of sepsis in this outbreak were caused by defective platelet containers, resulting in environmental contamination after pathogen reduction (*14*,*15*,*24*). However, several lines of evidence from this investigation suggest a common source of contamination occurring before pathogen reduction. First, WGS showed geographically and temporally dispersed isolates from varying sources, including patients, platelet components, and a platelet collection set manufacturer, were closely related genetically. Moreover, a possible novel ACBC species, not previously contained within public repositories, was identified in patients and the environment, irrespective of time and place (*13*,*25*). Second, implicated strains were identified before transfusion and storage of platelets that had not been pathogen reduced; those platelet components did not have the same final container as pathogen-reduced platelets, for which defects have been hypothesized as a contamination source (*15*,*24*). Contaminated platelet components were suspended in either 100% plasma or 65% PAS-C/35% plasma, suggesting other commonalities (e.g., saline or anticoagulant solutions) were sources of contamination, which was supported by environmental sampling and inspections identifying manufacturing deficiencies related to the assurance of sterility.

ACBC and *S. saprophyticus* are uncommon platelet contaminants and together have not previously been reported as polymicrobial contaminants implicated

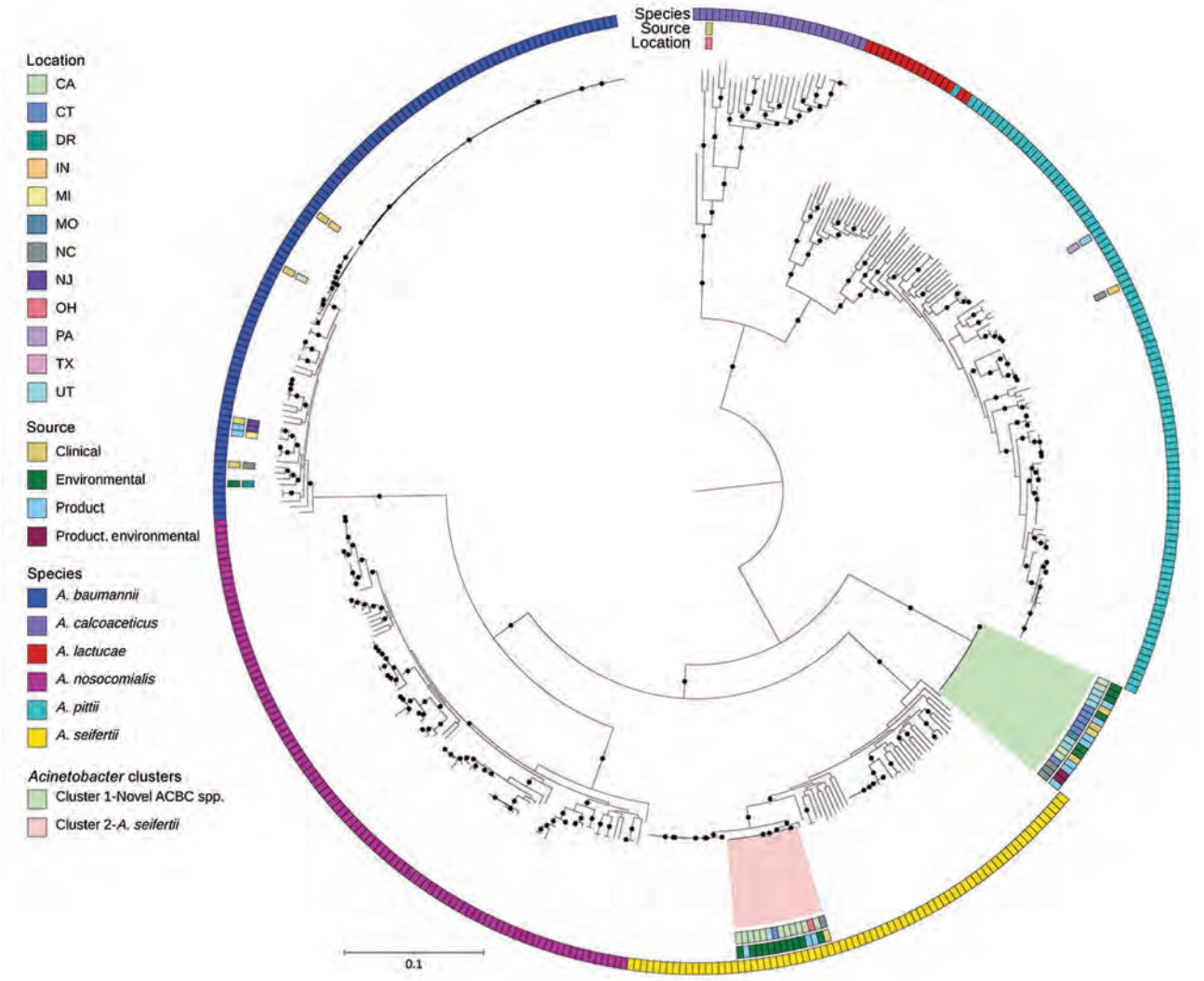

Figure 4. Public ACBC shown with study isolates from investigation of bacterial contamination of platelet blood products, United States, 2018–2022. Shown is a RaxML (https://cme.h-its.org)–generated phylogeny based on core genes of genomes from ACBC isolates from this study compared with all *A. calcoaceticus*, *A. lactucae*, and *A. seifertii* and a subsampled set of *A. baumannii*, *A. nosocomialis*, and *A. pittii* genomes from the National Center for Biotechnology Information RefSeq (https://www.ncbi.nlm.nih.gov/refseq) database, along with all *Staphylococcus saprophyticus* from the RefSeq database. Isolate location, isolate source, and species from National Center for Biotechnology Information database along with all *S. saprophyticus* isolates or by average nucleotide identity were layered onto the phylogeny. Pink and green indicate the 2 clusters from Figure 3, panel B. Black circles on branches indicate 100% support for the branch of 100 bootstraps. US states are identified by 2-letter postal codes. Scale bar indicates nucleotide substitutions per site. ACBC, *Acinetobacter calcoaceticus-baumannii*; DR, Dominican Republic.

in transfusion-transmitted sepsis (*2*,*3*,*21*). ACBC are widely distributed gram-negative organisms found in moist environments that can persist on surfaces and adhere to plastics (*26*). Although coagulase-negative *Staphylococcus* spp. are more frequent platelet contaminants, those bacteria are often identified as *S. epidermidis* and not *S. saprophyticus* (*6*,*18*). *S. saprophyticus* commonly colonizes the human urogenital tract and is a leading cause of urinary tract infections but is not typically implicated in transfusion-transmitted sepsis (*27*).

Both ACBC and *S. saprophyticus* have been shown to contaminate the environment and can form biofilms (*27*–*29*), although synergistic growth enhancement between ACBC and *S. saprophyticus* has not been observed (*30*). Effective pathogen reduction was demonstrated in platelet components inoculated with implicated strains of ACBC and *S. saprophyticus,* but that finding might not reflect real-world conditions in clinical practice during this investigation (*14*,*15*). However, 1 study detected residual viable bacteria after 7 days of storage in pathogen-reduced platelets experimentally inoculated with *L. adecarboxylata*, which

was attributed to a high inoculum (*26*). Certain spore-forming bacteria and nonenveloped viruses have also demonstrated resistance to pathogen reduction (*23*), and biofilm-forming bacteria might evade detection by bacterial culture or pathogen reduction (*31*).

One limitation of our findings is that, although efforts were made to identify cases or contaminated products, some might have gone unrecognized. Some patients lack clinical symptoms of transfusion-transmitted sepsis caused by varying inoculum size, asymptomatic infection, or misdiagnosis (*5*,*32*). Highlighting this variability is that, for some platelet collections associated with fatal sepsis in this investigation, platelet co-components from the same donation were transfused into 3 additional patients without incident. Pathogen-reduced platelets do not routinely undergo primary culture for bacteria before transfusion; consequently, the bacterial load is unknown. However, pathogen reduction of some platelet components during this investigation probably prevented some cases of transfusion-transmitted sepsis. The mechanisms of pathogen reduction evasion are unclear, and the effectiveness of pathogen reduction against biofilms is not completely understood.

Although most contaminated platelet components in this outbreak were collected by 1 blood establishment on the Amicus platform, 6 isolates were

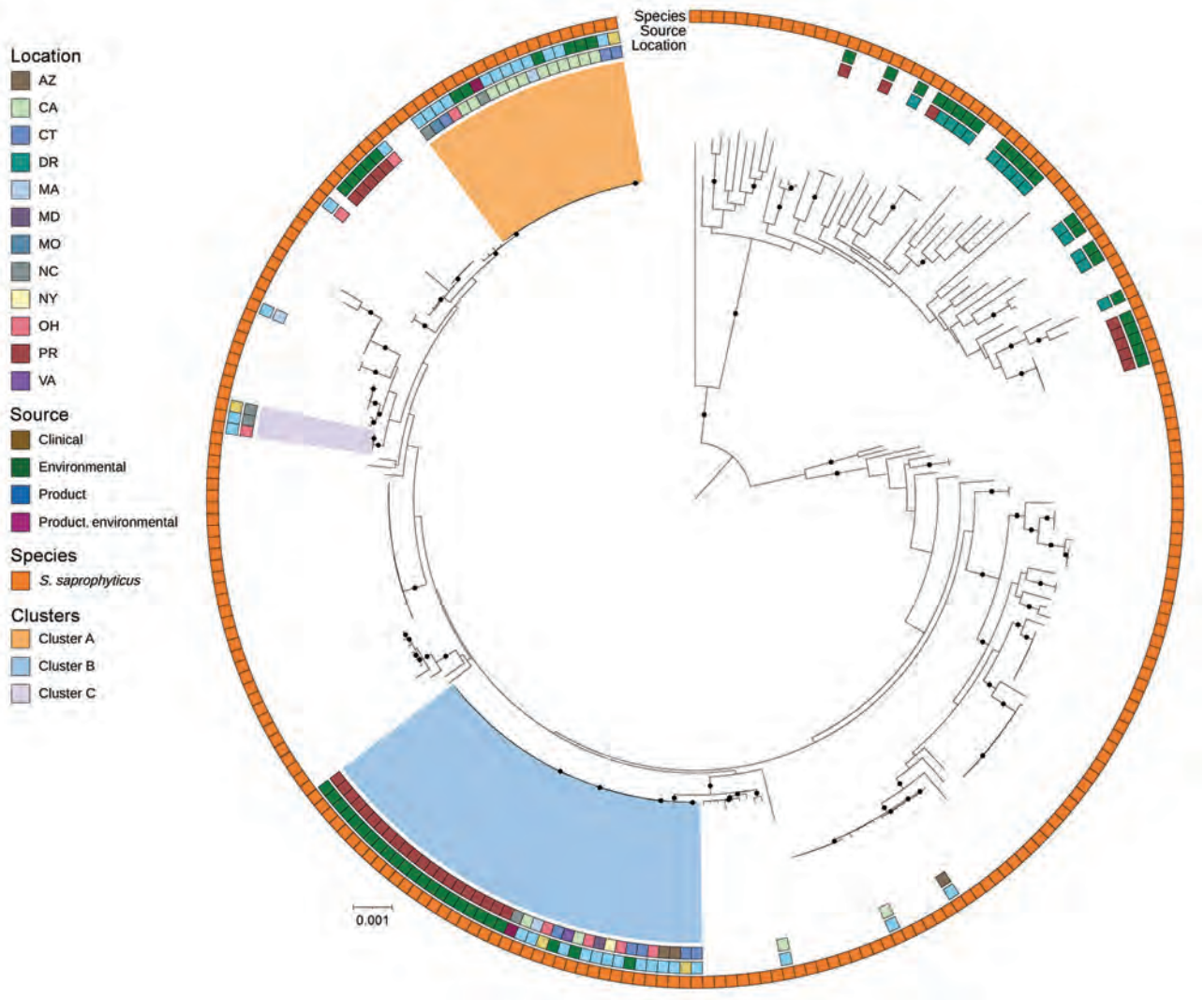

Figure 5. Public *Staphylococcus saprophyticus* genomes and study isolates from investigation of bacterial contamination of platelet blood products, United States, 2018–2022. Shown is a RaxML (https://cme.h-its.org)–generated phylogeny based on 1,808 core genes of all *S. saprophyticus* isolates from this study and all *S.saprophyticus* genomes from the National Center for Biotechnology Information RefSeq (https://www.ncbi.nlm.nih.gov/refseq) database. Isolate location, isolate source, and species from National Center for Biotechnology Information or by average nucleotide identity were layered onto the phylogeny. Light orange, blue, and purple indicate the 3 clusters from Figure 3, panel A. Black circles on branches indicate 100% support for the branch of 100 bootstraps. US states are identified by 2-letter postal codes. Scale bar indicates nucleotide substitutions per site. DR, Dominican Republic; PR, Puerto Rico.

interdicted from components collected by a second blood establishment on the Trima platform, and 2 of the 6 were closely related genetically to the *S. saprophyticus* cluster. However, those 2 isolates showed evidence of a common plasmid not identified in any other isolates in the cluster (data not shown). Furthermore, no epidemiologic links (e.g., shared materials or devices) were identified between this second establishment and the first establishment's outbreak-related transfusion transmitted sepsis cases or platelet components, despite association with the common *S. saprophyticus* strain. In contrast, strains associated with polymicrobial contamination were common among clinical cases of sepsis and the implicated manufacturing facility.

CDC and FDA continue to collaborate to ensure the safety of the blood supply. CDC has proposed additional studies to elucidate the effects of biofilm development on platelet bacterial risk control strategies (*33*). FDA and CDC will continue to monitor reports of bacterial contamination of platelets, and FDA will issue additional communications and take appropriate regulatory action as necessary. Despite these events, blood transfusion remains safer than ever because of bacterial mitigation strategies. Although such cases are uncommon, clinicians should maintain awareness of possible transfusion-transmitted sepsis even when using bacterial risk control strategies. Prompt recognition and reporting will help ensure identification of potential sources of contamination so that appropriate corrective actions can be taken.

About the Author

Dr. Kracalik is an epidemiologist in the National Center for Emerging and Zoonotic Infectious Diseases, Centers for Disease Control and Prevention, Atlanta, GA. His primary research interests are blood safety and zoonotic diseases.

References

1. Wagner SJ, Friedman LI, Dodd RY. Transfusion-associated bacterial sepsis. Clin Microbiol Rev. 1994;7:290–302. https://doi.org/10.1128/CMR.7.3.290
2. Eder AF, Kennedy JM, Dy BA, Notari EP, Weiss JW, Fang CT, et al.; American Red Cross Regional Blood Centers. Bacterial screening of apheresis platelets and the residual risk of septic transfusion reactions: the American Red Cross experience (2004–2006). Transfusion. 2007;47:1134–42. https://doi.org/10.1111/j.1537-2995.2007.01248.x
3. Kuehnert MJ, Roth VR, Haley NR, Gregory KR, Elder KV, Schreiber GB, et al. Transfusion-transmitted bacterial infection in the United States, 1998 through 2000. Transfusion. 2001;41:1493–9. https://doi.org/10.1046/j.1537-2995.2001. 41121493.x
4. Free RJ, Sapiano MRP, Chavez Ortiz JL, Stewart P, Berger J, Basavaraju SV. Continued stabilization of blood collections and transfusions in the United States: findings from the 2021 National Blood Collection and Utilization Survey. Transfusion. 2023;trf.17360. https://doi.org/10.1111/trf.17360
5. Hong H, Xiao W, Lazarus HM, Good CE, Maitta RW, Jacobs MR. Detection of septic transfusion reactions to platelet transfusions by active and passive surveillance. Blood. 2016;127:496–502. https://doi.org/10.1182/blood-2015-07-655944
6. Fenwick AJ, Gehrie EA, Marshall CE, Tobian AAR, Shrestha R, Kacker S, et al. Secondary bacterial culture of platelets to mitigate transfusion-associated sepsis: a 3-year analysis at a large academic institution. Transfusion. 2020;60:2021–8. https://doi.org/10.1111/trf.15978
7. Brecher ME, Hay SN. Bacterial contamination of blood components. Clin Microbiol Rev. 2005;18:195–204. https://doi.org/10.1128/CMR.18.1.195-204.2005
8. US Food and Drug Administration. Bacterial risk control strategies for blood collection establishments and transfusion services to enhance the safety and availability of platelets for transfusion. 2020 [cited 2023 Aug 2]. https://www.fda.gov/media/123448/download
9. Jones SA, Jones JM, Leung V, Nakashima AK, Oakeson KF, Smith AR, et al. Sepsis attributed to bacterial contamination of platelets associated with a potential common source—multiple states, 2018. MMWR Morb Mortal Wkly Rep. 2019;68:519–23. https://doi.org/10.15585/mmwr.mm6823a2
10. US Food and Drug Administration. Important information for blood establishments and transfusion services regarding bacterial contamination of platelets for transfusion. 2021 [cited 2023 Aug 2]. https://www.fda.gov/vaccines-blood-biologics/safety-availability-biologics/important-information-blood-establishments-and-transfusion-services-regarding-bacterial
11. US Food and Drug Administration. Important information for blood establishments and transfusion services regarding bacterial contamination of platelets for transfusion. 2022 [cited 2023 Aug 2]. https://www.fda.gov/vaccines-blood-biologics/safety-availability-biologics/important-information-blood-establishments-and-transfusion-services-regarding-bacterial-0
12. Stanton RA, Vlachos N, de Man TJ, Lawsin A, Halpin AL. Development and application of QuAISAR-H: a bioinformatics pipeline for short read sequences of healthcare-associated pathogens. Presented at: ASM Conference on Rapid Applied Microbial Next Generation Sequencing and Bioinformatics Pipelines; Tyson Falls, VA, USA; September 25, 2018.
13. Nevala-Plagemann C, Powers P, Mir-Kasimov M, Rose R. A fatal case of septic shock secondary to *Acinetobacter* bacteremia acquired from a platelet transfusion. Case Rep Med. 2019;2019:3136493. https://doi.org/10.1155/2019/3136493
14. Fridey JL, Stramer SL, Nambiar A, Moayeri M, Bakkour S, Langelier C, et al. Sepsis from an apheresis platelet contaminated with *Acinetobacter calcoaceticus/baumannii* complex bacteria and *Staphylococcus saprophyticus* after pathogen reduction. Transfusion. 2020;60:1960–9. https://doi.org/10.1111/trf.15951
15. Fadeyi EA, Wagner SJ, Goldberg C, Lu T, Young P, Bringmann PW, et al. Fatal sepsis associated with a storage container leak permitting platelet contamination with environmental bacteria after pathogen reduction. Transfusion. 2021;61:641–8. https://doi.org/10.1111/trf.16210
16. Food and Drug Administration. FDA dashboards. 2023 [cited 2023 Jan 31]. https://datadashboard.fda.gov/ora/firmprofile.htm?FEIi=2627511
17. Eder AF, Dy BA, DeMerse B, Wagner SJ, Stramer SL, O'Neill EM, et al. Apheresis technology correlates with

bacterial contamination of platelets and reported septic transfusion reactions. Transfusion. 2017;57:2969–76. https://doi.org/10.1111/trf.14308
18. Perez P, Salmi LR, Folléa G, Schmit JL, de Barbeyrac B, Sudre P, et al.; BACTHEM Group; French Haemovigilance Network. Determinants of transfusion-associated bacterial contamination: results of the French BACTHEM Case–Control Study. Transfusion. 2001;41:862–72. https://doi.org/10.1046/j.1537-2995.2001.41070862.x
19. LaVerda D, Shinefeld L, Best N, Lisitu J, Tambolleo G, Vallejo YR. Evaluation of an improved rapid bacterial assay with untreated and pathogen-reduced platelets: detection of *Acinetobacter* strains. Transfusion. 2021;61:2710–7. https://doi.org/10.1111/trf.16514
20. Kundrapu S, Srivastava S, Good CE, Lazarus HM, Maitta RW, Jacobs MR. Bacterial contamination and septic transfusion reaction rates associated with platelet components before and after introduction of primary culture: experience at a US Academic Medical Center 1991 through 2017. Transfusion. 2020;60:974–85. https://doi.org/10.1111/trf.15780
21. Haass KA, Sapiano MR, Savinkina A, Kuehnert MJ, Basavaraju SV. Transfusion-transmitted infections reported to the national healthcare safety network hemovigilance module. Transfus Med Rev. 2019;33:84–91. https://doi.org/10.1016/j.tmrv.2019.01.001
22. Heltberg O, Skov F, Gerner-Smidt P, Kolmos HJ, Dybkjaer E, Gutschik E, et al. Nosocomial epidemic of *Serratia marcescens* septicemia ascribed to contaminated blood transfusion bags. Transfusion. 1993;33:221–7. https://doi.org/10.1046/j.1537-2995.1993.33393174448.x
23. Cloutier M, De Korte D; ISBT Transfusion-Transmitted Infectious Diseases Working Party, Subgroup on Bacteria. Residual risks of bacterial contamination for pathogen-reduced platelet components. Vox Sang. 2022;117:879–86. https://doi.org/10.1111/vox.13272
24. Gammon RR, Reik RA, Stern M, Vassallo RR, Waxman DA, Young PP, et al. Acquired platelet storage container leaks and contamination with environmental bacteria: a preventable cause of bacterial sepsis. Transfusion. 2022;62:641–50. https://doi.org/10.1111/trf.16776
25. Crawford E, Kamm J, Miller S, Li LM, Caldera S, Lyden A, et al. Investigating transfusion-related sepsis using culture-independent metagenomic sequencing. Clin Infect Dis. 2020;71:1179–85. https://doi.org/10.1093/cid/ciz960
26. Wong D, Nielsen TB, Bonomo RA, Pantapalangkoor P, Luna B, Spellberg B. Clinical and pathophysiological overview of *Acinetobacter* infections: a century of challenges. Clin Microbiol Rev. 2017;30:409–47. https://doi.org/10.1128/CMR.00058-16
27. Lawal OU, Fraqueza MJ, Bouchami O, Worning P, Bartels MD, Gonçalves ML, et al. Foodborne origin and local and global spread of *Staphylococcus saprophyticus* causing human urinary tract infections. Emerg Infect Dis. 2021;27:880–93. https://doi.org/10.3201/eid2703.200852
28. Lawal OU, Barata M, Fraqueza MJ, Worning P, Bartels MD, Goncalves L, et al. *Staphylococcus saprophyticus* from clinical and environmental origins have distinct biofilm composition. Front Microbiol. 2021;12:663768. https://doi.org/10.3389/fmicb.2021.663768
29. Gedefie A, Demsis W, Ashagrie M, Kassa Y, Tesfaye M, Tilahun M, et al. *Acinetobacter baumannii* biofilm formation and its role in disease pathogenesis: a review. Infect Drug Resist. 2021;14:3711–9. https://doi.org/10.2147/IDR.S332051
30. Kerantzas CA, Merwede J, Snyder EL, Hendrickson JE, Tormey CA, Kazmierczak BI, et al. Assessment of polymicrobial interactions in bacterial isolates from transfused platelet units associated with sepsis. Transfusion. 2022;62:2458–63. https://doi.org/10.1111/trf.17136
31. Greco-Stewart VS, Brown EE, Parr C, Kalab M, Jacobs MR, Yomtovian RA, et al. *Serratia marcescens* strains implicated in adverse transfusion reactions form biofilms in platelet concentrates and demonstrate reduced detection by automated culture. Vox Sang. 2012;102:212–20. https://doi.org/10.1111/j.1423-0410.2011.01550.x
32. Jacobs MR, Good CE, Lazarus HM, Yomtovian RA. Relationship between bacterial load, species virulence, and transfusion reaction with transfusion of bacterially contaminated platelets. Clin Infect Dis. 2008;46:1214–20. https://doi.org/10.1086/529143
33. Centers for Disease Control and Prevention. FY23 broad agency announcement notice 75D301–23-R-72545. 2023 [cited 2023 Jan 31]. https://sam.gov/opp/15229982f7c348f69fd35e9a0add8aba/view

Address for correspondence: Sridhar V. Basavaraju, Centers for Disease Control and Prevention, 1600 Clifton Rd NE, Mailstop H16-3, Atlanta, GA 30329-4027, USA; email: etu7@cdc.gov

Effects of COVID-19 on Maternal and Neonatal Outcomes and Access to Antenatal and Postnatal Care, Malawi

Leonard Mndala, Chikondi Chapuma, Jennifer Riches, Luis Gadama, Fannie Kachale, Rosemary Bilesi, Malangizo Mbewe, Andrew Likaka, Moses Kumwenda, Regina Makuluni, Bertha Maseko, Chifundo Ndamala, Annie Kuyere, Laura Munthali, Deborah Phiri, Edward J.M. Monk, Marc Y.R. Henrion, Maria L. Odland,[1] David Lissauer[1]

We used national facility-level data from all government hospitals in Malawi to examine the effects of the second and third COVID-19 waves on maternal and neonatal outcomes and access to care during September 6, 2020–October 31, 2021. The COVID-19 pandemic affected maternal and neonatal health not only through direct infections but also through disruption of the health system, which could have wider indirect effects on critical maternal and neonatal outcomes. In an interrupted time series analysis, we noted a cumulative 15.4% relative increase (63 more deaths) in maternal deaths than anticipated across the 2 COVID-19 waves. We observed a 41% decrease in postnatal care visits at the onset of the second COVID-19 wave and 0.2% by the third wave, cumulative to 36,809 fewer visits than anticipated. Our findings demonstrate the need for strengthening health systems, particularly in resource-constrained settings, to prepare for future pandemic threats.

Maternal, newborn, and child health delivery services are critical, and many improvements in health outcomes have been achieved globally in the past decade (*1*). However, those gains likely were negatively affected by the COVID-19 pandemic and subsequent public health response. The pandemic disrupted global healthcare systems and healthcare delivery, even in the most well-resourced and resilient health systems (*2*). In the worst-case scenario, COVID-19's disruption of essential maternal, newborn, and child health interventions could result in an additional 1,157,000 child deaths and 56,700 maternal deaths in 118 low- and middle-income countries (*3*). For instance, in Nepal, the national COVID-19 lockdown led to an increase in stillbirth and neonatal mortality rates and decreases in quality of care in healthcare institutions (*4*).

Most countries in sub-Saharan Africa have struggling healthcare systems (*5*). Pandemics exacerbate existing challenges. For instance, the 2014 Ebola outbreak in West Africa greatly affected maternal and child health services and fewer women attended antenatal care visits, fewer institutional deliveries occurred, and child vaccination coverage was low (*6*). Although risks to achieving improvements in maternal, neonatal, and child health outcomes posed by COVID-19 are well recognized, little national-level evidence has been collected to elucidate the wider effects of COVID-19 waves on maternal, neonatal, and child health outcomes in sub-Saharan Africa (*3*).

In Malawi, a SARS-CoV-2 seroprevalence study of 5,085 blood samples from blood donors showed that seroprevalence was 70.2% (95% CI 62.2%–81.6%) by July 2021 (*7*). The Ministry of Health (MoH) prioritized the COVID-19 response, but because of existing challenges in the healthcare infrastructure, the pandemic

Author affiliations: Malawi-Liverpool-Wellcome Programme, Blantyre, Malawi (L. Mndala, C. Chapuma, J. Riches, M. Kumwenda, R. Makuluni, B. Maseko, C. Ndamala, A. Kuyere, L. Munthali, D. Phiri, E.J.M. Monk, M.Y.R. Henrion, M.L. Odland, D. Lissauer); University of Liverpool, Liverpool, UK (L. Mndala, C. Chapuma, J. Riches, M.L. Odland, D. Lissauer); Kamuzu University of Health Sciences, Blantyre (L. Gadama, M. Kumwenda); Ministry of Health, Lilongwe, Malawi (F. Kachale, R. Bilesi, M. Mbewe, A. Likaka); Universidade de Pernambuco, Recife, Brazil (A. Likaka); Liverpool School of Tropical Medicine, Liverpool (M.Y.R. Henrion); St. Olavs University Hospital, Trondheim, Norway (M.L. Odland)

DOI: https://doi.org/10.3201/eid2910.230003

[1]These authors contributed equally to this article.

greatly disrupted healthcare delivery (*8*). A paucity of data are available from sub-Saharan Africa to establish the effects of COVID-19 on maternal, neonatal, and child health. In response, Malawi MoH collaborated with the Malawi-Liverpool-Wellcome Programme (MLW) to implement the Maternal COVID-19 Surveillance (MATSurvey) online platform to routinely collect and monitor data on COVID-19 in maternity.

Limited research has been conducted in Malawi and sub-Saharan Africa using national real-time data collected during the peak of the pandemic to assess effects of COVID-19 on maternal and neonatal health and access to healthcare. We analyzed the effects of the second and third COVID-19 waves in Malawi on selected maternal and neonatal outcomes and access to care by using nationally collected data from all 33 government healthcare sites participating in MATSurvey.

Methods

Study Design

This study is a secondary retrospective cohort analysis of data gathered from a cohort of pregnant and recently pregnant women enrolled in the MATSurvey platform from September 6, 2020–October 31, 2021. Data from the platform are routinely collected for all women admitted in all 33 government healthcare facilities of Malawi, including all 27 government district hospitals, all 4 central hospitals, and 2 district health offices.

Data Source

MATSurvey was implemented by using available structures within Malawi's healthcare system. MATSurvey involved digitization of existing Maternal Death Surveillance and Response (MDSR) program tools and reviews. Digitization enabled electronic data capture in all government facilities during COVID-19, making data available in real-time for monitoring, evaluation, and response. Prior to MATSurvey, data collection under MDSR was paper-based. MATSurvey comprises all facilities under MDSR. The MDSR site coordinators are responsible for daily active case-finding using data from facility teams, clinical notes, hospital registers, and handover files. Cases include women who have died, suffered a maternal near-miss event (i.e., almost died from complications), or had suspected or confirmed COVID-19.

Site coordinators were trained in digital data collection and entry for a tailored electronic tablet application developed by the MLW team. Designated project coordinators provided oversight of the project from MLW remotely, together with MoH's quality management directorate zonal coordinators, to assist with timeliness in uploading data and addressing challenges. MLW and MoH conducted weekly data quality checks.

Definitions and Measurements

Using the COVID-19 epidemic curve for Malawi (Figure 1), we defined the baseline period as September 6–December 31, 2020; the second wave as January 1–June 19, 2021; and the third wave as June 20–October 31, 2021. We defined maternal death rate (deaths/1,000 live births) as the number of deaths from any cause related to or aggravated by pregnancy or its management, excluding accidental or incidental causes, during pregnancy and childbirth or within 42 days

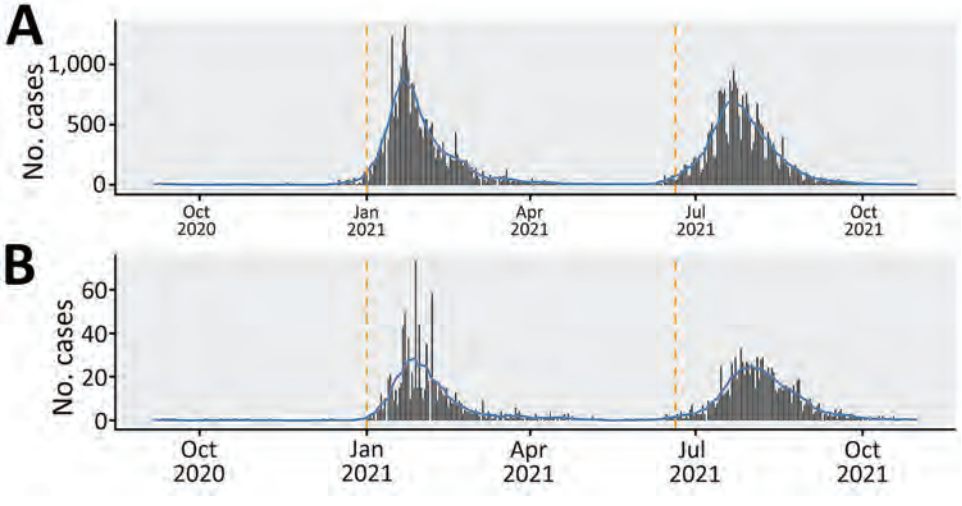

Figure 1. Epidemic data used in study of effects of COVID-19 on maternal and neonatal outcomes and access to antenatal and postnatal care, Malawi. A) Daily confirmed COVID-19 cases; B) daily confirmed COVID-19 deaths. The epidemiologic curve shows the beginning of second and third waves of COVID-19 in Malawi. Grey bars indicate daily case counts; blue lines indicate centered 14-day moving averages; orange vertical lines indicate proposed time points for the interruptions in the segmented time series analysis: January 1, 2021, just before the second COVID-19 wave; and June 20, 2021, just before the third COVID-19 wave. Data are from the Johns Hopkins University Center for Systems Science and Engineering (https://coronavirus.jhu.edu/map.html).

after termination of pregnancy, irrespective of the duration and site (e.g., ectopic) of the pregnancy. We defined neonatal death rate (deaths/1,000 live births) as the number of newborns up to 28 days of age who died before discharge. We defined stillbirth rate (stillbirths/1,000 live births) as the number of fetal deaths occurring during the antepartum and intrapartum period, after 28 weeks of pregnancy. We aggregated the number of antenatal clinic visits per week across the study period. We defined postnatal clinic visits as aggregated counts of visits per week across the study period. We defined the counterfactual scenario as the period during which no effects from second and third COVID-19 waves were seen.

Statistical Analysis

We aggregated data weekly across all facilities. We limited the date range of our analysis to September 6, 2020, after the end of the first COVID-19 wave in Malawi, to October 31, 2021, before the start of the fourth COVID-19 wave (Figure 1).

To assess the overall effects of the second and third pandemic waves on access to care and maternal and neonatal outcomes, we used an interrupted times series (ITS) regression approach for the time series obtained for each outcome (*9*). We used a negative binomial regression model for weekly reported clinic visits and maternal and neonatal outcomes. Those models included a linear trend over time for the logarithm of the rate of observed events. The ITS framework can foresee that a linear trend can be interrupted at ≥1 timepoints, both in overall level of events and in trend over time after interruptions. In our study, we allowed 2 interruptions: January 1, 2021, which was the start of second COVID-19 wave in Malawi; and June 20, 2021, the start of third COVID-19 wave. During the first COVID-19 wave in Malawi, MATSurvey was just being rolled out and not fully functional for capturing data. During that phase, data on COVID-19 in maternity were unavailable. Because of the paucity of data, we chose the period just after the first wave as the counterfactual period; that is, the period in which no effects of the second and third COVID-19 waves were seen. At each of the 2 interruption timepoints, we allowed both the level of the modeled events and the slope of the trajectory of number of events over time to change. For outcomes for which we estimated rates per 1,000 live births, the models also included an offset (i.e., a denominator) term for the logarithm of the number of weekly live births. To avoid ambiguity, and for the interest of mathematically inclined readers, we have made the precise model equations and code available (https://github.com/gitMarcH/MatSurv_ITS).

We also fitted models to data restricted to the time range up to the first interruption time point. Those models only included a constant term (the intercept), time, and the live birth denominator as an offset, if applicable. We used those models only for the first of the 3 time windows we considered in our analyses; that is, the period before the first interruption time point. By using those models to predict beyond the first interruption, the second COVID-19 wave, we were able to compare the counterfactual scenario of no effect on outcomes from the 2 COVID-19 waves against the observed events. To quantify the relative increase or decrease between the counterfactual model predictions and observed events, we divided the difference between both by the number of observed events. We characterized all outcomes in this study by a substantial amount of variation not explained by our models, which are most likely because covariates and confounders that are not recorded in the MATSurvey dataset. We quantified uncertainty in estimates by using the 95% CIs for the extrapolated model fits for the mean number of events for each outcome variable.

For model diagnostics, we inspected deviance residuals against fitted values and checked autocorrelations and partial autocorrelations for substantial deviations from model assumptions. We also computed pseudo R^2 values for every model. We chose January 1, 2021, and June 20, 2021, as timepoints by visually inspecting the epidemic curve (Figure 1). We performed analyses by using R version 4.1.2 (*10*). We fit negative binomial models for the ITS analyses by using the glm.nb() function from the library of Modern Applied Statistics with S (*11*).

Ethics Statement

Data were anonymized and made available to the research team by permission of MoH, Malawi, and the College of Medicine Research Ethics committee (protocol no. P.11/20/3186). Only aggregate data were made available to maintain patients' confidentiality. Patient consent was not required because MATSurvey is a national platform owned by MoH for routinely collecting data.

Results

During September 6, 2020–October 31, 2021, Malawi recorded 589 maternal deaths across all the healthcare facilities registered in MATSurvey. Of those deaths, 176 (29.9%) occurred during the baseline period, 208 (35.3%) occurred during the second COVID-19 wave, and 205 (34.8%) occurred during the third COVID-19 wave. During the same timeframe, Malawi recorded 6,701 neonatal deaths, of which 40.2% (n = 2,695)

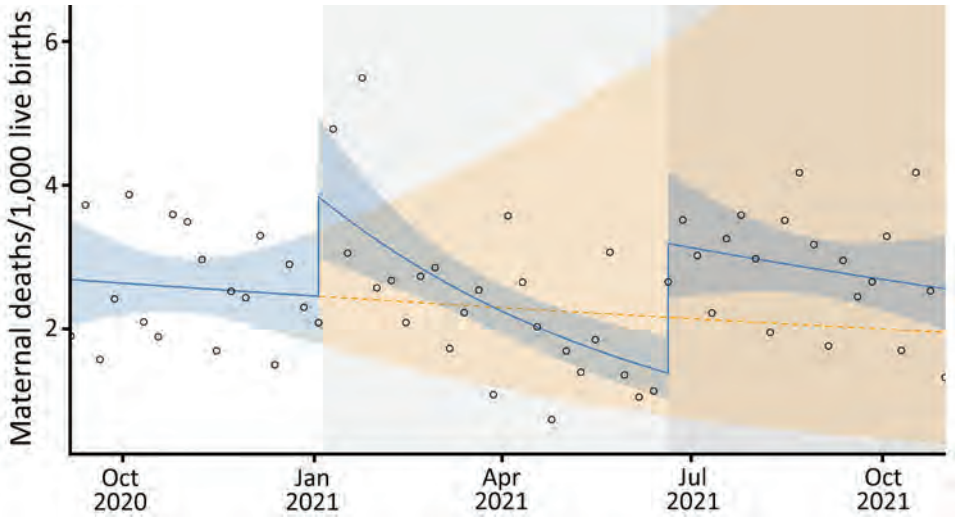

Figure 2. Maternal death rates in study of effects of COVID-19 on maternal and neonatal outcomes and access to antenatal and postnatal care, Malawi. Circles indicate observed data; blue lines indicate model fit from actual data, including step and slope changes during second (January 1, 2021) and third (June 20, 2021) COVID-19 waves. Dashed orange line indicates the counterfactual scenario of no second or third COVID−19 waves. Blue shaded areas indicate 95% CIs; yellow shaded areas indicate 95% CIs for the counterfactual scenario. Background shaded areas indicate the second (light gray) and third (dark gray) COVID−19 waves in Malawi. Pseudo R^2 = 0.06.

occurred during the second COVID-19 wave. The country reported 280,246 antenatal and 108,320 postnatal clinic visits. During the same timeframe, Malawi had 226,057 births, of which 67,377 (29.8%) were during the baseline, 88,685 (39.2%) were during the second wave, and 69,995 (31%) were during the third wave.

Maternal Death Rate

Compared with maternal deaths during September–December 2020 (baseline), a substantial increase occurred during January–October 2021, across the second and third COVID-19 waves (Figure 2). At the beginning of the second COVID-19 wave, we observed an increase in maternal deaths, which remained above the counterfactual scenario until around May 2021. We observed another increase in the outcome at the beginning of third wave, around July 2021.

The second COVID-19 wave led to a 57% increase in maternal death rate (rate ratio [RR] 1.57; p = 0.0228) compared with the counterfactual scenario. Maternal death rate increased 2-fold after the third COVID-19 wave (RR 2.31; p<0.001). The increase in maternal death rate across the second and third COVID-19 waves was accompanied by a sustained post–third wave effect (RR 1.03; p = 0.0408) (Table 1).

The total difference in maternal death rate between the counterfactual scenario and observed numbers from the beginning of the second through the third wave was −63 (95% CI −264 to 533). That finding represents an absolute increase by 63 maternal deaths and a relative increase of 15.4% during combined second and third waves of COVID-19 compared with the counterfactual scenario.

Neonatal Death Rate

At the beginning of the second COVID-19 wave, we observed no statistically significant change in the neonatal mortality rate (Figure 3). However, we saw a reduction at the beginning of the third wave. After the second COVID-19 wave, we saw a sustained decrease in the neonatal death rate, but we noted a sustained increase in neonatal death rate after the third wave (Table 2).

We observed a statistically nonsignificant drop in neonatal deaths at the interruption of both the second (RR 0.99; p = 0.9358) and third (RR 0.91; p = 0.2601) COVID-19 waves in Malawi. Both waves were associated with a change in time trend: a 2% drop occurred in the weekly trend during the second wave (RR 0.98; p = 0.0361), resulting in a slight decrease over time during that wave, then a 2% increase in the weekly trend, resulting again in a sustained increase in neonatal deaths over time during the period after the third wave (RR 1.02; p = 0.008).

The difference in neonatal mortality rates between the counterfactual scenario and observed out-

Table 1. Summary of regression analysis for maternal death rate in study of effects of COVID-19 on maternal and neonatal outcomes and access to antenatal and postnatal care, Malawi*

Variable	Estimate (95% CI)†	p value
Baseline, intercept	2.69 (2.00–3.63)	
COVID-19 wave 2	1.57 (1.06–2.30)	**0.0228**
COVID-19 wave 3	2.31 (1.54–3.47)	**0.0001**
Time, wk	0.99 (0.97–1.03)	0.7296
Post–COVID-19 wave 2	0.96 (0.93–0.99)	**0.0438**
Post–COVID-19 wave 3	1.03 (1.00–1.06)	**0.0408**

*Pseudo R^2 = 0.06. Bold text indicates statistical significance.
†The estimates are exponentiated model coefficients, i.e., the intercept estimate is the baseline incidence rate per 1,000 live births and all other estimates are rate ratios associated with the different variables.

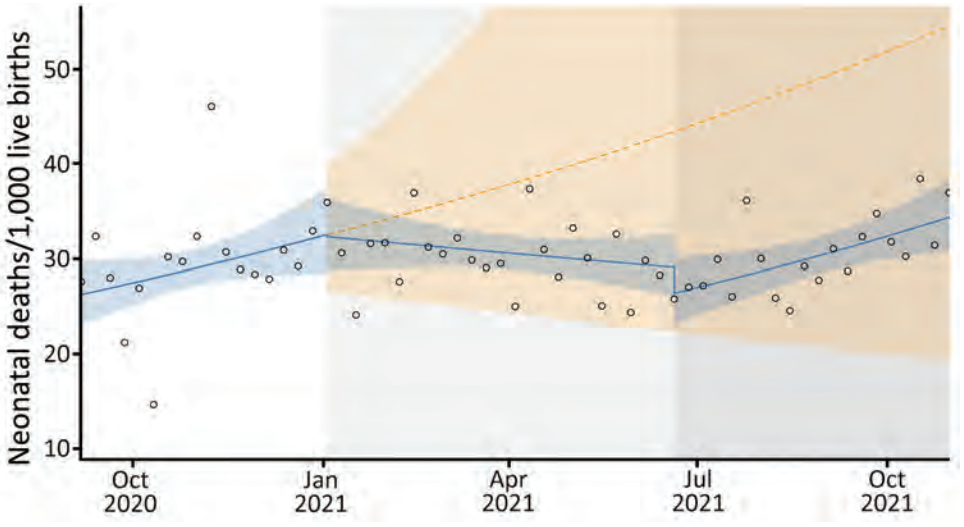

Figure 3. Neonatal death rates in study of effects of COVID-19 on maternal and neonatal outcomes and access to antenatal and postnatal care, Malawi. Circles indicate observed data; blue lines indicate model fit from actual data, including step and slope changes during second (January 1, 2021) and third (June 20, 2021) COVID-19 waves. Dashed orange line indicates the counterfactual scenario of no second or third COVID−19 waves. Blue shaded areas indicate 95% CIs; yellow shaded areas indicate 95% CIs for the counterfactual scenario. Background shaded areas indicate the second (light gray) and third (dark gray) COVID−19 waves in Malawi. Pseudo R^2 = 0.02.

comes from January 1–October 31, 2021, was 1,988 (95% CI −1,180 to 8,715). That finding translates to an absolute reduction of 1,988 and relative reduction of 41.4% neonatal deaths across the second and third COVID-19 waves.

Stillbirth Rate

We observed 131 (95% CI −1,032 to 1,863) fewer stillbirths per 1,000 live births compared with a scenario of no second and third COVID-19 waves. The drop in stillbirths was more of a sustained effect and not an immediate result of the second and third wave interruptions (Table 3; Figure 4). An immediate 30% increase in stillbirths occurred at the onset of the third COVID-19 wave (RR 1.30; p<0.001), but the increase was not sustained.

Antenatal and Postnatal Clinic Visits

During the beginning of the second and third COVID-19 waves, antenatal clinic visits increased (Figure 5), but we observed a sharp drop in postnatal clinic visits at the onset of the second wave (Figure 6). During the second and third COVID-19 waves, January 1, 2021–October 31, 2021, we observed an increase of 16,833 (95% CI 89,072–111,041) more antenatal clinic visits than during the period without the 2 waves. Although the differences were not statistically significant, during the second COVID-19 wave, we noted an 11% (RR 1.11; p = 0.1395) increase in antenatal clinic visits, but only a 3% (RR 1.03; p = 0.6187) increase occurred during the third COVID-19 wave.

Postnatal clinic visits dropped by 41% at the onset of the second COVID-19 wave (RR 0.59; p<0.001). A 0.2% decrease in postnatal care visits occurred at the onset of the third COVID-19 wave (RR 1.02; p = 0.0149), but although that decrease was not statistically significant, it was accompanied by a sustained post–third wave effect (Table 4). Postnatal clinic visits declined by 36,809 (95% CI 15,799–64,848) visits between the counterfactual scenario and observed outcome.

Table 2. Summary of regression analysis for neonatal death rate in study of effects of COVID-19 on maternal and neonatal outcomes and access to antenatal and postnatal care, Malawi*

Variable	Estimate (95% CI)†	p value
Baseline, intercept	25.93 (22.55–29.82)	
COVID-19 wave 2	0.99 (0.83–1.17)	0.9358
COVID-19 wave 3	0.91 (0.76–1.07)	0.2601
Time, wk	1.01 (0.99–1.02)	0.0691
Post COVID-19 wave 2	0.98 (0.96–0.99)	**0.0361**
Post COVID-19 wave 3	1.02 (1.0–1.03)	**0.0080**

*Pseudo R^2 = 0.02. Bold text indicates statistical significance.
†The estimates are exponentiated model coefficients, i.e., the intercept estimate is the baseline incidence rate per 1,000 live births and all other estimates are rate ratios associated with the different variables.

Discussion

Using an ITS regression analysis of aggregated time series data on COVID-19 in maternity, we estimated the total effects of the second and third COVID-19 waves on selected maternal and neonatal outcomes, and access to antenatal and postnatal care in Malawi. We found a statistically significant increase in the maternal death rate at the beginning of the second and third COVID-19 waves compared with a counterfactual scenario of no second and third COVID-19 waves. However, the neonatal death rate was largely unaffected by the 2 interruptions and only had a statistically significant sustained increase because of a time trend change in the period after the third wave.

Antenatal clinic visits were largely unaffected by the 2 pandemic waves, but the drop in postnatal care visits was statistically significant.

We observed a 57% increase in the maternal death rate at the first interruption (wave 2) and a >2-fold increase in maternal deaths at the second interruption (wave 3). After each of those increases, we noted a substantial, although statistically nonsignificant, waning of the death rate over the course of each wave. The SARS-CoV-2 Beta variant of concern was in circulation during the second wave in Malawi and the Delta variant was circulating during the third wave (*12*). In the United Kingdom, the Beta and Delta variants were associated with maternal deaths in pregnant and recently pregnant women (*13*), findings which are comparable to ours. Our results are also comparable to findings on a multinational cohort of pregnant women that reported that COVID-19 resulted in increased maternal deaths and exacerbated effects on women in low- and middle-income countries (*14*). Observed increased mortality rates at the beginning of the second and third pandemic waves could be the result of direct effects of COVID-19, such as respiratory failure, coupled with observed lack of invasive ventilation in healthcare facilities in Malawi. Another study in Malawi reported that shortness of breath had a statistically significant association with maternal death during the second and third COVID-19 waves (*15*).

Although the drop in neonatal death rate at the onset of both the second and third COVID-19 waves was not statistically significant, the sustained drop after the third COVID-19 wave was significant. Neonatal mortality rate remained below anticipated numbers compared with the counterfactual model of no association. A systematic review of evidence regarding maternal, fetal, and neonatal death associated with COVID-19 showed that direct COVID-19 infection of neonates was not associated with statistically significant mortality rates (*16*). Similarly, our data show that COVID-19 does not seem to have caused overall adverse effects on the outcomes of neonates in Malawi, suggesting that care during labor and the neonatal period was relatively available, despite the challenges to healthcare facilities caused by COVID-19.

Across the 2 COVID-19 waves, we observed fewer stillbirths than anticipated under the counterfactual model. We noted an increase in stillbirths at the onset of the third wave, but that was not sustained. Other studies have found no relationship between SARS-CoV-2 infection and stillbirths, which also appeared to be true for Malawi. In Nepal, the lockdown, and not necessarily COVID-19 infection, was associated with an increase in stillbirths (*4*). Different studies have also reported

Table 3. Summary of regression analysis for stillbirths in study of effects of COVID-19 on maternal and neonatal outcomes and access to antenatal and postnatal care, Malawi*

Variable	Estimate (95% CI)†	p value
Baseline, intercept	22.47 (22.14–27.04)	
COVID-19 wave 2	1.04 (0.91–1.18)	0.6225
COVID-19 wave 3	1.30 (1.14–1.47)	**0.0001**
Time, wk	1.00 (0.99–1.01)	0.7905
Post COVID-19 wave 2	0.99 (0.98–1.00)	0.1304
Post COVID-19 wave 3	1.00 (0.99–1.01)	0.5393

*Pseudo R^2 = 0.04. Bold text indicates statistical significance.
†The estimates are exponentiated model coefficients, i.e., the intercept estimate is the baseline incidence rate per 1,000 live births and all other estimates are rate ratios associated with the different variables.

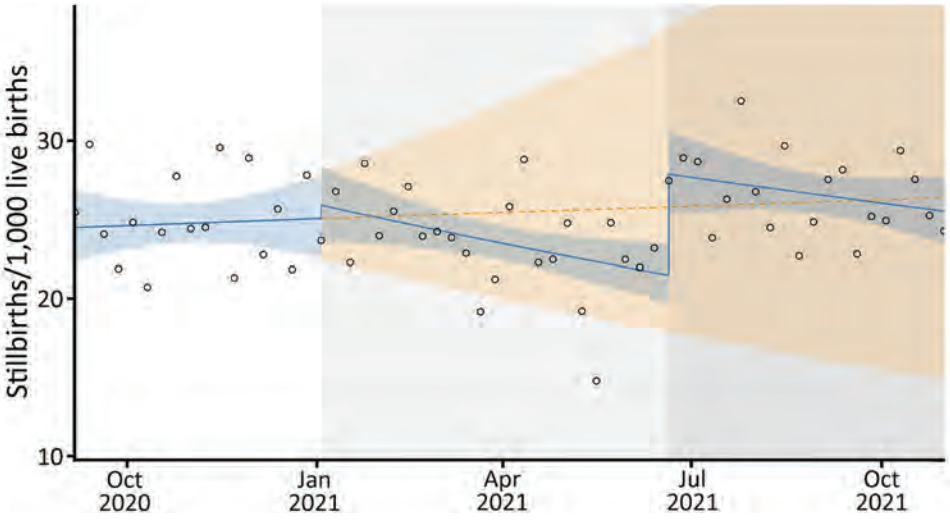

Figure 4. Stillbirth rates in study of effects of COVID-19 on maternal and neonatal outcomes and access to antenatal and postnatal care, Malawi. Circles indicate observed data; blue lines indicate model fit from actual data, including step and slope changes during second (January 1, 2021) and third (June 20, 2021) COVID-19 waves. Dashed orange line indicates the counterfactual scenario of no second or third COVID−19 waves. Blue shaded areas indicate 95% CIs; yellow shaded areas indicate 95% CIs for the counterfactual scenario. Background shaded areas indicate the second (light gray) and third (dark gray) COVID−19 waves in Malawi. Pseudo−R^2 = 0.04.

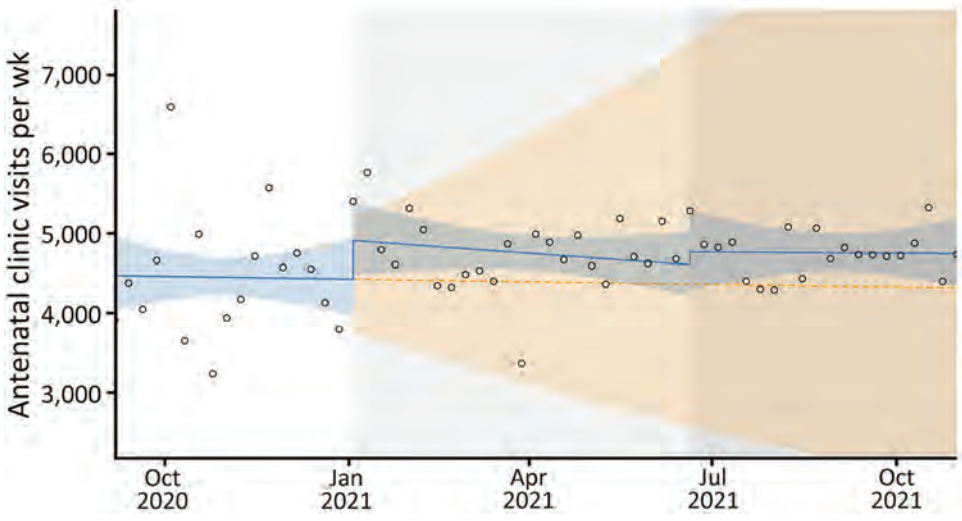

Figure 5. Antenatal clinic visits in study of effects of COVID-19 on maternal and neonatal outcomes and access to antenatal and postnatal care, Malawi. Circles indicate observed data; blue lines indicate model fit from actual data, including step and slope changes during second (January 1, 2021) and third (June 20, 2021) COVID-19 waves. Dashed orange line indicates the counterfactual scenario of no second or third COVID−19 waves. Blue shaded areas indicate 95% CIs; yellow shaded areas indicate 95% CIs for the counterfactual scenario. Background shaded areas indicate the second (light gray) and third (dark gray) COVID−19 waves in Malawi. Pseudo R^2 = 0.01.

increased preterm birth outcomes after SARS-CoV-2 infection, but not increases in stillbirths (*17*,*18*).

Despite the COVID-19 waves, antenatal clinic visits remained largely unaffected in Malawi. The country implemented a multisectoral response policy to respond the COVID-19 pandemic, which included risk communication, community engagement, and ensuring that critical services such as antenatal clinics remained robust (*19*).

Although antenatal clinic visits were largely unaffected, postnatal care clinical visits showed a sharp decline at the start of the second COVID-19 wave. About 6 weeks after discharge from facilities, many women did not return for care as recommended, which might be attributed to fear of SARS-CoV-2 infection, as seen among other patients in facilities (*20*). The reluctance to return for care might also have been linked to instituted facility-level policy changes that did not actively encourage women to return. Researchers in the United Kingdom called for vigilance to avoid disruptions and improve maternal postnatal healthcare amidst COVID-19 (*21*). However, evidence suggests that a substantial number of postnatal women became fearful of COVID-19 and more concerned about their wellbeing and that of their babies if exposed to SARS-CoV-2 in crowded environments (*20*). This fear likely explains why, in Malawi, postnatal care visits dropped substantially throughout our study period. Further qualitative

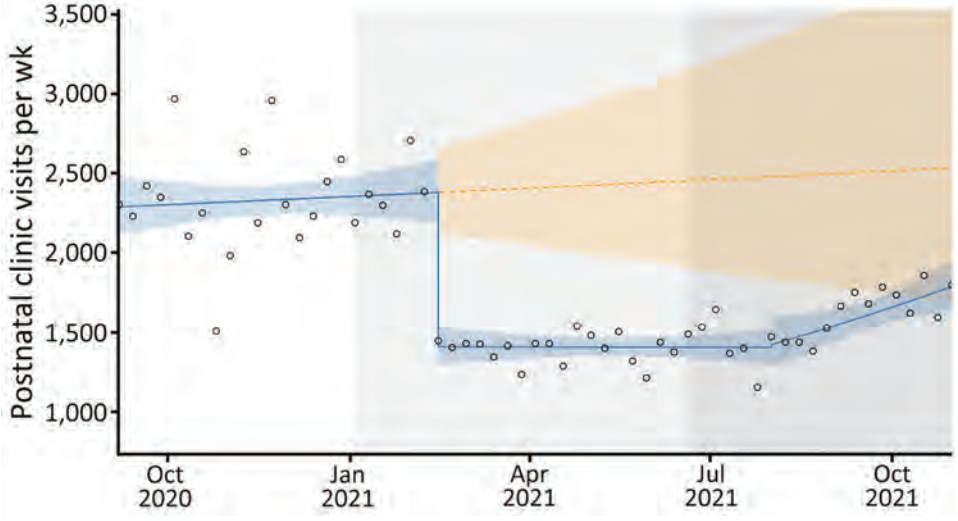

Figure 6. Postnatal clinic visits in study of effects of COVID-19 on maternal and neonatal outcomes and access to antenatal and postnatal care, Malawi. Circles indicate observed data; blue lines indicate model fit from actual data, including step and slope changes during second (January 1, 2021) and third (June 20, 2021) COVID-19 waves. Dashed orange line indicates the counterfactual scenario of no second or third COVID−19 waves. Blue shaded areas indicate 95% CIs; yellow shaded areas indicate 95% CIs for the counterfactual scenario. Background shaded areas indicate the second (light gray) and third (dark gray) COVID−19 waves in Malawi. Pseudo R^2 = 0.12.

Table 4. Summary of regression analysis for weekly postnatal visit rate in study of effects of COVID-19 on maternal and neonatal outcomes and access to antenatal and postnatal care, Malawi*

Variable	Estimate (95% CI)†	p value
Baseline, intercept	2,283.98 (2,100.42–2,483.58)	
COVID-19 wave 2	0.59 (0.53–0.66)	**0.0000**
COVID-19 wave 3	1.01 (0.88–1.16)	0.8521
Time, wk	1.00 (0.99–1.01)	0.5854
Post COVID-19 wave 2	0.99 (0.98–1.00)	0.6701
Post COVID-19 wave 3	1.02 (1.00–1.03)	**0.0149**

*Pseudo R^2 = 0.12. Bold text indicates statistical significance.
†The estimates are exponentiated model coefficients, i.e., the intercept estimate is the baseline rate, and all other estimates are rate ratios associated with the different variables.

research could examine the drop-in postnatal care visits and needed health education. The drop-in postnatal care visits also might have affected women's opportunities for critical postnatal interventions, such as contraception, which could have lasting effects that will require further evaluation and mitigation.

The first limitation of our study is that we attributed the baseline to a period when Malawi had already experienced the first COVID-19 wave. MATSurvey was not optimally functional before COVID-19 emerged, which is why we chose the period after the first wave as baseline in the interrupted regression analysis. Second, we chose to focus on 2 key interruptions, the second and third COVID-19 waves, because those presented the most critical scenarios in the country. Third, all the outcomes investigated in this study are characterized by substantial amounts of variation not explained by our models. Although some random variation existed, other drivers for variation in maternal and neonatal death, stillbirths, and antenatal and postnatal visits likely were not included in our data and hence could not be accounted for in our statistical models. A limitation of the dataset is that MATSurvey does not include data on possible confounders; hence, we could not adjust for those data in the ITS regression models. Fourth, our data might have risked overfitting, which we mitigated by choosing the 2 interruption time points in the regression models a priori, and we did not change those time points from outcome to outcome except for postnatal care visits, for which we had to account for the 6-week postnatal lag. Finally, our prediction 95% CIs for the hypothetical models are large and widen as the predictions stretched beyond January 1, 2021, the first interruption timepoint. Although not unexpected, because we were predicting beyond the data range used for fitting the model, the widening predictions mean considerable uncertainty exists regarding our estimates of differences between counterfactual model predictions and ITS regression fits. Those differences are reflected in the reported CIs but do not mean that interpretation of those findings needs to be nuanced, which affects all outcomes, but it is particularly acute for the maternal death outcome.

In conclusion, we used an ITS model to investigate the effects of the 2 most critical COVID-19 waves on maternal and neonatal health indicators in Malawi, which might also apply to other countries in sub-Saharan Africa. Further studies are needed to comprehend the burden of COVID-19 on maternal, neonatal, and child health outcomes. Nonetheless, our findings demonstrate the need for strengthening maternal, neonatal, and child healthcare systems to prepare for future pandemics, particularly in resource-constrained settings.

Acknowledgments

This work was made possible by the teams and partners working to deliver MATSurvey to high operational standard. We thank our team of government healthcare workers, particularly the safe motherhood coordinators (site coordinators) based at the healthcare facilities conducting MATSurvey, who ensure that the data are collected and uploaded timely and comprehensively.

Reasonable requests for anonymized data, aggregated by facility, can be made by contacting the Malawi Ministry of Health and the Malawi Liverpool Wellcome Programme, via the corresponding author.

This research was funded by The Bill and Melinda Gates Foundation (grant no. BMG618). The team is also supported by the National Institute for Health and Care Research (NIHR; DIPLOMATIC Ref:17/63/08 and SAFE Motherhood, NIHR134781; Global health research group and NIHR Professorship NIHR300808) using aid from the UK government to support global health research. The Wellcome Trust provided a strategic award to the Malawi Liverpool Wellcome Programme (award no. 206545/Z/17/Z) that, in part, covers the salary and operational costs of the Statistical Support Unit, headed by M.Y.R.H. The views expressed in this publication are those of the authors and not those of any of the funders.

Author contributions: L. Mndala, C.C., and D.L. conceptualized the project. D.L. and M.L.O. supervised the project. D.L. acquired funding and takes responsibility of this manuscript. D.P., M.Y.R.H., C.C., and L. Mndala curated data. M.Y.R.H. performed formal data analysis. L. Mndala conducted the literature search. L. Mndala, M.Y.R.H., D.L., M.L.O., J.R., and C.C. interpreted the data. L. Mndala and M.Y.R.H. drafted the manuscript. A.L., A.K., B.M., C.C., C.M., C.N., D.P., F.K., L. Munthali, M.K., M.M., R.B., R.M., L.G., and E.J.M.M. critically revised the manuscript for intellectual content. L. Mndala, D.P., and

M.Y.R.H. accessed and verified the data underlying the study. All authors read and approved final manuscript.

About the Author

Mr. Mndala is a PhD candidate in women's health at the University of Liverpool, Liverpool, UK, and is based at the Malawi-Liverpool-Wellcome Programme in Blantyre, Malawi. His research interests focus on maternal and child health.

References

1. World Health Organization. COVID-19: operational guidance for maintaining essential health services during an outbreak [cited 2022 Nov 14]. https://apps.who.int/iris/bitstream/handle/10665/331561/WHO-2019-nCoV-essential_health_services-2020.1-eng.pdf
2. Chmielewska B, Barratt I, Townsend R, Kalafat E, van der Meulen J, Gurol-Urganci I, et al. Effects of the COVID-19 pandemic on maternal and perinatal outcomes: a systematic review and meta-analysis. Lancet Glob Health. 2021; 9:e759–72. https://doi.org/10.1016/S2214-109X(21)00079-6
3. Roberton T, Carter ED, Chou VB, Stegmuller AR, Jackson BD, Tam Y, et al. Early estimates of the indirect effects of the COVID-19 pandemic on maternal and child mortality in low-income and middle-income countries: a modelling study. Lancet Glob Health. 2020;8:e901–8. https://doi.org/10.1016/S2214-109X(20)30229-1
4. Kc A, Gurung R, Kinney MV, Sunny AK, Moinuddin M, Basnet O, et al. Effect of the COVID-19 pandemic response on intrapartum care, stillbirth, and neonatal mortality outcomes in Nepal: a prospective observational study. Lancet Glob Health. 2020;8:e1273–81. https://doi.org/10.1016/S2214-109X(20)30345-4
5. World Health Organization Regional Office for Africa. The state of health in the WHO African Region: an analysis of the status of health, health services and health systems in the context of the Sustainable Development Goals 2018 [cited 2022 Nov 14]. https://apps.who.int/iris/handle/10665/275292
6. Delamou A, Ayadi AME, Sidibe S, Delvaux T, Camara BS, Sandouno SD, et al. Effect of Ebola virus disease on maternal and child health services in Guinea: a retrospective observational cohort study. Lancet Glob Health. 2017;5:e448–57. https://doi.org/10.1016/S2214-109X(17)30078-5
7. Mandolo J, Msefula J, Henrion MYR, Brown C, Moyo B, Samon A, et al. SARS-CoV-2 exposure in Malawian blood donors: an analysis of seroprevalence and variant dynamics between January 2020 and July 2021. BMC Med. 2021;19:303. https://doi.org/10.1186/s12916-021-02187-y
8. Soko RN, Burke RM, Feasey HRA, Sibande W, Nliwasa M, Henrion MYR, et al. Effects of coronavirus disease pandemic on tuberculosis notifications, Malawi. Emerg Infect Dis. 2021;27:1831–9. https://doi.org/10.3201/eid2707.210557
9. Lopez Bernal J, Cummins S, Gasparrini A. Interrupted time series regression for the evaluation of public health interventions: a tutorial. Int J Epidemiol. 2017;46:348–55. https://doi.org/10.1093/ije/dyw098
10. R Core Team. R: a language and environment for statistical computing. The R Foundation for Statistical Computing; Vienna: 2021.
11. Venables WN, Ripley BD. Modern applied statistics with S. New York, NY: Springer New York; 2002 [cited 2022 May 23]. http://link.springer.com/10.1007/978-0-387-21706-2
12. Anscombe C, Lissauer S, Thole H, Rylance J, Dula D, Menyere M, et al. A comparison of four epidemic waves of COVID-19 in Malawi; an observational cohort study. BMC Infect Dis. 2023;23:79. https://doi.org/10.1186/s12879-022-07941-y
13. Vousden N, Ramakrishnan R, Bunch K, Morris E, Simpson NAB, Gale C, et al. Severity of maternal infection and perinatal outcomes during periods of SARS-CoV-2 wildtype, alpha, and delta variant dominance in the UK: prospective cohort study. BMJ Med. 2022; 1:e000053. https://doi.org/10.1136/bmjmed-2021-000053
14. Villar J, Ariff S, Gunier RB, Thiruvengadam R, Rauch S, Kholin A, et al. Maternal and neonatal morbidity and mortality among pregnant women with and without COVID-19 infection: the INTERCOVID Multinational Cohort Study. Obstet Gynecol Surv. 2022;77:80–2. https://doi.org/10.1097/01.ogx.0000816508.60579.d5
15. Mndala L, Monk EJM, Phiri D, Riches J, Makuluni R, Gadama L, et al. Comparison of maternal and neonatal outcomes of COVID-19 before and after SARS-CoV-2 Omicron emergence in maternity facilities in Malawi (MATSurvey): data from a national maternal surveillance platform. Lancet Glob Health. 2022;10:e1623–31. https://doi.org/10.1016/S2214-109X(22)00359-X
16. Hessami K, Homayoon N, Hashemi A, Vafaei H, Kasraeian M, Asadi N. COVID-19 and maternal, fetal and neonatal mortality: a systematic review. J Matern Fetal Neonatal Med. 2022;35:2936–41. https://doi.org/10.1080/14767058.2020.1806817
17. Lokken EM, Huebner EM, Taylor GG, Hendrickson S, Vanderhoeven J, Kachikis A, et al.; Washington State COVID-19 in Pregnancy Collaborative. Disease severity, pregnancy outcomes, and maternal deaths among pregnant patients with severe acute respiratory syndrome coronavirus 2 infection in Washington State. Am J Obstet Gynecol. 2021; 225:77.e1–14. https://doi.org/10.1016/j.ajog.2020.12.1221
18. Delahoy MJ, Whitaker M, O'Halloran A, Chai SJ, Kirley PD, Alden N, et al.; COVID-NET Surveillance Team. Characteristics and maternal and birth outcomes of hospitalized pregnant women with laboratory-confirmed COVID-19—COVID-NET, 13 states, March 1–August 22, 2020. MMWR Morb Mortal Wkly Rep. 2020;69:1347–54. https://doi.org/10.15585/mmwr.mm6938e1
19. Mzumara GW, Chawani M, Sakala M, Mwandira L, Phiri E, Milanzi E, et al. The health policy response to COVID-19 in Malawi. BMJ Glob Health. 2021;6:e006035. https://doi.org/10.1136/bmjgh-2021-006035
20. Matsushima M, Tsuno K, Okawa S, Hori A, Tabuchi T. Trust and well-being of postpartum women during the COVID-19 crisis: depression and fear of COVID-19. SSM Popul Health. 2021;15:100903. https://doi.org/10.1016/j.ssmph.2021.100903
21. Bick D, Cheyne H, Chang YS, Fisher J. Maternal postnatal health during the COVID-19 pandemic: vigilance is needed. Midwifery. 2020;88:102781. https://doi.org/10.1016/j.midw.2020.102781

Address for correspondence: Leonard Mndala, Malawi-Liverpool-Wellcome Programme, Chipatala Ave, Chichiri, Blantyre 3, Malawi; email: leonardmndala@gmail.com

Emergence of SARS-CoV-2 Delta Variant and Effect of Nonpharmaceutical Interventions, British Columbia, Canada

Y.L. Elaine Chan, Michael A. Irvine, Natalie Prystajecky, Hind Sbihi, Marsha Taylor, Yayuk Joffres, Andrea Schertzer, Caren Rose, Louise Dyson, Edward M. Hill, Michael Tildesley, John R. Tyson, Linda M.N. Hoang, Eleni Galanis

In British Columbia, Canada, initial growth of the SARS-CoV-2 Delta variant was slower than that reported in other jurisdictions. Delta became the dominant variant (>50% prevalence) within ≈7–13 weeks of first detection in regions within the United Kingdom and United States. In British Columbia, it remained at ≤10% of weekly incident COVID-19 cases for 13 weeks after first detection on March 21, 2021, eventually reaching dominance after 17 weeks. We describe the growth of Delta variant cases in British Columbia during March 1–June 30, 2021, and apply retrospective counterfactual modeling to examine factors for the initially low COVID-19 case rate after Delta introduction, such as vaccination coverage and nonpharmaceutical interventions. Growth of COVID-19 cases in the first 3 months after Delta emergence was likely limited in British Columbia because additional nonpharmaceutical interventions were implemented to reduce levels of contact at the end of March 2021, soon after variant emergence.

Throughout the COVID-19 pandemic, SARS-CoV-2 variants have emerged through viral mutation. Variants demonstrating an increase in transmissibility or virulence; changes in clinical manifestations; or a decrease in the effectiveness of public health measures, diagnostics, vaccines, or therapeutics are designated variants of concern (VOCs) by the World Health Organization (*1*). By June 2021, a total of 4 SARS-CoV-2 variants had been designated VOCs (*1*). Designated a VOC in May 2021, Delta largely replaced the earlier Alpha, Beta, and Gamma VOCs because of its comparatively higher transmissibility (*2*). In India, where it was first detected, Delta outcompeted Alpha and drove an increase of COVID-19 cases beginning in March 2021 (*3*). By mid-August 2021, Delta represented >90% of genetically sequenced SARS-CoV-2 samples submitted to GISAID (https://www.gisaid.org), dominating on a global scale until its decline in favor of Omicron beginning in December 2021 (*4*,*5*).

By March 1, 2021, British Columbia (2021 population 5,214,805), Canada, had reported >80,000 COVID-19 cases and detected Alpha, Beta, and Gamma VOC cases among residents (*6*). The Delta VOC was first detected in British Columbia during the week of March 21, 2021, but did not grow to dominance (>50% prevalence) until 17 weeks later, during the week of July 18, 2021, after major relaxations in public health measures, or nonpharmaceutical interventions (NPIs).

Differences in factors such as NPIs, vaccination rates, competing variants in circulation, and population density and behavior may result in interjurisdictional differences in the transmission and growth rates of variants (*7*–*10*). The initial growth and time to dominance of Delta in British Columbia was slower than in jurisdictions such as England, Scotland, and several US states (*7*–*10*). In England, Delta grew to

Author affiliations: British Columbia Centre for Disease Control, Vancouver, British Columbia, Canada (Y.L.E. Chan, M.A. Irvine, N. Prystajecky, H. Sbihi, M. Taylor, Y. Joffres, A. Schertzer, C. Rose, J.R. Tyson, L.M.N. Hoang, E. Galanis); Public Health Agency of Canada, Ottawa, Ontario, Canada (Y.L.E. Chan, A. Schertzer); Simon Fraser University, Burnaby, British Columbia, Canada (M.A. Irvine); University of British Columbia, Vancouver (N. Prystajecky, H. Sbihi, C. Rose, L.M.N. Hoang, E. Galanis); University of Warwick, Coventry, UK (L. Dyson, E.M. Hill, M. Tildesley); Joint UNIversities Pandemic and Epidemiological Research (L. Dyson, E.M. Hill, M. Tildesley)

DOI: https://doi.org/10.3201/eid2910.230055

dominance ≈10 weeks after the fifth case was detected in mid-March 2021, reaching 62% prevalence among sequenced cases by mid-May 2021 (*7*). In Scotland, the Delta VOC rapidly replaced Alpha during April–May 2021 (*8*,*9*), and across 6 states in the United States, the average time from first detection of Delta to its dominance was ≈10 weeks (71 days, range 54–92 days) (*10*).

British Columbia and England are adequately comparable because they have universal healthcare systems, similar population age distribution (median age 42.8 years in British Columbia, 40 years for England and Wales in 2021), and similar temperate climates within the main metropolitan areas. Of note, key differences existed in public health policy and vaccination coverage between British Columbia and England around the time of Delta emergence; England ultimately experienced both a shorter time to dominance for Delta and higher subsequent growth in COVID-19 incidence (Appendix Figure 1, https://wwwnc.cdc.gov/EID/article/29/10/23-0055-App1.pdf). In British Columbia, circuit-breaker NPIs, including restricting travel outside the region of residence unless essential; suspending indoor dining, worship services, and adult group fitness activities; and expanding mask requirements in schools to younger age groups, were implemented on March 30, 2021, shortly after Delta variant was detected, in response to rising numbers of Alpha and Gamma variant cases (*11*). Those measures supplemented existing NPIs, which required physical distancing and masks in all public indoor settings, restricted gatherings, and encouraged workplaces to adopt remote working conditions (Appendix Table 1). During March–June 2021, the 7-day rolling COVID-19 incidence rate per 100,000 population in British Columbia peaked at 21.8 in mid-April 2021 before decreasing to a low of 1.0 at the end of June 2021.

Conversely, in the time surrounding Delta introduction and initial growth, England was in the early stages of reopening after lockdown and had begun gradually relaxing measures, including reopening schools to all students, replacing a stay-at-home order with a recommendation to stay local, and stepwise reopening of businesses and public buildings (*12*) (Appendix Table 1). England observed an initial decrease in its 7-day rolling COVID-19 incidence rate per 100,000 population from 77.0 in March 2021 to 20.7 for the beginning of May 2021, before seeing a substantial increase driven by Delta to 229.1 by the end of June 2021 (*13*) (Appendix Figure 1).

However, population COVID-19 vaccine coverage also differed between British Columbia and England; British Columbia had higher coverage among younger age groups (*14*,*15*). COVID-19 vaccination coverage overall and for persons ≥45 years of age were lower in British Columbia than in England during March–June 2021, but rates of first-dose coverage for persons 18–34 years of age in British Columbia exceeded those in England by May 2021 (Appendix Figure 2, panel A). Another key difference was the vaccine product used: most vaccine doses administered during March–June 2021 in British Columbia were the mRNA-based BNT162b2 (Pfizer-BioNTech, https://www.pfizer.com) or mRNA-1273 (Moderna, https://www.modernatx.com), and most administered in England were ChAdOx1 (Oxford-AstraZeneca, https://www.astrazeneca.com) (*16*).

The first objective of this study was to describe the emergence of the Delta VOC in British Columbia with respect to the presence of competing variants and case demographics, vaccination status, and travel history. The second objective was, through counterfactual modeling, to identify the main factors for the initially low rate of COVID-19 transmission in British Columbia after Delta variant introduction. Using England as the counterfactual scenario because of its similarities with British Columbia and the availability of public data from UK Health Security Agency, we explored the effects of differences in the proportion of Delta among all infections, public health measures, and vaccine coverage and type on the modeled number of overall COVID-19 cases in British Columbia.

Methods

SARS-CoV-2 Lineage Data

In British Columbia, SARS-CoV-2 quantitative PCR (qPCR) testing is offered by hospitals, private laboratories, and the British Columbia Centre for Disease Control (BCCDC) Public Health Laboratory (PHL), which serves as the reference laboratory for the province; VOC monitoring is performed primarily by the BCCDC PHL. During March 1–May 29, 2021 (US Centers for Disease Control and Prevention epidemiologic weeks [epiweeks] 9–21), a combined VOC testing strategy using both screening (i.e., targeted VOC single-nucleotide variant qPCR) and whole-genome sequencing (WGS) was applied to monitor VOC prevalence in BC (Appendix Table 2). During this period, the weekly percentage of samples undergoing VOC screening ranged from 80%–99% and the percentage undergoing WGS ranged from 31%–79%. During May 30–June 30, 2021 (epiweeks 22–26), WGS was attempted for all samples; 69%–79% of all weekly positive samples were successfully sequenced. VOC case definitions are provided (Appendix Table 3).

For samples that underwent both VOC screening and WGS, we used lineage results from WGS. We included only samples with ≥85% sequence coverage and no quality control flags in ncov-tools (https://github.com/jts/ncov-tools). We classified cases as having unknown lineage if samples did not undergo VOC screening or WGS, were screened VOC-negative or indeterminate and did not undergo WGS, or were not screened and failed WGS.

Study Population

We linked COVID-19 case investigation and SARS-CoV-2 lineage data by using the patient's full name, date of birth, and personal health number. We performed linkage using SAS version 9.4 (SAS Institute Inc., https://www.sas.com). We included all COVID-19 cases reported in British Columbia with case investigation information and specimen collection during March 1–June 30, 2021. For records with multiple specimen collection dates, we used the earliest positive date. For cases missing specimen collection date (n = 2,637; 4.0% of final study population), we used symptom onset date, followed by date of case report to the regional health authority. We performed data cleaning, analysis, and figure creation using R version 3.5.2 (The R Foundation for Statistical Computing, https://www.r-project.org).

Travel history information was collected during routine case investigation. Information on international travel was supplemented by reason for testing recorded in the BCCDC PHL database (e.g., international arrivals testing). Delta variant case-patients who had a travel history outside British Columbia were assumed to have acquired infection outside the province; those cases were considered Delta introductions.

COVID-19 vaccination status at time of case detection was linked from British Columbia's Provincial Immunization Registry using case identifiers. We considered case-patients fully vaccinated if symptom onset (or positive specimen collection if the onset date was not available) occurred ≥14 days after the second dose of BNT162b2, mRNA-1273, or ChAdOx1; additional doses were not yet approved or recommended during the study period. Case-patients were considered partially vaccinated if they were not fully vaccinated and onset or specimen collection occurred ≥21 days after first dose. Case-patients without any recorded vaccination or with onset or specimen collection <21 days after the first dose were considered unvaccinated.

Counterfactual Modeling Methods

We implemented counterfactual modeling using an established model of COVID-19 transmission dynamics in British Columbia (*17*). The model is an adapted susceptible-exposed-infected-recovered compartmental ordinary differential equation model. Additional modeled compartments included a quarantine compartment and a proportion of the population that participate in social distancing with analogous susceptible-exposed-infected-recovered compartments for the social distancing group. We used a Bayesian statistical model in the inference of the basic reproductive number, the fraction change in social distancing between predefined breakpoints, and a dispersion parameter associated with a negative binomial term to observed cases (*17*). We explored differences in the following factors on the modeled number of COVID-19 cases in British Columbia (Appendix Table 4).

Proportion of Delta variant Among All Infections

We extracted weekly data on the proportion of the Delta variant among cases in England from the July 23, 2021, UK Health Security Agency report (*18*) and included the proportion of all cases that were genotyped. Unlike in British Columbia, the proportion of cases of Delta in England transitioned from <5% to >80% during May–June 2021 (Appendix Figure 2, panel B). We incorporated logistic functions representing the relative proportion of Delta to represent the relative differences in growth between jurisdictions. We directly incorporated that function into the time-varying transmission term for each scenario, representing the per-contact transmissibility increasing in proportion to the changing composition of variants. Because we used the sampled proportion of Delta variant as input in the modeling, we did not directly explore reasons for their differences between jurisdictions within these scenarios.

Levels of Contact Leading to Transmission, Guided by Changes in NPIs

We constructed the transmission scenario for England on the basis of the fitted transmission estimate for British Columbia. We applied an increase in transmission rate to the England scenario after the March 30, 2021, circuit breaker measures were implemented in British Columbia, considering that those NPIs likely led to a reduction in cases in British Columbia but similar measures were not in place in England (Appendix Figure 1).

Vaccination Coverage and Majority Vaccine Product Administered

Data on age-dependent vaccination coverage extracted from the UK Government COVID-19 dashboard (*15*) (for England) and the Provincial Immunization

Registry (for British Columbia) included vaccination coverage by number of doses (1 or 2) and by age group (12–17 years, 18–24 years, 10-year bands for 25–74 years, and ≥75 years) (Appendix Figure 2, panel A). We derived parameters for estimated vaccine efficacy on the Delta variant by product and dose on the basis of previous values (Appendix Table 5) (*12*). To account for differences in vaccination scheduling, we collected data on proportion of vaccine coverage by first and second dose by age group from both jurisdictions and weighted them for British Columbia's population.

We fitted the model using a variational Bayes approach (*17*,*19*) to reported case data for British Columbia during March 1, 2020–July 12, 2021, with 4 transmission segments covering the study period, starting on January 25, March 29, April 5, and May 25, 2021 (Appendix Table 4). This work was conducted under the public health surveillance mandate of the BCCDC, and institutional review board approval was not sought. The planning, conduct, and reporting of this study was in line with the Declaration of Helsinki, as revised in 2013.

Results

Delta VOC Emergence

A total of 66,247 COVID-19 cases were reported in British Columbia during March 1–June 30, 2021; of those, 1,178 (1.8%) were Delta, 37,872 (57.2%) were other VOCs (Alpha, Beta, or Gamma), 6,930 (10.4%) were non-VOC, and 20,267 (30.6%) were of unknown lineage. During the study period, Alpha and Gamma were the most prevalent variants in British Columbia, codominating from April (epiweek 13) onwards; Alpha reached 46.1% of weekly incident cases (51.6% of cases with known lineage) during May 2–15 (epiweeks 18 and 19), and Gamma reached 40.0% of incident cases (48.8% of cases with known lineage) by the end of June 2021 (epiweek 26) (Figure 1). The prevalence of Beta was negligible, accounting for <20 incident cases (≤0.3%) per week.

The Delta VOC was first detected in British Columbia during epiweek 12; the earliest detected case had a specimen collection date of March 21, 2021. Delta case-patients were generally young (65.7% <40 years of age), and a slightly higher percentage were male than female (Table 1). Most Delta variant cases were in unvaccinated persons (83.2%), and most (86.4%) were identified as Pangolin (*20*) lineage B.1.617.2. The prevalence of the Delta variant reached its highest point at the end of the study period; during the last full epiweek (epiweek 25), 44 Delta cases occurred, which represented 10.1% of incident cases (12.9% of cases with known lineage) (Figure 1).

Overall, 14.2% (n = 167) of Delta case-patients had known history of travel outside BC; 91.6% (n = 153)

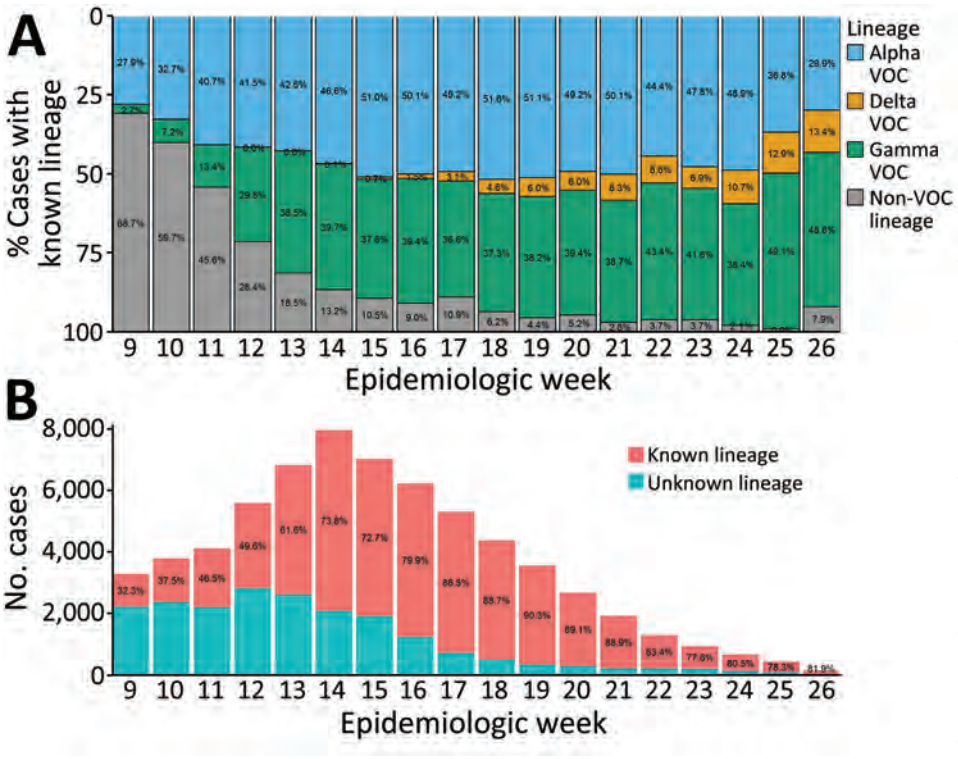

Figure 1. Percentage of COVID-19 cases by SARS-CoV-2 VOC lineage (A) and by known versus unknown lineage (B) reported in British Columbia, Canada, by epidemiologic week of specimen collection, March 1–June 30, 2021 (n = 66,247). Data are incomplete for epiweeks 9 and 26 because of study period date cutoffs. Beta VOC cases are not displayed in the top panel but are accounted for in the rounded percentages; Beta VOC cases did not account for >20 cases (<1% of cases with known lineage) per week in BC during the study period. COVID-19 cases of unknown lineage included cases with samples that did not undergo targeted VOC single-nucleotide variant (SNV) quantitative PCR (qPCR) screening or whole-genome sequencing (WGS), were negative or indeterminate on VOC SNV qPCR screening and did not undergo WGS, or did not undergo VOC SNV qPCR screening and failed WGS. VOC, variant of concern.

had traveled internationally and 8.4% (n = 14) had traveled only within Canada. On the evening of April 22, 2021, a ban on all direct commercial and private passenger flights from India and Pakistan was implemented throughout Canada (*21*,*22*). Most (82.4%; n = 126) international travel–related introductions of the Delta variant occurred before May 3, 2021 (accounting for day 10 postarrival qPCR testing for persons arriving in Canada before April 23) (Figure 2). At least half (50.8%; n = 64) of international travel–related Delta cases with specimen collection date before May 3, 2021, were in persons arriving from India, whereas 2 (7.4%) of 27 international travel–related Delta cases with specimens collected on or after May 3, 2021, were in persons who were known to have traveled from India (Table 2).

Counterfactual Modeling

Vaccine scheduling and coverage (i.e., timing of vaccination campaign rollout and percentage of population vaccinated) equivalent to that in England resulted in a lower counterfactual COVID-19 case rate in British Columbia than was observed across the study period, irrespective of vaccine product, NPIs, or proportional growth of the Delta variant (Figure 3; Appendix Figure 2). Modeled COVID-19 cases lowered further under the counterfactual scenario in which England's vaccine scheduling/coverage was combined with the British Columbia majority vaccine product. Within all NPI and proportion-of-Delta scenarios examined, modeled cases were lowest under England's vaccination scheduling/coverage combined with British Columbia's majority vaccination product (BNT162b2/mRNA-1273) and highest under British Columbia's vaccination coverage with England's majority vaccination product (ChAdOx1) (Figure 3).

Modeling indicates that, without the additional NPIs implemented at the end of March 2021 in British Columbia (Figure 3, panels A, C), a substantially higher COVID-19 caseload would have occurred in British Columbia under the province's vaccination schedule and coverage, especially if the proportional increase in Delta cases that occurred in England had occurred in British Columbia (Figure 3, panel A). Under England's vaccine scheduling and coverage, modeled British Columbia cases were still higher than those reported from June 2021 onward without British Columbia's additional NPIs if England's proportional increase of Delta had occurred (Figure 3, panel A). In the counterfactual scenario in which England's proportional increase of Delta occurred in the context of British Columbia's NPIs and vaccine coverage (Figure 3, panel B), modeled COVID-19 case rates were only slightly higher than reported and much lower than without British Columbia's NPIs (i.e., compared with Figure 3, panel A). Modeled COVID-19 case rates were lowest under British Columbia's NPI scenario and proportional increase of Delta across all vaccination scenarios (Figure 3, panel D).

Table 1. Pangolin lineage and patient demographics, vaccination status, and travel history for 1,178 SARS-CoV-2 Delta variant of concern cases reported in British Columbia, Canada, March 1–June 30, 2021

Characteristic	No. (%) Delta cases
Pangolin lineage*	
B.1.617.2	1,018 (86.4)
AY.18	44 (3.7)
AY.15	30 (2.5)
AY.10	22 (1.9)
AY.93	20 (1.7)
Other AY lineages	44 (3.7)
Patient demographics	
Age group, y	
<20	261 (22.2)
20–39	513 (43.5)
40–59	248 (21.1)
60–79	118 (10.0)
≥80	38 (3.2)
Sex	
F	553 (46.9)
M	622 (52.8)
Unknown	3 (0.3)
Vaccination status†	
Fully vaccinated	30 (2.5)
Partially vaccinated	168 (14.3)
Unvaccinated	980 (83.2)
Travel history	
International travel	153 (13.0)
Domestic travel outside BC	14 (1.2)
No known travel or only within BC	1011 (85.8)

*Pangolin version 4.0.5, Usher version 1.6, Pango version 1.6 (*20*). BC, British Columbia.
†Unadjusted proportions; vaccination status shown was at time of symptom onset or specimen collection. Patients were considered fully vaccinated if symptom onset (or positive specimen collection date if onset not available) occurred ≥14 d after second dose of BNT162b2 (Pfizer, https://www.pfizer.com), mRNA-1273 (Moderna, https://www.modernatx.com), or ChAdOx1 (AstraZeneca, https://www.astrazeneca.com). Patients were considered partially vaccinated if not fully vaccinated and onset/specimen collection date occurred ≥21 d after first dose. Persons without any recorded vaccine dose or with onset/specimen collection date <21 d after first dose were considered unvaccinated.

Discussion

The Delta VOC was first detected in British Columbia during March 21–27, 2021 (epiweek 12); the earliest cases were linked to international travel. Although the Delta variant had already been seeded in the community by the time the countrywide travel ban on direct flights to Canada from India was put in place (*21*), the ban appears to have reduced the number of travelers arriving from countries affected early by the Delta variant, thereby decreasing additional introductions (*23*). This targeted approach might have helped to slow early Delta variant growth in British

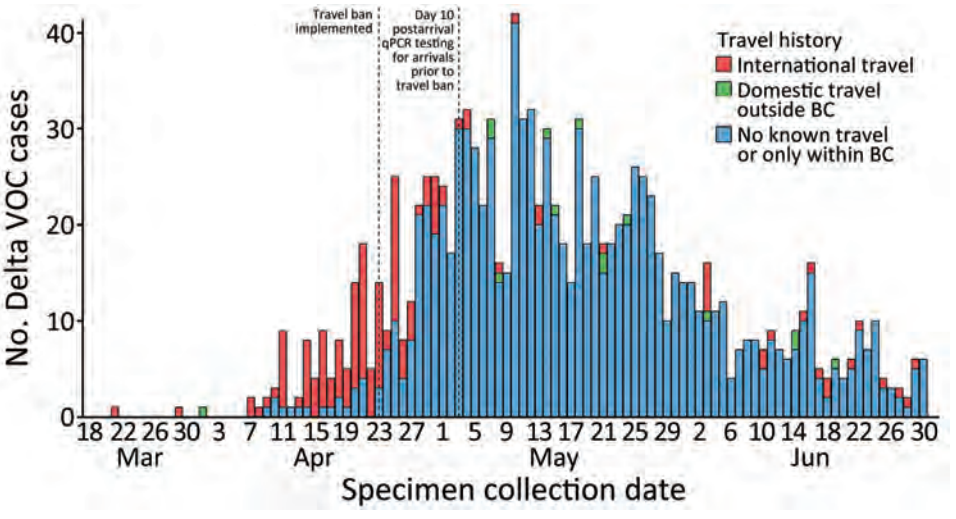

Figure 2. Epidemiologic curve of SARS-CoV-2 Delta VOC cases in British Columbia, Canada, by patient travel history, March 1–June 30, 2021 (n = 1,178). Delta VOC cases classified as having no known travel include 8 cases with missing travel information. Effective at 8:30 P.M. on April 22, 2021 (labeled as April 23 on figure), the government of Canada implemented a ban on all direct commercial and private passenger flights from India and Pakistan (*21*). The travel ban on direct flights from India remained in effect for the rest of the study period, whereas the ban on direct flights from Pakistan was in effect until June 21, 2021 (*21*,*22*). Travelers arriving before the federal travel ban were required to complete day 10 postarrival qPCR testing; as a result, travelers arriving before April 23 might have had specimens collected up to May 2, 2021. BC, British Columbia; qPCR, quantitative PCR; VOC, variant of concern.

Columbia, allowing time to increase population vaccination coverage (*23*).

Most Delta variant case-patients in our study were unvaccinated; 14% were partially vaccinated and 3% were fully vaccinated. Those proportions are reflective of the study period, during which the vaccination campaign in British Columbia was primarily focused on first dose rollout: population dose 1 coverage in British Columbia increased from 5% to 77% during the study period, but dose 2 coverage had only reached 28% by the end of the study. In British Columbia, vaccination rollout was primarily prioritized by age (*14*) and most Delta case-patients were young (<40 years). Studies have shown reduced vaccine effectiveness against symptomatic infection or high viral burden for Delta compared with Alpha (*24*,*25*), reiterating the importance of maximizing multidose coverage to improve conferred protection. On the basis of our counterfactual model, earlier population vaccine rollout akin to that done in England, which resulted in higher population dose 1 coverage (39%) by the start of the study period and 57% dose 2 coverage by the end (*15*), would likely have further decreased COVID-19 cases in British Columbia over the study period.

Our counterfactual modeling results suggest that the restrained early growth of COVID-19 cases in British Columbia after Delta was introduced was mainly because of decreased rates of contact from additional NPIs implemented 9 days after the first Delta case was detected, rather than from higher dose 1 vaccine coverage among younger persons or use of mRNA-based vaccines in British Columbia. Our findings are in line with those of McCrone et al. (*26*), who found that the key predictor for higher Delta growth rates between regions in England was increased levels of contact from population mobility and mixing because of the relaxation of NPIs. Results from a survey on behavioral and contact patterns in British Columbia (*27*) indicate that, whereas rates of contact during March–May 2021 either decreased or remained steady for all ages, contact rates increased in all age groups other than persons ≥65 years of age beginning in June 2021, coinciding with British Columbia's phased reopening (Appendix Figure 3).

Table 2. Information on country of origin for 153 SARS-CoV-2 Delta variant of concern cases reported in British Columbia, Canada, with known history of international travel in periods before and after travel ban and overall, March 1–June 30, 2021

	No. (%) Delta cases with international travel history		
Country of origin	Pre–travel ban period*	Post–travel ban period†	Overall
India	64 (50.8)	2 (7.4)	66 (43.1)
Other country	11 (8.7)	15 (55.6)	26 (17.0)
Missing information	51 (40.5)	10 (37.0)	61 (39.9)
Total for all Delta cases	126 (45.2)	27 (3.0)	153 (13.0)

*The Canadian travel ban on direct flights from India and Pakistan was implemented on the evening of April 22, 2021. Persons arriving in Canada before April 23, 2021, completed quantitative PCR testing 10 d after arrival. Therefore, pre–travel ban cases include Delta variant cases with specimen collection during March 21–May 2, 2021.
†Delta variant cases with specimen collection during May 3–June 30, 2021.

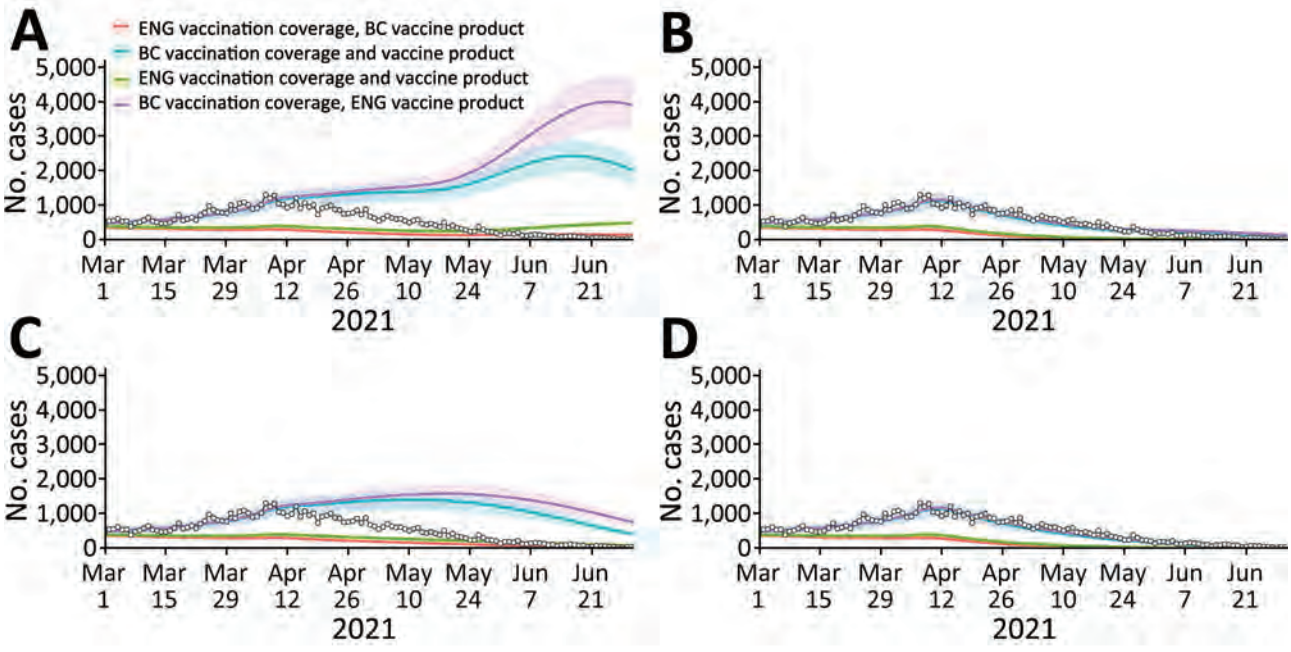

Figure 3. Retrospective counterfactual modeling of COVID-19 transmission in BC, Canada, March 1–June 30, 2021, compared with information from England. Model fitting for March 1, 2020, to July 12, 2021. A) England public health measures and proportion of Delta; B) BC public health measures and England proportion of Delta; C) England public health measures and BC proportion of Delta; D) BC public health measures and proportion of Delta. Each panel represents transmission scenarios derived from 1,000 variational Bayes samples, where measures that affect transmission and the proportion of Delta are reflective of BC or England. Each median line and 90% projection interval shading within each panel represents the vaccination scenario (i.e., population vaccine coverage and majority vaccine product of BC or England). The reported COVID-19 cases for BC are overlaid on each figure as white circles. BC, British Columbia.

Numerous studies have found NPIs to be associated with reduced COVID-19 transmission and thereby reduced illness, deaths, and strain on healthcare systems (*23*,*28*). Indeed, after a new phase of reopening began in British Columbia on July 1, 2021, including lifting the mask mandate for public indoor spaces and permitting countrywide recreational travel (Appendix Table 6) (*29*), British Columbia experienced a sharp rise in COVID-19 cases (Appendix Figure 4). In the weeks after July 1, 2021 (epiweek 26), a fourth wave of COVID-19 cases occurred in British Columbia, even though population vaccination coverage continued to increase. That wave was driven by the Delta variant, which rapidly grew to dominance, increasing to >70% of weekly incident COVID-19 cases by epiweek 29 (3 weeks later) and >85% by epiweek 30.

The Delta variant was first introduced at a time when British Columbia was experiencing a rise in Alpha and Gamma VOC cases, which required additional NPIs. Dominance of the Delta variant over previous VOCs has been widely reported (*3*,*7*,*8*), but the codominating Alpha and Gamma VOCs in circulation at the time of Delta introduction might have also helped to slow Delta's initial growth in British Columbia (*30*,*31*), which warrants further exploration. A limitation of this study is that the transmission model used is not multistrain but rather incorporates the increased transmissibility of a variant through modifying the time-varying per-contact transmissibility term to account for increasing prevalence of a more transmissible variant. As such, the time to dominance of a variant is fixed a priori and is not changed by model dynamics; the effect of precirculating strains cannot be fully assessed. The counterfactual model was instead intended to elucidate the effects of the change in the proportion of Delta on the number of reported COVID-19 cases.

Our counterfactual model used a simple modification of the rate of transmission to compare NPIs between British Columbia and England; other differences between the 2 jurisdictions that might have an effect on intercountry comparisons (e.g., demographics and contact patterns) were not considered. Rate of contact and probability of transmission per contact are highly dependent on population density and demographics, social factors, and geographic variation, which were not explicitly captured within these scenarios but were instead fitted to British Columbia reported case data

for the 2 transmission scenarios. Hence, the counterfactual model used does not allow for direct comparison of NPI strategies between jurisdictions. Comparison of COVID-19 cases and VOC growth between jurisdictions is further affected by differences in PCR testing rates, as well as VOC detection methods and approach. In this study, we assumed that testing rates were consistent over the study period in each jurisdiction; testing rates in British Columbia (*14*) and England (*32*) did not vary dramatically over this time, indicating relatively consistent case-finding.

In conclusion, spread from returning travelers resulted in community transmission of the emergent Delta VOC in British Columbia beginning in mid-to-late March 2021. However, growth of COVID-19 cases in the initial 3 months after Delta was detected was likely restrained because additional NPIs were implemented soon after variant introduction, including restricting interregional travel and expanding mandatory masking in schools to younger age groups. Our findings highlight the capacity of NPIs to reduce the spread of COVID-19, including highly transmissible variants such as Delta. Maximizing population-level COVID-19 vaccine coverage reduces rates of illness and death and is essential for return to prepandemic ways of life. However, NPIs remain vital for preventing COVID-19–associated burden, especially in the face of variants capable of vaccine escape. Future work should examine the effectiveness of different NPI strategies and the timing of implementing or relaxing NPIs in the context of vaccine coverage, variant-specific vaccine effectiveness, and public acceptance. Identifying the best balance of NPIs to achieve least restrictive means will minimize unintended social, economic, and health-related harms.

Acknowledgments

We thank the Medical Health Officers, epidemiology and surveillance teams, and case and contact management teams from British Columbia's regional health authorities for their collaboration and tremendous work in COVID-19 case investigation, management, and reporting. We also thank Mei Chong for assisting with data linkage and Prince Adu for providing results from the BC Mix COVID-19 Survey.

About the Author

Ms. Chan is a field epidemiologist with the Public Health Agency of Canada, placed at the British Columbia Centre for Disease Control (Vancouver, BC). Her research interests include the epidemiology and control of communicable diseases.

References

1. World Health Organization. Tracking SARS-CoV-2 variants [cited 2022 Dec 10]. https://www.who.int/en/activities/tracking-SARS-CoV-2-variants
2. Campbell F, Archer B, Laurenson-Schafer H, Jinnai Y, Konings F, Batra N, et al. Increased transmissibility and global spread of SARS-CoV-2 variants of concern as at June 2021. Euro Surveill. 2021;26:2100509. https://doi.org/10.2807/1560-7917.ES.2021.26.24.2100509
3. Mlcochova P, Kemp SA, Dhar MS, Papa G, Meng B, Ferreira IATM, et al.; Indian SARS-CoV-2 Genomics Consortium (INSACOG); Genotype to Phenotype Japan (G2P-Japan) Consortium; CITIID-NIHR BioResource COVID-19 Collaboration. SARS-CoV-2 B.1.617.2 Delta variant replication and immune evasion. Nature. 2021;599:114–9. https://doi.org/10.1038/s41586-021-03944-y
4. Elbe S, Buckland-Merrett G. Data, disease and diplomacy: GISAID's innovative contribution to global health. Glob Chall. 2017;1:33–46. https://doi.org/10.1002/gch2.1018
5. GISAID. Tracking of hCoV-19 variants [cited 2022 Dec 10]. https://www.gisaid.org/hcov19-variants
6. BC Centre for Disease Control. Weekly update on variants of concern (VOC): Sep 17, 2021 [cited 2022 Dec 10]. http://www.bccdc.ca/Health-Info-Site/Documents/VoC/VoC_weekly_09172021.pdf
7. Public Health England. SARS-CoV-2 variants of concern and variants under investigation in England: Technical briefing 23 [cited 2021 Sep 19]. https://assets.publishing.service.gov.uk/government/uploads/system/uploads/attachment_data/file/1018547/Technical_Briefing_23_21_09_16.pdf
8. Sheikh A, McMenamin J, Taylor B, Robertson C; Public Health Scotland and the EAVE II Collaborators. SARS-CoV-2 Delta VOC in Scotland: demographics, risk of hospital admission, and vaccine effectiveness. Lancet. 2021;397:2461–2. https://doi.org/10.1016/S0140-6736(21)01358-1
9. Public Health Scotland. Tracking the Delta variant in Scotland [cited 2023 Jun 25]. https://publichealthscotland.scot/our-blog/2021/november/tracking-the-delta-variant-in-scotland
10. Earnest R, Uddin R, Matluk N, Renzette N, Turbett SE, Siddle KJ, et al.; New England Variant Investigation Team. Comparative transmissibility of SARS-CoV-2 variants Delta and Alpha in New England, USA. Cell Rep Med. 2022;3:100583. https://doi.org/10.1016/j.xcrm.2022.100583
11. Office of the Premier. Three-week circuit breaker begins now to bend the curve, protect people [cited 2022 Dec 10]. https://news.gov.bc.ca/releases/2021PREM0023-000578
12. Scientific Advisory Group for Emergencies. SPI-M-O: summary of further modelling of easing restrictions–roadmap step 4 on 19th July 2021, 7 July 2021 [cited 2021 Aug 6]. https://www.gov.uk/government/publications/spi-m-o-summary-of-further-modelling-of-easing-restrictions-roadmap-step-4-on-19-july-2021-7-july-2021
13. UK Health Security Agency. Coronavirus (COVID-19) in the UK: cases in England [cited 2022 Feb 01]. https://coronavirus.data.gov.uk/details/cases?areaType=nation&areaName=England
14. BC Centre for Disease Control. British Columbia (BC) COVID-19 situation report: week 28: July 11–July 17, 2021 [cited 2022 Dec 10]. http://www.bccdc.ca/Health-Info-Site/Documents/COVID_sitrep/Week_28_2021_BC_COVID-19_Situation_Report.pdf
15. UK Health Security Agency. Coronavirus (COVID-19) in the UK: vaccinations in England [cited 2021 Aug 6]. https://coronavirus.data.gov.uk/details/vaccinations?areaType=nation&areaName=England

16. Department of Health & Social Care. Policy paper: UK COVID-19 vaccines delivery plan [cited 2022 May 15]. https://www.gov.uk/government/publications/uk-covid-19-vaccines-delivery-plan/uk-covid-19-vaccines-delivery-plan#supply-1
17. Anderson SC, Edwards AM, Yerlanov M, Mulberry N, Stockdale JE, Iyaniwura SA, et al. Quantifying the impact of COVID-19 control measures using a Bayesian model of physical distancing. PLOS Comput Biol. 2020;16:e1008274. https://doi.org/10.1371/journal.pcbi.1008274
18. Public Health England. SARS-CoV-2 variants of concern and variants under investigation in England: Technical briefing 19 [cited 2021 Aug 6]. https://assets.publishing.service.gov.uk/government/uploads/system/uploads/attachment_data/file/1005517/Technical_Briefing_19.pdf
19. Anderson SC, Edwards AM, Yerlanov M, Mulberry N, Stockdale JE, Falcao RC, et al. Bayesian SEIR modelling for multivariate COVID-19 case data [cited 2022 Dec 10]. https://seananderson.github.io/covidseir/index.html
20. O'Toole Á, Scher E, Underwood A, Jackson B, Hill V, McCrone JT, et al. Assignment of epidemiological lineages in an emerging pandemic using the pangolin tool. Virus Evol. 2021 Jul 30;7(2):veab064. https://doi.org/10.1093/ve/veab064 PMID 34527285
21. Transport Canada. Government of Canada suspends flights from India and Pakistan [cited 2022 Dec 10]. https://www.canada.ca/en/transport-canada/news/2021/04/government-of-canada-suspends-flights-from-india-and-pakistan.html
22. Public Health Agency of Canada. Government of Canada's first phase to easing border measures for travellers entering Canada [cited 2022 Dec 10]. https://www.canada.ca/en/public-health/news/2021/06/government-of-canadas-first-phase-to-easing-border-measures-for-travellers-entering-canada3.html
23. Wells CR, Sah P, Moghadas SM, Pandey A, Shoukat A, Wang Y, et al. Impact of international travel and border control measures on the global spread of the novel 2019 coronavirus outbreak. Proc Natl Acad Sci U S A. 2020;117:7504–9. https://doi.org/10.1073/pnas.2002616117
24. Lopez Bernal J, Andrews N, Gower C, Gallagher E, Simmons R, Thelwall S, et al. Effectiveness of Covid-19 Vaccines against the B.1.617.2 (Delta) Variant. N Engl J Med. 2021;385:585–94. https://doi.org/10.1056/NEJMoa2108891
25. Pouwels KB, Pritchard E, Matthews PC, Stoesser N, Eyre DW, Vihta KD, et al. Effect of Delta variant on viral burden and vaccine effectiveness against new SARS-CoV-2 infections in the UK. Nat Med. 2021;27:2127–35. https://doi.org/10.1038/s41591-021-01548-7
26. McCrone JT, Hill V, Bajaj S, Pena RE, Lambert BC, Inward R, et al.; COVID-19 Genomics UK (COG-UK) Consortium. Context-specific emergence and growth of the SARS-CoV-2 Delta variant. Nature. 2022;610:154–60. https://doi.org/10.1038/s41586-022-05200-3
27. Adu P, Binka M, Mahmood B, Jeong D, Buller-Tylor T, Jean Damascene M, et al. Quantifying contact patterns: development and characteristics of the British Columbia COVID-19 population mixing patterns survey. Int J Infect Dis. 2022;116:S30–1. https://doi.org/10.1016/j.ijid.2021.12.073
28. Scott N, Saul A, Spelman T, Stoove M, Pedrana A, Saeri A, et al. The introduction of a mandatory mask policy was associated with significantly reduced COVID-19 cases in a major metropolitan city. PLoS One. 2021;16:e0253510. https://doi.org/10.1371/journal.pone.0253510
29. Office of the Premier. B.C. shifts to Step 3 of restart plan [cited 2022 Dec 10]. https://news.gov.bc.ca/releases/2021PREM0043-001268
30. Lemey P, Ruktanonchai N, Hong SL, Colizza V, Poletto C, Van den Broeck F, et al. Untangling introductions and persistence in COVID-19 resurgence in Europe. Nature. 2021;595:713–7. https://doi.org/10.1038/s41586-021-03754-2
31. Russell A, O'Connor C, Lasek-Nesselquist E, Plitnick J, Kelly JP, Lamson DM, et al. Spatiotemporal analyses of 2 co-circulating SARS-CoV-2 variants, New York state, USA. Emerg Infect Dis. 2022;28:650–9. https://doi.org/10.3201/eid2803.211972
32. UK Health Security Agency. Coronavirus (COVID-19) in the UK: testing in England [cited 2022 Jul 15]. https://coronavirus.data.gov.uk/details/testing?areaType=nation&areaName=England

Address for correspondence: Y.L. Elaine Chan, British Columbia Centre for Disease Control, 655 W 12th Ave, Vancouver, BC V5Z 4R4, Canada; email: elaine.chan@bccdc.ca

Community Outbreak of *Pseudomonas aeruginosa* Infections Associated with Contaminated Piercing Aftercare Solution, Australia, 2021

Benjamin T. Trevitt, Anthea L. Katelaris, Catherine Bateman-Steel, Sandra Chaverot, Sinead Flanigan, Toni Cains, Elena Martinez, Andrew Ginn, Vitali Sintchenko, Arthur Jones, Kishen Lachireddy, Mark J. Ferson, Vicky Sheppeard

In April 2021, the South Eastern Sydney Local Health District Public Health Unit (Sydney, New South Wales, Australia) was notified of 3 patients with *Pseudomonas aeruginosa* infections secondary to skin piercings performed at the same salon. Active case finding through laboratories, clinician alerts, and monitoring hospital visits for piercing-related infections identified additional cases across New South Wales, and consumers were alerted. We identified 13 confirmed and 40 probable case-patients and linked clinical isolates by genomic sequencing. Ten confirmed case-patients had used the same brand and batch of aftercare solution. We isolated *P. aeruginosa* from opened and unopened bottles of this solution batch that matched the outbreak strain identified by genomic sequencing. Piercing-related infections returned to baseline levels after this solution batch was recalled. Early outbreak detection and source attribution via genomic sequencing are crucial for controlling outbreaks linked to contaminated products. Manufacturing standards for nonsterile cosmetic products and guidance for piercing aftercare warrant review.

Sporadic bacterial infections are a relatively common occurrence after nonmedical body piercing procedures, such as ear piercing (*1*). Localized infections occur at 10%–30% of new piercing sites (*1*), most commonly caused by *Staphylococcus aureus*, *Streptococcus pyogenes*, or *Pseudomonas aeruginosa* (*2*). Complications of piercing-related infections can range from minor superficial skin infections to abscess formation and necrosis requiring surgical intervention (*2*). Severe infections tend to occur in more avascular areas, such as auricular cartilage (*2*).

P. aeruginosa is a gram-negative bacterium commonly found in natural and built wet environments (*3*) and is a well-established cause of sporadic piercing-related infections. Infections tend to occur (on average) 2–4 weeks after piercing procedures (*4*) and have historically been attributed to exposure of piercing sites to swimming pools and fresh water, lack of adequate preoperative/intraoperative antisepsis of piercing sites, poor hand hygiene, and using contaminated solutions during or after piercing procedures (*3*,*5*–*8*). However, limited reports exist on *P. aeruginosa* infection outbreaks related to piercing (*3*,*9*)

In late April 2021, the South Eastern Sydney Local Health District Public Health Unit in Sydney, New South Wales (NSW), Australia, was notified by an ear, nose, and throat clinician that 3 patients had sought treatment for *P. aeruginosa* infections at 2 local hospital emergency departments after ear piercings. All piercings took place on April 1, 2021, at a newly opened skin penetration facility located in

Author affiliations: South Eastern Sydney Public Health Unit, Sydney, New South Wales, Australia (B.T. Trevitt, A.L. Katelaris, C. Bateman-Steel, S. Chaverot, S. Flanigan, T. Cains, M.J. Ferson, V. Sheppeard); University of Sydney, Sydney (B.T. Trevitt, E. Martinez, A. Ginn, V. Sintchenko, V. Sheppeard); Institute for Clinical Pathology and Medical Research New South Wales Health Pathology, Sydney (E. Martinez, A. Ginn, V. Sintchenko); St George Hospital, Sydney (A. Jones); Health Protection NSW, Sydney (K. Lachireddy); University of New South Wales, Sydney (M.J. Ferson)

DOI: https://doi.org/10.3201/eid2910.230560

southeastern Sydney. The identical pathogen, piercing date, and salon used by those 3 clients prompted an investigation into a potential common source. Environmental health officers initially inspected the implicated facility but did not find any store-specific practices or deficiencies that might have increased risk for piercing-related infections. We describe the methodology and outcome of this *P. aeruginosa* infection investigation, control measures implemented, and lessons learned.

Methods

Initial Case Definitions

We initially used broad case definitions to increase the sensitivity of active case finding. We defined a confirmed case-patient as a person who had a *P. aeruginosa* infection after a recent ear piercing and a probable case-patient as a person who had no cultures taken or no culture growth but had attended the implicated facility or other facilities of the same franchise or had used the same brand of aftercare solution.

Emergency Department Syndromic Surveillance

The NSW Public Health Rapid Emergency, Disease, and Syndromic Surveillance (PHREDSS) system monitors treatment sought at most public hospital emergency departments in the state in near-real time (*10*). Patients are coded according to their illness and discharge destination (e.g., admitted or discharged home) (*10*). We identified possible infection cases at hospitals via PHREDSS by using keyword searches of triage text: (infect*|cellulitis*) and (earring*|earing*|pierc*|peirc*).

Initial Investigations

We obtained details of procedures performed on confirmed case-patients, aftercare solutions used, notifications and complaints, and client lists from the initially implicated piercing salon. We identified additional cases of piercing-related infections in residents of greater Sydney, Wollongong, and Newcastle by examining the PHREDSS database.

Statewide Investigations and Case Finding

Beginning on April 30, 2021, weekly PHREDSS line lists of emergency department visits and admissions for piercing-related infections were provided to other public health units (PHUs) across NSW. We asked PHUs to review the medical records of patients on the PHREDSS list who were within their local health district and to contact patients who had positive *P. aeruginosa* cultures from clinical swab samples; PHUs gathered demographic and hospitalization data, determined when and where the patients had their piercing performed, and what aftercare solution (brand and batch) they had used. We also asked PHUs to obtain any available bottles of aftercare solution(s) used by the patient for laboratory testing. We alerted other states about the outbreak in NSW and asked them to report any confirmed or probable cases.

Microbiological Investigations and Whole-Genome Sequencing

Environmental health officers collected environmental samples and samples of aftercare solutions from the initial piercing salon for culture. We submitted specimens from case-patients and from opened and unopened bottles of aftercare solution to the Institute of Clinical Pathology and Medical Research–NSW Health Pathology for culturing and bacteria identification; positive culture isolates underwent whole-genome sequencing (WGS) by using the Illumina NextSeq platform (Illumina Corp., https://www.illumina.com), and their core genome multilocus sequence types (STs) were determined (*11*,*12*).

Ethics

This study was conducted as a public health investigation under the NSW Public Health Act 2010. Therefore, ethics approval was not required.

Results

The initial implicated facility was part of a nationwide franchise of piercing salons (franchise A), and this particular salon had opened on April 1, 2021, offering half-price piercings. The salon chain used Protat aftercare solution (Protat Tattoo Supplies, https://www.protatsupplies.com.au) from a single supplier. Unlike some aftercare solutions, Protat consists of natural preservatives, such as aloe vera, grapefruit seed extract, and *Melaleuca alternifolia* leaf oil, as well as saline containing benzalkonium chloride, which acts as an antimicrobial agent (*13*). The franchise's usual practice was to apply Protat immediately after piercing from a bottle that was then offered to the client to take home (the same bottle was not used for >1 client).

Descriptive Epidemiology

PHREDSS time series data showed an increase in emergency department visits for piercing infections in NSW beginning in April 2021 (Figure 1). Using the PHREDSS line lists, we identified 251 persons with a piercing-related infection via active case finding; 62 of those had *P. aeruginosa*–positive cultures.

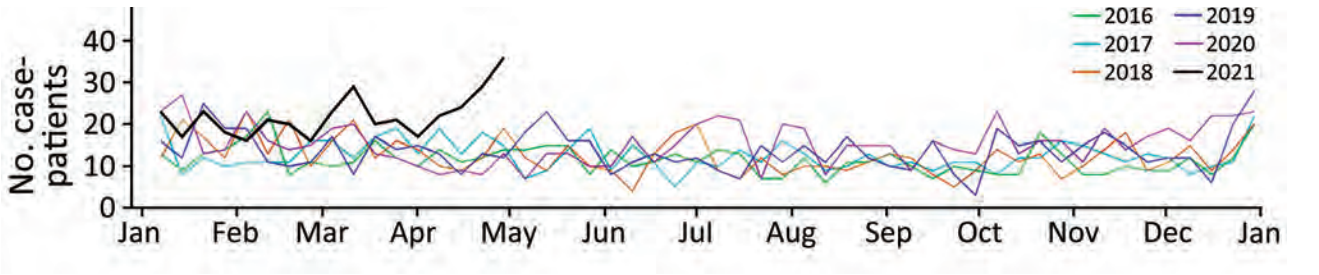

Figure 1. Weekly emergency department visits across New South Wales, Australia, by patients with piercing-site infections during 2016–2021 compiled for study of community outbreak of *Pseudomonas aeruginosa* infections associated with contaminated piercing aftercare solution. Data on emergency department visits and admissions for piercing-related infections were obtained from the New South Wales, Australia, Public Health Rapid Emergency, Disease, and Syndromic Surveillance system.

We sent samples from 15 previously opened bottles of Protat aftercare solution retrieved from case-patients for microbiological testing. Samples from 10 Protat bottles with the implicated batch number were tested; 9 were positive for *P. aeruginosa*, and 1 had no bacterial growth. The implicated batch had a use by date of October 1, 2023, and had been supplied to tattooing and piercing establishments during February 16–May 11, 2021 (*14*). Samples from 5 additional Protat bottles with different batch numbers were also tested and had no bacterial growth (Table 1).

We retrieved 11 unopened bottles of Protat aftercare solution from various chain stores in Sydney and Wollongong on May 14, 2021 (9 with the implicated batch number and 2 with different batch numbers). Samples from 3 unopened bottles of the implicated batch were positive for *P. aeruginosa* (850–2,000 CFU/mL); the remaining bottles had no growth Table 1). We received additional samples from 48 unopened Protat aftercare bottles with the implicated batch number from South Australia; 10 of those bottles were cultured and had no bacterial growth.

WGS was performed for 28 bacteria isolates (16 isolates from clinical samples, 3 from unopened bottles of Protat aftercare solution, and 9 from opened bottles of Protat aftercare solution); 27 of those isolates were *P. aeruginosa* and belonged to ST988. ST988 is a rare type that has not been identified previously in local isolate collections. Analysis identified 0–9 single-nucleotide polymorphism differences between the 27 isolate genomes (sequences with <25 single-nucleotide differences were regarded as a genomically linked cluster). Cluster analysis showed that all 27 submitted ST988 isolates were genomically linked. The remaining *P. aeruginosa* isolate was from a clinical sample and belonged to ST247 (Figure 2).

In total, we identified 13 case-patients who had *P. aeruginosa*–positive clinical isolates belonging to ST988 (2 case-patients had clinical samples taken from 2 different sites). Of the 13 case-patients with ST988 *P. aeruginosa* infections, 10 had used the implicated batch and 1 had used 2 different batches of Protat aftercare solution; information was not available for 2 cases. The case-patient with ST247 *P. aeruginosa* infection had used a different aftercare solution batch.

We reinterviewed the case-patient who reported using 2 different batches of Protat aftercare solution to confirm batch numbers. That case-patient had purchased those bottles 6 and 12 months earlier after other piercings and confirmed that additional aftercare solutions had not been purchased at the time of the latest piercing. However, a product was used in-store on their ear during the piercing procedure, and the case-patient was likely exposed to the implicated batch at that time.

Table 1. *Pseudomonas aeruginosa* detection rates in opened and unopened product bottles in study of community outbreak of infections associated with contaminated piercing aftercare solution, Australia, 2021*

Source	No. bottles tested	No. (%) positive bottles
Opened bottles	15	9 (60)
Implicated batch	10	9 (90)
Other batch	5	0
Unopened bottles	11	3 (27)
Implicated batch	9	3 (33)
Other batch	2	0
Total	26	12 (46)

*No. (%) positive bottles indicates positive growth of *P. aeruginosa* after sampling and culture. Solution was manufactured by Protat Tattoo Supplies (https://www.protatsupplies.com.au).

Outbreak Case Characteristics

After receiving the WGS analyses, we refined case definitions to be more specific. We used the confirmed case definition to determine associations with the suspected product, whereas the other case definitions tracked case incidence over time and assisted with ongoing case finding. We defined a confirmed case as a person in Australia with a body piercing infection caused by *P. aeruginosa* who had a piercing

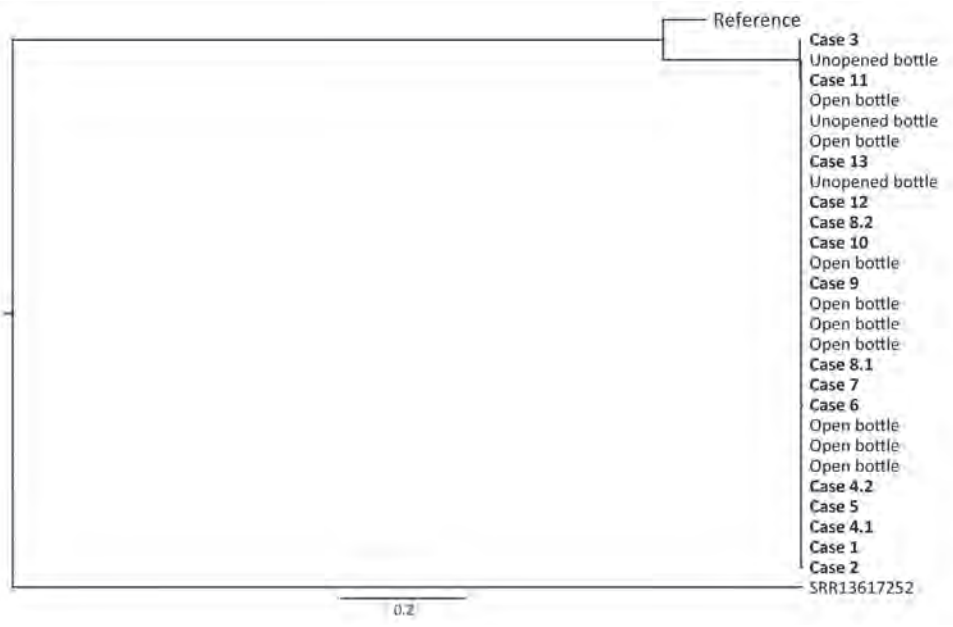

Figure 2. Phylogenetic analysis of *Pseudomonas aeruginosa* isolates collected in New South Wales in study of community outbreak of *P. aeruginosa* infections associated with contaminated piercing aftercare solution, Australia, 2021. Whole-genome sequencing was performed, and single-nucleotide polymorphisms were identified for 27 *P. aeruginosa* isolates from clinical specimens and opened or unopened bottles of Protat aftercare solution (Protat Tattoo Supplies, https://www.protatsupplies.com.au). Cluster analysis showed that all 27 sequences were genomically linked and belonged to sequence type 988. Reference indicates a representative sequence type 988 obtained from GenBank that was included in the analysis for comparison. The branch marked SRR13617252 indicates the *P. aeruginosa* mapping reference genome from the National Center for Biotechnology Information Sequence Read Archive database (https://www.ncbi.nlm.nih.gov/sra). Scale bar indicates nucleotide substitutions per site.

date after February 1, 2021, and ST988 detected in a clinical isolate. We defined a probable case either if a person in Australia had a body piercing infection caused by *P. aeruginosa* who had a piercing date after February 1, 2021, at a franchise A store but sequencing and typing data for a clinical isolate were not available; or the person had used Protat aftercare solution; or *P. aeruginosa* ST988 had been isolated from their aftercare product (regardless of store attended or product used). We defined a possible case as a person in Australia with a body piercing infection caused by *P. aeruginosa* who had a piercing date after February 1, 2021, but the piercing store was not a franchise A store and the aftercare product used was not Protat; a possible case was also defined as a person in Australia with a body piercing infection from which culture specimens were not collected or results were not available or had no bacterial growth, and the piercing was done at a franchise A store or the person used Protat aftercare solution. We defined a suspected case as a person in Australia with a body piercing infection caused by *P. aeruginosa* who had a piercing date after February 1, 2021, but the piercing location or aftercare product used was not known; a suspected case was also defined as a person in Australia with a body piercing infection and piercing date after February 1, 2021, but culture specimens were not collected or had no bacterial growth and the piercing site or use of aftercare solution was either not yet known, the store was not a franchise A store, or Protat aftercare solution was not used.

Of the 251 case-patients with piercing-related infections, 13 were confirmed, 40 were probable, 9 were possible, and 189 were suspected cases. Confirmed and probable cases predominantly comprised female patients (48/53, 91%) with a median age of 19.6 (range 15.5–59.6) years; 80% of those resided in metropolitan Sydney, Wollongong, or Newcastle. The median number of days between the piercing date and emergency department visit was 15 (range 3–35) days.

A higher percentage of confirmed and probable case-patients (30/53, 57%) required hospital admission compared with possible and suspected cases (9/198, 5%). In addition, confirmed and probable case-patients were more likely to have had piercings in cartilaginous areas, such as the tragus or helix, than possible and suspected cases and were much less likely to have been pierced in the earlobe or other noncartilaginous areas. We observed only minor differences in age, gender, and time (from piercing procedure to emergency department visit) between the confirmed/probable and possible/suspected groups. (Table 2)

All 13 confirmed case-patients attended either the initial implicated piercing facility or another franchise A facility and used Protat aftercare solution (Table 3). Of those, 10 case-patients were able to state specifically that they used the implicated batch of

Table 2. Differences in demographics, hospital admission status, and piercing characteristics according to case classification in study of community outbreak of *Pseudomonas aeruginosa* infections associated with contaminated piercing aftercare solution, Australia, 2021*

Characteristics	Confirmed or probable cases	Possible or suspected cases	Total no. (%) cases
Patient age, y, mean ±SD	23.6 ± 10.2	21.9 ±13.5	22.3 ±12.8
Patient sex			
F	48 (90.6)	175 (88.4)	223 (88.8)
M	5 (9.4)	23 (11.6)	28 (11.2)
Piercing site			
Ear, tragus/antitragus	2 (3.8)	5 (2.5)	7 (2.8)
Ear, helix/antihelix	18 (34.0)	26 (13.1)	44 (17.5)
Ear, lobule	4 (7.6)	51 (25.8)	55 (21.9)
Ear, not specified	28 (52.8)	79 (39.9)	107 (42.6)
Other†	1 (1.9)	37 (18.7)	38 (15.1)
Hospital admission status			
Admitted	30 (56.6)	9 (4.6)	39 (15.5)
Discharged	23 (43.4)	189 (95.5)	212 (84.5)
No. days from piercing to hospital visit, mean ±SD‡	14.1 ±7.2	14.7 ±9.8	14.4 ±9.1

*Values are no. (%) except as indicated.
†Includes breast, lip, nostril, and tongue.
‡Number of days could only be retrieved for a subset of case-patients through patient interviews and hospital records (n = 32 for confirmed or probable cases, n = 75 for possible or suspected cases).

Protat aftercare solution; 1 stated that the Protat aftercare solution they had used came from a different batch, and 2 stated they had used Protat aftercare solution postpiercing but were unable to identify the batch number. The case-patient who claimed to have used a different batch of Protat aftercare solution was likely administered the implicated batch immediately after piercing in the store (Table 3).

Outbreak Control Measures

On May 4, after identifying several additional *P. aeruginosa* piercing-related infections in clients who had attended franchise A stores across multiple NSW local health districts, the implicated franchisee agreed to cease using and selling Protat aftercare solution pending further investigation. NSW Health issued a clinician alert on May 13 to advise of an increase in hospital admissions because of *P. aeruginosa* infections after piercing procedures and to encourage clinicians to consider *P. aeruginosa* in patients with infections at piercing sites.

After confirmation of the presence of *P. aeruginosa* in unopened bottles of Protat aftercare solution, the distributor/manufacturer issued a voluntary recall of the contaminated batch from market shelves on May 14 and issued a product recall media release on May 31. On June 1, the Australian Competition and Consumer Commission published a recall notice for the implicated batch (*14*), which had been supplied to franchise A stores in NSW, Queensland, Victoria, and South Australia, as well as other tattooing and piercing establishments in all states of Australia and New Zealand. The commission also liaised with overseas regulators about the safety recall in Australia (*14*).

On May 28, after performing their own independent review, the manufacturer informed NSW Health that production/processing pathway testing of the implicated batch had detected a positive total microbial count, and results were PCR positive for *P. aeruginosa*. Root cause analysis conducted by the manufacturer identified several potential opportunities for contamination during manufacturing: handling of raw materials used for the manufacture of the product might have been compromised; flushing of the previous product out of the filling system

Table 3. Aftercare type and batch for confirmed and probable cases in study of community outbreak of *Pseudomonas aeruginosa* infections associated with contaminated piercing aftercare solution, Australia, 2021*

Source	Confirmed cases	Probable cases†	Confirmed and probable cases†
Protat	13 (100)	34 (85)	47 (89)
Implicated batch	10	20	30
Other batch	1	1	2
Unknown batch	2	13	15
Other brand	0	2 (5)	2 (4)
Not contactable	0	4 (10)	4 (8)
Total	13 (100)	40 (100)	53 (100)

*Values are no. (%). Implicated solution was manufactured by Protat Tattoo Supplies (https://www.protatsupplies.com.au).
†Case definitions for probable cases include Protat aftercare use for franchise A piercings; this case definition was used to help monitor the burden of disease during this outbreak and monitor the involvement of batches other than the implicated batch.

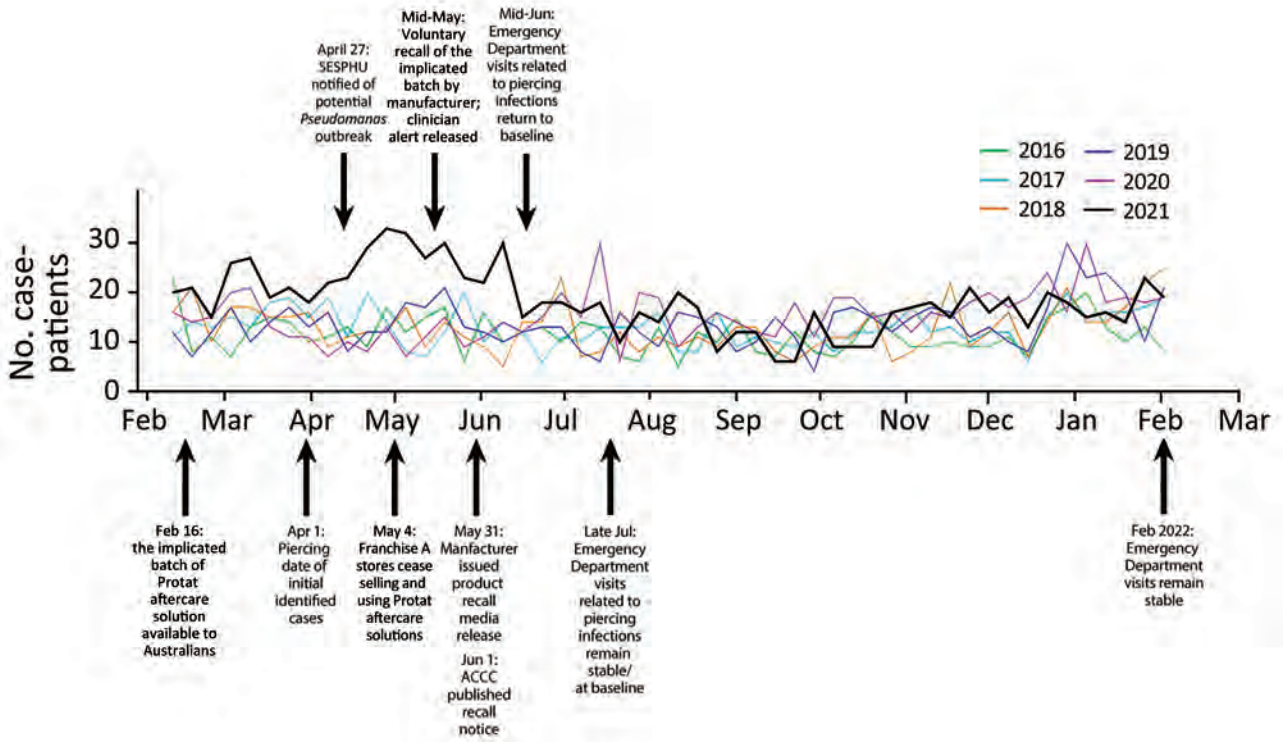

Figure 3. Timeline of key events during the community outbreak of *Pseudomonas aeruginosa* infections associated with contaminated piercing aftercare solution, Australia, 2021. Graph shows weekly numbers of *P. aeruginosa* infections in New South Wales during 2017–2022. Specific key events are shown for the 2021 outbreak of piercing-related *P. aeruginosa* infections. ACCC, Australian Competition and Consumer Commission; SESPHU, South Eastern Sydney Public Health Unit.

might not have been performed sufficiently; the spray ball in the mixing tank might have been contaminated; the mixing tank's lid might have been left open and unattended, potentially introducing contamination through water droplets; and the flow plate for tanks might have been contaminated when transfer connectors were switched between tanks. In addition, the prescribed microbial testing for this product was suspected to be insufficient.

In response to the contamination, the manufacturer began preservative challenge testing on the product formula; increased microbial testing for opportunistic pathogens, including *P. aeruginosa*, *S. aureus*, and *Candida* spp.; and performed antimicrobial disinfectant fogging of the manufacturing facilities. They also planned to take additional preventive actions to address the risk for future contamination, such as reassessing cleaning and hygiene procedures and maintenance and operation of equipment and parts; providing refresher training for all manufacturing and production operators, emphasizing vigilance and aseptic techniques; and potentially reformulating the product on the basis of challenge test results. The effect of the outbreak control measures was evident in the decline in emergency department visits beginning in late May 2021 and their return to baseline levels by mid-June 2021 (Figure 3).

Discussion

We found microbiological, environmental, and epidemiologic evidence linking a single batch of aftercare solution to a piercing-related *P. aeruginosa* infection outbreak across NSW during April–June 2021. The distinct whole-genome sequence type shared by 27 isolates from various sources, including clinical specimens and aftercare solution samples (both client-used and unopened bottles), established a single common source for this outbreak. Therefore, we successfully used WGS to establish a causative link between an aftercare product and a piercing-related *P. aeruginosa* infection outbreak.

Piercing-related *P. aeruginosa* infection outbreaks associated with aftercare solutions have been reported previously (*3*,*5*,*9*). In a 2016 outbreak in England, variable-number tandem-repeat (VNTR) typing was used to identify isolates from clinical samples collected from suspected case-patients and from environmental samples (opened and unopened bottles of aftercare solutions) to investigate possible links (*5*). The VNTR type for cases connected to that

2016 outbreak differed from cases unrelated to the outbreak and matched the VNTR type of isolates found in bottles of aftercare solution (*5*). In another outbreak in 2016 linked to a northwestern England piercing event, VNTR typing was also used to identify isolates from clinical samples of suspected case-patients, which matched isolates from water samples collected from the premises (*9*). Molecular subtyping was used to investigate an outbreak at an Oregon, USA, jewelry store in 2004 and successfully linked isolates from case-patients with *P. aeruginosa* piercing-related infections to isolates retrieved from a disinfectant bottle, as well as to isolates recovered from 2 workers and from wastewater located beneath sinks in the store (*3*).

Early recognition of the NSW outbreak and its subsequent effective management were partially attributed to the astuteness of the clinician who recognized and reported the cluster of *P. aeruginosa* piercing-related infections. Had this report not occurred, the outbreak might have gone unrecognized, and the cause might not have been identified as quickly, given that cases were dispersed geographically and the emergency department syndromic surveillance system was not routinely reviewed for this clinical syndrome. Furthermore, the successful investigation drew on the strengths of the NSW Public Health Network, which has conducted longstanding, real-time centralized surveillance of emergency departments, other health facilities, and public health units dispersed across the state. The network is well-placed to interact effectively with local patients and clinicians and also highlights effective coordination between clinical, public health, laboratory, and regulatory teams.

The first limitation of our study is that not all suspected case-patients had clinical isolates collected and not all probable cases had isolates retained for further characterization. Second, not all consumers had kept their bottles of aftercare solution or could recall the brand or batch number. Third, not all emergency departments in NSW are covered by PHREDDS; thus, some cases might have been missed. Nevertheless, sufficient evidence was available to issue timely clinician and consumer alerts and, eventually, a product recall, which prevented further infections.

Multiple outbreaks of *P. aeruginosa* infections from at least 2 continents have been caused by piercing aftercare products, suggesting that higher manufacturing standards might be required for such solutions. In Australia, although they are applied to recently penetrated skin, aftercare solutions are generally not regulated as therapeutic goods (*15*). Consumers expect aftercare solutions to be sterile, yet manufacturing processes reviewed in this investigation indicated that sterility could not be assured despite the manufacturer's intentions. Management of this outbreak has shown the importance of quality control and sterility assurance in manufacturing such solutions. Existing measures routinely and effectively imposed on regulated therapeutic goods to reduce contamination risk should also be applied to aftercare solutions, such as objectionable organism and microbial risk assessments and sterility testing and control (*16*–*19*). Early detection of pathogen clusters linked to contaminated products and source attribution via genomic sequencing are pivotal in controlling outbreaks, as is effective communication with stakeholders, including clients, health professionals, piercing franchises, and manufacturers.

Acknowledgments

We thank the Health Protection NSW staff, including Richard Broome, Shireen Durrani, Elaine Tennant, and Katherine Todd; NSW Health Public Health Rapid, Emergency, Disease and Syndromic Surveillance (PHREDSS) team; NSW Health Public Health Units; the store management; product distributor; and the product manufacturer for their cooperation.

About the Author

Dr. Trevitt is a public health medicine advanced trainee and is completing a master of biostatistics degree at the University of Sydney. He has interests in epidemiology, outbreak investigations, research, and managing drug and alcohol dependencies at a population level.

References

1. Patel M, Cobbs CG. Infections from body piercing and tattoos. Microbiol Spectr. 2015;3. https://doi.org/10.1128/microbiolspec.IOL5-0016-2015
2. Meltzer DI. Complications of body piercing. Am Fam Physician. 2005;72:2029–34.
3. Keene WE, Markum AC, Samadpour M. Outbreak of *Pseudomonas aeruginosa* infections caused by commercial piercing of upper ear cartilage. JAMA. 2004;291:981–5. https://doi.org/10.1001/jama.291.8.981
4. Manca DP, Levy M, Tariq K. Case report: infected ear cartilage piercing. Can Fam Physician. 2006;52:974–5.
5. Evans H, Bolt H, Heinsbroek E, Lloyd B, English P, Latif S, et al.; Outbreak Control Team. National outbreak of *Pseudomonas aeruginosa* associated with an aftercare solution following piercings, July to September 2016, England. Euro Surveill. 2018;23:1700795. https://doi.org/10.2807/1560-7917.ES.2018.23.37.1700795
6. Fisher CG, Kacica MA, Bennett NM. Risk factors for cartilage infections of the ear. Am J Prev Med. 2005;29:204–9. https://doi.org/10.1016/j.amepre.2005.06.003
7. More DR, Seidel JS, Bryan PA. Ear-piercing techniques

as a cause of auricular chondritis. Pediatr Emerg Care. 1999; 15:189–92. https://doi.org/10.1097/00006565-199906000-00007
8. Staley R, Fitzgibbon JJ, Anderson C. Auricular infections caused by high ear piercing in adolescents. Pediatrics. 1997;99:610–1. https://doi.org/10.1542/peds.99.4.610
9. MacPherson P, Valentine K, Chadderton V, Dardamissis E, Doig I, Fox A, et al. An outbreak of *Pseudomonas aeruginosa* infection linked to a "Black Friday" piercing event. PLoS Curr. 2017;9:ecurrents.outbreaks.51af24797f6f856a9861b5ddabc7db58. https://doi.org/10.1371/currents.outbreaks.51af24797f6f856a9861b5ddabc7db58
10. PHREDSS. 2017 [cited 2022 Jan 31]. https://www.health.nsw.gov.au/epidemiology/Pages/rapid-surveillance-using-PHREDSS.aspx
11. de Sales RO, Migliorini LB, Puga R, Kocsis B, Severino P. A core genome multilocus sequence typing scheme for *Pseudomonas aeruginosa.* Front Microbiol. 2020;11:1049. https://doi.org/10.3389/fmicb.2020.01049
12. Curran B, Jonas D, Grundmann H, Pitt T, Dowson CG. Development of a multilocus sequence typing scheme for the opportunistic pathogen *Pseudomonas aeruginosa.* J Clin Microbiol. 2004;42:5644–9. https://doi.org/10.1128/JCM.42.12.5644-5649.2004
13. Protat. Protat natural body piercing aftercare spray 50 mL safety data sheet. September 2022 [cited 2023 July 2]. https://protatsupplies.com.au/content/assets/Uploads/msds/Protat%20Natural%20Piercing%20Spray%2050ml.pdf
14. Australian Competition and Consumer Commission. Recalls. Protat Pty Ltd—Protat natural sea salt plus tea tree hygienic body piercing aftercare spray 50mL. July 2021 [cited 2022 Jan 31]. https://www.productsafety.gov.au/recalls/protat-pty-ltd-%E2%80%94-protat-natural-sea-salt-plus-tea-tree-hygienic-body-piercing-aftercare-spray-50ml
15. Australia Government Department of Health and Aged Care, Therapeutic Goods Administration. Australian Register of Therapeutic Goods (ARTG). 2023 [cited 2023 July 1]. https://www.tga.gov.au/resources/artg
16. Australian Government Department of Health and Aged Care, Therapeutic Goods Administration. Testing of therapeutic goods. December 2020 [cited 2023 July 2]. https://www.tga.gov.au/safety/product-testing-and-investigations/testing-therapeutic-goods
17. Sandle T. Pharmaceutical microbiology: essentials for quality assurance and quality control. Cambridge: Woodhead Publishing (Elsevier); 2016.
18. Stewart SE, Parker MD, Amézquita A, Pitt TL. Microbiological risk assessment for personal care products. Int J Cosmet Sci. 2016;38:634–45. https://doi.org/10.1111/ics.12338
19. Torbeck L, Raccasi D, Guilfoyle DE, Friedman RL, Hussong D. *Burkholderia cepacia*: this decision is overdue. PDA J Pharm Sci Technol. 2011;65:535–43. https://doi.org/10.5731/pdajpst.2011.00793

Address for correspondence: Benjamin Trevitt, South Eastern Sydney Public Health Unit, Locked Bag 88, Randwick, NSW 2031, Australia; email: benjamin.trevitt@health.nsw.gov.au

etymologia revisited

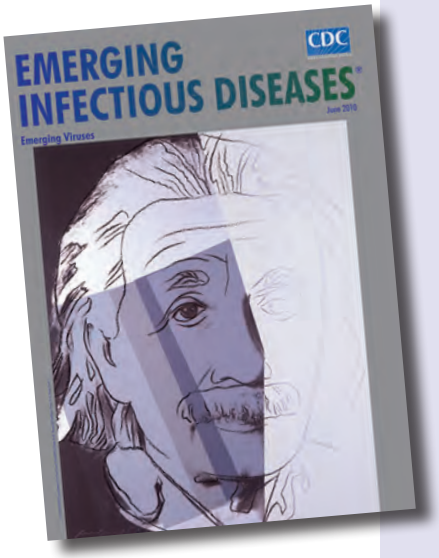

Originally published in June 2010

Lassa Virus

[lah sə] virus

This virus was named after the town of Lassa at the southern end of Lake Chad in northeastern Nigeria, where the first known patient, a nurse in a mission hospital, had lived and worked when she contracted this infection in 1969. The virus was discovered as part of a plan to identify unknown viruses from Africa by collecting serum specimens from patients with fevers of unknown origin. Lassa virus, transmitted by field rats, is endemic in West Africa, where it causes up to 300,000 infections and 5,000 deaths each year.

References:

1 Frame JD, Baldwin JM Jr, Gocke DJ, Troup JM. Lassa fever, a new virus disease of man from West Africa. I. Clinical description and pathological findings. Am J Trop Med Hyg. 1970;19:670–6
2. Mahy BW. The dictionary of virology, 4th ed. Burlington (MA): Elsevier; 2009.

https://wwwnc.cdc.gov/eid/article/16/6/et-1606_article

Characteristics of and Deaths among 333 Persons with Tuberculosis and COVID-19 in Cross-Sectional Sample from 25 Jurisdictions, United States

Scott A. Nabity, Suzanne M. Marks, Neela D. Goswami, Shona R. Smith, Evan Timme, Sandy F. Price, Lon Gross, Julie L. Self, Katelynne Gardner Toren, Masahiro Narita, Donna H. Wegener, Shu-Hua Wang, for the National Tuberculosis Controllers Association/CDC TB-COVID-19 Collaboration[1]

Little is known about co-occurring tuberculosis (TB) and COVID-19 in low TB incidence settings. We obtained a cross-section of 333 persons in the United States co-diagnosed with TB and COVID-19 within 180 days and compared them to 4,433 persons with TB only in 2020 and 18,898 persons with TB during 2017–2019. Across both comparison groups, a higher proportion of persons with TB–COVID-19 were Hispanic, were long-term care facility residents, and had diabetes. When adjusted for age, underlying conditions, and TB severity, COVID-19 co-infection was not statistically associated with death compared with TB infection only in 2020 (adjusted prevalence ratio 1.0 [95% CI 0.8–1.4]). Among TB–COVID-19 patients, death was associated with a shorter interval between TB and COVID-19 diagnoses, older age, and being immunocompromised (non-HIV). TB–COVID-19 deaths in the United States appear to be concentrated in subgroups sharing characteristics known to increase risk for death from either disease alone.

Tuberculosis (TB) and COVID-19 were leading infectious causes of illness and death globally in 2020. In the United States, >17 million COVID-19 cases and ≈7,000 TB cases were reported in 2020 (*1*). Both TB and COVID-19 are primarily respiratory illnesses with overlapping signs and symptoms, and the Centers for Disease Control and Prevention (CDC) lists TB as a medical risk factor for COVID-19–related disease severity and death (*2*). Few population-based reports of outcomes for persons with both TB and COVID-19 have been reported (*3*,*4*), and the definition of TB and COVID-19 co-diagnosis differs across studies. Those reports, and meta-analyses incorporating case reports and small observational series (*5*–*8*), have demonstrated higher mortality rates for persons with TB and COVID-19 compared with COVID-19 alone. Little has been published to adequately assess COVID-19 as a risk factor for poor TB outcomes. Furthermore, limited information is available from low TB incidence populations, including the United States. An analysis from California showed increased mortality rates for persons with TB and COVID-19 compared with TB only reported before the COVID-19 pandemic, particularly when TB and COVID-19 were diagnosed in close succession (*9*). That analysis indicated groups of persons who were disproportionately affected by both diseases, including Hispanic persons and those with diabetes or living in low health equity neighborhoods according to the California Healthy Places Index (*10*).

Author affiliations: California Department of Public Health, Richmond, California, USA (S.A. Nabity); Centers for Disease Control and Prevention, Atlanta, USA (S.A. Nabity, S.M. Marks, N.D. Goswami, S.F. Price, L. Gross, J.L. Self); Michigan Department of Health and Human Services, Lansing, Michigan, USA (S.R. Smith); Arizona Department of Health Services, Phoenix, Arizona, USA (E. Timme); Public Health–Seattle & King County, Seattle, Washington, USA (K. Gardner Toren, M. Narita); University of Washington, Seattle (M. Narita); National Tuberculosis Controllers Association, Atlanta (D.H. Wegener); The Ohio State University College of Medicine, Columbus, Ohio, USA (S.-H. Wang)

DOI: https://doi.org/10.3201/eid2910.230286

[1]Group members are listed at the end of this article.

The COVID-19 pandemic also affected TB epidemiology and program management across epidemiologic contexts (*11*). In the United States, reported TB incidence declined ≈20% in 2020 compared with 2019 (*12*). Limited information suggests that some persons with TB in the United States may have had more clinically severe disease in 2020 than before the COVID-19 pandemic (*13*), and TB diagnoses may have been delayed (*14*). We aimed to describe demographic, social, and clinical characteristics of persons with TB and COVID-19 in the United States, including risk for death, and to identify populations who may benefit most from integrated interventions.

Materials and Methods

Design and Population

We established a voluntary collaboration of US health jurisdictions to obtain a cross-sectional sample of persons with TB and COVID-19 diagnosed within 180 days (hereafter TB–COVID-19). We used the population-based National Tuberculosis Surveillance System (NTSS) for cases reported during 2017–2021 for standardized demographic, social, underlying conditions, and TB-specific diagnosis and treatment variables (*15*). Each jurisdiction captured a subset of the standardized data elements from the National Notifiable Disease Surveillance System for COVID-19 cases (*16*) and contributed them to this project. The core set of COVID-19 and TB surveillance data elements were consistent across jurisdictions. We included all persons with COVID-19 meeting the public health surveillance case definition for confirmed or probable COVID-19 (*17*) reported during January 1, 2020–June 30, 2021, who were also persons with TB reported in 2020 (i.e., persons with TB–COVID-19). Although the methods used by participating jurisdictions to identify persons with TB–COVID-19 varied (Appendix Table 1, https://wwwnc.cdc.gov/EID/article/29/10/23-0286-App1.pdf), each jurisdiction systematically identified their residents with co-diagnoses of TB and COVID-19 using personal identifiers. Of 26 participating jurisdictions, 11 (42.3%) used a software algorithm that included name and date of birth to match persons (several also included various combinations of sex, race/ethnicity, and place of residence), 8 (30.8%) had integrated surveillance systems (i.e., a given individual's TB and COVID-19 diagnoses were already linked to a single record), and 1 (3.8%) with an integrated surveillance system also performed a name-based software match (Appendix Table 1). Directly identifiable information in the surveillance registries was retained by participating jurisdictions and not shared with investigators in other jurisdictions or with CDC.

Each jurisdiction securely transmitted data on persons with TB–COVID-19 to CDC. We then excluded persons with TB–COVID-19 with unknown TB or COVID-19 diagnosis dates and for which diagnoses occurred >180 days apart, regardless of which disease was diagnosed first (Figure 1). For analysis of TB treatment outcomes, we excluded jurisdictions with incomplete TB case outcome data. To identify characteristics of persons with TB–COVID-19 that differed from persons with TB only, we compared them to characteristics of persons with TB reported in 2020 without COVID-19 (i.e., 2020 TB-only) and TB reported during the 3 most recent pre–COVID-19 years, 2017–2019 (i.e., 2017–2019 TB-only).

Data Elements

NTSS data included demographic, social, and clinical characteristics, and TB diagnosis and treatment outcomes. We used a composite all-cause death outcome that included TB diagnosed after death, death occurring before or during TB treatment, and death recorded on the COVID-19 case report form. We defined the TB diagnosis date as the earliest among positive smear or tissue collection, positive nucleic acid amplification test result, first culture specimen collected for phenotypic drug-sensitivity testing, or TB treatment start date. For the COVID-19 diagnosis date, we used the date of specimen collection of the first positive nucleic acid amplification test or antigen test. We defined persons with disseminated TB as having meningeal or miliary disease, both pulmonary and extrapulmonary disease, or having a positive culture for *Mycobacterium tuberculosis* complex from blood.

Analytic Methods

We compared characteristics of persons with TB–COVID-19 with those of persons with 2020 TB-only and 2017–2019 TB-only, calculating statistically significant differences of bivariate frequencies by using the Mantel-Haenszel χ^2 test (or Fisher exact test for small cell counts) with Bonferroni correction for multiple comparisons. We also calculated Clopper–Pearson binomial 95% CIs for some frequencies. For continuous variables, we assessed differences in parametric means by using t-tests. We used the Wilcoxon rank-sum test to compare nonparametric continuous variables. We calculated prevalence ratios (PRs) and 95% CIs by using log-binomial

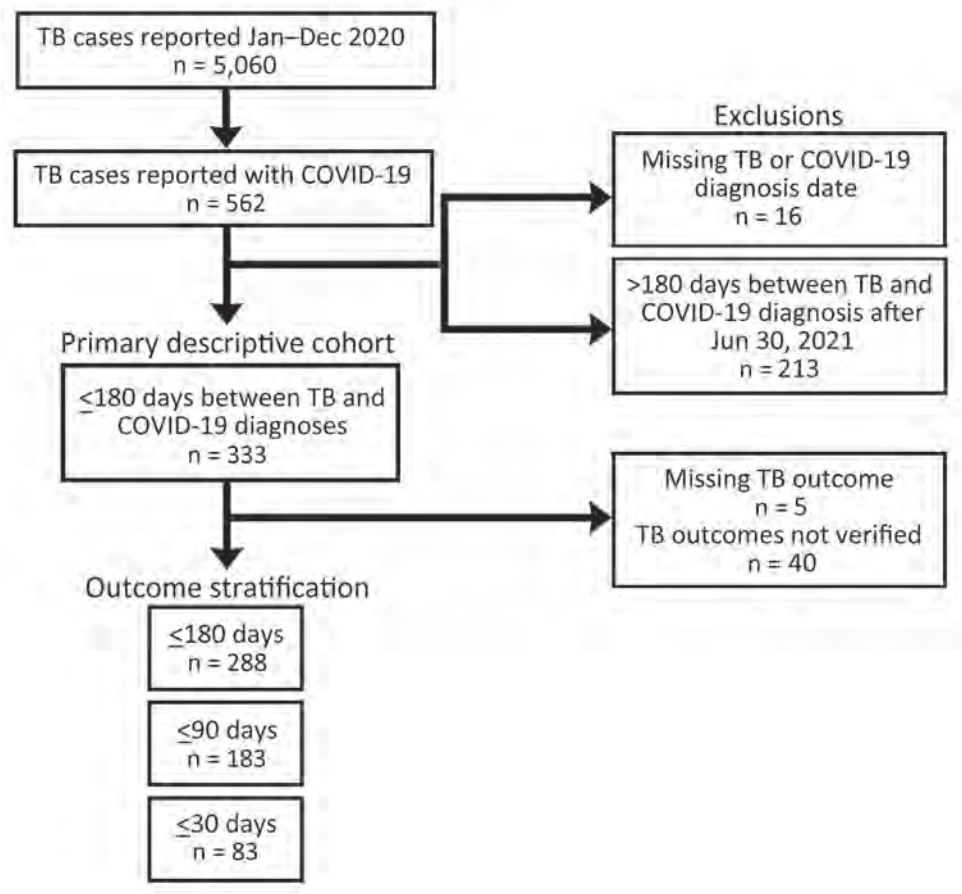

Figure 1. Analytic sample selection for persons with TB and COVID-19 co-diagnosed within 180 days (TB–COVID-19), 26 US jurisdictions, 2020. Three states performed registry matches with COVID-19 data up-to-date through an earlier date (January 24, 2021; February 2, 2021; August 31, 2021); 1 US state (North Dakota) that participated did not have TB–COVID-19 cases. The number of days between TB and COVID-19 diagnosis dates was calculated without regard for which disease was diagnosed first. Data from 2 jurisdictions (Puerto Rico and Los Angeles County; remainder of California included) were excluded because of incompleteness of outcomes data. TB, tuberculosis.

multivariable regression employing backward selection in logistic regression models to identify statistically significant ($\alpha = 0.05$) variables for inclusion in the log-binomial models. The final models included all variables reaching statistical significance and the COVID-19 co-diagnosis status as the exposure of interest. We did not assess interaction terms in multivariable models. Rather than exclude persons with missing covariate data, we classified missing values as unknown and retained them in the models. We stratified outcomes by the proximity in timing of TB and COVID-19 diagnoses (i.e., within 30, 90, and 180 days) and fit independent log-binomial models to each time interval.

Ethics Considerations

This activity was determined to meet the requirements of public health surveillance as defined in 45 CFR 46.102(l) (*2*). Informed consent was not required because the project was classified by CDC as nonresearch. Although most participating jurisdictions relied on the CDC project determination, some independently classified the activity as nonresearch.

Results

TB–COVID-19 Analytic Population

The 26 participating jurisdictions accounted for 62.9% of US TB cases in 2020 and 67.0% of the 2020 US population (*18*). The number of all TB cases reported in 2020 per participating jurisdiction ranged from 10 to 1,703: 12 jurisdictions (46.2%) reported <75 cases, 8 (30.8%) reported 75–149 cases, and 6 (23.1%) reported ≥150 cases. Participating jurisdictions reported ≈64% of the ≈46,353,000 COVID-19 cases reported in US states and territories reported during the observation period (*1*). Jurisdictions using more robust methods (i.e., a software algorithm or an integrated surveillance system) to identify persons with TB–COVID-19 (Appendix Table 1) accounted for 91.7% of the TB cases among the 26 participating jurisdictions.

One of 26 jurisdictions (North Dakota) did not identify persons with TB–COVID-19 meeting our criteria, and so we excluded numerator and denominator data for this jurisdiction from statistical analyses. The remaining 25 jurisdictions (23 US states; New York, NY; and Puerto Rico) identified 333 persons

with TB–COVID-19 meeting study criteria (Figures 1, 2). The number of persons with TB–COVID-19 identified per health jurisdiction ranged from 1 to 114 (Figure 2). The median age of persons with TB–COVID-19 was 55 years (interquartile range 35–69 years); 204 (61.3%) were male and 129 (38.7%) female, and 264 (79.3%) were non–US-born (Table 1, https://wwwnc.cdc.gov/EID/article/29/10/23-0286-T1.htm). Six (1.8%) persons were co-diagnosed with TB and COVID-19 on the same date, and 65 (19.5%) persons were co-diagnosed within 14 days (Figure 3). Of the 327 TB–COVID-19 cases diagnosed ≥1 day apart, 204 (62.4%) had TB diagnosed before COVID-19.

TB–COVID-19 Demographics Compared with 2020 TB-only and 2017–2019 TB-only

We did not find statistically significant (95% CI with Bonferroni correction) bivariate differences in persons with TB–COVID-19 relative to the 2020 TB-only and 2017–2019 TB-only comparison groups for sex, residence in a correctional facility, homelessness, or excessive alcohol use (Table 1). The TB–COVID-19 group had a higher proportion of Hispanic persons compared with both of the reference groups (Table 1). Higher proportions of persons with TB–COVID-19 also were residents of long-term care facilities at TB diagnosis compared with both reference groups.

TB–COVID-19 Clinical Characteristics Compared with 2020 TB-only and 2017–2019 TB-only

We did not find statistically significant differences, compared with either the 2020 TB-only or 2017–2019 TB-only reference group, for the proportion of persons with TB–COVID-19 by the status of a previous episode of TB, HIV infection, TB disease site (i.e., pulmonary-only, extrapulmonary, or both sites), or TB disease dissemination (Table 1). Compared with both reference groups, persons with TB–COVID-19 had a higher rate of diabetes and end-stage renal disease.

Multivariable Comparison of TB–COVID-19 Characteristics Compared with 2020 TB-only and 2017–2019 TB-only

In comparison to 2020 TB-only, persons with TB and COVID-19 diagnosed within 180 days were more likely to be in American Indian/Alaska Native (adjusted prevalence ratio [aPR] 5.3 [95% CI 2.1–13.4]) and, with borderline statistical significance, Native Hawaiian/Other Pacific Islander (aPR 2.3 [95% CI 1.0–5.3]) relative to non-Hispanic whites (Table 2). Persons with TB–COVID-19 also had a higher proportion of being non–US-born (aPR 1.5 [95% CI 1.1–2.1]), residing in long-term care facilities at TB diagnosis (aPR 2.5 [95% CI 1.6–4.0]), and having diabetes (aPR 1.6 [95% CI 1.3–2.0]). When comparing persons with TB–COVID-19 to 2017–2019 TB-only, those associations remained statistically significant; in addition, a higher proportion of persons with TB–COVID-19 also had end-stage renal disease (aPR 1.7 [95% CI 1.1–2.7]) and, with borderline statistical significance, acid-fast bacilli sputum smear positivity (aPR 1.3 [95% CI 1.0–1.6]) (Table 2).

Mortality Rates Compared with 2020 TB-only Patients

The occurrence of death at any time before or during TB treatment was 450/3,793 (11.9% [95% CI 10.8–12.9]) for 2020 TB-only. This rate compares with 48/288 (16.7% [95% CI 12.6–21.5]; unadjusted prevalence ratio [uPR] 1.4 [95% CI 1.1–1.8]) for persons co-diagnosed with TB and COVID-19 within 180 days, 39/183 (21.3% [95% CI 15.6–28.0]; uPR 1.8 [95% CI 1.3–2.5]) for those co-diagnosed within 90 days, and 17/83 (20.5% [95% CI 12.4–30.8]; uPR 1.7 [95% CI 1.1–2.7]) for those co-diagnosed within 30 days (Figure 4). After adjustment for age, comorbidities, and markers of TB disease severity, COVID-19 did not retain significance as an independent risk factor for all-cause mortality in persons with TB disease (Appendix Table 2). Significant cofactors were age ≥45 years, HIV infection (aPR 2.1 [95% CI 1.3–3.5]), end-stage renal disease (aPR 1.8 [95% CI 1.4–2.4]), TB disease dissemination (aPR 1.5 [95% CI 1.1–1.9]), and

Figure 2. Locations of 25 US jurisdictions contributing data for 333 persons with tuberculosis (TB) and COVID-19 co-diagnosed within 180 days (TB–COVID-19), 2020. Participating jurisdictions: Alabama (n = 5 cases), Arizona (n = 21), Arkansas (n = 9), California (n = 114), Colorado (n = 7), Indiana (n = 10), Iowa (n = 2), Kentucky (n = 6), Louisiana (n = 3), Massachusetts (n = 7), Michigan (n = 11), Minnesota (n = 14), Nevada (n = 4), New Hampshire (n = 1), New Jersey (n = 28), New Mexico (n = 4), New York State (n = 6); New York, NY (reporting separately; n = 37), North Carolina (n = 11), Ohio (n = 6), Puerto Rico (n = 2), South Carolina (n = 2), Tennessee (n = 11), Texas (n = 6), and Wisconsin (n = 6). North Dakota provided data but had no TB–COVID-19 cases reported.

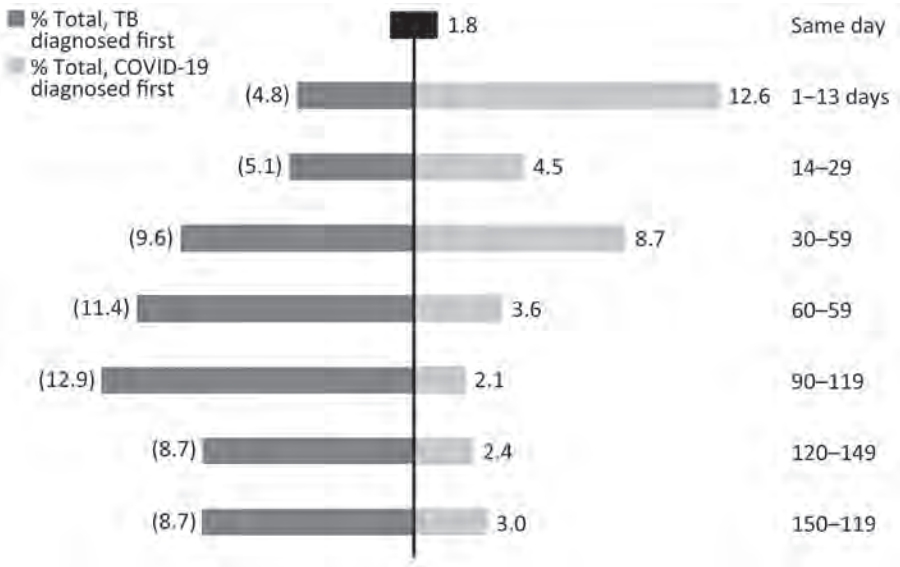

Figure 3. Frequency of 333 persons with TB and COVID-19 co-diagnosed (TB–COVID-19), by sequence and days between TB and COVID-19 diagnoses, 25 US jurisdictions, 2020. The percentage denominator accounts for all 333 persons. Individual percentages may not sum to 100% because of rounding. TB, tuberculosis.

sputum smear positivity for acid-fast bacilli (aPR 1.4 [95% CI 1.1–1.8]). We observed similar associations when persons had TB and COVID-19 diagnosed within shorter intervals (i.e., 30 and 90 days) (Appendix Table 2).

Risk Factors for Death among TB–COVID-19 Patients

Among the 288 persons with TB–COVID-19 with known mortality outcome (86.5% of all 333 persons with TB–COVID-19), death was associated with both TB and COVID-19 co-diagnoses being made within 90 days (aPR 2.3 [95% CI 1.1–4.8]), being immunocompromised (non-HIV) (aPR 2.7 [95% CI 1.1–6.4]), and age (Table 3). The adjusted risk for death increased with increasing age compared with ≤44 years: 45–64 years, aPR 5.6 (95% CI 1.6–19.8); 65–74 years, aPR 8.6 (95% CI 2.4–31.3); 75–84 years, aPR 12.6 (95% CI 3.5–45.7); and ≥85 years, aPR 25.0 (95% CI 6.9–91.1).

Table 2. Multivariable log-binomial regression of characteristics for 333 persons from 25 US jurisdictions who were diagnosed with TB–COVID-19 in 2020 and persons with TB only diagnosed in 2017–2019 or in 2020*

	2020 TB only		2017–2019 TB only	
Characteristic	uPR (95% CI)	aPR (95% CI)	uPR (95% CI)	aPR (95% CI)
Race/ethnicity†				
White	Referent	Referent	Referent	Referent
Black	0.8 (0.6–1.1)	1.1 (0.7–1.7)	0.9 (0.6–1.1)	1.2 (0.7–1.9)
Asian	0.7 (0.6–0.9)	0.8 (0.5–1.2)	0.7 (0.6–0.9)	0.8 (0.5–1.3)
Hispanic	1.6 (1.3–2.0)	1.4 (0.9–2.2)	1.6 (1.3–1.9)	1.4 (0.9–2.2)
NHOPI	2.4 (1.1–5.4)	2.3 (1.0–5.3)	2.2 (0.9–5.2)	2.9 (1.1–7.4)
American Indian/Alaska Native	3.4 (1.4–8.1)	5.3 (2.1–13.4)	2.3 (0.9–6.0)	3.4 (1.2–9.6)
Origin of birth				
US-born	Referent	Referent	Referent	Referent
Non–US-born	1.4 (1.1–1.8)	1.5 (1.1–2.1)	1.5 (1.1–1.9)	1.6 (1.1–2.2)
AFB sputum smear result				
Negative	Referent	NI	Referent	Referent
Positive	1.3 (1.0–1.5)		1.4 (1.1–1.7)	1.3 (1.0–1.6)
Missing/Unknown	0.9 (0.7–1.2)		0.9 (0.7–1.2)	1.0 (0.7–1.5)
Long-term care resident at TB diagnosis‡				
No	Referent	Referent	Referent	Referent
Yes	2.6 (1.6–4.2)	2.5 (1.6–4.0)	2.5 (1.5–4.1)	2.4 (1.4–4.0)
Diabetes				
No	Referent	Referent	Referent	Referent
Yes	1.8 (1.4–2.2)	1.6 (1.3–2.0)	2.0 (1.6–2.5)	1.8 (1.4–2.2)
End-stage renal disease				
No	Referent	NI	Referent	Referent
Yes	1.8 (1.2–2.7)		2.2 (1.4–3.4)	1.7 (1.1–2.7)

*Model adjusted for other variables in the table. aPR, adjusted prevalence ratio; AFB, acid-fast bacilli; NHOPI, Native Hawaiian and Other Pacific Islander; NI, not included in adjusted regression model because not statistically significant at 95% confidence level; TB, tuberculosis; TB–COVID-19, diagnosed with both TB and COVID-19 within 180 days; uPR, unadjusted prevalence ratio.
†Multiple race category not included because no persons with TB–COVID-19 reported multiple races.
‡Among persons ≥15 years of age.

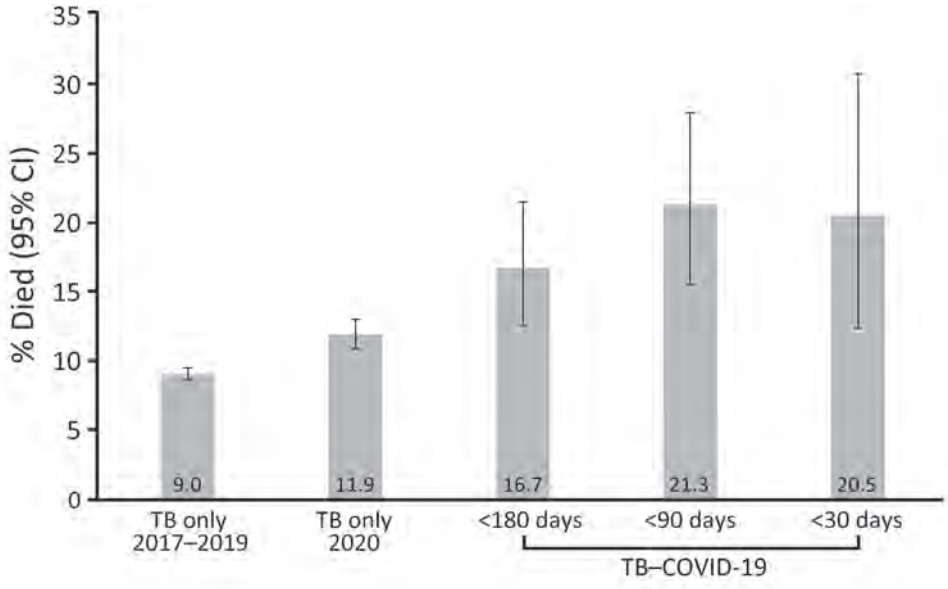

Figure 4. Unadjusted mortality rates for persons with TB only during 2017–2019 and during 2020 compared with persons with TB–COVID-19 during 2020, 25 US jurisdictions. Error bars indicate 95% CIs. TB, tuberculosis; TB–COVID-19, diagnosed with both TB and COVID-19 within 180 days.

Discussion

We report a large cohort of persons with TB–COVID-19 from a low TB–incidence setting (the United States) during the COVID-19 pandemic. Persons with TB and COVID-19 had overlapping sociodemographic and medical risk profiles known to be associated with each disease, including long-term care residence, diabetes, and end-stage renal disease. The frequency of death for persons with TB–COVID-19 was higher than persons with TB-only and depended on a shorter interval between TB and COVID-19 diagnoses (1 in 5 persons who had TB–COVID-19 co-diagnosed within 30 days died). However, COVID-19 was not independently associated with death among persons diagnosed with TB within 180 days when adjusted for age, underlying conditions, and TB disease severity, compared with those with 2020 TB-only patients. Among persons with TB–COVID-19, the timing of TB and COVID-19 co-diagnoses (i.e., within 90 days) remained a predictor of death, along with increasing age and being immunocompromised (non-HIV). Another analysis from California demonstrated an age-adjusted mortality rate ratio of 1.3 (95% CI 0.7–2.5) for deaths among TB–COVID-19 patients compared with 2017–2019 TB-only patients (*9*). That analysis did not adjust for underlying conditions (*9*). Increased mortality rates for persons with TB–COVID-19 has been repeatedly demonstrated in other settings when compared with persons with COVID-19 only (*5*–*8*). Other studies have demonstrated more severe COVID-19 disease classification among persons with TB–COVID-19 compared with persons diagnosed with COVID-19 without TB (*19*). However, few population-based studies have evaluated COVID-19 as a risk factor for all-cause mortality among persons with TB while adjusting for age, underlying conditions, and other potential confounders.

The baseline mortality rate for persons with TB was ≈9% annually in the United States in 2017 and 2018 (*18*). In our study, ≈17% of persons diagnosed with TB and COVID-19 within 180 days died. Nonetheless, in multivariable analysis corrected for age and underlying conditions, COVID-19 was not an independent predictor of death among persons with TB diagnosed within 180 days. Those findings suggest that poor outcomes for persons with TB–COVID-19 may be driven by the overlapping sociodemographic and medical risk factors common to each TB and COVID-19 that already place persons with TB at risk for death with TB, rather than the effect of COVID-19 coinfection alone. Compared with countries that have high TB prevalence, TB disease in the United States and other low TB incidence countries is more concentrated in older persons who have underlying conditions such as diabetes and renal disease (*18*). The timing of TB and COVID-19 co-diagnoses and its association with TB mortality warrants more investigation, given that our model demonstrated an association between a smaller diagnostic interval (90 days) and death among persons with TB–COVID-19. In addition to biological mechanisms to explain the association, persons with more severe COVID-19 may have been more likely to receive chest imaging and additional diagnostic testing to reveal concurrent TB.

Delayed TB diagnoses could have led to more severe TB disease at clinical evaluation in our analysis population. Another study from a low TB incidence setting showed a higher proportion of positive microscopic examinations during the COVID-19 pandemic compared

with historical trends (*20*), similar to the observation in this US cohort of persons with TB–COVID-19. This finding suggests longer delays until TB diagnosis during the COVID-19 pandemic. The timing of TB diagnosis after COVID-19 (a substantial proportion had TB diagnosed within 14 days after COVID-19) could also reflect delayed TB diagnoses, suggesting that COVID-19 could have brought persons with undiagnosed TB into care.

TB program participation was nonrandom, which limits the representativeness of results to the entire United States, perhaps especially related to race and ethnicity. Nonetheless, the cohort represented a cross-section of US jurisdictions with varying TB prevalence. An important distinction in comparison with other studies is that we were unable to compare outcomes for persons with TB–COVID-19 with those for persons with COVID-19 only. Other limitations are that the completeness of COVID-19 case reporting may have differed by jurisdiction and phase of the epidemic. Missing data may have lessened the accuracy of some descriptive characteristics; missing death dates precluded hazards analyses of time to death. Longitudinal case management for persons on TB treatment probably captured most, but potentially not all, deaths among persons with TB. Our definition for disseminated TB is intended to capture most cases resulting from hematogenous spread that might be associated with delayed diagnoses or poor outcomes. It may not reflect all disseminated TB characterized by isolated extrapulmonary lymphadenitis or TB misclassified because of incomplete tissue sampling. The Bonferroni correction may have raised the risk for type II error in bivariate comparisons, and the small number of persons with TB–COVID-19 and having sociodemographic characteristics potentially influencing outcomes (e.g., experiencing homelessness) limited our ability to describe them. Strengths include the high completeness of sociodemographic data available in NTSS (*15*). Still, some underlying conditions strongly associated with poor COVID-19 outcomes (e.g., cardiovascular disease and obesity) were not available.

In conclusion, this analysis of a US cohort of persons with TB–COVID-19 suggests deaths among persons with TB–COVID-19 in the United States is concentrated in subgroups having shared characteristics known to increase risk for death with either disease alone. Timely consideration for TB disease among persons with COVID-19 and TB risk factors should be reinforced. Because death was associated with shorter intervals between co-diagnoses, prioritizing additional early medical interventions for persons with concurrent disease processes who are at highest risk for death might improve outcomes. COVID-19 patients with severe disease may be given immunomodulating treatments that could reactivate latent TB infection. Therefore, COVID-19 patients with risk factors for TB infection could be considered for screening and treatment of latent TB infection. Last, integration of screening for TB infection (risk factor review and serum interferon gamma release assays testing) with community COVID-19 prevention efforts among subpopulations with shared risk profiles, as has been done for persons at increased risk for COVID-19 and diabetes (*21*), may expand high-yield opportunities to prevent TB.

National Tuberculosis Controllers Association/ CDC TB-COVID-19 Collaboration Members: Alabama Department of Public Health: Claire Payne; Arkansas Department of Health: Leonard Ntaate Mukasa, Virginia Maturino, Sandra E. Chai, Naveen Patil; California Department of Public Health: Emily Han, Pennan M. Barry, Seema Jain, Jennifer Flood; Colorado Department of Public Health and Environment: Juli Bettridge; Indiana Department of Health: Biak Chinpar, Sarah Bennett, Petia Boykova; Iowa Department of Health and Human Services: Allan Lynch; Kentucky Department of Public Health: Charles H. Rhea; Louisiana Department of Health: Andrew Smith, Kathryn Yoo; Massachusetts Department of Public Health: Andrew Tibbs, Kavita Gadani; Minnesota Department of Health: Katie Stinebaugh; New Hampshire Department of Health and Human Services: Carolyn R. Fredette, Elizabeth A. Talbot, Darlene Morse; New Jersey Department of Health: Julianna Wisniewski; New Mexico Department of Health: Brenda Montoya Denison; New York State Department of Health: Cheryl H. Kearns, Jamie Sommer; New York City Department of Health and Mental Hygiene: Soogyum Kim, Lisa Trieu; North Carolina Department of Health and Human Services: Daniela Ingram, Jennifer B. Wheeler; North Dakota Health & Human Services: Saurav Dahal; Ohio Department of Health: Sarah Mitchell, Sara Stokes; Puerto Rico Department of Health: Jose Calderon; South Carolina Department of Health & Environmental Control: Jesse S. Ellis; Tennessee Department of Health: Robert J. Cummins, Ben Katz; Texas Department of State Health Services: Anette Costa; Wisconsin Department of Health Services: Claire Leback; NTCA Working Group Members: Aakriti Pandita (University of Colorado), Matthew Dory (Maryland Department of Health), Maureen Murphy-Weiss (Columbus Public Health); CDC: Terence Chorba, Adam Langer, Farah Parvez, Benjamin Silk

Acknowledgments

We thank John A. Jereb, Susan McElhany, and Sabrina Nabinger.

Author contributions: All authors contributed to data interpretation and review and approval of the final manuscript. S.A.N., S.M.M., N.D.G., S.R.S., E.T., S.P., J.L.S., L.G., K.G.T., M.N., D.H.W., and S.H.W. conceived of the study design and analytic plan. The National Tuberculosis Controllers Association/CDC TB-COVID-19 Collaboration collected data. S.M.M. and S.P. curated and analyzed the data. S.A.N., S.M.M., and N.D.G. drafted the original manuscript. S.H.W., D.H.W., N.D.G., and S.A.N. coordinated the project.

About the Author

Dr. Nabity is a medical officer for CDC's Field Services Branch, Division of TB Elimination, National Center for HIV, Viral Hepatitis, STD, and TB Prevention, currently assigned to the California Department of Public Health Tuberculosis Control Branch. His primary research interests include the epidemiology of infectious diseases, including TB and COVID-19.

References

1. Johns Hopkins School of Public Health. Coronavirus Resource Center: cumulative cases. 2022 [cited 2022 Sep 23]. https://coronavirus.jhu.edu/data/cumulative-cases
2. Centers for Disease Control and Prevention. Underlying medical conditions associated with higher risk for severe COVID-19: information for healthcare professionals. 2022 [cited 2022 Sep 22]. https://www.cdc.gov/coronavirus/2019-ncov/hcp/clinical-care/underlyingconditions.html
3. Sy KTL, Haw NJL, Uy J. Previous and active tuberculosis increases risk of death and prolongs recovery in patients with COVID-19. Infect Dis (Lond). 2020;52:902–7. https://doi.org/10.1080/23744235.2020.1806353
4. Boulle A, Davies M-A, Hussey H, Ismail M, Morden E, Vundle Z, et al.; Western Cape Department of Health in collaboration with the National Institute for Communicable Diseases, South Africa. Risk factors for coronavirus disease 2019 (COVID-19) death in a population cohort study from the Western Cape Province, South Africa. Clin Infect Dis. 2021;73:e2005–15. https://doi.org/10.1093/cid/ciaa1198
5. Wang Y, Feng R, Xu J, Hou H, Feng H, Yang H. An updated meta-analysis on the association between tuberculosis and COVID-19 severity and mortality. J Med Virol. 2021;93:5682–6. https://doi.org/10.1002/jmv.27119
6. Aggarwal AN, Agarwal R, Dhooria S, Prasad KT, Sehgal IS, Muthu V. Active pulmonary tuberculosis and coronavirus disease 2019: a systematic review and meta-analysis. PLoS One. 2021;16:e0259006. https://doi.org/10.1371/journal.pone.0259006
7. Jindal R, Gupta M, Khan FR, Chaudhry G. Prevalence of co-morbidities and its association with mortality in Indian patients with COVID-19: a meta-analysis. Indian J Anaesth. 2022;66:399–418. https://doi.org/10.4103/ija.ija_845_21
8. Wang Q, Guo S, Wei X, Dong Q, Xu N, Li H, et al. Global prevalence, treatment and outcome of tuberculosis and COVID-19 coinfection: a systematic review and meta-analysis (from November 2019 to March 2021). BMJ Open. 2022;12:e059396. https://doi.org/10.1136/bmjopen-2021-059396
9. Nabity SA, Han E, Lowenthal P, Henry H, Okoye N, Chakrabarty M, et al. Sociodemographic characteristics, comorbidities, and mortality among persons diagnosed with tuberculosis and COVID-19 in close succession in California, 2020. JAMA Netw Open. 2021;4:e2136853. https://doi.org/10.1001/jamanetworkopen.2021.36853
10. Public Health Alliance of Southern California. The California Healthy Places Index. 2018 [cited 2021 Mar 12]. https://www.healthyplacesindex.org
11. Dheda K, Perumal T, Moultrie H, Perumal R, Esmail A, Scott AJ, et al. The intersecting pandemics of tuberculosis and COVID-19: population-level and patient-level impact, clinical presentation, and corrective interventions. Lancet Respir Med. 2022;10:603–22. https://doi.org/10.1016/S2213-2600(22)00092-3
12. Deutsch-Feldman M, Pratt RH, Price SF, Tsang CA, Self JL. Tuberculosis—United States, 2020. MMWR Morb Mortal Wkly Rep. 2021;70:409–14. https://doi.org/10.15585/mmwr.mm7012a1
13. Louie JK, Agraz-Lara R, Romo L, Crespin F, Chen L, Graves S. Tuberculosis-associated hospitalizations and deaths after COVID-19 shelter-in-place, San Francisco, California, USA. Emerg Infect Dis. 2021;27:2227–9. https://doi.org/10.3201/eid2708.210670
14. Narita M, Hatt G, Gardner Toren K, Vuong K, Pecha M, Jereb JA, et al. Delayed tuberculosis diagnoses during the coronavirus disease 2019 (COVID-19) pandemic in 2020—King County, Washington. Clin Infect Dis. 2021;73(Suppl 1):S74–6. https://doi.org/10.1093/cid/ciab387
15. Yelk Woodruff RS, Pratt RH, Armstrong LR. The US National Tuberculosis Surveillance System: a descriptive assessment of the completeness and consistency of data reported from 2008 to 2012. JMIR Public Health Surveill. 2015;1:e15. https://doi.org/10.2196/publichealth.4991
16. Council of State and Territorial Epidemiologists. Update to the standardized surveillance case definition and national notification for 2019 novel coronavirus disease (COVID-19). 2020 [cited 2023 Jan 9]. https://www.cste.org/resource/resmgr/ps/positionstatement2020/Interim-20-ID-02_COVID-19.pdf
17. Centers for Disease Control and Prevention. COVID-19 2020 interim case definition, approved August 5, 2020. 2020 [cited 2022 Sep 23]. https://ndc.services.cdc.gov/case-definitions/coronavirus-disease-2019-2020-08-05
18. Centers for Disease Control and Prevention. Reported tuberculosis in the United States, 2020. 2021 [cited 2022 Sep 23]. https://www.cdc.gov/tb/statistics/reports/2020/default.htm
19. Lucien MAB, Pierre K, Jean-Denis G, Rigodon J, Worrell CM, Couture A, et al. Epidemiology and risk factors related to severity of clinical manifestations of COVID-19 in outpatients: a retrospective study in Haiti. PLoS One. 2022;17:e0274760. https://doi.org/10.1371/journal.pone.0274760
20. Marchese V, Formenti B, Marchese L, Gregori N, Gardini G, Russo G, et al. COVID-19 effect on TB presentation and outcome. Int J Tuberc Lung Dis. 2022;26:375–7. https://doi.org/10.5588/ijtld.22.0036
21. Chapman LAC, Shukla P, Rodríguez-Barraquer I, Shete PB, León TM, Bibbins-Domingo K, et al. Risk factor targeting for vaccine prioritization during the COVID-19 pandemic. Sci Rep. 2022;12:3055. https://doi.org/10.1038/s41598-022-06971-5

Address for correspondence: Scott Nabity, California Department of Public Health, 850 Marina Bay Pkwy, Bldg P Fl 2, Richmond, CA 94804-6403, USA; email: hjq5@cdc.gov

Cycle Threshold Values as Indication of Increasing SARS-CoV-2 New Variants, England, 2020–2022

Rebecca E. Harrison, Ahmed Hamada, Nujcharee Haswell, Aigul Groves, Karina-Doris Vihta, Kerry Cella, Sarah Garner, Ann Sarah Walker, Anna C. Seale

Early detection of increased infections or new variants of SARS-CoV-2 is critical for public health response. To determine whether cycle threshold (Ct) data from PCR tests for SARS-CoV-2 could serve as an early indicator of epidemic growth, we analyzed daily mean Ct values in England, UK, by gene target and used iterative sequential regression to detect break points in mean Ct values (and positive test counts). To monitor the epidemic in England, we continued those analyses in real time. During September 2020–January 2022, a total of 7,611,153 positive SARS-CoV-2 PCR test results with Ct data were reported. Spike (S) gene target (S+/S–)–specific mean Ct values decreased 6–29 days before positive test counts increased, and S-gene Ct values provided early indication of increasing new variants (Delta and Omicron). Our approach was beneficial in the context of the first waves of the COVID-19 pandemic and can be used to support future infectious disease monitoring.

From identification of SARS-CoV-2 in December 2019 through September 22, 2022, ≈612 million confirmed cases and 6.5 million confirmed deaths were reported worldwide (*1*). During the COVID-19 pandemic, epidemic waves have usually been associated with emergence of a new variant. Assessing the emergence of any such new variant is critical for public health response. Although testing is essential for monitoring trends in detected cases, the diagnostic real-time quantitative reverse transcription PCR (qRT-PCR) tests also provide data pertaining to viral load and presence or absence of particular genes in the virus detected, which may further aid assessment of the likely course of the epidemic.

qRT-PCR results are sensitive, based on detection of SARS-CoV-2 RNA. Results are positive, negative, or indeterminate, based on a threshold for the number of replication cycles required for detection, the cycle threshold (Ct) (*2*,*3*). Typically, the higher the Ct value, the lower the viral load in the specimen (*4*).

Viral load is associated with infectivity and can be associated with severity of illness (*5*–*7*). Low Ct values have been associated with testing just after symptom onset (*8*–*11*), having the classic symptoms (e.g., cough/fever/anosmia/ageusia) (*4*), increased duration of viral shedding, (*12*,*13*), severe case of COVID-19 and increased risk for critical illness and death (*14*–*19*), older age (*20*–*22*), vaccination status (*23*), and higher secondary attack rate (*7*,*24*).

Individually, interpretation of Ct values as a proxy of infectiousness or severity of illness should be approached with caution. Results may be influenced by the time course of infection, additional technical factors during sampling, types of processing, and the specific assay used (*25*,*26*). However, in the population, Ct values as a proxy for viral load may provide information on the growth of the epidemic, if measured with a standardized assay.

On March 27, 2020, a new network of Lighthouse laboratories, was set up for SARS-CoV-2 testing in the United Kingdom (J.A. Douthwaite, unpub. data, https://www.researchsquare.com/article/rs-637020/v1). Four of those laboratories used the Thermo Fisher TaqPath RT-PCR test (*27*), which detects 3 SARS-CoV-2 gene targets: open reading frame (ORF)1, nucleocapsid (N), and spike (S). Ct values are

Author affiliations: United Kingdom Health Security Agency, London, UK (R.E. Harrison, A. Hamada, N. Haswell, A. Groves, K. Cella, S. Garner, A.C. Seale); University of Oxford, Oxford, UK (K.-D. Vihta, A.S. Walker); Warwick Medical School, University of Warwick, Coventry, UK (A.C. Seale); London School of Hygiene & Tropical Medicine, London (A.C. Seale)

DOI: https://doi.org/10.3201/eid2910.230030

available for each gene detected, and RT-PCR tests at TaqPath are standardized and thus comparable across laboratories. All 3 gene targets are not always detected, which can result from a sample of low quality or low viral load or from a virus having mutations in the ORF1ab, S, or N gene.

Over the course of the epidemic, and in particular with the emergence of the Alpha variant, which had S gene target failure (SGTF/S–) compared with the initial wild-type variant, the potential use of the S gene for identifying emergence of a new variant, combined with analysis of Ct values to investigate growth, became apparent. Data from both National Health Service (NHS) Test and Trace and from the UK COVID-19 Infection Survey (CIS) were thus assessed for the presence or absence of the S gene (*4*,*28*) (A.S. Walker, unpub. data, http://medrxiv.org/lookup/doi/10.1101/2021.01.13.21249721).

We describe use of Ct values with S gene target data for early detection and community growth of the Alpha, Delta, and Omicron (BA.1) SARS-CoV-2 variants in England; that approach was used in real-time monitoring for Delta and Omicron. We conducted our analysis to provide information for the outbreak response to the COVID-19 pandemic. Work was undertaken in accordance with national data regulations. We accessed and used only fully anonymized data from the UK Health Security Agency (UKHSA) in a secure research environment.

Methods

Data Source

We used data from the England national clinical and community testing program for September 1, 2020, through January 31, 2022 (*29*). We monitored SARS-CoV-2 RT-PCR tests processed at Taqpath laboratories at Milton Keynes, Glasgow Central, Alderley Park, and Newcastle. Samples were reported as positive if the algorithm was interpreted as positive for ≥1 of the N or ORF1ab genes by an assay-specific algorithm and decision mechanism that analyzes the raw assay data. The S gene was not considered a prerequisite for positivity because of mutations detected since mid-May 2020. TaqPath laboratories almost exclusively use community-based tests rather than healthcare-based tests.

Data Analyses

As part of routine monitoring, we prepared the data in SQL and conducted analyses in R (The R Project for Statistical Computing, https://www.r-project.org) and Python (https://www.python.org) during February 2020–February 2022 and present analyses through February 2022. We describe the total positive SARS-CoV-2 PCR tests, the proportion processed in Taqpath laboratories, and the changes in mean Ct values with different gene target combinations.

The absence of the S gene (S–) was a proxy for Alpha (September 1, 2020–January 28, 2021) and Omicron BA.1 (October 1, 2021–January 31, 2022), whereas the presence of the S gene (S+) with both other genes was a proxy for Delta (February 1, 2021–January 5, 2022). To confirm the use of the S gene as a proxy, we linked those data to whole-genome sequencing and rapid genotyping data, if available. Rapid genotyping was conducted 3–5 days after PCR and whole-genome sequencing data 10–14 days after PCR.

We recorded absolute numbers of positive test results and proportions by variant and measured 7-day rolling means of positive test results by variant by calendar period during which variants were detected and started to grow: Alpha (September 1, 2020–January 31, 2021), Delta (February 1, 2021–November 30, 2021), and Omicron (October 1, 2021–January 31, 2022). We restricted analysis of counts of S– and S+ to samples with Ct <30 because absence of S-gene detection above that threshold could reflect stochastic variation at low viral loads. Mean daily Ct values included all positive samples, including those with Ct >30, which enabled better detection of drops from high Ct values.

To detect trends and break points in Ct values and numbers of positive test results, we applied iterative sequential regression (ISR), which allows for changes in trend to be identified in real time through its sequential design (*28*), to daily mean Ct values and daily numbers of positive test results for each calendar period, broken down by S gene target profile (ORF1ab, N, and S+ vs. ORF1ab, N, and S–). If a model with 2 trends was a better fit compared with 1 trend, we fixed the change point and repeated the process (i.e., added more data and new models with this change point, as well as other potential change points after the initial one was fitted). That method enables efficient estimation of multiple changes in trend, unlike a traditional grid search algorithm. We set break points to be at least 14 days apart and used a gamma model because it seemed to be the most appropriate on the basis of its visual fit, despite the apparent dispersion constraints, and the negative binomial or Poisson may also be appropriate for the number of positive test results. We used results from the ISR model to describe days passed between break points in mean Ct trend and daily numbers of positive test results and the time taken for the break point to be identified by the ISR model.

Results

Emergence of Alpha from Wild-Type Variants

During April 2020–March 2021, a total of 3,312,159 PCR tests for SARS-CoV-2 were conducted in England through clinical and community testing streams; 27,902 (0.84%, 95% CI 0.83%–0.85%) tests were positive. Over that period, the percentage of swab samples with no S gene detected increased; >86% of those with Ct <30 had no S gene detected from November 16, 2020, through March 31, 2021, concurrent with emergence and expansion of Alpha (B.1.1.7) (although less complete dominance compared with later variants) (*4*). That finding led to use of the S gene Ct values, case numbers, and proportions as a proxy for monitoring positive tests that did or did not detect an S gene, according to both the UK Office of National Statistics Covid Infection Survey (ONS CIS) and UKHSA surveillance data (*4*,*28*). The S– characteristic was later also found to be a characteristic of Omicron BA.1. Other variants, such as Delta, Beta, and Gamma, usually do not have mutations in region of the S gene detected by the TaqPath assay primers, and so the PCR test will usually detect the S, ORF1ab, and N genes, described as S+.

Emergence of New Variants in Terms of S Gene and Growth (Ct Values)

During September 1, 2020–January 31, 2022, a total of 15,139,217 positive RT-PCR test results were reported in England, of which 7,611,153 (50.3%) had Ct values available for ORF1ab, N, or S gene targets from a TaqPath RT-PCR assay. Infections with S– virus were dominant from November 2020 through April 2021 (Alpha), and S+ infections became dominant after April 2021 (Delta), and then S– infections were dominant again between from 2021 through January 2022 (Omicron BA.1) (Figure 1). From January on, the BA.2 (S+) variant started to emerge. The sequence data and rapid genotyping results, when later available, were closely aligned (Appendix Figure, https://wwwnc.cdc.gov/EID/article/29/10/23-0030-App1.pdf).

Ct values in S+ tests slowly increased from September 2020 through March 2021 as wild-type SARS CoV-2 incidence decreased, and mean Ct values in S– tests decreased from September through December 2020 as Alpha increased. Ct values in S+ tests decreased as Delta incidence increased from May 2021. In December 2021, mean Ct values for S– tests again decreased rapidly, just as Omicron BA.1 incidence increased. (Figure 2).

Emergence of Alpha

From September 1, 2020, through January 31, 2021, daily S– test results (proxy Alpha) rose from 1 to 6,487, peaking at 22,936 on January 2, 2021. Sequencing of 169,823 (4.7%) of 3,617,137 viruses over this period showed that 78,410 (46.2%) were Alpha (Appendix Table 1). With the growth of Alpha, the daily mean Ct value for S– tests decreased from 26.1 on September 1, 2020, to 19.6 on December 20, 2020.

At that time, we were not using ISR in real time, but as we implemented the approach in mid-2021, we detected the first break point in mean daily Ct values in S– tests on November 22, 2020 (and it took 14 days for the ISR model to notice this break point), which was ≈6 days before incidence increased further. The drop in Ct value, if observed in real time, could have provided an early indicator of the Alpha increase. Retrospectively, we detected a break point for the plateau/increase in Ct values on December 24, 2020 (noticed 32 days later), and the peak in positive tests

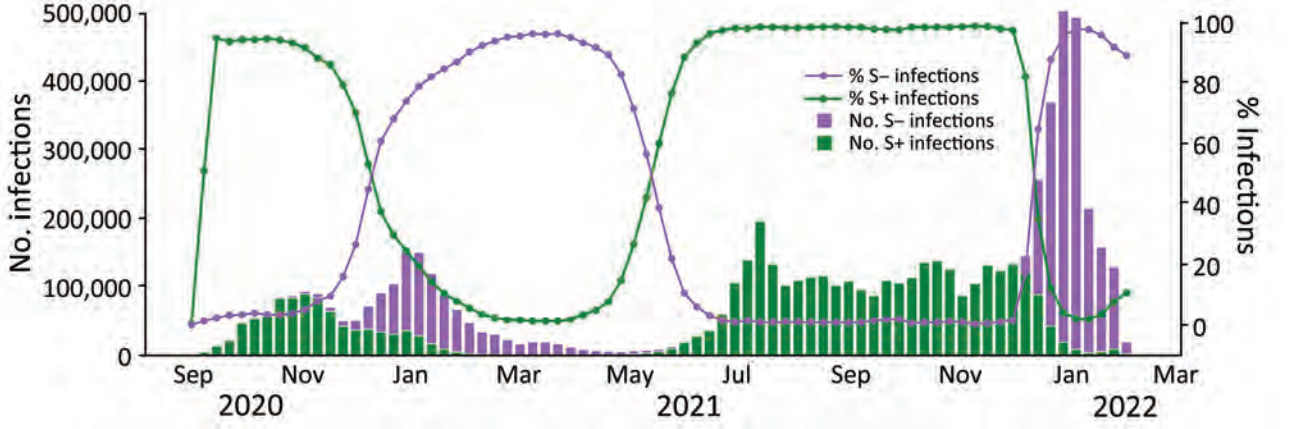

Figure 1. Weekly Taqpath reverse transcription quantitative PCR (*27*) gene detection (S+/S–) in SARS-CoV-2 infections, England, August 31, 2020–January 31, 2022. The chart excludes cycle threshold (Ct) values >30 for S– because when Ct >30, the S– may be caused by a sample of low quality or with low viral load rather than a reliable S– signal. Test results for which only 1 gene is detected are excluded. S, spike; S+, presence of S gene; S–, absence of S gene.

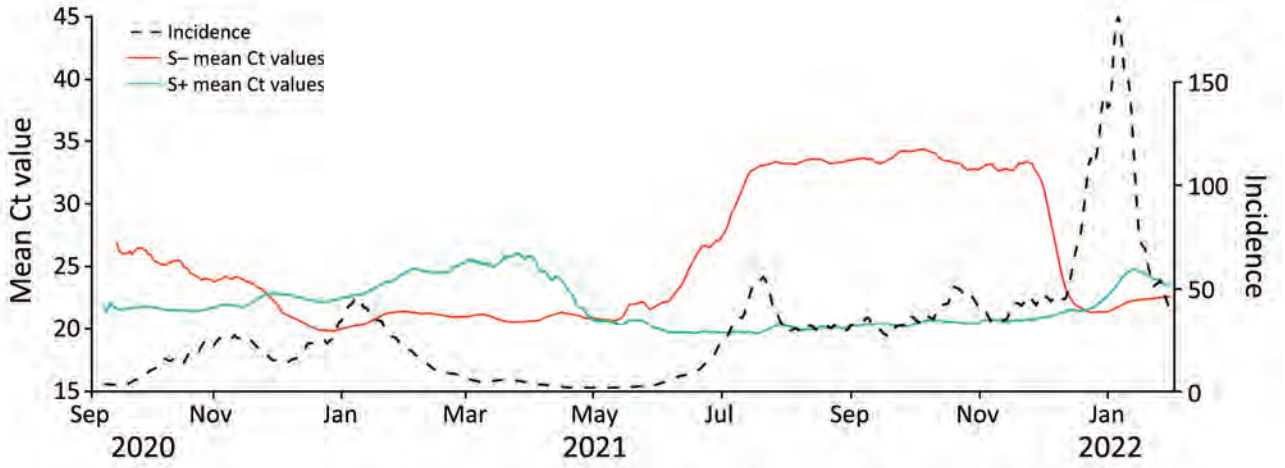

Figure 2. Daily mean Taqpath reverse transcription quantitative PCR (*27*) cycle threshold results by gene target profile (S+/S–) in SARS-CoV-2 infections, England, August 31, 2020–January 31, 2022. S+ indicates open reading frame ab1, nucleocapsid, and S detected; S– indicates open reading frame ab1 and nucleocapsid detected. Incidence, cases/100,000 population; S, spike; S+, presence of S gene; S–, absence of S gene.

11 days later on January 4, 2021 (noticed 16 days later) (Figure 3).

Emergence of Delta

From February 1, 2021, through November 30, 2021, daily S+ tests increased from 544, to 21,797, peaking at 35,866 on July 15, 2021. Sequencing of 1,546,168 (25.9%) of 5,965,964 viruses over that period showed that 1,273,965 (82.4%) were Delta (Appendix Table 1).

During this period, through regular analysis in real time, we first detected a break point in mean Ct values in S+ tests on March 23, 2021 (noticed 14 days later), ≈29 days before incidence started increasing. We detected a break point for the plateau/increase in Ct values on May 1, 2021 (noticed 16 days later), and the peak in positive test results 69 days later on July 9, 2021 (noticed 14 days later) (Figure 4). Use of gene target–specific data was particularly valuable for early detection of Delta growth at that time because overall case counts were declining in the country, masking growth of the new variant. The Beta and Gamma variants also emerged globally around this time, and our analyses provided early indication that these variants were not growing rapidly in England.

Emergence of Omicron

During October 1, 2021–January 31, 2022, the daily number of S– tests increased from 10 to 17,237, peaking at 108,438 on January 4, 2022. Sequencing of 1,961,850 (25.1%) of 7,800,924 viruses over that period showed that 1,120,807 (57.1%) were Omicron BA.1 (Appendix Table 1).

During that period, through regular analyses in real time, we first detected a break point in mean Ct values in S– tests on November 17, 2021 (noticed 14

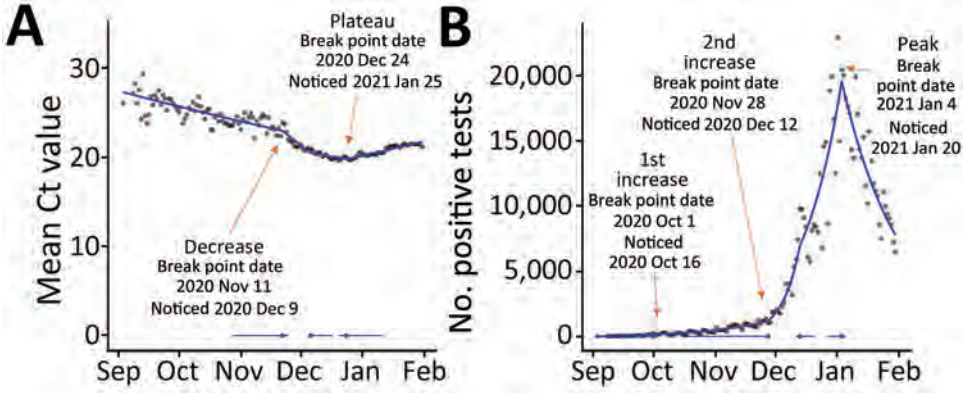

Figure 3. Emergence of novel Alpha variant of SARS-CoV-2 in England, showing mean Ct values (A) and positive results for SARS-CoV-2 S tests (B) for September 3, 2020–January 31, 2021, according to a gamma model. Break points detected through iterative sequential regression (ISR) that indicate significant changes in mean Ct values and positive test counts are labeled. Blue line represents estimated S– mean Ct value and positive test counts by ISR. Blue lines at the base of the graph represent 95% CIs around the break points estimated by the ISR model. Ct, cycle threshold; S, spike; S+, presence of S gene; S–, absence of S gene.

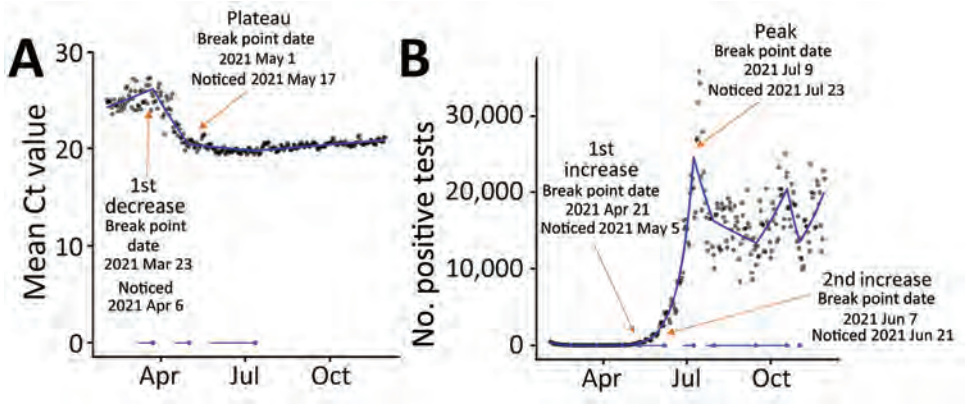

Figure 4. Emergence of novel Delta variant of SARS CoV-2 in England, showing mean Ct values (A) and positive test counts for SARS CoV-2 S-gene–positive tests (B) for February 1, 2020, through November 30, 2021, according to a gamma model. Break points detected through iterative sequential regression (ISR) that indicate significant changes in mean Ct values and positive tests are labeled. Blue line represents estimated S– mean Ct value and positive test counts by ISR. Blue lines at the base of the graph represent 95% CIs around the breakpoints estimated by the ISR model. Ct, cycle threshold; S, spike; S+, presence of S gene; S–, absence of S gene.

days later), ≈8 days before incidence started increasing. We again observed a drop in Ct value as a precursor to the start of the increasing number of positive test results. Over that period, mean Ct values for S– tests decreased from 34.5 to 22.9 from October 1, 2021, through January 31, 2022, dropping to a low of 21.0 on December 15, 2021 (Figure 5).

For S+ tests over the same period, we observed mean Ct values increase from 20.6 to 23.2 and daily positive tests decrease from 13,597 to 353. We also observed Ct values starting to drop again toward the middle of January 2022, resulting from emergence of Omicron BA.2.

Discussion

Detecting emergence and growth of new SARS CoV-2 variants is valuable for public health response. Starting in February 2022 in England, knowing the patterns for Alpha, we implemented routine monitoring of positive SARS-CoV-2 clinical test results in the community, by S gene status and mean Ct values, which subsequently provided an early indication of increased incidence for Delta and Omicron. We observed decreasing mean gene target –Ct values in surveillance data ≈6–29 days before variant-specific incidence increased in the population. Mean Ct values plateaued or slightly increased ≈1 month before peak case incidence.

Although the changes in Ct values and S gene data were useful early indicators of increasing incidence, they could not be interpreted in isolation. We needed confirmation of the use of the S gene as a proxy marker from genotyping and whole-genome sequencing. It was also fortuitous that for each new variant that became dominant in the United Kingdom during 2020–2021, its presence alternated with absence of the S gene. Tracking the growth of Delta in the United Kingdom by using S gene data was straightforward because no other S+ cases were in wide circulation at the time. A study in the United States, where Beta had gained traction along with Delta, was not able to use S gene data in the

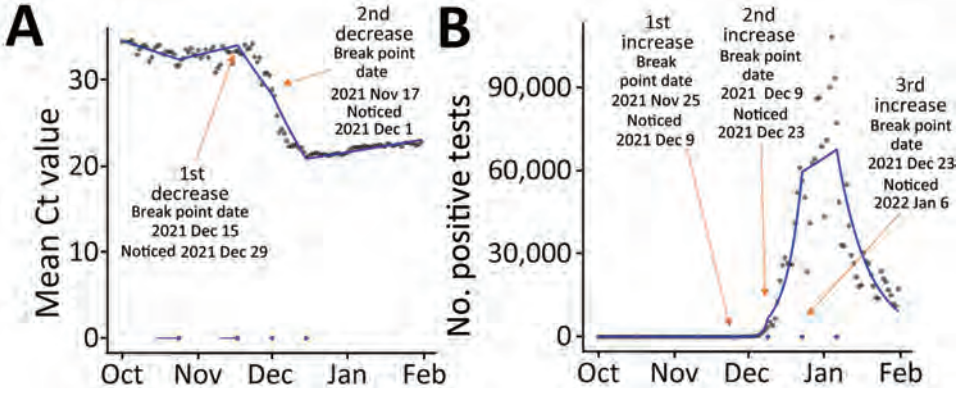

Figure 5. Emergence of novel Omicron (BA.1) variant of SARS CoV-2 in England, showing mean Ct values (A) and positive test counts for SARS CoV-2 S–tests (B) from October 1, 2021, through January 31, 2022, according to a gamma model. Break points detected through iterative sequential regression (ISR) that indicate significant changes in mean Ct values and positive tests are labeled. Blue line represents estimated S– mean Ct value and positive test counts by ISR. Blue lines at the base of the graph represent 95% CIs around the break points estimated by the ISR model. Ct, cycle threshold; S, spike; S+, presence of S gene; S–, absence of S gene.

same way that was possible here (*30*). The S gene is not, however, necessarily a prerequisite for using changes in Ct values to monitor emerging variants; although detection times may be slower, changes in Ct value trends should be detectable in positive tests, unrestricted by gene target (*31*). However, in the period that this work was undertaken (up to and including Omicron BA.1), we did not observe and thus analyze epidemic changes in which the S gene target did not change, and thus we cannot compare the time taken to detect changes by using this method without a change in gene target.

The sample size needed is also relevant to the technique. Although we do not present the results here, we were able to use ISR for the 9 regions of England to detect and compare rates of early growth in new variants. However, when this technique was attempted for all 309 lower tier local authorities, absolute and relative weekly S+/S– case numbers were usually more useful than Ct values for tracking growth because of the low number of positive test results during the emergence of a new variant at this geographic level. Going forward, to determine how quickly changes could be detected on a smaller scale, testing this approach on smaller datasets may be useful. Pandemic monitoring benefited by laboratories using a specific, standardized assay, although coverage varied regionally; coverage was notably lower in southwestern England. The use of the standardized TaqPath assay reduced data variation, which may be introduced if different assays or thresholds are used. A study in Bahrain used results from a variety of different assays and found utility of Ct values for predicting the pandemic trajectory to be lower than we did, although that finding may also be associated with their application of a different modeling technique (*32*). Further research would be needed to confirm those findings.

In the community testing data analyzed, testing tended to be conducted shortly after the appearance of symptoms, whereas for surveillance studies, such as the ONS CIS, testing was conducted across the period when a person tested positive on PCR (multiple weeks), leading to a greater range of Ct values. However, with the scale of community testing at the height of the pandemic in England, these data provided earlier indications of new variants than survey data and provided a more useful early indicator of growth of Delta or Omicron than lateral flow test/PCR test positivity, reflex assays, or sequencing. After a new variant was dominant, positivity and case rates became more useful for monitoring. The time delay for detecting a break point by using ISR was ≈2 weeks, but a change could be observed before then. For our analyses, we used gamma distributions, based on the best visual fit, although Poisson or negative binomial distributions may have been more appropriate for the daily count of positive tests. However, given the scale of the data in this analysis, the final fit by model is not likely to differ substantially.

Smaller studies have suggested that changes in Ct values can indicate changes in trajectory of the epidemic, including a study from Spain (*33*) that reported differential changes in mean Ct values and rate of positive tests in the first and second waves; a study from Pakistan (*34*), a study from Italy (*35*), and a study from Belgium (*36*) that reported a 17-day lag between changes in Ct values and positive tests, and a study from the United States that reported a 33-day lag between Ct values and cases (*37*). Our study, which used national surveillance data for >1 year, along with studies from ONS CIS and other studies in the United Kingdom (*4*,*28*) (A.S. Walker AS, unpub. data), provides evidence that using S-specific Ct values can identify emerging new variants and further evidence that Ct values can detect changes in incidence before positive test counts and sequencing data. We found that monitoring COVID-19 gene-specific Ct values in England was a useful early indicator for detecting epidemic growth and providing insight to support public health policy. This useful application of clinical testing data, although of maximal benefit in the context of the first waves of the COVID-19 pandemic, may have other applications for infectious disease monitoring.

The data used in this study are not publicly available because they were acquired under license/data sharing agreement from NHS Digital and UKHSA, under specific conditions of use. Individuals or organizations wishing to request access can request the data directly from NHS Digital (https://digital.nhs.uk/services/data-access-request-service-dars).

Funding was provided by the UK Government Department of Health and Social Care. K.-D.V. and A.S.W. are supported by the National Institute for Health Research (NIHR) Health Protection Research Unit in Healthcare Associated Infections and Antimicrobial Resistance at the University of Oxford in partnership with UKHSA (NIHR200915). A.S.W. is also supported by the NIHR Oxford Biomedical Research Centre and by core support from the Medical Research Council UK to the Medical Research Council Clinical Trials Unit (MC_UU_12023/22) and is an NIHR Senior Investigator.

The views expressed are those of the authors and not necessarily those of the NHS, NIHR, Department of Health, or UKHSA. The funder/sponsor did not have any role in the design and conduct of the study; collection, management, analysis, and interpretation of the data; preparation, review, or approval of the manuscript; and decision to submit the manuscript for publication.

About the Author

Ms. Harrison is a freelance epidemiologist with a research interest in infectious disease, reproductive health, and mental health in the public and private sectors.

References

1. World Health Organization. Coronavirus disease (COVID-19) weekly epidemiological update and weekly operational update. 2022 [cited 2022 Oct 4]. https://www.who.int/publications/m/item/weekly-epidemiological-update-on-covid-19—28-september-2022
2. Public Health England. Understanding cycle threshold (Ct) in SARS-CoV-2 RT-PCR [cited 2022 Feb 22]. https://assets.publishing.service.gov.uk/government/uploads/system/uploads/attachment_data/file/926410/Understanding_Cycle_Threshold__Ct__in_SARS-CoV-2_RT-PCR_.pdf
3. Caplan A, Bates KW, Brioni C, Santos A, Sabatini LM, Kaul KL, et al. Clinical characteristics and viral load dynamics of COVID-19 in a mildly or moderately symptomatic outpatient sample. PLoS One. 2021;16:e0258970. https://doi.org/10.1371/journal.pone.0258970
4. Walker AS, Pritchard E, House T, Robotham JV, Birrell PJ, Bell I, et al.; COVID-19 Infection Survey Team. Ct threshold values, a proxy for viral load in community SARS-CoV-2 cases, demonstrate wide variation across populations and over time. eLife. 2021;10:e64683. https://doi.org/10.7554/eLife.64683
5. Fox-Lewis A, Fox-Lewis S, Beaumont J, Drinković D, Harrower J, Howe K, et al. SARS-CoV-2 viral load dynamics and real-time RT-PCR cycle threshold interpretation in symptomatic non-hospitalised individuals in New Zealand: a multicentre cross sectional observational study. Pathology. 2021;53:530–5. https://doi.org/10.1016/j.pathol.2021.01.007
6. Liu Y, Yan LM, Wan L, Xiang TX, Le A, Liu JM, et al. Viral dynamics in mild and severe cases of COVID-19. Lancet Infect Dis. 2020;20:656–7. https://doi.org/10.1016/S1473-3099(20)30232-2
7. Lee LYW, Rozmanowski S, Pang M, Charlett A, Anderson C, Hughes GJ, et al. Severe acute respiratory syndrome coronavirus 2 (SARS-CoV-2) infectivity by viral load, S gene variants and demographic factors, and the utility of lateral flow devices to prevent transmission. Clin Infect Dis. 2022;74:407–15. https://doi.org/10.1093/cid/ciab421
8. Salvatore PP, Dawson P, Wadhwa A, Rabold EM, Buono S, Dietrich EA, et al. Epidemiological correlates of polymerase chain reaction cycle threshold values in the detection of severe acute respiratory syndrome coronavirus 2 (SARS-CoV-2). Clin Infect Dis. 2021;72:e761–7. https://doi.org/10.1093/cid/ciaa1469
9. Wölfel R, Corman VM, Guggemos W, Seilmaier M, Zange S, Müller MA, et al. Virological assessment of hospitalized patients with COVID-2019. Nature. 2020;581:465–9. https://doi.org/10.1038/s41586-020-2196-x
10. Howard-Jones AR, Maddocks S, Basile K, Dwyer DE, Branley J, Kok J. Prolonged PCR positivity in elderly patients infected with SARS-CoV-2. Pathology. 2021;53:914–6. https://doi.org/10.1016/j.pathol.2021.08.004
11. Shah S, Singhal T, Davar N, Thakkar P. No correlation between Ct values and severity of disease or mortality in patients with COVID 19 disease. Indian J Med Microbiol. 2021;39:116–7. https://doi.org/10.1016/j.ijmmb.2020.10.021
12. Aranha C, Patel V, Bhor V, Gogoi D. Cycle threshold values in RT-PCR to determine dynamics of SARS-CoV-2 viral load: an approach to reduce the isolation period for COVID-19 patients. J Med Virol. 2021;93:6794–7. https://doi.org/10.1002/jmv.27206
13. Zheng S, Fan J, Yu F, Feng B, Lou B, Zou Q, et al. Viral load dynamics and disease severity in patients infected with SARS-CoV-2 in Zhejiang province, China, January–March 2020: retrospective cohort study. BMJ. 2020;369:m1443. https://doi.org/10.1136/bmj.m1443
14. Fukushima T, Kabata H, Yamamoto R, Suhara T, Uwamino Y, Kondo Y, et al.; Keio Donner Project Team. The real-time reverse transcription-polymerase chain reaction threshold cycle values for severe acute respiratory syndrome coronavirus 2 predict the prognosis of coronavirus disease 2019 pneumonia. Respir Investig. 2021;59:360–3. https://doi.org/10.1016/j.resinv.2020.12.011
15. Rajyalakshmi B, Samavedam S, Reddy PR, Aluru N. Prognostic value of "cycle threshold" in confirmed COVID-19 patients. Indian J Crit Care Med. 2021;25:322–6. https://doi.org/10.5005/jp-journals-10071-23765
16. El Zein S, Chehab O, Kanj A, Akrawe S, Alkassis S, Mishra T, et al. SARS-CoV-2 infection: initial viral load (iVL) predicts severity of illness/outcome, and declining trend of iVL in hospitalized patients corresponds with slowing of the pandemic. PLoS One. 2021;16:e0255981. https://doi.org/10.1371/journal.pone.0255981
17. Faíco-Filho KS, Passarelli VC, Bellei N. Is higher viral load in SARS-CoV-2 associated with death? Am J Trop Med Hyg. 2020;103:2019–21. https://doi.org/10.4269/ajtmh.20-0954
18. Magleby R, Westblade LF, Trzebucki A, Simon MS, Rajan M, Park J, et al. Impact of severe acute respiratory syndrome coronavirus 2 viral load on risk of intubation and mortality among hospitalized patients with coronavirus disease 2019. Clin Infect Dis. 2021;73:e4197–205.
19. de la Calle C, Lalueza A, Mancheño-Losa M, Maestro-de la Calle G, Lora-Tamayo J, Arrieta E, et al. Impact of viral load at admission on the development of respiratory failure in hospitalized patients with SARS-CoV-2 infection. Eur J Clin Microbiol Infect Dis. 2021;40:1209–16. https://doi.org/10.1007/s10096-020-04150-w
20. Euser S, Aronson S, Manders I, van Lelyveld S, Herpers B, Sinnige J, et al. SARS-CoV-2 viral-load distribution reveals that viral loads increase with age: a retrospective cross-sectional cohort study. Int J Epidemiol. 2022;6;50:1795–1803.
21. Polese-Bonatto M, Sartor ITS, Varela FH, Giannini GLT, Azevedo TR, Kern LB, et al.; COVIDa Study Group. Children have similar reverse transcription polymerase chain reaction cycle threshold for severe acute respiratory syndrome coronavirus 2 in comparison with adults. Pediatr Infect Dis J. 2021;40:e413–7. https://doi.org/10.1097/INF.0000000000003300
22. Heald-Sargent T, Muller WJ, Zheng X, Rippe J, Patel AB, Kociolek LK. Age-related differences in nasopharyngeal severe acute respiratory syndrome coronavirus 2 (SARS-CoV-2) levels in patients with mild to moderate coronavirus disease 2019 (COVID-19). JAMA Pediatr. 2020;174:902–3. https://doi.org/10.1001/jamapediatrics.2020.3651

23. Puhach O, Adea K, Hulo N, Sattonnet P, Genecand C, Iten A, et al. Infectious viral load in unvaccinated and vaccinated patients infected with SARS-CoV-2 WT, Delta and Omicron. Nat Med. 2022;28:1491–1500. https://doi.org/10.1101/2022.01.10.22269010
24. Al Bayat S, Mundodan J, Hasnain S, Sallam M, Khogali H, Ali D, et al. Can the cycle threshold (Ct) value of RT-PCR test for SARS CoV2 predict infectivity among close contacts? J Infect Public Health. 2021;14:1201–5. https://doi.org/10.1016/j.jiph.2021.08.013
25. Singanayagam A, Patel M, Charlett A, Lopez Bernal J, Saliba V, Ellis J, et al. Duration of infectiousness and correlation with RT-PCR cycle threshold values in cases of COVID-19, England, January to May 2020. Euro Surveill. 2020;25:2001483. https://doi.org/10.2807/1560-7917.ES.2020.25.32.2001483
26. Falasca F, Sciandra I, Di Carlo D, Gentile M, Deales A, Antonelli G, et al. Detection of SARS-COV N2 gene: very low amounts of viral RNA or false positive? J Clin Virol. 2020;133:104660. https://doi.org/10.1016/j.jcv.2020.104660
27. Bridge JA. Reverse transcription-polymerase chain reaction molecular testing of cytology specimens: pre-analytic and analytic factors. Cancer Cytopathol. 2017;125:11–9. https://doi.org/10.1002/cncy.21762
28. Walker AS, Vihta KD, Gethings O, Pritchard E, Jones J, House T, et al. Tracking the emergence of SARS-CoV-2 Alpha variant in the United Kingdom. N Engl J Med. 2021;385:2582-5.
29. National Health ServiceS. Get tested for coronavirus (COVID-19) [cited 2022 Mar 17]. https://www.nhs.uk/conditions/coronavirus-covid-19/testing/get-tested-for-coronavirus
30. Smith BF, Graven PF, Yang DY, Downs SM, Hansel DE, Fan G, et al. Using spike gene target failure to estimate growth rate of the Alpha and Omicron variants of SARS-CoV-2. J Clin Microbiol. 2022;60:e0257321. https://doi.org/10.1128/jcm.02573-21
31. Hay JA, Kennedy-Shaffer L, Kanjilal S, Lennon NJ, Gabriel SB, Lipsitch M, et al. Estimating epidemiologic dynamics from cross-sectional viral load distributions. Science. 2021;373:eabh0635. https://doi.org/10.1126/science.abh0635
32. Abdulrahman A, Mallah SI, Alawadhi A, Perna S, Janahi EM, AlQahtani MM. Association between RT-PCR Ct values and COVID-19 new daily cases: a multicenter cross-sectional study. Infez Med. 2021;29:416–26. https://doi.org/10.53854/liim-2903-13
33. Rodríguez-Grande C, Catalán P, Alcalá L, Buenestado-Serrano S, Adán-Jiménez J, Rodríguez-Maus S, et al.; Gregorio Marañón Microbiology-ID COVID 19 Study Group. Different dynamics of mean SARS-CoV-2 RT-PCR Ct values between the first and second COVID-19 waves in the Madrid population. Transbound Emerg Dis. 2021;68:3103–6. https://doi.org/10.1111/tbed.14045
34. Shoaib N, Iqbal A, Shah FA, Zainab W, Qasim M, Zerqoon N, et al. Population-level median cycle threshold (Ct) values for asymptomatic COVID-19 cases can predict the trajectory of future cases. PLoS One. 2023;18:e0281899. https://doi.org/10.1371/journal.pone.0281899
35. Veronesi L, Colucci ME, Pasquarella C, Caruso L, Mohieldin Mahgoub Ibrahim M, Zoni R, et al. Virological surveillance of SARS-CoV-2 in an Italian northern area: comparison of real time RT PCR cycle threshold (Ct) values in three epidemic periods. Acta Biomed. 2020;91(9-S):19–21.
36. Yin N, Dellicour S, Daubie V, Franco N, Wautier M, Faes C, et al. Leveraging of SARS-CoV-2 PCR cycle thresholds values to forecast COVID-19 trends. Front Med (Lausanne). 2021;8:743988 https://doi.org/10.3389/fmed.2021.743988
37. Tso CF, Garikipati A, Green-Saxena A, Mao Q, Das R. Correlation of population SARS-CoV-2 cycle threshold values to local disease dynamics: exploratory observational study. JMIR Public Health Surveill. 2021;7:e28265. https://doi.org/10.2196/28265
38. World Health Organization. Coronavirus disease 2019 (COVID-19) situation report–52 [cited 2023 Jun 18]. https://www.who.int/docs/default-source/coronaviruse/situation-reports/20200312-sitrep-52-covid-19.pdf

Address for correspondence: Rebecca E. Harrison, UKHSA, Nobel House, 17 Smith Sq, London SW1P 3JR, UK; email: rebecca8harrison@gmail.com

Comprehensive Case–Control Study of Protective and Risk Factors for Buruli Ulcer, Southeastern Australia

Bridgette J. McNamara, Kim R. Blasdell, Arvind Yerramilli, Ina L. Smith, Simone L. Clayton, Michael Dunn, Ee Laine Tay, Katherine B. Gibney, Nilakshi T. Waidyatillake, Mohammad A. Hussain, Michael Muleme, Daniel P. O'Brien,[1] Eugene Athan[1]

To examine protective and risk factors for Buruli ulcer (BU), we conducted a case–control study of 245 adult BU cases and 481 postcode-matched controls across BU-endemic areas of Victoria, Australia. We calculated age- and sex-adjusted odds ratios for socio-environmental, host, and behavioral factors associated with BU by using conditional logistic regression. Odds of BU were >2-fold for persons with diabetes mellitus and persons working outdoors who had soil contact in BU-endemic areas (compared with indoor work) but were lower among persons who had bacillus Calmette–Guérin vaccinations. BU was associated with increasing numbers of possums and with ponds and bore water use at residences. Using insect repellent, covering arms and legs outdoors, and immediately washing wounds were protective; undertaking multiple protective behaviors was associated with the lowest odds of BU. Skin hygiene/protection behaviors and previous bacillus Calmette–Guérin vaccination might provide protection against BU in BU-endemic areas.

Buruli ulcer (BU) is a necrotizing infection of the skin and soft tissue caused by the environmental bacterium *Mycobacterium ulcerans* (*1*,*2*) and is 1 of 20 neglected tropical diseases recognized by the World Health Organization (*3*). BU often begins as a small papule or plaque with progressive ulceration if left untreated (*4*). The incubation period is ≈4–5 months, whereas the average delay from symptom onset to diagnosis is 1–2 months (*5*–*7*). Although sporadic cases have been noted globally, BU remains endemic in sub-Saharan Africa and more temperate southeastern Australia, 2 regions with vastly differing social and environmental conditions (*8*). In southeastern Australia, cases are most frequently detected in Mornington and Bellarine Peninsulas, regions on opposite sides of Port Philip Bay in Victoria state (*6*). BU case numbers have increased markedly in the previous decade in Victoria; disease-endemic areas within the region have expanded (*9*,*10*), but the reasons remain unclear.

The exact mechanisms of *M. ulcerans* transmission are elusive and might differ between endemic areas. Nevertheless, research has revealed certain key variables; leading theories involve insect bites or environmental contamination through minor trauma or existing wounds (*2*,*11*). In southeastern Australia, possums evidently play a crucial role as an animal reservoir that can sustain clinical disease and shed viable *M. ulcerans* through feces (*12*–*14*). Two species in particular, the common brushtail (*Trichosurus vulpecula*) and common ringtail (*Pseudocherius peregrinus*) possums, have been implicated as reservoir hosts. Furthermore, research in Australia reports mosquitoes as possible mechanical vectors (*15*–*17*).

Author affiliations: Barwon Health, Geelong, Victoria, Australia (B.J. McNamara, A. Yerramilli, M.A. Hussain, M. Muleme, D.P. O'Brien, E. Athan); University of Melbourne, Melbourne, Victoria, Australia (B.J. McNamara, K.B. Gibney, N.T. Waidyatillake, D.P. O'Brien); Commonwealth Scientific and Industrial Research Organisation, Geelong (K.R. Blasdell, S.L. Clayton, M. Dunn); Commonwealth Scientific and Industrial Research Organisation, Canberra, Australian Capital Territory, Australia (I.L. Smith); Department of Health, Melbourne (E.L. Tay); Peter Doherty Institute for Infection and Immunity, Melbourne (K.B. Gibney); Deakin University, Waurn Ponds, Victoria, Australia (N.T. Waidyatillake, E. Athan)

DOI: https://doi.org/10.3201/eid2910.230011

[1]These senior authors contributed equally to this article.

A previous questionnaire-based case–control study in Victoria showed that being bitten by mosquitoes increased the odds of *M. ulcerans* infection, whereas wearing protective clothing or applying insect repellent decreased the odds (*18*). In contrast, no convincing evidence exists that mosquitoes play a role in *M. ulcerans* transmission in West Africa. *M. ulcerans DNA* has been detected in environmental samples of other insects from aquatic areas in West Africa, such as water bugs (Hemiptera), dragonfly larvae (Odonata), and beetle larvae (Coleoptera) (*2*).

Environmental and climate factors also appear to play a critical role in *M. ulcerans* transmission dynamics. In Africa, cases of BU occur proximate to natural water bodies (*2*). Heavy rainfall and subsequent flooding have also been associated with increased detection of *M. ulcerans* in the environment and increased BU case numbers in certain regions (*9*,*19*). Environmental surveys, conducted as a separate part of this research project, showed that the odds of *M. ulcerans* bacteria existing within a property increased with the presence of certain native plant species, alkaline soil, and lower altitude, along with the presence of overhead powerlines and common ringtail possums (*14*).

Cleaning wounds immediately after trauma and the use of *Mycobacterium bovis* bacillus Calmette–Guérin (BCG) vaccination (for tuberculosis, also caused by a mycobacterium) might mitigate the risk of acquiring BU, although evidence regarding BCG vaccination is conflicting (*18*,*20*,*21*). In addition, BU lesions are common on exposed body areas, consistent with the premise that protective clothing might decrease BU risk by reducing insect bites and minor skin trauma that can cause potential inoculating events (*22*,*23*).

Determining risks and protective factors for BU is crucial to determine effective intervention and control strategies. Therefore, we conducted a case–control study to identify environmental, host, and behavioral risk and protective factors associated with BU in Victoria, Australia, where increasing cases and expanding BU-endemic areas have been observed.

Methods

Study Design and Participants

We performed a postcode matched, case–control study in BU-endemic areas surrounding Port Phillip Bay, Victoria, Australia (Figure 1; Appendix Table 1, https://wwwnc.cdc.gov/EID/article/29/10/23-0011-App1.pdf). Ethics approval was granted by the Victoria Department of Health Human Research Ethics Committee (project 10–18). We invited adults (≥18 years of age) to participate in the study who resided in Victoria and were notified to the Department of Health in Victoria as having laboratory-confirmed BU during June 2018–June 2020. We extracted case data from the Victoria Department of Health Public Health Events Surveillance System. We recruited case-patients via regular mail after receiving permission for contact from the patient's general practitioner or treating medical team. We restricted analysis to residents or holiday homeowners in the study areas (Figure 2).

We matched control participants (residents of Victoria ≥18 years of age) to patients according to residential postal codes within the study area. We selected controls from both the Victorian Population Health Survey (participants who had provided consent to be contacted for other research studies) and the electoral roll of Australia (when additional matched controls

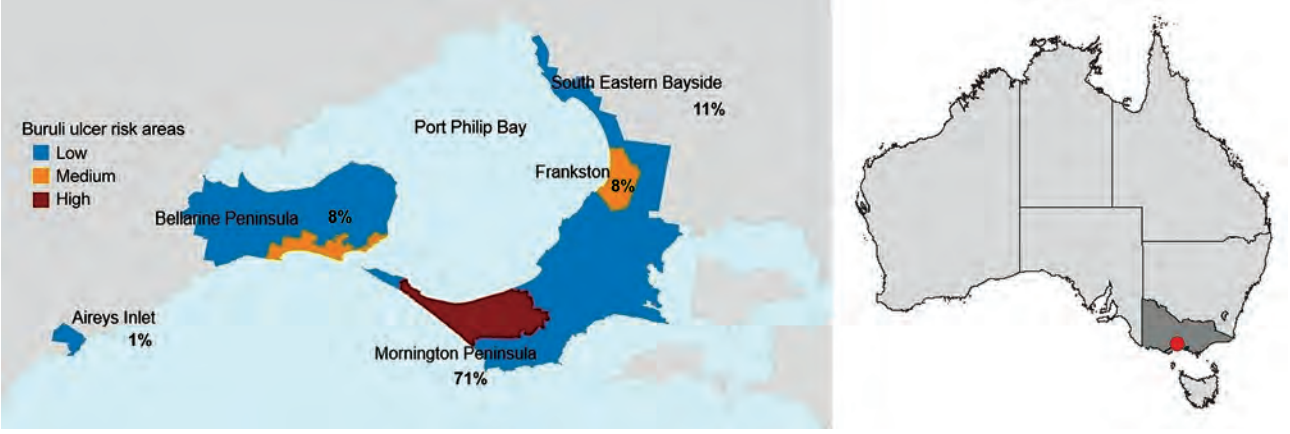

Figure 1. Locations of Buruli ulcer–endemic areas included in comprehensive case-control study of protective and risk factors for Buruli ulcer, Victoria, Australia. Colors indicate risk classifications at beginning of the study period, and numbers indicate percentage of total participating case-patients for each location within the study area. Full map of Australia shows study area in southeastern region.

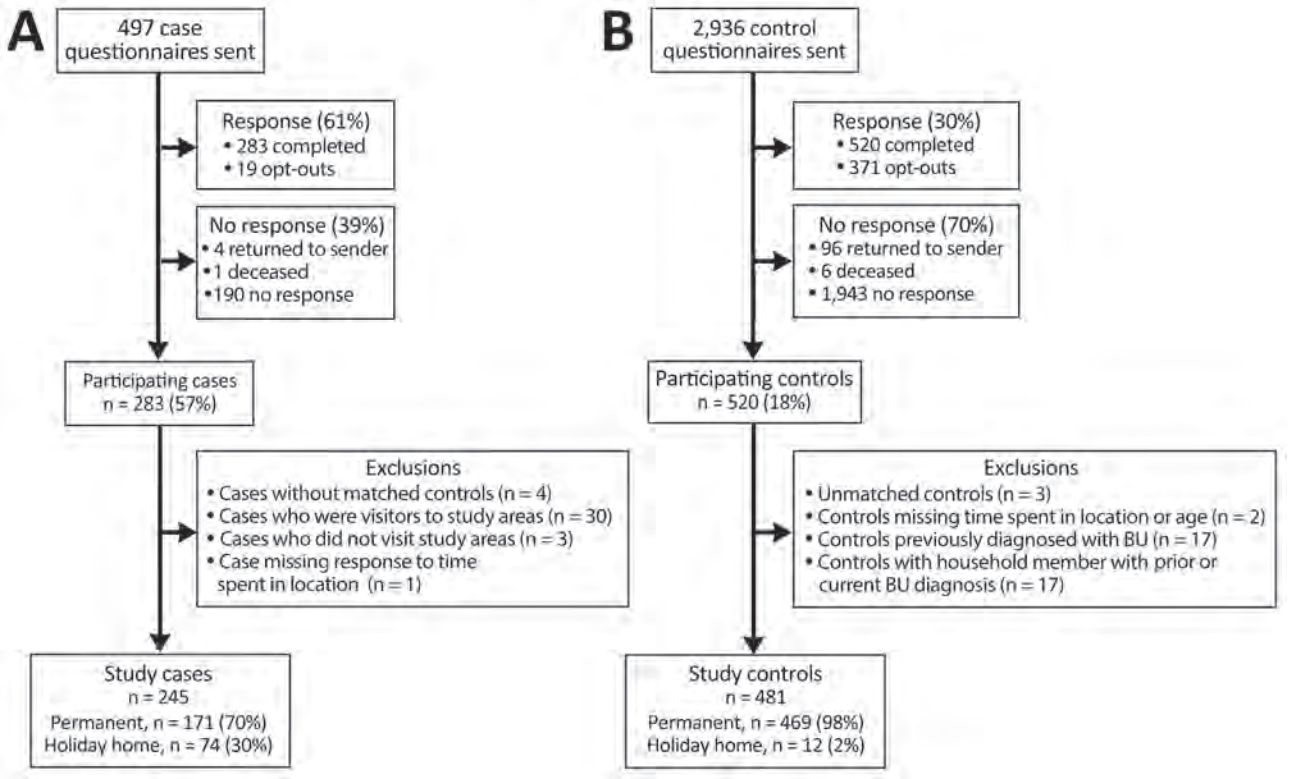

Figure 2. Flow diagrams of study recruitment, participation, and exclusion criteria in comprehensive case–control study of protective and risk factors for Buruli ulcer, southeastern Australia. A) Case-patient recruitment; B) control recruitment.

were required for a particular postcode). We excluded controls if they or a household member had been previously diagnosed with BU (Figure 2).

Participation for both patients and controls involved the return of a completed study questionnaire. In addition, a subsample of patients and controls were enrolled in an environmental survey of residential properties that investigated the presence of *M. ulcerans* (*14*).

Data Collection and Measurements

We used a self-administered questionnaire to examine the amount of time participants spent in the study areas, outdoor and lifestyle behaviors, insect exposure, medical history, and environmental characteristics of the participants' properties. We evaluated those details and formulated response and collapsed categories for analysis (Appendix Table 2). Participant-reported medications and conditions that might affect the immune system were reviewed by a physician specializing in infectious diseases (D.P.O.) to ascertain those likely to cause immunosuppression. We devised an occupational classification related to potential environmental exposure to *M. ulcerans* through employment by using participant responses to 2 questions: what proportion of your time do you spend outside as part of your occupation and are you in contact with the soil during your work? We examined the effects of working outdoors and having soil contact among participants whose employment was based in the study (disease-endemic) areas only.

Statistical Analysis

We evaluated host, environmental, and behavioral factors according to BU case status. We examined relationships between those factors and the likelihood of developing BU by using multivariable conditional logistic regression; cases and controls were matched by postcode. We calculated odds ratios adjusted for age and sex (aORs) and 95% CIs for the total participant sample (residents and holiday homeowners) and separately for residents only (Appendix Tables 3–11). Percentages of missing data were generally low (<3% for most factors); if missing data were >10%, we included a separate category for those participants with missing exposure data in the model unless otherwise stated. Given the expectation that participants might have multiple potentially protective health behaviors, we examined patterns and

clustering of those behaviors by using polychoric correlations and exploratory factor analysis (Appendix; Appendix Figures 2, 3).

We conducted a post-hoc sensitivity analysis to explore the robustness of the observed relationship between BCG vaccination and BU case status; we restricted analysis to participants 47–70 years of age who were within the age-range eligible for BCG vaccination as part of the routine vaccination schedule for schoolchildren in Victoria from the 1950s to 1985 (*24*). We analyzed those reporting receipt of BCG vaccination and those unsure of vaccination status as a single category (under the assumption of likely vaccination through routine vaccination) and compared them with age-matched participants reporting no BCG vaccination. We performed analyses by using Stata 15 (StataCorp LLC, https://www.stata.com) except for factor analysis, which we performed by using Stata 16.

Results

Demographic and Clinical Characteristics of Participants

We examined data from 245 (57% participation rate) BU case-patients and 481 (18%) postcode-matched control participants from across the BU-endemic areas; 171 (70%) patients and 469 (97.5%) controls were permanent residents in the study areas, and most (71%) were homeowners in high BU-endemic areas of Mornington Peninsula (Figure 1). Half (123/245) of case-patients were 60–79 years of age, signifying an overrepresentation when compared with all notified cases in the study areas (204/550 [37%] 60–79 years of age). In contrast, patients 18–39 years of age were underrepresented in our participant sample (35/245 [14%] compared with 134/550 [24%] among notified cases) (Appendix Table 12). We also observed an overrepresentation of controls 60–79 years of age and a large underrepresentation of controls 18–39 years of age when compared with population proportion estimates (Appendix Table 12). Male sex was associated with BU case status (57.6% of BU cases vs. 44.7% of controls; aOR 1.52 [95% CI 1.06–2.19]).

BU cases were reported predominantly during winter (44%) and spring (38%) (Table; Appendix Figure 1). The median time between symptom onset and diagnosis was 5 (interquartile range [IQR] 3–12) weeks; duration was longer for patients who were holiday homeowners (8 [IQR 4–13]) weeks than for those who were residents (4 [IQR 3–10] weeks; p<0.0001 by rank-sum test). An insect bite, wound, or injury to the affected area was reported in 36% of BU cases before ulcers appeared.

Host Factors

We evaluated associations between host factors and BU case status (Figure 3). Persons with a history of diabetes mellitus had a higher probability of developing BU than those without diabetes (aOR 2.26 [95% CI 1.13–4.49]). An association was observed with prednisolone therapy (aOR 2.56 [95% CI 1.28–5.13]); however, this result could be confounded by persons commencing prednisolone therapy during their BU treatment.

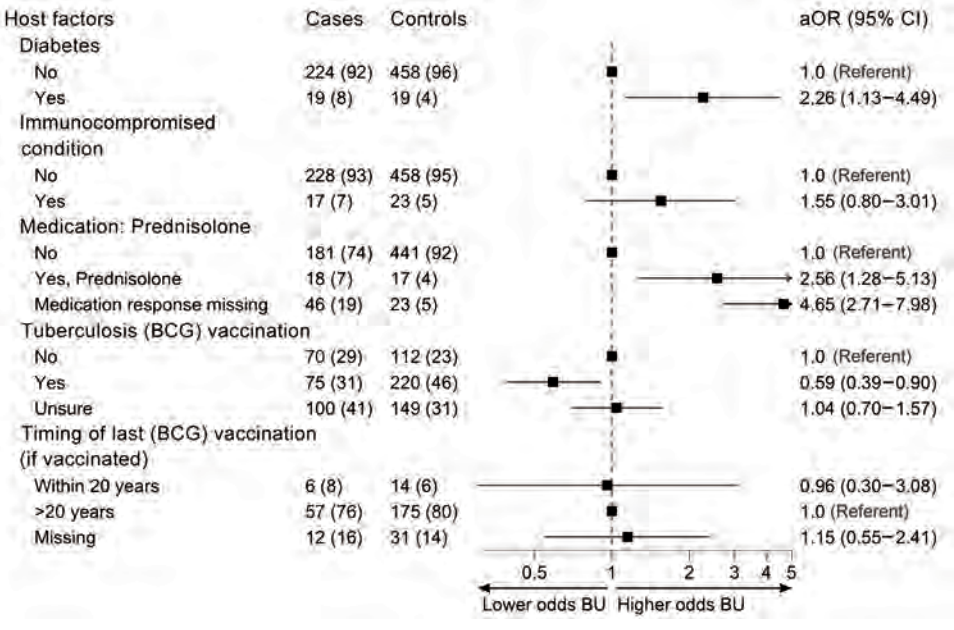

Figure 3. Odds of developing Buruli ulcer according to different host factors in comprehensive case–control study of protective and risk factors for Buruli ulcer, southeastern Australia. Host characteristics are shown for case-patients and control participants as no. (%). Odds ratios (adjusted according to age and sex) and 95% CIs are indicated. Vaccination was with *Mycobacterium bovis* BCG vaccine for tuberculosis. Immunocompromised conditions category was for any participant who reported a condition that had the potential to compromise the immune system (excluding diabetes and cancer [active or historical]; cancer status was not available in this study). aOR, adjusted odds ratio; BCG, bacillus Calmette-Guérin vaccine; BU, Buruli ulcer.

Receipt of BCG vaccination was associated with lower odds of BU (aOR 0.59 [95% CI 0.39–0.90]) than for participants reporting no BCG vaccination. No relationship between BU and vaccination timing (<20 or >20 years ago) was observed. Of note, 41% of patients and 31% of controls reported that they were unsure whether they had received the vaccination. In the sensitivity analysis that restricted participant age to 47–70 years (those unsure were assumed vaccinated), the observed association between BU and BCG vaccination persisted but was attenuated; aOR was 0.71 (95% CI 0.41–1.22) for the entire age-restricted participant sample (Appendix Table 11).

Environmental Factors

The presence of possums around the property was strongly associated with BU in residents (aOR 5.30 [95% CI 1.82–15.49]) and, to a lesser extent, in the entire participant sample (aOR 2.33 [95% CI 1.15–4.71]). The likelihood of developing BU increased with the number of possums reported around the residential property (Figure 4; Appendix Table 5); large amounts of possum feces (compared with none) (aOR 1.88 [95% CI 1.05–3.36]); and with the presence of tea trees (*Leptospermum* sp.), a common habitat for possums, on the property (aOR 1.72 [95% CI 1.10–2.69]).

Most (98%) properties used piped (town) water for drinking, bathing, and garden watering. Participants drinking filtered town water (274/721, 38% of total participants) had lower odds of developing BU than those not drinking filtered town water (aOR 0.64 [95% CI 0.46–0.90]). Of those not drinking filtered town water, 433/447 (97%) drank unfiltered town water, and 14 (3%) drank water from other sources only, such as tank or bottled water. Use of bore water by residents for bathing or garden watering was associated with BU (aOR 1.56 [95% CI 0.98–2.50]). Water sources around the property were not associated with BU case status, except for the presence of ponds (aOR 1.69 [95% CI 0.99–2.89]) for residents (Figure 4). We observed no associations between case status and the presence of other nonpossum wildlife or biting insects; use of garden products (mulch or potting mix)

Table. Characteristics of patients and disease manifestations in comprehensive case–control study of protective and risk factors for Buruli ulcer, southeastern Australia*

Characteristics	Cases, n = 245	Controls, n = 481
Age group, y		
18–39	35 (14)	38 (8)
40–59	68 (28)	125 (26)
60–79	123 (50)	278 (58)
≥80	19 (8)	40 (8)
Sex		
F	104 (42)	266 (55)
M	141 (58)	215 (45)
Employment status†		
Employed	124 (51)	211 (44)
Unpaid employment, unemployed	19 (8)	18 (4)
Retired	100 (41)	249 (52)
Notification dates		
Summer, Dec–Feb	26 (11)	NA
Autumn, Mar–May	18 (7)	NA
Winter, Jun–Aug	107 (44)	NA
Spring, Sep–Nov	94 (38)	NA
Duration of symptoms before diagnosis, wk		
Median (IQR)	5 (3–12)	NA
Missing data	21 (9)	NA
Days from notification to questionnaire completion		
Median (IQR)	56 (38–90)	NA
Insect bite/wound/injury to area before ulcer developed		
Yes	99 (40)	NA
No	42 (17)	NA
Unsure	88 (36)	NA
Missing data	16 (7)	NA
Type of bite/wound/injury in area before ulcer developed, n = 99		
Insect bite	51 (52)	NA
Wound/injury	30 (30)	NA
Mixed	6 (6)	NA
Other, unsure/missing data	12 (12)	NA
Time from wound/bite to ulcer, if yes, n = 87		
Median, weeks (IQR)	6 (3–13)	NA

*Values are no. (%) except as indicated. IQR, interquartile range; NA, not applicable.
†Unpaid employment included students and persons with home duties.

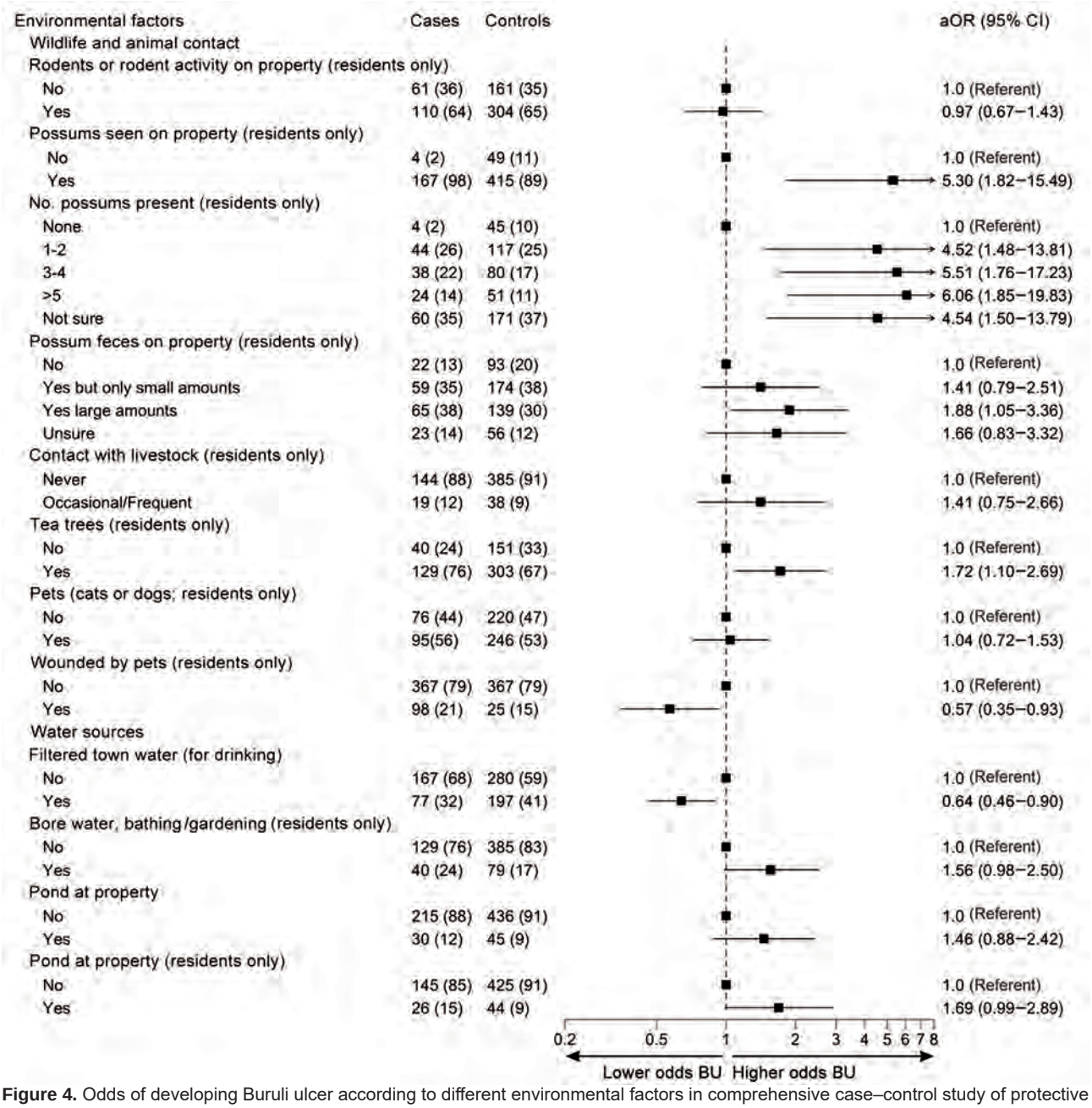

Figure 4. Odds of developing Buruli ulcer according to different environmental factors in comprehensive case–control study of protective and risk factors for Buruli ulcer, southeastern Australia. Environmental factors are shown for case-patients and control participants as no. (%). Odds ratios (adjusted according to age and sex) and 95% CIs are indicated. aOR, adjusted odds ratio; BU, Buruli ulcer.

among residents; or with earthworks, major renovations, or sewerage works near the property (Appendix Table 7).

Exposures

Working outdoors was associated with higher odds of BU than working indoors in BU-endemic areas (Figure 5); highest odds were associated with occupations involving soil contact (aOR 2.89 [95% CI 1.01–8.25]). Outdoor occupations that involved soil contact were commonly gardeners, carpenters, and other construction-related roles.

We found no association between gardening frequency and BU case status among residents (Figure 5); however, the entire participant sample comprising more holiday homeowner cases had lower odds for BU (aOR 0.50 [95% CI 0.34–0.74]). Participants partaking in outdoor activities (>95% of participants)

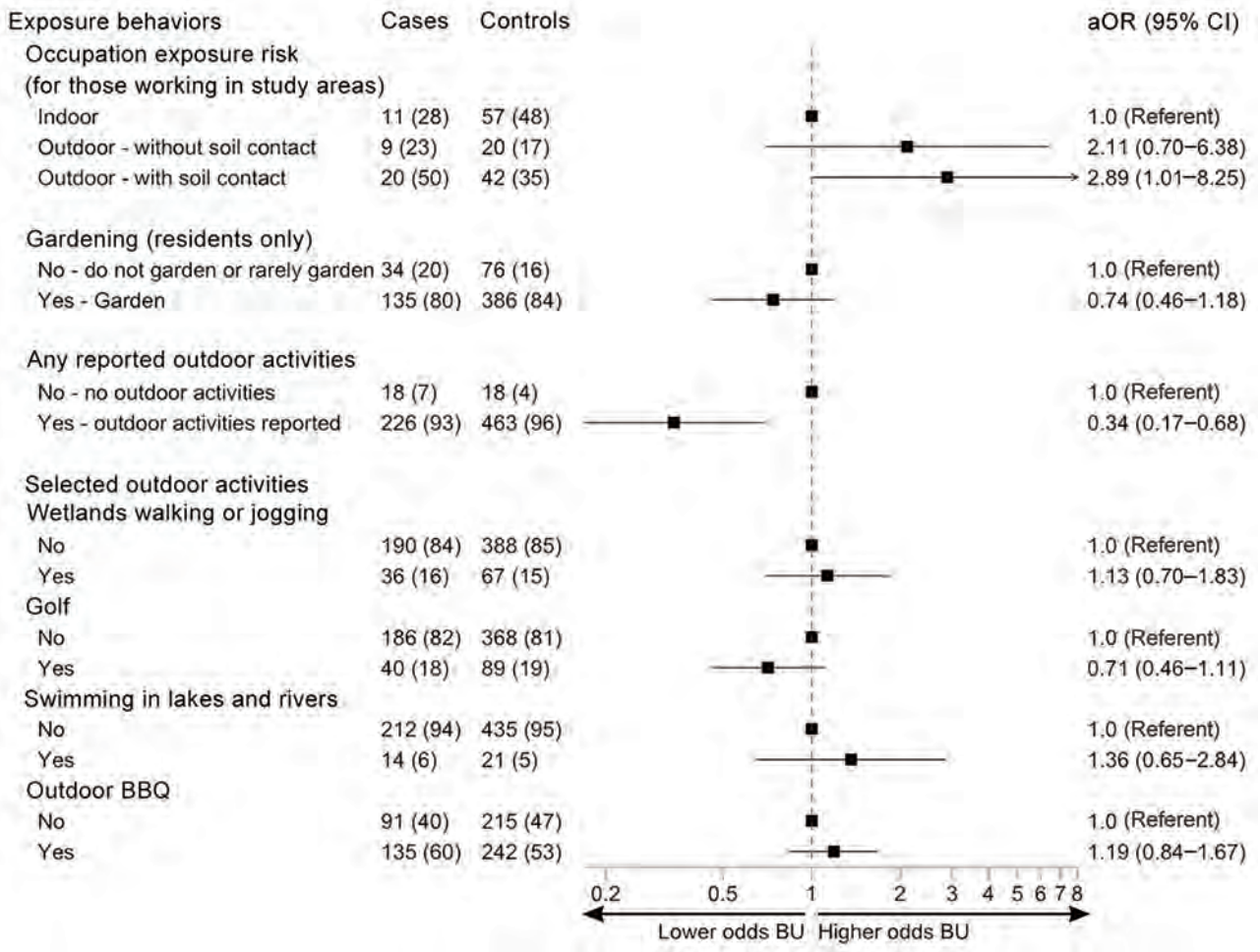

Figure 5. Odds of developing Buruli ulcer according to potential outdoor exposures in comprehensive case–control study of protective and risk factors for Buruli ulcer, southeastern Australia. Potential outdoor exposures are shown for case-patients and control participants as no. (%). Odds ratios (adjusted according to age and sex) and 95% CIs are indicated. aOR, adjusted odds ratio; BBQ, barbeque; BU, Buruli ulcer.

had a lower likelihood of developing BU than those not undertaking outdoor activities (aOR 0.34 [95% CI 0.17–0.68]). However, we observed no strong associations between participants undertaking individual activities (beach walks/jogging, wetland walks/jogging, bushwalking, golf, sports on an oval, swimming in local lakes/rivers, sailing, outdoor barbeques, or other activities) and those not undertaking the activity (Appendix Table 9).

Protective Behavioral Factors

We analyzed associations between protective health behaviors and BU case status (Figure 6). Several protective behaviors were associated with lower odds of developing BU: tending immediately to cuts and scratches received during outdoor activity by washing the area and then applying antiseptic or dressings (aOR 0.56 [95% CI 0.36–0.87]), wearing insect repellant during warmer months (aOR 0.62 [95% CI 0.43–0.89]), and covering arms and legs with clothing (aOR 0.59 [95% CI 0.36–0.90]). Participants who combined protective behaviors had the strongest correlations between tending to new wounds, covering preexisting wounds, washing hands after outdoor activity, and using gloves for gardening (Appendix Figures 2, 3). Combining protective behaviors was associated with lower odds of BU; we observed a gradient of decreasing odds for BU in those undertaking higher numbers of protective behaviors (Figure 6).

Discussion

We conducted a comprehensive case–control study in temperate, BU-endemic areas of Victoria, Australia, and found that the presence of possums or a pond on residential property was a key environmental factor

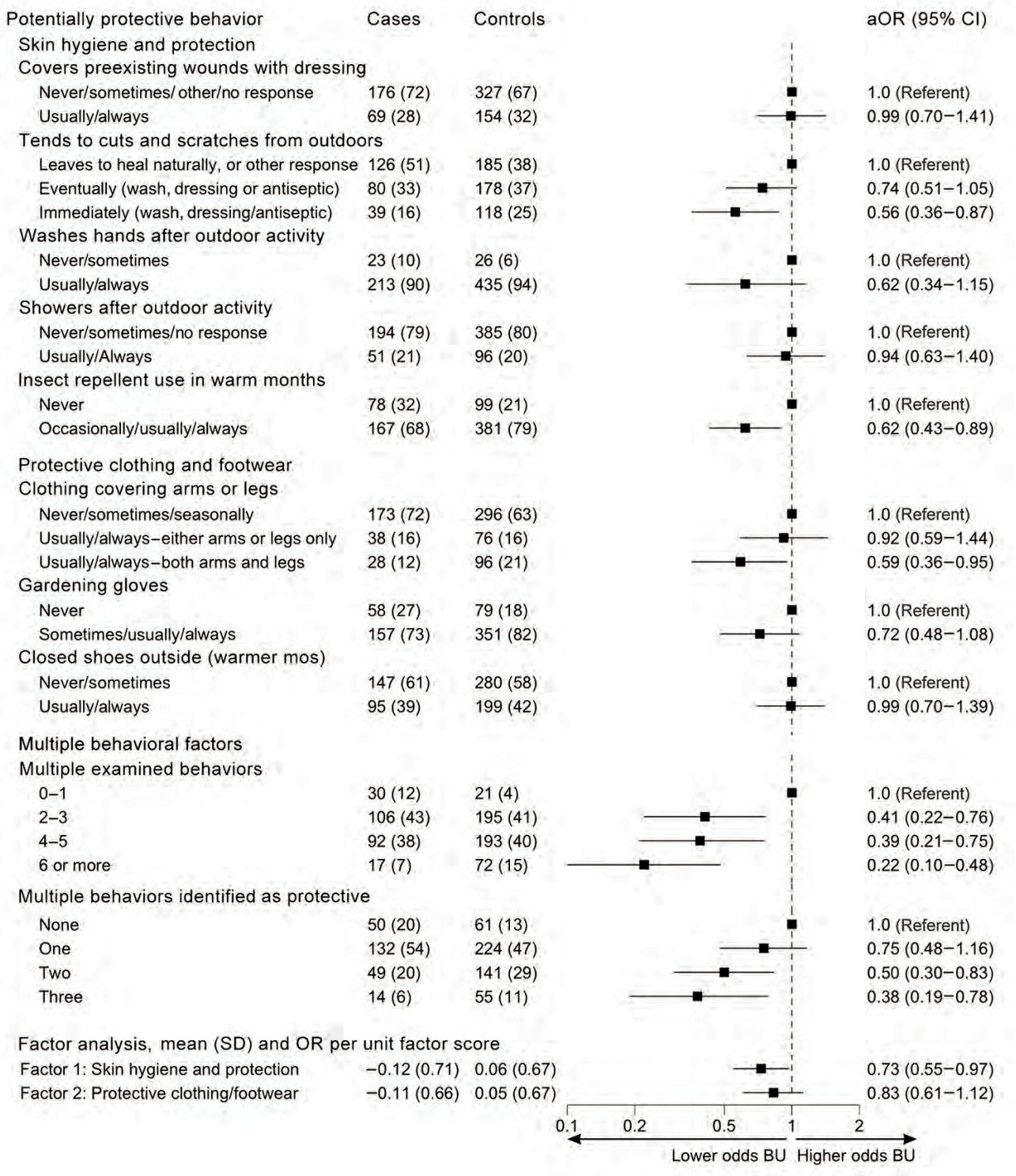

Figure 6. Odds of developing Buruli ulcer according to protective behavioral factors in comprehensive case-control study of protective and risk factors for Buruli ulcer, southeastern Australia. Potential protective behavioral factors are shown for case-patients and control participants as no. (%), except for factor analyses, which are shown as mean (SD). Odds ratios (adjusted according to age and sex) and 95% CIs are indicated. Includes binary variable for tending to outdoor cuts and scratches immediately (usually/always vs all other responses). aOR, adjusted odds ratio; BU, Buruli ulcer; OR, odds ratio.

for BU, whereas having diabetes mellitus and working outdoors (especially in contact with soil) were key host factors associated with higher probability of developing BU. We identified modifiable health behaviors for public health intervention relating to skin hygiene and protection, including tending immediately to outdoor cuts and scratches by cleaning and applying antiseptic or dressing, using insect repellant, and covering arms and legs with clothing. Moreover, undertaking multiple protective behaviors was associated with lower odds of developing BU. We found a protective association between BCG vaccination and BU, as well as the unexpected finding of a protective association for drinking filtered town water compared with unfiltered water, which warrants further investigation. We found no evidence for associations between BU and other hypothesized risks, including gardening, other outdoor leisure activities, pet ownership, major renovations or earthworks, or sewerage type or works.

Our findings strengthen the evidence for possums as a key mammal reservoir of *M. ulcerans* in Victoria (*12*,*14*). Possums can become infected with *M. ulcerans*; >40% of possum fecal samples collected in 1 BU-endemic area were positive for *M. ulcerans* DNA, and a considerable proportion of possums displayed BU skin lesions (*12*). The environmental survey component of this study found possum feces to be a key source of viable bacteria (*14*); *M. ulcerans* DNA was found in 23% and viable *M. ulcerans* bacteria in 5% of all ringtail possum fecal samples (*14*). According to participant responses, we found that increased likelihood of BU was associated with increasing numbers of possums at the participant's property and with increasing amounts of possum feces. The number of tea trees, a common possum habitat, on the property was also highly associated with BU case status.

The involvement of aquatic environments has been suggested for *M. ulcerans* transmission in BU-endemic areas of West Africa, but limited evidence has been found in Victoria (*2*,*11*). In our study, residential ponds and use of bore water were associated with BU. Contributions to BU incidence remain unclear for direct contact with contaminated water; ponds providing habitat for mosquitoes, which could act as mechanical vectors; or ponds attracting mammal reservoirs. The protective association found for piped, filtered town drinking water was unexpected; town water catchments for BU-endemic areas also provide water to many nonendemic metropolitan areas; thus, the protective association for water filtration might reflect other unmeasured confounding factors affecting BU risk. Furthermore, correlations between drinking filtered water and other potentially protective behaviors were relatively weak (correlation coefficient <0.18), and clustering of those behaviors does not appear to explain the association. Although *M. ulcerans* infection in the gastrointestinal tract of infected possums has been reported (*25*), whether *M. ulcerans* exposure via ingestion could result in BU skin lesions in humans is unclear. The relationship between bore water and BU might not indicate bore water use is a risk factor for BU; rather, bore water might be associated with the presence of *M. ulcerans* in the environment, such as in plants or possums.

Mosquitoes have been proposed as likely mechanical vectors for BU in Australia but are less likely candidates in West Africa (*11*). We did not find associations between reported levels of local mosquitoes or other biting insects and BU. However, we did find a protective association between BU and use of insect repellant, consistent with a previous case–control study on Bellarine Peninsula in Victoria, where 72% lower odds of BU were found among persons using insect repellent (*18*). In contrast to that study, we found a relatively higher percentage of persons reporting insect repellent use (68% vs. 31% of case-patients and 79% vs. 54% of controls). Our results indicate a positive public health development, given the role of mosquitoes in transmission of several arboviral diseases, and might be the result of local public health campaigns (*10*), such as Beat the Bite (https://www.betterhealth.vic.gov.au/sites/default/files/2021-10/Beat-the-bite-brochure.pdf).

Skin protection and skin hygiene behaviors were associated with lower odds of BU. We found that tending to cuts and scratches during outdoor activity by stopping immediately to wash the area and applying antiseptic or a dressing had the strongest protective association, which is consistent with previous studies in Australia (*18*) and Cameroon (*26*). However, our study adds new evidence suggesting a dose-response association that indicates the timeliness of tending to wounds might also help prevent BU; lower odds of BU were observed for immediate treatment compared with leaving the wound alone or tending eventually. Cuts and scratches obtained during outdoor activities or work might increase inoculating events with *M. ulcerans*, which might be present on the skin after contact with contaminated soil, plants, or water. Laboratory studies have demonstrated that a needle puncture or mosquito bite on contaminated skin was sufficient for *M. ulcerans* to enter the skin of mice and cause an ulcer (*15*). In our study, bites or wounds were reported in 40% of cases before ulcer

appearance; some participants recalled specific injuries to the area that preceded ulcer development.

The higher odds of BU in persons with diabetes is similar to findings for other mycobacterial diseases, such as tuberculosis and leprosy (*27*), and might reflect increased risk because of impaired cellular immunity (*28*). Targeted messaging highlighting the importance of protective measures might help prevent BU in persons with diabetes.

We showed that BCG vaccination was highly protective against BU (aOR 0.59 [95% CI 0.39–0.90]). Protective effects of BCG vaccination against tuberculosis and leprosy have been well established (*29*). The vaccine is derived from a live attenuated strain of *M. bovis* and shares epitopes with other nontuberculous mycobacteria (*20*). Previous case–control studies showed conflicting evidence that BCG vaccination prevents *M. ulcerans* infection (*29*–*32*). Two randomized controlled trials demonstrated a protective effect of BCG vaccination against BU (*33*,*34*); a lower incidence of BU in persons vaccinated with BCG compared with unvaccinated persons was observed in Uganda, with a combined relative risk estimate of 0.50 (95% CI 0.37–0.69) (*20*). However, both of those studies demonstrated only short-term efficacy up to 1 year after vaccination; longer-term follow up and analysis were not performed because of limited sample size. Using different antigenic strains of BCG might enhance or lengthen protection against nontuberculous mycobacteria or BU (*20*,*29*), whereas revaccination could also provide more sustained immunity to *M. ulcerans* infection, although this idea has not been comprehensively explored (*20*). Further research on the potential role of BCG vaccination for protection against BU is warranted.

A key strength of our study of BU risk factors is the use of a population-based notifiable disease database for case detection that ensured robust ascertainment of laboratory-confirmed BU from almost all BU-endemic locations in Victoria. Compared with a previous case–control study in the Bellarine Peninsula, Victoria (*18*), this study also examined a comprehensive list of environmental, host and behavioral risk, and protective factors, and we have identified new public health-related risk groups and environmental risk factors. The graded responses observed for certain individual protective behaviors as well as multiple combined behaviors offers strong evidence and support for causal inference despite the limitations of the observational study design.

The first limitation of our study is the potential for recall bias given the long disease incubation period, potential for differential recall if patients were more aware of hypothesized transmission pathways than controls, and potential effects of seasonality on recall by matched controls who were recruited after the patients. Second, potential selection bias was noted because of differential participation between patients and controls; younger patients were more likely to participate than younger control participants, and a greater proportion of holiday homeowners existed among BU cases. Despite those limitations, survey completion in this study was rapid (within 2 months of diagnosis for most cases) compared with the previous case–control study in Victoria (*18*), which had a median completion rate of 1.5 years postdiagnosis. We adjusted all analyses for age and sex, and the postcode-matched design helped account for unmeasured socioeconomic and environmental differences across the BU-endemic areas. By analyzing results for the entire cohort and separately for residents only, we found strong associations among the resident cohort and differential effects of home ownership. Finally, our findings are relevant to Victoria, Australia, and might offer insights relevant to other areas; however, those data might not be immediately generalizable to other parts of the world.

In conclusion, our study identifies environmental and host factors associated with BU and simple behaviors relating to skin hygiene and protection that appear to mitigate the risk of developing BU. We highlight areas that warrant further investigation, particularly the potential role of the BCG vaccine in mitigating BU risk. Our findings are essential to inform public health strategies for BU prevention, especially for persons at highest risk in BU-endemic areas who work outdoors and those with diabetes.

Acknowledgments

We thank Loretta Vaughen for help with accessing the Victoria Population Health Survey database, all persons who assisted with questionnaire deployment, and all project participants.

This study was funded by a National Health and Medical Research Council Partnership Project Grant (GNT1152807) led by Professor T. Stinear. The funder of the study had no role in study design, data collection, data analysis, data interpretation, or writing of the report.

Deidentified participant data and questionnaires may be shared on a collaborative basis upon reasonable request made to D.P.O. (daniel.o'brien@barwonhealth.org.au) or E.A. (eugene.athan@barwonhealth.org.au). Requesting researchers will be required to submit an analysis plan and obtain relevant ethics approval.

About the Author

Dr. McNamara is an epidemiologist at the Barwon South West Public Health Unit and honorary senior research fellow at the Centre for Epidemiology and Biostatistics at the University of Melbourne. Her research interests focus on social and health equity and applied epidemiology for disease outbreak management and primary prevention, particularly for Buruli ulcer and COVID-19.

References

1. MacCallum P, Tolhurst JC, Buckle G, Sissons HA. A new mycobacterial infection in man. J Pathol Bacteriol. 1948;60:93–122. PubMed https://doi.org/10.1002/path.1700600111
2. Merritt RW, Walker ED, Small PLC, Wallace JR, Johnson PDR, Benbow ME, et al. Ecology and transmission of Buruli ulcer disease: a systematic review. PLoS Negl Trop Dis. 2010;4:e911. https://doi.org/10.1371/journal.pntd.0000911
3. World Health Organization. Neglected tropical diseases. 2022 [cited 2022 Sep 17]. https://www.who.int/health-topics/neglected-tropical-diseases#tab=tab_1
4. Boyd SC, Athan E, Friedman ND, Hughes A, Walton A, Callan P, et al. Epidemiology, clinical features and diagnosis of *Mycobacterium ulcerans* in an Australian population. Med J Aust. 2012;196:341–4. https://doi.org/10.5694/mja12.10087
5. Trubiano JA, Lavender CJ, Fyfe JAM, Bittmann S, Johnson PDR. The incubation period of Buruli ulcer (*Mycobacterium ulcerans* infection). PLoS Negl Trop Dis. 2013;7:e2463. https://doi.org/10.1371/journal.pntd.0002463
6. Loftus MJ, Tay EL, Globan M, Lavender CJ, Crouch SR, Johnson PDR, et al. Epidemiology of Buruli ulcer infections, Victoria, Australia, 2011–2016. Emerg Infect Dis. 2018;24:1988–97. https://doi.org/10.3201/eid2411.171593
7. Quek TYJ, Henry MJ, Pasco JA, O'Brien DP, Johnson PDR, Hughes A, et al. *Mycobacterium ulcerans* infection: factors influencing diagnostic delay. Med J Aust. 2007;187:561–3. https://doi.org/10.5694/j.1326-5377.2007.tb01416.x
8. Simpson H, Deribe K, Tabah EN, Peters A, Maman I, Frimpong M, et al. Mapping the global distribution of Buruli ulcer: a systematic review with evidence consensus. Lancet Glob Health. 2019;7:e912–22. https://doi.org/10.1016/S2214-109X(19)30171-8
9. Yerramilli A, Tay EL, Stewardson AJ, Fyfe J, O'Brien DP, Johnson PDR. The association of rainfall and Buruli ulcer in southeastern Australia. PLoS Negl Trop Dis. 2018;12:e0006757. https://doi.org/10.1371/journal.pntd.0006757
10. Victoria Department of Health. Buruli ulcer is spreading. Health advisory November 8, 2022 [cited 2023 Jan 2]. https://www.health.vic.gov.au/health-advisories/buruli-ulcer-is-spreading
11. Muleta AJ, Lappan R, Stinear TP, Greening C. Understanding the transmission of *Mycobacterium ulcerans*: a step towards controlling Buruli ulcer. PLoS Negl Trop Dis. 2021;15:e0009678. https://doi.org/10.1371/journal.pntd.0009678
12. Fyfe JAM, Lavender CJ, Handasyde KA, Legione AR, O'Brien CR, Stinear TP, et al. A major role for mammals in the ecology of *Mycobacterium ulcerans*. PLoS Negl Trop Dis. 2010;4:e791. https://doi.org/10.1371/journal.pntd.0000791
13. Singh A, McBride WJH, Govan B, Pearson M. Potential animal reservoir of *Mycobacterium ulcerans*: a systematic review. Trop Med Infect Dis. 2018;3:56. https://doi.org/10.3390/tropicalmed3020056
14. Blasdell KR, McNamara B, O'Brien DP, Tachedjian M, Boyd V, Dunn M, et al. Environmental risk factors associated with the presence of *Mycobacterium ulcerans* in Victoria, Australia. PLoS One. 2022;17:e0274627. https://doi.org/10.1371/journal.pone.0274627
15. Wallace JR, Mangas KM, Porter JL, Marcsisin R, Pidot SJ, Howden B, et al. *Mycobacterium ulcerans* low infectious dose and mechanical transmission support insect bites and puncturing injuries in the spread of Buruli ulcer. PLoS Negl Trop Dis. 2017;11:e0005553. https://doi.org/10.1371/journal.pntd.0005553
16. Johnson PDR, Azuolas J, Lavender CJ, Wishart E, Stinear TP, Hayman JA, et al. *Mycobacterium ulcerans* in mosquitoes captured during outbreak of Buruli ulcer, southeastern Australia. Emerg Infect Dis. 2007;13:1653–60. https://doi.org/10.3201/eid1311.061369
17. Lavender CJ, Fyfe JAM, Azuolas J, Brown K, Evans RN, Ray LR, et al. Risk of Buruli ulcer and detection of *Mycobacterium ulcerans* in mosquitoes in southeastern Australia. PLoS Negl Trop Dis. 2011;5:e1305. https://doi.org/10.1371/journal.pntd.0001305
18. Quek TYJ, Athan E, Henry MJ, Pasco JA, Redden-Hoare J, Hughes A, et al. Risk factors for *Mycobacterium ulcerans* infection, southeastern Australia. Emerg Infect Dis. 2007;13:1661–6. https://doi.org/10.3201/eid1311.061206
19. Landier J, Constantin de Magny G, Garchitorena A, Guégan JF, Gaudart J, Marsollier L, et al. Seasonal patterns of Buruli ulcer incidence, Central Africa, 2002–2012. Emerg Infect Dis. 2015;21:1414–7. https://doi.org/10.3201/eid2108.141336
20. Zimmermann P, Finn A, Curtis N. Does BCG vaccination protect against nontuberculous mycobacterial infection? A systematic review and meta-analysis. J Infect Dis. 2018;218:679–87. https://doi.org/10.1093/infdis/jiy207
21. Fevereiro J, Sajjadi N, Fraga AG, Teixeira PM, Pedrosa J. Individual and clinical variables associated with the risk of Buruli ulcer acquisition: a systematic review and meta-analysis. PLoS Negl Trop Dis. 2020;14:e0008161. https://doi.org/10.1371/journal.pntd.0008161
22. Bratschi MW, Bolz M, Minyem JC, Grize L, Wantong FG, Kerber S, et al. Geographic distribution, age pattern and sites of lesions in a cohort of Buruli ulcer patients from the Mapé Basin of Cameroon. PLoS Negl Trop Dis. 2013;7:e2252. https://doi.org/10.1371/journal.pntd.0002252
23. Yerramilli A, Tay EL, Stewardson AJ, Kelley PG, Bishop E, Jenkin GA, et al. The location of Australian Buruli ulcer lesions—implications for unravelling disease transmission. PLoS Negl Trop Dis. 2017;11:e0005800. https://doi.org/10.1371/journal.pntd.0005800
24. Taylor JW, Curtis N, Denholm J. BCG vaccination: an update on current Australian practices. Aust J Gen Pract. 2020;49:651–5. https://doi.org/10.31128/AJGP-06-20-5490
25. O'Brien CR, Handasyde KA, Hibble J, Lavender CJ, Legione AR, McCowan C, et al. Clinical, microbiological and pathological findings of *Mycobacterium ulcerans* infection in three Australian possum species. PLoS Negl Trop Dis. 2014;8:e2666. https://doi.org/10.1371/journal.pntd.0002666
26. Landier J, Boisier P, Fotso Piam F, Noumen-Djeunga B, Simé J, Wantong FG, et al. Adequate wound care and use of bed nets as protective factors against Buruli ulcer: results from a case control study in Cameroon. PLoS Negl Trop Dis. 2011;5:e1392. https://doi.org/10.1371/journal.pntd.0001392
27. Bridson T, Govan B, Ketheesan N, Norton R. Overrepresentation of diabetes in soft tissue nontuberculous

mycobacterial infections. Am J Trop Med Hyg. 2016;95:528–30. https://doi.org/10.4269/ajtmh.16-0104
28. Berbudi A, Rahmadika N, Tjahjadi AI, Ruslami R. Type 2 diabetes and its impact on the immune system. Curr Diabetes Rev. 2020;16:442–9. https://doi.org/10.2174/1573399815666191024085838
29. Phillips RO, Phanzu DM, Beissner M, Badziklou K, Luzolo EK, Sarfo FS, et al. Effectiveness of routine BCG vaccination on Buruli ulcer disease: a case-control study in the Democratic Republic of Congo, Ghana and Togo. PLoS Negl Trop Dis. 2015;9:e3457. https://doi.org/10.1371/journal.pntd.0003457
30. Debacker M, Portaels F, Aguiar J, Steunou C, Zinsou C, Meyers W, et al. Risk factors for Buruli ulcer, Benin. Emerg Infect Dis. 2006;12:1325–31. https://doi.org/10.3201/eid1209.050598
31. Nackers F, Tonglet R, Slachmuylder V, Johnson RC, Robert A, Zinsou C, et al. Association between haemoglobin variants S and C and *Mycobacterium ulcerans* disease (Buruli ulcer): a case-control study in Benin. Trop Med Int Health. 2007;12:511–8. https://doi.org/10.1111/j.1365-3156.2006.01808.x
32. Raghunathan PL, Whitney EAS, Asamoa K, Stienstra Y, Taylor TH Jr, Amofah GK, et al. Risk factors for Buruli ulcer disease (*Mycobacterium ulcerans* infection): results from a case-control study in Ghana. Clin Infect Dis. 2005;40:1445–53. https://doi.org/10.1086/429623
33. Bradley WG, Hudgson P, Gardner-Medwin D, Walton JN. Myopathy associated with abnormal lipid metabolism in skeletal muscle. Lancet. 1969;293:495–8. https://doi.org/10.1016/S0140-6736(69)91593-1
34. Smith PG, Revill WD, Lukwago E, Rykushin YP. The protective effect of BCG against *Mycobacterium ulcerans* disease: a controlled trial in an endemic area of Uganda. Trans R Soc Trop Med Hyg. 1976;70:449–57. https://doi.org/10.1016/0035-9203(76)90128-0

Address for correspondence: Bridgette McNamara, Barwon South West Public Health Unit, Barwon Health, PO Box 281, Geelong, VIC 3220, Australia; email: Bridgette.mcnamara@barwonhealth.org.au

Candida auris Clinical Isolates Associated with Outbreak in Neonatal Unit of Tertiary Academic Hospital, South Africa

Dikeledi Kekana, Serisha D. Naicker, Liliwe Shuping, Sithembiso Velaphi, Firdose L. Nakwa, Jeannette Wadula, Nelesh P. Govender, for GERMS-SA[1]

Candida auris was first detected at a university-affiliated hospital in Johannesburg, South Africa, in 2009. We used whole-genome sequencing to describe the molecular epidemiology of *C. auris* in the same hospital during 2016–2020; the neonatal unit had a persistent outbreak beginning in June 2019. Of 287 cases with culture-confirmed *C. auris* infection identified through laboratory surveillance, 207 (72%) had viable isolates and 188 (66%) were processed for whole-genome sequencing. Clade III (118/188, 63%) and IV (70/188, 37%) isolates co-circulated in the hospital. All 181/188 isolates that had a fluconazole MIC ≥32 μg/mL had *ERG11* mutations; clade III isolates had VF125AL substitutions, and clade IV isolates had K177R/N335S/E343D substitutions. Dominated by clade III, the neonatal unit outbreak accounted for 32% (91/287) of all cases during the study period. The outbreak may have originated through transmission from infected or colonized patients, colonized healthcare workers, or contaminated equipment/environment.

Candida auris is a multidrug-resistant yeast that causes invasive infections with high associated mortality in acute and long-term healthcare facilities worldwide (*1*,*2*). Although *C. auris* was initially described in 2009 in Japan, the earliest cases of infection in South Africa were reported in 2014 (*3*). Those cases prompted a retrospective review of surveillance isolates that identified a case of *C. auris* bloodstream infection in 2009 at a Johannesburg academic hospital (*4*). The rapid emergence and international spread during 2014–2023, high crude mortality rates (30%–60%), and antifungal resistance make *C. auris* a global public health concern; the World Health Organization has designated it a critical-priority fungal pathogen (*5*,*6*).

Neonatal outbreaks caused by *C. auris* are occasionally documented, although early outbreaks in South Africa occurred mainly among critically ill adults (*7*). In more recent years, *C. auris* has caused outbreaks involving neonates and has subsequently become endemic in many hospitals in South Africa (*7*–*10*). *C. parapsilosis* has been a major pathogen causing late-onset sepsis among hospitalized neonates in low- and middle-income countries because of its ability to colonize the skin of hospitalized patients and healthcare workers, persist on hospital surfaces, and adhere to indwelling medical devices, characteristics that are also applicable to *C. auris* (*11*,*12*).

C. auris is classified into several genetically distinct clades. Clade I originated in South Asia, clade II in East Asia, clade III in Africa, clade IV in South America, and clade V in the Middle East (Iran) (*13*). All clades exhibit minimal intraclade genetic diversity but are separated from each other by tens to hundreds of thousands of single nucleotide polymorphisms (*13*,*14*). A possible sixth clade was reported from Singapore and Bangladesh in August 2023 (C. Suphavilai et al., unpub. data, https://www.medrxiv.org/content/10.1101/2023.08.01.23293435v1). Most clade isolates from Africa are resistant to fluconazole; some are resistant to other antifungal classes (*9*,*15*).

Author affiliations: National Institute for Communicable Diseases, Johannesburg, South Africa (D. Kekana, S.D. Naicker, L. Shuping, N.P. Govender); University of the Witwatersrand, Johannesburg (D. Kekana, S. Velaphi, F.L. Nakwa, J. Wadula, N.P. Govender); Chris Hani Baragwanath Academic Hospital, Johannesburg (S. Velaphi, F.L. Nakwa, J. Wadula); University of Cape Town, Cape Town, South Africa (N.P. Govender); University of Exeter, Exeter, United Kingdom (N.P. Govender)

DOI: http://doi.org/10.3201/eid2910.230181

[1]Members of GERMS-SA are listed at the end of this article.

Globally, echinocandin-resistant isolates are not as prevalent as azole- and polyene-resistant isolates, which is partly why echinocandins are recommended as first-line treatment (*5*).

We aimed to describe the molecular epidemiology of *C. auris* at a large tertiary academic hospital in Johannesburg, South Africa by using whole-genome sequencing (WGS), focusing on a persistent outbreak in the hospital's neonatal unit. For GERMS-SA, an ongoing surveillance program, we sought and obtained annual ethics approvals from several university ethics committees in South Africa. A detailed description of GERMS-SA surveillance methods has been published previously (*7*).

Materials and Methods

Study Setting and Definitions

We conducted the cross-sectional study at the 3,200-bed Chris Hani Baragwanath Academic Hospital (CHBAH) in Soweto, Johannesburg, South Africa. Affiliated with the University of the Witwatersrand, CHBAH provides a wide range of subspecialist inpatient and outpatient surgical, medical, pediatric and obstetrics/gynecology services. The hospital serves 1.5 million persons around Soweto and surrounding areas as a tertiary referral center. The hospital's neonatal unit caters to neonates requiring admission from ≈20,000 annual births within the hospital; 3,000 births from local district hospitals and 10,000 births from the local clinics annually; and those requiring surgical services from the southern Gauteng and North West Provinces (*16*). All *C. auris* isolates in this study were received from the onsite microbiology laboratory at CHBAH.

We included *C. auris* isolates from all patients admitted to the neonatal unit from June 12, 2019, through May 30, 2020 (overlapping with the neonatal unit outbreak, which began with an index case diagnosed on June 12, 2019), as well as isolates from patients admitted across the hospital from March 1, 2016, through July 31, 2020 (Figure 1). Specimens that were processed for routine microbiology culture and yielded *C. auris* were from blood, central venous catheter (CVC) tips, urine, and wound and burn swabs. We also included *C. auris* isolates that were cultured from swabs collected by targeted screening of high-risk contact patients in the neonatal unit (e.g., adjacent incubator, same cubicle, or both). For all case-patients with multiple isolates within a 30-day period, we used the first isolate for analysis. We obtained demographic and clinical data such as age, sex, ward location, and site of *Candida* infection from the GERMS-SA surveillance database. We defined neonates as <28 days of age, infants as 28 days to <12 months of age, children as 1–12 years of age, adolescents as 13–17 years of age, and adults as ≥18 years of age.

Culture, Identification, and Antifungal Susceptibility Testing

All isolates from invasive and noninvasive cases were first processed at the CHBAH onsite laboratory. If

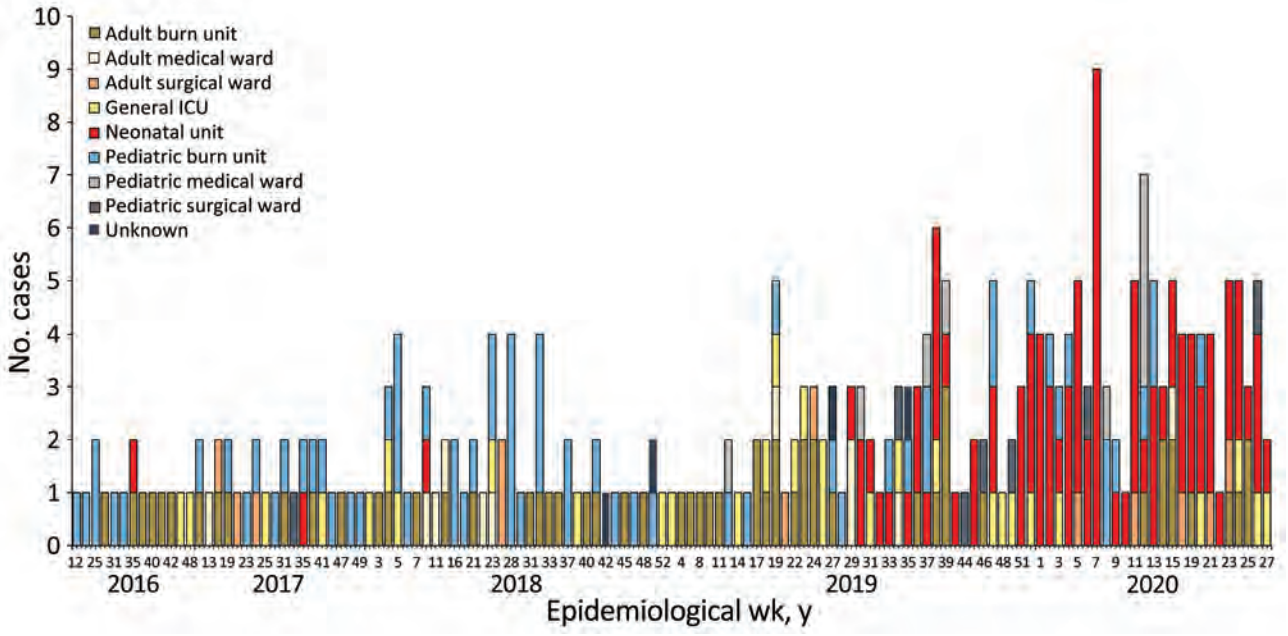

Figure 1. Epidemic curve by ward location for 287 laboratory-confirmed cases of *Candida auris* infection or colonization at an academic tertiary hospital, South Africa, March 2016–July 2020. ICU, intensive care unit.

yeasts were observed on microscopic direct examination or if fungal culture was specifically requested, we inoculated specimens onto Sabouraud agar (Diagnostic Media Products [DMP], https://www.nhls.ac.za). We used Vitek-2 (bioMérieux, https://www.biomerieux.com) and Microscan Walkaway (Beckman Coulter, www.beckmancoulter.com) for initial identification. We shipped cultures to the National Institute for Communicable Diseases (NICD) on Dorset transport medium or agar plates (DMP); we confirmed identification and performed antifungal susceptibility testing before storage (*16*,*17*). For this study, we retrieved *C. auris* isolates from −70°C freezer storage at the NICD and subcultured on Sabouraud agar to confirm viability, then cultured them onto chromogenic agar (DMP) to confirm purity (CHROMagar *Candida* powder was sourced from Mast Diagnostics, https://www.mastgroup.com). We conducted matrix-assisted laser desorption/ionization-time of flight mass spectrometry (Bruker Daltonics, https://www.bruker.com) to identify all *C. auris* isolates again before further testing. We performed antifungal susceptibility testing using commercial gradient diffusion (Etest, bioMérieux) or broth microdilution assays (Sensititre; Thermo Fisher, https://www.thermofisher.com). We used the Etest method to generate amphotericin B MICs because the gradient diffusion strip provides a wider range of MIC values than are generated by broth-microdilution testing; the wider range may help discriminate between susceptible and resistant isolates (*17*). We interpreted MICs using tentative breakpoints proposed by the US Centers for Disease Control and Prevention (*1*). All experiments included the quality control strains *C. parapsilosis* (ATCC 22019) and *C. krusei* (ATCC 6258), following M27-A3 (*18*) and M60 recommendations of the Clinical and Laboratory Standards Institute (*19*).

Whole-Genome Sequencing

We extracted DNA using the Zymo Research Quick-DNA Fungal/Bacterial miniprep kit (Zymo Research Corporation, https://www.zymoresearch.com) according to the manufacturer's instructions, with some exceptions. For example, we extracted DNA from yeast colonies directly instead of from a resuspension of yeast cells in water; we used 40 μL of elution buffer instead of the 100 μL recommended volume. We sent genomic DNA to the NICD Sequencing Core Facility for WGS. We performed sequencing of the 12.6 Mb-sized genome on 188 samples. We prepared genomic libraries using Nextera DNA Library Preparation (Illumina, https://www.illumina.com), followed by 2 × 300 bp sequencing on an Illumina NextSeq 500 platform to produce paired end reads.

Single-Nucleotide Polymorphism Calling and Phylogenetic Analysis

We assessed the quality of read data using FastQC version 0.11.9 (https://www.bioinformatics.babraham.ac.uk) and performed read filtering and trimming using PRINSEQ version 0.20.4 (http://prinseq.sourceforge.net) (*20*). We mapped the read data to a reference *C. auris* genome (clade III, B11221; National Center for Biotechnology Information [NCBI] BioProject accession no. PRJNA535510) using the Burrows-Wheeler data transformation algorithm version 0.7.17 (*21*). We performed variant calling (i.e., single-nucleotide polymorphism [SNP] analysis) using SAMtools version 1.11 (*21*) through the Northern Arizona SNP Pipeline (NASP) (http://tgennorth.github.io/NASP/install.html) (*22*). Filtering parameters involved removing positions that had <10× coverage, <90% variant allele calls and those within duplicated regions in the reference (*14*). We estimated a maximum parsimony phylogeny tree using MEGA software version 10.0.5 (https://www.megasoftware.net) and bootstrap analysis based on 1,000 replicates using the bestSNP alignment produced by the NASP pipeline (*23*). We included external sequences representing each clade (I–V) in the analysis to confirm the clade assignments of the isolates: clade I, PEKT02 (B8441, NCBI BioSample no. SAMN05379624) and SRR3883445 (B11214, NCBI BioSample no. SAMN05379602); clade II, PYFR01 (B11220, NCBI BioSample no. SAMN05379608); clade IV, PYGM01 (B11243, NCBI BioSample no. SAMN05379619); clade V, SRR9007776 (NCBI BioSample no. SAMN11570381). Also included in the analysis was a genome of the first South Africa isolate to be reported and sequenced from CHBAH in 2009 (*9*).

Phylodynamic Analysis of Clade III Neonatal Isolates

We created a root-to-tip regression plot using TempEst version 1.5.3 (*24*) to quantify the mutation rate and to assess the temporal signal of the outbreak strains. We inferred Bayesian phylogenies using BEAST version 1.8.4 (*25*) by applying a general time-reversible nucleotide substitution model under a strict molecular clock with the mutational rate obtained from the root-to-tip regression. We used the SNP alignment of the clade III isolates for both TempEst and BEAST. We chose a general time-reversible model as a nonspecific model for phylogenetic inference. The model assumes different rates of substitution for each nucleotide and different frequencies of nucleotide occurrence (*26*). Furthermore, we applied a coalescent exponential population prior distribution and used specimen collection dates (day, month, year) as tip

dates. We set the length of the Markov Chain Monte Carlo (MCMC) at 50,000,000 steps and logged parameters every 1,000 steps. We used Tracer version 1.7.1 (https://beast.community/tracer) to visualize and analyze the posterior MCMC samples. The effective sample size was >700, indicating that the MCMC runs had converged. We generated a maximum clade credibility tree with TreeAnnotator version 1.8.4 (https://beast.community/treeannotator) after discarding the first 10% as burn-in and visualized the tree using FigTree version 1.4.4 (http://tree.bio.ed.ac.uk/software/figtree). We also performed an exploratory analysis to reconstruct potential transmission routes in the hospital (Appendix, https://wwwnc.cdc.gov/EID/article/29/10/23-0181-App1.pdf).

Resistance Mutation Identification

We used CLC Genomics Workbench version 10 (QIAGEN, https://www.qiagen.com) to assess and identify mutations in resistant *C. auris* isolates. We extracted 2 genes from each resistant *C. auris* genome and assessed for any point mutations (i.e., substitutions, duplications): *ERG11*, which is transcribed into an azole target; and *FKS1*, an echinocandin target gene (*27*). We used a wild-type strain with no known mutations as a reference in the analysis to determine the presence of mutations (*C. auris* B8441, NCBI accession no. PEKT00000000). Susceptible isolates were also assessed for mutations in the same genes.

Results

Patient Characteristics

During the surveillance period, 287 culture-confirmed cases (invasive and noninvasive) were reported from the hospital from different wards; of those, 207 (72%) had viable isolates available for analysis. Most of the cases were from the neonatal unit (91/287, 32%), pediatric burn unit (66/287, 23%), and adult burn unit (57/287, 20%). The median age was 1.4 years (interquartile range [IQR] 22 days to 21 years; range 0 days to 85 years). Adults accounted for the highest proportion of cases (74/287, 26%) followed by neonates (62/287, 22%). More patients were male (54%, 155/287) than female (42%, 121/287; sex was unknown for 4% (11/287). Most isolates were from blood cultures (161/287, 56%), followed by skin swabs (33/287, 12%) (Table 1).

Table 1. Characteristics of 287 patients with *Candida auris* infection or colonization admitted to a large academic hospital in South Africa, 2016–2020

Characteristic	No. (%) isolates
Sex	
M	155 (54)
F	121 (42.2)
Unknown	11 (3.8)
Age group	
Neonates, ≤28 d	62 (21.6)
Infants, 28 d–12 mo	56 (19.5)
Children, 1–12 y	54 (18.8)
Adolescents, 13–17 y	11 (3.8)
Adults, ≥18 y	74 (25.8)
Unknown	30 (10.5)
Specimen type	
Blood	161 (56.1)
Skin swab	33 (11.5)
Arterial catheter tip	28 (9.8)
Central venous catheter tip	24 (8.4)
Urine	11 (3.8)
Tracheal aspirate	8 (2.8)
Tissue, not specified	6 (2.1)
Fluid aspirate, not specified	3 (1)
Skin scraping	1 (0.3)
Burn/wound swab	1 (0.3)
Unknown	11 (3.5)
Ward location	
Neonatal unit	91 (31.7)
Pediatric burn unit	66 (23)
Adult burn unit	57 (19.9)
General adult/pediatric intensive care unit	30 (10.5)
Adult surgical	12 (4.2)
Adult medical	11 (3.8)
Pediatric medical	9 (3.1)
Pediatric surgical	7 (2.4)
Unknown	4 (1.4)

Antifungal Susceptibility of Isolates

Most (199/207; 96%) of the isolates were resistant to fluconazole (MIC ≥32 μg/mL); 13 (6%) were considered resistant to amphotericin B (MIC ≥2 μg/mL). Multidrug-resistant isolates were also present; 2 (0.9%) isolates were resistant to both caspofungin and fluconazole and 3 (1.4%) were resistant to both fluconazole and amphotericin B. No isolates in this study were resistant to ≥3 antifungal classes (panresistant) (Table 2).

Phylogenetic and Resistant Mutation Analysis

Of 207 viable *C. auris* isolates, 200 were available for WGS. We excluded 12 sequences of poor quality from the analysis; WGS data of 188 isolates were available for bioinformatics analysis. Overall, 118 (63%) clustered with the Africa clade III reference and the remaining 70 (37%) with the South America clade IV reference (Figure 2). Isolates in this study did not cluster in any other clade. A total of 181 (96%) isolates had a fluconazole MIC value ≥32 μg/mL, and 186 (99%) had known resistance mutations in the *ERG11* gene; thus, 5 sequences from phenotypically susceptible isolates also housed resistance mutations (Table 3). Isolates for clade III had the VF125AL substitution that is specific to the clade. Isolates from clade IV had the substitutions K177R/N335S/E343D, which had been documented in this clade previously *(28)*. Some

Table 2. MIC distribution of *Candida auris* isolates (n = 207) from patients admitted to a tertiary academic hospital, South Africa, 2016–2020*

		No. isolates with MIC, μg/mL																
Drug	Breakpoint, μg/mL	0.008	0.015	0.03	0.06	0.12	0.25	0.5	1	2	4	8	16	32	64	128	256	Unk†	% Resistant
AFG	≥4		1		28	129	42	7											0
MFG	≥4			2	96	94	12	1	2										0
5FC	≥128	3			67	125	10	2											0
POS	NA	1	1	15	73	80	31	4	2										NA
VRC	NA				2	8	21	58	103	13	2								NA
ITC	NA			2	10	84	84	25	2										NA
FLC	≥32								1				7	13	34	73	79		96
AMB	≥2						1	9	135	61								1	42
AMB Etest‡	≥2		1	1	2	9	22	76	79	11	2							4	6.2

*AMB, amphotericin B; AFG, anidulafungin; FLC, fluconazole; ITC, itraconazole; MFG, micafungin; NA, not available; POS, posaconazole; unk, unknown; VRC, voriconazole; 5FC, flucytosine.
†Isolates missing data or not tested
‡MICs were determined using both broth microdilution and E-test method for amphotericin B.

isolates with the clade IV substitutions (27/70, 38%) had an additional E102K substitution.

The neonatal unit, the location of the outbreak starting in June 2019, was dominated by clade III isolates, whereas clade IV strains dominated the adult and pediatric burn units. We observed clade mixing in both burn units (Figure 3). Isolates from the neonatal unit constituted 37% (68/188) of the isolates in our phylogenetic tree.

Phylodynamic Analysis

We included only isolates from clade III, which was the clade responsible for the neonatal unit outbreak, in the following analysis. We created a root-to-tip regression plot to determine whether there was a positive correlation between the time the isolates were sampled and the number of substitutions along the tree topology. Linear regression estimates of the evolutionary rate equated to 1.3471×10^5 nt substitutions/site/year (correlation coefficient = 0.5). The rate was similar to that of an outbreak in Kenya caused by clade III isolates in which the calculated mutation of the outbreak strains was 1.8695 e−5 substitutions/site/year (*29*). The rate supported a strong temporal signal and was sufficient for further Bayesian molecular dating. The root-to-tip regression plot predicted the time to the most recent common ancestor (tMRCA) in 2018 based on the x intercept (Figure 4). The tMRCA for clade III in this hospital dated back to early 2014 (95% highest posterior density 2013 to mid-2015), whereas the tMRCA for the neonatal unit outbreak dated to 2018 (95% highest posterior density, mid-2017 to mid-2018), corresponding to the estimation from the root-to-tip regression analysis (Figure 5, https://wwwnc.cdc.gov/EID/article/29/10/23-0181-F5.htm). The exploratory analysis of the outbreak reconstruction of clade III revealed that infections were introduced into the neonatal unit from the adult burn unit, adult medical department, and an unknown ward (Appendix).

Discussion

Fluconazole-resistant clade III *C. auris* isolates caused a large persistent outbreak in the neonatal unit of a tertiary academic South Africa hospital beginning in June 2019 and continuing into 2023. WGS analysis of all viable surveillance isolates from this hospital during 2016–2020 revealed that clade IV *C. auris* isolates dominated in the adult and pediatric burn units with clade III and IV co-circulation. Phylodynamic analysis of the clade III neonatal outbreak isolates did not point to a specific source.

By 2016, *C. auris* was reported in >100 South Africa acute-care hospitals and had caused large outbreaks in some of these hospitals. *C. auris* had replaced other pathogens to become the third most common cause of candidemia in South Africa (*7*). Over our entire study period (i.e., March 2016–July 2020), the neonatal unit outbreak contributed to one third of all the cases at the hospital. Smaller *C. auris* outbreaks involving neonates have been reported previously in other hospitals in South Africa (*7*,*30*). Neonatal units in national central hospitals, such as CHBAH, have become fungal outbreak epicenters, driven by the innate vulnerability of very high-risk patients admitted to these units, occupancy routinely exceeding the approved bed capacity of the unit, and limited resources available for infection prevention and control or antimicrobial stewardship (*31*). Although the exact manner of *C. auris* introduction for this outbreak remains undetermined, temporal analysis of the outbreak strains placed tMRCA in early 2018, suggesting a relatively recent introduction (*10*,*32*). Continued surveillance until June 2022 has confirmed persistence of *C. auris* in the unit with sporadic cases of invasive infections.

Most isolates in our study belonged to Africa clade III (118/188, 63%) or the South America clade IV (70/188, 37%). The overall molecular epidemiology of *C. auris* in South Africa was determined in a

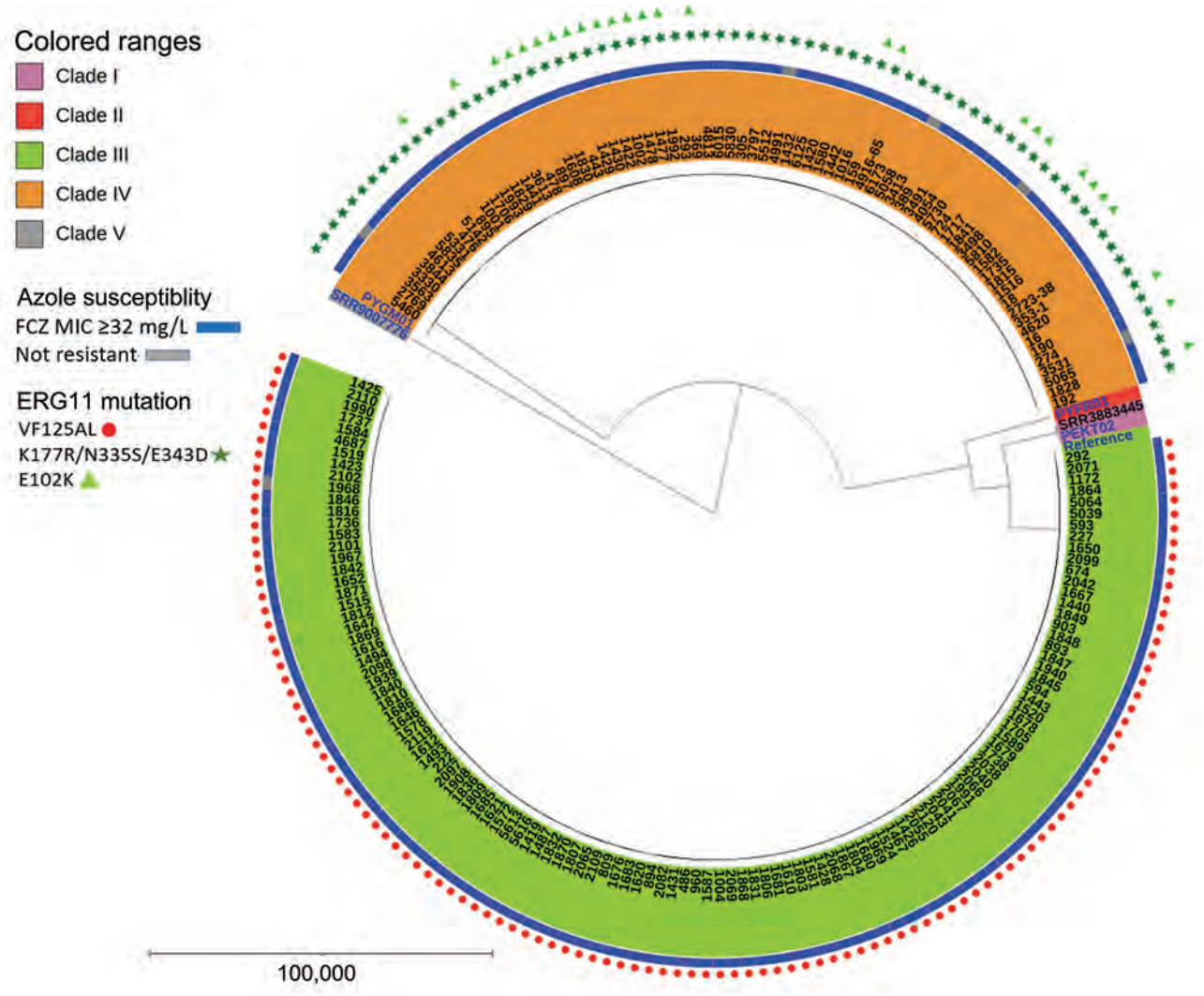

Figure 2. Phylogenetic tree depicting clade distribution and fluconazole resistance mutations of 188 invasive or colonizing South African *Candida auris* strains isolated from patients admitted to a large metropolitan hospital in South Africa, 2016–2020. The unrooted maximum-parsimony tree was created using MEGA software (https://www.megasoftware.net) using 287,338 single-nucleotide polymorphisms based on 1,000 bootstrap replicates. Scale bar indicates number of pairwise differences. FCZ, fluconazole.

WGS study which reported that 85% of isolates from 2009–2018 belonged to clade III, 12% belonged to clade I, and 3% to clade IV (*9*). An earlier global molecular epidemiology study reported only clade III isolates (n = 51) from South Africa (*33*). However, clade IV contributed to a proportionally larger case load in this hospital. Because the first reported isolate in South Africa in 2009 belonged to clade IV and was from CHBAH (*9*), we hypothesize that a clonal expansion of clade IV occurred in this hospital and those strains continued to circulate during our study period. Circulation of multiple *C. auris* clades in South Africa may be explained by global travel and trade (*34*–*36*). Furthermore, phylogeographic mixing of *C. auris* clades has been observed more often in recent years. Countries including Canada (clades I, II, and III), Kenya (clades I and III) and the United States (clades I, II, III, and IV) also reported cases caused by multiple *C. auris* clades (*10*).

Table 3. Clade proportions and frequency of antifungal drug resistance within the study population among 188 *Candida auris* isolates, South Africa

	No. (%) isolates				
Clade	All	Fluconazole resistant	Point mutation in *ERG11*	Point mutation in *FKS1*	Amphotericin B resistant
III	118 (62.5)	117 (99.1)	118 (100)	0	2 (2.8)
IV	70 (37.4)	66 (91.4)	70 (100)	0	1 (1.42)

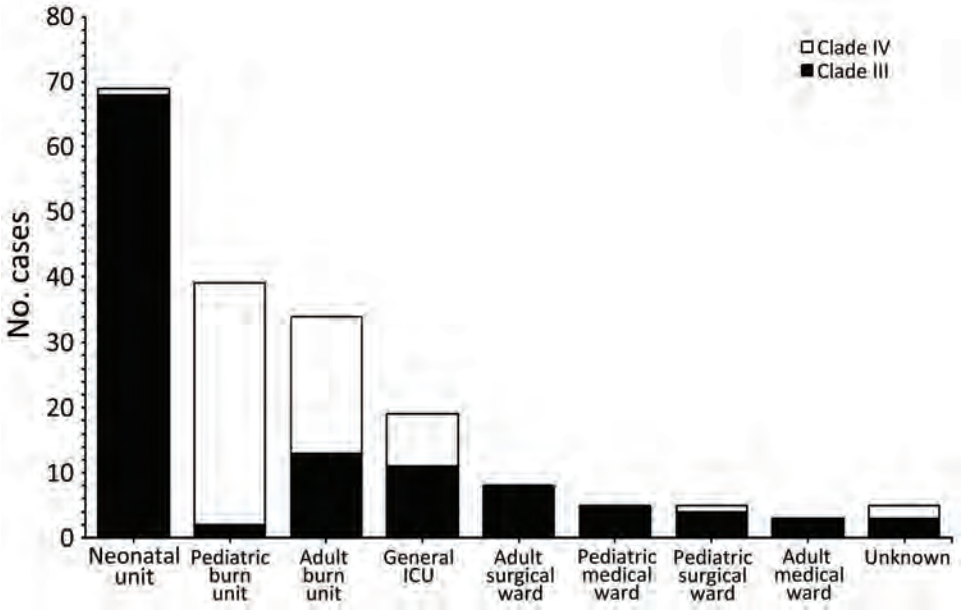

Figure 3. Clade distribution of 188 South African *Candida auris* isolates from patients admitted to a large metropolitan hospital classified by the patients' ward locations, South Africa, 2016–2020. ICU, intensive care unit.

Most isolates in our study were resistant to fluconazole. Fluconazole-susceptible isolates of *C. auris* are rare worldwide, especially within Africa clade III; this resistance limits the treatment options (*9*). Fluconazole-resistant *C. auris,* as a cause of healthcare-associated infections, adds costs to the health system since fluconazole is the least expensive and most accessible systemic antifungal agent (*8*,*37*). Amphotericin B resistance has been reported among *C. auris* isolates but remains rare while echinocandin resistance has also been reported, especially in clade I isolates (*37*). Echinocandins are recommended as first-line treatment for candidemia in adults, although amphotericin B deoxycholate, with better central nervous system penetration, is recommended for neonates who may develop *Candida* meningoencephalitis (*8*). We did not observe isolates resistant to all classes of antifungals in this study; however, 2 panresistant isolates were reported in South Africa in a previous study (*16*).

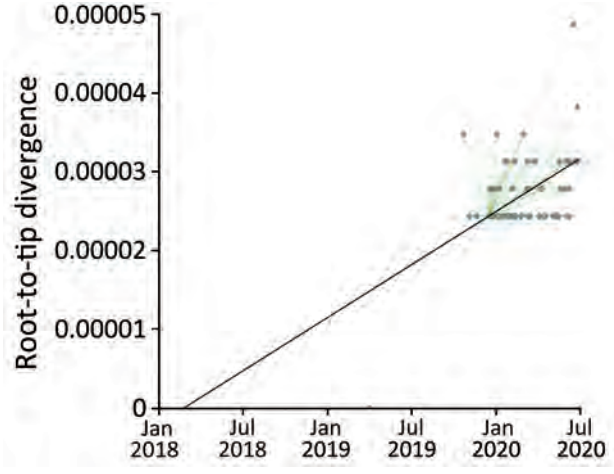

Figure 4. Root-to-tip regression analysis of 67 South African *Candida auris* outbreak isolates from the neonatal ward of a large metropolitan hospital in South Africa. Genetic distance is plotted against sampling time. Every data point represents a tip on the phylogeny. Black line indicates correlation coefficient for the regression. Green lines represent the evolutionary rate in substitutions/site/day.

Most of the fluconazole-resistant isolates in our study had clade-specific mutations in the *ERG11* gene that are known to contribute to resistance. The clade III *ERG11* mutation (VF125AL) seems to be universal across resistant isolates within the clade and has been seen in other clade III isolates from previous studies, even those isolated outside Africa (*33*); T.K. Price et al., unpub. data, https://doi.org/10.1101/2020.10.26.20214908). The *ERG11* gene–mediated mechanism of resistance to fluconazole for clade IV isolates varies, and isolates from different geographic areas have different *ERG11* mutations (*28*). Isolates in our study had the same substitutions as isolates originating from Colombia, which contained all 3 Erg11p substitutions (K177R, N335S, E343D), whereas azole resistance in clade I India/Pakistan isolates and some clade IV Colombia isolates was caused by Y132F or K143R substitutions (*28*). Of interest, the K177R, N335S, and E343D clade IV substitutions have not been shown to contribute to increased azole resistance even in Colombian isolates. Instead, other Colombian isolates had the substitutions I466M or Y501H that have been shown to contribute to resistance, which we did not see in the isolates in our study (*28*). Some sequences with the described clade IV substitutions had an additional E102K substitution in our study; this substitution

has not been documented or proven to contribute to decreased susceptibility in *C. auris* strains. There were cases in our study where susceptible isolates possessed resistant mutations especially in clade IV. It appears that clade IV isolates might have a more complex mechanism of resistance.

A limitation of our study was that we only included cultured isolates from laboratory-based surveillance from patients with routinely diagnosed invasive infections and a few with colonization. Thus, we sampled only a subset of all infections that would have occurred at this hospital. An extensive collection of isolates using systematic sampling in a prospective study, including invasive, colonizing, and environmental strains, would be needed to determine the full extent of transmission routes with a higher resolution and to avoid missing links. In addition, detailed clinical information and travel and hospital transfer data were not available for all cases; this information would have enabled us to potentially determine how the pathogen was introduced into the hospital. Another limitation in our study is that we did not account for recombination analysis, which might have introduced bias in the phylogenetic analysis.

In summary, we characterized *C. auris* isolates circulating in a major metropolitan public hospital in South Africa. Our data showed that clades III and IV co-circulated, and clade III was responsible for a large outbreak in the neonatal unit. Most isolates were resistant to fluconazole and carried previously published clade-specific *ERG11* mutations. We speculate that the neonatal unit outbreak may have originated from cross-unit transmission by infected or colonized patients, colonized healthcare workers, or contaminated equipment. Patient environments may have also served as reservoirs of infection.

Members of the GERMS-SA surveillance program who participated in surveillance and sending *Candida* isolates and data to the National Institute for Communicable Diseases: John Black, Vanessa Pearce (Eastern Cape Province); Masego Moncho, Motlatji Maloba (Free State Province); Anwar Hoosen, Charl Verwey, Charles, Feldman, Colin Menezes, David Moore, Dina Pombo, Gary Reubenson, Grace Ntlemo, Jeannette Wadula, Jeremy Nel, Maphoshane Nchabeleng, Merika Tsitsi, Moamokgethi Moshe, Mohammed Said, Nicolette du Plessis, Rispah Chomba, Sarah Stacey, Theunis Avenant, Trusha Nana, Vindana Chibabhai (Gauteng Province); Adhil Maharj, Douglas Wilson, Fathima Naby, Halima Dawood, Khine Swe Swe Han, Lisha Sookan, Nomonde Dlamini, Praksha Ramjathan, Prasha Mahabeer, Prathna Bhola, Romola Naidoo, Sumayya Haffejee, Surendra Sirkar, Yeishna Ramkillawan (KwaZulu-Natal Province); Ken Hamese, Ngoaka Sibiya, Phetho Mangena, Ruth Lekalakala (Limpopo Province); Greta Hoyland, Sindi Ntuli (MP); Pieter Jooste (Northern Cape Province); Ebrahim Variava, Ignatius Khantsi, Omphile Mekgoe (North West Province); Adrian Brink, Elizabeth Prentice, Kessendri Reddy, Andrew Whitelaw (Western Cape Province); Ebrahim Hoosien, Inge Zietsman, Terry Marshall, Xoliswa Poswa; Chetna Govind, Juanita Smit, Keshree Pillay, Sharona Seetharam, Victoria Howell; Catherine Samuel, Marthinus Senekal; Andries Dreyer, Louis Marcus, Warren Lowman; Anne von Gottberg, Anthony Smith, Azwifarwi Mathunjwa, Bhavani Moodley, Cecilia d'Abreu, Cecilia Miller, Cheryl Cohen, Farzana Ismail, Harry Moultrie, Husna Ismail, Jacqueline Weyer, Jackie Kleynhans, Jenny Rossouw, John Frean, Joy Ebonwu, Judith Mwansa-Kambafwile, Juno Thomas, Kate Bishop, Kerrigan McCarthy, Liliwe Shuping, Linda de Gouveia, Linda Erasmus, Lynn Morris, Lucille Blumberg, Marshagne Smith, Martha Makgoba, Michelle Groome, Mignon du Plessis, Mimmy Ngomane, Mokupi Manaka, Myra Moremi, Nazir Ismail, Nelesh Govender, Neo Legare, Nicola Page, Nombulelo Hoho, Olga Perovic, Phuti Sekwadi, Rindidzani Magobo, Rudzani Mashau, Ruth Mpembe, Sibongile Walaza, Siyanda Dlamini, Sunnieboy Njikho, Susan Meiring, Tiisetso Lebaka, Vanessa Quan, Wendy Ngubane.

Acknowledgments

We acknowledge Rhys Farrer and Nancy Chow for technical assistance and individuals from the Centre for Healthcare-Associated Infections, Antimicrobial Resistance and Mycoses at NICD: Agnes Sesoko, Amanda Shilubane, Boitumelo Kgoale, Boniwe Makwakwa, Daniel Desanto, Denver Jainarain, Ernest Tsotetsi, Gloria Molaba, Greg Greene, Ivy Rukasha, Juliet Paxton, Leandi Steynfaardt, Mabatho Mhlanga, Mbali Dube, Michelle Lowe, Mpho Thanjekwayo, Naseema Bulbulia, Nikiwe Valashiya, Nozuko Blasich, Ntombi Dube, Patrick Pitjeng, Phelly Matlapeng, Rosah Mabokachaba, Rotondwa Mudau, Rubeina Badat, Ruth Mogokotleng, Sabelle Jallow, Serisha Naicker, Siphiwe Kutta, Tsidiso Maphanga, and Wilhelmina Strasheim.

This work was supported in part by a Fogarty International Centre Global Infectious Disease research training grant from the National Institutes of Health to the University of Pittsburgh and National Institute for Communicable Diseases (D43TW011255) and by the South Africa-Pitt Public Health Genomic Epidemiology Training Program (SAPPHGenE) by providing financial support for degree purposes and non-degree training.

About the Author

Ms. Kekana is a bioinformatics scientist at the National Institute for Communicable Diseases, Johannesburg, South Africa. This research paper formed the basis of her master of science degree in medicine awarded by the University of the Witwatersrand in 2022. She is working on next-generation sequencing data analysis of viral genomes, including SARS-CoV-2, respiratory syncytial virus, and influenza virus.

References

1. Spivak ES, Hanson KE. *Candida auris*: an emerging fungal pathogen. J Clin Microbiol. 2018;56: e01588-17. https://doi.org/10.1128/JCM.01588-17
2. Sardi JCO, Scorzoni L, Bernardi T, Fusco-Almeida AM, Mendes Giannini MJS. *Candida* species: current epidemiology, pathogenicity, biofilm formation, natural antifungal products and new therapeutic options. J Med Microbiol. 2013;62:10–24. https://doi.org/10.1099/jmm.0.045054-0
3. Satoh K, Makimura K, Hasumi Y, Nishiyama Y, Uchida K, Yamaguchi H. *Candida auris* sp. nov., a novel ascomycetous yeast isolated from the external ear canal of an inpatient in a Japanese hospital. Microbiol Immunol. 2009;53:41–4. https://doi.org/10.1111/j.1348-0421.2008.00083.x
4. Govender NP, Patel J, Magobo RE, Naicker S, Wadula J, Whitelaw A, et al.; TRAC-South Africa group. Emergence of azole-resistant *Candida parapsilosis* causing bloodstream infection: results from laboratory-based sentinel surveillance in South Africa. J Antimicrob Chemother. 2016;71:1994–2004. https://doi.org/10.1093/jac/dkw091
5. Lockhart SR, Etienne KA, Vallabhaneni S, Farooqi J, Chowdhary A, Govender NP, et al. Simultaneous emergence of multidrug-resistant *Candida auris* on 3 continents confirmed by whole-genome sequencing and epidemiological analyses. Clin Infect Dis. 2017;64:134–40. https://doi.org/10.1093/cid/ciw691
6. World Health Organization. WHO fungal priority pathogens list to guide research, development and public health action. 2022 Oct 25 [cited 2023 Jan 15]. https://www.who.int/publications/i/item/9789240060241
7. van Schalkwyk E, Mpembe RS, Thomas J, Shuping L, Ismail H, Lowman W, et al.; GERMS-SA. Epidemiologic shift in candidemia driven by *Candida auris*, South Africa, 2016–2017. Emerg Infect Dis. 2019;25:1698–707. https://doi.org/10.3201/eid2509.190040
8. Govender NP, Avenant T, Brink A, Chibabhai V, Cleghorn J, du Toit B, et al. Federation of Infectious Diseases Societies of Southern Africa guideline: recommendations for the detection, management and prevention of healthcare-associated *Candida auris* colonisation and disease in South Africa. S Afr J Infect Dis. 2019;34:163. https://doi.org/10.4102/sajid.v34i1.163
9. Naicker SD, Maphanga TG, Chow NA, Allam M, Kwenda S, Ismail A, et al. Clade distribution of *Candida auris* in South Africa using whole genome sequencing of clinical and environmental isolates. Emerg Microbes Infect. 2021;10:1300–8. https://doi.org/10.1080/22221751.2021.1944323
10. Mashau RC, Meiring ST, Dramowski A, Magobo RE, Quan VC, Perovic O, et al.; Baby GERMS-SA. Culture-confirmed neonatal bloodstream infections and meningitis in South Africa, 2014-19: a cross-sectional study. Lancet Glob Health. 2022;10:e1170–8. https://doi.org/10.1016/S2214-109X(22)00246-7
11. Shuping L, Mpembe R, Mhlanga M, Naicker SD, Maphanga TG, Tsotetsi E, et al.; for GERMS-SA. Epidemiology of culture-confirmed candidemia among hospitalized children in South Africa, 2012-2017. Pediatr Infect Dis J. 2021; 40:730–7. https://doi.org/10.1097/INF.0000000000003151
12. Welsh RM, Bentz ML, Shams A, Houston H, Lyons A, Rose LJ, et al. Survival, persistence, and isolation of the emerging multidrug-resistant pathogenic yeast *Candida auris* on a plastic health care surface. J Clin Microbiol. 2017;55:2996–3005. https://doi.org/10.1128/JCM.00921-17
13. Muñoz JF, Gade L, Chow NA, Loparev VN, Juieng P, Berkow EL, et al. Genomic insights into multidrug resistance, mating and virulence in *Candida auris* and related emerging species. Nat Commun. 2018;9:5346. https://doi.org/10.1038/s41467-018-07779-6
14. Escandón P, Chow NA, Caceres DH, Gade L, Berkow EL, Armstrong P, et al. Molecular epidemiology of *Candida auris* in Colombia reveals a highly related, countrywide colonization with regional patterns in amphotericin B resistance. Clin Infect Dis. 2019;68:15–21.
15. Maphanga TG, Naicker SD, Kwenda S, Muñoz JF, van Schalkwyk E, Wadula J, et al.; for GERMS-SA. *In vitro* antifungal resistance of *Candida auris* isolates from bloodstream infections, South Africa. Antimicrob Agents Chemother. 2021;65:e0051721. https://doi.org/10.1128/AAC.00517-21
16. Chris Hani Baragwanath Academic Hospital [cited 2022 Sep 10]. https://www.chrishanibaragwanathhospital.co.za
17. Berkow EL, Lockhart SR, Ostrosky-Zeichner L. Antifungal susceptibility testing: current approaches. Clin Microbiol Rev. 2020;33:e00069-19. https://doi.org/10.1128/CMR.00069-19
18. Clinical and Laboratory Standards Institute (CLSI). Reference method for broth dilution antifungal susceptibility testing of yeasts, 4th edition (M27). Wayne (PA): The Institute; 2017.
19. Clinical and Laboratory Standards Institute (CLSI). Performance Standards for Antifungal Susceptibility Testing of Yeasts, 2nd edition (M60). Wayne (PA): The Institute; 2020.
20. Schmieder R, Edwards R. Quality control and preprocessing of metagenomic datasets. Bioinformatics. 2011;27:863–4. https://doi.org/10.1093/bioinformatics/btr026
20. Li H, Durbin R. Fast and accurate short read alignment with Burrows-Wheeler transform. Bioinformatics. 2009;25:1754–60. https://doi.org/10.1093/bioinformatics/btp324
21. Sahl JW, Lemmer D, Travis J, Schupp JM, Gillece JD, Aziz M, et al. NASP: an accurate, rapid method for the identification of SNPs in WGS datasets that supports flexible input and output formats. Microb Genomics. 2016;2:e000074.
22. Kumar S, Nei M, Dudley J, Tamura K. MEGA: a biologist-centric software for evolutionary analysis of DNA and protein sequences. Brief Bioinform. 2008;9:299–306. https://doi.org/10.1093/bib/bbn017
23. Rambaut A, Lam TT, Max Carvalho L, Pybus OG. Exploring the temporal structure of heterochronous sequences using TempEst (formerly Path-O-Gen). Virus Evol. 2016;2:vew007. https://doi.org/10.1093/ve/vew007
24. Drummond AJ, Rambaut A. BEAST: Bayesian evolutionary analysis by sampling trees. BMC Evol Biol. 2007;7:214. https://doi.org/10.1186/1471-2148-7-214
25. Choudhuri S. Phylogenetic analysis. In: Bioinformatics for beginners. San Diego: Academic Press; 2014. p. 209–18.
26. Frias-De-Leon MG, Hernandez-Castro R, Vite-Garin T, Arenas R, Bonifaz A, Castanomn-Olivares L, et al.

Antifungal resistance in *Candida*: molecular determinants. Antibiotics. 2020;9:1–16.
27. Healey KR, Kordalewska M, Jiménez Ortigosa C, Singh A, Berrío I, Chowdhary A, et al. Limited *ERG11* mutations identified in isolates of *Candida auris* directly contribute to reduced azole susceptibility. Antimicrob Agents Chemother. 2018;62:e01427-18. https://doi.org/10.1128/AAC.01427-18
28. Adam RD, Revathi G, Okinda N, Fontaine M, Shah J, Kagotho E, et al. Analysis of *Candida auris* fungemia at a single facility in Kenya. Int J Infect Dis. 2019;85:182–7. https://doi.org/10.1016/j.ijid.2019.06.001
29. Moema I, Ismail H, Van Schalkwyk E, Shuping L, Govender NP. Outbreak of culture-confirmed *Candida auris* bloodstream infection in the neonatal unit of a public-sector hospital, South Africa, July through September 2017. 2017 [cited 2023 Aug 21]. https://www.tephinet.org/learning/fead/outbreak-culture-confirmed-candida-auris-bloodstream-infection-neonatal-unit-public
30. van Schalkwyk E, Iyaloo S, Naicker SD, Maphanga TG, Mpembe RS, Zulu TG, et al. Large outbreaks of fungal and bacterial bloodstream infections in a neonatal unit, South Africa, 2012–2016. Emerg Infect Dis. 2018;24:1204–12. https://doi.org/10.3201/eid2407.171087
31. Michalski C, Kan B, Lavoie PM. Antifungal immunological defenses in newborns. Front Immunol. 2017;8:281. https://doi.org/10.3389/fimmu.2017.00281
32. Chow NA, Muñoz JF, Gade L, Berkow EL, Li X, Welsh RM, et al. Tracing the evolutionary history and global expansion of *Candida auris* using population genomic analyses. mBio. 2020;11:e03364–19. https://doi.org/10.1128/mBio.03364-19
33. Turbett ISE, Becker DSM, Belford MTB, Kelly RTM, Desrosiers MTL, Oliver RNE, et al. Evaluation of *Candida auris* acquisition in US international travellers using a culture-based screening protocol1. J Travel Med. 2022;29:taab186. https://doi.org/10.1093/jtm/taab186
34. Chow NA, Gade L, Tsay SV, Forsberg K, Greenko JA, Southwick KL, et al.; US Candida auris Investigation Team. Multiple introductions and subsequent transmission of multidrug-resistant *Candida auris* in the USA: a molecular epidemiological survey. Lancet Infect Dis. 2018;18:1377–84. https://doi.org/10.1016/S1473-3099(18)30597-8
35. Yadav V, Heitman J. On fruits and fungi: a risk of antifungal usage in food storage and distribution in driving drug resistance in *Candida auris.* MBio. 2022;13:e0073922. https://doi.org/10.1128/mbio.00739-22
36. Miot J, Leong T, Takuva S, Parrish A, Dawood H. Cost-effectiveness analysis of flucytosine as induction therapy in the treatment of cryptococcal meningitis in HIV-infected adults in South Africa. BMC Health Serv Res. 2021;21:305. https://doi.org/10.1186/s12913-021-06268-9
37. Bravo Ruiz G, Lorenz A. What do we know about the biology of the emerging fungal pathogen of humans *Candida auris*? Microbiol Res. 2021;242:126621.

Address for correspondence: Nelesh P. Govender, National Institute for Communicable Diseases, Centre for Healthcare-Associated Infections, Antimicrobial Resistance and Mycoses, Private Bag X4, Sandringham, Johannesburg 2132, South Africa; email: neleshg@nicd.ac.za

etymologia revisited

Originally published in March 2019

Streptomycin

strep'to-mi'sin

In the late 1930s, Selman Waksman, a soil microbiologist working at the New Jersey Agricultural Station of Rutgers University, began a large-scale program to screen soil bacteria for antimicrobial activity. By 1943, Albert Schatz, a PhD student working in Waksman's laboratory, had isolated streptomycin from *Streptomyces griseus* (from the Greek *strepto-* ["twisted"] + *mykēs* ["fungus"] and the Latin *griseus*, "gray").

In 1944, Willam H. Feldman and H. Corwin Hinshaw at the Mayo Clinic showed its efficacy against *Mycobacterium tuberculosis*. Waksman was awardeda Nobel Prize in 1952 for his discovery of streptomycin, although much of the credit for the discovery has since been ascribed to Schatz. Schatz later successfully sued to be legally recognized as a co-discoverer of streptomycin.

References:

1. Comroe JH Jr. Pay dirt: the story of streptomycin. Part I. From Waksman to Waksman. Am Rev Respir Dis. 1978;117:773–81.
2. Wainwright M. Streptomycin: discovery and resultant controversy. Hist Philos Life Sci. 1991;13:97–124.

https://wwwnc.cdc.gov/eid/article/25/3/et-2503_article

Sporadic Shiga Toxin–Producing *Escherichia coli*–Associated Pediatric Hemolytic Uremic Syndrome, France, 2012–2021

Gabrielle Jones, Patricia Mariani-Kurkdjian, Aurélie Cointe, Stéphane Bonacorsi, Sophie Lefèvre, François-Xavier Weill, Yann Le Strat

Shiga toxin–producing *Escherichia coli*–associated pediatric hemolytic uremic syndrome (STEC-HUS) remains an important public health risk in France. Cases are primarily sporadic, and geographic heterogeneity has been observed in crude incidence rates. We conducted a retrospective study of 1,255 sporadic pediatric STEC-HUS cases reported during 2012–2021 to describe spatiotemporal dynamics and geographic patterns of higher STEC-HUS risk. Annual case notifications ranged from 109 to 163. Most cases (n = 780 [62%]) were in children <3 years of age. STEC serogroups O26, O80, and O157 accounted for 78% (559/717) of cases with serogroup data. We identified 13 significant space-time clusters and 3 major geographic zones of interest; areas of southeastern France were included in ≥5 annual space-time clusters. The results of this study have numerous implications for outbreak detection and investigation and research perspectives to improve knowledge of environmental risk factors associated with geographic disparities in STEC-HUS in France.

Shiga toxin–producing *Escherichia coli* (STEC) bacteria are responsible for a spectrum of disease, ranging from simple to bloody diarrhea, and pose increased risk for severe complications, including hemolytic uremic syndrome (HUS) in children <5 years of age and the elderly (*1*). Although STEC infections represent a global burden that is difficult to characterize, in part because of differences in diagnostic capacity and disease surveillance systems, an estimated 2.8 million STEC infections and 3,890 STEC-HUS cases occur annually worldwide (*2*). Estimated notification rates of STEC infection in Europe during 2017–2021 ranged from 1.6 to 2.4 cases/100,000 population (*3*).

In France, STEC surveillance is conducted through voluntary clinical and microbiologic surveillance of HUS in children <15 years of age (*4*). Annual incidence rates for pediatric STEC-HUS in France remain relatively high, and in recent years have been close to estimated notification rates for all STEC infections in Europe (*5*). Since 1996, annual incidence rates have ranged from 0.6 to 1.5 cases/100,000 population (73 to 168 cases reported annually), and incidence has exceeded 4 cases/100,000 population in children <3 years of age (*5*). The primary serogroups identified in cases are O26, O80, and O157; an increase of serogroups O26 and O80 in the 2010s coincided with a decrease in O157 (*4*).

Ruminants are the primary reservoir, excreting STEC in their feces, thereby potentially contaminating food and their environment and posing a risk for STEC contamination in humans (*6*,*7*). Although STEC pose a substantial outbreak potential, most infections are sporadic; only 3% of cases reported in France during 2007–2016 were outbreak-associated (*4*). Determining the source of contamination for sporadic cases is difficult for numerous reasons, including limited epidemiologic data, the multiple potential sources of contamination, and gaps in knowledge about pathogen source–pathway interactions (*1*,*4*,*8*).

Annual incidence rates calculated from pediatric STEC-HUS surveillance in France show regional variations. Space–time cluster detection methods, which can be applied to epidemiologic surveillance for outbreak detection, are also of interest for studying sporadic infectious disease cases. Indeed, several

Author affiliations: Santé Publique France, Saint-Maurice, France (G. Jones, Y. Le Strat); Centre Hospitalier Universitaire Robert Debré, Assistance publique–Hôpitaux de Paris, Paris, France (P. Mariani-Kurkdjian, A. Cointe, S. Bonacorsi); Institut Pasteur, Université Paris-Cité, Paris (S. Lefèvre, F.-X. Weill)

DOI: https://doi.org/10.3201/eid2910.230382

recent studies illustrate such approaches for describing spatiotemporal disease patterns and identifying recurrent geographic clusters representing differences in baseline disease risk, including STEC infection, cryptosporidiosis, and salmonellosis (*8*–*12*).

The first objective of our study was to describe temporal trends and geographic distribution of sporadic pediatric STEC-HUS cases in France over a 10-year period. The second objective was to identify space–time clusters and describe geographic patterns of significantly higher risk for sporadic STEC-HUS at a fine geographic scale. Such data are crucial for enabling epidemiologic surveillance, including assessment of clusters requiring epidemiologic investigations. In addition, robust, statistically significant data identifying geographic disparities at a fine scale open perspectives for further research aiming to better understand potential environmental, sociodemographic, and even behavioral factors associated with observed differences.

Methods

Data Sources and Processing

Cases of suspected STEC-HUS in children <15 years of age are reported to Santé publique France (France's national public health agency) according to previously described clinical criteria (*4*). Surveillance data include demographic information (age, sex, and postal codes of residence and temporary stay), clinical data (diarrhea, date of diarrhea onset, and date of HUS diagnosis), results of stool analysis, and limited epidemiologic information (outbreak-related [community, childcare, or family setting] and primary at-risk exposures). In accordance with data protection procedures defined by France's oversight authority for privacy and data protection (Commission Nationale de l'Informatique et des Libertés), age, postal codes, dates of diarrhea onset, and HUS diagnosis are conserved indefinitely for surveillance purposes.

Microbiologic STEC surveillance is voluntary and coordinated by the National Reference Center (NRC) for *Escherichia coli*, *Salmonella* and *Shigella* (Institut Pasteur, Paris, France) and its associated laboratory (University Hospital Robert Debré, Assistance publique–Hôpitaux de Paris, Paris) (*4*). Over the entire study period, NRC conducted PCR testing of stool samples to detect virulence genes (*stx1, stx2, eae,* and *ehxA*) and O-antigen biosynthesis genes of the 10 most frequent STEC serogroups identified in France (O157, O26, O103, O145, O91, O121, O104, O55, O111, and O80 [in 2013]). NRC performed culture on all *stx*- or *eae*-positive stools. Serogrouping methods evolved over the study period (*13*,*14*) (Appendix, https://wwwnc.cdc.gov/EID/article/29/10/23-0382-App1.pdf).

We identified 1,419 notified pediatric STEC-HUS cases with symptom onset during January 1, 2012–December 31, 2021, from surveillance data. For cases with no diarrhea, we used date of HUS diagnosis. We defined sporadic cases as those having no documented epidemiologic link to other confirmed STEC or STEC-HUS cases. For cases of person-to-person transmission in a family or childcare setting, the first case was retained for analysis because the index case is considered a sporadic case potentially associated with geographically specific exposures. We excluded from analysis all foodborne or environmentally associated outbreak cases and cases in patients with reported international travel during the entire exposure period. We were able to link cases with whole-genome sequencing (WGS) data for 2018–2021. We retained in the analysis cases belonging to a WGS-linked cluster but with no common source of infection suspected from epidemiologic investigations. Also, we excluded cases with no postal code available because they could not be geocoded. Postal codes of temporary stay correspond to locations visited in France in the week before diarrhea onset. Furthermore, we restricted analyses to cases reported from mainland France. In total, we excluded 164 (12%) of 1,419 reported cases.

We used population data for children <15 years of age available for the period 2012–2018 from the National Institute for Statistics and Economic Studies. For the remaining study period of 2019–2021, we used the most recent census data available (2018). Geocoding of cases used postal code of residence or of temporary stay when available (n = 5).

We obtained all study data from anonymous surveillance data conserved by Santé publique France according to an ongoing authorization by the Commission Nationale de l'Informatique et des Libertés. No additional ethics approval was required.

Temporal and Spatial Analyses

We described temporal and spatial distributions for all cases and by subgroups for 2 variables of epidemiologic importance, age of patient and STEC serogroup. We defined 6 age groups on the basis of observed distribution in STEC-HUS incidence from surveillance data: <1 year, 1 year, 2 years, 3–4 years, 5–9 years, 10–14 years. Those groups were also statistically pertinent for calculation of standardized incidence rates. We conducted serogroup-specific subgroup analyses for the 3 most frequently identified serogroups in pediatric STEC-HUS cases in France,

O26, O80, and O157 (top-3 serogroups). For other serogroups, the number of isolates was insufficient for subgroup analysis (mean <5 isolates/year). We classified cases into 4 groups (Appendix): top-3 serogroups, other serogroup, no serogrouping, and ungroupable. We retained for overall analysis children with HUS but no microbiologic confirmation of STEC infection on the basis of clinical criteria (diarrhea before HUS) and the fact that in young children, HUS is largely associated with STEC infection (*4*).

We described temporal trends and spatial distribution by using age-standardized incidence rates calculated by the direct method. We represented spatial distribution at the administrative department level (n = 95). By using a moving average method, we decomposed monthly incidence rates into trend, season, and residual components through the decompose function with an additive model using R version 4.2 (The R Foundation for Statistical Computing, https://www.r-project.org).

Space-time Scan Statistics

We conducted a retrospective analysis for space-time cluster detection using SaTScan version 9.7 (https://www.satscan.org), including all cases and for each of the top-3 serogroups. We geocoded all cases to the établissement public de cooperation intercommunale (EPCI), a geographic unit that groups municipalities on the basis of administrative criteria (1,233 EPCI are in mainland France). The scan statistic tests whether cases are randomly distributed over space and time and identifies clusters for which a significant difference exists in the number of observed cases compared with expected cases (*15*,*16*). For each cluster, the main outputs were geographic information (coordinates of the center of the circle and radius); cluster time interval by date, population size, and number of observed and expected cases; relative risk; and p value. We considered clusters significant at $p \leq 0.05$.

We used a discrete Poisson model because of high spatial resolution of the geographic unit of analysis and the rare occurrence of STEC-HUS cases (≤1 case for most ECPIs). We included age as a covariable for all analyses. We chose different tuning parameters to assess their effect on results. On the basis of the sensitivity analysis, we restricted the maximum radius of the circular scan window to 100 km and maximum geographic cluster size to 10% of the population at risk. We set the time precision unit to days with a maximum cluster duration of 90 days to account for observed seasonality of STEC-HUS (*8*,*11*). We retained a minimum number of cases (cluster restriction) of 2. We performed space–time scans over the 10-year study period and annually. On the basis of the results of annual space–time scans, we calculated the cluster recurrence index developed by Boudou et al. to identify geographic areas where significant clusters occurred at least once during the study period (*10*). We conducted all statistical analyses by using R version 4.2 and SaTScan version 9.7 (*17*).

Results

Number of Cases over Time

A total of 1,255 sporadic pediatric STEC-HUS cases were reported during January 2012–December 2021; the annual number of cases ranged from 109 (in 2014 and in 2015) to 163 (in 2017) (Figure 1). Cases were distributed in 542 (44%) of 1,233 EPCIs. A sample was sent to NRC for 1,132 (90%) cases, and 717 (63%) of those had a STEC serogroup identified (Appendix Table 1, Figure 1). The top-3 serogroups accounted for 78% (559/717) of cases with serogroup data: O26, 228 cases (41%); O80, 149 cases (27%); and O157, 182 cases (33%). Approximately 23% (255/1,132) of cases were ungroupable. The 283 (23%) cases with no serogrouping consisted of 123 with no sample sent to NRC (24 [20%] with reported PCR detection of *stx* at the notifying hospital) and 160 that were negative at NRC (PCR *stx* or serologic tests). For the 259 cases with no *stx* detection or negative serologic tests, 95% (247) were in patients who had diarrhea before HUS.

We observed no overall trend in the annual number of sporadic cases notified or in age-standardized annual incidence rates during 2012–2021. However, for STEC O26 and O80, we observed a significant increasing trend, in parallel to a significant decreasing trend for O157 (Figures 1, 2).

The proportions of female and male case-patients were comparable over the entire study period (Figure 3). Most cases (780/1,255 [62%]) were in patients <3 years of age. Incidence rate varied by age group; the highest incidence was in children 1–2 years of age (4.9 cases/100,000 population) (Figure 3). Incidence rate by age varied slightly by serogroup; the highest incidence was in younger age groups (1–2 years) for STEC O80 (0.9 cases/100,000 population) and STEC O26 (1 case/100,000 population), compared with incidence in that age group for STEC O157 (0.2 cases/100,000 population).

Temporal and Spatial Distribution of Incidence Rates

Seasonal decomposition of all sporadic STEC-HUS cases confirmed seasonality with a distinct annual peak (Appendix Figure 2). Annual peaks also were observed for the top-3 serogroups but with associated

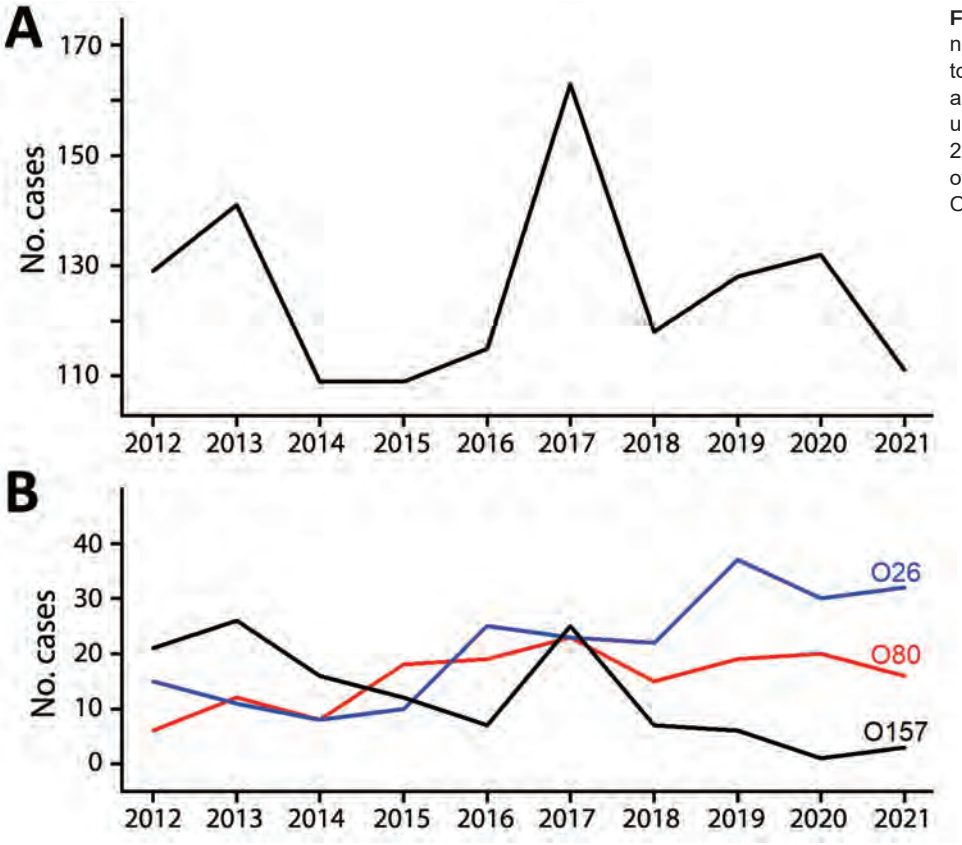

Figure 1. Annual reported number of sporadic Shiga toxin–producing *Escherichia coli*–associated pediatric hemolytic uremic syndrome cases, France, 2012–2021. A) All cases; B) cases of infection with serogroups O26, O80, and O157.

secondary and tertiary peaks between the primary seasonal peaks.

Seasonality was observed in monthly age-standardized incidence rates for each year of the study period. The highest incidence occurred in summer and early fall (July–October) (Figure 4). No clear spatial trends in annual age-standardized incidence rates were evident during the study period. The departments with the highest incidence rates varied from 1 year to the next (Figure 5).

We described spatial distribution for the top-3 serogroups over 2 periods (2012–2016 and 2017–2021) to account for a smaller number of cases. For STEC O26, we observed a geographic extension of cases when comparing the 2012–2016 period to the 2017–2021 period (Figure 6). We observed a similar evolution for STEC O80. For STEC O26 and STEC O80, departments in the eastern half of France had slightly higher incidence rates. For STEC O157, the highest incidence rates were primarily in departments in northwest France, regardless of the period.

Space–Time Scanning

Space–time scanning of all cases over the entire 10-year period identified 2 significant clusters occurring in 2019 and 2013, primarily in 2 regions in eastern France (Table 1; Figure 7). Scanning over the 10-year period by serogroup identified 2 significant clusters: STEC O26 (2019, southeast France) and STEC O80 (2017, northeast France) (Appendix Table 2, Figure 3). WGS data available for the isolates within the 2019 O26 space-time cluster identified 3 WGS-linked

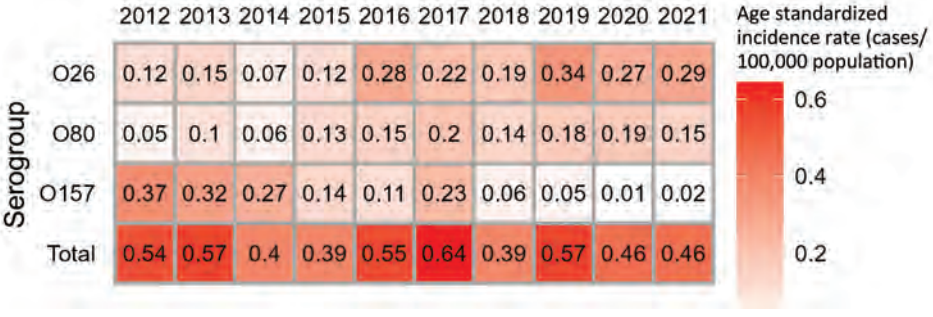

Figure 2. Age-standardized annual incidence rates of reported sporadic Shiga toxin–producing *Escherichia coli*–associated pediatric hemolytic uremic syndrome cases, for all cases and cases of infection with serogroups O26, O80, and O157, France, 2012–2021.

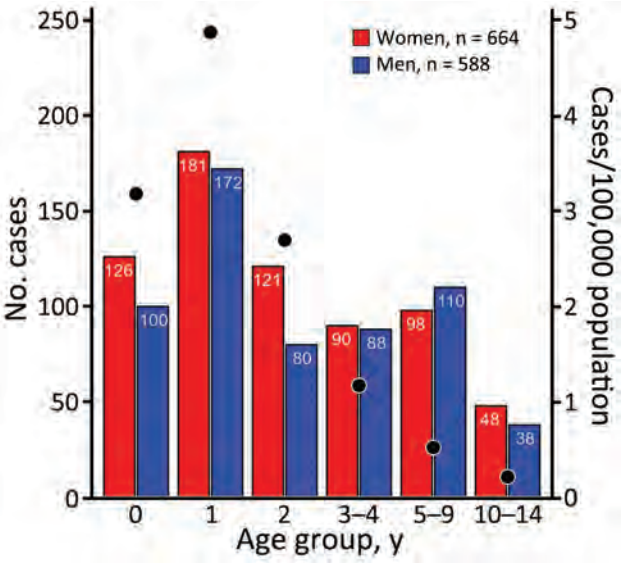

Figure 3. Number of reported sporadic Shiga toxin–producing *Escherichia coli*–associated pediatric hemolytic uremic syndrome cases, by age group and sex, and incidence rate, by age group (black dots), France, 2012–2021. Data were missing on sex for 3 cases (1 case each in patients <1 year, 3 years, and 4 years of age).

clusters of 2 isolates each (EnteroBase [https://enterobase.readthedocs.io] cgMLST scheme, HC5 level) (*14*). Short-read sequences are available in EnteroBase (identification nos. 201904732, 201904733, 201905626, 201905634, 201907203, and 201908310) and in the European Nucleotide Archive (study no. PRJEB50273). For each pair of WGS-linked isolates, epidemiologic investigations did not identify a suspected common source of infection.

Annual space–time scanning identified 13 significant space–time clusters (Table 2; Figure 8). We identified ≥1 significant cluster for each year, with the exception of 2014 and 2017, and detected a maximum of 3 significant clusters in 2018. Median cluster size was 10 cases (range 2–20 cases). Clusters occurred exclusively in the period of June–November, and most clusters corresponded to the seasonal peak observed in STEC-HUS notifications during July–October. Annual scanning by serogroup did not identify any significant space–time clusters.

The cluster recurrence index ranged from zero to 7 and identified an area of particularly high recurrence in southeast France; certain EPCIs were included in ≥5 clusters during the study period (Figure 9). Two additional major geographic zones were identified as hotspots, although to a lesser degree, in the northwest and northeast.

Discussion

During 2012–2021, a mean of 125 cases of sporadic pediatric STEC-HUS were reported in France annually. Incidence was highest in children <3 years of age, and particularly in children 1–2 years of age (an incidence 1.7 times greater than that observed in children <1 year of age and 2 times greater than that observed in children 2–3 years of age). Analysis of temporal trends by serogroup showed the increase of HUS-associated STEC O26 and STEC O80 in parallel to the decrease in STEC O157. Similar trends have been observed in other countries of Europe (*3*,*18*). Department-level age-standardized incidence rates showed geographic heterogeneity and no clear patterns when considering all STEC-HUS cases. Subgroup analysis showed the geographic extension of STEC O26 and STEC 80.

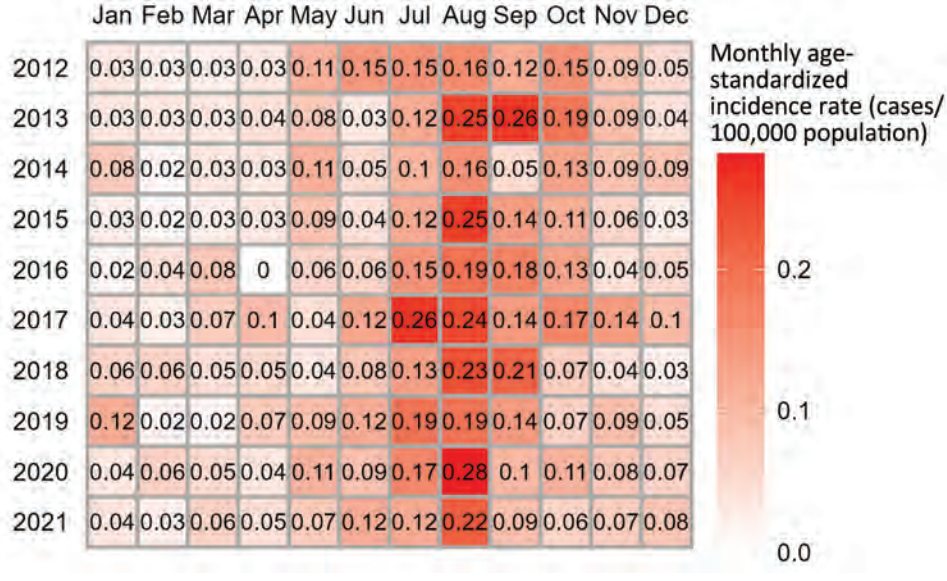

Figure 4. Monthly age-standardized incidence rates of reported sporadic Shiga toxin–producing *Escherichia coli*–associated pediatric hemolytic uremic syndrome cases, France, 2012–2021.

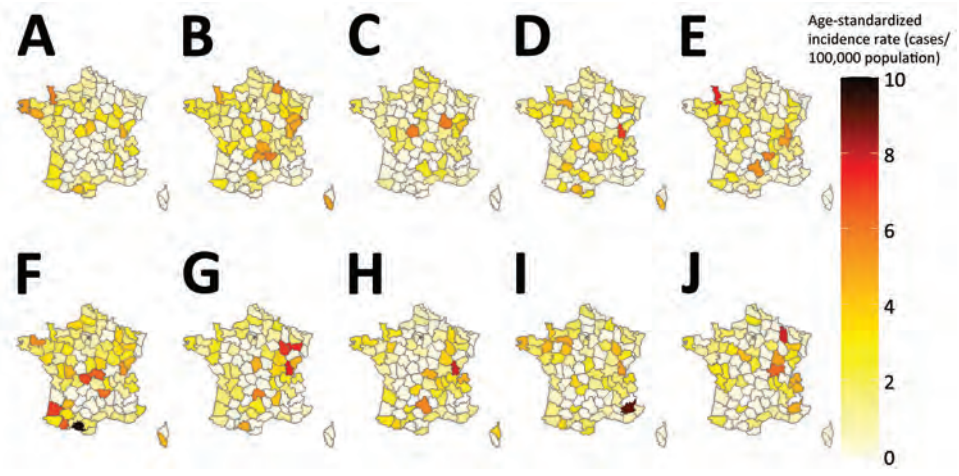

Figure 5. Geographic distribution of age-standardized incidence rates of all reported sporadic Shiga toxin–producing *Escherichia coli*–associated pediatric hemolytic uremic syndrome cases, France, 2012–2021. A) 2012; B) 2013; C) 2014; D) 2015; E) 2016; F) 2017; G) 2018; H) 2019; I) 2020; J) 2021.

Annual space–time scanning identified 13 significant clusters occurring over a 10-year period and confirmed geographic disparities in cases. Significant clusters occurred almost exclusively during the seasonal peak of STEC-HUS observed during July–October. Application of the cluster recurrence index identified several geographic zones of interest, in particular southeast France, with certain EPCIs included in ≥5 recurrent space–time clusters. This zone is in the second most densely populated region in France and includes a major city, Lyon, but also rural areas and high cattle density (*19*). To a lesser extent, we identified notable space–time clusters in regions in northwest and northeast France (1–2 clusters during the study period). In contrast to the southeast, those regions are less populated and have smaller population centers. As in southeast France, cattle density is higher than elsewhere in France (*19*).

One limitation of our analysis is that we hypothesized that sensitivity of reporting was constant over space and time for the 10-year study period. Previous studies estimated sensitivity of reporting at 66% during 2002–2003 and 85% during 2016–2017 (*20*; Santé publique France, unpub. data). Variations may have occurred in the sensitivity of reporting over time or between regions. In particular, the occurrence of outbreaks might improve reporting because of greater awareness among clinicians after outbreak events. Of note, several foodborne STEC-HUS outbreaks with wide media coverage occurred during 2018–2019 (*21*–*23*). However, several aspects of the surveillance system limit potential bias. In particular, the surveillance system has been in place since 1996 and has a stable network of specialized hospital units, enabling Santé publique France to be in regular contact with clinicians and maintain a high level of awareness for reporting of cases. In addition, an annual reminder is sent to all participating hospital units asking them to notify any cases missed during the previous year.

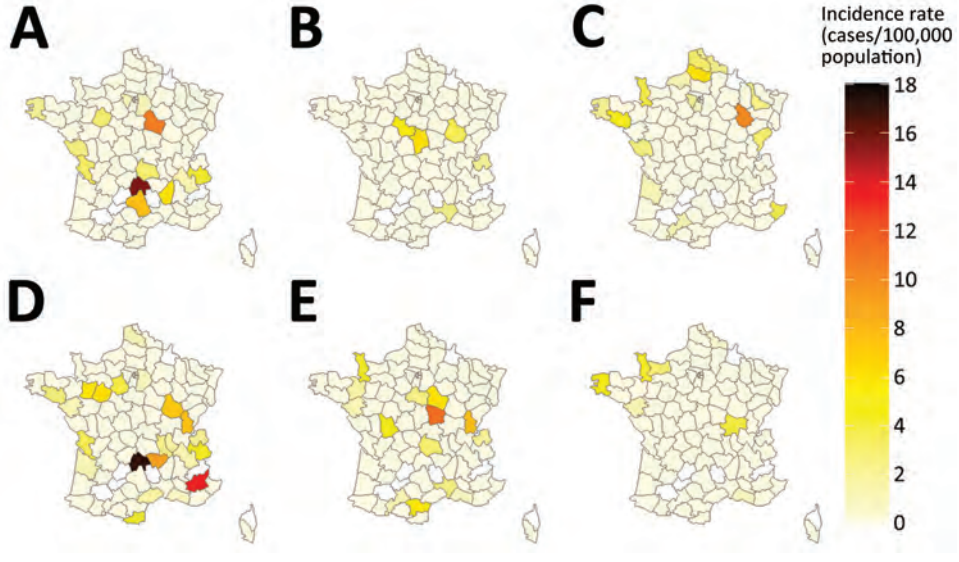

Figure 6. Geographic distribution of age-standardized incidence rates of reported sporadic Shiga toxin–producing *Escherichia coli*–associated pediatric hemolytic uremic syndrome cases caused by serogroups O26, O80, and O157, France, 2012–2021. A–C) Serogroups O26 (A), O80 (B), and O157 (C) during 2012–2016. D–F) Serogroups O26 (D), O80 (E), and O157 (F) during 2017–2021.

Table 1. Characteristics of significant clusters detected by space–time scanning of all reported sporadic Shiga toxin–producing *Escherichia coli*–associated pediatric hemolytic uremic syndrome cases, France, 2012–2021

Cluster ID	Start date	End date	Radius, km	Population	Observed no.	Expected no.	Relative risk	p value
2019 cluster A	2019 Jun	2019 Jun	96	1,073,339	20	2.8	7.2	0.00159
2013 cluster B	2013 Aug	2013 Oct	73	217,195	9	0.43	21.1	0.024

*ID, identification.

Therefore, our retrospective analysis is less likely to be affected by heterogeneous reporting.

Moreover, space–time analysis relied on EPCIs under the hypothesis that the at-risk STEC exposure occurred in the place of residence or in another reported place of exposure in France. However, case-patients may have more limited geographic movements corresponding to at-risk exposures that are not documented in surveillance data. In this case, the documented EPCI would not correspond to the actual geographic area of at-risk exposure, but because EPCIs corresponds to grouped municipalities, this factor should limit the potential bias.

Furthermore, microbiologic data was limited for some cases, and microbiologic surveillance evolved over the 10-year study period. Including cases based solely on clinical criteria may have resulted in non–STEC-related HUS. However, almost all case-patients had diarrhea before HUS, and detection of *stx* genes may be hindered by several factors, including antibiotic treatment and the delay between diarrhea onset and sampling. Because postdiarrheal HUS in young children is largely attributable to STEC infection, we considered the limited risk for including non–STEC-associated cases (*4*). In addition, the power of the serogroup analysis is probably reduced by the fact that not all reported cases had a stool sample sent to NRC for analysis or that no serogroup was identified for some cases. Introducing routine WGS data into epidemiologic surveillance in 2017 has improved characterization of isolates and detection of related strains and of potential outbreaks (e.g., those with diffuse or fewer cases) (*24*–*26*). As a result, the capacity to detect outbreak cases from pediatric STEC-HUS surveillance in France evolved, and during 2012–2016, cases belonging to smaller outbreaks possibly were not detected and would be misclassified as sporadic cases in our study. A possible result of such misclassification could be a greater number of space-time clusters identified during this period compared with 2017–2021. However, this difference did not occur; the number of space-time clusters per year is comparable between the periods before and after introduction of WGS. Also, although WGS results can suggest potential links between isolates, Besser et al. discussed the importance of epidemiologic investigations in the assessment of WGS-linked isolates (*24*), and the existence of a common source cannot be assumed. We therefore excluded WGS-linked isolates only if epidemiologic investigation suspected a common source of infection.

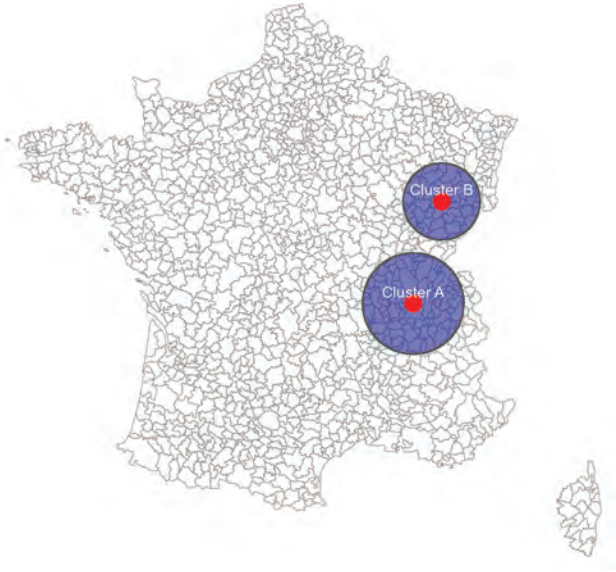

Figure 7. Significant clusters detected by space–time scanning of all reported sporadic Shiga toxin–producing *Escherichia coli*–associated pediatric hemolytic uremic syndrome cases, France, 2012–2021.

Space-time cluster detection is sensitive to the selection of parameters in SaTScan. Chen et al. discussed the challenges and potential effect of those parameter choices (*27*), and published studies offer limited guidance for parameter choice, in particular given differences in characteristics of diseases and study populations. To limit the influence of parameter choice on results, we conducted a sensitivity analysis, and our selected parameters produced robust results even when individual parameters, such as maximum population at risk, varied. We considered a maximum radius of 100 km for the scanning window as relevant for this study because the underlying hypothesis is that higher relative risk for sporadic STEC-HUS in certain geographic areas may be caused by unidentified environmental factors. Therefore, identifying clusters with unlimited radii is not epidemiologically relevant.

Our study adds to an existing body of research demonstrating the effect of applying scan statistics to describe spatiotemporal dynamics of sporadic disease, even for more rare occurrences. Our results

Table 2. Characteristics of significant clusters detected each year by space–time scanning of all reported sporadic Shiga toxin–producing *Escherichia coli*–associated pediatric hemolytic uremic syndrome cases, France, 2012–2021

Cluster ID	Start date	End date	Radius, km	Population	Observed no.	Expected no.	Relative risk	p value
2012 1	2012 Aug	2012 Oct	98	343,365	10	0.79	13.7	0.024
2012 2	2012 Jul	2012 Aug	38	111,646	6	0.15	41.7	0.024
2013 1	2013 Aug	2013 Oct	73	223,770	9	0.47	20.18	0.00748
2013 2	2013 Nov	2013 Nov	0	1,278	2	0.0002	10013.3	0.031
2015 1	2015 Aug	2015 Oct	98	1,090,917	18	2	10.56	0.0000253
2016 1	2016 Jun	2016 Sep	99	1,001,768	17	2.39	8.16	0.00215
2018 1	2018 Jun	2018 Sep	94	253,429	10	0.58	18.61	0.00196
2018 2	2018 Sep	2018 Sep	25	37,752	3	0.0058	527.19	0.031
2018 3	2018 Jul	2018 Sep	99	926,727	11	1.15	10.45	0.044
2019 1	2019 Jun	2019 Sep	96	1,082,597	20	2.94	7.88	0.000202
2020 1	2020 Jun	2020 Aug	86	333,046	10	0.75	14.3	0.017
2020 2	2020 Aug	2020 Aug	79	858,465	8	0.38	22.26	0.017
2021 1	2021 Jul	2021 Aug	99	999,909	10	0.66	16.46	0.00501

*ID, identification.

provide important insight into the epidemiologic context and have implications for outbreak detection and investigation and for research perspectives to improve knowledge of risk factors associated with geographic disparities in disease. The identification of several geographic areas with recurring clusters of sporadic STEC-HUS confirms statistically, and at a much finer geographic scale, previous observations of disparities in regional incidence of pediatric STEC-HUS in France (*4*,*19*). Taking into account geographic differences is relevant to analysis of surveillance data for outbreak detection purposes, in particular for evaluating epidemiologic signals and the decision to initiate investigations. The different geographic relative risks identified in this study will be integrated into SaTScan as part of ongoing research into its application for outbreak

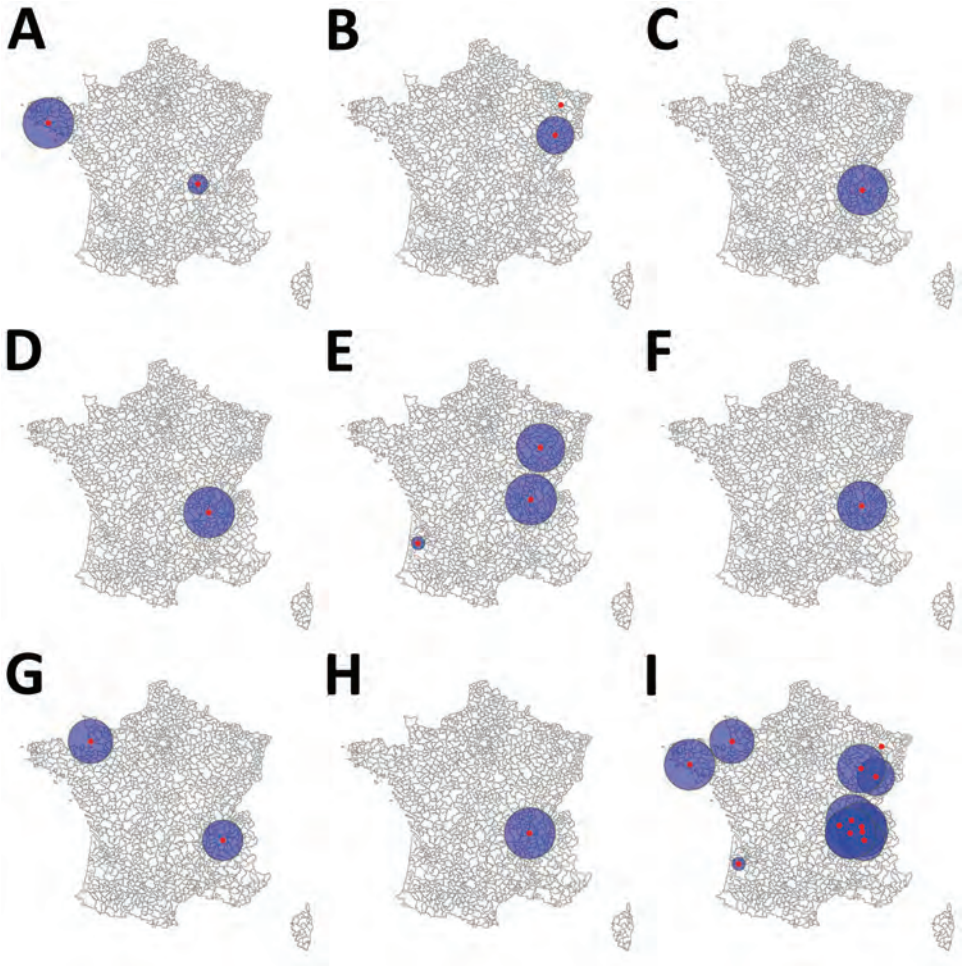

Figure 8. Significant clusters detected by annual space–time scanning of all reported sporadic Shiga toxin–producing *Escherichia coli*–associated pediatric hemolytic uremic syndrome cases, France, 2012–2021. A) 2012; B) 2013; C) 2015; D) 2016; E) 2018; F) 2019; G) 2020; H) 2021; I) 2012–2021.

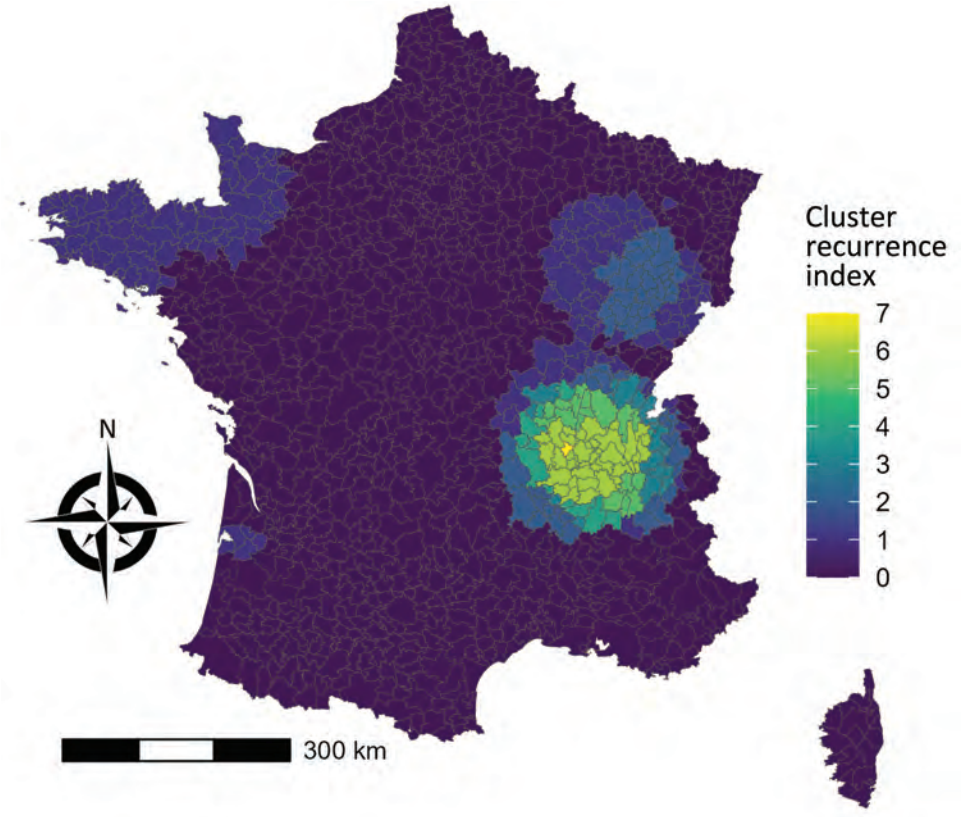

Figure 9. Cluster recurrence index of all reported sporadic Shiga toxin–producing *Escherichia coli*–associated pediatric hemolytic uremic syndrome cases, France, 2012–2021.

detection in France (*28*). Compared with WGS, statistical space-time cluster detection provides a reactive approach that can be applied to case notification data before WGS data are available (e.g., delays of ≈3 weeks in France) or in absence of strain isolation.

Our study also provides the necessary data and justification for further research on geographic factors associated with a higher baseline risk for STEC-HUS in France. Ecologic studies conducted in several countries using STEC surveillance data have identified significant associations with ruminant density, rural classification, and water sources, in particular private well usage (*9*,*29*–*32*). The findings of a study in France by Haus-Cheymol et al. suggested an association between pediatric STEC-HUS incidence and dairy cattle and calf density. The described geographic distribution of higher dairy cattle density in that study overlaps in part with the higher-risk geographic zones identified in our study in northwest and eastern France (*19*). However, the study merits an update because it is from the early 2000s, is limited to a more macroscopic geographic level, and covers a period before several observed evolutions in STEC epidemiology in France.

Our analysis also identified significant, recurring, space-time clusters consisting of cases with different serogroups. This finding suggests conditions favorable for STEC transmission that may contribute to higher risk for STEC-HUS, including geographic differences that could influence STEC risk because of different patterns of food and environmental exposures through a range of transmission pathways. We plan to use our results in further studies aimed at exploring the association with environmental parameters potentially underlying STEC-HUS risk in France. Conducting such a study at a finer geographic scale would aim to provide improved insight for public health professionals to target and adapt public health interventions, including communication with the general population, aimed at STEC prevention.

Acknowledgments

We thank Henriette de Valk and Harold Noel for their attentive reading of the manuscript and helpful suggestions.

About the Author

Ms. Jones is an epidemiologist for Santé publique France, the national public health agency of France, working in foodborne disease surveillance and outbreak investigation. Her primary research interests include surveillance of STEC infections and STEC-associated hemolytic uremic syndrome and viral gastroenteritis.

References

1. Joseph A, Cointe A, Mariani Kurkdjian P, Rafat C, Hertig A. Shiga toxin–associated hemolytic uremic syndrome: a narrative review. Toxins (Basel). 2020;12:67. https://doi.org/10.3390/toxins12020067
2. Majowicz SE, Scallan E, Jones-Bitton A, Sargeant JM, Stapleton J, Angulo FJ, et al. Global incidence of human Shiga toxin–producing *Escherichia coli* infections and deaths: a systematic review and knowledge synthesis. Foodborne Pathog Dis. 2014;11:447–55. https://doi.org/10.1089/fpd.2013.1704
3. European Centre for Disease Prevention and Control. STEC infection: annual epidemiological report for 2021. 2022 [cited 2023 Jan 15]. https://www.ecdc.europa.eu/sites/default/files/documents/AER%20STEC%20-%202021.pdf
4. Bruyand M, Mariani-Kurkdjian P, Le Hello S, King LA, Van Cauteren D, Lefevre S, et al.; Réseau français hospitalier de surveillance du SHU pédiatrique. Paediatric haemolytic uraemic syndrome related to Shiga toxin–producing *Escherichia coli*, an overview of 10 years of surveillance in France, 2007 to 2016. Euro Surveill. 2019;24:1800068. https://doi.org/10.2807/1560-7917.ES.2019.24.8.1800068
5. Jones G, Mariani-Kurkdjian P, Cointe A, Bonacorsi S, Lefèvre S, Pardos de la Gandara M, et al. Annual report for surveillance of hemolytic uremic syndrome in children under 15 years old, France 2021 [in French]. 2022 [cited 2022 Dec 1]. https://www.santepubliquefrance.fr/maladies-et-traumatismes/maladies-infectieuses-d-origine-alimentaire/syndrome-hemolytique-et-uremique-pediatrique/documents/bulletin-national/donnees-de-surveillance-du-syndrome-hemolytique-et-uremique-en-2021
6. Kintz E, Brainard J, Hooper L, Hunter P. Transmission pathways for sporadic Shiga-toxin producing *E. coli* infections: a systematic review and meta-analysis. Int J Hyg Environ Health. 2017;220:57–67. https://doi.org/10.1016/j.ijheh.2016.10.011
7. Augustin J-C, Kooh P, Mughini-Gras L, Guillier L, Thébault A, Audiat-Perrin F, et al. Risk factors for sporadic infections caused by Shiga toxin–producing *Escherichia coli*: a systematic review and meta-analysis. Microb Risk Anal. 2021;17:17. https://doi.org/10.1016/j.mran.2020.100117
8. Cleary E, Boudou M, Garvey P, Aiseadha CO, McKeown P, O'Dwyer J, et al. Spatiotemporal dynamics of sporadic Shiga toxin–producing *Escherichia coli* enteritis, Ireland, 2013-2017. Emerg Infect Dis. 2021;27:2421–33. https://doi.org/10.3201/eid2709.204021
9. Brehony C, Cullinan J, Cormican M, Morris D. Shiga toxigenic *Escherichia coli* incidence is related to small area variation in cattle density in a region in Ireland. Sci Total Environ. 2018;637-638:865–70. https://doi.org/10.1016/j.scitotenv.2018.05.038
10. Boudou M, Cleary E, ÓhAiseadha C, Garvey P, McKeown P, O'Dwyer J, et al. Spatiotemporal epidemiology of cryptosporidiosis in the Republic of Ireland, 2008–2017: development of a space-time "cluster recurrence" index. BMC Infect Dis. 2021;21:880. https://doi.org/10.1186/s12879-021-06598-3
11. Li X, Singh N, Havelaar AH, Blackburn JK. Geographical distribution and space-time clustering of human illnesses with major *Salmonella* serotypes in Florida, USA, 2017–2018. Epidemiol Infect. 2022;150:e175. https://doi.org/10.1017/S0950268822001558
12. Varga C, John P, Cooke M, Majowicz SE. Area-level clustering of Shiga toxin–producing *Escherichia coli* infections and their socioeconomic and demographic factors in Ontario, Canada: an ecological study. Foodborne Pathog Dis. 2021;18:438–47. https://doi.org/10.1089/fpd.2020.2918
13. King LA, Nogareda F, Weill F-X, Mariani-Kurkdjian P, Loukiadis E, Gault G, et al. Outbreak of Shiga toxin–producing *Escherichia coli* O104:H4 associated with organic fenugreek sprouts, France, June 2011. Clin Infect Dis. 2012;54:1588–94. https://doi.org/10.1093/cid/cis255
14. Zhou Z, Alikhan NF, Mohamed K, Fan Y, Achtman M; Agama Study Group. The EnteroBase user's guide, with case studies on *Salmonella* transmissions, *Yersinia pestis* phylogeny, and *Escherichia* core genomic diversity. Genome Res. 2020;30:138–52. https://doi.org/10.1101/gr.251678.119
15. Kulldorff M, Athas WF, Feuer EJ, Miller BA, Key CR. Evaluating cluster alarms: a space-time scan statistic and brain cancer in Los Alamos, New Mexico. Am J Public Health. 1998;88. https://doi.org/10.2105/AJPH.88.9.1377
16. Kulldorff M, Heffernan R, Hartman J, Assunção R, Mostashari F. A space-time permutation scan statistic for disease outbreak detection. PLoS Med. 2005;2:e59. https://doi.org/10.1371/journal.pmed.0020059
17. R Core Team. R: a language and environment for statistical computing. 2021 [cited 2022 Apr 1]. https://www.r-project.org
18. Cointe A, Birgy A, Mariani-Kurkdjian P, Liguori S, Courroux C, Blanco J, et al. Emerging multidrug-resistant hybrid pathotype Shiga toxin–producing *Escherichia coli* O80 and related strains of clonal complex 165, Europe. Emerg Infect Dis. 2018;24:2262–9. https://doi.org/10.3201/eid2412.180272
19. Haus-Cheymol R, Espie E, Che D, Vaillant V, DE Valk H, Desenclos JC. Association between indicators of cattle density and incidence of paediatric haemolytic-uraemic syndrome (HUS) in children under 15 years of age in France between 1996 and 2001: an ecological study. Epidemiol Infect. 2006;134:712–8. https://doi.org/10.1017/S095026880500542X
20. Espié E, Grimont F, Mariani-Kurkdjian P, Bouvet P, Haeghebaert S, Filliol I, et al. Surveillance of hemolytic uremic syndrome in children less than 15 years of age, a system to monitor O157 and non-O157 Shiga toxin–producing *Escherichia coli* infections in France, 1996–2006. Pediatr Infect Dis J. 2008;27:595–601. https://doi.org/10.1097/INF.0b013e31816a062f
21. Santé publique France. Two cases of hemolytic uremic syndrome with a probable link to consumption of contaminated reblochon cheese [in French]. 2018 Dec 20 [cited 2023 Dec 1]. https://www.santepubliquefrance.fr/les-actualites/2018/deux-cas-de-syndrome-hemolytique-et-uremique-en-lien-probable-avec-la-consommation-de-reblochon-contamine
22. Jones G, Lefèvre S, Donguy MP, Nisavanh A, Terpant G, Fougère E, et al. Outbreak of Shiga toxin–producing *Escherichia coli* (STEC) O26 paediatric haemolytic uraemic syndrome (HUS) cases associated with the consumption of soft raw cow's milk cheeses, France, March to May 2019. Euro Surveill. 2019;24:1900305. https://doi.org/10.2807/1560-7917.ES.2019.24.22.1900305
23. Jones G, de Valk H. Outbreak of Shiga toxin–producing *Escherichia coli* O26 linked to consumption of raw milk reblochon cheese, France, March–May 2018 [in French]. 2020 [cited 2022 Dec 1]. https://www.santepubliquefrance.fr/maladies-et-traumatismes/maladies-infectieuses-d-origine-alimentaire/syndrome-hemolytique-et-uremique-pediatrique/documents/rapport-synthese/epidemie-d-infections-a-escherichia-coli-o26-producteur-de-shiga-toxines-liees-a-la-consommation-de-reblochon-au-lait-cru.-france-mars-mai-2018

24. Besser JM, Carleton HA, Trees E, Stroika SG, Hise K, Wise M, et al. Interpretation of whole-genome sequencing for enteric disease surveillance and outbreak investigation. Foodborne Pathog Dis. 2019;16:504–12. https://doi.org/10.1089/fpd.2019.2650
25. Dallman TJ, Byrne L, Ashton PM, Cowley LA, Perry NT, Adak G, et al. Whole-genome sequencing for national surveillance of Shiga toxin–producing *Escherichia coli* O157. Clin Infect Dis. 2015;61:305–12. https://doi.org/10.1093/cid/civ318
26. Moura A, Criscuolo A, Pouseele H, Maury MM, Leclercq A, Tarr C, et al. Whole genome-based population biology and epidemiological surveillance of *Listeria monocytogenes*. Nat Microbiol. 2016;2:16185. https://doi.org/10.1038/nmicrobiol.2016.185
27. Chen J, Roth RE, Naito AT, Lengerich EJ, Maceachren AM. Geovisual analytics to enhance spatial scan statistic interpretation: an analysis of U.S. cervical cancer mortality. Int J Health Geogr. 2008;7:57. https://doi.org/10.1186/1476-072X-7-57
28. Robertson C, Nelson TA, MacNab YC, Lawson AB. Review of methods for space-time disease surveillance. Spat Spatio-Temporal Epidemiol. 2010;1:105–16. https://doi.org/10.1016/j.sste.2009.12.001
29. Frank C, Kapfhammer S, Werber D, Stark K, Held L. Cattle density and Shiga toxin–producing *Escherichia coli* infection in Germany: increased risk for most but not all serogroups. Vector Borne Zoonotic Dis. 2008;8:635–43. https://doi.org/10.1089/vbz.2007.0237
30. Elson R, Grace K, Vivancos R, Jenkins C, Adak GK, O'Brien SJ, et al. A spatial and temporal analysis of risk factors associated with sporadic Shiga toxin–producing *Escherichia coli* O157 infection in England between 2009 and 2015. Epidemiol Infect. 2018;146:1928–39. https://doi.org/10.1017/S095026881800256X
31. Odoi AWM, Martin SW, Michel P, Middleton D, Holt J, Wilson J. Investigation of clusters of giardiasis using GIS and a spatial scan statistic. Int J Health Geogr. 2004;3:11. https://doi.org/10.1186/1476-072X-3-11
32. Óhaiseadha C, Hynds PD, Fallon UB, O'Dwyer J. A geostatistical investigation of agricultural and infrastructural risk factors associated with primary verotoxigenic *E. coli* (VTEC) infection in the Republic of Ireland, 2008–2013. Epidemiol Infect. 2017;145:95–105. https://doi.org/10.1017/S095026881600193X

Address for correspondence: Gabrielle Jones, Santé publique France, Direction des Maladies Infectieuses, 12 rue du Val d'Osne, 94415 Saint-Maurice CEDEX, France; email: gabrielle.jones@santepubliquefrance.fr

Stability of Monkeypox Virus in Body Fluids and Wastewater

Claude Kwe Yinda,[1] Dylan H. Morris,[1] Robert J. Fischer, Shane Gallogly, Zachary A. Weishampel, Julia R. Port, Trenton Bushmaker, Jonathan E. Schulz, Kyle Bibby, Neeltje van Doremalen, James O. Lloyd-Smith, Vincent J. Munster

An outbreak of human mpox infection in nonendemic countries appears to have been driven largely by transmission through body fluids or skin-to-skin contact during sexual activity. We evaluated the stability of monkeypox virus (MPXV) in different environments and specific body fluids and tested the effectiveness of decontamination methodologies. MPXV decayed faster at higher temperatures, and rates varied considerably depending on the medium in which virus was suspended, both in solution and on surfaces. More proteinaceous fluids supported greater persistence. Chlorination was an effective decontamination technique, but only at higher concentrations. Wastewater was more difficult to decontaminate than plain deionized water; testing for infectious MPXV could be a helpful addition to PCR-based wastewater surveillance when high levels of viral DNA are detected. Our findings suggest that, because virus stability is sufficient to support environmental MPXV transmission in healthcare settings, exposure and dose-response will be limiting factors for those transmission routes.

Human mpox is an infectious zoonotic disease caused by monkeypox virus (MPXV) that was first discovered in 1958 in nonhuman primates in a laboratory setting (*1*). Even though exact animal reservoirs are unknown, small mammals are thought to maintain MPXV in West and Central Africa (*2*,*3*), where the virus is endemic (*4*) and periodic spillover into humans and limited onward transmission occur (*5*). Historically, MPXV cases have been identified sporadically outside of endemic regions, mostly related to travel, nosocomial contact, or contact with imported rodents (*6*).

Author affiliations: National Institute of Allergy and Infectious Diseases, Laboratory of Virology, Hamilton, Montana, USA (C.K. Yinda, R.J. Fischer, S. Gallogly, Z.A. Weishampel, J.R. Port, T. Bushmaker, J.E. Schulz, N. van Doremalen, V.J. Munster); University of California, Los Angeles, California, USA (D.H. Morris, J.O. Lloyd-Smith); University of Notre Dame, Notre Dame, Indiana, USA (K. Bibby)

DOI: https://doi.org/10.3201/eid2910.230824

There are 2 known clades of MPXV: clades I (formerly Congo Basin clade) and II (formerly West Africa clade) (*7*). In May 2022, the largest known human outbreak of mpox began; this multinational outbreak is caused by clade IIb MPXV. On July 23, 2022, the World Health Organization declared the human mpox outbreak a Public Health Emergency of International Concern (*8*). Since then, >87,000 laboratory-confirmed cases have been reported, most outside of endemic regions.

Human-to-human transmission of MPXV is likely to occur through direct contact or, potentially, fomites such as clothes, utensils, and bedding (*7*). During the ongoing outbreak, most cases have involved men who have sex with men (MSM). Sexual activity has been shown to be a likely route of transmission through skin-to-skin contact or sharing of body fluids. MPXV has been detected in a wide variety of samples including blood, saliva, urine, feces, semen, and skin, as well as rectal and oropharyngeal swab specimens (*9*,*10*). Environmental sampling detected low amounts of viable MPXV on household surfaces, even 15 days after initial discovery (*11*). In addition, MPXV genetic material has been detected in wastewater streams (*12*), prompting concern about risk of infection for wastewater workers or possible reverse spillover into populations (*13*). We evaluated stability in body fluids on surfaces and in wastewater of MPXV isolate hMPXV/USA/MA001/2022 (MA001), isolated in May 2022 from a human case-patient in Massachusetts, USA, and assessed the effectiveness of decontamination methods using chlorination.

Methods

We performed all experiments using 4.8×10^6 plaque forming units (PFU)/mL clade II MPXV MA001 under maximum containment conditions at Rocky Mountain Laboratories (Hamilton, MT, USA). We propagated the virus in VeroE6 cells in Dulbecco

[1]These authors contributed equally to this study.

modified Eagle medium (DMEM; Sigma-Aldrich, https://www.sigmaaldrich.com) supplemented with 10% fetal bovine serum, 1 mmol L-glutamine, 50 U/mL penicillin, and 50 μg/mL streptomycin (10% DMEM). We completed all experiments in triplicate at room temperature (21°C–23°C) unless otherwise indicated. We quantified MPXV using a plaque assay; limit of detection for all replicates was 2 PFU/mL. All experimental measurements are reported as medians across 3 replicates. We acquired human body fluids commercially from Lee BioSolutions Inc. (now Medix Biochemica USA Inc., https://www.leebio.com). Wastewater samples were collected from a municipal wastewater treatment plant in northern Indiana, USA, then shipped frozen overnight to Rocky Mountain Laboratories, where they were stored at –80°C until used as described elsewhere (*14*).

Stability of MPXV on Surfaces under Different Environmental Conditions

We evaluated the surface stability of MPXV MA001 on 15 mm polypropylene, AISI 316L alloy stainless steel disks, and cotton in conditions representing temperate fall (4°C/40% relative humidity [RH]), controlled room (21°C–23°C/40% RH), and tropical (28°C/65% RH) environments. We produced controlled environmental conditions in environmental chambers (MMM Group, https://www.mmm-medcenter.com) with protection from UV-B and UV-C exposure. After each environmental condition was established and maintained, we deposited 50 μL (7–10 drops) of MPXV stock containing 10^5 PFU on the surface of a disk. At time of deposition (day 0) and 7 additional predefined timepoints (1, 3, 5, 7, 10, 15, and 20 days after deposition), we recovered deposited virus by rinsing with 1 mL of DMEM supplemented with 2% fetal bovine serum, 1 mmol L-glutamine, 50 U/mL penicillin, and 50 μg/mL streptomycin (2% DMEM) and froze the samples at –80°C until time of titration.

MPXV Stability in Human Body Fluids

We measured stability of MPXV on surfaces by pipetting 50 μL of each body fluid containing 10^5 PFU of MPXV on surface plastic or in solution containing 2.0×10^6 PFU/mL (10^5 PFU/50 μL) stored in a screw-top vial at 21°C/40% RH. To determine the stability of MPXV in body fluids we spiked blood, semen, serum, saliva, urine, and feces with MPXV MA001. To determine the stability of the virus in body fluids deposited on surfaces and allowed to dry naturally, we aliquoted 50 μL of each fluid containing 10^5 PFU of MPXV onto a polypropylene disk and left them at 21°–23°C/40% RH. We recovered samples for each fluid at time of deposit and 1-, 3-, 5-, 7-, 10-, 15-, and 20-day timepoints by rinsing with 1 mL of 2% DMEM and froze the samples at −80°C until titrated. To determine the virus stability in solution, we initially prepared fluid containing 2.0×10^6 PFU/mL (10^5 PFU/50 μL). We stored solution samples (5 mL each) in screw-top vials at room temperature between sampling times. At time of deposition and 1-, 3-, 5-, 7-, 10-, 15-, and 20-day timepoints, we pipetted 50 μL of each fluid-virus mix into 1 mL of 2% DMEM and froze the samples at –80°C until time of titration.

MPXV Stability in Wastewater and Deionized Water

To assess the stability of MPXV in wastewater and deionized water, we diluted 50 μL of stock virus in 5 mL of wastewater (irradiated with 5 millirads to inactivate possible contaminants, 1:100) and deionized water (1:100 dilution) in triplicate. At time of deposition and 1-, 3-, 5-, 7-, 10-, 15-, and 20-day timepoints, we placed 100 μL of virus-spiked sample in 900 μL of DMEM supplemented with 2% DMEM and froze the samples at −80°C until time of titration. Physiochemical parameters of the wastewater have been reported elsewhere (*14*)

Wastewater Disinfection

To test the efficacy of free chlorine for disinfecting MPXV in wastewater, we diluted stock virus 100 times in wastewater and added 1.098 mL to each well in the top row of a deep-well 96-well plate. We took a sample from the solution before adding chlorine to obtain the initial virus concentration in the sample. For each concentration we added Acros Organics sodium hypochlorite (ThermoFisher, https://www.thermofisher.com) to 3 wells each to obtain initial doses of 0, 1, 5, or 10 parts per million (ppm). At initiation and 1-, 5-, 10-, 30-, and 60-minute timepoints, we added 100 μL samples of the wastewater solution to 100 μL of 0, 1, 5, and 10 ppm sodium thiosulfate solution to quench remaining free chlorine. We titrated the resulting solution and transferred it in total to 800 μL of DMEM supplemented with 2% DMEM. We froze samples at –80°C until time of titration.

Virus Quantification Using Endpoint Titration Plaque Assay

We thawed frozen samples and performed 10× serial dilutions. We added 250 μL of each dilution to a well of confluent Vero E6 cells in a 12-well plate and incubated them for 2 h. After 2 h, we added an additional 1 mL of 2% DMEM to each well. We incubated plates at 37°C with 5% CO_2 for 4 d. On day 4, we removed the medium from the wells and replaced it with 10%

formaldehyde for 10 min. After 10 min, we removed the formalin and replaced it with a 1% solution of crystal violet. The crystal violet remained on the cells for 10 min, at which point we removed it and rinsed the plates with water. After drying, we assessed the plates for plaques. We inferred individual titers and virus half-lives in a Bayesian framework (Appendix), modeling the plaque counts observed in titration wells as Poisson distributed, as reported elsewhere (*15*).

Results

In DMEM on surfaces, MPXV showed a biphasic pattern of initially slow, followed by rapid, decay. Because the transition in pace of decay typically occurred when all visible liquid had evaporated from the surface, consistent with observations for SARS-CoV-2 (*15*), we termed those periods the wet and dry phases. MPXV was less stable at higher temperatures, consistent with theoretical expectations (*15*) (Figure 1, panel A). It was more stable on stainless steel and polypropylene surfaces than on cotton, although recovering viable virus from a porous, absorbent surface like cotton may differ from recovery from nonporous, nonabsorbent surfaces, such as stainless steel (Figure 1, panel A). We calculated posterior median estimated half-lives ($T_{1/2}$) (interquartile range [IQR] 2.5%–97.5%) for the wet and dry phases (Appendix Table). $T_{1/2}$ on cotton during the dry phase could not be estimated for the 21°C–23°C room temperature and 28°C tropical conditions because we could detect no viable virus after the point of macroscopically observed drying of surfaces (Figure 1, panel A).

Next, we investigated the stability of MPXV in body fluids: blood, semen, serum, saliva, urine, and feces (Figure 2, panel A). We evaluated all matrices both on surfaces and in solution. Virus half-life showed no obvious differences between the wet and dry phases in blood, semen, and serum; half-lives during both phases were similar to half-lives in DMEM solution (Figure 2, panel B). In contrast, for saliva, urine, and feces on surfaces, virus half-lives were notably longer during the wet than the dry phase, and for all 3 secretions, half-lives were similar in solution (Figure 2, panel B).

MPXV in blood and semen showed little or no detectable decay either in solution or on surfaces during the 20-day test period (Figure 2, panel A; Appendix Table 1). Results for blood on surface and in solution varied notably. $T_{1/2}$ for blood in solution was 58.90 days (IQR 10.00–1,638.42 days) and on surfaces (dry

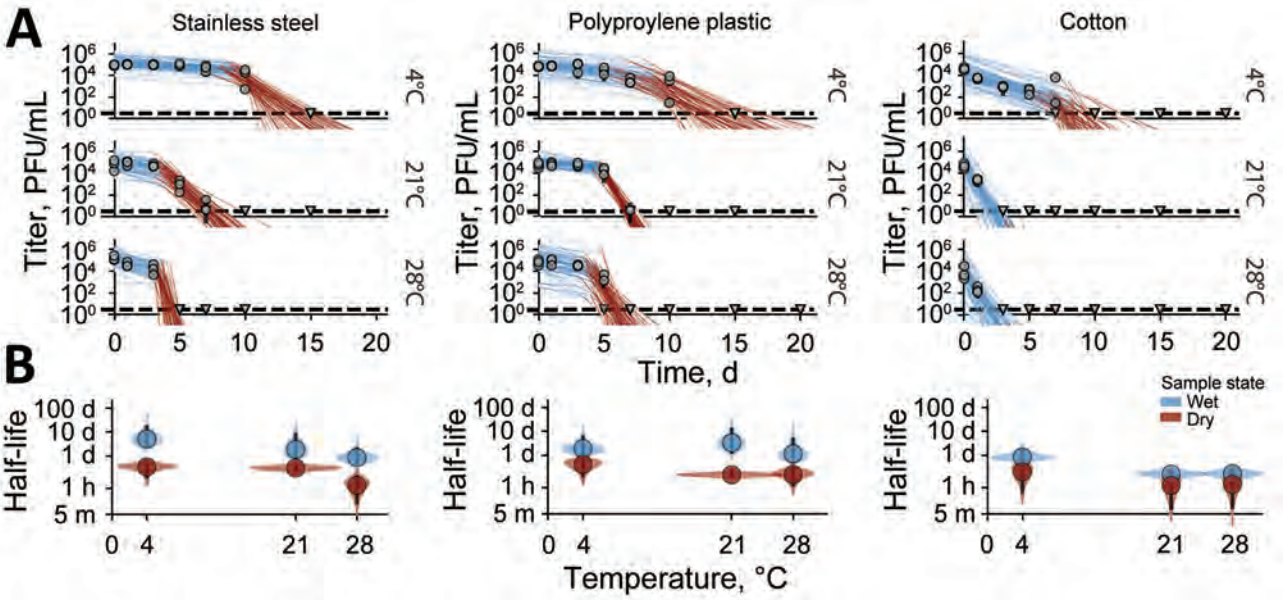

Figure 1. Monkeypox virus decay on cotton, polypropylene, and stainless steel under different environmental conditions. A) Regression lines showing predicted exponential decay of virus titers over time compared with measured (directly inferred) virus titers. Points show posterior median of measured titers; black lines show 95% credible intervals. Colored lines indicate random draws from the joint posterior distribution of exponential decay rate (negative of the slope) and intercept (initial virus titer), visualizing range of possible decay patterns for each experimental condition. Blue lines show virus titers during the inferred wet phase, when residual moisture remains visible on the surface; red lines show virus titers during the inferred dry phase, when evaporation has reached a state of quasi-equilibrium. The exact breakpoint was inferred from the data with a previous measurement from the last day of observable liquid. B) Inferred virus half-lives by surface and temperature condition. Dots show the posterior median half-life estimate and black lines show 68% (thick) and 95% (thin) credible intervals. Violin plots show the shape of posterior distribution. Blue show inferred virus half-lives on surfaces during wet phase and red on surfaces during dry phase.

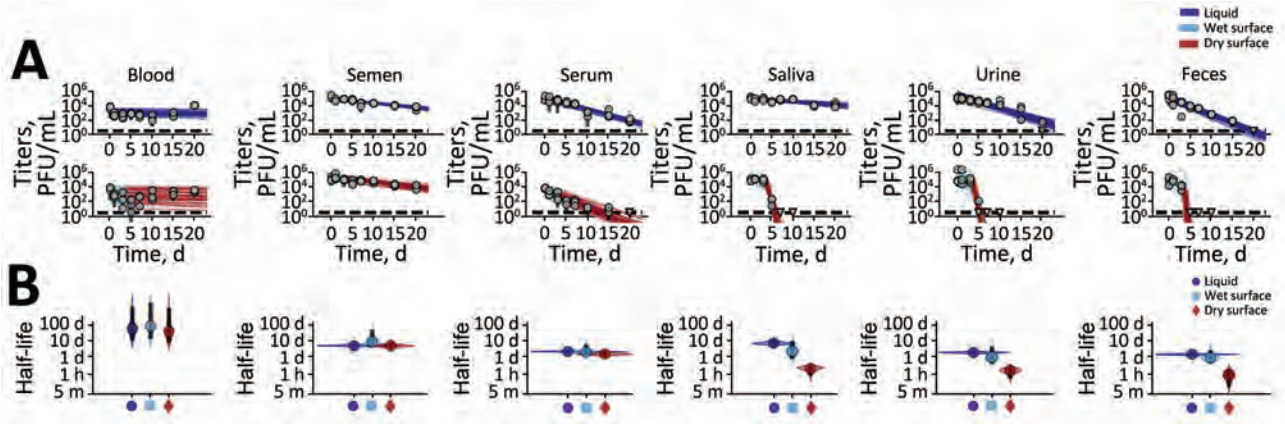

Figure 2. Monkeypox virus decay in human blood, semen, serum, saliva, urine, and feces solutions deposited on surfaces. A) Regression lines showing predicted exponential decay of virus titers over time compared with measured (directly inferred) virus titers. Points show posterior median measured titers; black lines show 95% credible intervals. Colored lines indicate random draws from joint posterior distribution of exponential decay rate (negative of the slope) and intercept (initial virus titer), visualizing range of possible decay patterns for each experimental condition. Top row shows experiments in bulk solution (liquid); bottom row shows experiments on surfaces. For surface experiments, light blue lines show the inferred titers during the wet phase, when visible residual moisture remains on the surface; red lines show the inferred dry phase, when evaporation has reached a state of quasi-equilibrium. The exact breakpoint was inferred from the data with a previous measurement from the last day of observable liquid. B) Inferred virus half-lives by condition and state. Dots show the posterior median half-life estimate and black lines show 68% (thick) and 95% (thin) credible intervals. Violin plots show the shape of posterior distribution. Dark blue show inferred virus half-lives in bulk solution, light blue on surfaces during wet phase, and red on surfaces during dry phase.

phase) was 38.75 days (IQR 6.75–1,234.38 days). $T_{1/2}$ for semen in solution was 4.63 days (IQR 3.94–5.70 days) and on surfaces (dry phase) was 4.57 days (IQR 3.35–7.09 days). MPXV in serum decayed over the test period, but with long half-lives of ≥1 days. $T_{1/2}$ for serum in solution was 1.93 days (IQR 1.71–2.27 days) and on surfaces (dry phase) was 1.32 days (IQR 0.98–1.78 days) (Figure 2, panels A, B).

MPXV had a long half-life in saliva, both in solution and on surfaces during the wet phase. $T_{1/2}$ for saliva in solution was 6.49 days (IQR 4.72–10.75 days) (Figure 2, panel B, Appendix Table 1) and on surfaces (wet phase) was 2.05 days (IQR 0.66–9.84 days), but it decayed rapidly during the dry phase: $T_{1/2}$ = 0.16 days (IQR 0.05–0.25 days). MPXV was less stable in urine and feces, but similar to results for some other body fluids, decay accelerated during the dry phase on surfaces (Figure 2, panel B). $T_{1/2}$ for urine in solution was 1.69 days (IQR 1.35–2.17 days); on surfaces (wet phase), 0.86 days (IQR 0.32–4.10 days); and on surfaces (dry phase), 0.11 days (IQR 0.03–0.21 days). $T_{1/2}$ for feces in solution was 1.28 days (IQR 1.07–1.53 days); on surfaces (wet phase), 0.76 days (IQR 0.35–2.51 days); and on surfaces (dry phase), 0.06 days (IQR 0.01–0.14 days).

Overall, MPXV was consistently at least as stable in bulk liquid environments as on surfaces, especially wet surfaces. Stability on wet versus dry surfaces differed notably for MPXV in saliva, urine, and feces but not for MPXV in blood, semen, and serum. On the basis of those differences in decay patterns for MPXV and for other viruses, as reported elsewhere (*16*), we hypothesized that a highly proteinaceous environment provides protection against decay of the virus, perhaps particularly during and after evaporation of residual water following deposition. To investigate this hypothesis, we assessed stability of MPXV in solution incorporating increasing percentages (0%, 40%, 80%, 100%) of serum mixed with DMEM. Virus stability (measured in half-lives) monotonically increased as a function of the percentage of serum (Figure 3).

Finally, we determined the stability of MPXV and effectiveness of sodium hypochlorite to inactivate MPXV in wastewater and deionized water (Figure 4). In untreated deionized water, MPXV did not decay during the sampling period: $T_{1/2}$ = 60.79 days (IQR 22.67–1078.62 days) (Figure 3). MPXV decayed to a meaningful level in wastewater, but with a half-life of multiple days ($T_{1/2}$ = 5.74 [IQR 4.58–8.05] days) (Figure 3; Appendix Figure 1). MPXV rapidly became inactivated in deionized water with added sodium hypochlorite; $T_{1/2}$ was 1.19 minutes (IQR 0.85–1.71 minutes) at 5 ppm free chlorine and 0.17 minutes (IQR 0.10–0.34 minutes) at 10 ppm. Higher chlorine concentrations were required for rapid inactivation of MPXV in contaminated wastewater samples: $T_{1/2}$ of viable virus was 8.13 minutes (IQR 6.45–10.50 minutes) at 5 ppm chlorine and 1.17 minutes (IQR 1.05–1.28 minutes) at 10

ppm. Differences in required chlorine concentrations could be because of high free-chlorine consumption by the wastewater (*17*). These results suggest that MPXV is quite stable in untreated water, including wastewater, but that wastewater can be disinfected quickly, substantially reducing levels of viable virus.

Discussion

Different studies investigating the stability of viruses of the genus *Orthopoxvirus* (family Poxiviridae) have arrived at similar conclusions as this study. Prolonged variola stability has been reported in scabs, vesicle and pustule fluids, lymph system, and purulent sores of patients (*18*). Also, investigations of variola in raw cotton and vaccinia in storm water and feces showed that a few virus particles may survive for long periods of time (*18*–*21*). Only a few studies have tested the stability of MPXV. An experimental study conducted on MPXV aerosol indicated the virus could remain viable in aerosol form for a prolonged period (*22*). Two other studies measuring stability and inactivation of MPXV showed the virus could be efficiently inactivated by alcohol- and aldehyde-based surface disinfectants. When World Health Organization–recommended alcohol-based hand rub solutions were used to test disinfection, MPXV displayed greater stability than all other emerging or reemerging enveloped viruses (*23*,*24*).

We found that MPXV indeed shows strong environmental persistence on surfaces and in solution. MPXV in some media (DMEM with human saliva, urine, and feces) showed clear biphasic decay on surfaces but not in others (blood, semen, and serum). The observed biphasic decay was indicative of stability kinetics differing from the virus initially deposited on surfaces in a liquid solution to virus remaining after macroscopic evaporation of the solution. Stability also varied depending on the various MPXV-containing fluids and wastewater we tested. MPXV persisting in clinical specimens (*25*–*27*) or tissues also suggested fluid-dependent rates of decay. More proteinaceous solutions, such as blood, serum, and semen, favored virus stability. We confirmed experimentally that the protective effect of serum was directly proportional to the concentration of serum. That finding was consistent with observations from other recent studies that environmental inactivation of viruses can be slowed by proteins in the solution and is strongly dependent on physicochemical properties of the medium (*16*).

Environmental risk assessment has typically focused on properties of the ambient environment (temperature, humidity, surface type for fomite transmission, ventilation rate for airborne transmission). Taken together with previous work on other viruses, our results suggest that route and type of contamination

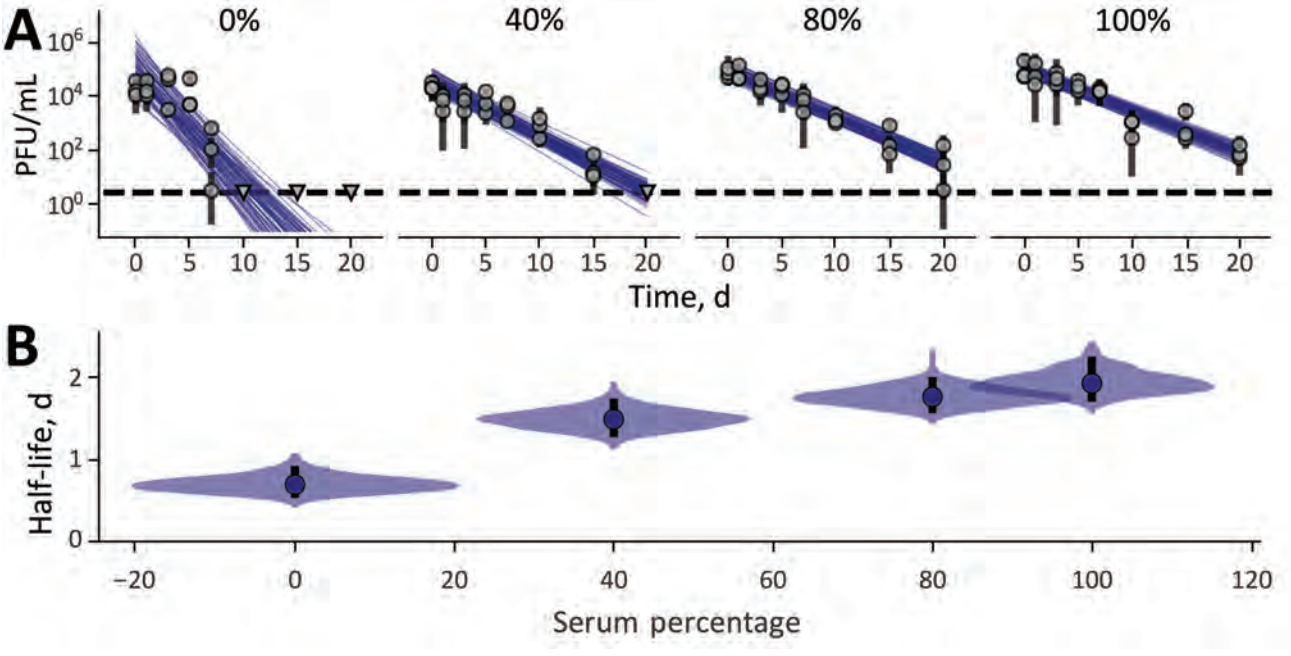

Figure 3. Monkeypox virus decay in different human serum dilutions in Dulbecco modified Eagle medium. A) Regression lines showing predicted exponential decay of virus titers over time compared with measured (directly inferred) virus titers. Points show posterior median measured titers; black lines show 95% credible intervals. Colored lines indicate random draws from joint posterior distribution of the exponential decay rate (negative of the slope) and intercept (initial virus titer), visualizing range of possible decay patterns for each experimental condition. B) Inferred virus half-lives by serum concentration. Dots show posterior median half-life estimate and black lines show 68% (thick) and 95% (thin) credible intervals. Violin plots show the shape of posterior distribution of virus half-lives.

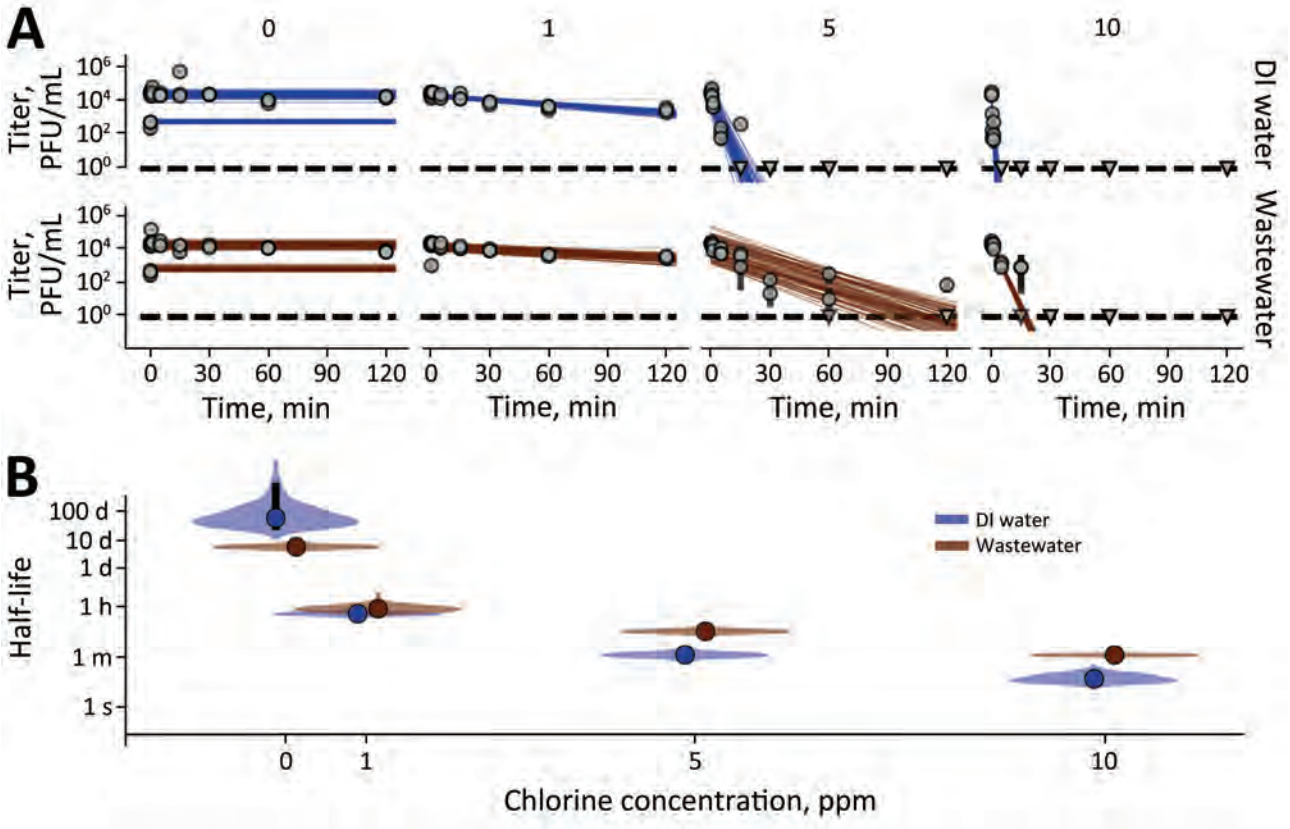

Figure 4. Monkeypox virus exponential decay and decontamination in wastewater and DI water. A) Regression lines showing predicted exponential decay of virus titer over time compared with measured (directly inferred) virus titers. Points show posterior median measured titers; black lines show 95% exponential decay rate (negative of the slope) and intercept (initial virus titer), visualizing range of possible decay patterns for each experimental condition. B) Inferred virus half-lives as a function of free chlorine concentration in parts per million. Violin plots show the shape of the posterior distribution of virus half-lives. Dots show credible intervals for posterior median half-life estimates and black lines show 68% (thick) and 95% (thin) credible intervals. Violin plots show the shape of posterior distribution. Dark blue show inferred virus half-lives in DI water and red in wastewater. DI, deionized; ppms, parts per million.

should also be considered, because viability of viruses may also depend on the body fluids from which they are shed. That factor may partly account for variability in persistence of environmental MPXV contamination on different surfaces (*11*) and in discrepancies between the longevity of MPXV on cotton in this study compared with results from epidemiologic investigations in which exudate (vesicular or pustular fluids) provided more virus-protective environments (*18*). So far, of the many cases reported among healthcare workers, only a few have been occupationally acquired (*28*–*32*), suggesting that risk for workplace transmission of MPXV to healthcare workers is notably low. In addition, many environmental surfaces are regularly exposed to UV light and common household disinfectants, which decrease viral infectivity. Nevertheless, persistence of MPXV in the environment suggests that precautions are required to avoid environmental and nosocomial transmission, in particular in hospital settings.

MPXV transmission and spread through sexual contact, especially among MSM, has been confirmed. That means long half-lives of viable MPXV in blood and semen increase risk of transmission through fluid exchange or skin-to-skin contact during sexual activity. Potential long-term viability in semen presents further implications for viral load in infected persons and for duration of infectiousness even after viral replication stops. Genetic material from other viruses, including Zika and Ebola, has been detected in semen months or years after initial infection, but how this relates to MPXV infectivity remains an open question (*33*). Estimated viral half-lives in our work are consistent with infectious MPXV remaining in semen for weeks after virus replication ends, as reported elsewhere (*34*,*35*). It should be noted however, that in patient blood, so far only DNA has been detected, and what roles blood and serum can play in MPXV transmission remains unclear (*36*).

Our finding that MPXV can remain infectious for weeks in untreated wastewater raises the potential for risk of exposure among sanitation workers, peridomestic animals, and wildlife (*13*). Given the suspected role of rodents as reservoirs of MPXV, this possibility raises hypothetical concerns about zoonotic reservoirs becoming established in previously nonendemic countries. However, we emphasize that dilution and chemical disinfection can mitigate these risks. Because previous studies only tested for viral DNA (*12*,*37*–*40*), we suggest that testing for infectious MPXV could be a valuable complement to PCR-based wastewater surveillance when significant quantities of viral DNA are detected.

In conclusion, our results suggest that MPXV stability is dependent on the surface, the environmental conditions, and the matrix of the virus. Overall, we found MPXV showed long half-lives in a variety of body fluids, both in bulk solutions and when deposited wet then allowed to dry on common clinical and residential surfaces, and half-lives approaching a week in untreated wastewater. Our findings suggest that, because virus stability is sufficient to support environmental or fomite transmission of MPXV, exposure and dose-response will be limiting factors for those transmission routes.

Acknowledgments

We thank Zachary Wiener, Todd Smith, Nicolle Baird, Christina Hutson, Fahim Atif, and Inger Damon for rapidly sharing the monkeypox virus strain used in this study. We thank Bernie Moss, Patricia Earl, Elaine Haddock, and the Rocky Mountain Laboratories institutional biosafety committee and biosafety office for helpful suggestions and support.

This work was supported by the Intramural Research Program of the National Institute of Allergy and Infectious Diseases of the National Institutes of Health. D.H.M. and J.O.L.-S. were supported by the National Science Foundation (DEB-2245631).

Conceptualization: C.K.Y., D.H.M., J.L.S., and V.M.; methodology: C.K.Y., T.B., R.J.F., S.G., Z.A.W., J.R.P., J.E.S., N.vD.; resources: K.B; supervision: N.vD., J.L.S. and V.J.M.; data curation: C.K.Y., D.H.M., S.G., Z.A.W. J.R.P. and R.J.F.; data analysis: C.K.Y., D.H.M., J.L.S., V.M.; writing: C.K.Y., D.H.M., J.L.S., V.M.; visualization: C.K.Y., and D.H.M.

About the Author

Dr. Yinda is a postdoctoral research fellow in the Laboratory of Virology of the National Institute of Allergy and Infectious Diseases. He is interested in emerging viruses and their transmission potential. Dr. Morris is a postdoctoral researcher in the Department of Ecology and Evolutionary Biology at the University of California, Los Angeles. He is interested in quantitative models of virus ecology and evolution.

References

1. Mwamba P, Tshioko K, Moudi A, V Mukinda, G.N. Mwema, D Messinger, et al. Human monkeypox in Kasai Oriental, Zaire (1996–1997). Eurosurveillance Monthly. 1997;2:33–5.
2. Nalca A, Rimoin AW, Bavari S, Whitehouse CA. Reemergence of monkeypox: prevalence, diagnostics, and countermeasures. Clin Infect Dis. 2005;41:1765–71. https://doi.org/10.1086/498155
3. Curaudeau M, Besombes C, Nakouné E, Fontanet A, Gessain A, Hassanin A. Identifying the most probable mammal reservoir hosts for monkeypox virus based on ecological niche comparisons. Viruses. 2023;15:727. https://doi.org/10.3390/v15030727
4. World Health Organization. Multi-country monkeypox outbreak: situation update [cited 2022 Jun 1]. https://www.who.int/emergencies/disease-outbreak-news/item/2022-DON396.
5. Rimoin AW, Mulembakani PM, Johnston SC, Lloyd Smith JO, Kisalu NK, Kinkela TL, et al. Major increase in human monkeypox incidence 30 years after smallpox vaccination campaigns cease in the Democratic Republic of Congo. Proc Natl Acad Sci U S A. 2010;107:16262–7. https://doi.org/10.1073/pnas.1005769107
6. Bunge EM, Hoet B, Chen L, Lienert F, Weidenthaler H, Baer LR, et al. The changing epidemiology of human monkeypox—a potential threat? A systematic review. PLoS Negl Trop Dis. 2022;16:e0010141. https://doi.org/10.1371/journal.pntd.0010141
7. Gigante CM, Korber B, Seabolt MH, Wilkins K, Davidson W, Rao AK, et al. Multiple lineages of monkeypox virus detected in the United States, 2021–2022. Science. 2022;378:560–5. https://doi.org/10.1126/science.add4153
8. World Health Organization. WHO Director-General declares the ongoing monkeypox outbreak a Public Health Emergency of International Concern. [cited 2022 Sep 19]. https://www.who.int/europe/news/item/23-07-2022-who-director-general-declares-the-ongoing-monkeypox-outbreak-a-public-health-event-of-international-concern
9. Peiró-Mestres A, Fuertes I, Camprubí-Ferrer D, Marcos MÁ, Vilella A, Navarro M, et al.; Hospital Clinic de Barcelona Monkeypox Study Group. Frequent detection of monkeypox virus DNA in saliva, semen, and other clinical samples from 12 patients, Barcelona, Spain, May to June 2022. Euro Surveill. 2022;27:2200503. https://doi.org/10.2807/1560-7917.ES.2022.27.28.2200503
10. Cassir N, Cardona F, Tissot-Dupont H, Bruel C, Doudier B, Lahouel S, et al. Observational cohort study of evolving epidemiologic, clinical, and virologic features of monkeypox in southern France. Emerg Infect Dis. 2022;28:2409–15. https://doi.org/10.3201/eid2812.221440
11. Morgan CN, Whitehill F, Doty JB, Schulte J, Matheny A, Stringer J, et al. Environmental persistence of monkeypox virus on surfaces in household of person with travel-associated infection, Dallas, Texas, USA, 2021. Emerg Infect Dis. 2022;28:1982–9. https://doi.org/10.3201/eid2810.221047
12. Wolfe MK, Yu AT, Duong D, Rane MS, Hughes B, Chan-Herur V, et al. Use of wastewater for mpox outbreak surveillance in California. N Engl J Med. 2023;388:570–2. https://doi.org/10.1056/NEJMc2213882

13. Maal-Bared R, Gerba C, Bibby K, Munakata N, Mehrotra AS, Brisolara KF, et al. The current multicountry monkeypox outbreak: what water professionals should know. ACS EST Water. 2022;2:1628–38. https://doi.org/10.1021/acsestwater.2c00287
14. Bivins A, Greaves J, Fischer R, Yinda KC, Ahmed W, Kitajima M, et al. Persistence of SARS-CoV-2 in water and wastewater. Environ Sci Technol Lett. 2020;7:937–42.
15. Morris DH, Yinda KC, Gamble A, Rossine FW, Huang Q, Bushmaker T, et al. Mechanistic theory predicts the effects of temperature and humidity on inactivation of SARS-CoV-2 and other enveloped viruses. eLife. 2021;10:e65902. https://doi.org/10.7554/eLife.65902
16. Lin K, Schulte CR, Marr LC. Survival of MS2 and Φ6 viruses in droplets as a function of relative humidity, pH, and salt, protein, and surfactant concentrations. PLoS One. 2020;15:e0243505. https://doi.org/10.1371/journal.pone.0243505
17. Greaves J, Fischer RJ, Shaffer M, Bivins A, Holbrook MG, Munster VJ, et al. Sodium hypochlorite disinfection of SARS-CoV-2 spiked in water and municipal wastewater. Sci Total Environ. 2022;807:150766. https://doi.org/10.1016/j.scitotenv.2021.150766
18. MacCallum FO, McDonald JR. Effect of temperatures of up to 45 degrees C on survival of variola virus in human material in relation to laboratory diagnosis. Bull World Health Organ. 1957;16:441–3.
19. MacCallum FO, McDonald JR. Survival of variola virus in raw cotton. Bull World Health Organ. 1957;16:247–54.
20. Essbauer S, Meyer H, Porsch-Ozcürümez M, Pfeffer M. Long-lasting stability of vaccinia virus (orthopoxvirus) in food and environmental samples. Zoonoses Public Health. 2007;54:118–24. https://doi.org/10.1111/j.1863-2378.2007.01035.x
21. Abrahão JS, Trindade GS, Ferreira JM, Campos RK, Bonjardim CA, Ferreira PC, et al. Long-lasting stability of vaccinia virus strains in murine feces: implications for virus circulation and environmental maintenance. Arch Virol. 2009;154:1551–3. https://doi.org/10.1007/s00705-009-0470-1
22. Verreault D, Killeen SZ, Redmann RK, Roy CJ. Susceptibility of monkeypox virus aerosol suspensions in a rotating chamber. J Virol Methods. 2013;187:333–7. https://doi.org/10.1016/j.jviromet.2012.10.009
23. Meister TL, Tao R, Brüggemann Y, Todt D, Steinmann J, Timm J, et al. Efficient inactivation of monkeypox virus by World Health Organization–recommended hand rub formulations and alcohols. Emerg Infect Dis. 2023;29:189–92. https://doi.org/10.3201/eid2901.221429
24. Meister TL, Brüggemann Y, Todt D, Tao R, Müller L, Steinmann J, et al. Stability and inactivation of monkeypox virus on inanimate surfaces. J Infect Dis. 2023;jiad127. https://doi.org/10.1093/infdis/jiad127
25. Pettke A, Filén F, Widgren K, Jacks A, Glans H, Andreasson S, et al. Ten-week follow-up of monkeypox case-patient, Sweden, 2022. Emerg Infect Dis. 2022;28:2074–7. https://doi.org/10.3201/eid2810.221107
26. Nörz D, Brehm TT, Tang HT, Grewe I, Hermanussen L, Matthews H, et al. Clinical characteristics and comparison of longitudinal qPCR results from different specimen types in a cohort of ambulatory and hospitalized patients infected with monkeypox virus. J Clin Virol. 2022;155:105254. https://doi.org/10.1016/j.jcv.2022.105254
27. Li Z, Li XX, Chen Y, Ruan Q, Huang X, Zhu G, et al. Persistence of monkeypox virus DNA in clinical specimens. J Infect. 2022;85:702–69.
28. Marshall KE, Barton M, Nichols J, de Perio MA, Kuhar DT, Spence–Davizon E, et al. Health care personnel exposures to subsequently laboratory–confirmed monkeypox patients—Colorado, 2022. Am J Transplant. 2022;22:2699–703. https://doi.org/10.1111/ajt.16681
29. Vaughan A, Aarons E, Astbury J, Brooks T, Chand M, Flegg P, et al. Human-to-human transmission of monkeypox virus, United Kingdom, October 2018. Emerg Infect Dis. 2020;26:782–5. https://doi.org/10.3201/eid2604.191164
30. Salvato RS, Rodrigues Ikeda ML, Barcellos RB, Godinho FM, Sesterheim P, Bitencourt LCB, et al. Possible occupational infection of healthcare workers with monkeypox virus, Brazil. Emerg Infect Dis. 2022;28:2520–3. https://doi.org/10.3201/eid2812.221343
31. Le Pluart D, Ruyer-Thompson M, Ferré VM, Mailhe M, Descamps D, Bouscarat F, et al. A healthcare-associated infection with monkeypox virus of a healthcare worker during the 2022 outbreak. Open Forum Infect Dis. 2022;9:ofac520. https://doi.org/10.1093/ofid/ofac520
32. Carvalho LB, Casadio LVB, Polly M, Nastri AC, Turdo AC, de Araujo Eliodoro RH, et al. Monkeypox virus transmission to healthcare worker through needlestick injury, Brazil. Emerg Infect Dis. 2022;28:2334–6. https://doi.org/10.3201/eid2811.221323
33. Feldmann H. Virus in semen and the risk of sexual transmission. N Engl J Med. 2018;378:1440–1. https://doi.org/10.1056/NEJMe1803212
34. Lapa D, Carletti F, Mazzotta V, Matusali G, Pinnetti C, Meschi S, et al.; INMI Monkeypox Study Group. Monkeypox virus isolation from a semen sample collected in the early phase of infection in a patient with prolonged seminal viral shedding. Lancet Infect Dis. 2022;22:1267–9. https://doi.org/10.1016/S1473-3099(22)00513-8
35. Lapa D, Carletti F, Colavita F, Nicastri E, Girardi E, Antinori A, et al. Viral replication and infectivity of monkeypox through semen—authors' reply. Lancet Infect Dis. 2022;22:1532–3. https://doi.org/10.1016/S1473-3099(22)00613-2
36. Reda A, Abdelaal A, Brakat AM, Lashin BI, Abouelkheir M, Abdelazeem B, et al. Monkeypox viral detection in semen specimens of confirmed cases: a systematic review and meta-analysis. J Med Virol. 2023;95:e28250. https://doi.org/10.1002/jmv.28250
37. de Jonge EF, Peterse CM, Koelewijn JM, van der Drift AR, van der Beek RFHJ, Nagelkerke E, et al. The detection of monkeypox virus DNA in wastewater samples in the Netherlands. Sci Total Environ. 2022;852:158265. https://doi.org/10.1016/j.scitotenv.2022.158265
38. La Rosa G, Mancini P, Veneri C, Ferraro GB, Lucentini L, Iaconelli M, et al. Detection of monkeypox virus DNA in airport wastewater, Rome, Italy. Emerg Infect Dis. 2023;29:193–6. https://doi.org/10.3201/eid2901.221311
39. Sharkey ME, Babler KM, Shukla BS, Abelson SM, Alsuliman B, Amirali A, et al. Monkeypox viral nucleic acids detected using both DNA and RNA extraction workflows. Sci Total Environ. 2023;890:164289. https://doi.org/10.1016/j.scitotenv.2023.164289
40. Girón-Guzmán I, Díaz-Reolid A, Truchado P, Carcereny A, García-Pedemonte D, Hernáez B, et al. Spanish wastewater reveals the current spread of monkeypox virus. Water Res. 2023;231:119621. https://doi.org/10.1016/j.watres.2023.119621

Address for correspondence: Vincent Munster, Chief Virus Ecology Section, Rocky Mountain Laboratories, NIAID, NIH, 903 S 4th St, Hamilton, MT 59840, USA; email: vincent.munster@nih.gov

Ancestral Origin and Dissemination Dynamics of Reemerging Toxigenic *Vibrio cholerae*, Haiti

Carla N. Mavian, Massimiliano S. Tagliamonte, Meer T. Alam, S. Nazmus Sakib, Melanie N. Cash, Monika Moir, Juan Perez Jimenez, Alberto Riva, Eric J. Nelson, Emilie T. Cato, Jayakrishnan Ajayakumar, Rigan Louis, Andrew Curtis, V. Madsen Beau De Rochars, Vanessa Rouzier, Jean William Pape, Tulio de Oliveira, J. Glenn Morris Jr.,[1] Marco Salemi,[1] Afsar Ali[1]

The 2010 cholera epidemic in Haiti was thought to have ended in 2019, and the Prime Minister of Haiti declared the country cholera-free in February 2022. On September 25, 2022, cholera cases were again identified in Port-au-Prince. We compared genomic data from 42 clinical *Vibrio cholerae* strains from 2022 with data from 327 other strains from Haiti and 1,824 strains collected worldwide. The 2022 isolates were homogeneous and closely related to clinical and environmental strains circulating in Haiti during 2012–2019. Bayesian hypothesis testing indicated that the 2022 clinical isolates shared their most recent common ancestor with an environmental lineage circulating in Haiti in July 2018. Our findings strongly suggest that toxigenic *V. cholerae* O1 can persist for years in aquatic environmental reservoirs and ignite new outbreaks. These results highlight the urgent need for improved public health infrastructure and possible periodic vaccination campaigns to maintain population immunity against *V. cholerae*.

The ancient disease cholera remains a major public health threat in countries lacking safe drinking water, optimal sanitation, and preventive hygiene practices (*1*). In Haiti, which had not had a cholera outbreak in >100 years, toxigenic *Vibrio cholerae* O1 was detected in October 2010, after a major earthquake in January 2010 that destroyed much of the nation's public health infrastructure. The first cholera epidemic wave in 2010 was likely caused by introduction of toxigenic *V. cholerae* O1 by peacekeeping troops from Nepal through contamination of Haiti's Artibonite River by sewage outflows from the camp used by the peacekeeping contingent (*2*–*4*). Initial disease transmission was associated with exposure to water in the Artibonite River, then transmission throughout the country by human movement, tracking along major highways, and subsequent reentry of the microorganism into the aquatic environment (*5*–*8*). During October 2010–February 2019, more than 820,000 cases and nearly 10,000 cholera deaths were reported in Haiti (*9*).

Despite ongoing surveillance, no clinical cholera cases were reported in Haiti from February 2019 through early September 2022, leading to assumptions that cholera had been eradicated (*10*). However, on September 25, 2022, two *V. cholerae* infections were identified in the Port-Au-Prince metropolitan area (*11*), after which the outbreak rapidly spread across the country. By May 12, 2023, the epidemic had resulted in 41,944 suspected cases in all 10 departments of the country; 38,420 hospitalizations and 685 deaths were reported (*12*). Full genome cholera sequences from an isolate sampled on September 30, 2022 (*13*), and 16 additional isolates collected from Centre, Grand-Anse, and Ouest Departments during September 30–October 31, 2022 (*14*), showed that the 2022 strains were homogeneous and closely related to the clinical and environmental strains circulating in Haiti since 2010.

Author affiliations: University of Florida, Gainesville, Florida, USA (C.N. Mavian, M.S. Tagliamonte, M.T. Alam, S.N. Sakib, M.N. Cash, J.P. Jimenez, A. Riva, E.J. Nelson, E.T. Cato, R. Louis, V.M. Beau De Rochars, J.G. Morris Jr., M. Salemi, A. Ali); Stellenbosch University, Stellenbosch, South Africa (M. Moir, T. de Oliveira); Case Western Reserve University School of Medicine, Cleveland, Ohio, USA (J. Ajayakumar, A. Curtis); Les Centres GHESKIO, Port-au-Prince, Haiti (V. Rouzier, J.W. Pape); Weill Cornell Medical College, New York, New York, USA (V. Rouzier, J.W. Pape); University of KwaZulu-Natal, Durban, South Africa (T. de Oliveira); Centre for the AIDS Programme of Research in South Africa (CAPRISA), Durban, South Africa (T. de Oliveira); University of Washington, Seattle, Washington, USA (T. de Oliveira)

DOI: https://doi.org/10.3201/eid2910.230554

[1]These senior authors contributed equally to this article.

Our research group has been monitoring the cholera epidemic in Haiti since 2010 (*15*). Our work has highlighted the role of the aquatic environment in the initial 2010 epidemic and the ongoing evolution of *V. cholerae* strains collected as part of longitudinal collection of water samples from rivers and estuarine sites (*6*–*8*,*16*–*18*). Yet, the underlying driver of recurrent toxigenic *V. cholerae* O1 outbreaks in endemic settings remains highly debated. One scenario suggests that periodic introduction and transmission of new cholera strains within human populations is the major driver and that environmental aquatic reservoirs play little or no role, providing only a transient medium for the bacteria to pass from one host to the next (*19*,*20*). An alternative perspective argues that toxigenic *V. cholerae* O1, akin to other *Vibrio* spp., can persist in aquatic reservoirs with seasonal and occasional spillover into human populations and then exponentially spread from person to person (*21*,*22*). We used whole-genome sequencing and Bayesian phylogenetics and phylogeography to reconstruct the origin and dissemination dynamic of toxigenic *V. cholerae* reemergence during the 2022 epidemic in Haiti.

Methods

For this study, we sequenced 42 clinical *V. cholerae* strains isolated during October–November 2022 and 48 previously unreported *V. cholerae* strains from clinical (n = 45) and environmental (n = 3) sources collected by our group during September 2017–June 2018, the last years of the previous epidemic wave. We used a Bayesian framework to construct phylogeny for those sequences, a large (n = 1,824) dataset of worldwide sequences, and publicly available sequences from strains isolated Haiti in 2022 (n = 17) and during 2010–2019 (n = 262, including 32 sequences from environmental isolates collected by our group) (*9*).

Sample Collection and *V. cholerae* Isolation

To isolate toxigenic *V. cholerae* O1, stool samples were collected and immediately transported to the laboratory of the Groupe Haitien d'Étude du Sarcome de Kaposi et des infections Opportunistes (GHESKIO) or to the University of Florida (UF) laboratory in Haiti. The UF laboratory processed all environmental samples. Samples were enriched in alkaline peptone water or directly inoculated samples onto thiosulfate-citrate-bile-sucrose agar plates, or both, as described previously (*6*,*7*,*16*,*17*,*23*). We further characterized each isolate by serology and performed initial genetic characterization by using PCR techniques targeting toxigenic *V. cholerae* genes (*6*).

We initiated *V. cholerae* environmental studies in 2012, collecting water samples each month from a series of 17 fixed environmental sampling sites in rural river and estuarine areas in Gressier and Leogane (Figure 1). We previously reported isolation of *V. cholerae* from 10 (59%) of the 17 collection sites and 17 (8.6%) of 197 surface water samples in 2013–2014 (*6*,*7*). *V. cholerae* isolation was seasonal and associated with higher surface water temperatures and increased rainfall (*6*,*7*). We did not see a correlation between fecal coliform counts and *V. cholerae* isolation, suggesting that the environmental toxigenic *V. cholerae* O1 we isolated were autochthonous and not associated with fecal contamination at the collection site (*6*,*7*). We subsequently expanded site locations to include multiple sites in the Port-au-Prince region; sites in Jacmel, on the southern coastline of Haiti; and sites along the Artibonite River, where cholera was introduced in 2010 (Figure 1). We isolated a total of 32 toxigenic *V. cholerae* O1 bacteria from aquatic environmental sites during 2012–2018.

Whole-Genome Mapping and SNP Calling

The UF Emerging Pathogens Institute (Gainesville, Florida, USA) performed high-quality full genome next-generation sequencing on 90 strains from 2017–2018 and 2022 by using previously described in-house protocols (*6*–*8*,*16*,*18*) (Appendix, https://wwwnc.cdc.gov/EID/article/29/10/23-0554-App1.pdf). We trimmed raw reads and genome assemblies from GenBank and the European Nucleotide Archive (ENA; https://www.ebi.ac.uk/ena) databases by using fastp version 0.22.0 (*24*). We analyzed reads by reference mapping to the 2010EL-1786 strain (GenBank accession nos. NC_016445.1 and NC_016446.1) as a reference for the Haiti dataset (*8*,*18*) or the N16961 strain (GenBank accession nos. NZ_CP028827.1 and NZ_CP028828.1) as reference for the global dataset (*19*,*20*). We used Snippy version 4.6.0 (https://github.com/tseemann/snippy) for mapping and variant calling and Gubbins version 3.2.1 (*25*) to scan consensus genome alignments for recombination. For the global dataset, we split the alignment into clusters we identified with fastBaps version 1.0.8 (*26*) before recombination analysis (Appendix).

Phylogenetic Inference with Worldwide *V. cholerae* Dataset

We inferred a maximum-likelihood phylogenetic tree by using IQ-TREE (*27*) to compare *V. cholerae* O1 strains from Haiti, including isolates from the 2022 outbreak, with 1,824 worldwide cholera strains collected during

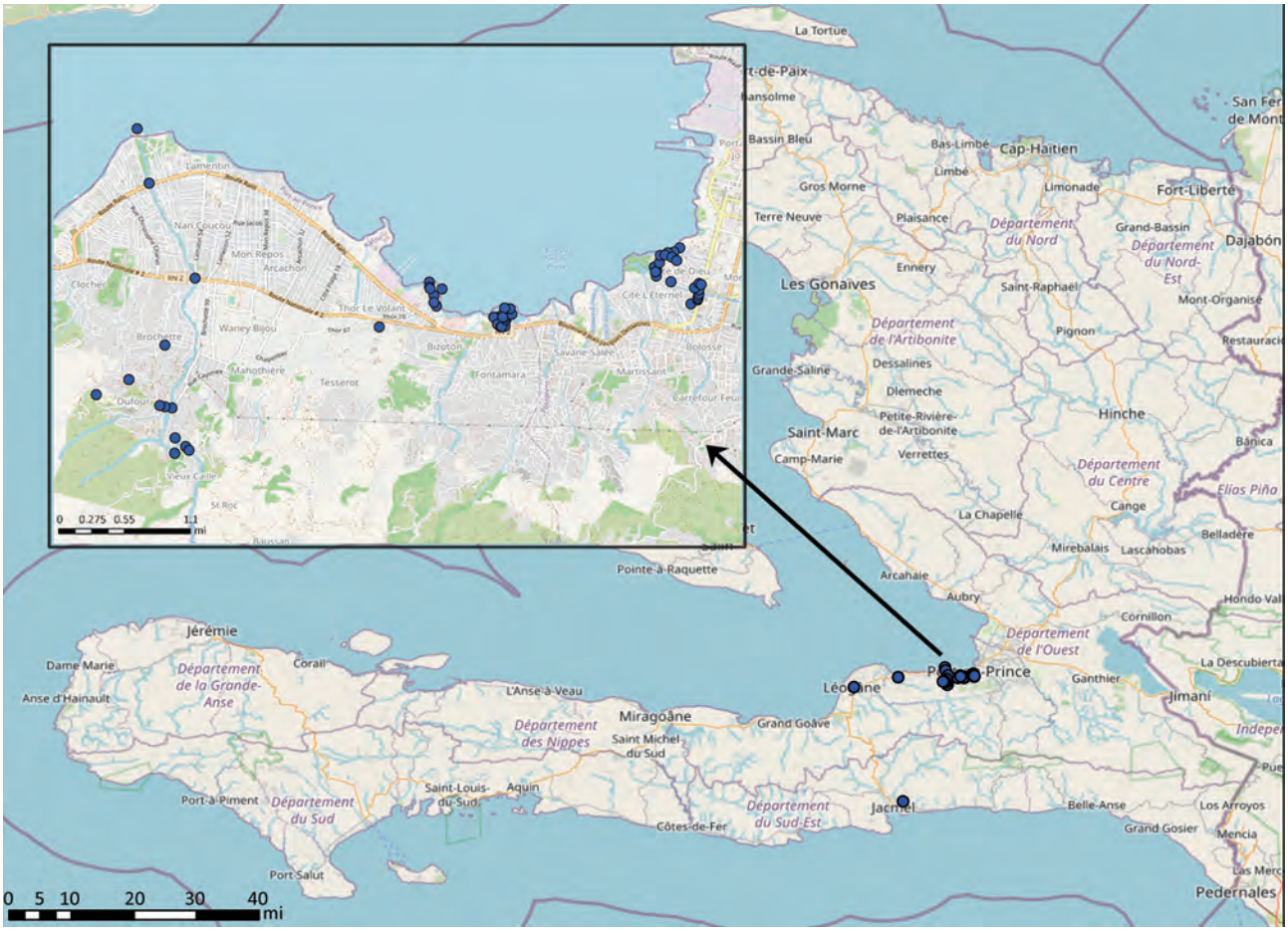

Figure 1. Selective sites of environmental sampling during used in a study of ancestral origin and dissemination dynamic of reemerging toxigenic *Vibrio cholerae*, Haiti. Blue dots indicate locations of environmental sampling sites for *V. cholerae* during 2012–2018. Inset shows detail of Port-au-Prince area sampling sites. Maps created by using OpenStreetMap (https://www.openstreetmap.org).

1957–2022. The global collection comprised strains from Europe (n = 22), the Americas (n = 593, excluding the Haiti strains), Asia (n = 465), Africa (n = 743), and Oceania (n = 1). Strains from the Americas included those from an outbreak in Argentina in the 1990s and an outbreak in Mexico during the 1990s–2013. Samples from Asia included strains from Bangladesh (1971–2011 and 2022), Nepal (1994, 2003, and 2010), and a wide range of strains from India collected during 1962–2017. The collection from Africa included strains from the 2015–2017 outbreak in the Democratic Republic of the Congo (*28*). Strains from the Middle East included strains from Yemen in 2017 (*29*). We determined the phylogenetic signal by using the likelihood mapping test in IQ-TREE (*27*). We used TreeTime (*30*) to obtain a maximum-likelihood tree scaled in time.

Phylodynamic Inference and Phylogeography

We used a Bayesian framework to infer a posterior distribution of trees and estimate the time of the most common ancestor of the sampled sequences. We considered strict or uncorrelated relaxed molecular clock models and constant or Bayesian skyline plot demographic priors. We ran Markov chain Monte Carlo samplers for 500 million generations, sampling every 50,000 generations, which was sufficient to achieve proper mixing of the Markov chain, as evaluated by effective sampling size >200 for all parameter estimates under a given model. We used BEAST version 1.10.4 (*31*) to perform Bayesian calculations. We obtained a maximum clade credibility (MCC) tree from the posterior distribution of trees by using optimal burn-in with TreeAnnotator in BEAST. For publishing purposes, we visualized the MCC phylogeny in R (The R Foundation for Statistical Computing, https://www.r-project.org) by using the ggtree package (*32*).

We performed Bayesian phylogeographic analysis in BEAST version 1.10.4 (*33*) by using groups as a discrete trait, an asymmetric transition (migration) model, Bayesian skyline plot as demographic prior,

and Bayesian stochastic search variable selection models. We considered rates yielding a Bayes factor (BF) >3 as well-supported diffusion rates (*34*) and BF >6 as decisive support (*35*), constituting the migration graph. We used DensiTree version 2 (R. Remco et al., unpub. data, https://doi.org/10.1101/012401) to graphically edit phylogenetic trees (Appendix).

Results

Epidemiology of 2022 Outbreak and Characterization of Toxigenic *V. cholerae* O1 Clinical Isolates

Our work focused on patients admitted to the GHESKIO cholera treatment center (CTC) in Port-au-Prince. GHESKIO CTC is near a portion of the city waterfront occupied by shantytowns (Figure 2, panel A), which were a key source of cases in the 2022 epidemic. Cases seen at GHESKIO CTC were concentrated among children (Figure 3, panel A), which aligned with national data reported by the Ministry of Public Health and Population in Haiti (*12*). Isolated *V. cholerae* strains were susceptible to antimicrobial agents commonly used to treat cholera (*22*), including doxycycline, ciprofloxacin, and azithromycin (Appendix Table 1). However, ciprofloxacin susceptibility was borderline and molecular analysis showed a DNA gyrase mutation in *gyrA* (Ser83Ile) and *parC* (Ser85Leu) that was previously described in clinical isolates from Haiti (*36*,*37*).

Epidemiologic curves of cumulative cases from the GHESKIO CTC showed an exponential outbreak followed by a plateau phase at the beginning of November 2022 (Figure 3, panel B), as noted in national data (*12*). When we mapped the GHESKIO CTC case data to neighborhoods, the major initial hotspots of the epidemic were Bolosse, Village de Dieu, and Cite Plus, all of which are proximate to or southwest of GHESKIO, and Waaf Jeremy, north of GHESKIO (Figure 2, panel A). During October 2022, at the beginning of the epidemic, case foci clearly moved from an initial concentration along the coast to inland areas on a week-by-week basis (Figure 2, panels C–F).

We obtained sequence data for 42 toxigenic *V. cholerae* O1 strains collected during October 3–November 21, 2022: 40 from GHESKIO CTC and 2 from a clinic at Fond Parisien, which is in a rural area ≈30 miles east of Port-au-Prince and near the border with the Dominican Republic (Figure 2, panel B). All strains were serotype Ogawa and carried the genes for cholera toxin and other key genes associated with cholera pathogenicity and virulence (Appendix Table

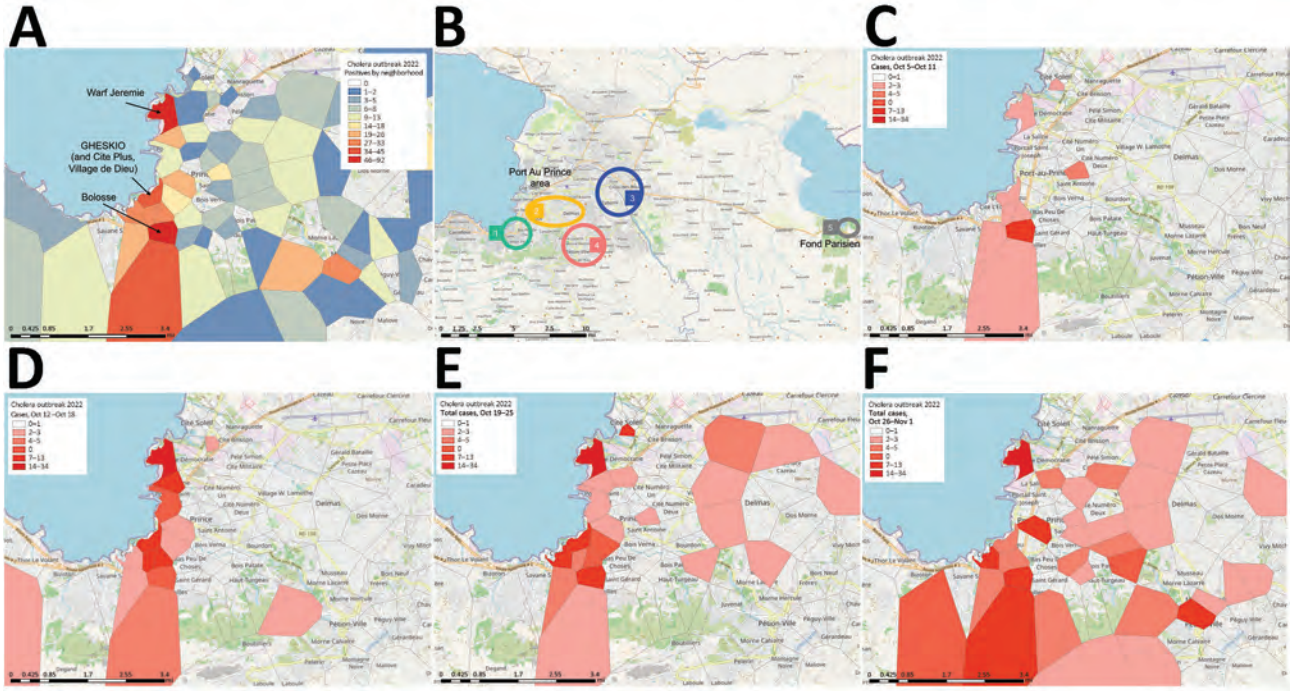

Figure 2. Temporal-spatial data on 2022 cholera cases in a study of ancestral origin and dissemination dynamic of reemerging toxigenic *Vibrio cholerae*, Haiti. Data were reported by GHESKIO CTC. A) Cumulative number of patients per Port-au-Prince neighborhood seen at the GHESKIO CTC during October–December 2022. B) Location of Fond Parisien site (no. 5 in gray circle) in relation to phylogeographic case groupings in Port-au-Prince neighborhoods: 1, GHESKIO area; 2, central eastern; 3, far eastern; 4, greater Pétion-Ville. C–F) Temporal and spatial distribution of the reported cholera cases by week: October 5–11 (C); October 12–18 (D); October 19–25 (E); October 26–November 1 (F). Maps created by using OpenStreetMap (https://www.openstreetmap.org). CTC, cholera treatment center; GHESKIO, Groupe Haitien d'Étude du Sarcome de Kaposi et des infections Opportunistes.

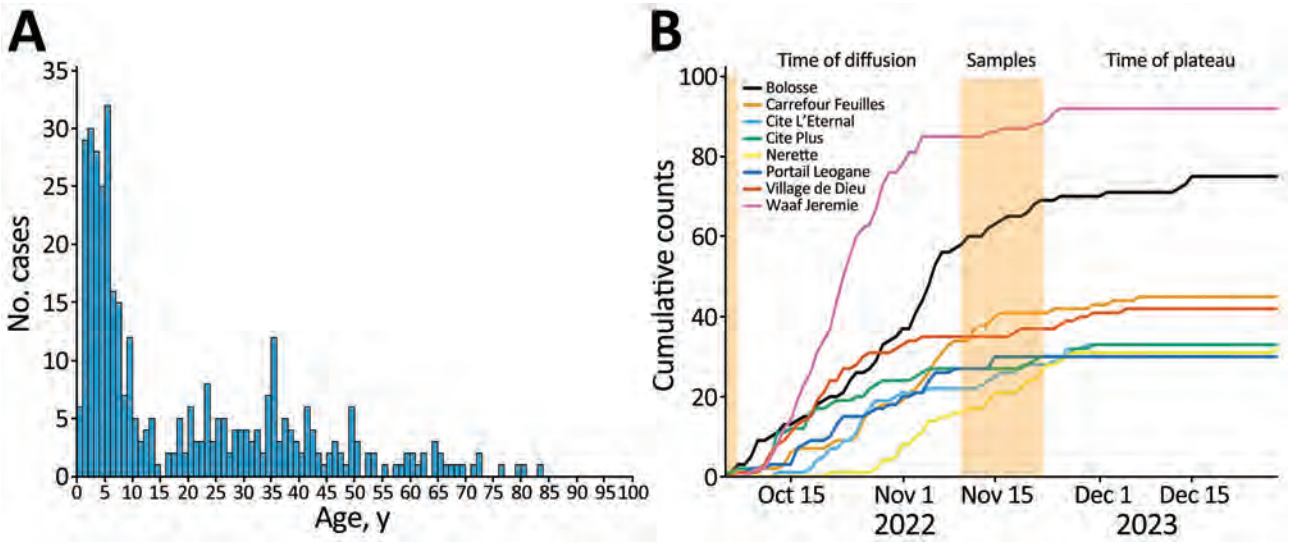

Figure 3. Characteristics of the 2022 cholera outbreak in Haiti based on reported positive cholera cases by GHESKIO. A) Age distribution of cases. B) Epidemiologic curves, by neighborhoods, of cumulative cases over time from the GHESKIO cholera treatment center. Orange shading indicates sampling interval of this study. GHESKIO, Groupe Haitien d'Étude du Sarcome de Kaposi et des infections Opportunistes.

2). All samples were collected between the end of the exponential phase and the beginning of the plateau phase of the epidemic (Figure 3, panel B). The UF institutional review board approved analysis and sequencing of the deidentified isolates.

We performed genomewide comparison of high-quality SNPs (SNPs) for those 42 sequences and 17 sequences from 2022 reported by others (*13*,*14*). Genomes were relatively homogenous and had a mean nucleotide distance in pair-wise comparisons of 1.26 high-quality SNPs, consistent with a single source introduction. However, 2022 cholera genomes from Haiti displayed 41–53 (median 24) high-quality SNP differences compared with the 2010EL-1786 reference strain. Compared with all previous strains from Haiti, a total of 5 mutations in coding segments of chromosome 1 were unique to the 2022 sequences, 1 synonymous and 4 nonsynonymous (Appendix Table 3). In addition, a 4-nt insertion caused a frameshift in the hypothetical gene HJ37_RS07360, resulting in a premature stop codon (Appendix Table 3).

As noted in prior publications (*13*,*14*), the maximum-likelihood phylogeny inferred from the genome-wide SNP alignment of 310 strains isolated in Haiti from 2010–2018, sequences from the 2022 outbreak (n = 59, including our 42 new sequences) and 1,824 worldwide reference sequences (Appendix Table 4) confirmed that the new cholera cases clustered within a well-supported (bootstrap >90%) monophyletic clade from Haiti (Appendix Figure 1). Those findings clearly demonstrate that the outbreak was caused by reignition of endemically circulating strains rather than outside introduction.

Bayesian Phylogeography Dissemination during Early Outbreak Phases

We reconstructed *V. cholerae* dispersal patterns for the 42 Haiti strains we sequenced and for which neighborhood of residence was known by using a Bayesian phylogeographic framework. Because of the short sampling time (October 3–November 21, 2022), we used a strict molecular clock and a fixed rate of 0.0179 SNP nucleotide substitutions per high-quality SNP site, which is similar to estimates obtained by previous studies (*8*,*16*,*18*), and the molecular clock analysis performed on our whole 2010–2022 Haiti dataset (Appendix). We used DensiTree to visualize the posterior distribution of trees obtained from phylogeography analysis to depict all probable migrations (Figure 4, panel A), from which we extracted migrations that were strongly supported by BFs of 5<BF<6 and BF>6 (Figure 4, panel B; Appendix Table 5). Cases included in the phylogeographic analysis tended to cluster in 4 general areas in Port-au-Prince (Figure 2, panel B; Figure 4, panel B). The snapshot of that phase of the outbreak provided by the phylogeography analysis is consistent with epidemiologic findings showing an epidemic hub within the Port-au-Prince administrative district and statistically significant (BF >6) migrations from group 2, corresponding to the central eastern neighborhoods of Port-au-Prince to other communes within the city and then to Fond Parisien

(Figure 4, panel B). We also observed well-supported (5<BF<6) migrations within Port-au-Prince with origins in group 1, corresponding to the GHESKIO environs, and in group 4, corresponding to greater Pétion-Ville (Figure 4, panel B).

Ancestral Origin of 2022 *V. cholerae* O1 Strains in Haiti

Toxigenic *V. cholerae* O1 strains sampled in Haiti during 2010–2014 were all Ogawa serotype, except for occasional sporadic Inaba strains. However, beginning in 2015, Inaba became the dominant clinical serotype, and by 2018 virtually all sampled clinical strains were serotype Inaba (*8*,*17*,*18*). During that time, toxigenic Ogawa strains were still detected from environmental sources (Figure 5; Appendix Figure 2, panels A, B). In contrast, all 2022 clinical strains were serotype Ogawa (Appendix Figure 2, panel C); thus, we sought to test the hypothesis that the new outbreak was linked to Ogawa strains persisting in the environment. Strong phylogenetic and temporal signals were detected in the whole dataset from Haiti, including clinical and environmental cholera samples collected during 2010–2022 (Appendix Figure 3). We inferred Bayesian MCC trees according to different molecular clock models and demographic priors (Appendix). To select the best fitting model, we compared path sampling and stepping-stone marginal likelihood estimates for each model pair by BF (Appendix Table 6). The MCC tree showed high support (posterior probability >0.9) for the 2022 strains sharing a most recent common ancestor (MRCA) with EnvJ515 environmental Ogawa strain (Figure 5, panels A, B), which was sampled in 2018 at a site on the Jacmel Estuary on Haiti's southeastern coast. Path sampling and stepping-stone model testing also showed that although the phylogeny model enforcing monophyly with environmental strain EnvJ515 had a lower posterior probability than the unconstrained tree, the BF between the 2 models was not statistically significant (Appendix Table 6). Enforcing monophyly of the 2022 clade with other Ogawa or Inaba strains sampled in 2018 always resulted in a BF decisively supporting the null hypothesis of common ancestry between the 2022 strains and EnvJ515 (Table).

The time to MRCA of 2022 outbreak strains was January 2022 (95% high posterior density interval of April 2021–July 2022), sharing a common ancestor with EnvJ515 in July 2018 (95% high posterior density interval May–July 2018) (Figure 5, panel B). Five high-quality SNPs in chromosome I and 1 in chromosome II differentiate the 2022 outbreak strains from EnvJ515; all are nonsynonymous mutations, and 2 affect hypothetical proteins (Appendix Table 7). We mapped an additional SNP difference in an intergenic region of chromosome II (Appendix Table 7). Although our focus was on EnvJ515, 2 other environmental Ogawa strains appear at the base of both the Ogawa and Inaba clades in the MCC tree: Env5156,

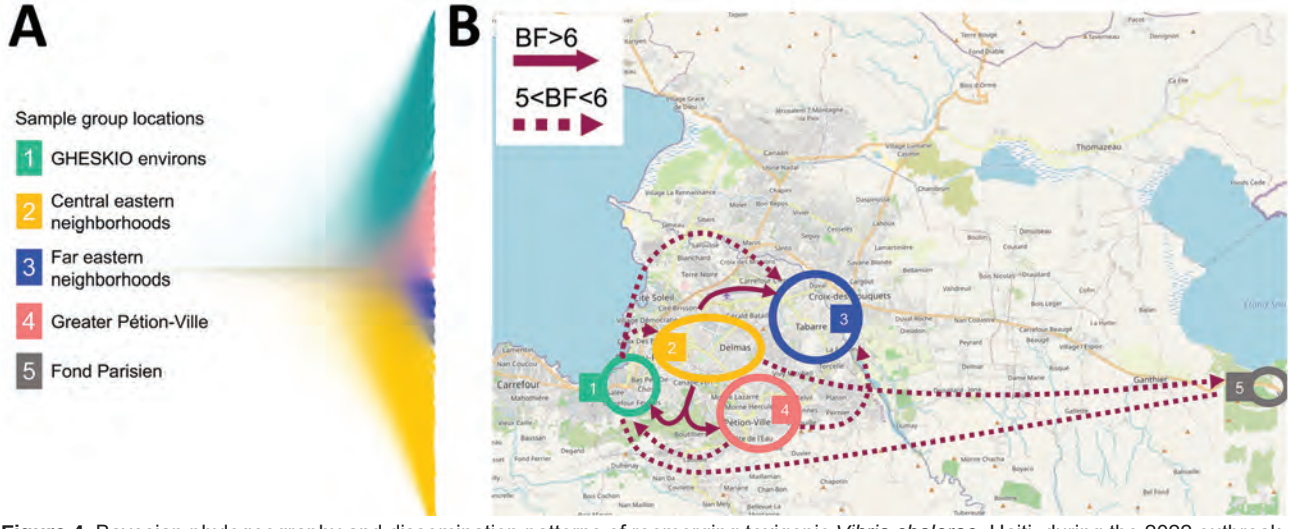

Figure 4. Bayesian phylogeography and dissemination patterns of reemerging toxigenic *Vibrio cholerae*, Haiti, during the 2022 outbreak. A) Bayesian DensiTree showing superimposed posterior distribution of trees inferred by the phylogeography analysis of *V. cholerae* full genomes from clinical cases sampled in Haiti during October 3–November 21. Colors indicate branches of samples grouped by location. B) Locations of case clusters delimited by colored circles. Solid- and broken-lined arrows indicate migration patterns among areas, as supported by Bayes factor and inferred from phylogeographic analysis by using a discrete trait asymmetric diffusion model. We considered rates yielding a BF >3 supported diffusion rates (*33*) and BF >6 decisive support (*34*), constituting the migration graph. Maps demonstrate major migrations of 5<BF<6 and BF >6. A list of all migrations supported by BF >3 are reported elsewhere (Appendix Table 5, https://wwwnc.cdc.gov/EID/article/29/10/23-0554-App1.pdf). BF, Bayes factor.

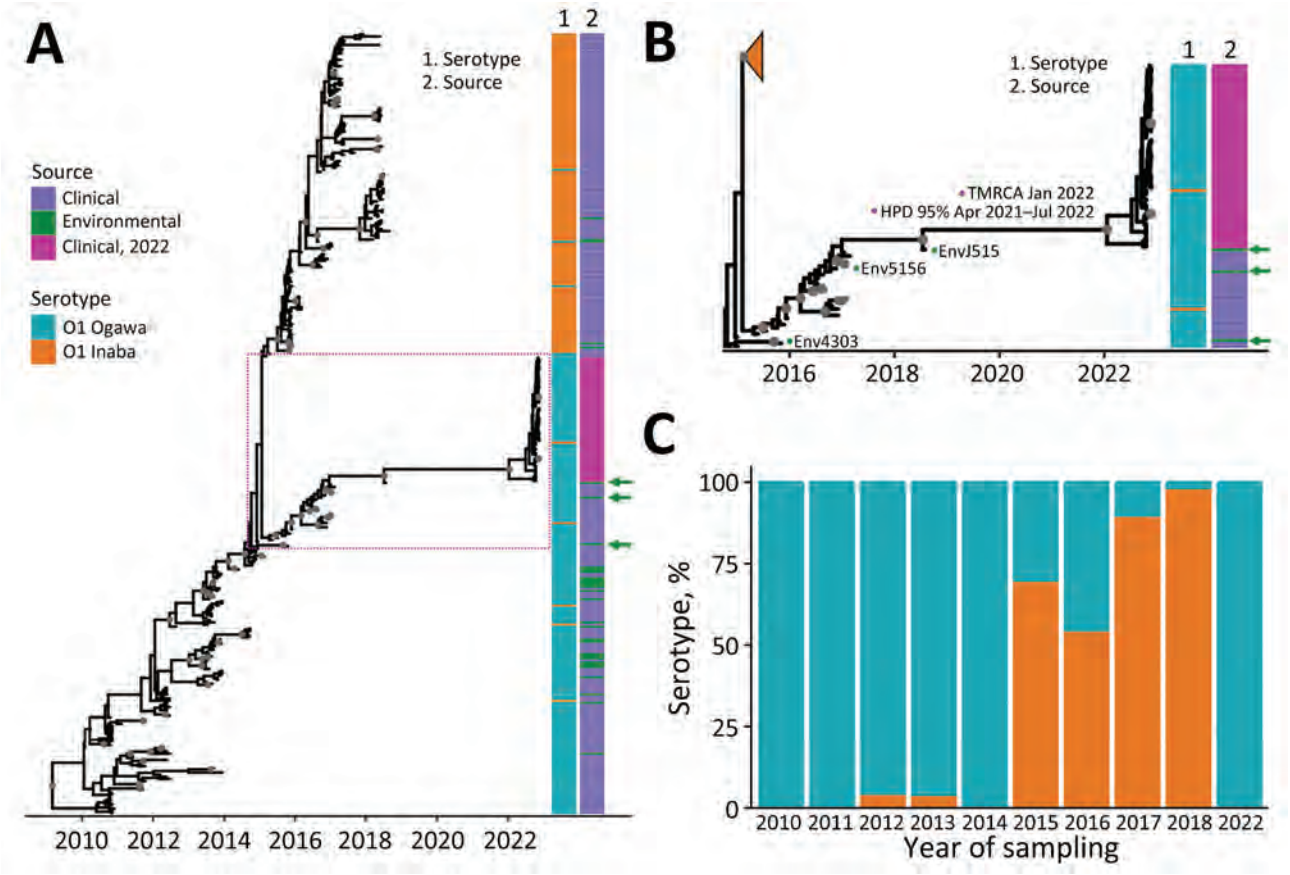

Figure 5. Inferred Bayesian phylogeny in a study of ancestral origin and dissemination dynamic of reemerging toxigenic *Vibrio cholerae*, Haiti. Phylogeny was inferred from 371 toxigenic *V. cholerae* O1 full genome clinical and environmental strains collected in Haiti during 2010–2022. A, B) Time-scaled phylogenies of *V. cholerae* serotypes inferred by enforcing a relaxed clock with Bayesian skyline demographic prior in BEAST version 1.10.4 (https://beast.community): A) Phylogeny of all isolates collected during 2010–2022. Dotted box denotes area detailed area shown in panel B. B) Detail of Ogawa clade from which the 2022 *V. cholerae* epidemic strains were derived. Gray circles indicate internal nodes supported by posterior probability >0.9. Branch lengths are scaled in time according to the x-axis. Time to MRCA of the 2022 Haiti isolates is shown at the node. Heatmaps denote clinical or environmental source and O1 serotype Ogawa or Inaba of the strains. Green arrows indicate the position of environmental strains basal to major clades. The collapsed orange clade refers to the monophyletic Inaba clade. Numbered green dots represent environmental *V. cholerae* O1 Ogawa isolates collected in Haiti; 2 were isolated from Jacmel Estuary, EnvJ515 in 2018 and Env4303 in 2015; Env5156 was isolated from a river in Leogane in 2016. C) Percentage of Ogawa and Inaba serotype isolates from samples collected in Haiti per year. HPD, high posterior density; MRCA, most recent common ancestor.

which was isolated in 2016 from Leogane, on the north coast of the southern peninsula; and Env4303, which was isolated in 2015 from the Jacmel estuary where EnvJ515 was isolated (Figure 5, panel B). The 2022 outbreak strains and EnvJ515, Env5156, and Env4303 shared 24 high-quality SNPs, among which 16 are in coding segments, 9 cause a nonsynonymous change, and 2 cause a frameshift (Appendix Table 8). Those high-quality SNPs are a subset of a total of 41 that EnvJ515, Env5156, and Env4303 have in common, highlighting the link between the 2022 outbreak strains and the Ogawa strains persisting in the aquatic environment since 2015 (Appendix Table 9). During 2015–2018, a total of 4 Inaba strains were isolated from environmental sites in Gressier and Carrefour (Figure 1). However, phylogenetic analysis showed those strains were intermixed with concurrently isolated Inaba clinical strains and were not closely related to the 2022 Ogawa clinical strains or 2015–2018 Ogawa environmental isolates (Figure 5, panel A).

Discussion

Our epidemiologic observations and phylogeographic analysis focused on cholera patients admitted to the GHESKIO CTC. Patient access to the GHESKIO CTC might have been influenced by transportation issues and local disruptions created by gang warfare in the city. Nonetheless, our overall observations support the

Table. Bayesian hypothesis testing of monophyly used in a study of ancestral origin and dissemination dynamic of reemerging toxigenic *Vibrio cholerae*, Haiti*

Monophyly testing†	lml(ML)$_{SS}$‡	Ln(BF)$_{SS}$§	lml(ML)$_{PS}$‡	Ln(BF)$_{PS}$§
Monophyly enforced with Ogawa 2014–2018 clade	–1,985.9	95.3	–1,988.4	94.5
MCC tree 2022 Haiti clade monophyletic with EnvJ515	–1,890.6		–1,893.9	
Monophyly enforced with Inaba 2018 clade	–1,987.9	97.3	–1,990.0	96.1
MCC tree 2022 Haiti clade monophyletic with EnvJ515	–1,890.6		–1,893.9	

*BF, Bayes factor; lml, log marginal likelihood; Ln, log; MCC, maximum clade credibility; ML, maximum-likelihood; SS, stepping-stone; PS, path sampling.
†The test compares the MCC tree topology in Figure 5, panel B (H_0), between 2022 environmental strains and 2018 environmental strain ENV515. Alternative topologies were obtained by enforcing monophyly with other strains (H_A).
‡log of marginal likelihood estimates, lml(MLE), obtained by SS or PS by using a strict molecular clock and a Bayesian skyline demographic prior, with or without enforcing monophyly between the 2022 Haiti strains and different clinical strains.
§log of BF comparing the null (H_0) and alternative (H_A) hypotheses.

hypothesis that the 2022 cholera outbreak in Haiti radiated from a single hub in Port-au-Prince, then spread exponentially, and was not caused by introduction of multiple *V. cholerae* strains. Of note, Bayesian hypothesis testing showed that the 2022 cholera strains shared a MRCA with an environmental lineage circulating in 2018. The location at the base of both Inaba and Ogawa clades of 2 other environmental Ogawa strains isolated in 2015 and 2016 is consistent with an established persistent environmental foci of this toxigenic *V. cholerae* O1 subclade (Figure 5, panels A, B). Of particular note, we isolated Ogawa strain Env4303 from the Jacmel estuary sampling site in 2015 and subsequently isolated EnvJ515 from the same site 3 years later, when virtually all clinical toxigenic *V. cholerae* O1 strains were serotype Inaba from a clearly distinct subclade. Our prior in vitro studies have demonstrated that toxigenic *V. cholerae* strains can survive in nutrient-poor aquatic environments for >700 days (*38*). Although the ecologic or strain factors driving persistence of *V. cholerae* strains within environmental reservoirs remain to be fully elucidated, persistence and subsequent spillover of strains from environmental foci into human populations in Haiti is supported not only by this study but also by prior phylodynamic studies from our group (*8*).

Jacmel, where EnvJ515 was isolated, is a popular local beach resort with easy access to Port-au-Prince and numerous restaurants, bars, and hotels lining the waterfront. Ten days before the first cholera case was reported September 25, 2022, Haiti had catastrophic flooding in the aftermath of hurricane Fiona (*39*), providing an ideal setting for environmental spillover of *V. cholerae* into water and food systems. Spread of the epidemic strain likely was further advanced by an abrupt interruption of the water supply by the national water company related to gang warfare and political unrest (*40*,*41*). That interruption resulted in an inability to provide potable water to shantytown areas of Port-au-Prince, a key area where the epidemic was identified. The shantytown areas are characterized by high-density, informal buildings and heavily polluted, open-air drainage channels coming from the city, which does not have a formal sewerage system or sewage treatment facilities. Those channels also drain water from the surrounding mountains and flow through the shantytown community into the harbor. Two major drainage channels pass through the areas near GHESKIO and Waaf Jeremy, areas that had particularly high case counts in the early weeks of the epidemic (Figure 2, panels C–F). Considering the local challenges with water and sanitation, introduction of *V. cholerae* into those areas, whether via the drainage channels or through human movement, almost certainly led to the emergence of initial cholera spatial hotspots and subsequent epidemic disease.

During the 2022 epidemic, infection rates appeared to be substantially higher among children 0–9 years of age, which is consistent with a lack of immunity to *V. cholerae* among this age group because they were not exposed to clinical cases in the preceding 3–4 years. Of note, clinical cases in the 2015–2019 outbreak almost exclusively were caused by *V. cholerae* Inaba serotype, and field-based studies suggest that initial Inaba infections protect against subsequent Ogawa infections (*42*). Thus, issues with cross-protection between the 2 serotypes and waning cholera immunity in the general population might have led to increased susceptibility to infection.

From a prevention standpoint, mathematical models we previously developed indicated that cholera eradication in Haiti will be difficult without substantive improvements to drinking water and sanitation infrastructure and that a clear potential for recurrence of epidemic disease from environmental reservoirs exists (*8*,*43*). Our previous modeling also underscored the potentially critical role that mass cholera vaccination can play in controlling epidemics (*44*). Although oral killed cholera vaccine has been used successfully in targeted campaigns in Haiti (*45*,*46*), efforts have not been made to immunize the entire country or to develop a long-term vaccination strategy. A major focus of prevention efforts in Haiti has been implementation of rapid response teams that go to homes of cholera patients and use sanitation

and chlorination of household water to try to minimize transmission within households (*47*). Those efforts clearly are needed, but the ongoing risk for recurrent outbreaks from environmental reservoirs urges more action.

In summary, our data support the concept that a previously circulating Ogawa lineage served as the ancestor of *V. cholerae* strains that reemerged during the 2022 cholera outbreak in Haiti, suggesting a crucial link to the aquatic ecosystem. Links to environmental reservoirs documented in this study highlight the urgent need for overall improvements in public health infrastructure and water sanitation in Haiti and potential need for periodic mass vaccination campaigns to maintain protective levels of population immunity.

This article was preprinted at https://doi.org/10.1101/2022.11.21.22282526.

Genomic sequences from this study have been deposited in the National Center for Biotechnology Information Sequence Read Archive under BioProject no. PRJNA900623. Global maximum-likelihood and maximum clade credibility trees are available at https://github.com/cmavian/CholeraHaiti2022.

Funding for these studies was provided in part by grants from the National Institute of Allergy and Infectious Diseases (grant nos. R01AI128750, R01AI123657, and R01AI097405, awarded to J.G.M.).

Author contributions: C.N.M., V.R., J.W.P., J.G.M.J., M.S., and A.A. conceptualized the study; C.N.M., M.S.T., M.T.A., M.N.C., M.M., J.P.J., A.R., S.N.S., E.J.N., E.T.C., T. dO., M.S., and A.A. developed the methodology; C.N.M., M.S.T., M.T.A., M.S., and A.A. conducted the investigation; C.N.M., J.P.J., and M.M. created visualizations; J.G.M.J. acquired funding; C.N.M., M.T.A., V.R., J.W.P., J.G.M.J., M.S., and A.A. provided project administration; C.N.M., J.G.M.J., M.S., and A.A. supervised the project; C.N.M., M.S., and A.A. wrote the original draft; C.N.M., M.S.T., M.T.A., M.N.C., V.M.B.D.R., V.R., J.W.P., T.dO., J.G.M.J., M.S., and A.A. wrote, reviewed, and edited the final manuscript.

About the Author

Dr. Mavian is a faculty member in the Department of Pathology, Immunology, and Laboratory Medicine at the University of Florida College of Medicine, Gainesville, FL, USA. Her research interests include intrahost and interhost evolution of HIV, emergence and spread of arboviruses in the Americas, and the evolutionary dynamics of *Vibrio cholerae* in the human population and aquatic ecosystems in Haiti.

References

1. World Health Organization. Cholera—global situation. 2022 [cited 2023 Feb 8]. https://www.who.int/emergencies/disease-outbreak-news/item/2022-DON426
2. Hendriksen RS, Price LB, Schupp JM, Gillece JD, Kaas RS, Engelthaler DM, et al. Population genetics of *Vibrio cholerae* from Nepal in 2010: evidence on the origin of the Haitian outbreak. MBio. 2011;2:e00157-11. https://doi.org/10.1128/mBio.00157-11
3. Piarroux R, Barrais R, Faucher B, Haus R, Piarroux M, Gaudart J, et al. Understanding the cholera epidemic, Haiti. Emerg Infect Dis. 2011;17:1161–8. https://doi.org/10.3201/eid1707.110059
4. Ivers LC, Walton DA. The "first" case of cholera in Haiti: lessons for global health. Am J Trop Med Hyg. 2012;86:36–8. https://doi.org/10.4269/ajtmh.2012.11-0435
5. Blackburn JK, Diamond U, Kracalik IT, Widmer J, Brown W, Morrissey BD, et al. Household-level spatiotemporal patterns of incidence of cholera, Haiti, 2011. Emerg Infect Dis. 2014;20:1516–9. https://doi.org/10.3201/eid2009.131882
6. Alam MT, Weppelmann TA, Longini I, De Rochars VM, Morris JG Jr, Ali A. Increased isolation frequency of toxigenic *Vibrio cholerae* O1 from environmental monitoring sites in Haiti. PLoS One. 2015;10:e0124098. https://doi.org/10.1371/journal.pone.0124098
7. Alam MT, Weppelmann TA, Weber CD, Johnson JA, Rashid MH, Birch CS, et al. Monitoring water sources for environmental reservoirs of toxigenic *Vibrio cholerae* O1, Haiti. Emerg Infect Dis. 2014;20:356–63. https://doi.org/10.3201/eid2003.131293
8. Mavian C, Paisie TK, Alam MT, Browne C, Beau De Rochars VM, Nembrini S, et al. Toxigenic *Vibrio cholerae* evolution and establishment of reservoirs in aquatic ecosystems. Proc Natl Acad Sci U S A. 2020;117:7897–904. https://doi.org/10.1073/pnas.1918763117
9. World Health Organization. Cholera—Haiti, 12 October 2022 [cited 2023 Aug 29]. https://www.who.int/emergencies/disease-outbreak-news/item/2022-DON415
10. DAI. Haiti declared free of cholera [cited 2023 Aug 29]. https://www.dai.com/news/haiti-declared-free-of-cholera
11. Vega Ocasio D, Juin S, Berendes D, Heitzinger K, Prentice-Mott G, Desormeaux AM, et al.; CDC Haiti Cholera Response Group. Cholera outbreak—Haiti, September 2022–January 2023. MMWR Morb Mortal Wkly Rep. 2023;72:21–5. https://doi.org/10.15585/mmwr.mm7202a1
12. Ministry of Public Health and Population. Epidemiological situation of cholera, 12 May 2023 [in French] [cited 2023 Aug 29]. https://www.mspp.gouv.ht
13. Rubin DHF, Zingl FG, Leitner DR, Ternier R, Compere V, Marseille S, et al. Reemergence of cholera in Haiti. N Engl J Med. 2022;387:2387–9. https://doi.org/10.1056/NEJMc2213908
14. Walters C, Chen J, Stroika S, Katz LS, Turnsek M, Compère V, et al. Genome sequences from a reemergence of *Vibrio cholerae* in Haiti, 2022 reveal relatedness to previously circulating strains. J Clin Microbiol. 2023;61:e0014223. https://doi.org/10.1128/jcm.00142-23
15. Ali A, Chen Y, Johnson JA, Redden E, Mayette Y, Rashid MH, et al. Recent clonal origin of cholera in Haiti. Emerg Infect Dis. 2011;17:699–701. https://doi.org/10.3201/eid1704.101973
16. Azarian T, Ali A, Johnson JA, Mohr D, Prosperi M, Veras NM, et al. Phylodynamic analysis of clinical and environmental *Vibrio cholerae* isolates from Haiti reveals diversification driven by positive selection. MBio. 2014;5:e01824-14. https://doi.org/10.1128/mBio.01824-14

17. Alam MT, Ray SS, Chun CN, Chowdhury ZG, Rashid MH, Madsen Beau De Rochars VE, et al. Major shift of toxigenic *V. cholerae* O1 from Ogawa to Inaba serotype isolated from clinical and environmental samples in Haiti. PLoS Negl Trop Dis. 2016;10:e0005045. https://doi.org/10.1371/journal.pntd.0005045
18. Paisie TK, Cash MN, Tagliamonte MS, Ali A, Morris JG Jr, Salemi M, et al. Molecular basis of the toxigenic *Vibrio cholerae* O1 serotype switch from Ogawa to Inaba in Haiti. Microbiol Spectr. 2023;11:e0362422. https://doi.org/10.1128/spectrum.03624-22
19. Weill FX, Domman D, Njamkepo E, Tarr C, Rauzier J, Fawal N, et al. Genomic history of the seventh pandemic of cholera in Africa. Science. 2017;358:785–9. https://doi.org/10.1126/science.aad5901
20. Domman D, Quilici ML, Dorman MJ, Njamkepo E, Mutreja A, Mather AE, et al. Integrated view of *Vibrio cholerae* in the Americas. Science. 2017;358:789–93. https://doi.org/10.1126/science.aao2136
21. Colwell RR, Huq A. Environmental reservoir of *Vibrio cholerae*. The causative agent of cholera. Ann N Y Acad Sci. 1994;740(1 Disease in Ev):44–54. https://doi.org/10.1111/j.1749-6632.1994.tb19852.x
22. Morris JG Jr. Cholera—modern pandemic disease of ancient lineage. Emerg Infect Dis. 2011;17:2099–104. https://doi.org/10.3201/eid1711.111109
23. Azarian T, Ali A, Johnson JA, Jubair M, Cella E, Ciccozzi M, et al. Non-toxigenic environmental *Vibrio cholerae* O1 strain from Haiti provides evidence of pre-pandemic cholera in Hispaniola. Sci Rep. 2016;6:36115. https://doi.org/10.1038/srep36115
24. Chen S, Zhou Y, Chen Y, Gu J. fastp: an ultra-fast all-in-one FASTQ preprocessor. Bioinformatics. 2018;34:i884–90. https://doi.org/10.1093/bioinformatics/bty560
25. Croucher NJ, Page AJ, Connor TR, Delaney AJ, Keane JA, Bentley SD, et al. Rapid phylogenetic analysis of large samples of recombinant bacterial whole genome sequences using Gubbins. Nucleic Acids Res. 2015;43:e15. https://doi.org/10.1093/nar/gku1196
26. Tonkin-Hill G, Lees JA, Bentley SD, Frost SDW, Corander J. Fast hierarchical Bayesian analysis of population structure. Nucleic Acids Res. 2019;47:5539–49. https://doi.org/10.1093/nar/gkz361
27. Nguyen LT, Schmidt HA, von Haeseler A, Minh BQ. IQ-TREE: a fast and effective stochastic algorithm for estimating maximum-likelihood phylogenies. Mol Biol Evol. 2015;32:268–74. https://doi.org/10.1093/molbev/msu300
28. Alam MT, Mavian C, Paisie TK, Tagliamonte MS, Cash MN, Angermeyer A, et al. Emergence and evolutionary response of *Vibrio cholerae* to novel bacteriophage, Democratic Republic of the Congo. Emerg Infect Dis. 2022;28:2482–90. https://doi.org/10.3201/eid2812.220572
29. Weill F-X, Domman D, Njamkepo E, Almesbahi AA, Naji M, Nasher SS, et al. Genomic insights into the 2016–2017 cholera epidemic in Yemen. Nature. 2019;565:230–3. https://doi.org/10.1038/s41586-018-0818-3
30. Sagulenko P, Puller V, Neher RA. TreeTime: maximum-likelihood phylodynamic analysis. Virus Evol. 2018;4:vex042. https://doi.org/10.1093/ve/vex042
31. Drummond AJ, Rambaut A. BEAST: Bayesian evolutionary analysis by sampling trees. BMC Evol Biol. 2007;7:214. https://doi.org/10.1186/1471-2148-7-214
32. Yu GC, Smith DK, Zhu HC, Guan Y, Lam TTY. GGTREE: an R package for visualization and annotation of phylogenetic trees with their covariates and other associated data. Methods Ecol Evol. 2017;8:28–36. https://doi.org/10.1111/2041-210X.12628
33. Drummond AJ, Suchard MA, Xie D, Rambaut A. Bayesian phylogenetics with BEAUti and the BEAST 1.7. Mol Biol Evol. 2012;29:1969–73. https://doi.org/10.1093/molbev/mss075
34. Lemey P, Rambaut A, Drummond AJ, Suchard MA. Bayesian phylogeography finds its roots. PLOS Comput Biol. 2009;5:e1000520. https://doi.org/10.1371/journal.pcbi.1000520
35. Xie W, Lewis PO, Fan Y, Kuo L, Chen MH. Improving marginal likelihood estimation for Bayesian phylogenetic model selection. Syst Biol. 2011;60:150–60. https://doi.org/10.1093/sysbio/syq085
36. Sjölund-Karlsson M, Reimer A, Folster JP, Walker M, Dahourou GA, Batra DG, et al. Drug-resistance mechanisms in *Vibrio cholerae* O1 outbreak strain, Haiti, 2010. Emerg Infect Dis. 2011;17:2151–4. https://doi.org/10.3201/eid1711.110720
37. Kim HB, Wang M, Ahmed S, Park CH, LaRocque RC, Faruque AS, et al. Transferable quinolone resistance in *Vibrio cholerae*. Antimicrob Agents Chemother. 2010;54:799–803. https://doi.org/10.1128/AAC.01045-09
38. Jubair M, Morris JG Jr, Ali A. Survival of *Vibrio cholerae* in nutrient-poor environments is associated with a novel "persister" phenotype. PLoS One. 2012;7:e45187. https://doi.org/10.1371/journal.pone.0045187
39. Haiti Libre. Haiti—FLASH: first effect of Hurricane Fiona on Haiti [cited 2023 Aug 29]. https://www.haitilibre.com/en/news-37687-haiti-flash-first-effect-of-hurricane-fiona-on-haiti.html
40. United Nations. 'Violent civil unrest' in Haiti hampers aid delivery, 16 Sep 2022 [cited 2023 Aug 29]. https://news.un.org/en/story/2022/09/1126861
41. The Guardian. They have no fear and no mercy: gang rule engulfs Haitian capital, 18 Sep 2022 [cited 2023 Aug 29]. https://www.theguardian.com/world/2022/sep/18/haiti-violence-gang-rule-port-au-prince
42. Ali M, Emch M, Park JK, Yunus M, Clemens J. Natural cholera infection-derived immunity in an endemic setting. J Infect Dis. 2011;204:912–8. https://doi.org/10.1093/infdis/jir416
43. Kirpich A, Weppelmann TA, Yang Y, Ali A, Morris JG Jr, Longini IM. Cholera transmission in Ouest Department of Haiti: dynamic modeling and the future of the epidemic. PLoS Negl Trop Dis. 2015;9:e0004153. https://doi.org/10.1371/journal.pntd.0004153
44. Kirpich A, Weppelmann TA, Yang Y, Morris JG Jr, Longini IM Jr. Controlling cholera in the Ouest Department of Haiti using oral vaccines. PLoS Negl Trop Dis. 2017; 11:e0005482. https://doi.org/10.1371/journal.pntd.0005482
45. Sévère K, Rouzier V, Anglade SB, Bertil C, Joseph P, Deroncelay A, et al. Effectiveness of oral cholera vaccine in Haiti: 37-month follow-up. Am J Trop Med Hyg. 2016;94:1136–42. https://doi.org/10.4269/ajtmh.15-0700
46. Pape JW, Rouzier V. Embracing oral cholera vaccine—shifting response to cholera. N Engl J Med. 2014;370:2067–9. https://doi.org/10.1056/NEJMp1402837
47. Ratnayake R, Finger F, Azman AS, Lantagne D, Funk S, Edmunds WJ, et al. Highly targeted spatiotemporal interventions against cholera epidemics, 2000–19: a scoping review. Lancet Infect Dis. 2021;21:e37–48. https://doi.org/10.1016/S1473-3099(20)30479-5

Address for correspondence: J. Glenn Morris Jr., Emerging Pathogens Institute, University of Florida, 2055 Mowry Rd, Gainesville, Florida 32610-0009, USA; email: jgmorris@epi.ufl.edu

Treponema pallidum Detection at Asymptomatic Oral, Anal, and Vaginal Sites in Adults Reporting Sexual Contact with Persons with Syphilis

Ei T. Aung, Christopher K. Fairley, Deborah A. Williamson, Francesca Azzato, Janet M. Towns, Rebecca Wigan, Eric P.F. Chow,[1] Marcus Y. Chen[1]

We investigated *Treponema pallidum* PCR positivity at mucosal sites (oral, anal, and vaginal sites) among adults who had sexual contact with a person with syphilis (syphilis contacts). All syphilis contacts had oral rinse and swab samples collected for testing. Men who have sex with men had anal swab and women had vaginal swab samples collected for testing, regardless of the presence of lesions. Of 407 persons tested, 42 (10%) had early syphilis diagnosed; of those, 19 (45%) tested positive by PCR from any anatomic site and had a positive serologic test. *T. pallidum* was positive from vaginal samples in 3 women, anal samples in 3 men, and oral cavity samples in 2 women and 3 men, without symptoms at those sites. Three women had no prior syphilis serologic test. *T. pallidum* detection at asymptomatic mucosal sites suggests early syphilis infections, particularly in cases that would conventionally be staged as latent syphilis of unknown duration.

Syphilis, caused by *Treponema pallidum*, results in substantial disease and death if left untreated. The World Health Organization (WHO) estimated a global burden of 6 million new syphilis infections in 2018, and syphilis remains a major public health challenge (*1*). High incidence of syphilis continues to persist among men who have sex with men (MSM) in high-income countries (*2*,*3*). Increases in syphilis among heterosexual populations and congenital syphilis have also been reported in many countries, including Australia (*4*). Early detection and treatment are essential in reducing the infectious period and transmission. Developing interventions aimed at improving syphilis control, including methods that can detect syphilis infection as early as possible, is essential.

To identify early syphilis infection, persons who are at risk for syphilis infection should undergo screening. The conventional method for syphilis screening involves serologic testing, which consists of detecting *T. pallidum* antibodies by using *T. pallidum*–specific and nonspecific tests (*5*,*6*). However, a challenge with this method is the window period between the infection onset and the appearance of antibodies in very early syphilis, which can lead to a negative serologic result during that period, causing the infection to go undetected. Moreover, the sensitivity and specificity of *T. pallidum*–specific and –nonspecific serologic tests for syphilis vary by stages of infection (*7*,*8*). For example, *T. pallidum*–nonspecific tests are less sensitive in detecting primary syphilis (62%–78%) than in detecting secondary syphilis (97%–100%) (*7*). *T. pallidum*–specific tests such as immunoassays have a wide range of sensitivities for detecting primary syphilis (78%–96%), varying according to the specific immunoassay used (*9*). Furthermore, those *T. pallidum*–specific immunoassays demonstrate persistent presence of treponemal antibodies in patients previously treated for syphilis (*9*), which can sometimes pose challenges in identifying a very early new syphilis infection when treponemal antibodies are present and

Author affiliations: Melbourne Sexual Health Centre, Alfred Health, Melbourne, Victoria, Australia (E.T. Aung, C.K. Fairley, J.M. Towns, R. Wigan, E.P.F. Chow, M.Y. Chen); Central Clinical School, Monash University, Melbourne (E.T. Aung, C.K. Fairley, J.M. Towns, E.P.F. Chow, M.Y. Chen); The Doherty Institute for Infection and Immunity, Melbourne (D.A. Williamson); Victorian Infectious Diseases Reference Laboratory, Melbourne (D.A. Williamson, F. Azzato); Melbourne School of Population and Global Health, The University of Melbourne, Melbourne (E.P.F. Chow)

DOI: https://doi.org/10.3201/eid2910.230660

[1]These senior authors contributed equally to this article.

T. pallidum–nonspecific tests are nonreactive. Therefore, laboratory methods that can enhance detection of very early syphilis infections are needed.

Nucleic acid amplification tests (NAATs) such as PCR for *T. pallidum* have been shown to be highly sensitive for the detection of primary syphilis lesions (*10*–*14*), showing sensitivity ranging from 80% to 95% (*13*–*17*). Recent studies have shown *T. pallidum* is detectable by PCR not only from primary syphilis lesions at genital sites but also from other sites and sample types, including the anal canal, oral cavity, saliva, and urine (*14*,*18*–*23*). A study from the Netherlands detected *T. pallidum* by PCR in various mucosal tissues and body fluids in the early stages of syphilis, even in the absence of lesions (*20*). Those findings indicate that PCR can detect *T. pallidum* in the early stages of syphilis, with or without lesions at various mucosal sites. Consequently, PCR may be useful in detecting syphilis in asymptomatic persons at high risk before seroconversion takes place.

In this study, we undertook PCR testing for *T. pallidum* from adults who reported sexual contact with a person with syphilis by using oral, vaginal, and anal samples, even when symptoms and signs of syphilis were not reported from those sites. We hypothesized that some of those persons would have very early syphilis infection and *T. pallidum* would be detectable from those sites in the absence of lesions. We sought to determine whether PCR detection at those locations might precede the appearance of syphilis antibodies on serologic testing.

Methods

In this cross-sectional study, we included men and women who reported sexual contact with a person with syphilis infection (hereafter, syphilis contacts), provided consent to having PCR testing for syphilis, and visited the Melbourne Sexual Health Centre (MSHC) during November 2018–March 2020. The study was approved by the Alfred Hospital Ethics Committee, Melbourne, Australia (project no. 474/18). MSHC is a public sexual health and HIV clinic in the state of Victoria, Australia, and provides ≈50,000 consultations/year. The clinic has an electronic medical record system that stores demographic and epidemiologic data.

Clients seeking care at the clinics were evaluated by a nurse after their registration. The nurse typically collects a brief account of the clients' current condition and adds this information to their medical records before assigning them to healthcare professionals. Persons who had been in sexual contact with someone diagnosed with syphilis were identified on the basis of their own report. Those persons were notified about their exposure through either anonymous text messages or direct communication from the persons who had been in contact with them.

Contacts of syphilis were provided with a plain-language participant information sheet explaining PCR testing from mucosal sites. Verbal consent was obtained from those who agreed to have the *T. pallidum* PCR tests from the mucosal sites. The clinicians collected oral swab samples (all participants), anal swab samples (MSM only), and vaginal swab samples (women only) by using the Universal Transport Medium swab (Copan Italia, https://www.copangroup.com) for *T. pallidum* PCR testing. Participants also self-collected an oral rinse by gargling 10 mL of sterile water for *T. pallidum* PCR (i.e., mucosal screening PCR tests). *T. pallidum* PCR testing also was performed on swab samples taken from any syphilis lesions present (i.e., lesion PCR tests).

Participants who reported having symptoms suggestive of syphilis, such as anogenital or oral lesions, were examined by the clinician at the respective sites, and swab samples were taken from any lesion for *T. pallidum* PCR testing. Vaginal examinations were performed by using speculum if a woman reported any genital lesions or symptoms, and anoscopic examination was performed where a participant reported an anorectal lesion. Whether or not a participant required vaginal speculum or anoscopic examination was a decision made by the clinician on clinical grounds. We collected data on clinical examination findings retrospectively.

All participants had syphilis serologic testing performed and were offered syphilis treatment with intramuscular benzathine penicillin (2.4 mU single dose) or doxycycline (100 mg 2×/d for 2 weeks) for those with penicillin allergy. The participants were offered routine chlamydia and gonorrhea testing according to sexual transmitted infection (STI) testing guidelines depending on their sexual risk (*25*,*26*). If persons were diagnosed with syphilis infection and considered to have latent syphilis of unknown duration, they were asked to return for further treatment with a total of 3 doses of weekly benzathine penicillin (or 4 weeks of doxycycline for those with penicillin allergy).

We defined MSM as men who have sex with men or with transwomen and bisexual as either men or women who had sex with both men and women (including transgender persons). We defined heterosexual as either men or women who had sex only with the opposite sex. We defined sexuality on the basis of

self-reported sexual practice in the last 12 months and not on sexual identity.

E.T.A. reviewed medical records to capture information on types of partners (regular vs. casual), type of sex (anal, vaginal, or oral sex), condom use (condomless vs. with condoms), and signs and symptoms of syphilis at consultation. The information on types of partners was self-reported, and no formal definition of regular and casual partners was used in the study. Some participants might have defined regular partners as romantic partners (e.g., boyfriends or husbands) or casual sexual partners as regular contacts without romantic attachment (*24*).

Laboratory Methods

We tested specimens at the Victorian Infectious Diseases Reference Laboratory (VIDRL; Melbourne, VIC, Australia), by using a TaqMan real-time PCR (ThermoFisher, https://www.thermofisher.com) targeting the *polA* gene of *T. pallidum* (*15*). We extracted DNA by using the Quick DNA/RNATM MagBead Extraction kit (Zymo Research, https://www.zymoresearch.com) on the Tecan Freedom EVO 100 automated system (Tecan, https://lifesciences.tecan.com). The PCR was designed at VIDRL by using the Primer Express software program (ThermoFisher, https://www.thermofisher.com), and the details of the *T. pallidum* PCR testing are described elsewhere (*15*). For a positive *T. pallidum* PCR sample, we reported a cycle threshold, which reflects the amount of nucleic acid in the sample.

We assessed serologic testing for syphilis by using a chemiluminescence immunoassay (CLIA) (DiaSorin, https://www.diasorin.com) and then confirmed results by using *T. pallidum* Particle Agglutination assay (TPPA) (https://www.fujirebio.com) and Rapid Plasma Reagin (RPR) (Becton Dickinson, https://www.bd.com). We performed routine screening for chlamydia and gonorrhea with NAAT by using Hologic Panther System Aptima Combo 2 assay (Hologic https://www.hologic.com) on the urine samples, vaginal swab samples, pharyngeal swab samples, and anal swab samples. We performed those screenings in line with MSHC testing guidelines and Australia's STI guidelines (*25*,*26*). We obtained separate anal and oral swab samples for *T. pallidum* PCR and chlamydia and gonorrhea testing. We tested for herpes simplex virus from genital lesions by using an in-house TaqMan real-time PCR, targeting the glycoprotein B gene. We tested for *Mycoplasma genitalium* by using the ResistancePlus MG Assay (SpeeDx, https://plexpcr.com). We performed HIV screening by using the DiaSorin Liaison XL Murex HIV Ab/Ag chemiluminescence immunoassay (4th generation) and confirmed results by using Western blot.

Identifying of Syphilis Cases

We identified all new syphilis cases by using laboratory classifications for early infectious syphilis and latent syphilis from the Australia Department of Health and the US Centers for Disease Control and Prevention (*27*,*28*). Of note, early latent syphilis in Australia is defined as syphilis infection acquired within the previous 24 months with no clinical evidence of syphilis (*28*). Staging of syphilis was undertaken by a senior sexual health physician, who determined the staging on the basis of the medical record and laboratory results, including results from external healthcare services.

Statistical Analysis

We reported categorical variables as frequencies and percentages and continuous variables as medians and interquartile ranges (IQRs). We defined syphilis diagnosis as testing positive by *T. pallidum* PCR, serologic testing, or both. We calculated 95% CIs for syphilis diagnoses by using a binomial proportion CI. The study was stopped in March 2020 because of the COVID-19 pandemic. We performed all analyses by using Stata version 16 (StataCorp LLC, https://www.stata.com).

Results

A total of 407 contacts had ≥1 specimen for PCR screening (oral and anal in MSM, oral in heterosexual men, and oral and vaginal in women). Of the 407 contacts, 339 were MSM, 22 were heterosexual men, 20 were heterosexual women, 1 was a bisexual woman, and 25 were bisexual men. Among the contacts living with HIV (16%, n = 67), most were MSM (94%, n = 63); one third of contacts (33%, n = 134) were using HIV preexposure prophylaxis. One fifth of the contacts (20%, n = 85) had a history of syphilis infection, and a small number (9%, n = 35) reported ever injecting drugs. The median age of the syphilis contacts was 32 years (IQR 27–40 years).

Nearly half (47%, n = 193) of the contacts reported having a casual partner as their syphilis contact, whereas 35% (n = 144) reported a regular partner as the contact. Most (71%, n = 290) contacts reported condomless sex during anal or vaginal sex, and 17% (n = 69) had signs or symptoms suggestive of syphilis (Table 1).

A total of 42 contacts (10%, 95% CI 8%–14%) had syphilis infection diagnosed (case-patients) (Figure). Of those, 33 were MSM, 5 were women, 2 were heterosexual men, and 3 were bisexual men. Syphilis

Table 1. Possible syphilis symptoms described by 69 patients in retrospective study of men and women who visited the Melbourne Sexual Health Centre, Melbourne, Victoria, Australia, during November 2018–March 2020*

Symptom	No. patients
Oral symptoms, n = 15	
Oral ulcers: mouth ulcers, gum ulcers, tongue ulcers†	11
Lip sores or ulcers	4
Anal symptoms, n = 18	
Anal or perianal ulcers/blisters/lesions, painful and painless	7
Anal lump	2
Anal or perianal rash, red rash	1
Anal pain: severe, discomfort, associated with mucous discharge	5
Tenesmus	2
Anal itch†	1
Penile or genital symptoms, n = 17	
Penile lesions/sores on glans penis, foreskin	8
Penile rash, including red spots, pimple-like	5
Penis lump	2
Scrotal lump and rash, flaky skin†	2
Nonorogenital symptoms, n = 18	
Body rash: torso, back, flank, palms, soles‡	12
Rash/sores on shin, leg, thigh	4
Lump on eyelid, conjunctivitis	2
Systemic symptoms, n = 21	
Headache	3
Fever, including night sweats, chills	6
Fatigue/lethargy	2
Influenza-like symptoms, unwell, sore throat	5
Blurred vision	2
Tinnitus	1
Swollen lymph nodes: groin, submental	2

*Some participants presented with >1 symptom, and therefore, the total would not add up to 69.
†The participant had tongue ulcer, flaky skin on scrotum and itchy anus with PCR positive test results from tongue, scrotum, and anus.
‡Some descriptions include spots, itchy papules, and red patches.

was detected by positive serologic testing alone in the absence of positive PCR in 21 cases (50%, 95% CI 34%–66%). Nineteen cases (45%, 95% CI 30%–61%) were detected by positive serologic tests together with positive *T. pallidum* PCR; 9 of those case-patients had *T. pallidum* detected by PCR from ≥1 mucosal sites (oral, anal, or vaginal) in the absence of lesions at these sites (Table 2). The remaining 10 of the 19 case-patients had signs and symptoms suggestive of syphilis and were *T. pallidum*–positive from mucosal sites, lesions sites, or both (Table 3). Of the 42 syphilis case-patients, 2 had *T. pallidum* PCR detected from penile lesions with a negative serologic test. Because those 2 case-patients had *T. pallidum* PCR detected only from lesion PCR tests, they are not discussed further.

Syphilis Cases Detected by *T. pallidum* PCR and Serologic Testing

Among the 9 asymptomatic case-patients (i.e., PCR positive and no visible lesions), 4 were women, 4 were MSM, and 1 was a bisexual man. The median age was 27 years (IQR 24–31 years). *T. pallidum* PCR was detected from ≥1 of the mucosal screening PCR tests (58% [95% CI 37%–78%], 14/24): oral swab, oral rinse, anal swab, or vaginal swab (Table 2). The RPR titer ranged from nonreactive to 1:256 (median RPR 1:32, IQR 1:8–1:128).

Among the 10 symptomatic case-patients (i.e., PCR positive and visible lesions), 1 was a woman, 8 were MSM, and 1 was a bisexual man. The median age was 32 years (IQR 24–39 years). In this group, 69% (95% CI 52%–83%, 27/39) of *T. pallidum* PCR specimens were positive from the mucosal screening PCR tests, the lesion PCR tests, or both. The RPR titer ranged from 1:32 to 1:256 (median RPR 1:64, IQR 1:32–1:128) (Table 3). Of the 10 symptomatic case-patients, 7 had positive PCR from mucosal screening sites with or without positive PCR from lesion sites. Among these 7 case-patients, 5 had positive PCR only from mucosal screening sites; 3 had signs and symptoms of secondary syphilis. Two case-patients had positive PCR from both mucosal screening sites and lesion sites (Table 3).

Syphilis Cases Detected by Positive Serologic Tests in the Absence of *T. pallidum* PCR Detection

Twenty-one case-patients had positive syphilis serologic tests but no positive *T. pallidum* screening results (lesion PCR was not performed) (Table 4). This group included 19 MSM, 1 heterosexual man, and 1 bisexual man. The median age in this group was 33 years (IQR

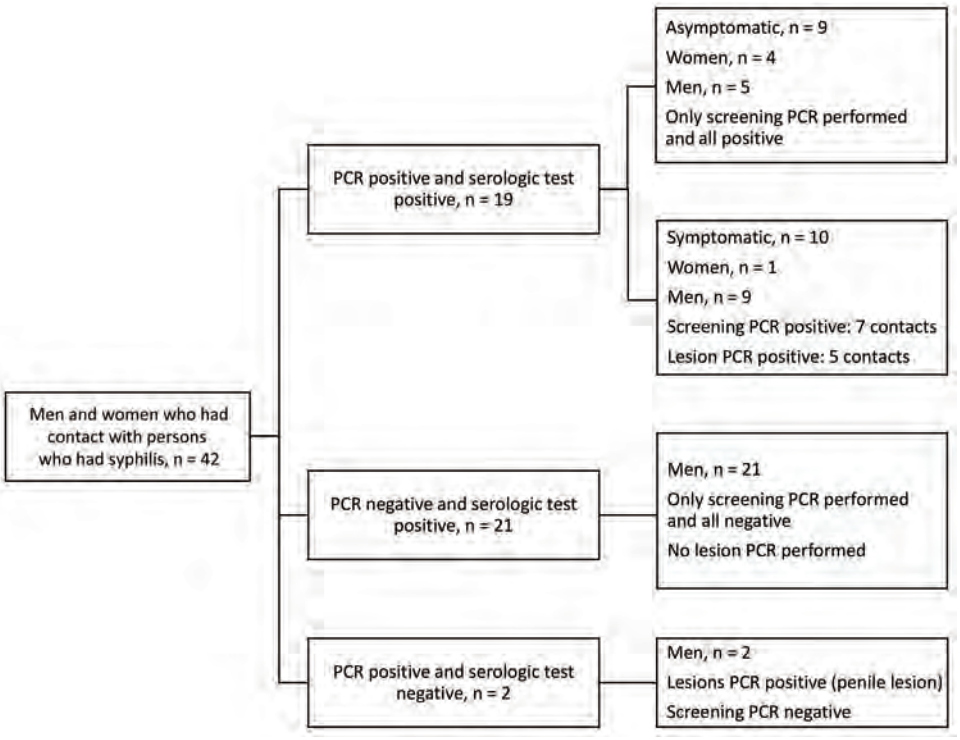

Figure. Flowchart of syphilis infections among men and women who had contact with persons who had syphilis, categorized by positive PCR and serologic test results and presence or absence of symptoms, in retrospective study of patients who visited the Melbourne Sexual Health Centre, Melbourne, Victoria, Australia, during November 2018–March 2020.

28–40 years). Most (86%, 18/21) were asymptomatic for syphilis except 3 case-patients. Two men with symptoms had secondary syphilis diagnosed and had a generalized body rash. One man with symptoms had a headache and blurred vision, consistent with symptoms of neurosyphilis, and a resolving body rash. *T. pallidum* lesion PCR tests were not performed on the 3 men with symptoms. The RPR titer ranged from nonreactive to 1:128 (median RPR 1:4, IQR nonreactive to 1:32).

Positivity of *T. pallidum* PCR

The positivity of *T. pallidum* PCR from the mucosal screening tests (oral, anal, and vaginal sites) was 3% (95% CI 2%–5%; n = 24) from 776 specimens, whereas the positivity from the suspected syphilis lesions was 16% (95% CI 7%–30%; n = 8) from 50 specimens tested from various sites, such as the penis, perianal, scrotum, and tongue (Table 5). The concordance of oral rinse (2%, 8/387) and oral swab (3%, 11/352) PCR was 99% (n = 352/355).

Table 2. Characteristics of 9 syphilis patients without signs or symptoms of syphilis who had PCR detection of *Treponema pallidum* from oral, anal, or vaginal sites in retrospective study of men and women who visited the Melbourne Sexual Health Centre, Melbourne, Victoria, Australia, during November 2018–March 2020*

Group by sexual practice	HIV/PrEP status	Signs on examination	Mucosal PCR sites (value if positive†)			Serologic test results		Previous serologic test results (RPR titer if reactive)	Staging of syphilis
			Oral cavity	Vagina	Anal	Current RPR titer	Previous syphilis serologic test		
Woman‡	Neg	No	–	+ (31)	ND	1:8	8 y	Negative	Primary
Woman§	Neg	ND	–	+ (36)	ND	1:2	None	NA	Primary
Woman‡	Neg	No	+ (33)	ND	ND	1:128¶	None	NA	Primary
Woman‡	Neg	ND	+ (32)	+ (37)	ND	1:16	None	NA	Early latent
Bisexual man	Neg	ND	–	NA	+ (35)	Nonreactive#	8 mo	Negative	Early latent
MSM	Neg	No	–	NA	+ (26)	1:32	12 mo	Negative	Early latent
MSM	HIV	No	+ (30)	NA	–	1:256¶	10 mo	+ (1:8)	Primary
MSM	HIV	No	+ (36)	NA	–	1:128¶	10 mo	Negative	Primary
MSM	PrEP	No	+ (36)	NA	+ (32)	1:32	2 mo	Nonreactive	Primary

*MSM, men who have sex with men; NA, not applicable; ND, not done; neg, HIV-negative and not taking PrEP; PrEP, preexposure prophylaxis for HIV; RPR, rapid plasma reagin; woman, heterosexual woman; –, negative by *T. pallidum* PCR; +, positive by *T. pallidum* PCR.
†Cycle threshold value of *T. pallidum* PCR.
‡The regular partners (of ≥1 year duration) had early syphilis (primary and secondary) diagnosed.
§The casual partner had secondary syphilis diagnosed.
¶These 3 patients had high RPR titers with oral PCR detection. We attribute oral PCR detection to shedding after dissemination of *T. pallidum* on the basis of the high RPR titer, although this finding could be attributable to occult lesions in the oral cavity.
#Positive *T. pallidum*–specific antibodies and nonreactive RPR with negative *T. pallidum*–specific antibodies 8 months prior.

Table 3. Characteristics of 10 syphilis patients with signs and symptoms of syphilis who had a positive serologic test and *Treponema pallidum* PCR detection from mucosal sites or lesion sites in retrospective study of patients who visited the Melbourne Sexual Health Centre, Melbourne, Victoria, Australia, during November 2018–March 2020*

Group by sexual practice	HIV/PrEP status	Signs on examination	Mucosal PCR sites (value if positive†)			Serologic test results			Previous serologic test results (RPR titer if reactive)	Staging of syphilis
			Oral cavity	Vagina	Anus	Lesion PCR sites (value if positive†)	Current RPR titer	Previous syphilis serologic test		
Woman	Neg	Oral ulcers	+ (36)	–	–		1:64	24 mo	Negative	Primary
MSM	Neg	Tender anal ulcers	–	NA	+ (30)		1:16	3 wks	1:1	Primary
MSM	HIV	Torso and hand rash	+ (31)	NA	+ (30)		1:64	5 mo	Nonreactive	Secondary
MSM	PrEP	Torso rash, penis and perianal rash	+ (34)	NA	+ (30)		1:128	2 mo	Nonreactive	Secondary
MSM‡	Neg	Maculopapular rash on torso and soles	–	NA	+ (26)		1:256	12 mo	Unknown	Secondary
MSM‡	Neg	Ulcer on tongue, scrotal rash	+ (32)	NA	+ (36)	Tongue, + (30); scrotum, + (39)	1:32	26 mo	Unknown	Primary
MSM	HIV	Penile ulcer	+ (34)	NA	+ (40)	Penis, + (34)	1:128	4 mo	Negative	Primary
Bisexual man	Neg	Penile ulcers	–	NA	–	Penis, + (38)	1:32	15 mo	Negative	Primary
MSM	HIV	Penile ulcers, torso rash	–	NA	–	Penis, + (36)	1:64	12 mo	Negative	Secondary
MSM	HIV	Palms and feet rash, ulcers on penis, and nodules on scrotum	–	NA	–	Penis, + (36) scrotum, –; palms, –; soles, –	1:128	16 mo	1:1	Secondary

*MSM, men who have sex with men; NA, not applicable; ND, not done; neg, HIV negative and not taking PrEP; PrEP, preexposure prophylaxis for HIV; RPR, rapid plasma reagin; woman, heterosexual woman; –, negative by *T. pallidum* PCR; +, positive by *T. pallidum* PCR.
†Cycle threshold value of *T. pallidum* PCR.
‡These 2 patients had syphilis treated at other clinics previously, but the exact RPR at that time is unknown.

Presence or Absence of Signs and Symptoms of Syphilis

Among 338 asymptomatic contacts, 8% (27, 95% CI 5–11) had syphilis infection diagnosed on the basis of positive serologic tests with or without positive *T. pallidum* PCR results. Of the 338 contacts, 56% (180/338) received an examination. Among 69 contacts with signs and symptoms of syphilis, 22% (15, 95% CI 13–33) had syphilis infection diagnosed on the basis of positive serologic tests, positive *T. pallidum* PCR, or both.

Co-infection with Other STIs

A total of 32 contacts (8%, 32/407) had ≥1 STI other than syphilis diagnosed. All of them were MSM, and among them, 6 had syphilis diagnosed. Five had syphilis diagnosed on positive PCR and serologic testing, whereas 1 had syphilis diagnosed on a positive serologic test alone. Among the 32 contacts, 17 were positive for chlamydia, and 12 contacts were positive for gonorrhea. Five contacts were positive for *Mycoplasma genitalium* infection, and 2 contacts tested positive for anal herpes simplex virus. Among the STIs other than syphilis, anorectal chlamydia was the most common infection (n = 15).

Discussion

In this study of men and women reporting sexual contact with a person with syphilis, we did not identify any persons with PCR detection of *T. pallidum* from oral, anal, or vaginal sites where serologic testing was negative, indicating that using PCR for screening of syphilis contacts at mucosal sites might not provide any additional benefit over existing syphilis screening using serologic testing. However, we found a proportion of men and women who tested positive for *T. pallidum* by PCR from the oral cavity, anus, or vagina in the absence of signs or symptoms of syphilis at those sites or elsewhere. In some cases, serologic testing for syphilis was positive in the absence of negative serologic testing within the previous 2 years. Those persons would conventionally be staged as having latent syphilis of unknown duration, and they probably were treated for possible late latent infection. However, detection of *T. pallidum* by PCR from oral, anal, or vaginal sites, in conjunction with the syphilis contact status,

suggests that those infections probably were early asymptomatic infections.

The findings indicate that PCR-based testing for *T. pallidum* at mucosal sites may be useful in assisting with staging of syphilis infection. Consequently, this approach could provide guidance to clinicians and patients regarding treatment duration. Furthermore, *T. pallidum* PCR testing at mucosal sites has the potential to aid in partner notification, particularly in cases where an early infectious syphilis is diagnosed and the duration of infection is uncertain. *T. pallidum* PCR may complement current methods of staging, which rely on various factors, including the presence of signs of early syphilis, the patient's history of syphilis and treatment, sexual history (including contact with a partner with syphilis infection), and past and current laboratory results (including serologic testing and direct detection methods using molecular assays).

We identified several asymptomatic women who had positive syphilis serologic testing and PCR detection of *T. pallidum* from the mucosal screening sites (the vagina, oral cavity, or both). Those women had never been serologically tested for syphilis before or had been tested >2 years previously. We also identified several asymptomatic MSM who had positive syphilis serologic testing and PCR detection of *T. pallidum* from the anus, oral cavity, or both. In contrast to the women, all those men had been serologically tested for syphilis within the previous 2 years. The difference in serologic testing between women and men reflects frequent serologic screening for syphilis being well established among MSM in Australia but less so among women in urban centers because syphilis has only emerged as a major public health concern among women in that setting in recent years.

Several studies have examined the role of NAAT in syphilis screening (*20*,*29*). A US study compared the use of transcription-mediated amplification (TMA) assay performed on rectal and pharyngeal mucosa in MSM with routine serologic testing and found 2 additional syphilis cases diagnosed on TMA testing before positive serologic testing (*29*). Patients in both cases had TMA detection in rectal swabs: 1 did not have symptoms, and the other had anal symptoms. In contrast, our study did not identify syphilis cases diagnosed on *T. pallidum* PCR from mucosal sites before positive serologic testing.

Table 4. Characteristics of 21 syphilis patients with positive serologic tests in the absence of PCR detection from mucosal sites or lesion sites in retrospective study of patients who visited the Melbourne Sexual Health Centre, Melbourne, Victoria, Australia, during November 2018–March 2020*

Group by sexual practice	HIV/PrEP status	Signs and symptoms of syphilis	Current RPR titer	Previous syphilis serologic test	Previous serologic test result (RPR titer if reactive)	Staging of syphilis
MSM	Neg	No	1:4	8 mo	Nonreactive	Early latent
MSM†	PrEP	No	Nonreactive	18 mo	Nonreactive	Early latent
MSM	PrEP	No	Nonreactive	10 mo	Negative	Early latent
MSM	PrEP	Not examined	Nonreactive	3 mo	Negative	Early latent
MSM	Neg	No	1:16	5 mo	Nonreactive	Early latent
MSM	HIV	No	Nonreactive	6 mo	Negative	Early latent
MSM	PrEP	No	1:128	4 mo	Negative	Early latent
MSM	Neg	No	1:32	12 mo	Negative	Early latent
MSM	Neg	Not examined	1:64	4 mo	Negative	Early latent
MSM	HIV	Not examined	1:64	1 mo	Negative	Early latent
MSM	PrEP	Not examined	1:4	8 mo	1:1	Early latent
Heterosexual man	Neg	Not examined	1:8	8 mo	Negative	Early latent
Bisexual man	Neg	Macular rash on palms	1:32	None	None	Secondary
MSM	Neg	Rash/papules on penis, maculopapular rash on hands and back	1:32	14 mo	Nonreactive	Secondary
MSM	PrEP	Not examined	Nonreactive	11 mo	Negative	Early latent
MSM§	Neg	Blurred vision and headache, Resolved body rash before presentation	1:64	19 mo	Negative	Secondary/ neurosyphilis
MSM	HIV	Not examined	1:4	3 mo	Nonreactive	Early latent
MSM	PrEP	No	Nonreactive	6 mo	Negative	Early latent
MSM‡	Neg	No	1:2	None	None	Late latent
MSM	PrEP	Not examined	Nonreactive	1 mo	Negative	Early latent
MSM	HIV	Not examined	1:32	2 mo	Nonreactive	Early latent

*MSM, men who have sex with men; neg, HIV negative and not taking PrEP; nonreactive, nonreactive RPR; PrEP, preexposure prophylaxis for HIV; RPR, rapid plasma reagin.
†IgM was reactive on serologic test.
‡Treated for late latent syphilis.
§Subsequently had neurosyphilis diagnosed.

Table 5. Patients testing positive on *Treponema pallidum* PCR at mucosal screening sites and lesion sites in retrospective study of patients who visited the Melbourne Sexual Health Centre, Melbourne, Victoria, Australia, during November 2018–March 2020

Sites tested by *T. pallidum* PCR	No. tested	No. (%) positive by *T. pallidum* PCR
Mucosal sites*	776	24 (3.0)
Oral cavity†	405	12 (3.0)
No oral symptoms	339	8 (2.4)
Oral symptoms present	66	4 (6.1)
Anal swab	352	9 (2.6)
No anal symptoms	291	4 (1.4)
Anal symptoms present	61	5 (8.2)
Vaginal swab	19	3 (13.6)
No vaginal symptoms	18	3 (16.7)
Vaginal symptoms present	1	0
Lesion sites‡	50	8 (16.0)
Penile swab	23	6 (26.0)
Other sites (perianal: 13)	27	2§ (7.4)

*Oral cavity, anus, and vagina.
†Specimens tested from oral cavity were oral swab, oral rinse, or both. Oral swab was positive in 11/352 (3%) samples. Oral rinse was positive in 8/397 (2%) samples.
‡Penis, perianal, labia, mouth ulcer, palms, soles, pubic, right groin, scrotum, and tongue.
§Positive PCR from specimens tested at tongue and scrotum.

In our study, we found that 40% of the 42 confirmed early syphilis cases among men and women had PCR detection of *T. pallidum* from ≥1 of the mucosal sites (oral, anus, and vagina), with or without lesions at these sites. Of note, we show PCR detection of *T. pallidum* in asymptomatic women. *T. pallidum* detection by PCR in women has been shown in other studies but predominantly from genital lesions (*16*,*30*–*32*). The presence of *T. pallidum* at those mucosal sites may represent the site of inoculation (and hidden primary lesions) or dissemination from a distant site (*19*). Several other recent studies showed that *T. pallidum* can be detected from the oral cavity or anus of men and women with early syphilis infection (*18*–*23*). Detection of *T. pallidum* by PCR was reported in ≈24% of 200 MSM with confirmed early syphilis infection with or without lesions at the oral cavity and anus (*18*). Those studies suggest that syphilis probably is infectious from oral, anal, and vaginal sites in the absence of local signs and symptoms.

The first limitation of our study is that it was terminated prematurely because of the COVID-19 pandemic, which limited the sample size. The number of women in the study was small because the clinic population was predominantly male, and fewer women attended. The sexual partners reported by contacts might not have actually had syphilis, given that we were unable to confirm their diagnosis; if so, we may have overestimated syphilis infections in this study group. Not all contacts who self-reported that they were asymptomatic had examination of oral, vaginal, and anal sites by the clinician (46% did not undergo examination), which could have led to occult lesions at those sites being missed. The *T. pallidum* PCR we used might have lower sensitivity than other *T. pallidum* molecular assays, such as TMA, resulting in a lower number of PCR-positive mucosal screening tests (*29*,*33*). Further, current data are not sufficient to indicate that *T. pallidum* PCR positivity at a mucosal site is a proof of early syphilis infection. *T. pallidum* might reflect contamination from very recent sexual intercourse with a person with syphilis infection, such as residual semen at the mucosal site.

Overall, we conclude that *T. pallidum* PCR screening from mucosal sites (oral, anus, and vagina) may not have added benefit over screening using serologic testing. It may, however, have a role in assisting with syphilis staging, particularly in the absence of syphilis lesions. A positive PCR result from asymptomatic mucosal sites may help identify early infections in persons who would otherwise be classified as having latent syphilis of unknown duration. However, such an interpretation requires a correlation with additional sexual behavioral information and the broader clinical context. *T. pallidum* PCR screening at mucosal sites may be especially relevant in populations that do not undergo regular syphilis screening with serologic testing.

Acknowledgments

We thank Darren Lee, who assisted with data entry and registry of specimens at VIDRL. We also acknowledge the clinicians from the Melbourne Sexual Health Centre who assisted with collection of specimens.

The data for this study are not publicly available because of privacy and ethical restrictions; however, data will be made available on reasonable request to the corresponding author, with the permission of the Alfred Hospital Ethics Committee. Restrictions apply to the availability of the data, which were used under license for this study.

This study was supported by Australia's National Health and Medical Research Council (NHMRC) Partnership Project Grant (APP2003399). E.P.F.C. is supported by an NHMRC Emerging Leadership Investigator Grant (GNT1172873). D.A.W. is supported by an NHMRC Investigator Grant (APP1174555). C.K.F. is supported by an NHMRC Leadership Investigator Grant (GNT1172900). M.Y.C. and J.M.T. are supported by an NHMRC Partnership Project Grant (APP2003399). E.T.A. is supported by an Australia Government's Research Training Program scholarship from Monash University and a Research Entry Scholarship from the Chapter of Sexual Health Medicine, Royal Australasian College of Physicians.

Author contributions: M.Y.C. and E.P.F.C. designed the study. M.Y.C., E.P.F.C., C.K.F. and R.W. coordinated the study and contributed to the development of the study protocol. D.A.W. and F.A. performed laboratory testing. E.T.A. collected data, performed the analysis of the data, performed chart review, wrote the first draft of the manuscript, and revised the manuscript. All authors reviewed and edited the manuscript. All authors read and approved the final manuscript.

About the Author

Dr. Aung is a sexual health physician and a PhD candidate at Melbourne Sexual Health Centre and Monash University, Australia. Her research focuses on syphilis epidemiology and early detection.

References

1. World Health Organization. Report on global sexually transmitted infection surveillance, 2018. Geneva: World Health Organization; 2018.
2. Tsuboi M, Evans J, Davies EP, Rowley J, Korenromp EL, Clayton T, et al. Prevalence of syphilis among men who have sex with men: a global systematic review and meta-analysis from 2000–20. Lancet Glob Health. 2021;9:e1110–8. https://doi.org/10.1016/S2214-109X(21)00221-7
3. Kojima N, Klausner JD. An update on the global epidemiology of syphilis. Curr Epidemiol Rep. 2018;5:24–38. https://doi.org/10.1007/s40471-018-0138-z
4. Aung ET, Chen MY, Fairley CK, Higgins N, Williamson DA, Tomnay JE, et al. Spatial and temporal epidemiology of infectious syphilis in Victoria, Australia, 2015–2018. Sex Transm Dis. 2021;48:e178–82. https://doi.org/10.1097/OLQ.0000000000001438
5. Luo Y, Xie Y, Xiao Y. Laboratory diagnostic tools for syphilis: current status and future prospects. Front Cell Infect Microbiol. 2021;10:574806.
6. Peeling RW, Mabey D, Kamb ML, Chen X-S, Radolf JD, Benzaken AS. Syphilis. Nat Rev Dis Primers. 2017;3:17073.
7. Tuddenham S, Katz SS, Ghanem KG. Syphilis laboratory guidelines: performance characteristics of nontreponemal antibody tests. Clin Infect Dis. 2020;71(Suppl 1):S21–42. https://doi.org/10.1093/cid/ciaa306
8. Park IU, Tran A, Pereira L, Fakile Y. Sensitivity and specificity of treponemal-specific tests for the diagnosis of syphilis. Clin Infect Dis. 2020;71(Suppl 1):S13–20. https://doi.org/10.1093/cid/ciaa349
9. Park IU, Fakile YF, Chow JM, Gustafson KJ, Jost H, Schapiro JM, et al. Performance of treponemal tests for the diagnosis of syphilis. Clin Infect Dis. 2019;68:913–8. https://doi.org/10.1093/cid/ciy558
10. Heymans R, van der Helm JJ, de Vries HJ, Fennema HS, Coutinho RA, Bruisten SM. Clinical value of *Treponema pallidum* real-time PCR for diagnosis of syphilis. J Clin Microbiol. 2010;48:497–502. https://doi.org/10.1128/JCM.00720-09
11. Gayet-Ageron A, Lautenschlager S, Ninet B, Perneger TV, Combescure C. Sensitivity, specificity and likelihood ratios of PCR in the diagnosis of syphilis: a systematic review and meta-analysis. Sex Transm Infect. 2013;89:251–6. https://doi.org/10.1136/sextrans-2012-050622
12. Gayet-Ageron A, Ninet B, Toutous-Trellu L, Lautenschlager S, Furrer H, Piguet V, et al. Assessment of a real-time PCR test to diagnose syphilis from diverse biological samples. Sex Transm Infect. 2009;85:264–9. https://doi.org/10.1136/sti.2008.034314
13. Shields M, Guy RJ, Jeoffreys NJ, Finlayson RJ, Donovan B. A longitudinal evaluation of *Treponema pallidum* PCR testing in early syphilis. BMC Infect Dis. 2012;12:353. https://doi.org/10.1186/1471-2334-12-353
14. Zhou C, Zhang X, Zhang W, Duan J, Zhao F. PCR detection for syphilis diagnosis: status and prospects. J Clin Lab Anal. 2019;33:e22890. https://doi.org/10.1002/jcla.22890
15. Leslie DE, Azzato F, Karapanagiotidis T, Leydon J, Fyfe J. Development of a real-time PCR assay to detect *Treponema pallidum* in clinical specimens and assessment of the assay's performance by comparison with serological testing. J Clin Microbiol. 2007;45:93–6. https://doi.org/10.1128/JCM.01578-06
16. Costa-Silva M, Coutinho D, Sobrinho-Simões J, Azevedo F, Lisboa C. Cross-sectional study of *Treponema pallidum* PCR in diagnosis of primary and secondary syphilis. Int J Dermatol. 2018;57:46–9. https://doi.org/10.1111/ijd.13823
17. Theel ES, Katz SS, Pillay A. Molecular and direct detection tests for *Treponema pallidum* subspecies *pallidum*: a review of the literature, 1964–2017. Clin Infect Dis. 2020;71(Suppl 1):S4–12. https://doi.org/10.1093/cid/ciaa176
18. Towns JM, Leslie DE, Denham I, Wigan R, Azzato F, Williamson DA, et al. *Treponema pallidum* detection in lesion and non-lesion sites in men who have sex with men with early syphilis: a prospective, cross-sectional study. Lancet Infect Dis. 2021;21:1324–31. https://doi.org/10.1016/S1473-3099(20)30838-0
19. Towns JM, Chow EPF, Wigan R, Fairley CK, Williamson D, Azzato F, et al. Anal and oral detection of *Treponema pallidum* in men who have sex with men with early syphilis infection. Sex Transm Infect. 2022;98:570–4. https://doi.org/10.1136/sextrans-2021-055370
20. Nieuwenburg SA, Zondag HCA, Bruisten SM, Jongen VW, Schim van der Loeff MF, van Dam AP, et al. Detection of *Treponema pallidum* DNA during early syphilis stages in peripheral blood, oropharynx, ano-rectum and urine as a proxy for transmissibility. Clin Infect Dis. 2022;75:1054–62. https://doi.org/10.1093/cid/ciac056
21. Tantalo LC, Mendoza H, Katz DA, Sahi SK, Marra CM. Detection of *Treponema pallidum* DNA in oropharyngeal swabs and whole blood for syphilis diagnosis. Sex Transm Dis. 2021;48:915–8. https://doi.org/10.1097/OLQ.0000000000001476

22. Wang C, Hu Z, Zheng X, Ye M, Liao C, Shang M, et al. A new specimen for syphilis diagnosis: evidence by high loads of *Treponema pallidum* DNA in saliva. Clin Infect Dis. 2021;73:e3250–8. https://doi.org/10.1093/cid/ciaa1613
23. Yang CJ, Chang SY, Wu BR, Yang SP, Liu WC, Wu PY, et al. Unexpectedly high prevalence of *Treponema pallidum* infection in the oral cavity of human immunodeficiency virus-infected patients with early syphilis who had engaged in unprotected sex practices. Clin Microbiol Infect. 2015;21:787.e1–7. https://doi.org/10.1016/j.cmi.2015.04.018
24. Bellhouse C, Walker S, Fairley CK, Chow EP, Bilardi JE. Getting the terminology right in sexual health research: the importance of accurately classifying fuck buddies among men who have sex with men. Sex Transm Infect. 2018;94:487–9. https://doi.org/10.1136/sextrans-2016-053000
25. The Australasian Society for HIV, Viral Hepatitis and Sexual Health Medicine. Australian STI management guidelines for use in primary care. 2021 [cited 2023 Aug 1]. https://www.sti.guidelines.org.au
26. Melbourne Sexual Health Centre. Testing guidelines. 2021 [cited 2023 Aug 1]. https://www.mshc.org.au/health-professionals/testing-guidelines
27. Workowski KA, Bachmann LH, Chan PA, Johnston CM, Muzny CA, Park I, et al. Sexually transmitted infections treatment guidelines, 2021. MMWR Recomm Rep. 2021;70:1–187. https://doi.org/10.15585/mmwr.rr7004a1
28. Public Health Laboratory Network Australian Government Department of Health. Syphilis laboratory case definition, 2012 [cited 2023 Feb 20]. http://www.health.gov.au/internet/main/publishing.nsf/Content/cda-phln-syphilis.htm
29. Golden M, O'Donnell M, Lukehart S, Swenson P, Hovey P, Godornes C, et al. *Treponema pallidum* nucleic acid amplification testing to augment syphilis screening among men who have sex with men. J Clin Microbiol. 2019;57:e00572–19. https://doi.org/10.1128/JCM.00572-19
30. Mehta SD, Pradhan AK, Green SJ, Naqib A, Odoyo-June E, Gaydos CA, et al. Microbial diversity of genital ulcers of HSV-2 seropositive women. Sci Rep. 2017;7:15475. https://doi.org/10.1038/s41598-017-15554-8
31. Noguchi H, Tokumitsu T, Kuroki E, Minematsu E, Asada Y, Kuroda S, et al. Detection of *Treponema pallidum* by immunocytochemistry of cervical smear: a case report. Diagn Cytopathol. 2021;49:E443–6. https://doi.org/10.1002/dc.24849
32. Grange PA, Gressier L, Dion PL, Farhi D, Benhaddou N, Gerhardt P, et al. Evaluation of a PCR test for detection of *Treponema pallidum* in swabs and blood. J Clin Microbiol. 2012;50:546–52. https://doi.org/10.1128/JCM.00702-11
33. Getman D, Lin M, Barakat N, Skvoretz R, Godornes C, Swenson P, et al. Analytical performance characteristics of a new transcription-mediated amplification assay for *Treponema pallidum*. J Clin Microbiol. 2021;59:e0051121. https://doi.org/10.1128/JCM.00511-21

Address for correspondence: Ei T Aung, Melbourne Sexual Health Centre, 580 Swanston St, Carlton, 3053, Victoria, Australia; email: eaung@mshc.org.au

etymologia revisited

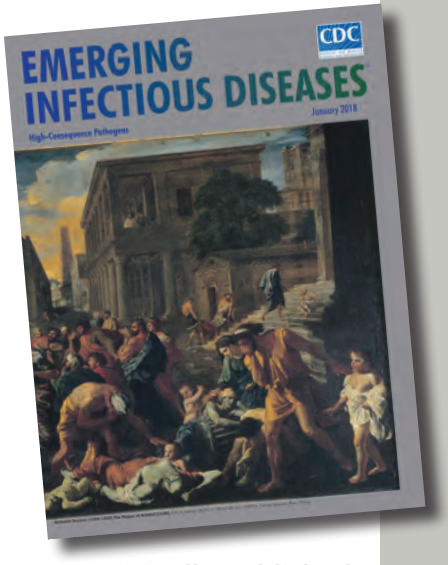

Originally published in January 2018

Plague
[plāg]

Plague (from the Latin *plaga*, "stroke" or "wound") infections are believed to have been common since at least 3000 BCE. Plague is caused by the ancestor of current *Yersinia* (named for Swiss bacteriologist Alexandre Yersin, who first isolated the bacterium) *pestis* strains. However, this ancestral *Y. pestis* lacked the critical *Yersinia* murine toxin (*ymt*) gene that enables vectorborne transmission. After acquiring this gene (sometime during 1600–950 BCE), which encodes a phospholipase D that protects the bacterium inside the flea gut, *Y. pestis* evolved the ability to cause pandemics of bubonic plague. The first recoded of these, the Justinian Plague, began in 541 ACE and eventually killed more than 25 million persons.

References:

1. Alexandre Yersin BW. Etymologia: yersinia. Emerg Infect Dis. 2010;16:496.
2. Centers for Disease Control and Prevention. History of plague [cited 2017 Oct 19]. https://www.cdc.gov/plague/history/index.html.
3. Rasmussen S, Allentoft ME, Nielsen K, Orlando L, Sikora M, Sjögren K-G, et al. Early divergent strains of Yersinia pestis in Eurasia 5,000 years ago. Cell. 2015;163:571–82.

https://wwwnc.cdc.gov/eid/article/24/1/et-2401_article

Managing Risk for Congenital Syphilis, Perth, Western Australia, Australia

Hannah MacKenzie, Suzanne P. McEvoy, Timothy J. Ford

The recent resurgence of infectious syphilis across many high-income countries has been accompanied by a shift in demographics, including infections increasing among women of reproductive age. Consequently, several high-income countries are reporting increasing cases of congenital syphilis, a disease associated with a range of health and social consequences and a disease that is treatable, is preventable, and could be eliminated. To prevent congenital syphilis in the large cosmopolitan city of Perth, Western Australia, Australia, multilevel coordinated action was undertaken, including increased frequency of syphilis screening of pregnant women, workforce education and community engagement, regular interagency meetings to manage syphilis during pregnancy, use of a dynamic electronic syphilis register, use of synoptic (structured) reporting to guide management at delivery (neonatal management plans), and congenital syphilis case reviews. Other jurisdictions facing increasing syphilis cases should consider adopting these measures to reduce the risk for congenital syphilis.

Syphilis is a highly contagious sexually transmitted infection (STI) caused by *Treponema pallidum*, which has substantial short- and long-term health complications if untreated (*1*). The first line of treatment is intramuscular injection with long-acting benzathine penicillin, although reinfection can occur (*2*). Prompt contact tracing can help reduce the risk for reinfection and disease spread among sexually active persons.

Congenital syphilis is caused by transplacental *T. pallidum* transmission from mother to fetus during pregnancy (*1*,*2*). It can result in a wide spectrum of health consequences, including miscarriage, premature birth, stillbirth, low birth weight, and perinatal death, as well as brain, nerve, and organ damage (*3*–*5*). Children with congenital syphilis may face long-term disability and accompanying health, education, and societal costs. Although vertical transmission to the fetus can happen at any time during pregnancy, the risk depends on the stage of maternal syphilis and stage of gestation at which the pregnant woman acquires the infection. Untreated, the risk for vertical transmission is 70%–100% among women with primary or secondary syphilis, 40% for those with early latent disease, 10% for late latent disease, and negligible for tertiary syphilis (*5*,*6*). Characteristically, pregnant women are screened for syphilis at their first antenatal visit. Further testing may not occur during pregnancy, which may result in missed new onset illness (*7*–*9*) and substantial risk to the fetus. Fortunately, congenital syphilis is preventable and treatable (*10*) through timely detection, treatment, contact tracing, and appropriate monitoring during pregnancy.

In 2007, the World Health Organization (WHO) launched an initiative for the "elimination of congenital syphilis as a public health problem" (*11*). More recently, WHO strategic directions to reduce STIs (*12*) offer guidance for the response to rising syphilis cases: to deliver high-quality, evidence-based, people-centered services; optimize systems, sectors, and partnerships; generate and use data to drive decisions for action; engage empowered communities and civil society; and foster innovations for impact.

Of concern, cases of congenital syphilis remain elevated in many low- and middle-income countries and are resurging in several high-income countries that had previously made gains toward elimination. During the past decade, rates of infectious syphilis have increased in Australia, the United States, Japan, and Canada (*6*,*13*–*18*), accompanied by increasing cases among women of reproductive age (*6*,*13*,*15*,*17*–*19*) and cases of congenital syphilis (*6*,*13*,*16*,*17*,*19*,*20*).

Author affiliations: Western Australia Department of Health, Perth, Western Australia, Australia (H. MacKenzie, S.P. McEvoy); Metropolitan Communicable Disease Control, Perth (S.P. McEvoy); Perth Children's Hospital, Perth (T.J. Ford); University of Western Australia, Perth (T.J. Ford)

DOI: https://doi.org/10.3201/eid2910.230432

In the United States, the rate of congenital syphilis increased annually since 2013, increasing 8-fold to 77.9/100,000 live births by 2021 (*17*,*19*). In that year, 46 states and the District of Columbia reported ≥1 cases of congenital syphilis (*17*).

In Australia, the rate of infectious syphilis cases increased by 316%, from 5.0/100,000 population in 2010 to 20.8/100,000 population in 2020 (*21*). In 2011, an outbreak mainly affecting Indigenous Australians began in northeastern Australia (*22*) and then migrated across the north and into northern Western Australia in 2014–2016 (*22*,*23*). Starting in 2012, cases of infectious syphilis increased in major cities, initially among men and, since 2015, among women. The rate of infectious syphilis cases among men in Australia increased by 36% from 2016 to 2020, and the rate among women of reproductive age rose by 109% (*15*).

We describe the changing demographics among the rising cases of infectious syphilis in Perth, Western Australia, Australia, and the resulting local policy initiatives implemented to reduce the risk for congenital syphilis, including the preliminary outcomes of a holistic multiagency antenatal program for pregnant women with syphilis. This information could be applied in other jurisdictions facing a resurgence of syphilis, particularly those with similar socioeconomic profiles.

Setting

Perth, population ≈2.1 million, is the capital city of the state of Western Australia, located on the southwestern coast of Australia. The city is culturally diverse; 2% of residents are Indigenous Australians, 60.9% of residents have ≥1 parent born overseas, 40.5% of residents were born overseas, and a non-English language is used in 23.7% of households. The median weekly household income in Perth (Australian dollars) is $1,865, which is above the national equivalent ($1,746) (*24*).

In Western Australia, under Public Health Act 2016, syphilis of all stages and congenital syphilis are notifiable to the Western Australia Department of Health by the medical or nurse practitioner attending the patient and the reporting laboratory (*25*). Those notifications are then assigned to the local public health unit for follow-up and action.

Definitions

In Australia, the term culturally and linguistically diverse (CALD) is used to describe persons and populations with particular cultural or linguistic affiliations. The definition often differs according to the indicators collected by the reporting organization (*26*) but may include characteristics such as country of birth, spoken English proficiency, and main language spoken at home (*27*). The term Indigenous Australians describes Aboriginal people (descendants from the original inhabitants of Australia) and Torres Strait Islander people (from the Torres Strait Islands, located northeast of Australia). In Western Australia, the descendants of the original inhabitants are Aboriginal people.

Infectious syphilis encompasses primary, secondary, early latent, and probable infectious syphilis. Those stages cover up to 2 years from the putative time of acquisition (*2*).

Data Sources

With approval from the corresponding data custodians, we obtained data on syphilis in Perth for 2001–2021 from the Western Australian Notifiable Infectious Diseases Database. We calculated rates by

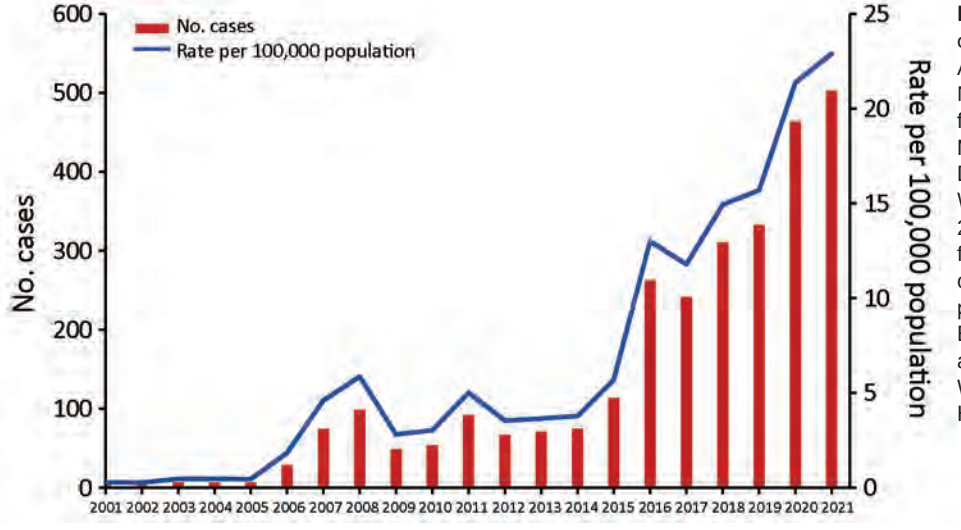

Figure 1. Infectious syphilis cases over time, Perth, Western Australia, Australia, 2001–2021. Numbers of cases were obtained from the Western Australian Notifiable Infectious Diseases Database, Department of Health Western Australia (January 2022); rates were calculated from the Australian Bureau of Statistics census-derived population data from the Epidemiology Branch, Public and Aboriginal Health Division, Western Australia Department of Health (February 2023).

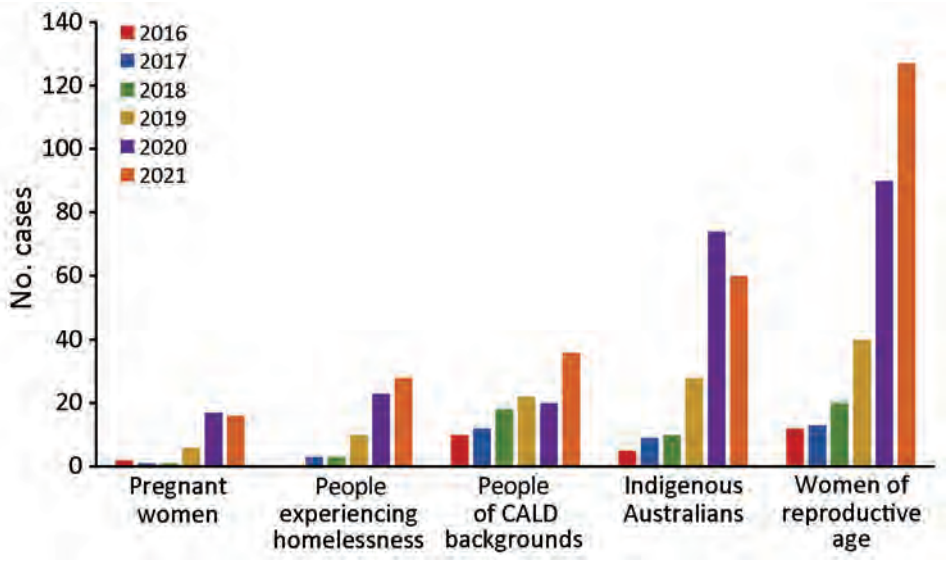

Figure 2. Number of infectious syphilis cases among pregnant women, persons experiencing homelessness, persons of CALD backgrounds, Indigenous Australians, and women of reproductive age, Perth, Western Australia, Australia, 2016–2021. Categories are not mutually exclusive (e.g., a person may fall into >1 category). Data obtained from the Western Australian Notifiable Infectious Diseases Database, Department of Health Western Australia (January 2022) and the Metropolitan Communicable Disease Control Syphilis Register, Metropolitan Communicable Disease Control (January 2022). CALD, culturally and linguistically diverse (persons born in a country other than Australia and who speak a non-English language at home).

using the Australian Bureau of Statistics census-derived population data from the Epidemiology Branch within the Western Australia Department of Health. We extracted data about pregnant women and persons experiencing homelessness with syphilis from the Metropolitan Communicable Disease Control (MCDC) Syphilis Register.

Contextualizing the Policy

In Perth, the number and rate of infectious syphilis cases have risen substantially, particularly since 2015, reaching 22.9 cases/100,000 population in 2021 (Figure 1). From 2001 through 2005, there were very few cases; the rate remained <0.5/100,000 population. In 2006, the rate increased to 1.8/100,000 population and fluctuated over the next decade, reaching 5.7/100,000 population in 2015; in this period, cases were predominantly among men who have sex with men. From 2015 through 2021, cases of infectious syphilis surged by 312%, coinciding with spread to the heterosexual population, outbreaks in northern Australia, the introduction and rising use of dating apps, and reports of transactional sex for illicit drugs or accommodation. Cases continued to increase despite various COVID-19 pandemic restrictions (*13*), as has been observed elsewhere (*17*,*18*).

Case escalation since 2015 has been accompanied by a rise in the number and proportion of cases among priority populations, including women of reproductive age and the subset who are pregnant, persons experiencing homelessness, persons of CALD backgrounds, and Indigenous Australians (Figure 2). The proportion of cases among Indigenous Australians has increased considerably, from 1.9% in 2016 to 15.9% in 2020 and to 11.9% in 2021.

For women of reproductive age, cases of infectious syphilis have risen from 2.8 cases/100,000 population in 2016 to 28.7/100,000 population in 2021. Likewise, cases among pregnant women in Perth rose 8-fold from 2016 through 2021, and there were 5 cases of congenital syphilis from 2018 through 2021 and only 2 cases in the preceding 10-year period.

Establishing Priority Areas

In July 2020, the Western Australian Chief Health Officer declared a syphilis outbreak in Perth (*28*), which prompted an organized, cross-agency collaborative effort, including establishing the Metropolitan Syphilis Outbreak Response Team (MSORT), a multiagency team with the primary goals of controlling the outbreak in Perth and preventing congenital syphilis. The response is underpinned by a local action plan (*28*) consisting of 5 priority areas: prevention, education, and community engagement; workforce development; testing, treatment, and contact tracing; surveillance and reporting; and antenatal and postnatal care (Table) (*28*). Although the action plan was informed by the WHO 5 strategic directions in relation to STIs (*12*), the priorities were determined by national initiatives (*29*) and a local consultation process involving stakeholders across health sectors, including government and nongovernment organizations and community health and hospital services (*30*).

MSORT has been pivotal in raising awareness about the outbreak, developing clinician alerts and

health promotion materials, educating the workforce, and revising guidelines (*5*,*31*–*34*). Moreover, the local public health unit, MCDC, works closely with local service providers and has helped establish multidisciplinary committees involving primary health, community health services, and hospitals to deliver additional outreach and services for priority groups, including pregnant women, Indigenous Australians, and persons experiencing homelessness.

Table. Local initiatives implemented to tackle the syphilis outbreak in Perth, Western Australia, Australia*

Priority area of the Metropolitan Action Plan (*28*)	Descriptions of initiatives
Prevention, education, and community engagement	Syphilis outbreak campaigns to increase awareness among health professionals and the community, including accessible educational resources that reduce stigma and are guided by cultural considerations Education of community organizations and community members (e.g., Indigenous, homeless and CALD persons) Education of cases and contacts by MCDC public health nurses, Indigenous health professionals and midwife Indigenous health team engagement and outreach with community members and persons experiencing homelessness Indigenous health team outreach service collaborates with other agencies (e.g., Indigenous community health and health services for persons experiencing homelessness)
Workforce development	Establishment of MSORT, a multiagency team to lead a coordinated outbreak response Diversification of MCDC workforce to address population and workforce needs, with a focus on priority populations, including establishment of Indigenous health, clinical midwifery, and general practitioner roles Project officer employed to facilitate the development of contextualized models of care and health promotion materials guided by stakeholder engagement for priority groups, including CALD persons Epidemiologist employed to help facilitate enhanced surveillance and reporting Public health staff engaging with and delivering education to a wide range of health professionals and services, focusing on specialty services that see high priority and/or atypical cases General practitioner delivering education to primary healthcare doctors and nurses MCDC midwife providing education to health professionals in maternity services Development of educational resources and clinician alerts to inform health professionals Establishment of regular multiagency SIP and SAPH case management meetings to oversee management of these priority groups
Testing, treatment and contact tracing	Template letter about syphilis treatment, partner notification and repeat testing sent to the test requesting health professional Evidence from the congenital syphilis case reviews informed adoption of 3-test routine screening of all pregnant women Frontline services engaged in case management and supporting contact tracing Engagement with laboratories to improve timeliness of results, particularly for antenatal requests, and changes to reporting algorithms to prevent missed notifications and diagnoses Improved processes for ordering parallel testing when monitoring RPRs in pregnant women Systematic approach to obtaining maternal and infant syphilis results through a reporting protocol to the MCDC SIP team from hospital obstetric services
Surveillance and reporting	Electronic syphilis public health management register developed to meet the needs of a syphilis outbreak, which has enabled better monitoring and identification of priority populations, including testing, treatment, and contact tracing efforts The register is used to generate automated reports (e.g., quarterly reports, individual summaries for case management meetings, and synoptic reports [neonatal management plans]) Automated alerts remind MCDC staff to confirm receipt of treatment or repeat testing for priority cases
Antenatal and postnatal care	Local STI, antenatal and obstetric guidelines changed to recommend syphilis screening for all pregnant women at initial visit, 28 weeks, and 36 weeks of gestation (or birth if earlier) Proactive public health management of pregnant women with syphilis and their sexual contacts Monthly multiagency meetings to ensure appropriate care and follow-up of pregnant women with syphilis Routine synoptic reporting (neonatal management plans) to guide syphilis testing and management of neonates and their mothers at delivery Interagency congenital syphilis case reviews to identify gaps in service delivery and inform service improvement

*CALD, culturally and linguistically diverse; MCDC, Metropolitan Communicable Disease Control; MSORT, Metropolitan Syphilis Outbreak Response Team; RPR, rapid plasma reagin; SAPH, Syphilis Among People Experiencing Homelessness; SIP, Syphilis In Pregnancy; STI, sexually transmitted infection.

Learning from Missed Opportunities

Analyzing congenital syphilis cases can identify opportunities for improved processes and service delivery to prevent future cases. Each case of congenital syphilis is a sentinel event. In Western Australia, all cases are reviewed by a panel consisting of health professionals and other relevant service providers involved in the management of the mother and infant (or fetus, in instances of stillbirth). The purpose of the reviews is not to attribute blame but rather to review the clinical and public health management of the mother and infant to develop recommendations and a plan for service improvement (*30*,*35*). The reviews also provide an opportunity to increase awareness and deliver education (*31*,*35*).

A public health report, which summarized 8 congenital syphilis cases and 1 near miss occurring across the state of Western Australia from January 2019 through June 2021, highlighted that congenital syphilis is generally not attributable to a single factor and encompasses complex social issues, health disparity, access difficulties, and varying levels of healthcare (*31*). Of the neonates with congenital syphilis born to women residing in Perth, the reviews identified pregnant women who tested negative for syphilis at their first antenatal visit but received no repeat syphilis testing during the remainder of their pregnancy, leaving infection acquisition undetected (*31*). In some instances, atypical or subtle clinical manifestations of syphilis remained undetected or misdiagnosed during the antenatal period.

Dynamic Electronic Syphilis Register

An effective response to any disease is reliant on efficient access to an accurate and comprehensive data surveillance system. To meet the needs of monitoring, reporting, responding to, and managing the syphilis outbreak, MCDC developed an electronic syphilis public health management register. The database can be used to review rapid plasma reagin (RPR) trends, treatment history, and contact tracing status, including identification of reinfections among past case-patients and contacts named on multiple occasions. Data completeness is supported by mandatory notification requirements.

The register has streamlined processes for case management, including a range of automated functions to generate enhanced surveillance reports, case summaries for meetings that include key points of discussion, handover, and neonatal management plans, as well as alerts for repeat testing, which trigger active public health follow-up with the responsible clinician. Furthermore, it enables monitoring of changing demographic profiles, including cases among CALD persons, persons experiencing homelessness, and persons who inject drugs or engage in transactional sex. Because cases among these population groups can be complex, to inform resource allocation, public health staff at MCDC review automated quarterly reports that include trends in demographic profiles.

Improving Reporting and Timeliness of Syphilis Test Results

The approach to notification of syphilis cases varied by laboratory. Some laboratories reported all positive syphilis test results (even if the RPR was negative), and others reported only according to minimum RPR cutoffs. To improve consistency for women of reproductive age, positive syphilis serology results regardless of the RPR are now reported by all laboratories because cases of early infectious syphilis and untreated early and late latent syphilis were occasionally missed.

Efficient reporting of, and access to, syphilis results help ensure timely case management, which is particularly valuable when managing syphilis in pregnant women, for whom prompt diagnosis, treatment, and contact tracing are pivotal for preventing congenital syphilis. Engaging with local laboratories to improve timeliness from specimen collection to reporting has led to development of an urgent syphilis testing protocol for pregnant women who attend major maternity hospitals and have not accessed regular antenatal care.

Regular parallel RPR monitoring during pregnancy is useful for monitoring treatment response and diagnosing reinfection. In some instances, MCDC staff members identified delays in parallel RPR testing for pregnant women with syphilis. Consultation with local laboratories has led to a revised protocol for this cohort to avoid preventable delays.

Workforce Development and Community Engagement

Because syphilis is often considered to be a rare condition in Australia (*36*), educating health professionals and the community of its resurgence is critical. Health professionals need to know how to diagnose the disease (clinical features and testing), manage cases and sexual contacts, and follow current guidelines. Local doctors and nurses have delivered education to a wide range of healthcare professionals; efforts have been focused on professionals who receive high-priority or atypical cases, such as dentists and oral surgeons, ophthalmologists, mental health professionals,

antenatal service providers, emergency department workers, and general practitioners.

Progressively, local frontline services have become more engaged in opportunistic screening, case management, and contact tracing. For example, opportunistic syphilis screening is now offered to persons entering correctional facilities, and the emergency department at one tertiary hospital has established enhanced screening practices and instigated patient management plans.

Whenever a case of infectious syphilis is notified to MCDC, public health nurses advise healthcare professionals over the phone and by template letter about treatment, partner notification, and repeat testing. When needed, persons with syphilis and their sexual contacts will also be interviewed and counseled. Although effective, those methods are resource intensive and can be difficult to maintain.

The Western Australian Department of Health has developed syphilis campaigns that have raised community awareness of the outbreak. The campaigns aim to reduce STI stigma and are guided by cultural considerations. Educational resources and clinician alerts for health professionals have promoted the "test, treat and trace" message, the value of additional routine testing of pregnant women, and access to culturally guided care (*34*). Outgoing emails from MCDC are accompanied by a signature block with an embedded link to local syphilis guidelines.

To focus on local population needs, the MCDC workforce has been expanded and includes public health doctors and nurses, a general practitioner, a clinical midwife, Indigenous health professionals, an epidemiologist, and a project officer. The team has developed effective collaborations with many local health and community organizations and members. The general practitioner delivers syphilis education to primary physicians and practice nurses. The midwife manages cases in pregnant women, liaising closely with clinicians and providing education to the pregnant women and their sexual contacts. The Indigenous healthcare professionals provide a vital outreach role and help Indigenous Australians and persons experiencing homelessness receive care in culturally safe ways (*37*). They support access to testing and treatment, including transportation assistance, where necessary, and they help to find hard-to-reach case-patients and contacts. The epidemiologist undertakes surveillance and reporting functions, examines the timeliness of treatment delivery, and analyzes the success of contact tracing efforts. The project officer develops models of care, engages with CALD community organizations and members, and provides health promotion materials that are easy to read and consumer focused.

Substantial progress has been made to enhance service delivery and accessibility for high-priority populations affected by syphilis in Perth; however, further actions are needed to ensure accessible care for all. Because of resource constraints amid a pandemic, work has only recently commenced to enhance service delivery for CALD populations (*28*). Ongoing work will be required to ensure that service provision continues to align with community needs.

Expanding Routine Pregnancy Screening

The WHO STI guideline (*38*), Centers for Disease Control and Prevention STI guidelines (*39*), and Australian Government pregnancy care guidelines (*23*) recommend screening all pregnant women for syphilis at their first antenatal visit. To date, recommendations regarding additional testing have been based on risk (depending on the woman's demographic profile) and background local syphilis epidemiology (*23*,*39*). More recently, data have demonstrated that testing only 1 time (during early pregnancy) may result in missed cases in which maternal syphilis is acquired later in gestation, particularly in areas where incidence of syphilis is increasing (*8*,*9*,*40*).

Risk factors can be challenging or absent, and cases may be missed if risk factors are relied on to guide testing. Because of the complexities that surround identifying risk factors (*41*) and findings from local congenital syphilis reviews, local STI, antenatal, and obstetric guidelines now recommend screening all pregnant women in Perth at their initial visit, at 28 weeks, and at 36 weeks of gestation (or delivery, if earlier) (*5*,*30*,*32*). Three-test screening for syphilis in all pregnant women helps normalize testing, recognizes that pregnant women remain sexually active, mitigates against unrecognized risk factors, and offers an opportunity to detect syphilis in pregnant women who have no or subtle signs and symptoms (*41*). Locally, universal screening at 28 weeks has already helped prevent at least 4 congenital syphilis cases since its introduction during 2021.

Enhancing Interagency Collaboration

In late 2020, MCDC introduced interagency and multidisciplinary case management meetings for 2 priority populations: Syphilis In Pregnancy (SIP) and Syphilis Among People Experiencing Homelessness. All pregnant women who received a diagnosis of syphilis during pregnancy, have a history of inadequately treated syphilis, or have completed treatment for infectious syphilis within the 12 months preced-

ing pregnancy are monitored by the SIP committee. The monthly meetings are a collaboration between public health professionals, sexual health physicians, an infectious diseases pediatrician, a neonatologist, midwives, an obstetrician, Indigenous health services, homeless health services, and health professionals from the Department of Justice when needed. Items considered are treatment decisions, access issues, risk assessment of the fetus, neonatal management plans, and contact tracing. This monthly collaboration enables timely support while maximizing the use of finite resources.

Supporting Optimal Management during Delivery

Early on, the SIP committee found that guidelines (*5*,*42*) for investigating and managing deliveries were not always followed, an issue that has also been described in other jurisdictions in Australia (*14*,*43*). That finding led to development of neonatal management plans, which are synoptic reports generated from the Syphilis Register with data for pregnant women with syphilis at ≈32–34 weeks of gestation (including demographics, stage of syphilis, results, treatment, contact tracing, and level of risk). Based on the data, a risk category (no, low- or high-risk for congenital syphilis) is assigned at the appropriate monthly meeting. Recommended maternal and neonatal investigations and treatment are based on risk category, and contact details of specialist services are provided (*5*,*42*). To guide management at delivery, the neonatal management plan is filed in the women's maternity hospital record before 36 weeks of gestation and discussed with the woman at an antenatal appointment.

Those plans have been well received by local maternity units and are now actively sought for pregnant women with syphilis who deliver in Perth. Hospital obstetric services report back to the MCDC SIP team, providing feedback on maternal and infant syphilis testing, information about the clinical examination of the neonate, and confirmation about any relevant treatment given to the infant.

Resourcing

Existing resources were used to support initiatives where possible. However, public health personnel developed a detailed business case and submitted it to the Western Australia Department of Treasury to expand the workforce, including at MCDC. Although successful, funding was limited to an initial 2-year period. In addition, MCDC received a modest 1-time grant for workforce development, which enabled increased education and outreach to clinicians and to Indigenous health and CALD service providers.

Preliminary Outcomes

From January 1, 2021, through September 30, 2022, the SIP committee monitored 63 pregnant women to the time of delivery or transfer to another health service region. No woman in the program delivered an infant with congenital syphilis.

Over the same period, 49 neonatal management plans were prepared as the program was consolidated. Of the 39 plans recommending infant treatment and mother/infant investigation at delivery (low- or high-risk plans), investigation recommendations were followed for 29 mother/infant pairs (74%), and treatment recommendations were followed for 36 (92%) infants. For a cohort in the Northern Territory of Australia, a similar risk-based approach to neonatal management has been implemented, although without formal generation of a synoptic report, which identified that only 52% of at-risk neonates received appropriate testing and 42% received adequate treatment at birth (*43*).

The program has enabled better monitoring of other health issues during pregnancy because of high attendance at antenatal appointments and, where required, has helped link women to social and community support for nonhealth issues, including housing. The holistic multiagency nature of this program, along with increased antenatal screening, community engagement with priority populations and key organizations, and strengthened collaboration with frontline services, have contributed to the positive outcomes.

Conclusions

The re-emergence of syphilis in Perth, and in locations in other high-income countries, has been accompanied by increasing case diversity and substantial involvement of women of reproductive age. Multilevel coordinated action that aligns with population needs is required to address this re-emerging disease effectively. Key elements include interagency collaboration, community engagement, workforce education, enhanced screening, ready access to treatment, contact tracing support, and surveillance and reporting. As rates of syphilis across the world increase, we urge other jurisdictions experiencing similar case loads to consider ways to reduce cases of congenital syphilis. Moreover, given that adherence to management guidelines in the evaluation of mother/infant pairs at delivery is suboptimal, implementing structured neonatal management plans can support optimal evidence-based care at birth. In our setting, the efforts that were successful in preventing additional cases of congenital syphilis were conducting

multiagency meetings for managing pregnant women with syphilis, using a dynamic electronic syphilis register, adopting synoptic reporting to guide management at delivery, undertaking community outreach and engagement with health services, and increasing routine syphilis screening during pregnancy.

About the Author

Dr. MacKenzie is in her third year of advanced training for membership in the Australian Faculty of Public Health Medicine and is based at the Public and Aboriginal Health Division at the Department of Health, Western Australia.

References

1. American Public Health Association. In: Heymann DL, editor. Control of Communicable Disease Manual. Washington (DC); American Public Health Association; 2015.
2. Australian Government. Syphilis—CDNA national guidelines for public health units. 2018 [cited 2022 Aug 30]. https://www.health.gov.au/resources/publications/syphilis-cdna-national-guidelines-for-public-health-units
3. Centers for Disease Control and Prevention. Congenital syphilis—CDC fact sheet. 2022 Apr [cited 2022 Aug 30]. https://www.cdc.gov/std/syphilis/stdfact-congenital-syphilis.htm
4. Victoria State Government, Department of Health. Congenital syphilis. 2020 Jul [cited 2022 Aug 30]. https://www.health.vic.gov.au/infectious-diseases/congenital-syphilis
5. Government of Western Australia, North Metropolitan Health Service, Women and Newborn Health Service. Obstetrics and gynaecology clinical practice guideline: syphilis in pregnancy. 2021 [cited 2022 Mar 25]. https://www.kemh.health.wa.gov.au/For-Health-Professionals/Clinical-Guidelines/Obs-Gyn-Guidelines
6. Government of Canada. Syphilis in Canada: technical report on epidemiological trends, determinants and interventions. 2020 Nov [cited 2022 Apr 4]. https://www.canada.ca/en/services/health/publications/diseases-conditions/syphilis-epidemiological-report.html#21
7. Wu MX, Moore A, Seel M, Britton S, Dean J, Sharpe J, et al. Congenital syphilis on the rise: the importance of testing and recognition. Med J Aust. 2021 Oct [cited 2022 Jan 18]. https://www.mja.com.au/journal/2021/215/8/congenital-syphilis-rise-importance-testing-and-recognition
8. Cooper JM, Porter M, Bazan JA, Nicholson LM, Sánchez PJ. Re-emergence of congenital syphilis in Ohio. Pediatr Infect Dis J. 2018;37:1286–9. https://doi.org/10.1097/INF.0000000000001995
9. Matthias JM, Rahman MM, Newman DR, Peterman TA. Effectiveness of prenatal screening and treatment to prevent congenital syphilis, Louisiana and Florida, 2013–2014. Sex Transm Dis. 2017;44:498–502. 10.1097/OLQ.0000000000000638 https://doi.org/10.1097/OLQ.0000000000000638
10. World Health Organization. Mother-to-child transmission of syphilis [cited 2022 Aug 30]. https://www.who.int/teams/global-hiv-hepatitis-and-stis-programmes/stis/prevention/mother-to-child-transmission-of-syphilis
11. World Health Organization. The global elimination of congenital syphilis: rationale and strategy for action [cited 2022 Oct 17] https://www.who.int/publications/i/item/the-global-elimination-of-congenital-syphilis-rationale-and-strategy-for-action
12. World Health Organization. Global health sector strategies on, respectively, HIV, viral hepatitis and sexually transmitted infections for the period 2022–2030. 2022 [cited 2022 Oct 17]. https://www.who.int/publications/i/item/9789240053779
13. Government of Western Australia, North Metropolitan Health Service. Epidemiology of notifiable infectious diseases in metropolitan Perth: Annual report 2020. 2021 [cited 2022 Mar 25]. https://www.nmhs.health.wa.gov.au/~/media/HSPs/NMHS/Documents/Public-Health/Report-of-notifiable-infectious-diseases-in-metropolitan-Perth-2020.pdf
14. Wu M, Seel M, Britton S, Dean JA, Lazarou M, Safa H, et al. Addressing the crisis of congenital syphilis: Key findings from an evaluation of the management of syphilis in pregnancy and the newborn in South-East Queensland. Aust N Z J Obstet Gynaecol. 2022;62:91–7. 10.1111/ajo.13424 https://doi.org/10.1111/ajo.13424
15. Kirby Institute. Sexually transmissible infections [cited 2022 Aug 30]. https://data.kirby.unsw.edu.au/STIs
16. Centers for Disease Control and Prevention. Tables—sexually transmitted disease surveillance, 2019. 2021 [cited 2021 Dec 1]. https://www.cdc.gov/std/statistics/2019/tables.htm
17. Centers for Disease Control and Prevention. Table 1—sexually transmitted diseases—reported cases and rates of reported cases, United States, 1941–2021 [cited 2023 Jun 20]. https://www.cdc.gov/std/statistics/2021/tables/1.htm
18. International Society for Infectious Diseases. PRO/EDR> Syphilis—Japan: (HS) increasing cases, RFI. ProMED. 2022 [cited 2022 Aug 30]. https://www.promedmail.org, archive no. 20220404.8702405.
19. Centers for Disease Control and Prevention. National overview of sexually transmitted diseases, 2021. 2023 May [cited 2023 Jun 20]. https://www.cdc.gov/std/statistics/2021/overview.htm#Syphilis
20. International Society for Infectious Diseases. PRO/EDR> Syphilis—Japan (03): rising incidence. ProMED. 2022 [cited 2022 Aug 30]. https://www.promedmail.org, archive no. 20211106.8699489.
21. Australian Government, Department of Health. National Notifiable Diseases Surveillance System (NNDSS): public datasets [cited 2021 Aug 2]. http://www9.health.gov.au/cda/source/cda-index.cfm
22. Australian Government, Department of Health. Multijurisdictional Syphilis Outbreak (MJSO) surveillance report—consolidated reports February to November 2020. 2020 [cited 2022 Aug 31]. https://www.health.gov.au/resources/publications/multijurisdictional-syphilis-outbreak-mjso-surveillance-report-consolidated-reports-february-to-november-2020
23. Australian Government, Department of Health and Aged Care. Syphilis. 2019 Jun [cited 2022 May 25]. https://www.health.gov.au/resources/pregnancy-care-guidelines/part-f-routine-maternal-health-tests/syphilis
24. Australian Bureau of Statistics. Greater Perth 2021 census all persons QuickStats [cited 2022 Sep 1]. https://abs.gov.au/census/find-census-data/quickstats/2021/5GPER
25. Government of Western Australia, Department of Justice, Parliamentary Counsel's Office. Public Health Act 2016 [cited 2023 Jun 20]. https://www.legislation.wa.gov.au/legislation/statutes.nsf/main_mrtitle_13791_homepage.html
26. Government of Western Australia, Sport, and Cultural Industries, Office of Multicultural Interests. Western

Australians from culturally and linguistically diverse backgrounds: a profile [cited 2023 Jun 20]. https://www.omi.wa.gov.au/docs/librariesprovider2/statistics/wa-cald-profile-2021.pdf
27. Australian Bureau of Statistics. Standards for statistics on cultural and language diversity. 2022 Feb [cited 2023 Jun 20]. https://www.abs.gov.au/statistics/standards/standards-statistics-cultural-and-language-diversity/latest-release
28. Government of Western Australia, Department of Health. Metropolitan syphilis outbreak response action plan 2021. 2021 [cited 2022 Aug30]. https://www.health.wa.gov.au/~/media/Corp/Documents/Health-for/Sexual-health/SORG/Metropolitan-Syphilis-Outbreak-Response-Action-Plan.pdf
29. Australian Government Department of Health and Aged Care. National response to syphilis. 2023 Jun 2 [cited 2023 Jun 20]. https://www.health.gov.au/our-work/national-response-to-syphilis#strategies
30. Government of Western Australia, Department of Health. Western Australian Syphilis Action Plan 2023–2025. Australia; 2023 [cited 2023 Jun 20]. https://www.health.wa.gov.au/~/media/Corp/Documents/Health-for/Sexual-health/SORG/WA-Syphilis-Outbreak-Response-Action-Plan-2023-25.pdf
31. Government of Western Australia, Department of Health. Silver book —STI/BBV management guidelines. 2020 [cited 2022 Apr 4]. https://ww2.health.wa.gov.au/Silver-book
32. Government of Western Australia. Public Health Review of Congenital Syphilis cases in WA Jan 2019-June 2021: summary report. Australia; 2021 [cited 2022 May 25]. https://www.health.wa.gov.au/~/media/Corp/Documents/Health-for/Sexual-health/SORG/Public-Health-Review-of-Congenital-Syphilis-Cases-in-WA-Report_Final.pdf
33. Government of Western Australia, North Metropolitan Health Service. GP antenatal shared care. 2021 [cited 2022 Feb 8]. https://www.kemh.health.wa.gov.au/For-Health-Professionals/Antenatal-shared-care
34. Government of Western Australia, Department of Health. WA syphilis outbreak response. 2022 Aug [cited 2022 Aug 31]. https://ww2.health.wa.gov.au/Articles/U_Z/WA-Syphilis-outbreak-response
35. Government of Western Australia. Guidelines for public health review of congenital syphilis case. 2022 Mar [cited 2022 Apr 4]. https://www.health.wa.gov.au/~/media/Files/Corporate/general-documents/Sexual-Health/PDF/Guidelines-for-review-of-congenital-syphilis.pdf
36. Royal Australian College of General Practitioners. Syphilis is making a comeback: what GPs need to know. 2021 Apr [cited 2022 Aug 30]. https://www1.racgp.org.au/newsgp/clinical/syphilis-is-making-a-comeback-what-gps-need-to-kno
37. Bertilone CM, McEvoy SP, Gower D, Naylor N, Doyle J, Swift-Otero V. Elements of cultural competence in an Australian Aboriginal maternity program. Women Birth. 2017;30:121–8. https://doi.org/10.1016/j.wombi.2016.09.007
38. World Health Organization. WHO guideline on syphilis screening and treatment for pregnant women. 2017 [cited 2022 May 25]. https://www.who.int/publications/i/item/9789241550093
39. Centers for Disease Control and Prevention. Syphilis during pregnancy. 2021 Jul [cited 2022 Aug 30]. https://www.cdc.gov/std/treatment-guidelines/syphilis-pregnancy.htm
40. Op de Coul EL, Hahné S, van Weert YW, Oomen P, Smit C, van der Ploeg KPB, et al. Antenatal screening for HIV, hepatitis B and syphilis in the Netherlands is effective. BMC Infect Dis. 2011;11:185. https://doi.org/10.1186/1471-2334-11-185
41. MacKenzie H, McEvoy S, Porter M. Congenital syphilis on the rise: the importance of testing and recognition [cited 2022 Aug 31]. https://www.mja.com.au/journal/2022/217/1/congenital-syphilis-rise-importance-testing-and-recognition
42. Government of Western Australia, Child and Adolescent Health Service. 2021 Jun. Syphilis: investigation and management of the neonate born to a mother with syphilis [cited 2022 Nov 9]. https://www.cahs.health.wa.gov.au/~/media/HSPs/CAHS/Documents/Health-Professionals/Neonatology-guidelines/Syphilis-Investigation-and-Management-of-the-Neonate-Born-to-a-Mother-with-Syphilis.pdf
43. McLeod C, Su JY, Francis JR, Ishwar A, Ryder N. Notification and management of congenital syphilis in the Northern Territory 2009 to 2014. Commun Dis Intell Q Rep. 201530;39:E323-8.

Address for correspondence: Suzanne P. McEvoy, Metropolitan Communicable Disease Control, 3/311 Wellington St, Perth, Western Australia, Australia; email: suzanne.mcevoy@health.wa.gov.au

Estimated Costs of 4-Month Pulmonary Tuberculosis Treatment Regimen, United States

Carla A. Winston, Suzanne M. Marks, Wendy Carr

We estimated direct costs of a 4-month or 6-month regimen for drug-susceptible pulmonary tuberculosis treatment in the United States. Costs were $23,000 per person treated. Actual treatment costs will vary depending on examination and medication charges, as well as expenses associated with directly observed therapy.

In 2022, the Centers for Disease Control and Prevention (CDC) published recommendations for a 4-month tuberculosis (TB) treatment option using rifapentine and moxifloxacin for persons ≥12 years of age with drug-susceptible pulmonary TB (*1*,*2*). By using published data sources for US healthcare costs for TB, we estimated costs per person treated with the 4-month treatment regimen and a standard 6-month regimen (*3*).

TB treatment consists of an intensive phase for bactericidal and sterilizing activity, followed by a continuation phase to ensure sterilization. Compared with a standard 6-month regimen, the 4-month regimen replaces rifampin and ethambutol in the 8-week daily intensive phase with high-dose rifapentine and moxifloxacin. The 4-month regimen continuation phase of 9 weeks of daily rifapentine, isoniazid, and moxifloxacin compares with a continuation phase of 18 weeks of daily rifampin and isoniazid for the 6-month regimen. For both regimens, recommendations are to administer treatment under directly observed therapy (DOT) for 5 of 7 weekly doses throughout treatment (*1*,*3*).

The Study

We estimated direct healthcare costs to treat 1 person with drug-susceptible TB (Table). Direct healthcare costs include inpatient and outpatient costs associated with diagnosis and treatment and exclude societal costs such as the value of lost patient productivity. All costs for this analysis were based on published unit cost data and updated to 2021 dollars by using Bureau of Economic Analysis Personal Consumption Expenditures indices for hospital and outpatient services (*4*). Overall, TB outcomes and adverse events were similar in the clinical trial of the 4-month regimen compared with the 6-month regimen (*2*); therefore, we assumed the percentage of persons hospitalized at any point during TB diagnosis and treatment was equivalent across regimens. We assumed hospitalization costs of persons with TB on both regimens to be equivalent at $17,432 in 2021 dollars, reflecting an estimated 49% of persons with TB hospitalized at $1,482 per day for an average 24 days and including 20% for physician costs, on the basis of previous publications (*5*–*7*). We added outpatient TB disease costs, including examination costs, clinic supplies, medication costs, and DOT costs, to drug-susceptible TB inpatient costs. We used medication costs based on US Department of Veterans Affairs acquisition costs (*8*) for maximum adult doses (isoniazid 300 mg, $0.19/dose; rifampin 600 mg, $2.45/dose; rifapentine 1,200 mg, $14.44/dose; pyrazinamide 2,000 mg, $17.88/dose; ethambutol 1,600 mg, $1.13/dose; moxifloxacin 400 mg, $2.35/dose) and applied them to 7-day-per-week dosing. DOT costs assumed clinical follow-up and personnel costs at $24/visit updated to $28/visit in 2021 dollars, on the basis of in-person observation 5 days per week (*6*).

We estimated examination costs by using Centers for Medicare and Medicaid Services average allowable charges for laboratory (*9*) and physician services (*10*). Baseline examination costs before initiating therapy, regardless of regimen, assumed 3 sputum smears for acid-fast bacilli at $5.39 per smear and 3 cultures for *Mycobacterium tuberculosis* at $10.80 per culture, 1 phenotypic drug-susceptibility test panel to include at least each drug in the regimen at $7.31 per drug, 1 rapid molecular drug-resistance detection panel to

Author affiliation: Centers for Disease Control and Prevention, Atlanta, Georgia, USA

DOI: https://doi.org/10.3201/eid2910.230314

Table. Input characteristics and direct treatment costs estimated for pulmonary drug-susceptible TB treatment, United States*

Characteristic	4-month regimen		6-month regimen	
	Intensive phase	Continuation phase	Intensive phase	Continuation phase
Time (doses)	8 wks (56 doses)	9 wks (63 doses)	8 wks (56 doses)	18 wks (126 doses)
Anti-TB medications	Isoniazid 300 mg, rifapentine 1,200 mg, pyrazinamide 2,000 mg, moxifloxacin 400 mg	Isoniazid 300 mg, rifapentine 1,200 mg, moxifloxacin 400 mg	Isoniazid 300 mg, rifampin 600 mg, pyrazinamide 2,000 mg, ethambutol 1,600 mg	Isoniazid 300 mg, rifampin 600 mg
No. daily pills†	15	11	12	4
No. DOT clinic visits‡	40	45	40	90
Costs§				
Examination	370		402	
Clinic supply	74		80	
Medication	3,023		1,546	
DOT	2,354		3,600	
Subtotal outpatient costs	5,820		5,628	
Subtotal inpatient costs¶	17,432		17,432	
Total estimated direct treatment costs	23,252		23,060	

*DOT, directly observed therapy; TB, tuberculosis.
†Pill count assumed anti-TB medications plus 1 daily pyridoxine (vitamin B6) tablet for persons taking isoniazid.
‡DOT administered 5 of 7 weekly doses throughout treatment.
§In 2021 US dollars.
¶Inpatient costs assumed equivalent across regimens because TB outcomes and adverse events were similar according to clinical trial data.

include at least each drug in the regimen at $41.68 per drug, 1 two-view chest radiograph at $34.20, 1 complete blood count at $7.77, 1 comprehensive metabolic panel at $10.56, and 1 liver function test at $8.17. We assumed smears and cultures were repeated monthly throughout treatment and yielded $16/month in additional laboratory costs.

Conclusions

In the absence of data from programmatic use of the 4-month regimen, estimated total direct costs of the 4-month and 6-month regimens in the United States based on published sources were similar, at $23,000 per person treated for pulmonary drug-susceptible TB. Hospitalization during diagnosis and treatment accounted for three-quarters of total costs. Because we assumed that hospitalization proportion was equal for the 4-month and 6-month regimens on the basis of adverse events reported during the clinical trial (*2*), inpatient costs were equal between regimens. Cost differences between the regimens were driven by higher drug costs in the 4-month regimen and by higher outpatient costs for length of follow-up and DOT in the 6-month regimen. In terms of drugs, rifapentine costs more per dose than rifampin, but fewer total doses are required for the 4-month regimen. Lower rifapentine prices would decrease costs associated with the 4-month regimen. The longer treatment regimen results in additional clinical follow-up assumptions, including 2 additional smears and 2 additional cultures, and greater DOT costs compared with the shorter regimen. However, some TB programs limit DOT in the continuation phase (e.g., 3 times/week) of the 6-month regimen, or may opt to use video DOT, which costs less than in-person DOT, for either the 4-month or 6-month regimen (*3*,*11*,*12*). Although we estimated molecular drug-susceptibility testing for moxifloxacin in this analysis as having equivalent cost to other drug-susceptibility tests, it might not yet be widely available in first-line testing because fluoroquinolones have historically been used primarily for drug-resistant TB treatment (*3*). Susceptibility testing for moxifloxacin as a first-line drug could result in start-up costs, changes in workflow, or a need for clinical validation if tests are not already in use by or accessible to local programs. CDC's Molecular Detection of Drug Resistance service offers sequencing at no charge to US public health laboratories to enhance early detection of mutations (*13*).

Societal costs attributable to lost patient productivity are likely to be higher for the 6-month versus the 4-month regimen as a function of longer healthcare engagement. Because this analysis focused on healthcare system costs, we did not include patient or larger societal costs such as costs associated with premature death or sequelae from TB. Adverse event reporting and death while receiving treatment during the clinical trial was statistically equivalent between the 4-month and 6-month regimens, with no signals of higher likelihood of relapse with the shorter regimen (*2*). On the basis of the trial data, we therefore could expect societal costs from premature death to be similar across regimens, thus providing no differentiation between regimens; however, post-TB disease or death was not assessed. Prior analyses, updated to 2021 dollars, assumed $29.55 for patient time for travel to and from the clinic and $3.64/dose for doses administered under in-person DOT and an additional $2.45 value per daily

dose of patient time in physically ingesting medication (*6*). Including patient costs for in-person DOT would yield ≈$1,500 ($1,456) greater costs for the 6-month regimen compared with the shorter regimen. Video DOT might mitigate patient costs (*11*,*12*).

Treatment shortening that has similar success and safety in producing favorable TB outcomes has potential advantages from the healthcare perspective and may be appealing to persons with TB if it reduces healthcare engagement. Actual treatment costs will vary across different settings (*14*) depending on examination and medication charges and the method of DOT for treatment support. Because of the limits of the data available to us, which are published list prices for unit costs, we were unable to estimate uncertainty around cost estimates for components of TB care. We encourage TB programs and researchers to report primary data collection on healthcare system costs and costs experienced by persons with TB to provide better data for costs for the new 4-month regimen in diverse real-world settings.

About the Author

Dr. Winston is associate director for science at CDC's National Center for HIV, Viral Hepatitis, STD, and Tuberculosis Prevention, Division of Tuberculosis Elimination. Her primary research interests are clinical and programmatic interventions to prevent and treat infectious diseases.

References

1. Carr W, Kurbatova E, Starks A, Goswami N, Allen L, Winston C. Interim guidance: 4-month rifapentine-moxifloxacin regimen for the treatment of drug-susceptible pulmonary tuberculosis—United States, 2022. MMWR Morb Mortal Wkly Rep. 2022;71:285–9. https://doi.org/10.15585/mmwr.mm7108a1
2. Dorman SE, Nahid P, Kurbatova EV, Phillips PPJ, Bryant K, Dooley KE, et al.; AIDS Clinical Trials Group; Tuberculosis Trials Consortium. Four-month rifapentine regimens with or without moxifloxacin for tuberculosis. N Engl J Med. 2021;384:1705–18. https://doi.org/10.1056/NEJMoa2033400
3. Nahid P, Dorman SE, Alipanah N, Barry PM, Brozek JL, Cattamanchi A, et al. Executive summary: official American Thoracic Society/Centers for Disease Control and Prevention/Infectious Diseases Society of America clinical practice guidelines: treatment of drug-susceptible tuberculosis. Clin Infect Dis. 2016;63:853–67. https://doi.org/10.1093/cid/ciw566
4. US Bureau of Economic Analysis. Price indexes for Personal Consumption Expenditures (PCE) for hospital and outpatient healthcare services, Table 2.4.4 [cited 2023 Feb 17]. https://apps.bea.gov/iTable/?reqid=19&step=2&isuri=1&categories=survey#eyJhcHBpZCI6MTksInN0ZXBzIjpbMSwyLDNdLCJkYXRhIjpbWyJjYXRlZ29yaWVzIiwiU3VydmV5Il0sWyJOSVBBX1RhYmxlX0xpc3QiLCI2OSJdXX0=
5. Aslam MV, Owusu-Edusei K, Marks SM, Asay GRB, Miramontes R, Kolasa M, et al. Number and cost of hospitalizations with principal and secondary diagnoses of tuberculosis, United States. Int J Tuberc Lung Dis. 2018;22:1495–504. https://doi.org/10.5588/ijtld.18.0260
6. Shepardson D, Marks SM, Chesson H, Kerrigan A, Holland DP, Scott N, et al. Cost-effectiveness of a 12-dose regimen for treating latent tuberculous infection in the United States. Int J Tuberc Lung Dis. 2013;17:1531–7. https://doi.org/10.5588/ijtld.13.0423
7. Taylor Z, Marks SM, Ríos Burrows NM, Weis SE, Stricof RL, Miller B. Causes and costs of hospitalization of tuberculosis patients in the United States. Int J Tuberc Lung Dis. 2000;4:931–9.
8. US Department of Veterans Affairs. Office of Procurement, Acquisition and Logistics. National Acquisition Center [cited 2023 Feb 17]. https://www.va.gov/opal/about/nac.asp
9. US Centers for Medicare and Medicaid Services. 2021 laboratory fee schedule [cited 2023 Feb 17]. https://www.cms.gov/Medicare/Medicare-Fee-for-Service-Payment/ClinicalLabFeeSched/Clinical-Laboratory-Fee-Schedule-Files
10. US Centers for Medicare and Medicaid Services. 2021 physician fee schedule [cited 2023 Feb 17]. https://www.cms.gov/medicare/physician-fee-schedule/search/license-agreement?destination=/medicare/physician-fee-schedule/search%3F
11. Beeler Asay GR, Lam CK, Stewart B, Mangan JM, Romo L, Marks SM, et al. Cost of tuberculosis therapy directly observed on video for health departments and patients in New York City; San Francisco, California; and Rhode Island (2017–2018). Am J Public Health. 2020;110:1696–703. https://doi.org/10.2105/AJPH.2020.305877
12. Mangan JM, Woodruff RS, Winston CA, Nabity SA, Haddad MB, Dixon MG, et al. Recommendations for use of video directly observed therapy during tuberculosis treatment—United States, 2023. MMWR Morb Mortal Wkly Rep. 2023;72:313–6. https://doi.org/10.15585/mmwr.mm7212a4
13. US Centers for Disease Control and Prevention. Molecular detection of drug resistance [cited 2023 Feb 17]. https://www.cdc.gov/tb/topic/laboratory/default.htm
14. Campbell JR, Nsengiyumva P, Chiang LY, Jamieson F, Khadawardi H, Mah HK, et al. Costs of tuberculosis at 3 treatment centers, Canada, 2010–2016. Emerg Infect Dis. 2022;28:1814–23. https://doi.org/10.3201/eid2809.220092

Address for correspondence: Carla Winston; Centers for Disease Control and Prevention, 1600 Clifton Rd NE, Mailstop H24-4, Atlanta, GA 30329-4027, USA; email: ctw3@cdc.gov

Human Tularemia Epididymo-Orchitis Caused by *Francisella tularensis* Subspecies *holartica*, Austria

Maximilian Seles, Julia Altziebler, Gregor Gorkiewicz, Lisa Kriegl, Stefan Hatzl
Sascha Ahyai, Romana Klasinc, Ines Zollner-Schwetz, Robert Krause

A previously healthy man in Austria had tularemia epididymo-orchitis develop, leading to unilateral orchiectomy. *Francisella tularensis* subspecies *holartica* was detected by 16S rRNA gene sequencing analysis of inflamed granulomatous testicular tissue. Clinicians should suspect *F. tularensis* as a rare etiologic microorganism in epididymo-orchitis patients with relevant risk factors.

Tularemia is a highly pathogenic zoonosis caused by the gram-negative intracellular bacterium *Francisella tularensis* (*1*). *F. tularensis* subspecies *tularensis* (type A) and *holarctica* (type B) are the main causative agents for tularemia in humans and animals; type B is present in Europe and Asia (*2*). Humans are infected through bites of arthropods (including ticks that are the primary vector of tularemia), as well as by inhaling infectious aerosols, handling infected animals, or ingesting contaminated water or food (*3*). Tularemia cases caused by inadvertent exposure among laboratory personnel have also been reported (*4*).

Clinical manifestations of tularemia in humans might result in ulceroglandular, oculoglandular, glandular, oropharyngeal, pulmonary, or typhoidal forms of disease. We report a case of tularemia epididymo-orchitis in a healthy man that led to unilateral orchiectomy.

The Study

In July 2022, a previously healthy 69-year-old man (nature filmmaker) came to an outpatient clinic in Austria because of fever (temperature up to 39°C), chills, malaise, headache, and lower abdominal pain after traveling to southern Slovenia, Cres island (Croatia), and northern Styria (Austria) 1 month earlier. The patient reported several tick bites but no further animal contact. Clinical examination showed a small ulcerative lesion on the lower left back, which was initially suspected to be an infected insect bite.

Laboratory tests showed leukocytosis (13.6×10^9 cells/L), increased C-reactive protein (CRP) of 85 mg/L, a serum creatinine level of 1.17 mg/mL, and an estimated low glomerular filtration rate of 63 mL/min/1.73m^2. The patient was admitted and initially given amoxicillin/clavulanic acid, which was subsequently changed to piperacillin/tazobactam plus moxifloxacin 3 days later because of persistent fever and sudden testicular swelling and pain, as well as an increased CRP level (357 mg/L) and leukocyte count (22.5×10^9 cells/L).

Computed tomography of the thorax, abdomen, and pelvis showed bilateral epididymo-orchitis and an enlarged right testicle with hyperperfusion and nonperfused areas and a hypoperfused left testicle (Figure 1). In addition, a pulmonary infiltration (diameter 5 mm) in the left lower lobe and diverticulitis were detected. Results of blood and urine cultures were negative. Urine antigen test results for *Legionella* sp. and pneumococci showed negative results. Antibodies specific for *Brucella* spp., *Leptospira* spp., and HIV were not detected.

The patient was transferred to the Medical University of Graz, where piperacillin/tazobactam was continued and moxifloxacin stopped. During the next few days, sonographic examinations showed an enlarged and inhomogenous and hyperperfused right testicle with clinical epididymitis but decreasing CRP

Author affiliations: Medical University of Graz, Graz, Austria (M. Seles, J. Altziebler, G. Gorkiewicz, L. Kriegl, S. Hatzl, S. Ahyai, I. Zollner-Schwetz, R. Krause); Medical University of Vienna, Vienna, Austria (R. Klasinc)

DOI: https://doi.org/10.3201/eid2910.230436

Figure 1. Computed tomography of patient who had human tularemia epididymo-orchitis caused by *Francisella tularensis* subspecies *holartica*, Austria. Coronal image shows the right testicle (arrow) during the arterial phase with hyperperfusion and nonperfused areas (abscess).

levels. Persistent pain and progressive inflammation observed by testicular ultrasound, including suspected abscess, led to unilateral orchiectomy (right testicle) 14 days after admission. Intraoperatively, the testicle and the spermatic cord showed massive inflammation. The orchiectomy was performed without any complications.

The leukocyte count returned to the reference range, and the CRP level decreased to 68 mg/L after surgery. Histopathologic examination showed a chronic granulomatous epididymo-orchitis with abundant suppurative granulomas located between destroyed seminiferous tubules in addition to diffuse mixed interstitial inflammatory infiltrate (Figure 2). PCRs results for *Mycobacterium tuberculosis* complex and atypical mycobacteria were negative. A 16S rRNA gene sequencing analysis of testicular tissue using an IonTorrent Platform (https://www.thermofisher.com) showed abundant bacterial DNA with 100% homology for *F. tularensis* subspecies *holartica* (78% of generated reads) (*1*).

Subsequently, a commercially available ELISA (Virion/Serion, https://www.virion-serion.de) detected IgM and IgG for a panel of human pathogens in serum or plasma (cutoff value >15 units/mL for IgG and IgM) and indicated the presence of *F. tularensis* lipopolysaccharide. *F. tularensis* antibody levels were 136 units/mL for IgG and >400 units/mL for IgM. The patient received doxycycline plus moxifloxacin for 2 months. At a 6-month follow-up, the patient had no additional complaints.

Conclusions

In Austria, antibodies against *F. tularensis* are found in 0.5% of healthy adults (*5*), and annual cases range between 0 and 58 (*2*,*6*). In clinically apparent infections, the most frequent manifestations of human tularemia are ulceroglandular or glandular forms. The oculoglandular, oropharyngeal, or pulmonary forms have been less frequently reported (*2*). In the case we report, the patient did not report any direct animal contact or use of unprocessed water or food during his nature filming activities. However, initial examination showed a small ulcerative lesion on the lower left back, which presumably was the initial tularemia skin lesion.

Worldwide, tularemia orchitis has been reported in hares (including 1 case with epididymo-orchitis) (*7*,*8*), a squirrel (*9*), and a marmoset (*10*). Infectious human epididymo-orchitis is usually caused by *Neisseria gonorrhoeae*, *Chlamydia trachomatis*, *Ureaplasma* spp., *Mycoplasma genitalium*, *Escherichia coli*, *Pseudomonas aeruginosa*, and other gram-negative bacteria,

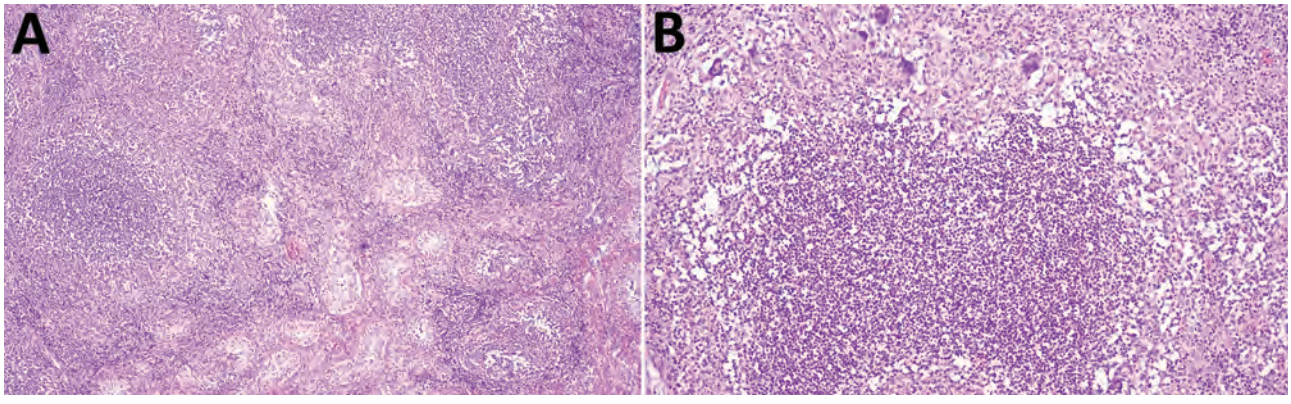

Figure 2. Granulomatous epididymo-orchitis in patient who had human tularemia epididymo-orchitis caused by *Francisella tularensis* subspecies *holartica*, Austria. A) Diffuse chronic granulomatous inflammation in the interstitium and between the seminiferous tubule. Hematoxylin and eosin stain; original magnification ×20. B) Suppurative granuloma with epithelioid cells and single giant cells in testicular tissue. Hematoxylin and eosin stain; original magnification ×100.

as well as *Staphylococcus aureus* in elderly persons. Granulomatous epididymo-orchitis is rare and usually caused by *Mycobacterium tuberculosis* or *Brucella* spp. Other rare etiologic agents include fungi, *Shistosoma* spp., or *Orientia tsutsugamushi* (*11*–*13*). *F. tularensis* has not been previously reported as a causative microorganism for epididymo-orchitis.

Patients who have epididymo-orchitis typically have acute onset unilateral scrotal pain, swelling, and erythema, and treatment with ceftriaxone combined with doxycycline or levofloxacin is recommended (*13*). Tularemia is treated with fluorochinolones, doxycycline, or aminoglycosides depending on disease severity. Our patient empirically received piperacillin/tazobactam with moxifloxacin, but moxifloxacin was discontinued after 3 days. During piperacillin/tazobactam monotherapy, CRP levels decreased, but sonography and clinical status worsened, leading to unilateral orchiectomy. We assume that the empirical application of moxifloxacin for 3 days lowered systemic inflammatory parameters but was too short for improvement of the testicular infection. Ultimately, the etiology of epididymo-orchitis could be elucidated by 16S rRNA gene sequencing analysis, which in this case led to successful directed therapy with doxycycline and moxifloxacin. Because of impaired renal function, aminoglycosides were not considered. Furthermore, serologic analysis confirmed this unusual case of tularemia.

The specific source of tularemia in this case remains unknown because *F. tularensis* subsp. *holartica* was prevalent in all countries visited by the patient before his infection (tularemia cases are reported from Austria and Slovenia and, rarely, from Croatia) (*14*). Nevertheless, our findings indicates that, in patients suspected of having tularemia by medical history (e.g., arthropod bites, animal contact) or clinical examination (e.g., ulcer, rash, lymphadenopathy), clinicians should consider *F. tularensis* as a rare etiologic microorganism in epididymo-orchitis.

About the Author

Dr. Seles is a urologic surgeon at the Medical University of Graz, Graz, Austria. His primary research interests are renal and penile cancer, endometriosis, and rare diseases.

References

1. Kim DY, Reilly TJ, Schommer SK, Spagnoli ST. Rabbit tularemia and hepatic coccidiosis in wild rabbit. Emerg Infect Dis. 2010;16:2016–7. https://doi.org/10.3201/eid1612.101013
2. Seiwald S, Simeon A, Hofer E, Weiss G, Bellmann-Weiler R. Tularemia goes west: epidemiology of an emerging infection in Austria. Microorganisms. 2020;8:1–13. https://doi.org/10.3390/microorganisms8101597
3. Maurin M, Gyuranecz M. Tularaemia: clinical aspects in Europe. Lancet Infect Dis. 2016;16:113–24. https://doi.org/10.1016/S1473-3099(15)00355-2
4. Boodman C, Richert Q, Lother S, Kasper K, Fanella S, Lagacé-Wiens P, et al. Inguinal ulceroglandular tularemia caused by *Francisella tularensis* subspecies *holarctica,* Canada. Emerg Infect Dis. 2021;27:1228–9. https://doi.org/10.3201/eid2704.203262
5. Tobudic S, Nedomansky K, Poeppl W, Müller M, Faas A, Mooseder G, et al. Seroprevalence for *Coxiella burnetii*, *Francisella tularensis*, *Brucella abortus* and *Brucella melitensis* in Austrian adults: a cross-sectional survey among military personnel and civilians. Ticks Tick Borne Dis. 2014;5:315–7. https://doi.org/10.1016/j.ttbdis.2013.12.007
6. Federal Ministry, Republic of Austria. Social Affairs, Health, Care and Consumer Protection. Annual report on notifiable diseases 2021 [in German] [cited 2023 Jul 24]. https://www.sozialministerium.at/dam/jcr:789e0910-5bad-45ca-a42d-bc07c533fa5a/Surveillance%202021_Jahresstatistik.pdf
7. Origgi FC, Pilo P. *Francisella tularensis* clades B.FTN002-00 and B.13 are associated with distinct pathology in the European brown hare (*Lepus europaeus*). Vet Pathol. 2016;53:1220–32. https://doi.org/10.1177/0300985816629718
8. Gregoire F, Cassart D, Desmecht DJ, Madani N, Linden A. Meningitis and orchitis in a hare (*Lepus europaeus*) infected with *Francisella tularensis*. Vet Rec Case Rep. 2016;4. https://doi.org/10.1136/vetreccr-2016-000306
9. Nelson DD, Haldorson GJ, Stanton JB, Noh SM, Bradway DS, Mansfield KG, et al. *Francisella tularensis* infection without lesions in gray tree squirrels (*Sciurus griseus*): a diagnostic challenge. J Vet Diagn Invest. 2014;26:312–5. https://doi.org/10.1177/1040638713520541
10. Splettstoesser WD, Mätz-Rensing K, Seibold E, Tomaso H, Al Dahouk S, Grunow R, et al. Re-emergence of *Francisella tularensis* in Germany: fatal tularaemia in a colony of semi-free-living marmosets (*Callithrix jacchus*). Epidemiol Infect. 2007;135:1256–65. https://doi.org/10.1017/S0950268807008035
11. Chirwa M, Davies O, Castelino S, Mpenge M, Nyatsanza F, Sethi G, et al. United Kingdom British association for sexual health and HIV national guideline for the management of epididymo-orchitis, 2020. Int J STD AIDS. 2021;32:884–95. https://doi.org/10.1177/09564624211003761
12. Saha A, Sarkar S, Patil A, Besra B, Saha C. Epididymo-orchitis in scrub typhus. Indian J Pediatr. 2018;85:1035–6. https://doi.org/10.1007/s12098-018-2682-4
13. Workowski KA, Bachmann LH, Chan PA, Johnston CM, Muzny CA, Park I, et al. Sexually transmitted infections treatment guidelines, 2021. MMWR Recomm Rep. 2021;70:1–187. https://doi.org/10.15585/mmwr.rr7004a1
14. European Food Safety Authority; European Centre for Disease Prevention and Control. The European Union One Health 2021 Zoonoses Report. EFSA J. 2022;20:e07666.

Address for correspondence: Robert Krause, Medical University of Graz, Auenbruggerplatz 15, A-8036 Graz, Austria; email: robert.krause@medunigraz.at

Listeria monocytogenes Transmission from Donated Blood to Platelet Transfusion Recipient, Italy

Maria Gori, Luca Bolzoni, Erika Scaltriti, Lilia Andriani, Vito Marano, Francesca Morabito, Clara Fappani, Danilo Cereda, Enza Giompapa, Rosa Chianese, Paola Lanzini, Livia Antonietta Martinelli, Silvia Bianchi, Antonella Amendola, Stefano Pongolini, Elisabetta Tanzi

We report *Listeria monocytogenes* infection in a patient in Italy who was transfused with pooled platelet concentrate. Genomic analysis revealed that *L. monocytogenes* isolates from the donor blood unit, the transfused platelets, and the patient's blood culture were genetically closely related, confirming transfusion transmission. Additional surveillance and secondary bacterial screening could improve transfusion safety.

Listeria monocytogenes is a gram-positive, primarily foodborne pathogen responsible for severe invasive infections (*1*), especially in immunocompromised patients. The treatment for some immunodeficiency conditions can require the administration of blood products, which pose additional risks for patients' health, although not generally connected with *L. monocytogenes* bacteremia. One case of transfusion-transmitted *L. monocytogenes* infection has been reported in the literature (*2*). Conversely, 2 case reports describe platelet products contaminated by *L. monocytogenes*, but the contamination was intercepted before transfusion (*3*,*4*). We describe a case of transfusion-related *L. monocytogenes* infection in a patient who received a pooled-platelet concentrate.

Author affiliations: Università degli Studi di Milano, Milan, Italy (M. Gori, C. Fappani, S. Bianchi, A. Amendola, E. Tanzi); Istituto Zooprofilattico Sperimentale della Lombardia e dell'Emilia-Romagna (IZSLER), Parma, Italy (L. Bolzoni, E. Scaltriti, S. Pongolini); Azienda Socio Sanitaria Territoriale della Valtellina e dell'Alto Lario, Sondrio, Italy (L. Adriani, V. Marano, F. Morabito, P. Lanzini); Directorate General for Health, Lombardy Region, Milan (D. Cereda); Agenzia di Tutela della Salute della Montagna, Sondrio (E. Giompapa, L.A. Martinelli); Agenzia Regionale Emergenza Urgenza, Milan (R. Chianese); Azienda Socio Sanitaria Territoriale dei Sette Laghi, Varese, Italy (R. Chianese)

DOI: https://doi.org/10.3201/eid2910.230746

The Study

On June 13, 2022, a 78-year-old woman was admitted to an emergency department in the Lombardy Region of northern Italy, reporting persistent fever, nausea, and vomiting. According to her medical history, she had gastric adenocarcinoma and had undergone total gastrectomy with splenectomy on February 15, 2021, and postoperative anemia was subsequently observed. In September 2021, she experienced cancer progression in the liver and, beginning in March 2022, she underwent chemotherapy with trifluridine/tipiracil.

At the time of her emergency admission, hematological tests revealed a severe pancytopenia, likely due to chemotherapy. Her hemoglobin level was 8 g/dL (reference range 12–16 g/dL), platelet count was 27,000/μL (reference range 150,000–450,000/μL), procalcitonin was 1.51 ng/mL (reference range 0.00–0.50 ng/mL), prothrombin time was 1.33 (reference range 0.80–1.20), activated partial thromboplastin time was 0.66 (reference range 0.80–1.20), and C-reactive protein was 318.7 mg/L (reference range 0.0–5.0 mg/L). Clinicians administered granulocyte growth factor therapy, transfusion treatment with concentrated red blood cells, and empirical antibiotic therapy with piperacillin-tazobactam. Blood cultures incubated in the BD BACTEC FX system (Becton Dickinson, https://www.bd.com) showed no growth.

On June 14, 2022, the patient underwent a transfusion of buffy coat–pooled platelet derived from 5 different donors. After transfusion of ≈150 mL of platelet products, the woman experienced chills,

nausea, and fever of 37.8°C. Treatment was stopped and hydrocortisone was administered, based on the diagnosis of transfusion reaction. The adverse reaction was reported to the Italian National Blood Centre on June 20, 2022. Antibiotic therapy was boosted with meropenem. A second blood culture yielded positive results 25 hours after collection, and *L. monocytogenes* was identified by matrix-assisted laser desorption/ionization time-of-flight mass spectrometry (Bruker Daltonics, https://www.bruker.com).

The isolate was susceptible to ampicillin, erythromycin, meropenem, penicillin, and trimethoprim/sulfamethoxazole. In response to this finding, on June 15, 2022, antibiotic therapy was adjusted to ampicillin/sulbactam and gentamicin and was continued for 21 days. Within 24 hours of adjusting antimicrobial drug therapy, the patient was afebrile. Because no additional complications were reported during hospitalization, the patient was discharged on July 5, 2022, hemodynamically stable. The woman died of progressive cancer on October 22, 2022.

We tested each of the 5 donated platelet units for bacterial contamination by using the BacT/ALERT 3D system (bioMérieux, https://www.biomerieux.com). We detected contamination in a single-donor unit, which we subsequently cultured and found positive for *L. monocytogenes*. The other blood component units obtained from the same unit (donated on June 9, 2022) were destroyed, and no other patients were transfused from them. The donor was recalled on June 16, 2022, but, because of quarantine for COVID-19, did not arrive at the transfusion center until June 28, 2022. The donor was investigated for possible risk factors related to the bacterial infection, such as consumption of contaminated food (none were identified) and confirmed the absence of gastrointestinal or febrile symptoms at the time of donation. Despite consideration of the time elapsed since donation, blood was drawn for cultures; results were negative.

The *L. monocytogenes* isolates recovered from the buffy coat platelet concentrate, the transfused patient's blood cultures, and the single-donor unit were sent to the regional reference laboratory (RRL) of Lombardy Region, Italy. On the basis of Ministry of Health provisions, RRLs in Italy perform whole-genome sequencing (WGS) to characterize *L. monocytogenes* isolates (*5*). We extracted genomic DNA by using the Maxwell HT 96 gDNA Blood Isolation System (Promega, http://www.promega.com) and conducted WGS on the Nextseq 550 system (Illumina, http://www.illumina.com). We performed in silico sequence type (ST) and PCR serogroup detection by using Institut Pasteur's BIGSdb-*Lm* (*6*), which revealed that the 3 isolates belonged to ST1 and PCR serogroup 4b. We performed comparative genomics to analyze allele distances in core-genome multilocus sequence typing (cgMLST) by using Pasteur's cgMLST allelic scheme (*6*) and analyzed SNPs by using the CFSAN SNP Pipeline version 2.1.1 (*7*). We observed neither allelic nor SNP differences. Four other ST1 clinical strains isolated in Lombardy Region in 2022 showed distances of 0–1 allele in cgMLST and 0–2 SNPs differences to the isolates involved in the transfusion-associated case. We used the strain originated from the donated blood unit (BioSample no. ERS15898914) as a reference for SNP analysis. The size of the core alignment between all 7 genomes was 2,930,365 bp, 98.7% of the reference strain's length. Trace-back investigation revealed that no other patients from the 2022 Lombardy outbreak had a history of blood transfusion. Moreover, epidemiologic investigation forms of the infected patients did not identify any food products as a common source of infection.

Conclusions

Current guidelines in transfusion medicine in Italy recommend testing for hepatitis B and C viruses, HIV, and serologic markers of *Treponema pallidum*. Mandatory tests do not consider bacterial contamination (*8*). Although both gram-positive and gram-negative organisms have reportedly caused transfusion-associated sepsis (*9*), the use of pathogen-reduction technology is not mandatory and was not applied on the platelets transfused to our patient.

Contamination of blood products commonly occurs because of introduction of skin microbiota at the phlebotomy site or donations by asymptomatic donors with transient bacteremia (*9*,*10*). The environment also can be a source of contamination, particularly when bag containers are breached during transfusion product processing, transport, or storage (*11*). Bacterial contamination is a higher risk in platelet products because platelets must be stored at room temperature to maintain viability and function, which could facilitate the growth of a wide spectrum of bacteria. Approximately 1 of every 1,000–3,000 platelet units are estimated be contaminated with bacteria (*12*–*14*).

In the case we described, bloodborne transmission was strongly supported by WGS-based typing, which confirmed that the *L. monocytogenes* isolates recovered from the transfused patient's blood cultures, the platelet concentrate, and the blood donor's platelet unit were genetically closely related. Although the source of the contamination was unclear, one explanation could be

environmental contamination of the donated blood unit. Several cases of contamination of transfusion products by environmental bacteria have been described (*12*). *L. monocytogenes* is widespread in the environment and could have entered the blood unit via undetected defects or damages in the storage container. Another explanation could be a transient bacteremia experienced by the donor who was asymptomatic at the time of donation, such as in a previously described case (*2*). Questionnaires administered to assess blood donors' health and medical history are not useful to identify *L. monocytogenes* infection because healthy persons will generally be asymptomatic. Indeed, persons with transient asymptomatic bacteremia, or who are in the recovery phase of an infection, still can qualify as blood donors.

In conclusion, bacterial contamination of donated blood and blood components still represents a major public health issue globally. This case highlights the need to improve safety in transfusion medicine by implementing surveillance activities and additional measures, such as secondary testing and pathogen-reduction technology.

Acknowledgments

We thank Elena Briozzo, Elisa Meroni, Serena Giulia Domenighini, Daniela Colzani, Francesca Antoniazzi, Alessandro Stefano Bertolini, and the laboratory staff of Clinical Pathology and Microbiology Unit Azienda Socio Sanitaria Territoriale Valtellina Alto Lario for their assistance in this investigation. We also thank Mirella Pontello for suggestions that helped us improve the quality of the paper.

The planning, conduction, and reporting of this study was in line with the Declaration of Helsinki, as revised in 2013. Ethical review and approval and patient consent were waived for this study because it was carried out as part of listeriosis surveillance performed by law in accordance with the Ministry of Health's Decree of March 7, 2022 (*8*).

Raw reads of the sequenced *Listeria monocytogenes* ST1 isolates of this study were deposited in the publicly available European Nucleotide Archive (https://www.ebi.ac.uk/ena) under project no. PRJEB62146, including transfused patient's blood cultures (BioSample no. ERS15898909), platelet concentrate (no. ERS15898912), donated blood unit (no. ERS15898914), and cluster-related human cases (nos. ERS15933521, ERS15898910, ERS15898911, and ERS15898914).

This research was funded by Ministero della Salute, grant no. IZSLER 12/19 (Ricerca Corrente PRC2019012) and Lombardy Region (DGR XI/3450, 28 July 2020).

Author contributions: M.G. performed laboratory analysis, analyzed the data, and wrote the manuscript. L.B. and E.S. conducted genomic and bioinformatics analysis, analyzed the data, and collaborated in the writing of the manuscript. L.A., V.M., and F.M. acquired and managed clinical data. C.F. and S.B. collaborated in the laboratory analysis and in the interpretation of the results. D.C. coordinated epidemiological surveillance activities. E.G., R.C., P.L., and L.A.M. collaborated in the epidemiological investigation. A.A. critically revised the manuscript. S.P. supervised genomic and bioinformatics analysis and critically revised the manuscript. E.T. supervised epidemiological and molecular investigation and critically revised the manuscript. All the authors reviewed and approved the final manuscript.

About the Author

Dr. Gori is a research fellow in the Department of Health Sciences, Università degli Studi di Milano, Milan, Italy. Her research focuses on the molecular surveillance of infectious diseases with a major impact on public health.

References

1. Koopmans MM, Brouwer MC, Vázquez-Boland JA, van de Beek D. Human listeriosis. Clin Microbiol Rev. 2023;36:e0006019. https://doi.org/10.1128/cmr.00060-19
2. Tolomelli G, Tazzari PL, Paolucci M, Arpinati M, Landini MP, Pagliaro P. Transfusion-related *Listeria monocytogenes* infection in a patient with acute myeloid leukaemia. Blood Transfus. 2014;12:611–4.
3. Guevara RE, Tormey MP, Nguyen DM, Mascola L. *Listeria monocytogenes* in platelets: a case report. Transfusion. 2006;46:305–9. https://doi.org/10.1111/j.1537-2995.2006.00718.x
4. Menon M, Graves L, McCombs K, Hise K, Silk B, Kuehnert M, et al. *Listeria monocytogenes* in donated platelets: a potential transfusion-transmitted pathogen intercepted through screening. Transfusion. 2013;53:1974–8. https://doi.org/10.1111/trf.12097
5. Ministry of Health. General Directorate of Health Prevention circular note on surveillance and prevention of listeriosis (no. 0008252–13/03/2017-DGPRE-DGPRE-P) [in Italian] [cited 2022 Apr 22]. https://www.iss.it/documents/20126/0/Listeriosi+-+Prima+Nota+Circolare+Ministero+della+Salute.pdf/6e18fcf8-b7b4-19ff-d6c3-c849899400aa?t=1582305476785
6. Moura A, Criscuolo A, Pouseele H, Maury MM, Leclercq A, Tarr C, et al. Whole genome-based population biology and epidemiological surveillance of *Listeria monocytogenes*. Nat Microbiol. 2016;2:16185. https://doi.org/10.1038/nmicrobiol.2016.185
7. Davis S, Pettengill JB, Luo Y, Payne J, Shpuntoff A, Rand H, et al. CFSAN SNP Pipeline: an automated method for constructing SNP matrices from next-generation sequence data. PeerJ Comput Sci. 2015;1:e20. https://doi.org/10.7717/peerj-cs.20
8. Ministry of Health. Official gazette of the Italian Republic, decree November 2, 2015. Provisions relating to

the quality and safety requirements of blood and blood components (no. 15A09709). GU general series no. 300; 28 Dec 2015; Supplementary ordinance no. 69 [in Italian] [cited 2022 Apr 22]. https://www.gazzettaufficiale.it/eli/id/2015/12/28/15A09709/sg
9. Allain JP, Bianco C, Blajchman MA, Brecher ME, Busch M, Leiby D, et al. Protecting the blood supply from emerging pathogens: the role of pathogen inactivation. Transfus Med Rev. 2005;19:110–26. https://doi.org/10.1016/j.tmrv.2004.11.005
10. Busch MP, Bloch EM, Kleinman S. Prevention of transfusion-transmitted infections. Blood. 2019;133(17): 1854–64. https://doi.org/10.1182/blood-2018-11-833996
11. Horth RZ, Jones JM, Kim JJ, Lopansri BK, Ilstrup SJ, Fridey J, et al. Fatal sepsis associated with bacterial contamination of platelets—Utah and California, August 2017. MMWR Morb Mortal Wkly Rep. 2018;67:718–22. https://doi.org/10.15585/mmwr.mm6725a4
12. Fadeyi EA, Wagner SJ, Goldberg C, Lu T, Young P, Bringmann PW, et al. Fatal sepsis associated with a storage container leak permitting platelet contamination with environmental bacteria after pathogen reduction. Transfusion. 2021;61:641–8. https://doi.org/10.1111/trf.16210
13. Levy JH, Neal MD, Herman JH. Bacterial contamination of platelets for transfusion: strategies for prevention. Crit Care. 2018;22:271. https://doi.org/10.1186/s13054-018-2212-9
14. Brecher ME, Hay SN. Bacterial contamination of blood components. Clin Microbiol Rev. 2005;18:195–204. https://doi.org/10.1128/CMR.18.1.195-204.2005

Address for correspondence: Elisabetta Tanzi, Università degli Studi di Milano, Via Carlo Pascal 36, 20133, Milan, Italy; email: elisabetta.tanzi@unimi.it

Imported Toxigenic *Corynebacterium Diphtheriae* in Refugees with Polymicrobial Skin Infections, Germany, 2022

Benedikt Daniel Spielberger, Anna Hansel, Alea Nazary, Eva-Maria Kleißle, Claus-Georg Lehr, Marcel Utz, Juliana Hofer, Siegbert Rieg,[1] Winfried V. Kern[1]

During August–December 2022, toxigenic *Corynebacterium diphtheriae* was isolated from 25 refugees with skin infections and 2 refugees with asymptomatic throat colonization at a refugee reception center in Germany. None had systemic toxin-mediated illness. Of erosive/ulcerative skin infections, 96% were polymicrobial. Erosive/ulcerative wounds in refugees should undergo testing to rule out cutaneous diphtheria.

Diphtheria is a potentially lethal upper respiratory tract infection that causes systemic illness associated with toxemia. Cases are mostly caused by toxigenic *Corynebacterium diphtheriae* and, rarely, by *C. ulcerans* through animal-to-human transmission (*1*). Although <500 cases have been detected in Europe during 2010–2019 (*2*), outbreaks have been reported in resource-limited settings (e.g., in refugee camps or in settings of waning immunization coverage) (*3*,*4*). During June–October 2022, a total of 371 diphtheria cases were detected in Europe; most (147 cases) were in Germany. Ongoing cases in 2023 and a fatal case in Belgium in June 2023 reported by the European Centre for Disease Prevention and Control (ECDC) highlight the need for further awareness (https://www.ecdc.europa.eu/en/publications-data/communicable-disease-threats-report-2-8-july-2023-week-27; https://www.ecdc.europa.eu/en/publications-data/communicable-disease-threats-report-30-january-5-february-2023-week-5; https://www.ecdc.europa.eu/en/publications-data/communicable-disease-threats-report-11-17-june-2023-week-24).

Author affiliation: University Medical Centre and Faculty of Medicine Freiburg, Freiburg, Germany

DOI: https://doi.org/10.3201/eid2910.230285

Since 2015, the University Medical Centre Freiburg has run an outpatient clinic at the refugee reception center in Freiburg, which in late 2022 detected an unusually high number of skin infections in refugees. After the initial case of cutaneous *C. diphtheriae* infection was detected, the University Medical Centre consulted with the local health authorities, and subsequent patients with skin wounds or erosive/ulcerative lesions were tested for throat colonization and skin infection with *C. diphtheriae*. Contacts of patients with confirmed cases (roommates, other close contacts) were identified and screened for *C. diphtheriae* skin infection and throat colonization. Our retrospective analysis was approved by the ethics committee of the University Medical Centre Freiburg (22-1493-S1-retro). Anonymized photographs were taken with the verbal consent of the patients.

The Study

In the beginning of the analysis period, we detected *C. diphtheriae* by using Columbia blood agar with fosfomycin plates and, after sufficient production, with tellurite agar. We confirmed isolates as *C. diphtheriae* by using matrix-assisted laser desorption/ionization time-of-flight mass spectrometry and using Bruker MALDI Biotyper (*5*). We detected the diphtheria toxin gene by using a conventional PCR assay (*6*). We sent all isolates for confirmation to the consiliary laboratory at Landesamt für Gesundheit Bayern (LGL Bayern, Oberschleißheim, Germany), where Elek test and multilocus-sequence typing (MLST) were additionally performed for several isolates.

During August 1, 2022, through December 31, 2022, *C. diphtheriae* was detected in 27 refugees. Of

[1]These senior authors contributed equally to this article.

those, 25 had sought care because of nonhealing skin lesions or wounds. Screening of 154 contacts (throat swabs) identified 2 asymptomatic carriers of *C. diphtheriae* without skin lesions. All patients were male, and most were young (mean 24 years, range 18–49 years). Three patients stated that they were minors but were classified as adults by local health authorities. Most patients were born in Afghanistan (15 persons) or Syria (11 persons); 1 refugee reported Morocco as his country of birth. Of the 18 (67%) refugees who were asked about their escape route, all stated that they had fled via Balkan states (Table 1; Appendix Table 1, https://wwwnc.cdc.gov/EID/article/29/10/23-0285-App1.pdf).

Cutaneous lesions persisted for a mean of 22.5 days; ≈70% persisted >14 days, and the overall range was wide, 3–60 days. Available detailed histories of the cause and circumstances of the primary manifestation indicated waterway crossings and forest habitation as the probable infection mode. The lesions were predominantly localized at the extremities: lower thigh (17 [63%]), feet and ankles (11 [41%]), hands (8 [32%]), and upper thigh (2 [7%]). In addition, genital lesions were observed in 2 refugees (7%) (Table 1; Appendix Table 1). Skin wounds appeared as partly punched-out, partly erosive lesions with erythematous margins (Figure panels A, B). Grayish mucous membranes or purulent lesions were detectable in isolated cases only.

Clinical differentiation between skin infections caused by *Staphylococcus aureus*, *Streptococcus pyogenes*, or both (Figure panel C) or wounds with evidence of *C. diphtheriae* was difficult. In addition to *C. diphtheriae*, both *S. aureus* and *S. pyogenes* were detected in 21 (84%) of the 25 refugees. In 3 (12%) refugees, *C. diphtheriae* and *S. pyogenes* were detected; in 1, only *C. diphtheriae* was detected. All 25 skin infections were colonized with toxin-producing *C. diphtheriae* as shown by positive PCR for the *tox* gene or positive Elek test through the consiliary laboratory (Table 2; Appendix Table 1). The 2 cases of *C. diphtheriae* throat colonization were

Table 1. Demographics and clinical manifestations of 27 refugees with imported toxigenic *Corynebacterium diphtheriae* in polymicrobial skin infections, Germany, 2022*

Study population	No. (%)
Mean age at first assessment (range), y	24 (18–49)
Suspected unaccompanied minor refugee	3 (11)
Country of birth	
Afghanistan	15 (56)
Syria	11 (41)
Morocco	1 (4)
Route of escape	
Asked about route	18 (67)
Answered Balkan	18 (100)
Clinical manifstations	
Any skin ulcer	25 (93)
Lower thigh	17 (63)
Knee	3 (11)
Upper thigh	2 (7)
Feet	11 (41)
Hands	8 (30)
Genitals	2 (7)
Patients without skin wounds	2 (7)
And with *C. diphtheriae* in throat swab specimen	2 (100)
Mean duration of wounds (range), d	22.5 (3–60)

*Values are no. (%) except as indicated. All patients were male.

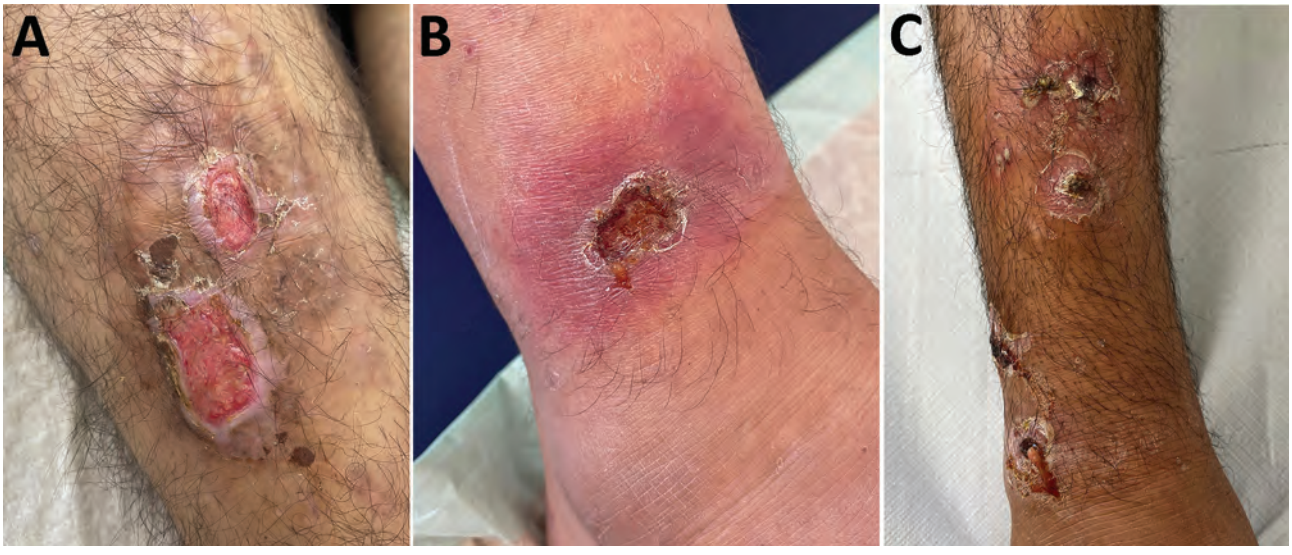

Figure. Clinical manifestations of *Corynebacterium diphtheriae* skin infections in patients at a refugee reception center in Freiburg. Germany, 2022. A) Chronic erosive skin lesions at the ventral lower thigh. Toxigenic *C. diphtheriae*, methicillin-sensitive *Staphylococcus aureus* (MSSA), and *Streptococcus pyogenes* were grown from skin swab samples. B) Ulcerative lesion with erythematous halo just above the right ankle. *C. diphtheriae*, MSSA, and *S. pyogenes* were detected from skin swab samples. C) Ecthymata at the lower leg without detection of *C. diphtheriae* but with growth of MSSA and *S. pyogenes*.

Table 2. Microbiology test results for 27 refugees with imported toxigenic *Corynebacterium diphtheriae* in polymicrobial skin infections, Germany, 2022*

Microbiology result	No. (%)
No. *C. diphtheriae* isolates	27
Any skin wound	25 (93)
Skin wounds with toxigenic *C. diphtheriae*	25
Toxigenic *C. diphtheriae* in skin wound and throat swab	5 (20)
Any throat swab with *C. diphtheriae*	7 (26)
And without skin wounds	2 (29)
Patients without skin wounds	2 (7)
And wth *C. diphtheriae* in throat swab	2 (100)
Contact persons screened	154
Co-colonization of skin infections (% of all skin wounds)	
C. diphtheriae, *Staphylococcus. aureus*, *Streptococcus pyogenes*	21 (84)
C. diphtheriae, *S. pyogenes*, no *S. aureus*	3 (12)
C. diphtheriae, no *S. pyogenes*, no *S. aureus*	1 (4)
Antimicrobial resistance	
Total *S. aureus* isolates	21
MSSA	11 (52)
Community-acquired MRSA	10 (48)
Hospital-acquired MRSA	0
Total no. *S. pyogenes* isolates	24
Resistance to clindamycin	3 (13)

*Values are no. (%) except as indicated. MRSA, methicillin-resistant *S. aureus*; MSSA, methicillin-sensitive *S. aureus*.

nontoxigenic. Among the 21 *S. aureus* isolates, 10 (48%) were methicillin resistant. Of the 24 *S. pyogenes* isolates, 3 (13%) showed resistance to clindamycin (Table 2). According to current European Committee on Antimicrobial Susceptibility Testing (https://www.eucast.org) recommendations, all *C. diphtheriae* isolates showed in vitro susceptibility to penicillin at increased exposure, and all but 2 isolates showed sensitivity to erythromycin or clindamycin (*7*). MLST was available for 16 isolates; sequence types 377 or 574 were identified 6 times, and sequence type 384 was identified 4 times. We established no correlation between country of origin and sequence type.

Detection of toxin-producing *C. diphtheriae* from throat swab samples was successful in 5 (20%) of the 25 patients with cutaneous lesions. No systemic illnesses associated with toxemia were observed in our cohort.

Conclusions

Our report adds details about the clinical picture of cutaneous diphtheria among refugees from Afghanistan, Syria, and Morocco in Germany. In this cohort, 100% of cutaneous infections were caused by toxigenic *C. diphtheriae*, which is a higher proportion than the 27% toxigenic cutaneous infections reported in 270 cases published over the past 65 years (Appendix Table 2). This magnitude indicates a common source of infection or increased risks for transmission while fleeing (*8*,*9*).

Nearly all skin infections in this cohort were polymicrobial, caused by *C. diphtheriae*, *S. aureus*, and *S. pyogenes*. Co-infections with *S. pyogenes* have been reported in the literature for 151 (56%) cases and with *S. aureus* for 110 (41%); methicillin resistance was noted in 19 (7%) cases (Appendix Table 2). Only 1 report indicates a rate of co-pathogens in the magnitude of that found in our cohort (*10*). Similar to a previous report from Germany, the isolates were broadly drug susceptible (*11*); susceptibility to penicillin seemed to be higher than that reported from Spain during 2014–2019 (*12*).

Another finding was that one fifth of the refugees with cutaneous diphtheria were concurrently colonized with toxigenic *C. diphtheriae* in the throat while remaining systemically asymptomatic. Such concurrent throat plus skin colonization may be highly relevant for transmission and should be identified.

Although in their rapid risk assessment the ECDC considered the overall risk for the residing population in refugee-accepting countries to be very low, several steps are crucial for preventing spread and casualties (*13*). Toxin-mediated systemic disease can be effectively prevented by universal immunization against diphtheria toxin. Refugee infants are particularly at risk because of the reported low rates of receiving a third dose of diphtheria-tetanus-pertussis vaccine in Afghanistan (81%) and Syria (48%) (*14*). Furthermore, waning immunity against vaccine-preventable diseases, especially for pertussis and diphtheria, is reported where antibody levels drop to prevaccination levels 5–6 years after vaccination (*15*).

Our report, in conjunction with material from ECDC, could be informative for migrants and healthcare workers with regard to identifying cutaneous diphtheria (*13*). These findings supplement recommendations for contact tracing, screening for throat colonization, and using personal protective equipment when changing dressings or taking swab specimens.

Workers at refugee reception centers should pay attention to chronic erosive/ulcerative wounds in refugees. They should conduct adequate microbiological investigations to rule out cutaneous diphtheria, even if *S. aureus* or *S. pyogenes* have already been identified, and should screen persons, including contact persons, for throat colonization. Booster vaccinations or full immunizations against diphtheria toxin and antimicrobial prophylaxis should be given in accordance with ECDC guidelines in risk settings when cases of diphtheria are suspected (*13*).

Acknowledgments

We thank the local health authorities in Freiburg, Germany, and the consiliary laboratory for diphtheria at LGL Bayern, Oberschleißheim, Germany, for discussing transmission and infection control issues.

About the Author

Dr. Spielberger works in pediatric infectious diseases. He has a strong interest in improving care for refugee minors and is head of the pediatric outpatient clinic at the refugee reception center in Freiburg.

References

1. Sharma NC, Efstratiou A, Mokrousov I, Mutreja A, Das B, Ramamurthy T. Diphtheria. Nat Rev Dis Primers. 2019;5:81. https://doi.org/10.1038/s41572-019-0131-y
2. Muscat M, Gebrie B, Efstratiou A, Datta SS, Daniels D. Diphtheria in the WHO European Region, 2010 to 2019. Euro Surveill. 2022;27:2100058. https://doi.org/10.2807/1560-7917.ES.2022.27.8.2100058
3. Hardy IR, Dittmann S, Sutter RW. Current situation and control strategies for resurgence of diphtheria in newly independent states of the former Soviet Union. Lancet. 1996;347:1739–44. https://doi.org/10.1016/S0140-6736(96)90811-9
4. Polonsky JA, Ivey M, Mazhar MKA, Rahman Z, le Polain de Waroux O, Karo B, et al. Epidemiological, clinical, and public health response characteristics of a large outbreak of diphtheria among the Rohingya population in Cox's Bazar, Bangladesh, 2017 to 2019: a retrospective study. PLOS Med. 2021;18:e1003587.
5. Hsieh SY, Tseng CL, Lee YS, Kuo AJ, Sun CF, Lin YH, et al. Highly efficient classification and identification of human pathogenic bacteria by MALDI-TOF MS. Mol Cell Proteomics. 2008;7:448–56. https://doi.org/10.1074/mcp.M700339-MCP200
6. Nakao H, Popovic T. Development of a direct PCR assay for detection of the diphtheria toxin gene. J Clin Microbiol. 1997;35:1651–5. https://doi.org/10.1128/jcm.35.7.1651-1655.1997
7. The European Committee on Antimicrobial Susceptibility Testing. Breakpoint tables for interpretation of MICs and zone diameters, version 13.1, 2023 [cited 2023 July 10]. https://www.eucast.org/fileadmin/src/media/PDFs/EUCAST_files/Breakpoint_tables/v_13.1_Breakpoint_Tables.pdf
8. Sing A, Heesemann J. Imported cutaneous diphtheria, Germany, 1997–2003. Emerg Infect Dis. 2005;11:343–4. https://doi.org/10.3201/eid1102.040560
9. Kofler J, Ramette A, Iseli P, Stauber L, Fichtner J, Droz S, et al. Ongoing toxin-positive diphtheria outbreaks in a federal asylum centre in Switzerland, analysis July to September 2022. Euro Surveill. 2022;27:2200811 https://doi.org/10.2807/1560-7917.ES.2022.27.44.2200811
10. May MLA, McDougall RJ, Robson JM. *Corynebacterium diphtheriae* and the returned tropical traveler. J Travel Med. 2014;21:39–44. https://doi.org/10.1111/jtm.12074
11. Marosevic DV, Berger A, Kahlmeter G, Payer SK, Hörmansdorfer S, Sing A. Antimicrobial susceptibility of *Corynebacterium diphtheriae* and *Corynebacterium ulcerans* in Germany 2011–17. J Antimicrob Chemother. 2020;75:2885–93. https://doi.org/10.1093/jac/dkaa280
12. Hoefer A, Pampaka D, Herrera-León S, Peiró S, Varona S, López-Perea N, et al. Molecular and epidemiological characterization of toxigenic and nontoxigenic *Corynebacterium diphtheriae*, *Corynebacterium belfantii*, *Corynebacterium rouxii*, and *Corynebacterium ulcerans* isolates identified in Spain from 2014 to 2019. J Clin Microbiol. 2021;59:e02410-20. https://doi.org/10.1128/JCM.02410-20
13. European Center for Disease Prevention and Control. Increase of reported diphtheria cases among migrants in Europe due to *Corynebacterium diphtheriae* [cited 2023 Jul 10]. https://www.ecdc.europa.eu/en/publications-data/increase-reported-diphtheria-cases-among-migrants-europe-due-corynebacterium
14. World Health Organization. WHO and UNICEF estimates of immunization coverage: 2021 revision [cited 2023 Feb 17]. https://www.who.int/teams/immunization-vaccines-and-biologicals/immunization-analysis-and-insights/global-monitoring/immunization-coverage/who-unicef-estimates-of-national-immunization-coverage
15. Gao H, Lau EHY, Cowling BJ. Waning immunity after receipt of pertussis, diphtheria, tetanus, and polio-related vaccines: a systematic review and meta-analysis. J Infect Dis. 2022;225:557–66. https://doi.org/10.1093/infdis/jiab480

Address for correspondence: Benedikt Daniel Spielberger, University Medical Center Freiburg, Mathildenstr. 1, 79106 Freiburg, Germany; email: benedikt.spielberger@uniklinik-freiburg.de

Expansion of Invasive Group A *Streptococcus* $M1_{UK}$ Lineage in Active Bacterial Core Surveillance, United States, 2019–2021

Yuan Li, Joy Rivers, Saundra Mathis, Zhongya Li, Sopio Chochua, Benjamin J. Metcalf, Bernard Beall, Jennifer Onukwube, Christopher J. Gregory, Lesley McGee

From 2015–2018 to 2019–2021, hypertoxigenic $M1_{UK}$ lineage among invasive group A *Streptococcus* increased in the United States (1.7%, 21/1,230 to 11%, 65/603; p<0.001). $M1_{UK}$ was observed in 9 of 10 states, concentrated in Georgia (n = 41), Tennessee (n = 13), and New York (n = 13). Genomic cluster analysis indicated recent expansions.

The $M1_{UK}$ lineage of group A *Streptococcus* (GAS) is a hypertoxigenic clone within the serotype M1 GAS strain and has been associated with increased scarlet fever and invasive GAS (iGAS) disease incidence in the United Kingdom since 2014 (*1*–*3*). $M1_{UK}$ carries 27 characteristic lineage-defining single-nucleotide variants (SNVs) that distinguish it from other globally circulating M1 GAS clones (*1*). By 2020, $M1_{UK}$ had also became the dominant clone among M1 GAS in England (*3*), the Netherlands (*4*), and Australia (*5*) and showed substantial presence in Canada (*6*).

In the United States, $M1_{UK}$ was identified as a minor clone of M1 iGAS isolates in the Active Bacterial Core surveillance (ABCs) system, a laboratory- and population-based surveillance system for invasive bacterial infections that is currently implemented in 10 US states (*7*), in 2015–2018 (*8*). Using genomic surveillance data in ABCs, we investigated the trend of $M1_{UK}$ in 2019–2021 and documented the characteristics of iGAS infections caused by $M1_{UK}$.

The Study

We identified iGAS cases through ABCs and mapped whole-genome sequencing reads of M1 isolates against the M1 reference genome MGAS5005 to identify M1UK based on previously reported characteristic M1UK SNVs (1). We constructed phylogenetic trees by using kSNP3.0 software (9). We identified genomic clusters by using a hierarchical cluster analysis with a cutoff value of 10 SNVs as described (10). We evaluated change of M1UK proportion among M1 iGAS over time by using the χ^2 test for trend in proportions (trend test). We used the Fisher exact test to assess equality of proportions. All p values were 2 sided, and we considered p<0.05 statistically significant. We performed all analyses by using R software version 3.4.3 (The R Foundation for Statistical Computing, https://www.r-project.org).

We submitted all whole-genome sequencing data files of the study isolates to the National Center for Biotechnology Information Sequence Read Archive (BioProject no. PRJNA395240). Accession numbers of the 86 $M1_{UK}$ isolates are provided (Appendix Table 4, https://wwwnc.cdc.gov/EID/article/29/10/23-0675-App1.pdf).

During 2019–2021, a total of 603 cases of M1 iGAS infections were documented through ABCs. Among those cases, 65 (11%) were caused by the $M1_{UK}$ clone (Figure 1, panel A), and the percentage was significantly higher than that observed during 2015–2018 (1.7%, 21/1,230; p<0.001). The trend test indicated a significant increasing trend in the $M1_{UK}$ proportion among M1 iGAS isolates during 2015–2021 (p<0.001). During 2015–2021, most $M1_{UK}$ cases (67/86) were concentrated in 3 states: Georgia (41 cases,) Tennessee (13 cases), and New York (13 cases), although the $M1_{UK}$ clone was found in 9 of the 10 ABCs sites (Figure 1, panel B). Nearly one third of all $M1_{UK}$ infections (28/86) occurred in the first quarter of 2020 (Figure 1, panel B). During 2015–2021, a total of 12 iGAS isolates

Author affiliation: Centers for Disease Control and Prevention, Atlanta, Georgia, USA

DOI: https://doi.org/10.3201/eid2910.230675

were identified as the intermediate lineages, containing 13 (n = 4) or 23 (n = 8) of the 27 characteristic $M1_{UK}$ SNVs (Appendix Figure 1), and they did not show significant expansion from 2015–2018 through 2019–2021 (p = 0.07).

Phylogenetic analysis of the 86 $M1_{UK}$ isolates showed 9 distinctive genomic clusters (Figure 2). Each genomic cluster contained 2–21 genomically closely related isolates, and collectively those clusters accounted for 74 (86%) of all $M1_{UK}$ isolates (Figure 2). For 2 $M1_{UK}$ isolates within a same cluster, the median pairwise genomic distance was 3 SNVs (interquartile range [IQR] 1.5–6), consistent with continued transmission from a recent introduction event. However, for 2 $M1_{UK}$ isolates not in the same cluster, the median pairwise genomic distance was 33 SNVs (IQR 28–38), indicating some degree of genomic diversity within $M1_{UK}$, although not as much as the diversity observed among 100 randomly selected globally circulating M1 GAS clone isolates in ABCs, 2015–2021 (median 63 SNVs, IQR 49–115). (Appendix Figure 1).

The clusters displayed clear signatures of temporal and geographic relatedness (Appendix Figure 2). For example, the largest cluster, cluster_1, showed a sharp increase of cases at the beginning of 2020, followed by a rapid decrease. The second largest cluster, cluster 2, showed relatively stable case numbers spanning from the third quarter of 2018 to the third quarter of 2020. Within a genomic cluster, most $M1_{UK}$ iGAS were identified in 1 or 2 states, suggesting a localized spread of the infection.

Overall, $M1_{UK}$ and non-$M1_{UK}$ M1 isolates had many common genetic features of the contemporary M1 *S. pyogenes* strain (Table). The $M1_{UK}$ clone had a higher proportion of isolates that had the streptococcal pyrogenic exotoxin gene *speC* (4.7% [4/86] vs. 1.4% [24/1,747]; p = 0.039), the super antigen A gene *ssa* (2.3% [2/86] vs. 0.1% (2/1,747]; p = 0.012), and the extracellular streptodornase D gene *sda1* (also known as *sdaD2*; 100% [86/86] vs. 92% [1,613/1,747]; p = 0.002). The *speC* and *ssa* genes were found in 4 nonclustered $M1_{UK}$ isolates, of which 2 isolates had both genes, suggesting acquisition of prophage ΦHKU488.vir (*5*).

Patients infected by the $M1_{UK}$ strain showed similar age, sex, and syndrome distribution compared with patients infected by non-$M1_{UK}$ M1 GAS (Table), except that $M1_{UK}$ isolates were more likely to be found in patients with pneumonia (33% vs. 22%; p = 0.033). The case-fatality rate was high for $M1_{UK}$ iGAS infection (22%) although it was not significantly different from that of non-$M1_{UK}$ M1 iGAS (15%; p = 0.089). In subgroup analysis stratified by time (2015–2018, 2019–2021) and location (GA, TN, and NY only), $M1_{UK}$ isolates were associated with higher proportions of *speC*, *ssa*, *sda1*, and pneumonia compared with non-$M1_{UK}$ isolates in all 3 subgroups (Appendix Tables 1–3), except for *speC* in 2019–2021. The difference in subgroup analysis was generally not statistically significant, potentially caused by smaller sample size and reduced power in a subgroup.

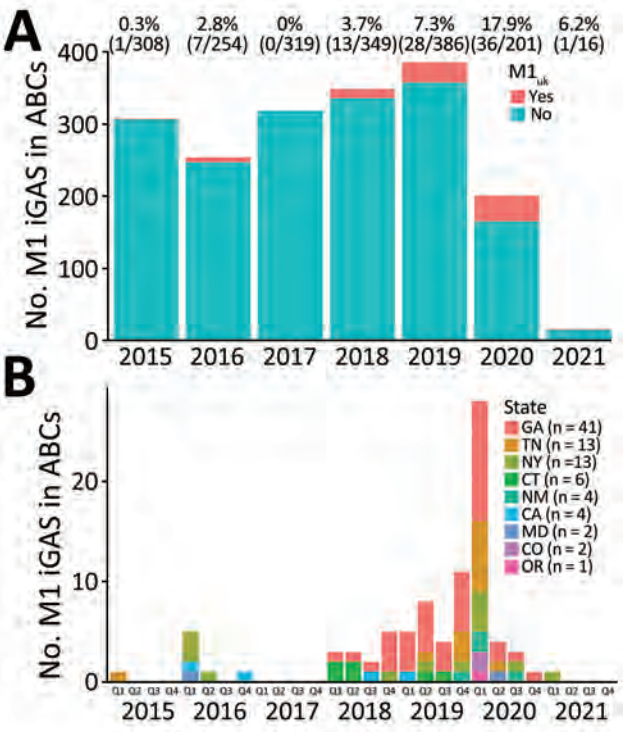

Figure 1. Expansion of $M1_{UK}$ lineage in serotype M1 iGAS in the United States, 2015–2021. A) Counts and percentages of $M1_{UK}$ isolates among M1 iGAS isolates in ABCs during 2015–2021. B) Number of $M1_{UK}$ infections over time in 9 states that are part of the ABCs system. Key shows total number of $M1_{UK}$ infections during 2015–2021 for each state. ABCs, Active Bacterial Core Surveillance System; iGAS, invasive group A *Streptococcus* disease; Q, quarter.

Conclusions

This study demonstrates a substantial increase of $M1_{UK}$ lineage during 2019–2021 in the ABCs sites in the United States. Additional data are needed to determine variance in $M1_{UK}$ iGAS incidence across states outside the 10 states in ABCs. The proportion of $M1_{UK}$ iGAS in ABCs remains much lower than that reported in England (*3*), Australia (*5*), and the Netherlands (*4*). We documented the mode of expansion for the $M1_{UK}$ lineage in the United States by determining whether the 86 $M1_{UK}$ iGAS cases could be explained by 1 recent introduction or multiple ones. We tracked the shape and characteristics of epidemiologic curves for each

cluster, which could help understand different patterns of disease transmission. The increase was associated with the formation and expansion of multiple genomic clusters in which each cluster was mostly found in only 1 or 2 states. The results suggested that the $M1_{UK}$ clone might have been introduced and

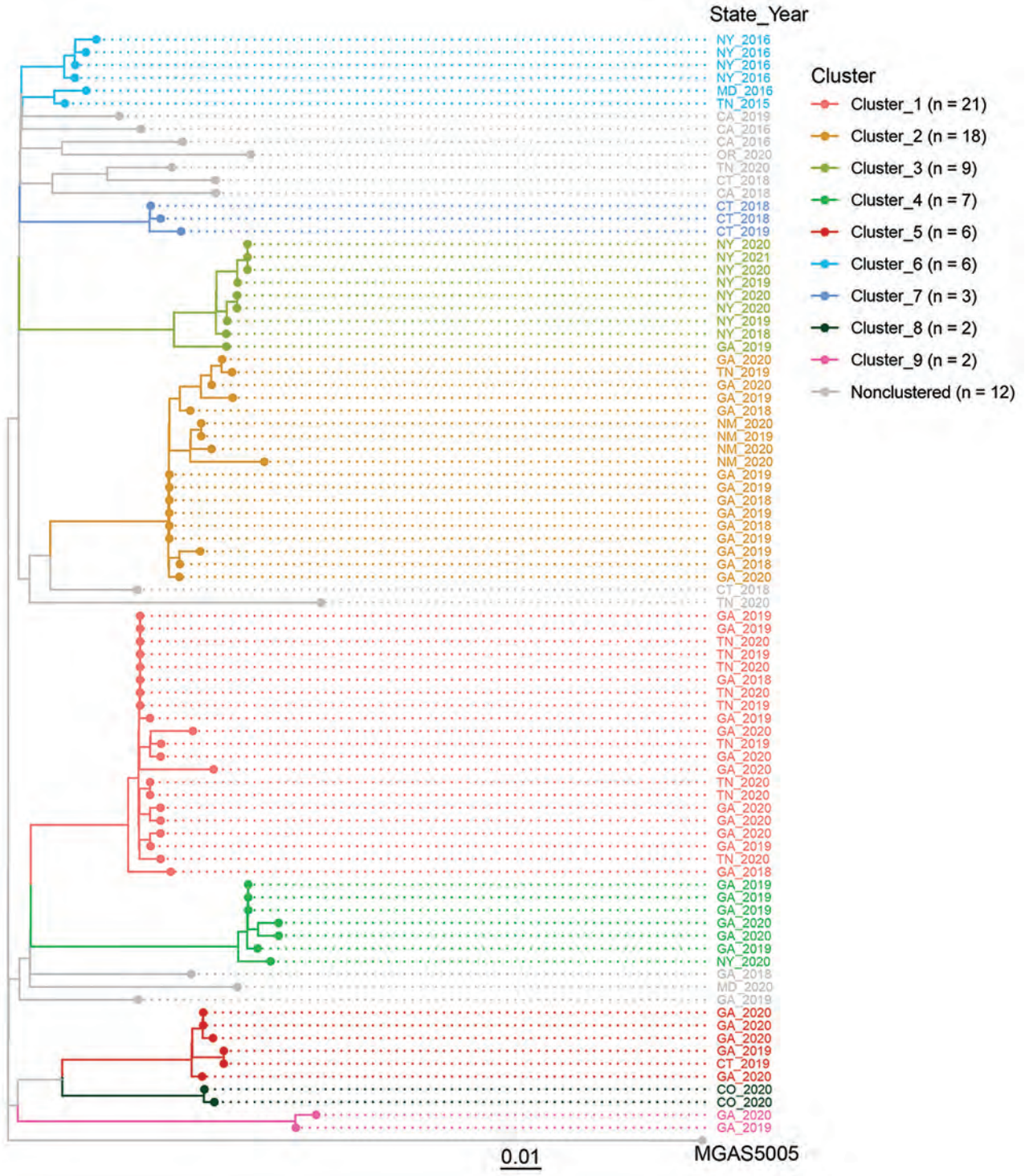

Figure 2. Genomic clusters of $M1_{UK}$ invasive group A *Streptococcus* disease, United States, 2015–2021. Core-genome phylogenetic tree of 86 $M1_{UK}$ invasive group A *Streptococcus* disease isolates and the reference M1 genome MGAS5005 was based on 462 core single-nucleotide variant sites generated by kSNP3.0 software (*9*). Tip colors indicate 9 groups of genomically closely related isolates (genomic clusters). Key shows total number of $M1_{UK}$ isolates in each cluster. Scale bar indicates expected nucleotide substitutions per site.

Table. Strain and patient features of $M1_{UK}$ iGAS compared with other M1 iGAS in ABCs, United States, 2015–2021

Characteristic	M1 iGAS, no. (%) cases		p value†
	$M1_{UK}$, n = 86	Non-$M1_{UK}$, n = 1,747	
Strain feature‡			
Antimicrobial susceptibility			
Penicillin nonsusceptible	0	0	1.000
Erythromycin nonsusceptible	0	21 (1.2)	0.621
Clindamycin nonsusceptible	0	20 (1.1)	1.000
Tetracycline nonsusceptible	0	18 (1)	1.000
Levofloxacin nonsusceptible	0	9 (0.5)	1.000
Pyrogenic exotoxin genes			
speA	86 (100)	1,720 (98.5)	0.635
speC	4 (4.7)	24 (1.4)	0.039
speG	86 (100)	1747 (100)	1.000
speH	0	1 (0.1)	1.000
speI	0	1 (0.1)	1.000
speJ	86 (100)	1,747 (100)	1.000
speK	0	2 (0.1)	1.000
speL	0	0	1.000
speM	0	0	1.000
Ssa	2 (2.3)	2 (0.1)	0.012
smeZ	85 (98.8)	1,737 (99.4)	0.411
Other virulence factors			
hasA hyaluronic acid synthetase, capsule	86 (100)	1,03 (97.5)	0.266
Virulence-associated DNase, SDA1§	86 (100)	1,613 (92.3)	0.002
Patient characteristic			
Age, y			
<18	12 (14)	233 (13.3)	0.871
18–34	5 (5.8)	178 (10.2)	0.266
35–49	19 (22.1)	333 (19.1)	0.484
50–64	21 (24.4)	445 (25.5)	0.899
65–74	15 (17.4)	289 (16.5)	0.768
≥75	14 (16.3)	269 (15.4)	0.762
Sex			
M	41 (47.7)	955 (54.7)	0.223
F	45 (52.3)	792 (45.3)	0.223
Clinical syndrome			
Cellulitis	25 (29.1)	633 (36.2)	0.205
Bacteremia without focus	11 (12.8)	276 (15.8)	0.544
Pneumonia	28 (32.6)	384 (22.0)	0.033
Necrotizing fasciitis	5 (5.8)	147 (8.4)	0.546
Streptococcal toxic shock syndrome	7 (8.1)	95 (5.4)	0.328
Death	19 (22.1)	260 (14.9)	0.089

*ABCs, Active Bacterial Core Surveillance System; iGAS, invasive group A *Streptococcus* disease.
†By Fisher exact test.
‡All strain features, including antimicrobial susceptibility, pyrogenic exotoxin genes, and other virulence factors, were inferred from whole-genome sequencing data.
§Detecting genetic marker for the *sda1* gene (GenBank accession no. AY452036.1), which is identical to the *sdaD2* gene (M5005_Spy1415; GenBank accession no. AAZ52033.1).

circulated in different geographic locations in the United States, rather than spreading from a recent single introduction event.

In 2020, *emm*1 was the leading cause of iGAS only in Georgia and New York in ABCs. In that year, the proportion of $M1_{UK}$ isolates among *emm1* iGAS was 38% (16/42) in Georgia and 25% (5/20) in New York. It appeared that $M1_{UK}$ lineage followed the same state preferences as M1 in general. In recent years, there were rapidly expanding clusters of *emm* types that were not historically so prevalent within several different states, mostly pattern E lineages (*emm*11,49,82,92,60) and pattern D lineages (*emm*83,59,81), which was associated with increasing proportions of disadvantaged persons and led to drastic changes in *emm* type distributions in those states (*11,12*).

Although the *speC* and *ssa* genes were associated with $M1_{UK}$ isolates, they were present in <5% of these isolates, and the biologic role of this association is unclear. It is crucial to monitor the spread of this variant and the associated virulence determinants to inform development of effective prevention and treatment strategies.

This study used the *Streptococcus pyogenes* multilocus sequence typing website (https://pubmlst.org/organisms/streptococcus-pyogenes) hosted at the University of Oxford.

This study was supported by the Centers for Disease Control and Prevention. Major support was provided by the Centers for Disease Control and Prevention Emerging Infections Program and the Advanced Molecular Detection Initiative.

Y.L., L.M., and B.B. contributed to study design; all authors contributed to data collection; Y.L. performed data analysis, produced the table and figures, and wrote the manuscript; and J.R., S.M., Z.L., S.C., B.J.M., B.B., J.O., C.J.G., and L.M. contributed to data analysis and interpretation. All authors reviewed and edited the manuscript.

About the Author

Dr. Yuan Li is a microbiologist and bioinformatician in the National Center for Immunization and Respiratory Diseases, Centers for Disease Control and Prevention, Atlanta, GA. His primary research interests are integration of laboratory and epidemiologic data to inform disease surveillance, outbreak responses, and vaccine strategies.

References

1. Lynskey NN, Jauneikaite E, Li HK, Zhi X, Turner CE, Mosavie M, et al. Emergence of dominant toxigenic M1T1 *Streptococcus pyogenes* clone during increased scarlet fever activity in England: a population-based molecular epidemiological study. Lancet Infect Dis. 2019;19:1209–18. https://doi.org/10.1016/S1473-3099(19)30446-3
2. Alcolea-Medina A, Snell LB, Alder C, Charalampous T, Williams TG, Tan MK, et al.; Synnovis Microbiology Laboratory Group. The ongoing *Streptococcus pyogenes* (group A *Streptococcus*) outbreak in London, United Kingdom, in December 2022: a molecular epidemiology study. Clin Microbiol Infect. 2023;29:887–90. https://doi.org/10.1016/j.cmi.2023.03.001
3. Zhi X, Li HK, Li H, Loboda Z, Charles S, Vieira A, et al. Emerging invasive group A *Streptococcus* $M1_{UK}$ lineage detected by allele-specific PCR, England, 2020. Emerg Infect Dis. 2023;29:1007–10. https://doi.org/10.3201/eid2905.221887
4. Rümke LW, de Gier B, Vestjens SMT, van der Ende A, van Sorge NM, Vlaminckx BJ, et al. Dominance of $M1_{UK}$ clade among Dutch M1 *Streptococcus pyogenes*. Lancet Infect Dis. 2020;20:539–40. https://doi.org/10.1016/S1473-3099(20)30278-4
5. Davies MR, Keller N, Brouwer S, Jespersen MG, Cork AJ, Hayes AJ, et al. Detection of *Streptococcus pyogenes* $M1_{UK}$ in Australia and characterization of the mutation driving enhanced expression of superantigen SpeA. Nat Commun. 2023;14:1051. https://doi.org/10.1038/s41467-023-36717-4
6. Demczuk W, Martin I, Domingo FR, MacDonald D, Mulvey MR. Identification of *Streptococcus pyogenes* $M1_{UK}$ clone in Canada. Lancet Infect Dis. 2019;19:1284–5. https://doi.org/10.1016/S1473-3099(19)30622-X
7. Centers for Disease Control and Prevention. Active Bacterial Core Surveillance, Emerging Infections Program Network. 2020 [cited 2023 Aug 18]. https://www.cdc.gov/abcs
8. Li Y, Nanduri SA, Van Beneden CA, Beall BW. $M1_{UK}$ lineage in invasive group A streptococcus isolates from the USA. Lancet Infect Dis. 2020;20:538–9. https://doi.org/10.1016/S1473-3099(20)30279-6
9. Gardner SN, Slezak T, Hall BG. kSNP3.0: SNP detection and phylogenetic analysis of genomes without genome alignment or reference genome. Bioinformatics. 2015;31:2877–8. https://doi.org/10.1093/bioinformatics/btv271
10. Li Y, Dominguez S, Nanduri SA, Rivers J, Mathis S, Li Z, et al. Genomic characterization of group A streptococci causing pharyngitis and invasive disease in Colorado, USA, June 2016–April 2017. J Infect Dis. 2022;225:1841–51. https://doi.org/10.1093/infdis/jiab565
11. Valenciano SJ, Onukwube J, Spiller MW, Thomas A, Como-Sabetti K, Schaffner W, et al. Invasive group A streptococcal infections among people who inject drugs and people experiencing homelessness in the United States, 2010–2017. Clin Infect Dis. 2021;73:e3718–26. https://doi.org/10.1093/cid/ciaa787
12. Metcalf B, Nanduri S, Chochua S, Li Y, Fleming-Dutra K, McGee L, et al. Cluster transmission drives invasive group A *Streptococcus* disease within the United States and is focused on communities experiencing disadvantage. J Infect Dis. 2022;226:546–53. https://doi.org/10.1093/infdis/jiac162

Address for correspondence: Yuan Li, Centers for Disease Control and Prevention, 1600 Clifton Rd NE, Mailstop H18-1, Atlanta, GA 30329-4027, USA; email: yqh8@cdc.gov

Estimate of COVID-19 Deaths, China, December 2022–February 2023

Zhanwei Du, Yuchen Wang, Yuan Bai, Lin Wang, Benjamin John Cowling, Lauren Ancel Meyers

China announced a slight easing of its zero-COVID rules on November 11, 2022, and then a major relaxation on December 7, 2022. We estimate that the ensuing wave of SARS-CoV-2 infections caused 1.41 million deaths in China during December 2022–February 2023, substantially higher than that reported through official channels.

For almost 3 years, China maintained a zero-COVID policy that effectively suppressed SARS-CoV-2 transmission. China began rolling back those rules on November 11, 2022, and ended most restrictions on December 7, 2022 (China Focus, 2023, https://english.news.cn/20221207/ca014c043bf24728b8dcbc0198565fdf/c.html), in response to the reduced severity of the Omicron variant or the growing socioeconomic and political costs of the restrictions. COVID-19 immediately surged; China reported nearly 82,000 COVID-19–related deaths during December 16, 2022–February 17, 2023 (*1*).

In December 2022, China disbanded its national COVID testing system and twice modified its criteria for classifying COVID-19–related deaths (*2*,*3*). The resulting uncertainties in reported occurrences and low official death counts have spurred speculation that official mortality reports from China substantially underestimate the full burden of the December 2022–January 2023 wave (*4*). In early December of 2022, the Chinese Center for Disease Control and Prevention (China CDC) launched a sentinel household surveillance program, tracking SARS-CoV-2 test positivity in 420,000 people in 22 provinces across China (*5*). We used those data to estimate a plausible range for the total number of COVID-19–related deaths during December 2022–January 2023. We classified a death as COVID-19–related if it occurred within 28 days of confirmed infection (*6*).

Author affiliations: World Health Organization Collaborating Center for Infectious Disease Epidemiology and Control, School of Public Health, University of Hong Kong, Hong Kong, China (Z. Du, Y. Bai, B.J. Cowling); Laboratory of Data Discovery for Health Limited, Hong Kong Science and Technology Park, Hong Kong (Z. Du, Y. Wang, Y. Bai, B.J. Cowling); University of Cambridge, Cambridge, UK (Y. Wang); University of Texas at Austin, Austin, Texas, USA (L.A. Meyers); Santa Fe Institute, Santa Fe, New Mexico, USA (L.A. Meyers)

DOI: http://doi.org/10.3201/eid2910.230585

The Study

We estimated COVID-19–related deaths by using an individual-based simulation that incorporated daily test positivity reports from the China CDC sentinel household surveillance system during December 16, 2022–January 19, 2023. We also incorporated age-specific vaccination and boosting rates reported in China and published estimates of infection fatality rates, vaccine effectiveness, and rates of immunity waning. We built a stochastic model to generate COVID-19 death reports from infections occurring during December 8, 2022–January 19, 2023, in a population of 1 million persons whose ages were randomly assigned according to the national age distribution in China. Each simulation was based on the reported SARS-CoV-2 test positivity rate (*5*) to stochastically determine the number of persons who would have initially tested positive on that day. Those testing positive were assigned a vaccination history generated stochastically from the daily age-specific vaccination rates reported in China (*7*) and given a level of vaccine-acquired protection against death based on the date of their last dose and published estimates for vaccine effectiveness (*7*). The simulation used that value and the age-specific infection-fatality rate (Leung K, Leung GM, Wu J, unpub. data, https://www.medrxiv.org/content/10.1101/2022.12.14.22283460) to determine probabilistically whether the patiet died from COVID-19 (Appendix, https://wwwnc.cdc.gov/

EID/article/29/10/23-0585-App1.pdf). Results were based on 1,000 model simulations. We conducted sensitivity analyses for assumed age-specific vaccine effectiveness (VE) against death, population size, and increase in infection-fatality rates as the healthcare system in China reached capacity.

The sentinel surveillance report from China CDC suggests that roughly 90% of China's population were infected during the focal 35-day period (*5*). This large and rapid wave caused ≈1.41 (95% credibility interval [CrI] 1.14–1.73) million deaths across China; 0.80 (95% CrI 0.60–1.05) million of those deaths occurred among adults >80 years of age. Estimated COVID-19 mortality rates (per 1 million population) ranged from roughly 0 (95% CrI 0–17) among children <9 years of age to 22,400 (95% CrI 16,500–30,000) among adults >80 years of age (Figure; Appendix Tables 2, 3).

Conclusions

COVID-19 deaths are related to a variety of health complications, including septic shock, multiorgan failure, respiratory failure, heart failure, and secondary infections (*8*). China's official reports may underestimate the COVID-19 death toll by a factor of 17 (95% CrI 14–22). Our analyses suggest that, in barely a month, COVID-19 killed >1 million persons in China. The difference between China's official mortality reports and our estimates may stem from delays in hospital reporting (*9*), omission of deaths happening outside of hospitals (*2*), gaps in China's vital registration system (*4*), or intentional reclassification after the insurance industry in China largely stopped covering COVID-19 in December 2022 (South China Morning Post, December 17, 2022, https://www.scmp.com/news/china/science/article/3203695/chinas-covid-19-patients-face-insurance-battle-over-pandemic-related-payouts).

As our findings indicate, the relaxation of China's zero-COVID policies in late 2022 precipitated an explosive wave of infections that caused an estimated 1,000 (95% CrI 843–1,230) deaths/1 million population. By comparison, during the large Omicron

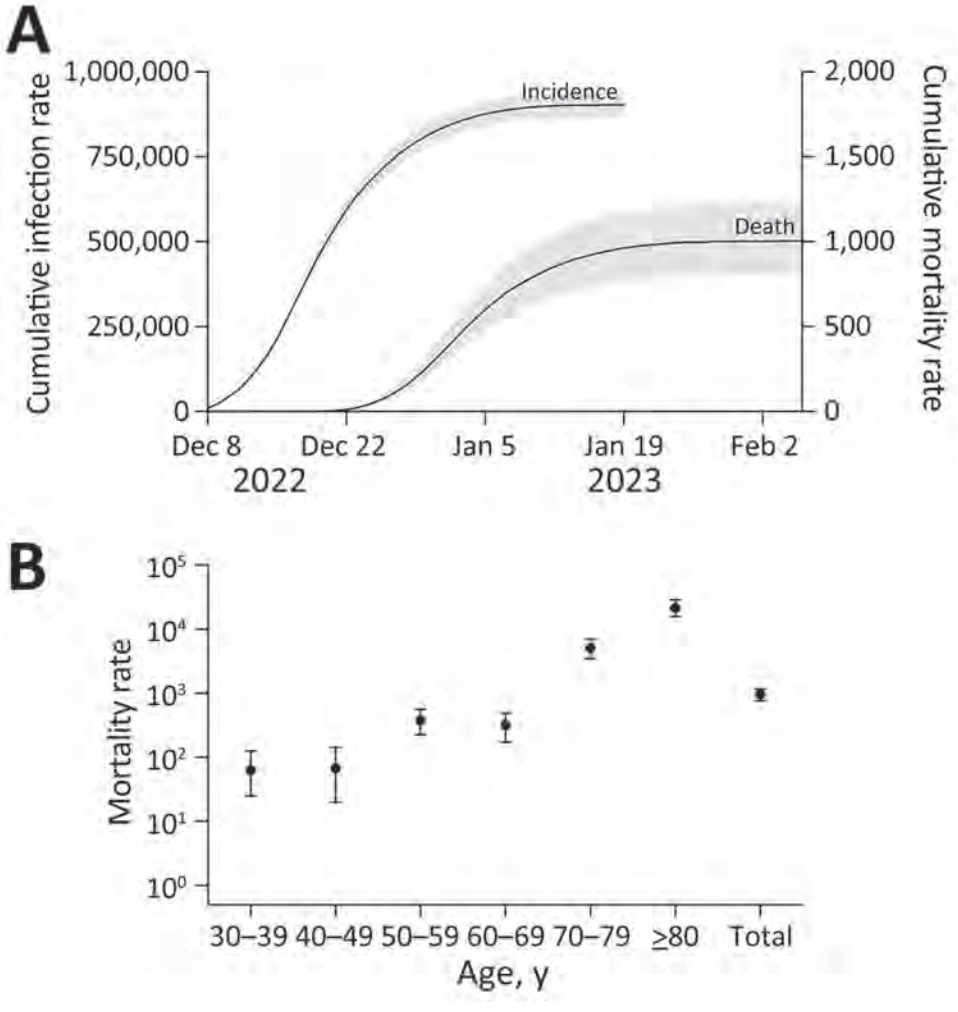

Figure. Estimated SARS-CoV-2 infection incidence in China during December 16, 2022–January 19, 2023, and resulting COVID-19 mortality rates. A) Estimated cumulative infection and mortality rates (per 1 million population) during December 8, 2022–February 7, 2023, based on test positivity data from the Chinese Center for Disease Control and Prevention sentinel community surveillance system, reported on January 26, 2023 (*5*). Gray shading indicates 95% credibility intervals derived from 1,000 stochastic simulations. B) Estimated age-specific COVID-19 mortality rates (deaths/1 million population, log scale), based on simulations that incorporate vaccine timing, coverage, effectiveness, and waning in each age group.

surges in early 2022, reported maximum 52-day mortality rates (deaths/1 million population) were 345 for the United States, 144 for the United Kingdom, and 1,166 for Hong Kong (*1*). Hong Kong's high COVID-19 mortality rate may have resulted from its large proportion of older adults and relatively low vaccination rates in this vulnerable group; 26% of Hong Kong's population is >60 years of age, and only 49% of that population had received ≥2 doses of a SARS-CoV-2 vaccine before March 2022 (*10*). By comparison, 90% of Australia's population >60 years of age, which comprises 22% of the total population, were double-vaccinated by March 2022; the peak 52-day mortality rate in Australia was roughly 88% lower than that of Hong Kong (137 deaths/1 million population) (*10*).

The unprecedented speed and severity of the wave in China is not surprising, given lack of infection-acquired immunity, moderate effectiveness of vaccines commonly administered in China, relatively low vaccine coverage in the oldest populations, and limited access to effective antiviral drugs. Mainland China had among the lowest estimated levels of excess mortality during the COVID-19 pandemic in 2020 and 2021 compared with 74 other countries worldwide (*11*), perhaps because of China's dynamic zero-COVID strategy. The abrupt relaxation of zero-COVID rules without measures to protect high-risk populations likely led to the surge in hospitalizations and deaths we examined. As of June 21, 2023, the cumulative reported mortality rate in China is 85 deaths/1 million persons, considerably lower than rates for countries such as the United States (3,332/1 million persons), which sustained high levels of mortality before December 2022, and Japan (603/1 million persons), which experienced a substantial wave starting in December 2022, around the same time as China (E. Mathieu et al., 2020, https://ourworldindata.org/coronavirus). Our estimates suggest that China's true death toll is closer to 1,014 deaths/1 million persons, roughly double that of Japan and 30% of that of the United States.

Our estimates are robust to moderate changes in the assumed age-specific vaccine efficacy and infection-fatality rates (Appendix Table 4). If the large surge in COVID-19 hospitalizations in late 2022 and early 2023 compromised patient care, we may have significantly underestimated the overall mortality rate. Assuming that COVID-19 mortality increased by a factor of 3.39 during China's 3-day peak in reported test positivity (based on an estimate from a COVID-19 healthcare surge in Hong Kong in March 2022 [*12*]), our estimate of overall mortality increases to 2.11 (95% CrI 1.71–2.60) million.

Our findings rely on the validity of data from the China CDC's sentinel household surveillance program, which might have some quality issues (e.g., double counting of persons who test multiple times). China CDC reports include graphs of daily positivity in this sample that enable rapid approximation of epidemic trends on a national scale (*5*). In addition, we assume that reported vaccinations were the only source of prior immunity and that all infections were by Omicron variants; surveillance data suggest that only 0.4% of specimens collected during this period were not Omicron (*5*).

In summary, our study suggests that the official mortality reports from China substantially underestimate the full burden of the December 2022–January 2023 COVID-19 wave, raising concerns about the accuracy and transparency of China's reporting system, as well as potential underestimation of reports from other countries that limit data collection and reporting. The decision to relax China's zero-COVID policies without adequate measures to protect high-risk populations had severe consequences. Other countries prioritized vaccines for older age groups and other vulnerable populations (*13*), and many studies have indicated that targeting medical countermeasures and protective measures toward groups with high infection-fatality rates can be life and cost saving (*14*,*15*). We expect that the true toll of COVID-19 in China will become clearer as additional epidemiologic data become available.

This work was supported by grants from the US Centers for Disease Control and Prevention (U01IP001136) and US National Institutes of Health (R01AI151176) and the AIR@InnoHK Programme from Innovation and Technology Commission of the Government of the Hong Kong Special Administrative Region. The funders had no role in the design and conduct of the study; collection, management, analysis, and interpretation of the data; preparation, review, or approval of the manuscript; or decision to submit the manuscript for publication.

B.J.C. consults for AstraZeneca, GlaxoSmithKline, Moderna, Pfizer, Roche, and Sanofi Pasteur.

About the Author

Dr. Du is a research assistant professor in the School of Public Health, LKS Faculty of Medicine, The University of Hong Kong, Hong Kong, China. He develops mathematical models to elucidate the transmission dynamics, surveillance, and control of infectious diseases.

References

1. Mathieu E, Ritchie H, Rodés-Guirao L, Appel C, Giattino C, Hasell J, et al. Coronavirus pandemic (COVID-19). Our World in Data. 2020 Mar 5 [cited 2023 Feb 4]. https://ourworldindata.org/covid-cases
2. China CDC. National epidemic situation of COVID-19 disease (2023–01–15). 2023 [cited 2023 Feb 14]. https://www.chinacdc.cn/jkzt/crb/zl/szkb_11803/jszl_13141/202301/t20230115_263381.html
3. National Health Commission. Transcript of press conference of the State Council's joint prevention and control mechanism for the novel coronavirus pneumonia outbreak (December 20, 2022). 2023 [cited 2023 Feb 1]. http://www.nhc.gov.cn/xcs/s3574/202212/a9510969ad85461297016f6ad1c87770.shtml
4. Lewis D. China's COVID wave has probably peaked, model suggests. Nature. 2023;613:424–5. https://doi.org/10.1038/d41586-023-00075-4
5. Chinese Center for Disease Control and Prevention. COVID-19 clinical and surveillance data—Dec 9, 2022 to Jan 23, 2023, China. 2023 Jan 26 [cited 2023 Jan 28]. https://en.chinacdc.cn/news/latest/202301/t20230126_263523.html
6. Nyberg T, Ferguson NM, Nash SG, Webster HH, Flaxman S, Andrews N, et al.; COVID-19 Genomics UK (COG-UK) consortium. Comparative analysis of the risks of hospitalisation and death associated with SARS-CoV-2 omicron (B.1.1.529) and delta (B.1.617.2) variants in England: a cohort study. Lancet. 2022;399:1303–12. https://doi.org/10.1016/S0140-6736(22)00462-7
7. Cai J, Deng X, Yang J, Sun K, Liu H, Chen Z, et al. Modeling transmission of SARS-CoV-2 Omicron in China. Nat Med. 2022;28:1468–75. https://doi.org/10.1038/s41591-022-01855-7
8. Gundlapalli AV, Lavery AM, Boehmer TK, Beach MJ, Walke HT, Sutton PD, et al. Death certificate–based ICD-10 diagnosis codes for COVID-19 mortality surveillance—United States, January–December 2020. MMWR Morb Mortal Wkly Rep. 2021;70:523–7. https://doi.org/10.15585/mmwr.mm7014e2
9. Liu J, Zhang L, Yan Y, Zhou Y, Yin P, Qi J, et al. Excess mortality in Wuhan city and other parts of China during the three months of the covid-19 outbreak: findings from nationwide mortality registries. BMJ. 2021;372:n415. https://doi.org/10.1136/bmj.n415
10. Smith DJ, Hakim AJ, Leung GM, Xu W, Schluter WW, Novak RT, et al. COVID-19 Mortality and vaccine coverage—Hong Kong Special Administrative Region, China, January 6, 2022–March 21, 2022. MMWR Morb Mortal Wkly Rep. 2022;71:545–8. https://doi.org/10.15585/mmwr.mm7115e1
11. Wang H, Paulson KR, Pease SA, Watson S, Comfort H, Zheng P, et al.; COVID-19 Excess Mortality Collaborators. Estimating excess mortality due to the COVID-19 pandemic: a systematic analysis of COVID-19-related mortality, 2020–21. Lancet. 2022;399:1513–36. https://doi.org/10.1016/S0140-6736(21)02796-3
12. Wong JY, Cheung JK, Lin Y, Bond HS, Lau EHY, Ip DKM, et al. Intrinsic and effective severity of COVID-19 cases infected with the ancestral strain and Omicron BA.2 variant in Hong Kong. J Infect Dis. 2023 Jun 27 [Epub ahead of print]. https://doi.org/10.1093/infdis/jiad236
13. Hale T, Angrist N, Goldszmidt R, Kira B, Petherick A, Phillips T, et al. A global panel database of pandemic policies (Oxford COVID-19 Government Response Tracker). Nat Hum Behav. 2021;5:529–38. https://doi.org/10.1038/s41562-021-01079-8
14. Wang X, Du Z, Huang G, Pasco RF, Fox SJ, Galvani AP, et al. Effects of cocooning on coronavirus disease rates after relaxing social distancing. Emerg Infect Dis. 2020;26:3066–8. https://doi.org/10.3201/eid2612.201930
15. Wang X, Du Z, Johnson KE, Pasco RF, Fox SJ, Lachmann M, et al. Effects of COVID-19 vaccination timing and risk prioritization on mortality rates, United States. Emerg Infect Dis. 2021;27:1976–9. https://doi.org/10.3201/eid2707.210118

Address for correspondence: Lauren Ancel Meyers, Department of Integrative Biology, University of Texas at Austin, 2415 Speedway #C0930, Austin, TX 78712, USA; email: laurenmeyers@austin.utexas.edu

Mpox in Children and Adolescents during Multicountry Outbreak, 2022–2023

Ana Hoxha,[1] Steven M. Kerr,[1] Henry Laurenson-Schafer, Nikola Sklenovská, Bernadette Basuta Mirembe, Ingrid Hammermeister Nezu, Patricia Ndumbi, Julia Fitzner, Maria Almiron, Marcelo Vila, Richard Pebody, Aisling M. Vaughan, Joana M. Haussig, Luis Alves de Sousa, Okot Charles Lukoya, Olaniyi Felix Sanni, Pierre Nabeth, Jeremias Domingos Naiene, Masaya Kato, Tamano Matsui, Krutika Kuppalli, Peter Omondi Mala, Rosamund F. Lewis, Olivier le Polain de Waroux, Boris I. Pavlin; WHO Mpox surveillance and Analytics Team

The 2022–2023 mpox outbreak predominantly affected adult men; 1.3% of reported cases were in children and adolescents <18 years of age. Analysis of global surveillance data showed 1 hospital intensive care unit admission and 0 deaths in that age group. Transmission routes and clinical manifestations varied across age subgroups.

Mpox is a zoonotic disease caused by monkeypox virus (MPXV) and previously found primarily in forested areas of Central and West Africa (*1*,*2*). In May 2022, a multicountry outbreak of mpox emerged; as of May 2023, there were >87,500 cases and 141 deaths reported from 111 World Health Organization (WHO) member countries (*3*). Globally 1.3% of reported cases during the outbreak have been in children and adolescents <18 years of age (*3*). During 1970–2021, mpox cases in Central Africa were predominately (54%–90%) reported in children (*4*–*6*), and children experienced more severe disease and adverse outcomes than adults (*6*,*7*).

After the first cases of mpox from countries without a history of the disease were reported to WHO in May 2022, a global surveillance system was established to collect aggregated data on probable and confirmed cases, as well as detailed case-based information on demographics, medical history, clinical manifestations, exposure factors, and testing (*8*). We describe epidemiologic and clinical characteristics of mpox in case-patients <18 years of age using surveillance data reported by all WHO regions during January 1, 2022–May 22, 2023 (https://www.who.int/publications/i/item/WHO-MPX-Surveillance-2022.4).

The Study

During the study period, 1.3% (1,118/84,614) of confirmed mpox cases globally were in patients <18 years of age. Most (61.8%, 691) were from the WHO Region of the Americas, followed by the African Region (30.3%, 339), the European Region (7.5%, 84), the Eastern Mediterranean Region, (<1%, 3), and the Western Pacific Region (<1%, 1) (Figure 1). No cases in patients <18 years of age were reported from the South-East Asia Region. Countries in the African Region reported mpox cases before the global outbreak (Figure 1), whereas reports of mpox cases in Europe and in the Americas began in May 2022 and peaked in July–August 2022. In Europe and the Americas, the epidemic curve of case-patients <18 years of age closely mimics the overall regional curves (*3*). The global percentage of case-patients <18 years of age has consistently remained low (0%–3%). By May 2023, overall case

Author affiliations: Health Emergencies Programme, World Health Organization (WHO), Geneva, Switzerland (A. Hoxha, H. Laurenson-Schafer, N. Sklenovska, B.B. Mirembe, I.H. Nezu, P. Ndumbi, J. Fitzner, K. Kuppalli, P.O. Mala, R.F. Lewis, O. le Polain de Waroux, B.I. Pavlin); CPC Analytics, Berlin, Germany (S.M. Kerr); WHO Regional Office for the Americas, Washington, DC, USA (M. Almiron, M. Vila); WHO Regional Office for Europe, Copenhagen, Denmark (R. Pebody, A.M. Vaughan); European Centre for Disease Prevention and Control, Solna, Sweden (J.M. Haussig, L. Alves de Sousa); WHO Regional Office for Africa, Brazzaville, Republic of the Congo (O.C. Lukoya, O.F. Sanni); WHO Regional Office for the Eastern Mediterranean, Cairo, Egypt (P. Nabeth, J.D. Naiene); WHO Regional Office for South-East Asia, Delhi, India (M. Kato); WHO Regional Office for the Western Pacific, Manila, Philippines (T. Matsui)

DOI: http://doi.org/10.3201/eid2910.230516

[1]These first authors contributed equally to this article.

counts were low across all regions; the Americas, the Eastern Mediterranean Region, and the Western Pacific Region reported sporadic case-patients <18 years of age. Among the 1,102 case-patients <18 years with available information, 59.3% (654) were male and 40.7% (448) female (Appendix Figure, https://wwwnc.cdc.gov/EID/article/29/10/23-0516-App1.pdf).

MPXV has 2 distinct clades, I and II (*9*). Virus clade information was not available for most cases and was assumed on the basis of the reporting country or subnational area and circulating clades in 2022, as reported by countries on GISAID (https://www.gisaid.org) or Nextstrain (https://nextstrain.org), in published literature, or to WHO. Of the 297 cases of mpox from countries reporting clade I, all age groups had a similar sex distribution (Appendix Figure, panel A). Of the 805 cases of mpox from countries reporting clade II, there were more male than female case-patients (269 vs. 104) among those 13–17 years of age. (For cases from Cameroon, 4 from eastern Cameroon are included in the clade I distribution, 1 from western Cameroon is included in the clade II distribution, and 1 for which we had no detailed geographic information was excluded.) Of case-patients with available hospitalization data, 47/335 (14.0%) were hospitalized and 1 was admitted to the intensive care unit; none was reported to have died.

Data on self-reported sexual behavior were limited for mpox case-patients <18 years of age. However, 37/166 (22.3%) of case-patients 13–17 years of age self-identified as men who have sex with men (MSM) (Table 1). Eleven cases involved persons living with

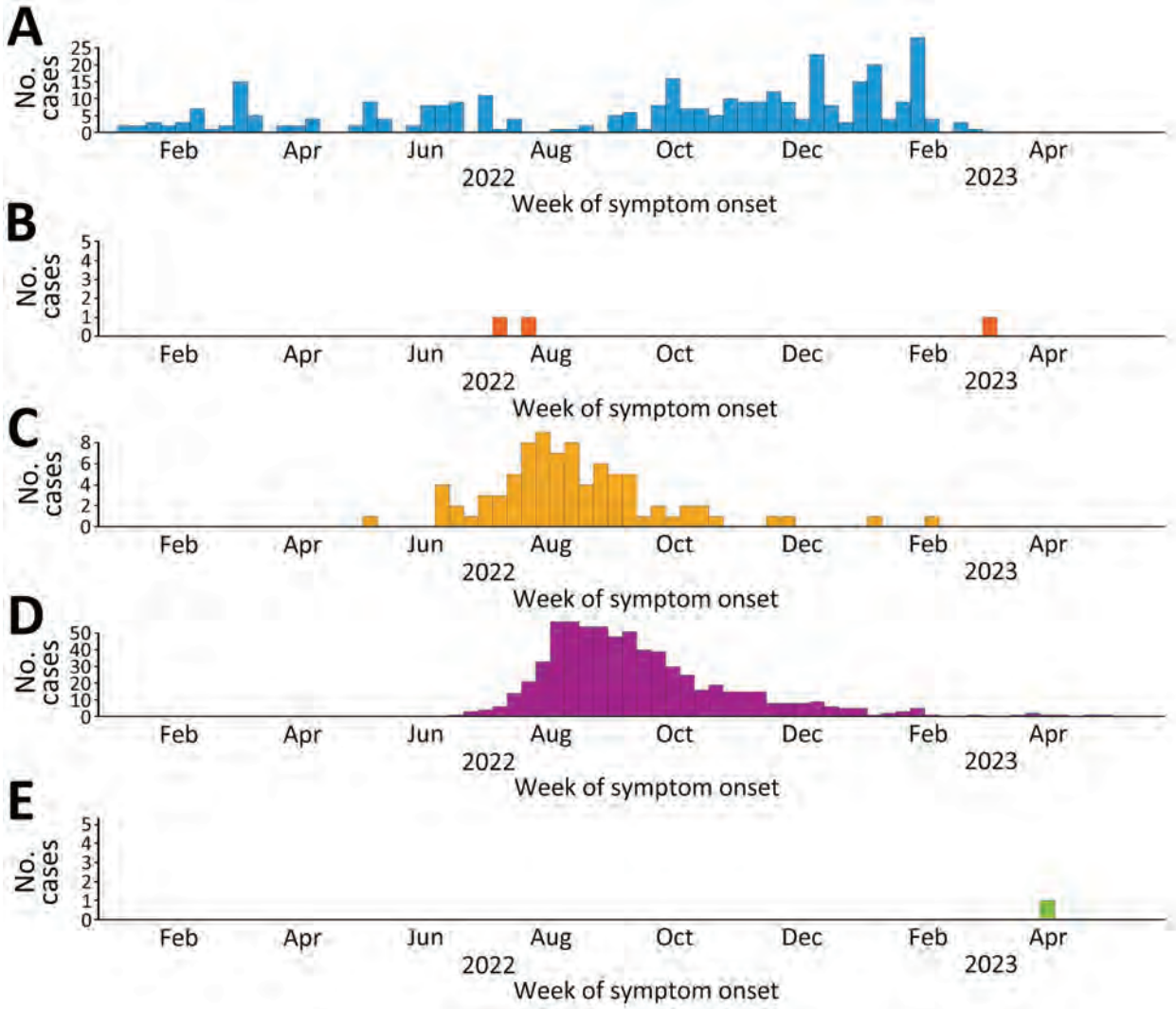

Figure 1. Epidemic curves of mpox cases among children and adolescents <18 years of age, grouped by World Health Organization regions, January 2022–May 2023. Dates represent the week of symptom onset, or the week of diagnosis or reporting if the date of symptom onset is unknown. A) African Region; B) Eastern Mediterranean Region; C) European Region; D) Region of the Americas; E) Western Pacific Region.

Table 1. Main epidemiologic characteristics of mpox in children and adolescents reported globally, January 2022–May 2023*

Characteristic	No. (%) case-patients, by age group			
	0–4 y	5–12 y	13–17 y	Total
Total	328 (29.3)	353 (31.6)	437 (39.1)	1,118 (100)
Sex				
M	168 (51.2)	182 (51.6)	304 (69.6)	654 (58.5)
F	154 (47.0)	170 (48.2)	124 (28.4)	448 (40.1)
Unknown	6 (1.8)	1 (0.3)	9 (2.1)	16 (1.4)
Sexual behavior				
MSM	0	0	37 (8.5)	37 (3.3)
Non-MSM	0	43 (12.2)	119 (27.2)	162 (14.5)
Unknown	328 (100.0)	310 (87.8)	281 (64.3)	919 (82.2)
HIV status				
HIV+	0	2 (0.6)	9 (2.1)	11 (1.0)
HIV–	84 (25.6)	94 (26.6)	163 (37.3)	341 (30.5)
Unknown	244 (74.4)	257 (72.8)	265 (60.6)	766 (68.5)
Immunosuppressed				
Yes	1 (0.3)	2 (0.6)	4 (0.9)	7 (0.6)
No	116 (35.4)	119 (33.7)	176 (40.3)	411 (36.8)
Unknown	211 (64.3)	232 (65.7)	257 (58.8)	700 (62.6)
Known epidemiological link				
Yes	26 (7.9)	18 (5.1)	23 (5.3)	67 (6.0)
No	41 (12.5)	51 (14.4)	134 (30.7)	226 (20.2)
Unknown	261 (79.6)	284 (80.5)	280 (64.1)	825 (73.8)

*Percentages are calculated by column for each epidemiologic characteristic grouping. Unknown means that the information for the variable is missing. MSM, men who have sex with men.

HIV, 1 of whom was immunosuppressed. Another 6 case-patients reported immunosuppression, as defined by their care providers, that was caused by undisclosed medical conditions. Overall, 67/293 (22.9%) of cases with information provided had a stated epidemiologic link to a known mpox case.

Case-patients 0–12 years of age were exposed to MPXV mainly through physical person-to-person contact (excluding sexual contact) or contact with fomites, whereas exposure through sexual encounter was exclusively reported by those 13–17 years of age (Figure 2). Among the older group, some of whom self-identified as MSM, sexual transmission may explain the unequal sex distribution of clade II cases (Appendix Figure, panel B). The type of transmission was reported as other in 32/118 (27.1%) of cases, without additional information.

Among cases with data, 472/542 (87.1%) experienced symptoms (Table 2). We excluded from analysis cases reported to be symptomatic but without any specific symptom. The presence of any rash, which consisted of ≥1 rash symptoms (on the body, oral, genital, or unknown location), was the predominant symptom for all age groups (325/542, 60%); genital rash was present in 54/229 (23.6%) of case-patients 13–17 years of age and 19/313 (6.1%) of those <13 years of age ($p<0.00001$). Among case-patients 13–17 years of age who reported being infected through sexual contact, genital rash was present in 15/34 (44.1%). Genital rash may be indicative of the transmission route of mpox but can also be present when transmission has not occurred through sexual contact. After rash, the most reported symptoms were fever (270/542, 49.8%) and headache (158/542, 29.2%). Lymphadenopathy has been reported as a common mpox symptom (*1*,*6*); it was reported in 60/542 (11.1%) of cases in our study.

Conclusions

During this outbreak, countries with high caseloads reported most of the case-patients <18 years of age, however, the percentage of pediatric and adolescent patients in those countries was lower than that for adults. The percentage of patients <18 years of age was lower than had been feared early in the outbreak, amid concerns that the epidemic could shift from primarily affecting MSM to a more generalized epidemic spread, including among school-age children. Epidemiologic and clinical characteristics were similar for the age groups 0–4 and 5–12 years, whereas case-patients 13–17 years of age, who are more likely to be sexually active, commonly reported MSM sexual behavior, exposure through sexual contact, and having more genital lesions.

Studies from the Netherlands (*10*), Spain (*11*), England (*12*), and the United States (*13*,*14*) have described MPXV infection among children and adolescents during this outbreak. Consistent with our findings, most cases in those studies reported no intensive care unit admissions or deaths; WHO is aware of the death of an infant from mpox clade I for which data are not available (*3*). Our results differ from historical reports of mpox in children, in which they have been described as at higher risk for adverse events and

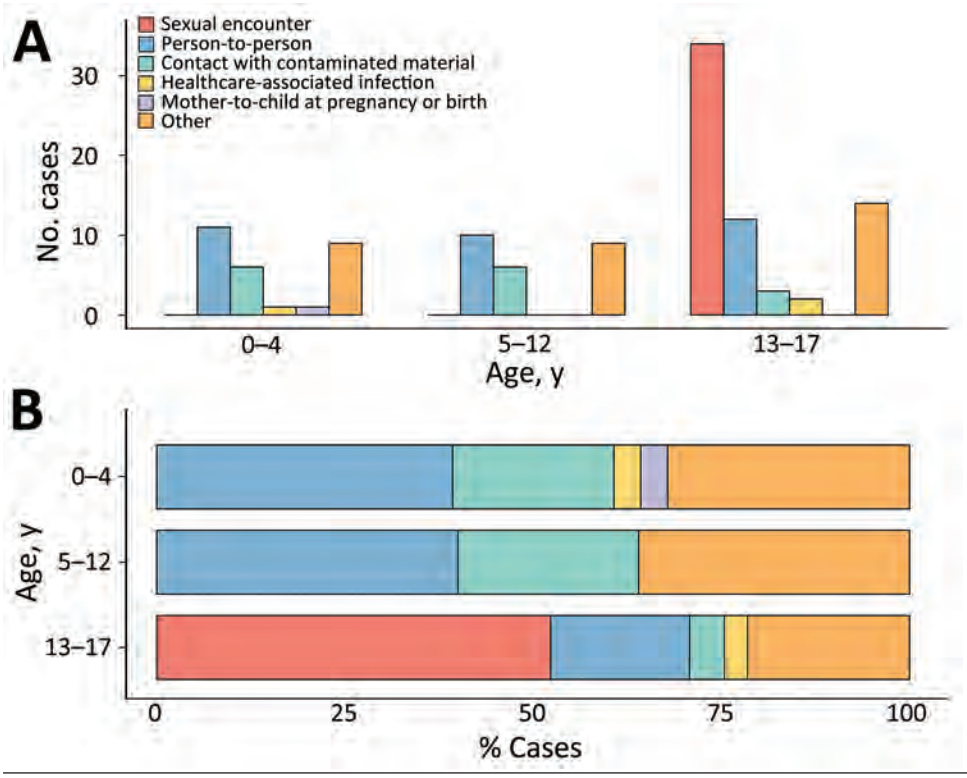

Figure 2. Mpox cases by transmission type by age group among children and adolescents <18 years of age, as reported globally to the World Health Organization, January 2022–May 2023. A) Absolute numbers; B) percentage among all cases with available information.

death related to disease (*15*). A previous study using the same surveillance data found higher odds of hospitalization for children <5 years of age than for those 15–45 years of age (*8*). The lower observed severity in children and adolescents in this outbreak than for previous outbreaks may be caused by a combination of increased ascertainment of mild cases, differing access to healthcare between settings, differing health status of the host populations, and lower virulence of clade IIb MPXV; clade I MPXV infection has been reported to be associated with higher severity than clade II (*1*).

Our study is based on surveillance data and likely underestimates the true number of case-patients <18 years of age, particularly in Africa (*8*). Disease severity may be underestimated because countries may not have updated case outcomes if hospitalization or death was delayed. Finally, data completeness varied

Table 2. Main symptoms of mpox in children and adolescents reported globally among cases with symptom data, January 2022–May 2023*

Characteristic	No. (%) case-patients, by age group			
	0–4 y	5–12 y	13–17 y	Total
Total	156 (28.8)	157 (28.9)	229 (42.3)	542 (100)
Any symptoms				
Yes	124 (79.5)	132 (84.1)	216 (94.3)	472 (87.1)
No	32 (20.5)	25 (15.9)	13 (5.7)	70 (12.9)
Any rash				
Yes	77 (49.4)	84 (53.5)	164 (71.6)	325 (60.0)
No	79 (50.6)	73 (46.5)	65 (28.4)	217 (40.0)
Genital rash				
Yes	8 (5.1)	11 (7.0)	54 (23.6)	73 (13.5)
No	148 (94.9)	146 (93.0)	175 (76.4)	469 (86.5)
Fever				
Yes	66 (42.3)	73 (46.5)	131 (57.2)	270 (49.8)
No	90 (57.7)	84 (53.5)	98 (42.8)	272 (50.2)
Headache				
Yes	18 (11.5)	44 (28.0)	96 (41.9)	158 (29.2)
No	138 (88.5)	113 (72.0)	133 (58.1)	384 (70.8)
Any lymphadenopathy				
Yes	4 (2.6)	11 (7.0)	45 (19.7)	60 (11.1)
No	152 (97.4)	146 (93.0)	184 (80.3)	482 (88.9)

*Percentages are calculated by column for each symptom.

among regions and countries; thus, our results may not be representative of each setting.

This study highlights the need for thorough epidemiologic investigation of mpox in children and adolescents. Clinicians should consider mpox as a possible diagnosis in these age groups when they have indicative symptoms, even with no known epidemiologic link to another case.

Acknowledgments

We thank all WHO Member States and their health workers for their engagement and detailed reporting of case-based information to WHO and other regional institutions, in line with temporary recommendations issued by the WHO Director-General under the Public Health Emergency of International Concern within the framework of the International Health Regulations (IHR 2005). Reporting to WHO was made possible through a global collaborative effort involving healthcare professionals, epidemiologists, and public health workers from across the world, to whom we are deeply grateful. For the WHO European Region, we used data reported by countries to ECDC and WHO through The European Surveillance System (TESSy; https://www.ecdc.europa.eu/en/publications-data/european-surveillance-system-tessy).

This work was supported by the World Health Organization contingency fund for emergencies.

About the Author

Dr. Hoxha is an infectious disease epidemiologist working for WHO Geneva, with special interest in surveillance systems, outbreak investigation, emergency response and epidemiological methods for public health. Mr. Kerr is a data analyst with CPC Analytics supporting the WHO Hub for Pandemic and Epidemic Intelligence in Berlin. His interests include disease modeling, monitoring and evaluation of global health surveillance, and global health disparities.

References

1. Gessain A, Nakoune E, Yazdanpanah Y. Monkeypox. 2022. 387:1783–93. https://www.nejm.org/doi/full/10.1056/NEJMra2208860
2. World Health Organization. Epidemiology of human monkeypox (mpox)— worldwide, 2018–2021. 2023 [cited 2023 Mar 23]. https://apps.who.int/iris/handle/10665/365630
3. World Health Organization. 2022–23 mpox (monkeypox) outbreak: global trends. 2023 [cited 2023 May 24]. https://worldhealthorg.shinyapps.io/mpx_global
4. Besombes C, Mbrenga F, Schaeffer L, Malaka C, Gonofio E, Landier J, et al. National monkeypox surveillance, Central African Republic, 2001–2021. Emerg Infect Dis. 2022;28:2435–45. https://doi.org/10.3201/eid2812.220897
5. Lourie B, Bingham PG, Evans HH, Foster SO, Nakano JH, Herrmann KL. Human infection with monkeypox virus: laboratory investigation of six cases in West Africa. Bull World Health Organ. 1972;46:633. **PMID:** 4340223
6. Ježek Z, Szczeniowski M, Paluku KM, Mutombo M. Human monkeypox: clinical features of 282 patients. J Infect Dis. 1987;156:293–8 https://doi.org/10.1093/infdis/156.2.293
7. Jezek Z, Marennikova SS, Mutumbo M, Nakano JH, Paluku KM, Szczeniowski M. Human monkeypox: a study of 2,510 contacts of 214 patients. J Infect Dis. 1986;154:551–5. https://doi.org/10.1093/infdis/154.4.551
8. Laurenson-Schafer H, Sklenovská N, Hoxha A, Kerr SM, Ndumbi P, Fitzner J, et al.; WHO mpox Surveillance and Analytics team. Description of the first global outbreak of mpox: an analysis of global surveillance data. Lancet Glob Health. 2023;11:e1012–23. https://doi.org/10.1016/S2214-109X(23)00198-5
9. Ulaeto D, Agafonov A, Burchfield J, Carter L, Happi C, Jakob R, et al. New nomenclature for mpox (monkeypox) and monkeypox virus clades. Lancet Infect Dis. 2023;23:273–5 https://doi.org/10.1016/S14733099(23)00055-5
10. Tutu van Furth AM, van der Kuip M, van Els AL, Fievez LCR, van Rijckevorsel GGC, van den Ouden A, et al. Paediatric monkeypox patient with unknown source of infection, the Netherlands, June 2022. Euro Surveill. 2022;27:2200552. https://doi.org/10.2807/1560-7917.ES.2022.27.29.2200552
11. Aguilera-Alonso D, Alonso-Cadenas JA, Roguera-Sopena M, Lorusso N, Miguel LGS, Calvo C. Monkeypox virus infections in children in Spain during the first months of the 2022 outbreak. Lancet Child Adolesc Health. 2022;6:e22–3. https://doi.org/10.1016/S2352-4642(22)00250-4
12. Ramnarayan P, Mitting R, Whittaker E, Marcolin M, O'Regan C, Sinha R, et al.; NHS England High Consequence Infectious Diseases (Airborne) Network. Neonatal monkeypox virus infection. N Engl J Med. 2022;387:1618–20. https://doi.org/10.1056/NEJMc2210828
13. Saunders KE, Van Horn AN, Medlin HK, Carpenter A, Lee PA, Gutierrez L, et al. Monkeypox in a young infant—Florida, 2022. MMWR Morb Mortal Wkly Rep. 2022;71:1220–1. https://doi.org/10.15585/mmwr.mm7138e3
14. Hennessee I, Shelus V, McArdle CE, Wolf M, Schatzman S, Carpenter A, et al.; California Department of Public Health Monkeypox Pediatric Working Group; CDC Monkeypox Pediatric Working Group. Epidemiologic and clinical features of children and adolescents aged <18 years with monkeypox—United States, May 17–September 24, 2022. MMWR Morb Mortal Wkly Rep. 2022;71:1407–11. https://doi.org/10.15585/mmwr.mm7144a4
15 Bunge EM, Hoet B, Chen L, Lienert F, Weidenthaler H, Baer LR, et al. The changing epidemiology of human monkeypox— potential threat? A systematic review. PLoS Negl Trop Dis. 2022;16:e0010141. https://doi.org/10.1371/journal.pntd.0010141

Address for correspondence: Ana Hoxha, World Health Organization, Avenue Appia 20, 1211 Geneva, Switzerland; email: hoxhaa@who.int

Outbreak of Sexually Transmitted Nongroupable *Neisseria meningitidis*–Associated Urethritis, Vietnam

Hao Trong Nguyen,[1] Thanh V. Phan,[1] Hau Phuc Tran, Thao Thi Phuong Vu, Nhi Thi Uyen Pham, Tho Thi Thanh Nguyen, Ha Manh Bui, Bao Hac Duong, Thu Nguyen Anh Luu, Nguyen Nhat Pham, Phuc Duy Nguyen, Tu Ngoc Le, Thu Quang Le, Dai Thi Trang Vo, Lan Trong Phan, Nghia Van Khuu, Quang Duy Pham, Thuong Vu Nguyen

We report on an outbreak of nongroupable *Neisseria meningitidis*–associated urethritis, primarily among men who have sex with men in southern Vietnam. Nearly 50% of *N. meningitidis* isolates were resistant to ciprofloxacin. This emerging pathogen should be considered in the differential diagnosis and management of urethritis.

Urogenital and anorectal infections caused by *Neisseria meningitidis* have been reported in several countries and found to be more prevalent among men who have sex with men (MSM) than among heterosexual men or women (*1*–*3*). During 2013–2016, rising numbers of a novel clade of nongroupable *N. meningitidis* (NmNG) urethritis were reported in multiple US cities and have been termed US NmNG urethritis clade (*4*). Two cases of US NmNG urethritis were also documented among MSM in the United Kingdom in 2019 (*5*). We report an outbreak of urethritis associated with US NmNG urethritis clade among men in southern Vietnam.

The Study

We conducted a matched case–control study to investigate *N. meningitidis* urethritis and risk factors in men seeking treatment for urinary discharge at Ho Chi Minh City Hospital of Dermato-Venereology (HHDV; Ho Chi Minh City, Vietnam). Cases of *N. meningitidis* urethritis were confirmed by either real-time PCR or culture of urethral discharge. Controls were matched to case-patients by age range and sexual orientation (Appendix, https://wwwnc.cdc.gov/EID/article/29/10/22-1596-App1.pdf). During September 2019–December 2020, we recruited 19 case-patients and 76 controls from HHDV (Appendix Figure 1). We collected information on sociodemographic factors, sexual behaviors, and medical history by face-to-face interviews and from medical records (Appendix). The HHDV institutional review board approved the study.

We identified *N. meningitidis* by using bacterial culture and real-time PCR targeting the *sodC* gene (*6*) and determined serogroups by using latex agglutination and real-time PCR. We performed antimicrobial susceptibility testing according to Clinical and Laboratory Standards Institute guidelines (*7*). We conducted whole-genome sequencing, then analyzed multilocus sequence types (MLST) in PubMLST (https://pubmlst.org/organisms/neisseria-spp). We used BEAST (http://beast.community) to estimate the time of bacterial arrival in Vietnam and to conduct antimicrobial-resistance typing (Appendix). We performed conditional logistic regression to assess risk factors for US NmNG urethritis clade by using Stata 14 (StataCorp LLC, https://www.stata.com). We used a log likelihood-ratio test to select the best-fitting model (Appendix).

The mean age of case-patients was lower than that of controls (26.9 vs. 27.8 years). Condom use was low in both case-patients and controls before pyuria developed (5.3% of case-patients, 2.7% of

Author affiliations: Ho Chi Minh City Hospital of Dermato-Venereology, Ho Chi Minh City, Vietnam (H.T. Nguyen, T.T.P. Vu, N.T.U. Pham, T.T.T. Nguyen, H.M. Bui, B.H. Duong, T.N.A. Luu, N.N. Pham); Pasteur Institute of Ho Chi Minh City, Ho Chi Minh City (T.V. Phan, H.P. Tran, P.D. Nguyen, T.N. Le, T.Q. Le, D.T.T. Vo, L.T. Phan, N.V. Khuu, Q.D. Pham, T.V. Nguyen)

DOI: https://doi.org/10.3201/eid2910.221596

[1]These first authors contributed equally to this article.

Table 1. Correlates of several selected factors among male patients with *Neisseria meningitidis* US NmNG urethritis and controls, Vietnam*

Variables	Cases, n = 19	Controls, n = 76	Univariable analysis† OR (95% CI)	p value	Multivariable analysis† aOR (95% CI)	p value
Mean age, y	26.9	27.8	0.90 (0.75–1.07)	0.232	NA	
Mean years of education	10.8	11.0	0.96 (0.75–1.23)	0.760		
Currently living in Ho Chi Minh City	14 (73.4)	56 (73.7)	1.00 (0.30–3.28)	>0.999		
Living arrangements						
Live with a female partner	1 (5.3)	22 (30.1)	Referent		Referent	
Live with a male partner	8 (42.1)	10 (13.7)	17.03 (1.83–158.26)	0.013	14.41 (1.01–204.62)	0.049
Other, e.g., live alone, or with friends or family	3 (15.8)	12 (16.4)	5.44 (0.65–45.54)	0.118	7.0 (0.61–80.24)	0.118
Ever had sex with						
Male sexual partners	14 (73.7)	49 (64.5)	Referent			
Female sexual partners	4 (21.1)	16 (21.1)	0.41 (0.02–7.54)	0.551		
Both male and female partners	1 (5.3)	11 (14.5)	0.17 (0.01–3.17)	0.238		
Ever had oral sex	19 (100.0)	74 (97.4)	NA			
Ever participated in group sex	1 (5.3)	2 (2.6)	2 (0.18–22.06)	0.571		
During past 12 mo						
Oral or vaginal sex with female partner	4 (21.1)	44 (57.9)	0.10 (0.02–0.47)	0.004	0.13 (0.02–0.87)	0.035
Oral or anal sex with male partner	15 (78.9)	39 (51.3)	10.57 (1.28–87.34)	0.029	NA	
Any casual partners	5 (26.3)	34 (44.7)	0.39 (0.12–1.32)	0.131	NA	
Commercial sex worker partner	3 (15.8)	28 (36.8)	0.30 (0.08–1.15)	0.078		
Drunkenness during sex	3 (15.8)	23 (30.3)	0.33 (0.07–1.65)	0.177		
Sex with a foreign-born partner in the past month	3 (15.8)	1 (1.3)	12.0 (1.25–115.36)	0.031	26.78 (1.03–697.82)	0.048
Condom use during sex before symptom onset‡	1 (5.3)	2 (2.7)	1.81 (0.16–20.08)	0.628		
Used social media sites to find sexual partners	13 (68.4)	32 (42.1)	4.07 (1.17–14.13)	0.027	NA	
Ever used ATS§	1 (5.3)	4 (5.3)	1.00 (0.10–10.07)	>0.999		

*Values are no. (%) except as indicated. ATS, amphetamine-type stimulants; aOR, adjusted odds ratio; NA, not applicable; OR, odds ratio.
†Conditional logistic regression.
‡Symptoms were pyuria, dysuria, or both.
§Ecstasy, crystal meth (methamphetamine), or other substances used to increase excitement when having sex (also called chemsex).

Table 2. Correlates of demographic characteristics, STI symptoms and pathogens among male patients with *N. meningitidis* US NmNG urethritis and controls, Vietnam*

Variables	Cases, n = 19	Controls, n = 76	Univariable analysis† OR (95% CI)	p value	Multivariable analysis† aOR (95% CI)	p value
Mean age, y	26.9	27.8	0.90 (0.75–1.07)	0.232	NA	
Mean years of education	10.8	11.0	0.96 (0.75–1.23)	0.760	NA	
Medical examination ≥3 d after symptom onset	13 (68.4)	11 (14.5)	18.41 (4.04–83.86)	<0.001	16.00 (2.00–127.54)	0.009
Symptoms						
Pyuria	2 (10.5)	10 (13.2)	0.79 (0.16–3.79)	0.764	NA	
Dysuria	13 (68.4)	65 (85.5)	0.39 (0.12–1.19)	0.098	NA	
Burning sensation during urination	2 (10.5)	57 (75.0)	0.05 (0.01–0.22)	<0.001	0.08 (0.01–0.46)	0.005
Discharge	4 (21.1)	16 (21.1)	1.00 (0.26–3.89)	>0.999		
Time between symptom onset and medical consultation, d						
Mean	4.7	3.0	1.92 (1.18–3.13)	0.009	NA	
Median (range)	5 (3–12)	3 (1–14)				
History of meningococcal vaccine						
Ever	0	1 (1.3)	NA			
Never	12 (63.2)	51 (67.1)	NA			
Do not know, do not remember	7 (36.8)	24 (31.6)	NA			
Positive tests						
HIV	2 (10.5)	6 (7.9)	1.36 (0.26–7.20)	0.716	NA	
Syphilis	2 (10.5)	3 (3.9)	2.67 (0.45–15.96)	0.283	NA	
Gonorrhea	0 (0.0)	75 (98.7)	NA		NA	
Chlamydia	4 (21.1)	7 (9.2)	2.57 (0.67–9.83)	0.168	3.83 (0.37–39.43)	0.258
Ureaplasma	1 (5.3)	8 (10.5)	0.48 (0.06–4.01)	0.502	NA	
Mycoplasma	1 (5.3)	10 (13.2)	0.39 (0.04–3.10)	0.372	NA	

*Values are no. (%) except as indicated. aOR, adjusted odds ratio; NA, not applicable; OR, odds ratio.
†Conditional logistic regression.

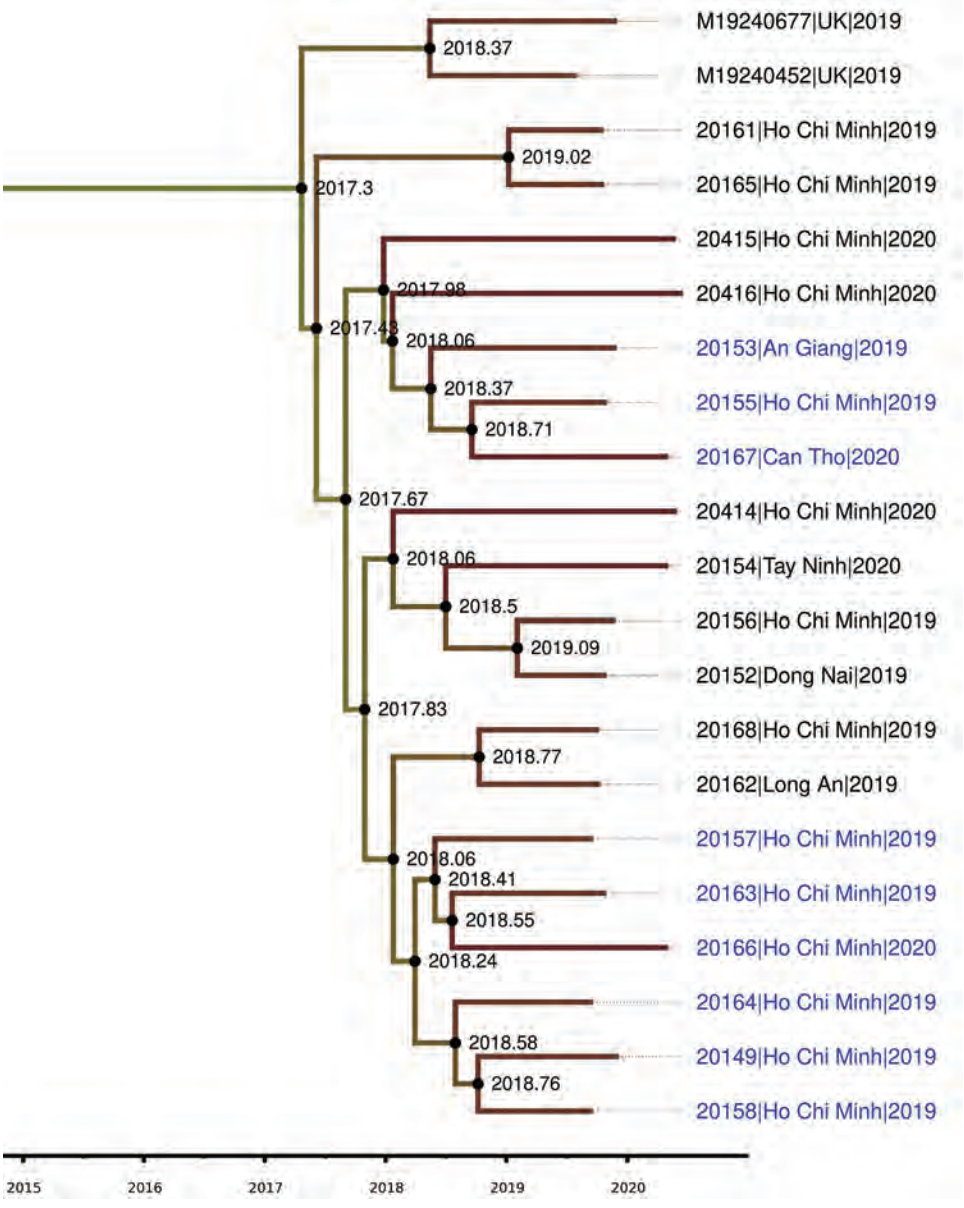

Figure 1. Phylogenetic tree of isolates from an outbreak of sexually transmitted nongroupable *Neisseria meningitidis*–associated urethritis, Vietnam. Phylogenetic tree was constructed using Baysian Skygrid model, performing with BEAST/BEAGLE version 1.10.4 (https://beast.community/beagle), and displaying with FigTree version 1.4.4 (http://tree.bio.ed.ac.uk/software/Figtree). Blue text indicates ciprofloxacin-resistant strains. Scale bar indicates the time of evolutionary history.

controls). More case-patients than controls lived with male partners (42.1% vs. 13.7%) and had sex with foreign-born persons (15.8% vs. 1.3%). Multivariate analysis results showed that persons living with male partners (adjusted odds ratio [aOR] 14.41, 95% CI 1.01–204.62) and having sex with foreign-born persons (aOR 26.78, 95% CI 1.03–697.82) were more likely to contract US NmNG urethritis (Table 1). Moreover, most (79%) case-patients reported sex with male partners. Persons having oral or vaginal sex with female partners in the past 12 months were less likely to have US NmNG urethritis (aOR 0.13, 95% CI 0.02–0.87). Those findings suggest that the US NmNG outbreak was concentrated within the MSM population.

Among 19 case-patients, 7 were co-infected with ≥1 other pathogen: 2 (11%) cases of syphilis, 4 (21%) cases of chlamydia, and 1 (0.1%) case involving both ureaplasma and mycoplasma. Ten (83%) case-patients without co-infections and 6 (86%) with co-infections experienced ≥1 symptom. Pyuria was reported in 2 (29%) co-infected case-patients, and dysuria was reported in 10 (83%) case-patients without co-infections and 3 (43%) with co-infections (Appendix Table 1). Most participants had not received meningococcal

vaccines, nor recalled being vaccinated against *N. meningitidis* (Table 2). The prevalence of HIV, syphilis, and chlamydia infections was higher among case-patients compared to controls but not statistically significant, whereas gonorrhea was only found in controls (98.7%) (Table 2). Multivariate analysis showed that those who had US NmNG urethritis were less likely to report burning sensations during urination (odds ratio [OR] 0.08, 95% CI 0.01–0.46) and more likely to delay seeking treatment (OR 16.0, 95% CI 2.0–127.54) (Table 2).

In this study, uncomplicated gonorrhea was treated with a single 500-mg intramuscular dose of ceftriaxone, followed by either a 7-day course of doxycycline (100 mg 2×/day) or a single 1,000-mg dose of azithromycin. In Vietnam, gonococci isolated in 2011 and during 2015–2016 increasingly resisted antimicrobial drugs except for ceftriaxone, spectinomycin, and azithromycin (*8*). Moreover, 98.3% of *N. gonorrhoeae* isolates were ciprofloxacin-resistant (*9*). In a national survey conducted in Vietnam, 30% of persons reported purchasing antibiotics primarily for addressing symptoms, including genitourinary manifestations, and 81.7% did so without a prescription; ciprofloxacin was among the top 5 antimicrobial drugs acquired (*10*). In another study among MSM in Vietnam, 64% reported ever taking antibiotics without a prescription (*11*).

The US NmNG urethritis clade in our study displayed intermediate susceptibility to penicillin, with MIC values ranging from 0.125–0.38 mg/L. Nine of the 19 isolates demonstrated resistance to ciprofloxacin (MIC 0.19–3.0 μg/mL). MLST analysis revealed that the isolates belonged to the sequence type 11 complex (Appendix Table 2). A phylogenetic tree displayed the isolates from Vietnam and the United Kingdom forming a monophyletic clade with those from Ohio, USA, one of the 2 US NmNG urethritis clades (*12*) (Appendix Figure 2). BEAST analysis estimated that the time of most recent common ancestor of Vietnam and UK isolates appeared between 2016 and 2018 (median 2017.3; 95% high posterior density interval 2016.4–2018.1), with a Bayesian posterior probability of 1.0 (Figure 1; Appendix Figure 3).

All isolates carried the penA_316 allele and point mutations that reduced their susceptibility to penicillin (*13*). Nine ciprofloxacin-resistant isolates

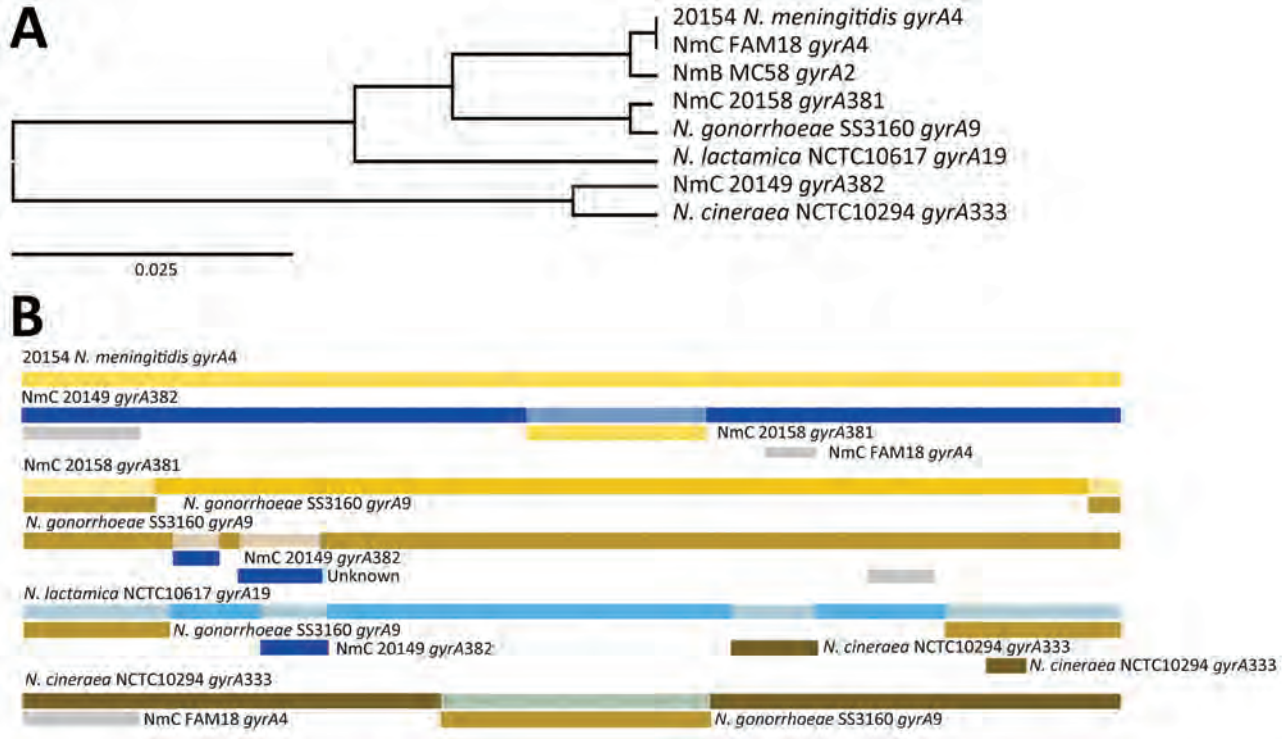

Figure 2. Whole-genome analysis of isolates from an outbreak of sexually transmitted nongroupable *Neisseria meningitidis*–associated urethritis, Vietnam. Comparison generated in RDP4 (https://rdp4.software.informer.com) for full length of 2,751-bp. A) Tree shows the genetic relationship between isolate 20158_*gyrA381* and gonococci_*gyrA9* using unweighted pair group method with arithmetic mean of the region derived from their parents, beginning at 1 to ending breakpoint at 337 bp. B) Bars show potential recombination breakage points identified with at least 1 of the 7 methods contained in RDP4. NmB, *N. meningitidis* B; NmC, *N. meningitidis* C.

exhibited 2 new alleles in *gyrA*, assigned as *gyrA*_381 (n = 8), which had dual mutations at T91F and D95A, and *gyrA*_382, which had monomutation at T91I. We used RDP4 (https://rdp4.software.informer.com) to analyze the full 2,751-bp length and found that *gyrA*_381 received a fragment containing a mutation from gonococci (Figure 2). Our study revealed that isolates containing mutations at both T91F and D95A in the *gyrA* gene displayed a high level of resistance to ciprofloxacin, similar to that found in *N. gonorrhoeae* (*14*). Moreover, isolate 20158 had a mutation at S87R of *parC* and the *gyrA*_381 allele had an elevated MIC of 3 μg/mL.

The emergence of ciprofloxacin-resistant *N. meningitidis* US NmNG urethritis clade in Vietnam is a major concern, especially considering ciprofloxacin resistance is rare in the United Kingdom and United States (*4*,*5*). A previous study observed that strains with MICs ≥0.064 mg/L were correlated with alterations in *gyrA* (*15*). Hence, when specimens cannot be cultured, *gyrA*-sequencing can be particularly useful in predicting susceptibility of ciproloxacin.

Conclusions

We report an outbreak of US NmNG urethritis among men in Vietnam, predominantly MSM. Having sex with foreign-born persons and living with male partners were factors strongly associated with the disease. Isolates in this outbreak might have originated from the Ohio (USA) clade and were mainly resistant to ciprofloxacin, which is commonly used for prophylaxis against invasive meningococcal diseases in Vietnam.

Symptoms among patients with US NmNG urethritis were milder than those in controls with gonococcal urethritis. Because US NmNG urethritis is less likely than gonococcal urethritis to manifest symptoms, clinicians should consider *N. meningitidis* when managing patients with urethral discharge. Bacterial culture should be routinely performed on urethritis specimens that test *N. gonorrhoeae*–negative by nucleic acid amplification tests to determine whether the infection is caused by *N. meningitidis*. More studies with larger sample sizes should be conducted to provide a more comprehensive picture of the burden and clinical symptoms of US NmNG urethritis.

In conclusion, our findings emphasize the importance of ongoing monitoring of appropriate use of antibiotics and antimicrobial resistance to prevent the further spread of resistant US NmNG urethritis clade. Thus, clinicians should be aware of this emerging bacterium and include US NmNG in the differential diagnosis for urethitis.

Acknowledgments

We thank colleagues from Pasteur Institute of Ho Chi Minh's Laboratory of Respiratory Bacteria and Ho Chi Minh City Hospital of Dermato-Venereology for assisting in the data collection and testing of specimens. We thank Wendy Aft and Minh-Thu Hoang Nguyen for carefully editing the first manuscript. We also thank Richard Yanagihara for his valuable comments and thoroughly editing the revised manuscript.

The findings and conclusions in this publication are those of the authors and do not necessarily represent the official position of the government of Vietnam, the Ministry of Health, the Pasteur Institute of Ho Chi Minh City, and the Ho Chi Minh City Hospital of Dermato-Venereology.

Authors contributions: H.T.N., T.V.P., Q.D.P., and T.V.N. conceived the work and designed the study. H.T.N. oversaw the data collection at the hospital, and T.V.P.was responsible for testing the specimens. T.V.N., H.T.N, T.V.P., and H.P.T.oversaw the study, interpreted the results and compiled the manuscript. T.T.PU, N.T.U.P., T.T.TN., H.M.B, B.H.D., T.N.A.L, and N.N.P. conducted data collection from patients and assisted in data management and analysis. P.D.N, N.V.K, T.N.L., Q.D.P., T.Q.L., H.P.T., D.V.T.T., and L.T.P contributed to data management and analysis. All authors approved the final manuscript.

About the Authors

Dr. H.T. Nguyen is a senior researcher in Ho Chi Minh City Hospital of Dermato-Venereology, Vietnam. His research interests include clinical dermatology and sexually transmitted diseases. Mr. Phan is a microbiologist at Pasteur Institute in Ho Chi Minh City, Vietnam. His research interests focus on the agents that cause bacterial meningitis, particularly *Neisseria meningitidis* and *Streptococcus pneumoniae*.

References

1. Maini M, French P, Prince M, Bingham JS. Urethritis due to *Neisseria meningitidis* in a London genitourinary medicine clinic population. Int J STD AIDS. 1992;3:423–5. https://doi.org/10.1177/095646249200300604
2. Hayakawa K, Itoda I, Shimuta K, Takahashi H, Ohnishi M. Urethritis caused by novel *Neisseria meningitidis* serogroup W in man who has sex with men, Japan. Emerg Infect Dis. 2014;20:1585–7. https://doi.org/10.3201/eid2009.140349
3. Givan KF, Keyl A. The isolation of *Neisseria* species from unusual sites. Can Med Assoc J. 1974;111:1077–9.
4. Retchless AC, Kretz CB, Chang H-Y, Bazan JA, Abrams AJ, Norris Turner A, et al. Expansion of a urethritis-associated *Neisseria meningitidis* clade in the United States with concurrent acquisition of *N. gonorrhoeae* alleles. BMC Genomics. 2018;19:176. https://doi.org/10.1186/s12864-018-4560-x

5. Brooks A, Lucidarme J, Campbell H, Campbell L, Fifer H, Gray S, et al. Detection of the United States *Neisseria meningitidis* urethritis clade in the United Kingdom, August and December 2019—emergence of multiple antibiotic resistance calls for vigilance. Euro Surveill. 2020;25:2000375. https://doi.org/10.2807/1560-7917.ES.2020.25.15.2000375
6. World Health Organization. Laboratory methods for the diagnosis of meningitis caused by *Neisseria meningitidis, Streptococcus pneumoniae*. Geneva: The Organization; 2011.
7. Clinical and Laboratory Standards Institute. Performance standards for antimicrobial susceptibility testing; thirtieth informational supplement (M100–S30). Wayne (PA): The Institute; 2020.
8. Lan PT, Golparian D, Ringlander J, Van Hung L, Van Thuong N, Unemo M. Genomic analysis and antimicrobial resistance of *Neisseria gonorrhoeae* isolates from Vietnam in 2011 and 2015–16. J Antimicrob Chemother. 2020;75:1432–8. https://doi.org/10.1093/jac/dkaa040
9. Adamson PC, Van Le H, Le HHL, Le GM, Nguyen TV, Klausner JD. Trends in antimicrobial resistance in *Neisseria gonorrhoeae* in Hanoi, Vietnam, 2017–2019. BMC Infect Dis. 2020;20:809. https://doi.org/10.1186/s12879-020-05532-3
10. Nguyen TTP, Do TX, Nguyen HA, Nguyen CTT, Meyer JC, Godman B, et al. A national survey of dispensing practice and customer knowledge on antibiotic use in Vietnam and the implications. Antibiotics (Basel). 2022;11:1091. https://doi.org/10.3390/antibiotics11081091
11. Dong HV, Hoa NT, Minh NXB, Trung NV, May F, Giang LM, et al. Antibiotic usage and commensal pharyngeal *Neisseria* of MSM in Hanoi, Vietnam. Sex Transm Infect. 2017;93:A52–3. https://doi.org/10.1136/sextrans-2017-053264.131
12. Bazan JA, Peterson AS, Kirkcaldy RD, Briere EC, Maierhofer C, Turner AN, et al. Notes from the field: increase in *Neisseria meningitidis*-associated urethritis among men at two sentinel clinics—Columbus, Ohio, and Oakland County, Michigan, 2015. MMWR Morb Mortal Wkly Rep. 2016;65:550–2. https://doi.org/10.15585/mmwr.mm6521a5
13. Taha MK, Vázquez JA, Hong E, Bennett DE, Bertrand S, Bukovski S, et al. Target gene sequencing to characterize the penicillin G susceptibility of *Neisseria meningitidis*. Antimicrob Agents Chemother. 2007;51:2784–92. https://doi.org/10.1128/AAC.00412-07
14. Unemo M, Shafer WM. Antimicrobial resistance in *Neisseria gonorrhoeae* in the 21st century: past, evolution, and future. Clin Microbiol Rev. 2014;27:587–613. https://doi.org/10.1128/CMR.00010-14
15. Hong E, Thulin Hedberg S, Abad R, Fazio C, Enríquez R, Deghmane AE, et al. Target gene sequencing to define the susceptibility of *Neisseria meningitidis* to ciprofloxacin. Antimicrob Agents Chemother. 2013;57:1961–4. https://doi.org/10.1128/AAC.02184-12

Address for correspondence: Thuong Vu Nguyen, Department for Disease Control and Prevention, Pasteur Institute in Ho Chi Minh City, 167 Pasteur St, District 03, Ho Chi Minh City 700901, Vietnam; email: nguyenthuong@yahoo.com or thuongnv@pasteurhcm.edu.vn

etymologia revisited

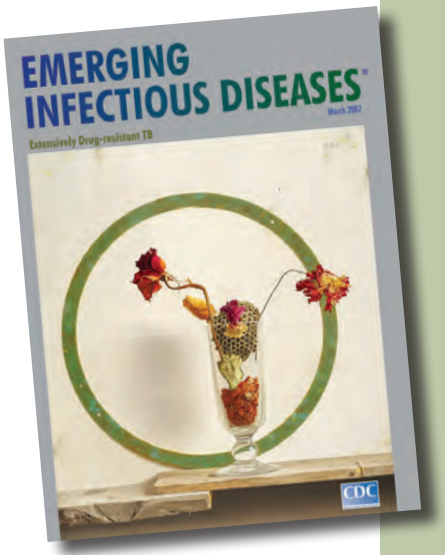

Originally published in March 2007

Norovirus

[nor'-o-vi'rəs]

Genus of viruses that cause viral gastroenteritis. Noroviruses are named after the original strain, "Norwalk virus," which caused an outbreak of acute gastroenteritis among children at an elementary school in Norwalk, Ohio, in 1968. Numerous outbreaks of disease with similar symptoms have been reported since, and the etiologic agents were called "Norwalk-like viruses" or "small round-structured viruses." Noroviruses are transmitted primarily through the fecal-oral route and are highly contagious; as few as 10 viral particles may infect a person.

Reference

Mahy BWJ. A dictionary of virology. London: Academic Press; 2001; http://www.cdc.gov/ncidod/dvrd/revb/gastro/norovirus-qa.htm; http://www.medicinenet.com/norovirus_infection/article.htm

https://wwwnc.cdc.gov/eid/article/13/3/e1-1303_article

Pseudomonas aeruginosa High-Risk Sequence Type 463 Co-Producing KPC-2 and AFM-1 Carbapenemases, China, 2020–2022

Piaopiao Zhang,[1] Wenhao Wu,[1] Nanfei Wang, Haiting Feng, Jie Wang, Fang Wang, Yan Zhang, Hongchao Chen, Qing Yang, Yan Jiang,[2] Tingting Qu[2]

We report the clonal spread and evolution of high-risk *Pseudomonas aeruginosa* sequence type 463 co-producing KPC-2 and AFM-1 carbapenemases isolated from hospital patients in China during 2020–2022. Those strains pose a substantial public health threat and surveillance and stricter infection-control measures are essential to prevent further infections.

Carbapenemase-producing *Pseudomonas aeruginosa* poses a global threat to public health. Epidemics caused by this pathogen are associated with high-risk clones (e.g., sequence type [ST] 235, ST277, ST175, ST233 and ST111), particularly those clones producing metallo-β-lactamases; Verona integron-encoded metallo-β-lactamase and imipenemase are the most prevalent carbapenemase types (*1*,*2*). A *Klebsiella pneumoniae* carbapenemase (KPC)–producing clone, ST463, has emerged and become predominant in carbapenemase-producing *P. aeruginosa* populations in China (*3*). Three *P. aeruginosa* strains co-producing KPC and *Alcaligenes faecalis* metallo-β-lactamase (AFM) were reported in 2022 and attributed to ST463 (*4*,*5*). During 2020–2022, we observed the clonal spread of ST463 carbapenem-resistant *P. aeruginosa* (CRPA) co-producing KPC-2 and AFM-1 (KPC-2–AFM-1 CRPA) in a hospital in China, which caused infections with high mortality. We report on KPC-2–AFM-1 CRPA emergence and driving forces that caused dissemination.

The Study

During September 2020–June 2022, 192 nonduplicated CRPA isolates were collected from 192 patients admitted to a tertiary hospital in Zhejiang, China. Among those isolates, carbapenemase-producing *Pseudomonas aeruginosa* belonging to 10 different STs reached an overall prevalence of 41.1% (79/192) (Appendix Figure 1, https://wwwnc.cdc.gov/EID/article/29/10/23-0509-App1.pdf). We investigated KPC-2–AFM-1 CRPA strains isolated from 8 patients; 3 strains were colonizers and 5 were associated with infections (Table). The patients (6 men, 2 women) were 45–90 years of age, and all had complicated conditions and a history of intensive care unit admission. Antimicrobial drugs active against KPC-2–AFM-1 CRPA (colistin in monotherapy) were given to 4 patients; 5 infected patients eventually died; the remaining 3 patients, who only had bacterial colonization, were discharged (Table).

All 8 isolates were ST463, had identical resistance genes (Appendix Table 1) and type III secretion system genotype *exoU*+/*exoS*+, and differed by 5–30 single-nucleotide polymorphisms, indicating clonal dissemination (Appendix Figure 2). Each strain had 1 chromosome and a plasmid containing the β-lactamase gene bla_{KPC-2}. Alignment of the 8 plasmids showed an identical backbone, but we noted major

Author affiliations: The First Affiliated Hospital of Zhejiang University School of Medicine, Hangzhou, China (P. Zhang, W. Wu, N. Wang, H. Feng, J. Wang, F. Wang, Y. Zhang, H. Chen, Q. Yang, T. Qu); Zhejiang University School of Medicine Sir Run Run Shaw Hospital, Hangzhou (Y. Jiang); Key Laboratory of Microbial Technology and Bioinformatics of Zhejiang Province, Hangzhou (Y. Jiang)

DOI: https://doi.org/10.3201/eid2910.230509

[1]These authors contributed equally to this article.

[2]These senior authors contributed equally to this article.

Table. Demographics and clinical characteristics of 8 patients infected by *Pseudomonas aeruginosa* high-risk sequence type 463 co-producing KPC-2 and AFM-1 carbapenemases, China, 2020–2022*

Patient no.	Strain	Age, y/sex	Ward	Underlying conditions	Sample isolation date	Sample type	Infection type	Therapy†	Outcome/Date
1	ZY94	90/M	ICU	Chronic kidney disease	2021 Feb 9	Sputum	Pulmonary infection	IMP, PTZ, COL	Death/2021 Feb 10
2	ZY156	77/M	ED	Acute toxic encephalopathy	2021 Feb 25	Urine	Urinary tract colonization	SCF	Discharge/2021 Mar 13
3	ZY1012	63/F	ICU	Intraabdominal malignancy	2021 Jul 26	Ascites	Intraabdominal infection	CZA, LEV, COL	Death/2021 Aug 20
4	ZY1075	79/M	ICU	Chronic cardiopulmonary disease	2021 Aug 12	Urine	Urinary tract colonization	NA	Discharge/2021 Aug 13
5	ZY1167	71/M	ICU	Hematologic malignancy	2021 Aug 28	Sputum	Pulmonary infection	IMP, PTZ, COL	Death/2021 Sep 13
6	ZY1214	45/M	Cardiac surgery	Aortic dissection	2021 Aug 31	Urine	Urinary tract colonization	SCF	Discharge/2021 Sep 8
7	ZY36	61/M	ICU	Chronic kidney disease	2022 Jan 9	Sputum	Pulmonary infection	IMP, SCF, COL	Death/2022 Jan 17
8	ZY1710	90/F	Geriatrics	Gallbladder carcinoma	2022 Apr 16	Sputum	Pulmonary infection	IMP	Death/2022 Apr 17

*AFM, *Alcaligenes faecalis* metallo-β-lactamase; COL, colistin; CZA, ceftazidime/avibactam; ED, emergency department; ICU, intensive care unit; IMP, imipenem; KPC, *Klebsiella pneumoniae* carbapenemase; LEV, levofloxacin, NA, not applicable (none); PTZ, piperacillin/tazobactam; SCF, cefperazone/sulbactam.
†Therapy began after bacterial isolation and identification.

differences within the insertion region; the conserved core bla_{KPC-2} genetic platform insertion sequence (IS) *Kpn27*–bla_{KPC-2}–IS*Kpn6* in plasmid p94 remained intact, whereas IS*Kpn6* and several genes immediately upstream (IS*Kpn6*–open reading frame–*klcA*–open reading frame) were absent in the other 7 plasmids (Appendix Figure 3, panel A), forming a novel genetic context for bla_{KPC-2}. All plasmids were designated as type I plasmids (*6*) but had a 16-kb deletion of a mobilization-related operon within the backbone (Appendix Figure 3, panel B), supporting their nontransferability, which was confirmed by conjugation assays.

Using phylogenetic analysis of 125 ST463 genomes (68 from the National Center for Biotechnology Information Reference Sequence database [https://www.ncbi.nlm.nih.gov/refseq] and 57 from our collection), we found that those genomes were divided into 2 clades (Figure 1). Collection dates for strains in clade 1 were much earlier than those for clade 2. Clade 1 was primarily represented by clones from the United States, and clade 1 isolates did not harbor bla_{KPC} or bla_{AFM}. The larger clade 2 originated in China and most isolates in this clade carried bla_{KPC}; we also detected bla_{AFM} in clade 2. Independent evolution of ST463 clones in China might be correlated with sequential acquisition of bla_{KPC} and bla_{AFM}. Paired single-nucleotide polymorphism distances for clade 2 strains in a minimum spanning tree were mainly 0–60 (Appendix Figure 2), demonstrating a high degree of relatedness among those isolates and clonal transmission of KPC-producing *P. aeruginosa* ST463 in China. The 8 KPC-2–AFM-1 CRPAs clustered with 3 bla_{AFM}-carrying strains and formed a separate subclade inside clade 2 that was surrounded by bla_{AFM}-negative, KPC-producing *P. aeruginosa*. Therefore, we inferred that ST463 KPC-2–AFM-1 CRPA clones probably arose from ST463 KPC-producing *P. aeruginosa*.

We could not map the genome sequences of clade 1 strains to the reference plasmid p94 (0% coverage), indicating the absence of type I plasmids in ST463 clones outside of China. Using BLAST (https://blast.ncbi.nlm.nih.gov), we retrieved 40 homologous plasmids that had >50% coverage and >95% identity to p94; all were type I plasmids carried by 14 different *P. aeruginosa* STs (Appendix Figure 4), suggesting an extensive horizontal transfer of type I plasmids within a narrow host range. Plasmid phylogeny revealed that all bla_{KPC-2}–encoding plasmids clustered together in an independent branch, and separation of that branch from closely related bla_{KPC-2}–negative plasmids might be associated with acquisition of bla_{KPC-2} (Appendix Figure 5). The presence of multiple copies of IS*26* in the bla_{KPC-2}–adjacent region beyond the core platform indicated a critical role for IS*26* elements in remodeling and resistance evolution of type I plasmids in the ST463 lineage (Appendix Figure 4) (*7*). We deduced an underlying evolutionary pathway: an ST463 *P. aeruginosa* progenitor initially acquired a highly transferable type I plasmid, which subsequently evolved into a resistance plasmid through IS*26*-mediated insertion events involving a bla_{KPC-2}–carrying region, then by chromosomal integration of bla_{AFM-1} to form KPC-2–AFM-1 CRPA. To further verify this hypothesis, we conducted a genomic comparison between ZY94 and the 1755 strain, which carried neither bla_{KPC} nor bla_{AFM} but was phylogenetically closest to the KPC-2–AFM-1

CRPA cluster (Figure 1). The genome of 1755 was also composed of 1 chromosome and 1 plasmid (p1755). Plasmid p94 was highly homologous (coverage 81%, identity 99.76%) to p1755 and might have evolved from p1755 via IS*26*-mediated intermolecular transposition of a bla_{KPC-2}–carrying translocatable unit that targeted an existing copy of IS*26* (Appendix Figure 6, panel A). Comparisons between their chromosomes identified a redundant bla_{AFM-1}–containing, multidrug-resistance fragment bracketed by IS*5564* in the same orientation, which was flanked by two 6-bp (GCTAGA) target site duplications (Appendix Figure 6, panel B), indicating a site-specific insertion event.

All 8 isolates were resistant to β-lactams and β-lactam/β-lactamase inhibitors, including carbapenems, ceftazidime/avibactam, fluoroquinolones, and gentamicin, and were only susceptible to amikacin and intermediately susceptible to colistin. We observed synergistic inhibitory effects against all 8 strains when we used combinations of ceftazidime/avibactam and aztreonam (Appendix Table 1). Compared with *P. aeruginosa* strain ATCC27853, all strains showed 4-fold higher MICs for chlorhexidine, a commonly used medical disinfectant, suggesting chlorhexidine tolerance (Appendix Table 1) (*8*).

All 8 strains exhibited small colony variant phenotypes together with strong biofilm formation capacities (Appendix Table 2). To assess their stability, desiccation resilience, and virulence, we selected strains ZY94 (infecting strain) and ZY1214 (colonizing strain) for further experiments. After we subcultured in antimicrobial drug–free Luria-Bertani broth for 10

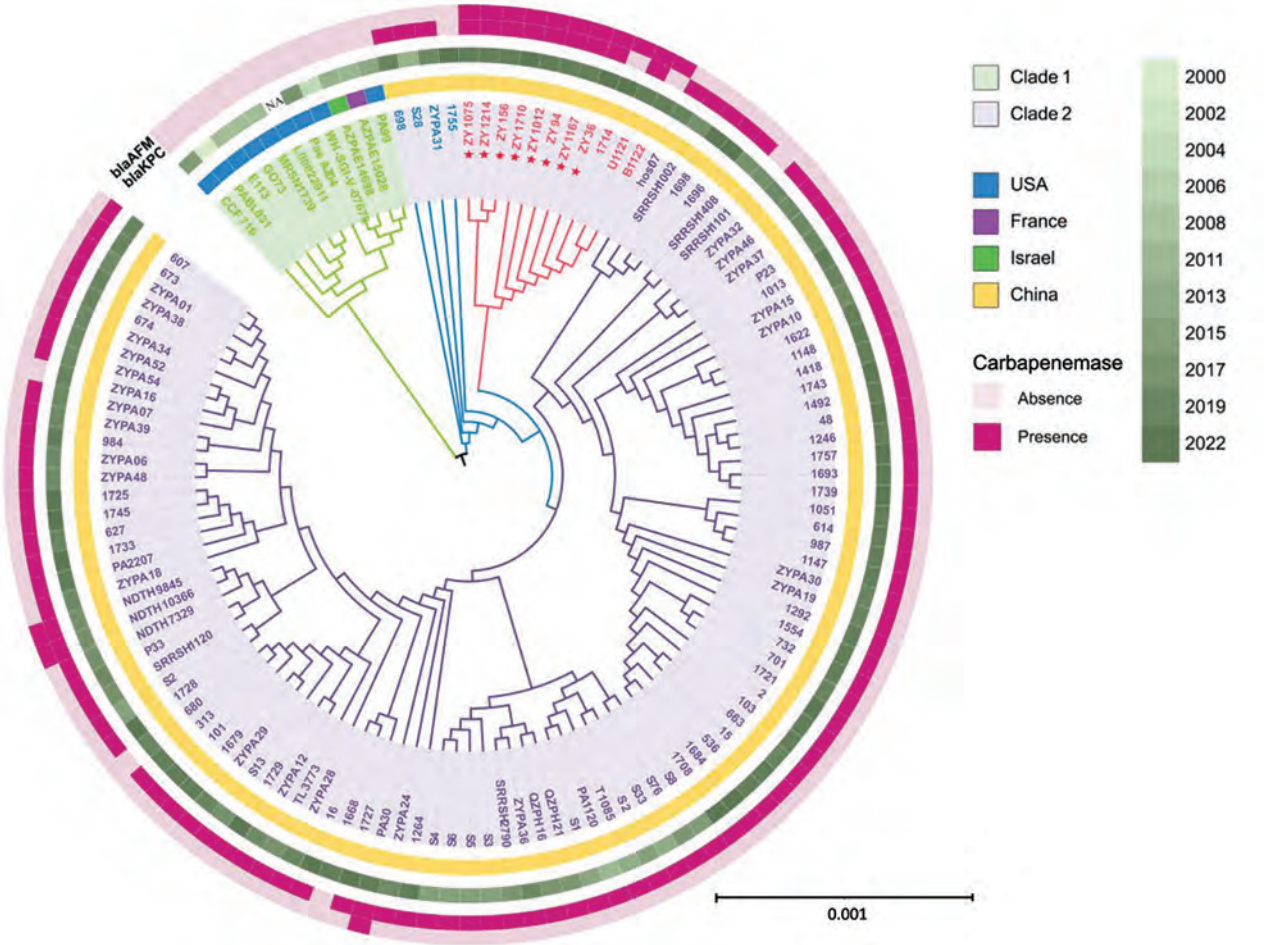

Figure 1. Phylogenetic analysis of *Pseudomonas aeruginosa* high-risk sequence type 463 strains co-producing KPC-2 and AFM-1 carbapenemases, China, 2020–2022. Core-genome phylogenetic tree was built for 125 *P. aeruginosa* sequence type 463 strains and rooted in the midpoint. Red asterisks indicate the 8 carbapenem-resistant *P. aeruginosa* strains co-producing KPC-2 and AFM-1 from a hospital in China. Presence and absence of bla_{AFM} and bla_{KPC} genes are indicated in the outermost 2 rings. Collection year, indicated by different shades of green, and location where each strain was isolated are indicated in the middle rings. The innermost shaded ring indicates strains belonging to clade 1 or 2. Scale bar indicates nucleotide substitutions per site. AFM, *Alcaligenes faecalis* metallo-β-lactamase; *bla*, β-lactamase; KPC, *Klebsiella pneumoniae* carbapenemase; NA, not available.

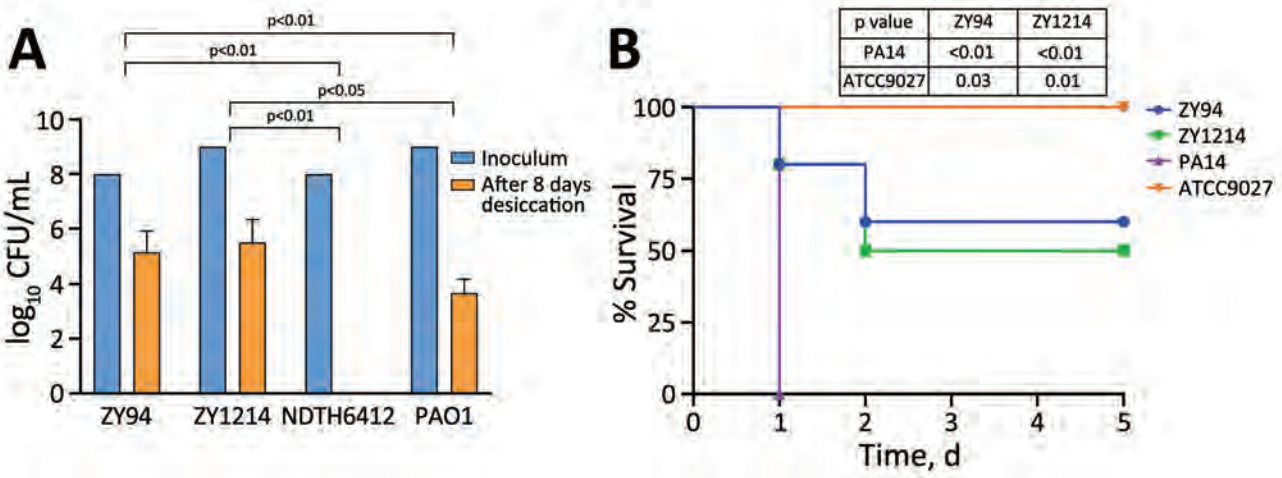

Figure 2. Desiccation tolerance and virulence analyses of *Pseudomonas aeruginosa* high-risk sequence type 463 co-producing KPC-2 and AFM-1 carbapenemases, China, 2020–2022. A) Carbapenem-resistant *P. aeruginosa* strains ZY94 and ZY1214 isolated from hospital patients in China were evaluated for desiccation tolerance. Results are given as mean (SD) CFU/mL for each isolate before and after 8 days of desiccation. Laboratory reference strain PAO1 and *P. aeruginosa* NDTH6412, which belongs to high-risk international sequence type 235, were used as controls. B) Virulence was determined by using Kaplan-Meier survival curves of mice intraperitoneally challenged with 1×10^7 CFUs of strain ZY94 or ZY1214, hypervirulent strain PA14, or nonvirulent *P. aeruginosa* strain ATCC9027. Mice (10 per group) were monitored for 5 days and the number of dead mice was assessed each day. Mantel-Cox log rank tests were used to calculate p values for survival curve comparisons between the different strains. AFM, *Alcaligenes faecalis* metallo-β-lactamase; CFUs, colony forming units; KPC, *Klebsiella pneumoniae* carbapenemase.

days, ZY94 and ZY1214 retained stable small colony variant phenotypes; their bla_{KPC-2}–carrying plasmid and bla_{AFM-1} gene were both stably inherited (stability was 93% for ZY94 and 95% for ZY1214). Both strains survived for 8 days on a dry polystyrene surface at higher rates than strains PAO1 and NDTH6412 (Figure 2, panel A). Furthermore, in mouse intraperitoneal challenge models (Appendix), ZY94 and ZY1214 strains had significantly higher (≈50%) lethality than ATCC9027 ($p<0.05$), but were less virulent than the PA14 strain (Figure 2, panel B).

Conclusions

We documented the persistent clonal spread of ST463 KPC-2–AFM-1 CRPAs in a hospital in China and provided insights into a potential evolutionary pathway for KPC-2–AFM-1 CRPA formation. Extensive drug resistance, disinfectant and desiccation resilience, strong biofilm formation, and high stability constituted strategies for those strains to defend against host and clinical challenges, thereby driving persistent transmission of this high-risk clone. Infections caused by such pathogens might lead to high death rates, especially in immunocompromised or critically ill patients, highlighting the urgent need for effective infection prevention and control policies. ST463 KPC-2–AFM-1 CRPA strains pose a substantial public health threat because of their extensive drug resistance, considerable pathogenicity, and ability to persist in the environment. Targeted surveillance and stricter infection-control measures are essential to prevent further infection outbreaks.

This study was supported by the Natural Science Foundation of Zhejiang Province (grant no. TGY23H010005) and Scientific Research Fund of Zhejiang Provincial Education Department (grant no. Y202146838).

This study was approved by the institutional review board of the First Affiliated Hospital of Zhejiang University School of Medicine in China (approval no. IIT20210120B).

About the Author

Dr. Zhang is a resident doctor at the First Affiliated Hospital of Zhejiang University School of Medicine, in Hangzhou, Zhejiang, China. Her primary research interests are antimicrobial drug resistance and *Pseudomonas aeruginosa* epidemiology.

References

1. Del Barrio-Tofiño E, López-Causapé C, Oliver A. *Pseudomonas aeruginosa* epidemic high-risk clones and their association with horizontally-acquired β-lactamases: 2020 update. Int J Antimicrob Agents. 2020;56:106196. https://doi.org/10.1016/j.ijantimicag.2020.106196
2. Reyes J, Komarow L, Chen L, Ge L, Hanson BM, Cober E, et al.; Antibacterial Resistance Leadership Group and Multi-Drug Resistant Organism Network Investigators. Global epidemiology and clinical outcomes of

carbapenem-resistant *Pseudomonas aeruginosa* and associated carbapenemases (POP): a prospective cohort study. Lancet Microbe. 2023;4:e159–70. https://doi.org/10.1016/S2666-5247(22)00329-9

3. Hu Y, Liu C, Wang Q, Zeng Y, Sun Q, Shu L, et al. Emergence and expansion of a carbapenem-resistant *Pseudomonas aeruginosa* clone are associated with plasmid-borne *bla* $_{KPC-2}$ and virulence-related genes. mSystems. 2021; 6:e00154-21. https://doi.org/10.1128/mSystems.00154-21
4. Li Y, Zhu Y, Zhou W, Chen Z, Moran RA, Ke H, et al. *Alcaligenes faecalis* metallo-β-lactamase in extensively drug-resistant *Pseudomonas aeruginosa* isolates. Clin Microbiol Infect. 2022;28:880.e1–8. PubMed https://doi.org/10.1016/j.cmi.2021.11.012
5. Zhang P, Wang J, Shi W, Wang N, Jiang Y, Chen H, et al. In vivo acquisition of *bla*$_{KPC-2}$ with low biological cost in *bla*$_{AFM-1}$–harboring ST463 hypervirulent *Pseudomonas aeruginosa* from a patient with hematologic malignancy. J Glob Antimicrob Resist. 2022;31:189–95. https://doi.org/10.1016/j.jgar.2022.09.004
6. Zhu Y, Chen J, Shen H, Chen Z, Yang QW, Zhu J, et al. Emergence of ceftazidime- and avibactam-resistant *Klebsiella pneumoniae* carbapenemase-producing *Pseudomonas aeruginosa* in China. mSystems. 2021;6:e0078721. https://doi.org/10.1128/mSystems.00787-21
7. He S, Hickman AB, Varani AM, Siguier P, Chandler M, Dekker JP, et al. Insertion sequence IS*26* reorganizes plasmids in clinically isolated multidrug-resistant bacteria by replicative transposition. mBio. 2015;6:e00762. https://doi.org/10.1128/mBio.00762-15
8. Sahin S, Mogulkoc MN, Kürekci C. Disinfectant and heavy metal resistance profiles in extended spectrum β-lactamase (ESBL) producing *Escherichia coli* isolates from chicken meat samples. Int J Food Microbiol. 2022;377:109831. https://doi.org/10.1016/j.ijfoodmicro.2022.109831

Address for correspondence: Tingting Qu, The First Affiliated Hospital of Zhejiang University School of Medicine, No.79 Qingchun Rd, Hangzhou 310000, China; email: qutingting@zju.edu.cn

Seafood-Associated Outbreak of *ctx*-Negative *Vibrio mimicus* Causing Cholera-Like Illness, Florida, USA

Meer T. Alam,[1] Sarah R. Stern,[1] Devin Frison, Katie Taylor, Massimiliano S. Tagliamonte, S. Sakib Nazmus, Taylor Paisie, Nicole B. Hilliard, Riley G. Jones, Nicole M. Iovine, Kartik Cherabuddi, Carla Mavian, Paul Myers, Marco Salemi, Afsar Ali,[2] J. Glenn Morris, Jr.[2]

Vibrio mimicus caused a seafood-associated outbreak in Florida, USA, in which 4 of 6 case-patients were hospitalized; 1 required intensive care for severe diarrhea. Strains were *ctx*-negative but carried genes for other virulence determinants (hemolysin, proteases, and types I–IV and VI secretion systems). Cholera toxin–negative bacterial strains can cause cholera-like disease.

Vibrio mimicus, named because of its close metabolic and genetic similarity to *V. cholerae*, is recognized globally as a cause of foodborne and waterborne diarrheal disease (*1*–*4*). Limited data indicate that *V. mimicus* incidence is lower than that reported for *V. parahaemolyticus* and non-O1/non-O139 *V. cholerae* but comparable to that of *V. fluvialis* (*3*,*4*). Although some *V. mimicus* strains produce cholera toxin (CTX) or a cholera-like toxin or have genes from the *ctx* complex, most do not (*1*,*5*). Nonetheless, *V. mimicus* can cause severe, cholera-like illness; the hospitalization rate among case-patients reported in 2014 (the most recent year for which data are available) to the Centers for Disease Control and Prevention is 57% (*3*). We report a seafood-associated outbreak caused by *V. mimicus* in Florida, USA, in which 4 of 6 patients required hospitalization.

Author affiliations: University of Florida Emerging Pathogens Institute, Gainesville, Florida, USA (M.T. Alam, M.S. Tagliamonte, S.N. Sakib, T. Paisie, C. Mavian, M. Salemi, A. Ali, J.G Morris, Jr.); University of Florida College of Public Health and Health Professions, Gainesville (M.T. Alam, S.S. Nazmus, A. Ali); University of Florida College of Medicine, Gainesville (S.R. Stern, K. Taylor, M.S. Tagliamonte, T. Paisie, R.G. Jones, N.M. Iovine, K. Cherabuddi, C. Mavian, M. Salemi, J.G. Morris, Jr.); Florida Department of Health in Alachua County, Gainesville (D. Frison, P. Myers); University of Florida Health and Shands Hospital, Gainesville (N.B. Hilliard, N.M. Iovine, K. Cherabuddi)

DOI: https://doi.org/10.3201/eid2910.230486

The Study

In June 2019, the Florida Department of Health in Alachua County (DOH-Alachua; Gainesville, FL, USA) received reports of multiple cases of diarrheal illnesses associated with eating at a local seafood restaurant. Six case-patients were subsequently identified who met the case definition of having eaten seafood at the implicated restaurant within a 2-day time window and who experienced acute onset of diarrhea within 96 hours of the reported meal or had a clinical diagnosis of vibriosis. Median case-patient age was 35.5 years; median incubation period was 24 (range 7–32) hours. All 6 case-patients had diarrhea; other signs/symptoms were vomiting (6 case-patients), headache (3 case-patients), and nausea (3 case-patients). Four patients were hospitalized, 3 at the University of Florida Heath Science Center (UFHealth; Gainesville). Among the UFHealth patients, 1 was admitted to the intensive care unit because of a diarrheal purge of 7–8 L. That patient was 39 years of age, had a history of hypertension and type 2 diabetes mellitus, and fully recovered after treatment with volume repletion and 4 days of doxycycline and ceftriaxone.

DOH-Alachua determined that the foods most commonly consumed by case-patients were steamed blue crab (5 case-patients), steamed snow crab (5 case-patients), and steamed shrimp (4 case-patients). Only

[1]These first authors contributed equally to this article.

[2]These senior authors contributed equally to this article.

1 case-patient reported eating oysters. A joint environmental health assessment by DOH-Alachua, the Florida DOH regional environmental epidemiologist, and the Florida Department of Business and Professional Regulation documented multiple food safety violations (i.e., substantive overall sanitation issues, thawing frozen shrimp overnight at room temperature, returning cooked crabs to crates that previously held live crabs), and a lack of required state-approved employee education.

Fecal samples from the patients hospitalized at UFHealth were initially screened by using a culture-independent diagnostic PCR technique (BioFire FilmArray GI Panel; BioFire Diagnostics, https://www.biofiredx.com), which indicated possible *V. cholerae* and non-*cholerae Vibrio* spp. In follow-up studies at the University of Florida Emerging Pathogens Institute, fecal samples were plated on thiosulfate citrate bile-salts sucrose agar after enrichment in alkaline peptone water (pH 8.5) (Appendix, https://wwwnc.cdc.gov/EID/article/29/10/23-0486-App1.pdf). Green colonies, reflecting the lack of sucrose fermentation, characteristic of *V. mimicus*, grew from 2 of 3 samples. We confirmed that the isolates were *V. mimicus* by using convergent PCR primers (*6*); we designated the strains as D461B_US_2019 and E3_US_2019. Isolates were susceptible to doxycycline, azithromycin, ciprofloxacin, and ceftriaxone (Appendix Table 1).

Neither strain carried genes encoding CTX (*ctx*A or *ctx*B) or other accessory genes linked to the CTX phage. However, both strains elicited strong hemolysis/hemolytic activity against sheep blood as measured by standard assays (Appendix Figure 1). Strains also exhibited protease activity, motility, and biofilm formation (Appendix Figures 2, 3). Whole-genome sequencing and bioinformatic analysis detected genes for a variety of possible virulence determinants, including hemolysin, various proteases, and types I–IV and VI secretion systems (Appendix Table 2). Strains carried both a heat stable and heat labile toxin, which showed >98% nucleotide and amino acid identity to similar genes in a *V. mimicus* strain (SCCF01) that was hypervirulent for freshwater catfish in China (*7*). In an earlier genomic study of 2 *ctx*-negative *V. mimicus* strains, Hasan et al. (*1*) reported the presence of genetic elements of the pre-CTX prophage (including *ace* and *zot*, implicated as contributors to diarrhea associated with CTX-negative *V. cholerae* strains [*8*]) and the VSP-II pathogenicity island, neither of which were present in our Florida *V. mimicus* strains. They also noted a gene cluster similar to that of the *V. cholerae* VPI-2 pathogenicity island; we found an identical gene cluster in our strains.

In a phylogenetic analysis based on the core genome (*9*) (Appendix), the 2 Florida strains clustered within a single, well-supported clade consistent with their high similarity, indicating a very recent common origin (Figure). Although the maximum-likelihood tree of available *V. mimicus* sequences shows several independent lineages of strains sampled worldwide with no apparent geographic structure, the closest lineages to the Florida strains were clinical isolates from the United Kingdom, as well as clinical and environmental strains from the United States, albeit with no strong bootstrap support.

Conclusions

V. mimicus is present either as a free-living microorganism or in biofilm in the aquatic/estuarine environment; infection is strongly associated with seafood consumption (*4*,*10*,*11*). For this outbreak, we could not identify a single source for the infection, given that case-patients had eaten a variety of seafoods and there were sufficient breakdowns in food safety practices within the kitchen to make cross-contamination of multiple foods highly likely. Although oysters have been implicated as a *V. mimicus* source, only 1 case-patient reported eating oysters, making oysters an unlikely primary source of infection. We also note the risk inherent in placing cooked seafood back into containers in which live seafood has been shipped, a practice linked with previous *V. mimicus* and other *Vibrio* spp. outbreaks (*12*).

Most hospitals and commercial laboratories have now moved to use of culture-independent diagnostic techniques, resulting in a strikingly increased number of cases of *Vibrio*-associated infections reported in the United States (*13*). The outbreak reported here highlights the utility of such techniques for providing a quick, preliminary diagnosis of a possible *Vibrio* infection as well as problems with such systems. Exact isolate speciation was not possible with the system used by UFHealth, and speciation subsequently required careful classical microbiological approaches (with enrichment procedures) to isolate and identify the organism, without which this outbreak caused by a less common *Vibrio* species would almost certainly have been missed.

V. mimicus evolved from a common *V. cholerae* ancestor with a prototypic sixth pandemic genomic backbone (*1*). Although most *V. mimicus* strains have not retained the *ctx* genes (the primary virulence factor responsible for the severe diarrhea seen in

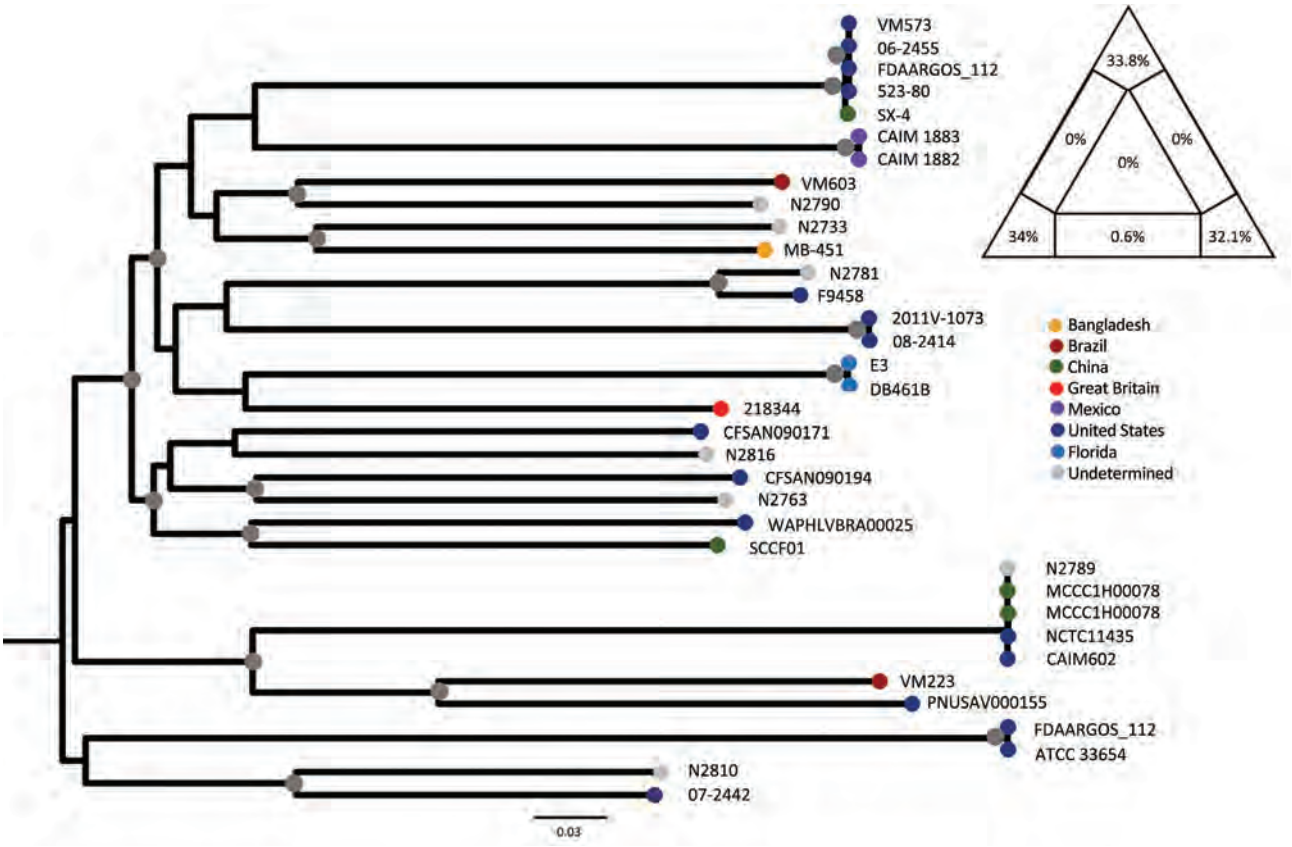

Figure. Maximum-likelihood tree of *Vibrio mimicus* strains. The tree was calculated by using 35 sequences; the best evolutionary model was selected by Bayesian information criterion. Nodes marked by a gray circle have bootstrap support (1,000 replicates) >90%. Scale bar represents the number of substitutions per site. The phylogenetic signal of the alignment was determined by likelihood mapping, as shown by the triangle in the top right corner. A complete explanation is provided online (https://wwwnc.cdc.gov/EID/article/29/10/23-0486-F1.htm).

cholera), the 2 strains isolated in this outbreak carried a wide variety of potential virulence determinants, showing varying degrees of similarity with potential virulence factors reported for other *V. mimicus* strains (*1*,*7*). Common to many other *Vibrio* species (including *V. cholerae*), *V. mimicus* has a superintegron (*1*,*14*), which can serve as a capture system for acquiring DNA from the surrounding environment and may have contributed to the accumulation of virulence genes. We did not see evidence of distinct clinical and environmental lineages (associated with *V. cholerae* and *V. parahaemolyticus*), underscoring the idea that most *V. mimicus* strains, regardless of origin, have the potential for carrying genes capable of causing illness in humans.

Although incidence data for *V. mimicus* are limited, partially because of diagnostic difficulties, *Vibrio* case numbers are clearly increasing with rising surface water temperatures (*13*,*15*,*16*). Thus, diagnostic capabilities for *V. mimicus* and other *Vibrio* species need to be enhanced. There also needs to be recognition that strains that do not carry cholera toxin can cause cholera-like disease and that further work is needed to more clearly identify the pathogenic mechanisms by which such strains cause illness.

Laboratory studies were funded through internal funding sources at the University of Florida and the University of Florida Emerging Pathogens Institute.

About the Authors

Dr. Alam is an investigator in the Cholera Laboratory at the University of Florida Emerging Pathogens Institute, where he oversees studies of *V. cholerae* and other *Vibrio* species, including recent studies in Haiti and the Democratic Republic of the Congo. Dr. Stern is a resident physician at Atrium Health/Wake Forest Baptist and Wake Forest University School of Medicine, in Wake Forest, North Carolina.

References

1. Hasan NA, Grim CJ, Haley BJ, Chun J, Alam M, Taviani E, et al. Comparative genomics of clinical and environmental

Vibrio mimicus. Proc Natl Acad Sci U S A. 2010;107:21134–9. https://doi.org/10.1073/pnas.1013825107
2. Chitov T, Kirikaew P, Yungyune P, Ruengprapan N, Sontikun K. An incidence of large foodborne outbreak associated with *Vibrio mimicus*. Eur J Clin Microbiol Infect Dis. 2009;28:421–4. https://doi.org/10.1007/s10096-008-0639-7
3. Centers for Disease Control and Prevention. National Enteric Disease Surveillance: COVIS Annual Summary, 2014 [cited 2022 Jul 25]. https://www.cdc.gov/nationalsurveillance/pdfs/covis-annual-summary-2014-508c.pdf
4. Louisiana Office of Public Health. Vibrios [cited 2022 Jul 27]. https://ldh.la.gov/assets/oph/Center-PHCH/Center-CH/infectious-epi/Annuals/Vibrios_LaIDAnnual.pdf
5. Shinoda S, Nakagawa T, Shi L, Bi K, Kanoh Y, Tomochika K, et al. Distribution of virulence-associated genes in *Vibrio mimicus* isolates from clinical and environmental origins. Microbiol Immunol. 2004;48:547–51. https://doi.org/10.1111/j.1348-0421.2004.tb03551.x
6. Kim H-J, Ryu J-O, Lee S-Y, Kim E-S, Kim H-Y. Multiplex PCR for detection of the *Vibrio* genus and five pathogenic *Vibrio* species with primer sets designed using comparative genomics. BMC Microbiol. 2015;15:239. https://doi.org/10.1186/s12866-015-0577-3
7. Yu Z, Wang E, Geng Y, Wang K, Chen D, Huang X, et al. Complete genome analysis of *Vibrio mimicus* strain SCCF01, a highly virulent isolate from the freshwater catfish. Virulence. 2020;11:23–31. https://doi.org/10.1080/21505594.2019.1702797
8. Trucksis M, Galen JE, Michalski J, Fasano A, Kaper JB. Accessory cholera enterotoxin (Ace), the third toxin of a *Vibrio cholerae* virulence cassette. Proc Natl Acad Sci U S A. 1993;90:5267–71. https://doi.org/10.1073/pnas.90.11.5267
9. Guardiola-Avila I, Sánchez-Busó L, Acedo-Félix E, Gomez-Gil B, Zúñiga-Cabrera M, González-Candelas F, et al. Core and accessory genome analysis of *Vibrio mimicus*. Microorganisms. 2021;9:191. https://doi.org/10.3390/microorganisms9010191
10. Abioye OE, Osunla AC, Okoh AI. Molecular detection and distribution of six medically important *Vibrio* spp. in selected freshwater and brackish water resources in Eastern Cape Province, South Africa. Front Microbiol. 2021;12:617703. https://doi.org/10.3389/fmicb.2021.617703
11. Álvarez-Contreras AK, Quiñones-Ramírez EI, Vázquez-Salinas C. Prevalence, detection of virulence genes and antimicrobial susceptibility of pathogen *Vibrio* species isolated from different types of seafood samples at "La Nueva Viga" market in Mexico City. Antonie van Leeuwenhoek. 2021;114:1417–29. https://doi.org/10.1007/s10482-021-01591-x
12. Centers for Disease Control and Prevention. Notes from the field: *Vibrio mimicus* infection from consuming Crayfish—Spokane, Washington, June, 2010. Morb Mortal Wkly Rep. 2010;59:1374.
13. Centers for Disease Control and Prevention. FoodNet Fast [cited 2022 Jul 25]. https://wwwn.cdc.gov/foodnetfast
14. Mazel D, Dychinco B, Webb VA, Davies J. A distinctive class of integron in the *Vibrio cholerae* genome. Science. 1998; 280:605–8. https://doi.org/10.1126/science. 280.5363.605
15. Trinanes J, Martinez-Urtaza J. Future scenarios of risk of *Vibrio* infections in a warming planet: a global mapping study. Lancet Planet Health. 2021;5:e426–35. https://doi.org/10.1016/S2542-5196(21)00169-8
16. Brehm TT, Berneking L, Sena Martins M, Dupke S, Jacob D, Drechsel O, et al.; German Vibrio Study Group. Heatwave-associated *Vibrio* infections in Germany, 2018 and 2019. Euro Surveill. 2021;26:2002041. https://doi.org/10.2807/1560-7917.ES.2021.26.41.2002041

Address for correspondence: J. Glenn Morris, Jr., Emerging Pathogens Institute, PO Box 100009, Gainesville, FL 32610, USA; email: jgmorris@epi.ufl.edu

Influenza A(H5N1) Virus Infections in 2 Free-Ranging Black Bears (*Ursus americanus*), Quebec, Canada

Benjamin T. Jakobek, Yohannes Berhane, Marie-Soleil Nadeau, Carissa Embury-Hyatt, Oliver Lung, Wanhong Xu, Stéphane Lair

Wholly Eurasian highly pathogenic avian influenza H5N1 clade 2.3.4.4b virus was isolated from 2 free-ranging black bears with meningoencephalitis in Quebec, Canada. We found that isolates from both animals had the D701N mutation in the polymerase basic 2 gene, previously known to promote adaptation of H5N1 viruses to mammal hosts.

Since its arrival in North America during December 2021, the Eurasian highly pathogenic avian influenza (HPAI) virus subtype H5N1, clade 2.3.4.4b, has been associated with a high mortality rate for wild birds all over the continent (*1*). Affected bird species include mainly waterfowl and colonial nesting marine birds, as well as scavenger birds, such as gulls, eagles, vultures, and corvids (*2*,*3*). As with several other subtypes, HPAI H5N1 can potentially infect persons, although clinical cases in humans have been limited (*4*). However, this virus has been shown to be pathogenic for different species of wild mammals, including red fox, striped skunk, mink, raccoon, and seals (*5*–*7*). Infections with influenza A(H1N1) viruses have been described in captive sloth bears (*8*). We report and describe infections by HPAI H5N1 virus in 2 black bears (*Ursus americanus*) found in Quebec, Canada, during the summer of 2022.

Author affiliations: Centre Québécois sur la Santé des Animaux Sauvages/Canadian Wildlife Health Cooperative, St. Hyacinthe, Quebec, Canada (B.T. Jakobek, S. Lair); Université de Montréal, St. Hyacinthe (B.T. Jakobek, S. Lair); University of Saskatchewan Western College of Veterinary Medicine, Saskatoon, Saskatchewan, Canada (Y. Berhane); Canadian Food Inspection Agency National Centre for Foreign Animal Disease, Winnipeg, Manitoba, Canada (Y. Berhane, C. Embury-Hyatt, O. Lung, W. Xu); University of Manitoba, Winnipeg (Y. Berhane, O. Lung); Ministère de l'Agriculture, des Pêcheries et de l'Alimentation Laboratoire de Santé Animale, St. Hyacinthe (M.-S. Nadeau)

DOI: https://doi.org/10.3201/eid2910.230548

The Study

Two young-of-the-year black bear cubs (likely born in January–February) were observed wandering on a road within the Forillon National Park in Gaspé, Quebec, Canada (48°51′39″N, 64°13′26″W), on June 14, 2022. The cubs, which were active and quite vocal, were not attended by their dam. Shortly afterward, an adult female bear with unusual behavior was reported ≈200 m from the cubs. This female was wandering between vehicles, fell into a river, and began circling. Upon the arrival of park officials, the animal was in lateral recumbency and convulsing in a ditch.

Because of the severity of the neurologic signs present and concern for public safety, the bear was anesthetized and then euthanized. The 2 cubs, presumed to be orphaned, were also euthanized. The carcasses of the adult female and 1 of the cubs were subsequently frozen. The adult female was thawed a few days later and examined on site. Different organs were sampled, refrozen and shipped, along with the originally frozen cub, to the Canadian Wildlife Health Cooperative Quebec regional center for further macroscopic examination, which was performed on July 7, 2022.

Macroscopic examination of viscera of the adult female show no notable findings, other than extensive postmortem changes. The cub (a 5.1-kg female) was thin and had limited fat stores. A mild mesenteric lymphadenomegaly was present, and the cerebrum appeared to be diffusely congested.

Histopathologic examination of tissues sampled from the adult female showed multifocal infiltration of the meninges by numerous lymphoplasmacytic cells, which extended into the Virchow–Robin spaces, forming perivascular cuffing. Neuronal necrosis associated with satellitosis and glial nodules was commonly observed. Aggregates of polymorphonuclear cells in the cerebral substance and areas of neuropile vacuolization with axonal degeneration were also present. The cub had similar, but of lower intensity and predominantly neutrophilic in nature, cerebral inflammatory and degenerative lesions, in addition to fibrinoid neutrophilic vasculitis. Small necrotic foci surrounded by granulocytes and mononuclear cells were also occasionally seen in the liver of the cub.

Influenza A virus (IAV) antigen was detected by using immunohistochemical staining (Appendix, https://wwwnc.cdc.gov/EID/article/29/10/23-0548-App1.pdf) in brain and liver cells; liver cells were observed only in the bear cub (Figure 1). Brain tissues from both animals were negative for rabies virus by the direct rapid immunohistochemical test (*9*).

We extracted RNAs from brain tissues and tracheo-rectal swab specimens from both animals and found that they were positive for IAV genomic material by using matrix and H5 gene specific real-time reverse transcription PCRs (*10*,*11*). We isolated H5N1 viruses from brain samples collected from both bears in 9-day-old embryonated specific pathogen-free chicken eggs. We amplified all 8 genome segments of the virus directly from clinical samples and isolates and were sequenced by using the Oxford Nanopore platform as described (*12*), and the Rapid Barcoding Kit 96 (https://www.nanoporetech.com). We basecalled raw Nanopore signal data and demultiplexed with Guppy v5.1.12 (https://timkahlke.github.io) using the super-accurate basecalling model. We then analyzed and assembled the basecalled reads by using the CFIA-NCFAD/nf-flu v3.1.0 (https://zenodo.org/record/7011213#.ZBs5cXbMIuU) nextflow workflow.

The hemagglutinin (HA) gene of the virus belonged to Eurasian goose/Guangdong (Gs/GD) lineage HPAI H5N1 clade 2.3.4.4b and had the cleavage site motif of PLREKRRKR/GLF, compatible with HPAI viruses (Figure 2). All 8 genome segments of the viruses from both bears contained wholly Eurasian IAVs similar to the Newfoundland-like H5N1 viruses, which came from Europe to Canada by the Atlantic

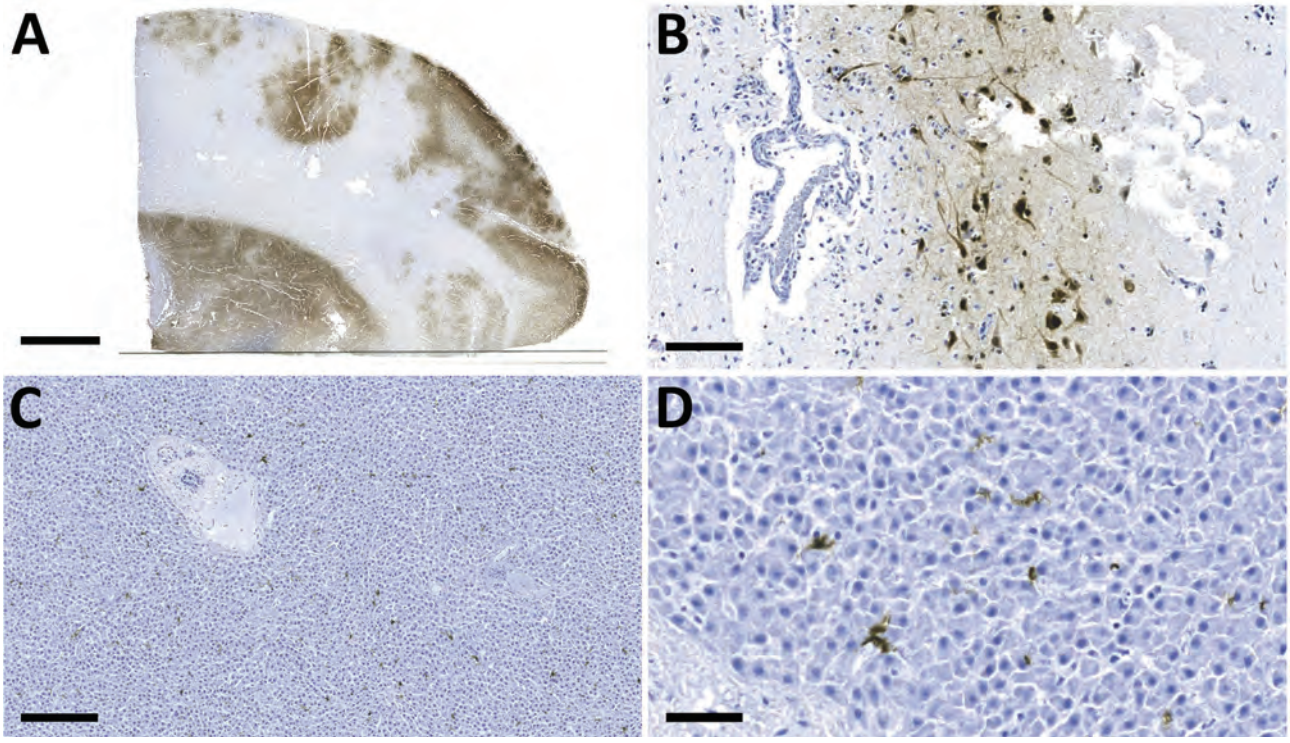

Figure 1. Detection of influenza A virus antigen in black bears by immunohistochemical analysis, Quebec, Canada. A) Brain tissue, showing abundant viral antigen detected multifocally throughout the section and observed primarily in gray matter areas. Scale bar indicates 5 mm. B) Brain immunostaining within neurons and surrounding neuropil. Scale bar indicates 100 μm. C) Liver tissue, showing viral antigen within individual cells. Scale bar indicates 200 μm. D) Liver tissue, showing that cells have the morphologic appearance of Kuppfer cells. Scale bar indicates 50 μm. Monoclonal antibody and diaminobenzidine stained, Gill's hematoxylin counterstained.

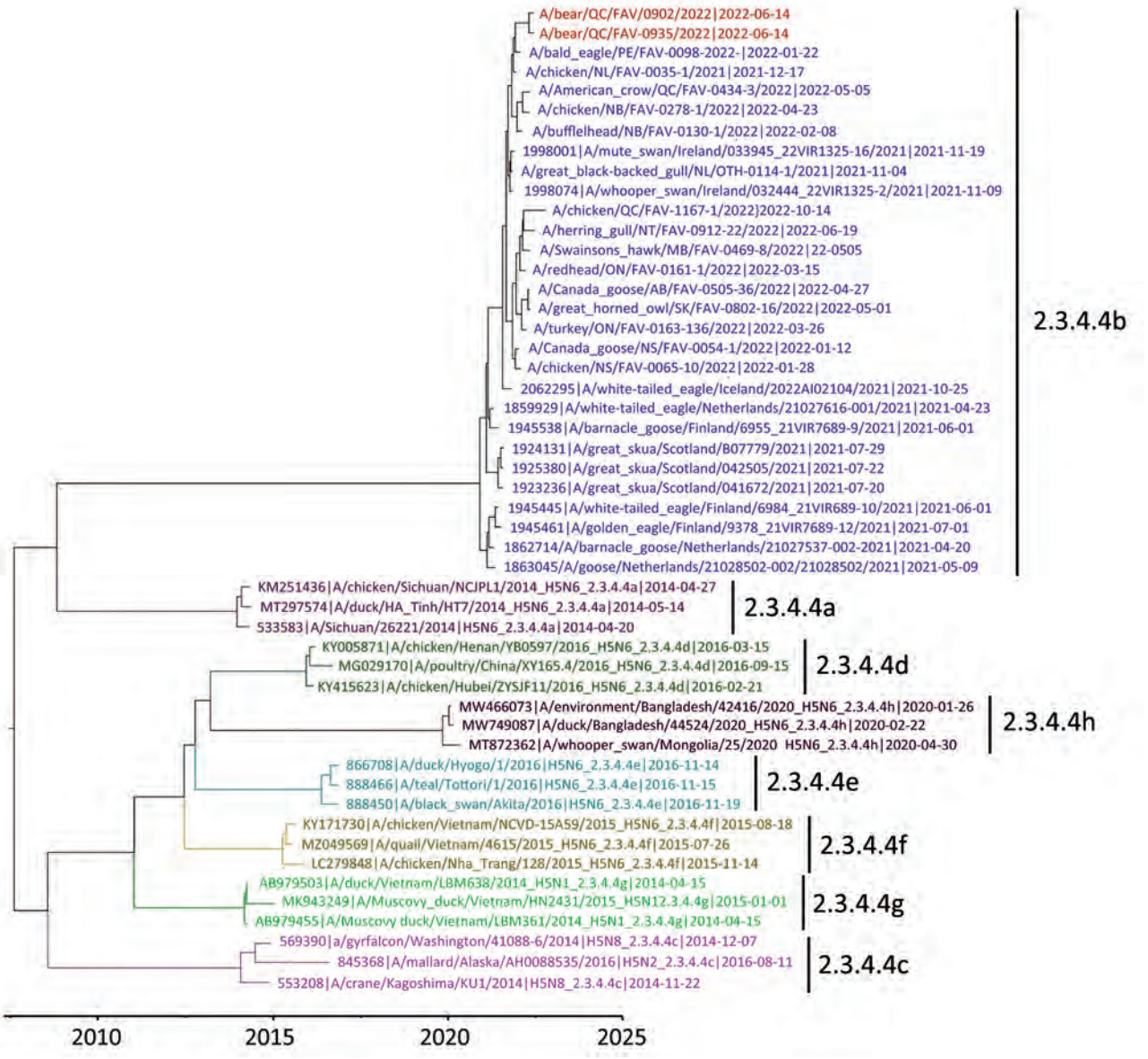

Figure 2. Maximum-clade credibility tree for influenza A virus antigen in black bears by immunohistochemical analysis, Quebec, Canada, inferred by using Bayesian and Markov Chain Monte Carlo analyses for the H5 hemagglutinin gene. Shown are relationships among black bear strains from this investigation (red), European 2021 H5 clade 2.3.4.4b HPAI strains (blue), and early Canada wild bird and poultry strains (purple). Colors and labels indicate the other H5 clade 2.3.4.4 subgroups.

Flyway in 2021 (*1*). Both bears had mammalian adaptive mutations (D701N) in the polymerase basic protein 2 subunit of the RNA polymerase complex.

We conducted a Bayesian phylogenetic analysis to identify phylogenetic relatedness of the H5 HA gene between black bears and Eurasian-origin H5N1 HPAIVs, as well as representative subgroups of clade 2.3.4.4. (Appendix). The maximum clade credibility tree of the H5 HA gene showed that the HA genes of black bear samples were grouped with the current outbreak 2.3.4.4b subgroup (Figure 2). The HA genes were most closely related to those of early H5N1 HPAIVs isolated from eastern Canada provinces, as well as strains circulating in northwestern Europe during winter 2021. Those genes were also more similar to those the fully Eurasian lineages observed in red foxes than to those observed in striped skunks and mink (*5*) and were not closely related to the New England–specific lineages documented in New England seals (*7*). Full genome sequences of both isolates were deposited in the GISAID database (https://www.gisaid.org) under accession nos. EPI_ISL_1747865 and EPI_ISL_17478584.

Conclusions

The described black bears were within the Atlantic Americas avian flyway, where Eurasian lineage H5N1 viruses were detected in 2021 (*1*). The global epizootic of the HPAI H5N1 virus belonging to clade 2.3.4.4b has led to an exceptional number of animal deaths, particularly in domestic poultry and wild birds (*12*).

As opportunistic omnivores, black bears might be found scavenging on carcasses of dead animals, including birds. Within 5 km and in the 3 weeks preceding the euthanasia of both bears, several dead wild birds tested positive for the Eurasian lineage of HPAI H5N1, including common murre (*Uria aalge*), American crow (*Corvus brachyrhynchos*), northern gannet (*Morus bassanus*), and razorbill (*Alca torda*) (Canadian Wildlife Health Cooperative internal database, https://www.cwhc-rcsf.ca). Suspected deaths of seals caused by HPAI H5N1 had occurred around the same time that the bears were found; however, those seal carcasses were >300 km away, and no suspected or confirmed seal deaths caused by HPAI H5N1 have been reported in seal populations in the Gaspé Peninsula (*13*). Therefore, it is suspected that the adult female black bear in this study was infected through spillover directly from infected bird carcasses because black bears in the Gaspé Peninsula share habitat with marine birds for which there have been confirmed deaths caused by HPAI H5N1 (*13*; Canadian Wildlife Health Cooperative internal database) during the same period.

Although H5N1 virus transmission has been documented in mink and ferrets, transmission of the virus between mammals is generally inefficient (*14*). Therefore, the possibility that the virus that affected these black bears was transmitted from 1 bear to another, or from another mammal species, is much less probable than transmission from birds. Although HPAI virus infections in mammals might occur secondary to other infections, no other infectious agents were identified in either of the black bears.

Acknowledgments

We thank the employees of the Complex de Diagnostic et d'Épidémiosurveillance Vétérinaire du Québec for their contributions and work, M. Fisher for sequencing and sequence data processing, and the Parks Canada wildlife officials for their involvement in this study.

Support was provided to O.L. by the Canadian Safety and Security Program (CSSP-2018-TA-2362) for the Oxford Nanopore GridION sequencer.

About the Author

Dr. Jakobek is a veterinary resident in wildlife health management with the Canadian Wildlife Health Cooperative and the Faculté de Médecine Vétérinaire at the Université de Montréal, Saint-Hyacinthe, Quebec, Canada. His primary research interests are wildlife disease epidemiology and conservation medicine.

References

1. Caliendo V, Lewis NS, Pohlmann A, Baillie SR, Banyard AC, Beer M, et al. Transatlantic spread of highly pathogenic avian influenza H5N1 by wild birds from Europe to North America in 2021. Sci Rep. 2022;12:11729. https://doi.org/10.1038/s41598-022-13447-z
2. Prosser DJ, Schley HL, Simmons N, Sullivan JD, Homyack J, Weegman M, et al. A lesser scaup (*Aythya affinis*) naturally infected with Eurasian 2.3.4.4 highly pathogenic H5N1 avian influenza virus: movement ecology and host factors. Transbound Emerg Dis. 2022;69:e2653–60. https://doi.org/10.1111/tbed.14614
3. Nemeth NM, Ruder MG, Poulson RL, Sargent R, Breeding S, Evans MN, et al. Bald eagle mortality and nest failure due to clade 2.3.4.4 highly pathogenic H5N1 influenza A virus. Sci Rep. 2023;13:191. https://doi.org/10.1038/s41598-023-27446-1
4. World Health Organization. Human infection with avian influenza A(H5) viruses. Avian Influenza Weekly Update Number 887.
5. Alkie TN, Cox S, Embury-Hyatt C, Stevens B, Pople N, Pybus MJ, et al. Characterization of neurotropic HPAI H5N1 viruses with novel genome constellations and mammalian adaptive mutations in free-living mesocarnivores in Canada. Emerg Microbes Infect. 2023;12:2186608. https://doi.org/10.1080/22221751.2023.2186608
6. Horimoto T, Maeda K, Murakami S, Kiso M, Iwatsuki-Horimoto K, Sashika M, et al. Highly pathogenic avian influenza virus infection in feral raccoons, Japan. Emerg Infect Dis. 2011;17:714–7. https://doi.org/10.3201/eid1704.101604
7. Puryear W, Sawatzki K, Hill N, Foss A, Stone JJ, Doughty L, et al. Highly of highly pathogenic avian influenza A (H5N1) in New England seals, United States. Emerg Infect Dis. 2023;29:786–91. https://doi.org/10.3201/eid2904.221538
8. Boedeker NC, Nelson MI, Killian ML, Torchetti MK, Barthel T, Murray S. Pandemic (H1N1) 2009 influenza A virus infection associated with respiratory signs in sloth bears (*Melursus ursinus*). Zoonoses Public Health. 2017;64:566–71. https://doi.org/10.1111/zph.12370
9. Saturday GA, King R, Fuhrmann L. Validation and operational application of a rapid method for rabies antigen detection. US Army Med Dep J. 2009;(Jan–Mar):42–5.
10. Spackman E, Senne DA, Myers TJ, Bulaga LL, Garber LP, Perdue ML, et al. Development of a real-time reverse transcriptase PCR assay for type A influenza virus and the avian H5 and H7 hemagglutinin subtypes. J Clin Microbiol. 2002;40:3256–60. https://doi.org/10.1128/JCM.40.9.3256-3260.2002
11. Weingartl HM, Berhane Y, Hisanaga T, Neufeld J, Kehler H, Emburry-Hyatt C, et al. Genetic and pathobiologic characterization of pandemic H1N1 2009 influenza viruses from a naturally infected swine herd. J Virol. 2010;84:2245–56. https://doi.org/10.1128/JVI.02118-09
12. Adlhoch C, Fusaro A, Gonzales JL, Kuiken T, Marangon S, Niqueux É, et al.; European Food Safety Authority; European

Centre for Disease Prevention and Control; European Union Reference Laboratory for Avian Influenza. Avian influenza overview December 2021–March 2022. EFSA J. 2022;20:e07289.
13. Canadian Food Inspection Agency, National Emergency Operation Centre, Geographic Information System Services. Highly pathogenic avian influenza—wild birds [cited 2023 Apr 11]. https://cfia-ncr.maps.arcgis.com/apps/dashboards/89c779e98cdf492c899df23e1c38fdbc
14. Imai M, Herfst S, Sorrell EM, Schrauwen EJA, Linster M, De Graaf M, et al. Transmission of influenza A/H5N1 viruses in mammals. Virus Res. 2013;178:15–20. https://doi.org/10.1016/j.virusres.2013.07.017

Address for correspondence: Stéphane Lair, Centre Québécois sur la Santé des Animaux Sauvages/Canadian Wildlife Health Cooperative, Faculté de Médecine Vétérinaire, Université de Montréal, 3200 Rue Sicotte, St. Hyacinthe, QB J2S 2M2, Canada; email: stephane.lair@umontreal.ca

Limited Outbreak of Highly Pathogenic Influenza A(H5N1) in Herring Gull Colony, Canada, 2022

Liam U. Taylor, Robert A. Ronconi, Hayley A. Spina, Megan E.B. Jones, C. Brandon Ogbunugafor, Andrea J. Ayala

In summer 2022, highly pathogenic influenza A(H5N1) virus reached the herring gull (*Larus argentatus* subspecies *smithsonianus*) breeding colony on Kent Island, New Brunswick, Canada. Real-time monitoring revealed a self-limiting outbreak with low mortality. Proactive seabird surveillance is crucial for monitoring such limited outbreaks, protecting seabirds, and tracing zoonotic transmission routes.

Highly pathogenic avian influenza (HPAI) viruses pose a near-term threat to commercial poultry and a long-term risk for human pandemics (*1*,*2*). Recent outbreaks of HPAI A(H5N1) virus have also caused mass mortality events in vulnerable seabird populations (3). Because outbreaks are difficult to predict, knowledge of HPAI in wild birds is often limited to cross-sectional surveillance or post hoc records of mass mortality events (*4*–*6*).

Beginning in December 2021, an HPAI H5N1 virus strain spread from Eurasia into Canada, subsequently infecting wild, commercial, and backyard bird populations across North America (*4*) (https://www.usgs.gov/centers/nwhc/science/distribution-highly-pathogenic-avian-influenza-north-america-20212022). During summer 2022, we studied the life history of American herring gulls (*Larus argentatus* subspecies *smithsonianus*) at the Kent Island breeding colony in New Brunswick, Canada (Figure 1). Thus, we had an unusual opportunity to monitor emerging disease symptoms and deaths in a wild population. We report timelines, clinical details, and epidemiologic observations from a laboratory-confirmed HPAI outbreak that caused a relatively low death rate within a seabird colony.

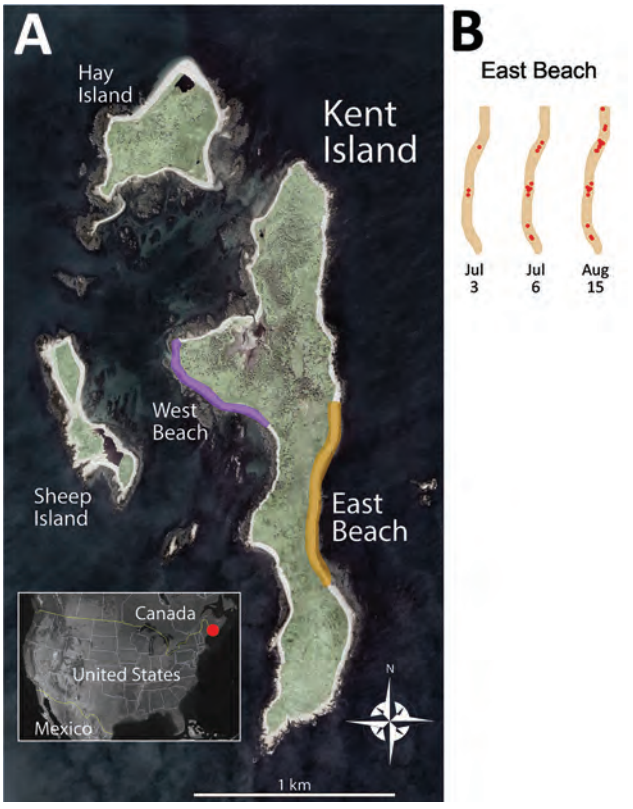

Figure 1. Location of gull breeding colony on Kent Island, New Brunswick, Canada, in study of limited outbreak of highly pathogenic influenza A(H5N1) in herring gull colony, 2022. A) Inset shows location of Kent Island in Canada. The main study site was on East Beach (yellow strip), and a secondary site was on West Beach (purple strip). Intermittent monitoring occurred across Kent, Hay, and Sheep Islands. Satellite image from Google Earth (https://earth.google.com). B) Accumulating carcass locations (red points) for 3 timepoints on East Beach.

Author affiliations: Yale University, New Haven, Connecticut, USA (L.U. Taylor, C.B. Ogbunugafor, A.J. Ayala); Canadian Wildlife Service, Dartmouth, Nova Scotia, Canada (R.A. Ronconi); Environment and Climate Change Canada, Dartmouth (R.A. Ronconi); University of Guelph, Guelph, Ontario, Canada (H.A. Spina); University of Prince Edward Island, Charlottetown, Prince Edward Island, Canada (M.E.B. Jones); Canadian Wildlife Health Cooperative, Charlottetown (M.E.B. Jones)

DOI: https://doi.org/10.3201/eid2910.230536

Table 1. Summary of influenza-related herring gull deaths on Kent Island and neighboring islands in study of limited outbreak of highly pathogenic influenza A(H5N1), Canada, 2022*

Area	Census count† (±SD)	No. censuses conducted	No. deaths	Death rate,‡ %	Survey schedule
Kent Island, East Beach	526 (169)	110	22	4.2	1–3×/d, Jun 1–Aug 15, Sep 2
Kent Island, West Beach	221 (60)	88	15	6.8	1–2×/d, Jun 1–Jul 7, Jul 22–Aug 14, Sep 2
Kent Island, total§	3,077 (937)	10	66–87	2.1–2.8	1×/wk, Jun 1–Jul 7, Jul 15 (partial), Jul 22–Aug 14, Sep 2 (partial)
Sheep Island	900	1	25	2.8	Jul 5 (boat count), Jul 14 (partial), Aug 29
Hay Island	617 (267)	2	41	6.7	Jun 21, Aug 7

*Mean counts are of adult herring gulls >10 months of age. Partial surveys covered only part of the survey area.
†Census counts varied with time, tide, and seasonal fluctuations for both breeding and nonbreeding populations.
‡Calculated according to mean census count. Our assumption that all intact adult gull carcasses were influenza-related might have raised death rate estimates, whereas intermittent surveys and imperfect carcass detection might have lowered death rate estimates.
§Ranges for number of deaths and death rate are provided because of possible double counting of untagged carcasses by 2 observers outside of the main study sites.

The Study

We monitored herring gulls on Kent Island (latitude 44.5828°N, longitude 66.7568°W; Figure 1). Gulls nest across the ≈100-ha island and on adjacent Hay and Sheep Islands (Figure 1). Herring gulls on Kent Island generally migrate north from eastern North America in early May, lay eggs in mid-May, hatch chicks in mid-June, and fledge chicks in August (*7*,*8*).

During June 1–August 15, 2022, we surveyed the main study area on East Beach (Figure 1) 1–3 times/day, conducting full census counts, monitoring disease symptoms, and individually marking carcasses. Other areas of Kent Island were surveyed on an intermittent schedule (Table 1). We assumed that all generally intact adult carcasses were virus-induced deaths because sudden deaths of adult birds are rare in breeding colonies. Because injuries and deaths are common among chicks, we were unable to assess virus-induced deaths in chicks except for suspected cases C1–C3 (Appendix, https://wwwnc.cdc.gov/EID/article/29/10/23-0536-App1.pdf).

We did not observe illness in the colony during a preliminary visit to Kent Island (May 24–27). On the morning of June 27, we spotted a lethargic adult herring gull on East Beach that died that afternoon (Table 2; Figure 2). Disease symptoms and deaths spiked at 9 deaths during July 4–8 (Figure 2). We observed 9 more deaths that accumulated more slowly through August 15; a final check on September 2 revealed only 1 new carcass. The total number of East Beach cases was 25, resulting in 22 confirmed deaths (4.2% site mortality; Tables 1, 2). Daily checks of West Beach for part of the summer showed a similar timeline and effect as that observed on East Beach (Tables 1, 2). Total carcass counts across Kent, Sheep, and Hay Islands indicated a <10% mortality rate (Table 2).

During the summer 2022 breeding season, colony populations declined beginning in July (Figure 2). We assume that gulls exited the breeding colony because of normal seasonal phenology (*8*) rather than offsite deaths. Boat surveys of the surrounding Grand Manan archipelago (mid-June, mid-July) noted only 3 dead adult herring gulls in the water, and no mass mortality was reported on nearby beaches (1 dead HPAI virus–positive herring gull was found on Grand Manan on July 4; https://cfia-ncr.maps.arcgis.com/

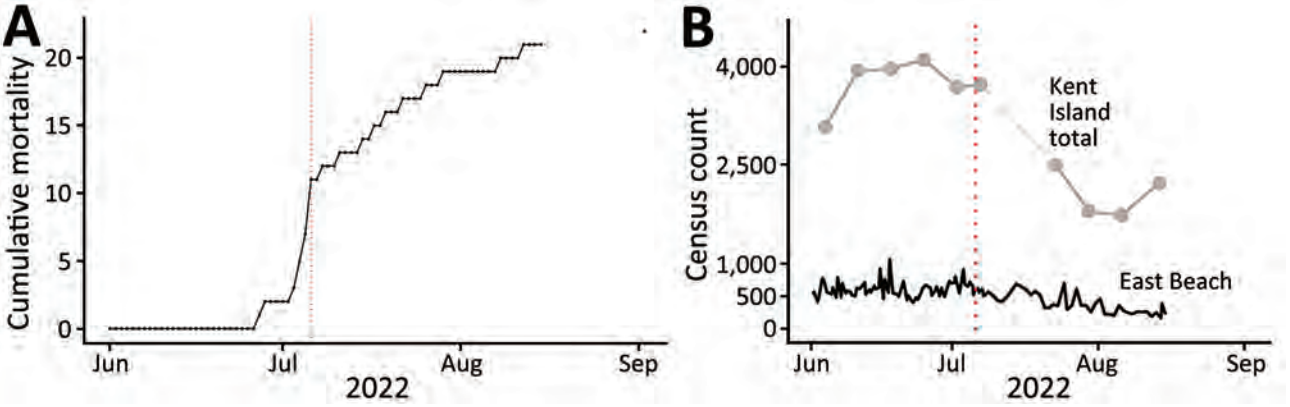

Figure 2. Adult herring gull deaths (cumulative, end-of-day) on East Beach, Kent Island, New Brunswick, Canada, in study of limited outbreak of highly pathogenic influenza A(H5N1) in herring gull colony, 2022. A) Cumulative mortality of herring gulls on East Beach during summer 2022. B) Census counts (number of breeding and nonbreeding adult herring gulls) from 1–3 surveys/day on East Beach and weekly total counts from surveys of the entire island. Red dotted lines mark July 6, the date of maximum gull deaths on East Beach.

apps/dashboards/89c779e98cdf492c899df23e1c38fdbc). Censuses in June 2023 confirmed that the Kent Island herring gull population had returned for another breeding season (mean 4,290 herring gulls).

We collected case descriptions, images, and videos of herring gull adults and chicks from Kent Island (Appendix). Putative HPAI clinical signs in herring gulls matched those observed after experimental inoculations of HPAI H5N1 in related species (*9*,*10*). Neurologic symptoms progressed from lethargy and drooped wings to incoordination, head tremors, torticollis, and immobility over the course of hours or days. During the peak of the outbreak, dozens of additional birds displayed putative minor symptoms (e.g., slumped postures, hesitancy to fly) that were difficult to track and could not be linked to subsequent death. One bird manifesting severe neurologic distress apparently recovered within hours (case 27).

We collected 3 carcasses of adult symptomatic birds (case 8, case 20, and 1 euthanized bird in southwest Kent Island on July 15) along with 3 chicks (cases C1–C3). Carcasses were collected under Canadian Wildlife Service permit no. SS2506 (to R.A.R.). All 3 adults and 1 chick (case C2) tested positive for a Eurasian strain of HPAI H5N1 virus (Appendix).

All sick or dead adult gulls throughout June and July were ≥4 years old according to plumage, matching the usual minimum breeding age for the species (Table 2) (*8*). Plumage-based censuses suggested 3%–6% of colony birds were 1–3 years of age (data not shown). Those younger birds were not breeding, and only 2 were found dead on East Beach later in the

Table 2. Putative highly pathogenic influenza A(H5N1) virus cases in herring gulls on East Beach and West Beach study areas in study of limited outbreak on Kent Island, Canada, 2022*

			First seen sick		Last seen alive		Found dead	
Case no.	Location	Age,† y	Date	Time	Date	Time	Date	Time
1	East Beach	≥4	Jun 27	≈09:30	Jun 27	≈09:30	Jun 27	≈16:30
2	East Beach	≥4	NA	NA	NA	NA	Jun 28	≈17:00
6	East Beach	≥4	Jul 2	12:11	Jul 2	12:11	Jul 3	09:38
8	East Beach	≥4	Jul 3	09:49	Jul 5	13:22	Jul 5	17:52
11	East Beach	≥4	Jul 3	20:30	Jul 3	20:30	Jul 4	08:57
12	East Beach	≥4	Jul 4	09:14	Jul 4	14:10	Jul 5	08:46
15	East Beach	≥4	Jul 4	13:51	Jul 4	17:09	Missing	NA
16	East Beach	≥4	Jul 4	14:21	Jul 5	13:22	Jul 6	12:01
18	East Beach	4	NA	NA	NA	NA	Jul 4	17:13
20	East Beach	≥4	Jul 5	08:51	Jul 6	16:46	Jul 6	19:39
24	East Beach	≥4	Jul 5	17:45	Jul 5	18:18	Jul 6	11:34
26	East Beach	≥4	Jul 5	17:10	Jul 6	11:36	Missing	NA
27	East Beach	4	Jul 6	11:54	Jul 6	19:53	Recovered?	NA
28	East Beach	≥4	NA	NA	NA	NA	Jul 6	11:58
31	East Beach	≥4	Jul 8	16:23	Jul 8	16:23	Jul 8	19:50
32	East Beach	≥4	Jul 10	16:30	Jul 10	19:45	Jul 11	16:42
33	East Beach	≥4	NA	NA	NA	NA	Jul 15	16:06
34	East Beach	≥4	NA	NA	NA	NA	Jul 17	16:25
35	East Beach	≥4	NA	NA	NA	NA	Jul 19	16:30
36	East Beach	≥4	Jul 21	07:39	Jul 21	16:26	Jul 22	09:46
37	East Beach	≥4	Jul 25	13:45	Jul 25	13:45	Jul 26	10:28
38‡	East Beach	≥4	Jul 26	10:25	Jul 26	10:25	Jul 29	08:36
39	East Beach	1	NA	NA	NA	NA	Aug 8	10:13
40	East Beach	1	NA	NA	NA	NA	Aug 12	08:13
NA	East Beach	NA	NA	NA	NA	NA	Sep 2	NA
4	West Beach	4	NA	NA	NA	NA	Jul 1	11:45
5	West Beach	≥4	Jul 1	16:18	Jul 1	16:18	Jul 1	17:20
9	West Beach	≥4	Jul 3	16:41	Jul 3	16:41	Jul 4	10:20
10	West Beach	≥4	Jul 3	16:43	Jul 3	16:43	Jul 4	10:25
13	West Beach	≥4	Jul 4	10:04	Jul 4	10:04	Jul 4	14:49
14	West Beach	≥4	NA	NA	NA	NA	Jul 4	10:11
19	West Beach	≥4	NA	NA	NA	NA	Jul 5	09:46
22	West Beach	≥4	NA	NA	NA	NA	Jul 5	17:15
25	West Beach	≥4	NA	NA	NA	NA	Jul 5	16:20
NA	West Beach	≥4	NA	NA	NA	NA	Jul 7	NA
NA	West Beach	≥4	NA	NA	NA	NA	Jul 7	NA
NA	West Beach	≥4	NA	NA	NA	NA	Jul 23	NA
NA	West Beach	NA	NA	NA	NA	NA	Sep 2	NA
NA	West Beach	NA	NA	NA	NA	NA	Sep 2	NA
NA	West Beach	NA	NA	NA	NA	NA	Sep 2	NA

*Case details are provided in the Appendix (https://wwwnc.cdc.gov/EID/article/29/10/23-0536-App1.pdf). Some carcasses were not numbered. NA, not applicable.
†Estimated according to plumage (*8*) when noted.

summer (Table 2). From 16 fully-tracked cases (Table 2) and surveys conducted 1–3 times/day, we showed the mean time (±SD) from first seen sick to last seen alive was 7.8 ±15.0 hours; the mean time from first seen sick to found dead was 20.9 ±14.9 hours.

We calculated the basic reproduction number (R_0) by using daily East Beach incidence data (June 1–August 15), gamma-distributed generation times from poultry data (4.8 ±0.58 days) (*11*), and the exponential growth rate method from the R package R0 (*12*). Overall R_0 was 1.02 (95% CI 0.95–1.11). R_0 was 8.23 (95% CI 3.97–21.11) if estimated from the rising incidence period (June 1–July 6) but fell to 0.84 (95% CI 0.64–1.07) if estimated from the falling incidence period (July 7–August 15).

HPAI was suspected or confirmed in 4 other species breeding on Kent Island (Appendix): great black-backed gulls (*Larus marinus*), Canada geese (*Branta canadensis*), common eiders (*Somateria mollissima*), and American crows (*Corvus brachyrhynchos*). Unlike the mostly intact gull carcasses on Kent Island (Appendix Table 1), many carcasses on Hay Island were partially consumed. Likely predators or scavengers were great black-backed gulls and bald eagles (*Haliaeetus leucocephalus*). Beginning in July, we noted gray seals (*Halichoerus grypus*) loitering offshore at East Beach. Seals rarely interacted with adult seabirds but harassed herring gull chicks paddling from shore.

Conclusions

A Eurasian lineage of HPAI H5N1 virus swept through the Kent Island herring gull colony starting in late June 2022. The outbreak appeared to slow within weeks (Figure 2) and resulted in <10% apparent colony mortality rate (Table 1). Low carcass disturbance (Appendix Table 1) and disease resistance or recovery (case 27) might have limited HPAI virus infections in the gulls. Furthermore, our islandwide censuses suggest 2022 population sizes were <25% of historical size across the same island area (Table 1) (*13*). Low densities might have reduced intraspecific transmission by limiting social interactions with infected conspecifics. However, we observed possible interspecific exposure routes through cohabitation (e.g., common eiders), predation/scavenging (e.g., bald eagles), and interactions between chicks and marine mammals (e.g., gray seals). Those pathways are consistent with global HPAI virus transmission between populations, including recent spillover events in mammals (*14*,*15*).

The current understanding of HPAI virus transmission in wild birds involves circulation in migratory waterfowl or roving gulls (*6*) and mass mortality events within seabird colonies (*3*,*5*). Our study suggests that limited outbreaks in seabird colonies could play an important role in HPAI transmission chains. Post hoc surveillance of mass mortality is insufficient if seabird colonies can circulate HPAI without mass mortality. Therefore, we propose that more proactive monitoring of seabirds for HPAI virus infections will be critical for guarding commercial poultry (*1*), averting potentially catastrophic zoonotic transmission (*2*), and protecting vulnerable seabirds, including gulls.

Acknowledgments

We thank Patricia Jones, Ian Kyle, Sarah Mueller, Sarah Dobney, and the students, staff, and faculty at the Bowdoin Scientific Station on Kent Island for fieldwork support; Yen-Hua Huang for providing helpful comments on the manuscript; and the Atlantic Region Canadian Wildlife Health Cooperative for assistance with laboratory testing.

Confirmatory laboratory test results were obtained from Canada's interagency surveillance program for avian influenza viruses in wild birds, a partnership that includes Environment and Climate Change Canada, the Canadian Food Inspection Agency, Canadian Wildlife Health Cooperative, and other federal, provincial, territorial, indigenous, and academic partners involved in wildlife, domestic animal, and human health (see website for full list of partners: https://cfia-ncr.maps.arcgis.com/apps/dashboards/89c779e98cdf492c899df23e1c38fdbc).

This work was supported by the National Science Foundation graduate research fellowship program (no. DGE1752134 to L.U.T.), National Science Foundation postdoctoral fellowship in biology (no. 2010904 to A.J.A.), the W.R. Coe Fund from Yale University, and Environment and Climate Change Canada.

This is contribution no. 293 of the Bowdoin Scientific Station.

About the Author

Mr. Taylor is a PhD candidate in the Department of Ecology and Evolutionary Biology at Yale University. He studies how social development influences, and is influenced by, the life history evolution of birds, with a focus on delayed reproduction and delayed plumage maturation in lekking manakins and colony-breeding gulls.

References

1. Alexander DJ. An overview of the epidemiology of avian influenza. Vaccine. 2007;25:5637–44. https://doi.org/10.1016/j.vaccine.2006.10.051
2. Horimoto T, Kawaoka Y. Pandemic threat posed by avian influenza A viruses. Clin Microbiol Rev. 2001;14:129–49. https://doi.org/10.1128/CMR.14.1.129-149.2001

3. Rijks JM, Leopold MF, Kühn S, In 't Veld R, Schenk F, Brenninkmeijer A, et al. Mass mortality caused by highly pathogenic influenza A(H5N1) virus in sandwich terns, the Netherlands, 2022. Emerg Infect Dis. 2022;28:2538–42. https://doi.org/10.3201/eid2812.221292
4. Caliendo V, Lewis NS, Pohlmann A, Baillie SR, Banyard AC, Beer M, et al. Transatlantic spread of highly pathogenic avian influenza H5N1 by wild birds from Europe to North America in 2021. Sci Rep. 2022;12:11729. https://doi.org/10.1038/s41598-022-13447-z
5. Banyard AC, Lean FZX, Robinson C, Howie F, Tyler G, Nisbet C, et al. Detection of highly pathogenic avian influenza virus H5N1 clade 2.3.4.4b in great skuas: a species of conservation concern in Great Britain. Viruses. 2022;14:212. https://doi.org/10.3390/v14020212
6. Hill NJ, Bishop MA, Trovão NS, Ineson KM, Schaefer AL, Puryear WB, et al. Ecological divergence of wild birds drives avian influenza spillover and global spread. PLoS Pathog. 2022;18:e1010062. https://doi.org/10.1371/journal.ppat.1010062
7. Anderson CM, Gilchrist HG, Ronconi RA, Shlepr KR, Clark DE, Fifield DA, et al. Both short and long distance migrants use energy-minimizing migration strategies in North American herring gulls. Mov Ecol. 2020;8:26. https://doi.org/10.1186/s40462-020-00207-9
8. Nisbet ICT, Weseloh DV, Hebert CE, Mallory ML, Poole AF, Ellis JC, et al. Herring gull (*Larus argentatus*). In: Rodewald PG, editor. Birds of North America. Ithaca (NY, USA): Cornell Lab of Ornithology; 2017.
9. Ramis A, van Amerongen G, van de Bildt M, Leijten L, Vanderstichel R, Osterhaus A, et al. Experimental infection of highly pathogenic avian influenza virus H5N1 in black-headed gulls (*Chroicocephalus ridibundus*). Vet Res. 2014;45:84. https://doi.org/10.1186/s13567-014-0084-9
10. Brown JD, Stallknecht DE, Beck JR, Suarez DL, Swayne DE. Susceptibility of North American ducks and gulls to H5N1 highly pathogenic avian influenza viruses. Emerg Infect Dis. 2006;12:1663–70. https://doi.org/10.3201/eid1211.060652
11. Kim WH, Cho S. Estimation of the basic reproduction numbers of the subtypes H5N1, H5N8, and H5N6 during the highly pathogenic avian influenza epidemic spread between farms. Front Vet Sci. 2021;8:597630. https://doi.org/10.3389/fvets.2021.597630
12. Boelle PY, Obadia T. R0: estimation of R0 and real-time reproduction number from epidemics. 2022 [cited 2023 Mar 1]. https://CRAN.R-project.org/package=R0
13. Bennett JL, Jamieson EG, Ronconi RA, Wong SNP. Variability in egg size and population declines of herring gulls in relation to fisheries and climate conditions. Avian Conserv Ecol. 2017;12:16. https://doi.org/10.5751/ACE-01118-120216
14. Runstadler JA, Puryear W. A brief introduction to influenza A virus in marine mammals. Methods Mol Biol. 2020;2123:429–50. https://doi.org/10.1007/978-1-0716-0346-8_33
15. Rijks JM, Hesselink H, Lollinga P, Wesselman R, Prins P, Weesendorp E, et al. Highly pathogenic avian influenza A(H5N1) virus in wild red foxes, the Netherlands, 2021. Emerg Infect Dis. 2021;27:2960–2. https://doi.org/10.3201/eid2711.211281

Address for correspondence: Liam U. Taylor. 21 Sachem St, Environmental Science Center, Yale University, New Haven, CT 06511, USA; email: liam.taylor@yale.edu

Antimicrobial Resistance in Slaughterhouses, Kenya

Katie A. Hamilton, Sam M. Njoroge, Kelvin Momanyi,[1] Maurice K. Murungi, Christian O. Odinga, Nicholas Bor, Allan F. Ogendo, Josiah Odaba, Joseph G. Ogola, Eric M. Fèvre, Laura C. Falzon

Slaughterhouses are hotspots for the transmission of antimicrobial-resistant pathogens. We conducted stakeholder discussions on antimicrobial-resistant pathogens within the slaughterhouse setting. Butchers were described as powerful stakeholders; challenges included limited funding and staff, inadequate infrastructure, and limited laboratory capacity. Slaughterhouse workers understood that their work increased their risk for exposure.

Antimicrobial resistance (AMR) in bacteria is one of the most serious global health threats of this century (*1*). Slaughterhouses act as disease hotspots because of frequent interactions between humans and animals (*2*), particularly in rural areas, such as western Kenya (*3*). Recent work showed that slaughterhouse workers are exposed to several zoonotic pathogens (*4*–*6*). However, little is known about the workplace risk for exposure to antimicrobial-resistant bacteria within the slaughterhouse context and the implications of workplace AMR exposure for public health and food safety in the region. This study engaged stakeholders in discussions on AMR within the slaughterhouse setting, with the objective of using baseline information to develop contextually relevant educational material and inform future research and improvements in work conditions.

The Study

This work was embedded within a larger surveillance study conducted in Busia, Bungoma, and Kakamega counties in western Kenya (*7*). In total, we conducted 6 stakeholder discussions exploring AMR in the slaughterhouse context. First, we held focus group discussions (3–9 participants) with the county veterinary officers, subcounty veterinary officers, and meat inspectors in each of the 3 counties. Focus group discussions lasted 2–3 hours, during which other topics not reported in this study (i.e., legislation and animal welfare) were also discussed. Next, we held 3 workshops for slaughterhouse workers from Bungoma (n = 60), Kakamega (n = 90), and Busia (n = 40). Participants were distributed into groups, with a maximum of 20 participants per group, and discussions lasted 45–60 minutes.

The purpose and modus operandi of the discussions were explained, and written consent was obtained from each participant. Discussions were held in English or Kiswahili, as required, and were led by moderators who used an interview guide with broad, open-ended questions (Appendix 1, https://wwwnc.cdc.gov/EID/article/29/10/23-0017-App1.pdf). All discussions were recorded and later transcribed verbatim, and translated from Kiswahili to English as needed, by an investigator. Two investigators (K.A.H., L.C.F.) thematically analyzed all transcripts, and inductively derived findings by using an interpretive–descriptive approach to identify themes emerging from the data (*8*). Each investigator coded all transcripts separately, before discussion and consensus on the main themes (Figure 1; Appendix 2, https://wwwnc.cdc.gov/EID/article/29/10/23-0017-App2.xlsx).

From the focus group discussions, we identified stakeholders who play a role in AMR within the slaughterhouse context and how they relate to each other (Figure 2). Butchers emerged as prominent and powerful stakeholders who exerted pressure on others, sometimes impeding them from carrying out

Author affiliations: University of Liverpool, Liverpool, UK (K.A. Hamilton, E.M. Fèvre, L.C. Falzon); International Livestock Research Institute, Nairobi, Kenya (K.A. Hamilton, S.M. Njoroge, K. Momanyi, M.K. Murungi, C.O. Odinga, N. Bor, A.F. Ogendo, J. Odaba, L.C. Falzon); Kenya Medical Research Institute, Nairobi (S.M. Njoroge); County Government of Busia, Busia, Kenya (A.F. Ogendo); University of Nairobi, Kenya (J.G. Ogola); University of Helsinki, Helsinki, Finland (J.G. Ogola); County Government of Bungoma, Bungoma, Kenya (J.G. Ogola)

DOI: https://doi.org/10.3201/eid2910.230017

[1]Current affiliation: Transdisciplinary Consultants Ltd., Nairobi, Kenya.

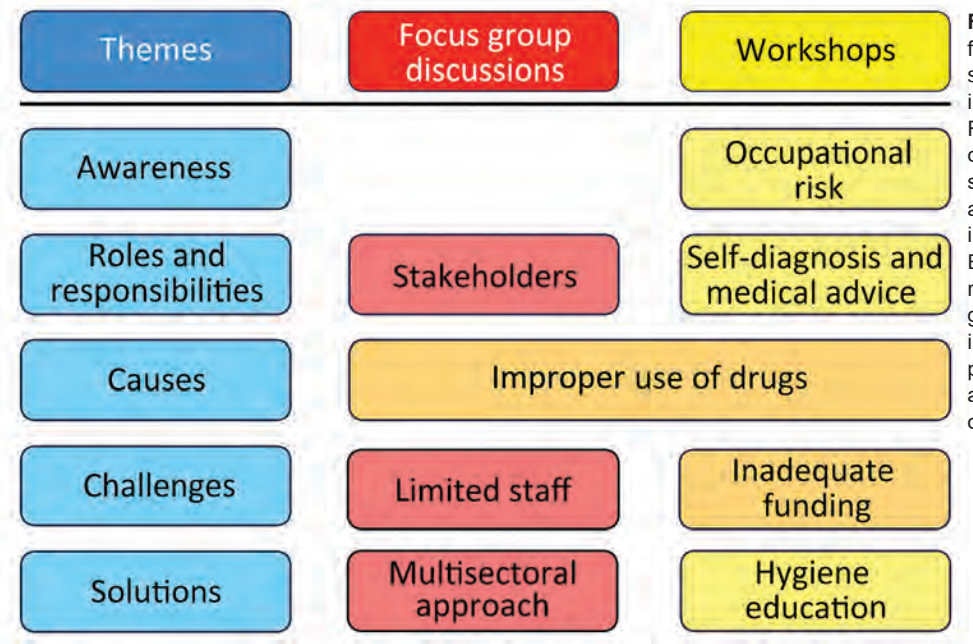

Figure 1. Themes identified from focus groups and in workshops in study of antimicrobial resistance in slaughterhouses, Kenya. Focus group discussions included county veterinary officers, subcounty veterinary officers, and meat inspectors; workshops included slaughterhouse workers. Blue indicates overall themes; red indicates results from focus group participants; yellow indicates results from workshop participants; orange indicates answers shared by both groups of participants.

their work properly. For instance, a meat inspector stated, "Because you will find a carcass has already been prepared, you come and inspect you find the injection sites are all full of drugs, now when you tell this person this animal is supposed to be condemned, my friend you will be looking for trouble, you might even be forced to run."

Participants recognized improper use of drugs as a factor driving resistance. Improper use included underdosing or overdosing animals and indiscriminate prescribing by professionals, such as medics and veterinarians. For example, a county veterinary officer stated, "If we vets also continue looking at all animals like they are 'antibiotic deficient,' that is the disease we treat, this problem will continue escalating."

Focus groups also identified challenges in dealing with bacterial AMR related to limited staff and inadequate funding, which led to underinvestments in infrastructure and equipment. Some slaughterhouses did not have access to reliable sources of clean water or lacked a perimeter fence, compromising biosecurity. Some slaughterhouse waste was disposed of indiscriminately, contaminating the surrounding environment. Participants cited the absence of surveillance to detect resistant pathogens and the lack of legislation requiring observance of withdrawal periods (periods during which animals are kept from the food chain while medications leave the body) on the farm as further hinderances.

Many participants noted that efforts to combat AMR required a multisectoral approach involving many stakeholders. In particular, they mentioned medics as a key group to include in public sensitization efforts because of the respect they command in the community.

In workshops for slaughterhouse workers, participants recognized they should seek medical advice before purchasing drugs, but admitted to often self-medicating or administering medications without a prescription because drugs, including some antibiotics, could be purchased directly from a chemist without prescription. The most popular antibiotic purchased for humans was amoxicillin and the most popular for livestock was oxytetracycline (Appendix 1).

Participants had experienced drug failure with antimalarial drugs in humans and with ectoparasitic and anthelmintic drugs in livestock. They understood that drugs often did not work because of misdiagnosis or misuse, including underdosing or not finishing the course. Participants provided various reasons for not finishing the course. A slaughterhouse worker in Bungoma said, "Sometimes you visit the chemist or clinic where a dose is prescribed for you but you don't have enough cash so maybe the drugs cost like 600 and you have 200. So, because the doctor wants money, they tell you to go with a little drug and ask after how many days will you get the money? You tell him tomorrow. You take the drugs for a few days and notice a change then stop, which also contributes because you have not finished the dose."

The workers understood that resistance was caused by a germ, and therefore transmitted in similar ways. They were also aware that their work increased

their risk of infection because of their frequent contact with animals. A slaughterhouse worker in Busia said, "So, maybe there are diseases that affect the animals and is [sic] undergoing treatment. The animal is taken to the slaughterhouse without completing the treatment, when slaughtering the animal, there is the interaction between human and the animal. In case there are injury to the human, there may be mixing of blood of the animal and human blood and hence we can also be affected."

Hygiene, both personal and at the workplace, was recognized as a key element in dealing with resistance. However, the uncertainty and poor pay associated with slaughterhouse work did not enable workers to purchase the required clothing and equipment. A slaughterhouse worker from Kakamega said, "...the pay you get is just enough to make ends meet but anything outside can't be covered. The pay is too little for people who do hardy work in the slaughterhouse."

Education was considered essential to understanding and mitigating the risk for bacterial AMR. For instance, a slaughterhouse worker in Busia stated, "Educate us on how we would be handling maybe the meat before it reaches [consumption]… Which other ways are we handling where, educating us on getting a knife, cutting meat, how to hang the meat so that it doesn't get bacteria from the ground, like you said, dust usually contains bacteria, so you educate us before undertaking the work."

Conclusions

Our analysis identified butchers as powerful stakeholders; elsewhere butchers have been described as uncooperative and profit-driven (*9*,*10*). However, their influence could be leveraged to positively influence others, and they should be included in future education campaigns or intervention strategies. Limited finances were a recurring theme, leading to poor health-seeking behaviors despite interviewees being aware of recommended good practices. Many slaughterhouse workers understood how diseases are transmitted and the importance of hygiene measures, suggesting that engagement activities previously conducted in this area (*7*,*11*) or developed as part of this work (*12*) have been effective. However, translation of knowledge into practice is often hampered by the limited resources and external pressures that the workers face.

In conclusion, long-term investments in slaughterhouses are needed to create an enabling environment that reduces the occupational risk to workers and safeguards the food they produce (*13*). Those

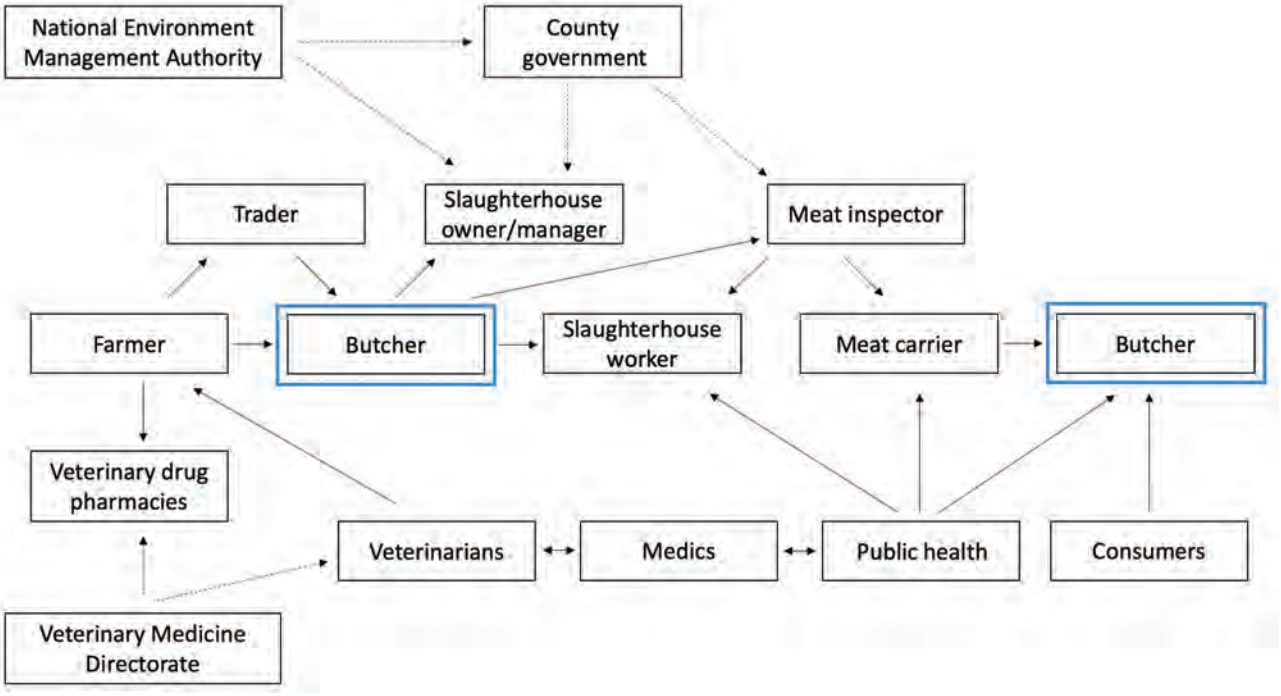

Figure 2. Relationship between stakeholders in study of antimicrobial resistance in slaughterhouses, Kenya. The chart shows relationships within the slaughterhouse context identified in focus group discussions conducted with county veterinary officers, subcounty veterinary officers, and meat inspectors, and in workshops conducted with slaughterhouse workers in western Kenya. Dotted arrows indicate stakeholders with authority to introduce or enforce regulations; solid arrows indicate relationships between stakeholders. Blue boxes indicate a stakeholder whose influence could be leveraged to positively influence others. Further information about stakeholders can be found in Appendix 1 (https://wwwnc.cdc.gov/EID/article/29/10/23-0017-App1.pdf).

investments need to be accompanied by investments in laboratory networks and surveillance efforts to better detect and mitigate AMR spread within the slaughterhouse context (*14*).

Acknowledgments

We thank the county veterinary officers, subcounty veterinary officers, meat inspectors, and slaughterhouse workers who participated in this study.

This study received support from the CGIAR One Health initiative, Protecting Human Health through a One Health Approach, which was supported by contributors to the CGIAR Trust Fund (https://www.cgiar.org).

K.A.H., S.M.N., K.M., M.K.M., C.O.O., N.B., J.O., E.M.F., and L.C.F. were all supported by The Zoonoses in Livestock in Kenya (ZooLinK) project supported by the Biotechnology and Biological Sciences Research Council, the Department for International Development, the Economic and Social Research Council, the Medical Research Council, the Natural Environment Research Council, and the Defence Science and Technology Laboratory, under the Zoonoses and Emerging Livestock Systems (ZELS) program (grant no. BB/L019019/1).

About the Author

Dr. Hamilton is a postdoctoral research scientist at the Institute of Infection, Veterinary & Ecological Sciences, University of Liverpool, UK and International Livestock Research Institute, Nairobi, Kenya. Her current interests include the antimicrobial landscape within communities, in particular the antimicrobial resistance relationship between animals and humans, and the use of waste-based epidemiology as a surveillance tool for antimicrobial resistance genes and emerging diseases in lower- and middle-income countries.

References

1. World Health Organization. Global Antimicrobial Resistance and Use Surveillance System (GLASS) [cited 2023 Aug 12]. https://www.who.int/initiatives/glass
2. Fasanmi OG, Ayodeji IO, Oloso NO, Fasina FO. Retrospective studies of abattoir zoonoses in Nigeria: public health implications. Perspect Agric Vet Sci Nutr Nat Resour. 2017;12:1–12. https://doi.org/10.1079/PAVSNNR201712058
3. Cook EAJ, de Glanville WA, Thomas LF, Kariuki S, Bronsvoort BMC, Fèvre EM. Working conditions and public health risks in slaughterhouses in western Kenya. BMC Public Health. 2017;17:14. https://doi.org/10.1186/s12889-016-3923-y
4. Cook EAJ, de Glanville WA, Thomas LF, Kariuki S, Bronsvoort BMC, Fèvre EM. Risk factors for leptospirosis seropositivity in slaughterhouse workers in western Kenya. Occup Environ Med. 2017;74:357–65. https://doi.org/10.1136/oemed-2016-103895
5. Cook EAJ, de Glanville WA, Thomas LF, Kiyong'a A, Kivali V, Kariuki S, et al. Evidence of exposure to *C. burnetii* among slaughterhouse workers in western Kenya. One Health. 2021;13:100305. https://doi.org/10.1016/j.onehlt.2021.100305
6. Cook EAJ, Gitahi N, de Glanville WA, Thomas LF, Kariuki S, Kang'ethe E, et al. Prevalence and risk factors for exposure to *Toxoplasma gondii* in slaughterhouse workers in western Kenya. BMC Infect Dis. 2021;21:944. https://doi.org/10.1186/s12879-021-06658-8
7. Falzon LC, Alumasa L, Amanya F, Kang'ethe E, Kariuki S, Momanyi K, et al. One Health in action: operational aspects of an integrated surveillance system for zoonoses in western Kenya. Front Vet Sci. 2019;6:252. https://doi.org/10.3389/fvets.2019.00252
8. Maykut P, Morehouse R. Beginning qualitative research: a philosophical and practical guide. 1st ed. London: Routledge; 1994.
9. Murungi MK, Muloi DM, Muinde P, Githigia SM, Akoko J, Fèvre EM, et al. The Nairobi pork value chain: mapping and assessment of governance, challenges, and food safety issues. Front Vet Sci. 2021;8:581376. https://doi.org/10.3389/fvets.2021.581376
10. Ameso EA, Bukachi SA, Olungah CO, Haller T. Ethnography of the slaughterhouse: a case of Nanyuki slaughterhouse in Laikipia County, Rift Valley, Kenya. Pastoralism. 2017;7:32. https://doi.org/10.1186/s13570-017-0107-z
11. Falzon LC, Ogola JG, Odinga CO, Naboyshchikov L, Fèvre EM, Berezowski J. Electronic data collection to enhance disease surveillance at the slaughterhouse in a smallholder production system. Sci Rep. 2021;11:19447. https://doi.org/10.1038/s41598-021-98495-7
12. Murungi MK, Momanyi K, Odinga CO, Bor N, Ogendo A, Ogola J, et al. Antimicrobial resistance (AMR) educational video, 2019 [cited 2023 Aug 12]. https://www.youtube.com/watch?v=T472S-zYZf0&t=0s
13. Grace D, Dipeolu M, Alonso S. Improving food safety in the informal sector: nine years later. Infect Ecol Epidemiol. 2019;9:1579613. https://doi.org/10.1080/20008686.2019.1579613
14. Bett K, Vijaykumar C, Slotin J, Kiambi S, Wesangula E, Tanui E, et al. People power: using citizen-generated data to address antimicrobial resistance in Kenya [cited 2023 Aug 12]. https://www.data4sdgs.org/sites/default/files/2021-09/AMR-report-V4.pdf

Address for correspondence: Katie A. Hamilton or Laura C. Falzon; Institute for Infection, Veterinary and Ecological Sciences, University of Liverpool, Liverpool, L69, 3BX, UK; e-mail: Katie.Hamilton@liverpool.ac.uk or Laura.Falzon@liverpool.ac.uk

Human-to-Human Transmission of Andes Virus Modeled in Syrian Hamsters

Silke A. Riesle-Sbarbaro, Norman Kirchoff, Katharina Hansen-Kant, Alice Stern, Andreas Kurth, Joseph B. Prescott

Several occurrences of human-to-human transmission of Andes virus, an etiological agent of hantavirus cardiopulmonary syndrome, are documented. Syrian hamsters consistently model human hantavirus cardiopulmonary syndrome, yet neither transmission nor shedding has been investigated. We demonstrate horizontal virus transmission and show that Andes virus is shed efficiently from both inoculated and contact-infected hamsters.

Hantavirus cardiopulmonary syndrome (HCPS) is a sporadic, lethal (>40% fatality rates) zoonotic disease, which in South America is primarily caused by Andes virus (ANDV) (*1*). HCPS is prevalent where the natural rodent reservoir, the long-tailed colilargo (*Oligoryzomys longicaudatus*), is present. Zoonotic transmission was thought to occur exclusively through exposure to aerosolized infectious particles from excreta or secreta of infected reservoirs (*2*). However, unique to ANDV among hantaviruses, person-to-person transmission events have been described, highlighting the potential importance of onward transmission for outbreaks (*3*–*5*).

Syrian hamsters (*Mesocricetus auratus*) infected with ANDV uniquely mimic many aspects of humans with ANDV-HCPS disease (*6*,*7*). This model has been crucial for understanding HCPS immunopathology and for developing potential therapeutic treatments (*8*–*11*). Although disease modeling in hamsters has been characterized extensively, studies of virus shedding and transmission are absent. In this study, we investigated whether horizontal transmission can be modeled in ANDV-infected hamsters.

The Study

To model ANDV shedding and transmission between hamsters, we placed 6 pairs of intranasally-inoculated (200 PFU equivalences of ANDV-9717869) hamsters in clean cages 1 day postinoculation (dpi). To increase contact events, we then introduced 6 pairs of naive hamsters (i.e., contacts) to the inoculated hamsters (6 cages) (Appendix Figure 1, https://wwwnc.cdc.gov/EID/article/29/10/23-0544-App1.pdf). Infectious work was performed within the Biosafety Level 4 facility at the Robert Koch Institute (Berlin, Germany). Animal experiments were approved by Landesamt für Gesundheit und Soziales (permit no. G0142/21). Approval of animal experimentation within Biosafety Level 4 facilities at the Robert Koch Institute was granted by the Regional Office for Health and Social Affairs, Berlin.

We implanted all hamsters with temperature-logging transponders (IPTT-300 Temperature Transponder; Plexx, https://www.plexx.eu). Throughout the experiment, we observed hamsters daily to assess disease signs. Pathognomonic acute disease signs (*6*,*11*) were a criterion for euthanasia, and surviving animals were euthanized at 40 dpi. At 27 dpi, one naive animal (c1-n1) was euthanized for unrelated illness (Table 1). Under isoflurane sedation, all animals were routinely weighed and sampled (oral and rectal mucosa and, opportunistically, urine). We collected blood and tissue samples at euthanasia. ANDV RNA copies and nucleocapsid IgG were measured as reported (*10*).

Irrespective of inoculation route, infected hamsters typically succumb uniformly to disease (*6*); however, 16.7% of the inoculated cohort survived, potentially because of the lower intranasal infection efficacy (>8-fold inoculum dose required) than that of an intramuscular infection (Table 1). Hamster c6-i2 recovered from moderate disease, and hamster c1-i1 remained healthy. All inoculated hamsters seroconverted (Table 1) and shed abundant ANDV RNA through tested routes until being euthanized (Figure 1, panels A–D; Figure 2; Appendix Figure 2, panel A). Onset of shedding averaged 6 dpi (5 dpi orally and

Author affiliation: Robert Koch Institute, Berlin, Germany

DOI: https://doi.org/10.3201/eid2910.230544

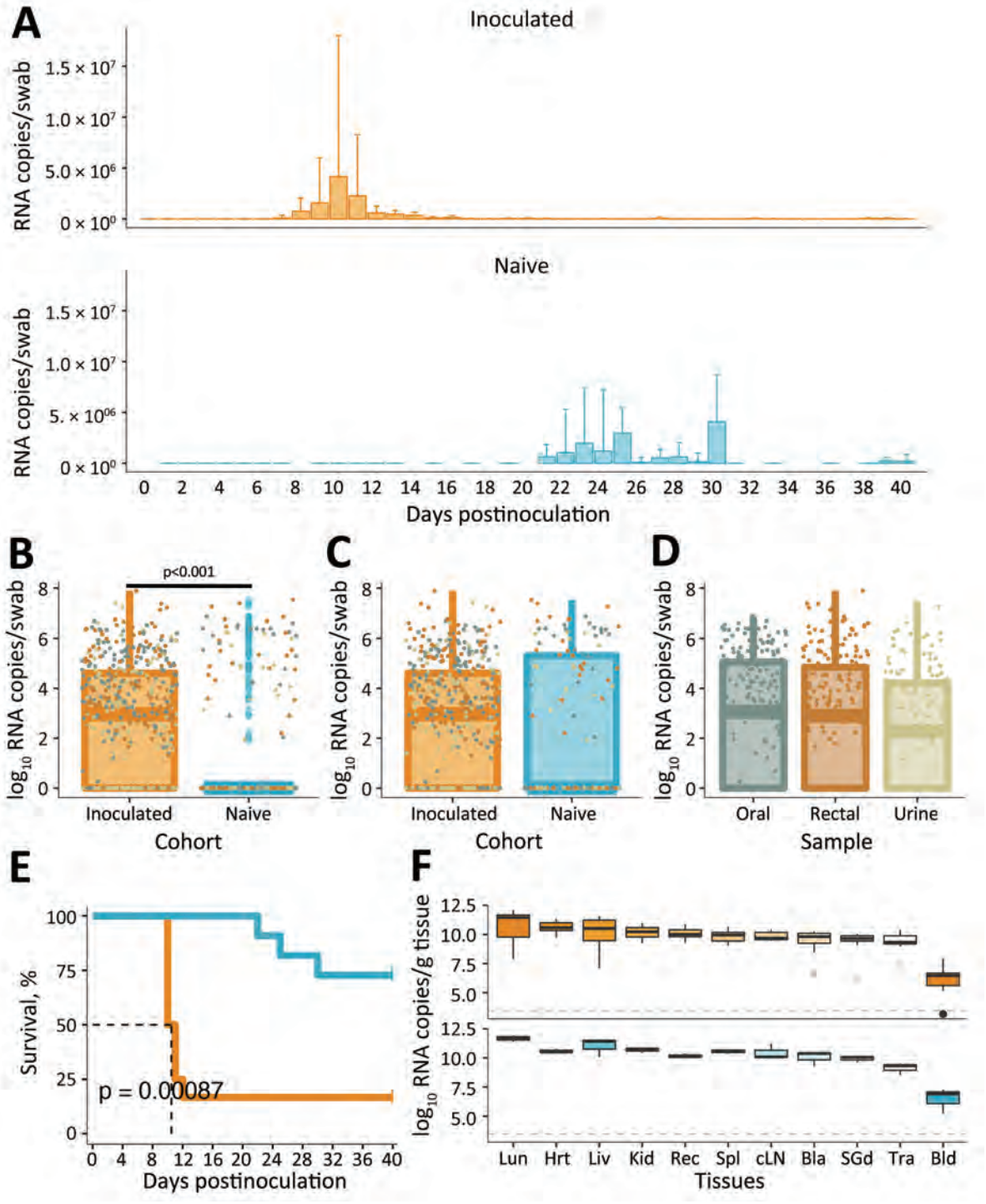

Figure 1. Dissemination and shedding of Andes virus (ANDV) in secretions and excretions of infected Syrian hamsters. A) ANDV RNA small segment loads in oral and rectal mucosa and urine sampled per day postinoculation throughout the experiment. B–C) Total ANDV RNA detected in all shedding routes (oral and rectal mucosa and urine), compared between cohorts (B) and between infected animals of each cohort (C) after adjustment of incubation days (AID). D) Comparison of ANDV RNA load between oral and rectal mucosa samples and urine samples from infected animals, using AID. Individual oral, rectal and urine samples are shown as points. Geometric mean RNA loads are displayed for $\log_{10}$ transformed data in panels B–D; error bars indicate SDs. E) Statistical analysis of survival between cohorts. Significance of Mantel-Cox log-rank test is shown within the plot ($p<0.001$). F) ANDV RNA distribution shown per gram of tissue or milliliter of blood. As reference, the horizontal grey line shows the inoculum dose. Bla, bladder; Bld, blood; cLN, cervical lymph node; Hrt, heart; Kid, kidney; Liv, liver; Lun, lung; Rec, rectum; SGd, submandibular salivary gland; Spl, spleen; Tra, trachea.

6 dpi rectally and in urine). Shedding was detected as early as 1 dpi in oral mucosa and urine, and peak shedding occurred consistently 1 day before euthanasia. Horizontal ANDV transmission was evidenced in 45% of the naive cohort (5/11 contacts), but HCPS developed in only 3 hamsters before the predetermined experimental endpoint (Table 1). Survival was significantly different between cohorts (Figure 1, panel E); inoculated hamsters had a median survival of 10.5 dpi and a 7.6-fold greater chance of death than infected

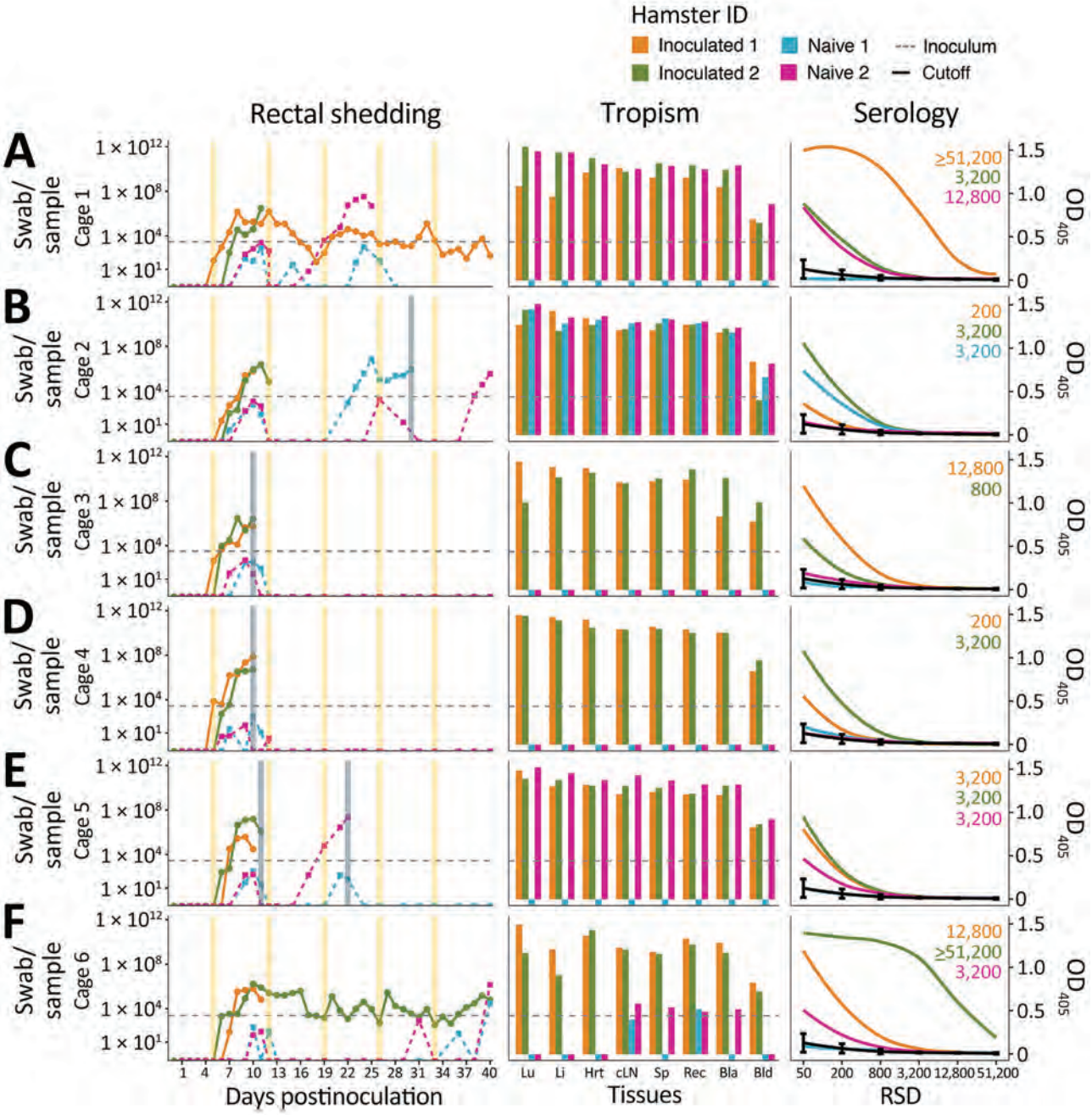

Figure 2. Timeline of Andes virus (ANDV) shedding and transmission between inoculated and naive Syrian hamster pairs from each cage. Panels A–F show data for cages 1–6. Left column displays shedding of ANDV RNA loads per rectal mucosa swab sample. Shedding loads of individual animals are shown as color-coded lines. Vertical shades show routine (yellow) or extra (grey) cage changes. Middle column displays tissue distribution of ANDV RNA per gram of tissue or milliliter of blood. The dashed horizontal grey line shows the inoculum dose. Right column displays results of nucleocapsid ELISA of serum collected at euthanasia. Antinucleocapsid serum titers are noted for animals that seroconverted. The assay cutoff is shown as a black curve with vertical line-ranges (mean ±3 SD) of each serum dilution. To improve figure visualization, the y-axes in panels A–C were $\log_{10}$-transformed. Bla, bladder; Bld, blood; cLN, cervical lymph node; Hrt, heart; ID, identification; Li, liver; Lu, lung; OD_{405}, Optical density at 405 nm; Rec, rectum; RSD, reciprocal serum dilutions; Sp, spleen.

Table 1. Study design and disease progression in study of human-to-human transmission of Andes virus modeled in Syrian hamsters*

Cage no.	Inoculated	Ab titer	Status	Naive	Ab titer	Status
1	c1-i1	≥51200	Infected	c1-n1	Excluded	
	c1-i2	3200	Disease	c1-n2	12800	Disease
2	c2-i1	200	Disease	c2-n1	3200	Disease
	c2-i2	3200	Disease	c2-n2	Negative	Infected
3	c3-i1	12800	Disease	c3-n1	Negative	Uninfected
	c3-i2	800	Disease	c3-n2	Negative	Uninfected
4	c4-i1	200	Disease	c4-n1	Negative	Uninfected
	c4-i2	3200	Disease	c4-n2	Negative	Uninfected
5	c5-i1	3200	Disease	c5-n1	Negative	Uninfected
	c5-i2	3200	Disease	c5-n2	3200	Disease
6	c6-i1	12800	Disease	c6-n1	Negative	Uninfected
	c6-i2	≥51200	Recovered	c6-n2	3200	Infected
Total infected			100%		45%	
Total HCPS			83%		27%	

*AB, antibody; HCPS, Hantavirus-induced cardiopulmonary syndrome.

contacts (Table 2). However, ANDV was transmitted to 2 other contacts; animal c2-n2 likely evidenced a transmission chain from c2-n1, which potentially had the longest incubation time in this experiment (≥18 days). Hamster c2-n2 had abundant and disseminated ANDV RNA in tissue samples (Figure 2, middle column) but was the only infected contact that failed to mount an anti-N antibody response (Figure 2, right column). Animal c6-n2 was likely infected after a late transmission from the persistent shedding of animal c6-i2. Infection of c6-n2 was strongly suggested by the increasing ANDV RNA in rectal mucosa at 40 dpi, which was above intracage cross-contamination levels (Figure 2, panel F, left column). In addition, we detected intermediate loads of ANDV RNA in 4 tissue samples, and this hamster seroconverted (Table 1; Figure 2, panel F, middle and right columns).

Overall, virus replication and dissemination were not different between inoculated animals and infected contacts. Aside from hamster c6-n2, which was likely in an early phase of infection, all infected animals showed virus distribution consistent with previous studies (*7*,*11*); lung and liver samples harbored the highest ANDV RNA loads at euthanasia (Figure 1, panel F). Pairwise tissue comparison among cohorts revealed no significant differences in ANDV RNA loads in animals that became infected (Appendix Figure 3). Likewise, after adjusting incubation days in the naive cohort (Appendix Figure 4), shedding loads did not differ between infected animals of either cohort (Figure 1, panels B–C) or by route of shedding (Figure 1, panel D) or shedding duration (Appendix Figure 5). Yet, shedding onset was delayed in contact animals (by 9–30 adjusted incubation days). Other parameters (i.e., periodic weight loss and temperature variation) did not differ significantly between cohorts of infected animals (Appendix Figures 6, 7).

Conclusions

Reports of human-to-human ANDV transmission in recent decades (*3*–*5*), which could be driven by specific mutations of ANDV (*12*), highlight the importance of this phenomenon. In a 2018–2019 outbreak in Chubut Province, Argentina, for example, 33 persons were estimated to be infected after chains of transmissions started from 1 infectious person (*5*). The potential for human-to-human transmission has drastic implications for public health. Not only is spillover from reservoirs a consideration, but human transmission chains add further complexity in outbreak settings, requiring additional control measures, potential quarantine of infected persons and contacts, and additional precautions in dealing with HCPS patients.

We established an efficient model of ANDV transmission between hamsters and a method for monitoring infection. Moreover, because ANDV shedding loads did not differ by route in infected hamsters and oral shedding began 1 day earlier than with other routes, this model can be further simplified. We describe ANDV shedding kinetics in infected Syrian hamsters, but because of the known difficulties in Andes virus isolation (*13*), we cannot accurately determine infectious shedding kinetics. Still, infectious particles were shed from ≥4 of the inoculated animals, 1 of which was a persistent shedder. New World hantaviruses are thought to persistently infect and be

Table 2. Hazard risks of survival and relative risk of infection of the naïve cohort compared to the inoculated cohort in study of human-to-human transmission of Andes virus modeled in Syrian hamsters*

Cohort	Deaths, %	Infected, %	HR (95% CI)	p value	RR (95% CI)	p value
Naive	27	45	0.13 (0.03−0.5)	0.003	0.45 (0.2–0.9)	0.017

*HR, hazard risk; RR, relative risk.

intermittently shed from reservoir hosts (*2*). However, persistent shedding has not been reported in humans or animal models. Although ANDV RNA has been detected in body fluids of humans with HCPS (*14*), infectious virus has only been isolated from blood (presymptomatic) (*1*). Unfortunately, because of the study endpoint, we could not evaluate prolonged infectious shedding from an asymptomatic animal (c1-i1).

We also demonstrate that infectious ANDV was serially shed from an infected hamster to a naive hamster, then on to another naive hamster (cage 2). Viral shedding onset was delayed in the naive cohort, particularly for serial transmission. This delay could be because of our rudimentary adjusted incubation day threshold or could be a consequence of the transmission route, the transmitted dose (*7*), or even virus adaptation (*13*). Further studies are warranted to elucidate accurate incubation periods, transmission rates, and routes (e.g., contact, fomite, or aerosol). Increasing the experimental time frame also could have improved the results of this study.

Disease could not be verified for 2 infected contact animals. Whether disease would have developed to an extent requiring euthanasia is uncertain. In the case of hamster c2-n2, the high viral abundance and dissemination, paired with a lack of ANDV-specific antibodies could have enabled disease progression; favorable prognosis in humans is correlated with a strong IgG response early in disease (*15*).

In summary, our results demonstrate that the Syrian hamster is an appropriate model for horizontal transmission of ANDV. We demonstrated clear pathogenesis and further horizontal transmission in contact animals.

This work was funded by Robert Koch Institute.

About the Author

Dr. Riesle-Sbarbaro is a veterinarian and a postdoctoral researcher working in the Centre for Biological Threats and Special Pathogens at Robert Koch Institute, Berlin, Germany. Her research interests include comparative infection profiles of filoviruses to study potential reservoir hosts.

Reference

1. Galeno H, Mora J, Villagra E, Fernandez J, Hernandez J, Mertz GJ, et al. First human isolate of Hantavirus (Andes virus) in the Americas. Emerg Infect Dis. 2002;8:657–61. https://doi.org/10.3201/eid0807.010277
2. Schountz T, Prescott J. Hantavirus immunology of rodent reservoirs: current status and future directions. Viruses. 2014;6:1317–35. https://doi.org/10.3390/v6031317
3. Martinez VP, Bellomo C, San Juan J, Pinna D, Forlenza R, Elder M, et al. Person-to-person transmission of Andes virus. Emerg Infect Dis. 2005;11:1848–53. https://doi.org/10.3201/eid1112.050501
4. Padula PJ, Edelstein A, Miguel SDL, López NM, Rossi CM, Rabinovich RD. Hantavirus pulmonary syndrome outbreak in Argentina: molecular evidence for person-to-person transmission of Andes virus. Virology. 1998;241:323–30. https://doi.org/10.1006/viro.1997.8976
5. Martínez VP, Di Paola N, Alonso DO, Pérez-Sautu U, Bellomo CM, Iglesias AA, et al. "Super-spreaders" and person-to-person transmission of Andes virus in Argentina. N Engl J Med. 2020;383:2230–41. https://doi.org/10.1056/NEJMoa2009040
6. Safronetz D, Ebihara H, Feldmann H, Hooper JW. The Syrian hamster model of hantavirus pulmonary syndrome. Antiviral Res. 2012;95:282–92. https://doi.org/10.1016/j.antiviral.2012.06.002
7. Hooper JW, Larsen T, Custer DM, Schmaljohn CS. A lethal disease model for hantavirus pulmonary syndrome. Virology. 2001;289:6–14. https://doi.org/10.1006/viro.2001.1133
8. Williamson BN, Prescott J, Garrido JL, Alvarez RA, Feldmann H, Barría MI. Therapeutic efficacy of human monoclonal antibodies against Andes virus infection in Syrian hamsters. Emerg Infect Dis. 2021;27:2707–10. https://doi.org/10.3201/eid2710.210735
9. Prescott J, DeBuysscher BL, Brown KS, Feldmann H. Long-term single-dose efficacy of a vesicular stomatitis virus-based Andes virus vaccine in Syrian hamsters. Viruses. 2014;6:516–23. https://doi.org/10.3390/v6020516
10. Prescott J, Safronetz D, Haddock E, Robertson S, Scott D, Feldmann H. The adaptive immune response does not influence hantavirus disease or persistence in the Syrian hamster. Immunology. 2013;140:168–78. https://doi.org/10.1111/imm.12116
11. Safronetz D, Zivcec M, Lacasse R, Feldmann F, Rosenke R, Long D, et al. Pathogenesis and host response in Syrian hamsters following intranasal infection with Andes virus. PLoS Pathog. 2011;7:e1002426. https://doi.org/10.1371/journal.ppat.1002426
12. Bellomo CM, Alonso DO, Pérez-Sautu U, Prieto K, Kehl S, Coelho RM, et al. Andes virus genome mutations that are likely associated with animal model attenuation and human person-to-person transmission. MSphere. 2023;8:e0001823. https://doi.org/10.1128/msphere.00018-23
13. Prescott J, Feldmann H, Safronetz D. Amending Koch's postulates for viral disease: when "growth in pure culture" leads to a loss of virulence. Antiviral Res. 2017;137:1–5. https://doi.org/10.1016/j.antiviral.2016.11.002
14. Godoy P, Marsac D, Stefas E, Ferrer P, Tischler ND, Pino K, et al. Andes virus antigens are shed in urine of patients with acute hantavirus cardiopulmonary syndrome. J Virol. 2009;83:5046–55. https://doi.org/10.1128/JVI.02409-08
15. Valdivieso F, Vial P, Ferres M, Ye C, Goade D, Cuiza A, et al. Neutralizing antibodies in survivors of Sin Nombre and Andes hantavirus infection. Emerg Infect Dis. 2006;12:166–8. https://doi.org/10.3201/eid1201.050930

Address for correspondence: Joseph B. Prescott, Robert Koch Institute, Seestrasse 10, 13353, Berlin, Germany; email: PrescottJ@rki.de

Angiostrongylus cantonensis Infection in Brown Rats (*Rattus norvegicus*), Atlanta, Georgia, USA, 2019–2022

Nicole L. Gottdenker, Rafael Antonio Nascimento Ramos, Hassan Hakimi, Brittany McHale, Sam Rivera, Bryce M. Miller, Elizabeth W. Howerth, Caitlin E. Burrell, Justin M. Stilwell, Rita McManamon, Guilherme G. Verocai

Rat lungworm (*Angiostrongylus cantonensis*), a zoonotic parasite invasive to the United States, causes eosinophilic meningoencephalitis. *A. cantonensis* harbors in rat reservoir hosts and is transmitted through gastropods and other paratenic hosts. We discuss the public health relevance of autochthonous *A. cantonensis* cases in brown rats (*Rattus norvegicus*) in Atlanta, Georgia, USA.

Rat lungworm, *Angiostrongylus cantonensis* (Strongylida: Metastrongyloidea), causes eosinophilic meningoencephalitis (neural angiostrongyliasis) in humans and other accidental mammal hosts. This vectorborne nematode has an indirect life cycle in which several rodent species, including *Rattus* spp., serve as definitive hosts (*1*). Rodents become infected by ingesting terrestrial gastropods acting as intermediate hosts infected with third-stage larvae (L3). In the rodent host, L3 migrate through vasculature to the central nervous system and after 2 molts become adult nematodes that migrate to the pulmonary artery (*1*). After mating, females lay eggs that hatch first-stage larvae (L1) in lung airspaces. L1 ascend the trachea, pass into the digestive system after being swallowed by the host rat, and exit the body through feces (*1*). Subsequently, gastropods ingest nematode L1 after which the larvae develop to the infective L3 stage. Paratenic hosts, such as fish, frogs, and crustaceans, can also harbor *A. cantonensis* L3, which can be transferred to rodents and accidental hosts (*2*).

A. cantonensis, originally described in Asia, where most human infections are reported, is now endemic in different regions of the world (*2*). In the United States, *A. cantonensis* was initially reported in Hawaii (*3*), and later in Texas, Louisiana, Alabama, and Florida, likely introduced by infected rats and gastropods through trade routes, such as on merchant ships (*3*–*7*). We confirm autochthonous *A. cantonensis* infection in brown rats (*Rattus norvegicus*) in Atlanta, Georgia, USA, and briefly discuss the relevance of these findings to human and animal health.

The Study

We collected tissue samples (brain, heart, liver, kidney, lung, spleen, skeletal muscle, skin, gastrointestinal tract, adrenal gland, and gonads) from 33 wild brown rats found dead during 2019–2022 on the grounds of a zoological facility located in Atlanta, Fulton County, Georgia (33°44′1.536″N; 84°22′19.416″W). We stored samples in 10% neutral buffered formalin and processed them for routine histopathologic evaluation as part of opportunistic monitoring of wildlife found dead on zoo grounds. Of the rats we histologically evaluated, 7/33 (21.2%) had nematodes in heart, pulmonary artery, and brain tissues (Table; Figure).

Where intravascular nematodes were observed, we extracted genomic DNA from paraffin-embedded tissue sections using QIAamp DNA

Author Affiliations: University of Georgia College of Veterinary Medicine, Athens, Georgia, USA (N.L. Gottdenker, B. McHale, B.M. Miller, E.W. Howerth, C.E. Burrell, R. McManamon); Texas A&M University School of Veterinary Medicine and Biomedical Sciences, College Station, Texas, USA (R.A.N. Ramos, H. Hakimi, G.G. Verocai); Zoo Atlanta, Atlanta, Georgia, USA (S. Rivera); Mississippi State University College of Veterinary Medicine, Starkville, Mississippi, USA (J.M. Stilwell)

DOI: https://doi.org/10.3201/eid2910.230706

Table. Histopathologic findings of *Angiostrongylus cantonensis* nematode infection and molecular confirmation in brown rats (*Rattus norvegicus*), Atlanta, Georgia, USA, 2019–2022*

ID, age class/sex	Case submission date	Histopathologic findings	GenBank accession no.
Case 1, adult/M	2019 Feb 19	Brain: hemorrhagic and lymphohistiocytic meningoencephalitis with intralesional nematodiasis (adult nematodes, presumptive *Angiostrongylus* spp.)	OQ793715
Case 2, adult/F	2021 Feb 12	Lung: severe multifocal chronic nodular nematodiasis (adult nematodes and larvated ova, presumptive *Angiostrongylus* spp.)	OQ793716
Case 3, juvenile/ unknown	2021 Jan 20	Heart: intravascular (i.e., cardiac chamber, pulmonary artery) nematodiasis	NA
Case 4, Age unknown/unknown	2021 Aug 24	Lung: pulmonary arterial nematodiasis; pulmonary hemorrhage and edema	NA
Case 5, adult/unknown	2022 Apr 25	Heart and pulmonary artery: cardiac nematodiasis with endothelial pulmonary aortic subendothelial myxomatous change Lung: nematode cross section with similar characteristics to heart nematodes	NA
Case 6, adult/unknown	2022 Aug 09	Heart and pulmonary artery: intraventricular and intra-arterial nematodiasis Lung: moderate intraluminal, peritracheal, and pulmonary hemorrhage	OQ793717
Case 7, adult/M	2022 Oct 18	Lung: eosinophilic pulmonary arteritis with degenerate intraluminal nematodes	OQ793718

*Pre- or postmortem predation of some rats might have occurred before rats were found. Thus, representative samples of all organs might not have been available for evaluation and in some cases, sex or age class could not be determined. ID, identification; NA, not available.

FFPE Tissue Kit (QIAGEN, https://www.qiagen.com) according to manufacturer recommendations. PCR reactions targeted a 200-bp segment of the mitochondrial cytochrome oxidase subunit 1 gene (*cox1*). We performed a 25 μL reaction containing 0.25 μmol each of primers CO1ACF7 (5′-TGCCTGCTTTTGGGATTGTTAGAC-3′) and CO1ACR7 (5′-TCACTCCCGTAGGAACCGCA-3′), 1× GoTaq Green Master Mix (Promega Corporation, https://www.promega.com), and 2.5 μL of DNA template (*8*). Cycling procedure involved initial denaturation at 95°C for 2 min, then 40 cycles at 95°C for 30 s, 50°C for 30 s, 72°C for 90 s, and a final extension at 72°C for 5 min. We used nuclease-free water as a negative control and DNA of *Dirofilaria immitis* as a positive control. We purified PCR

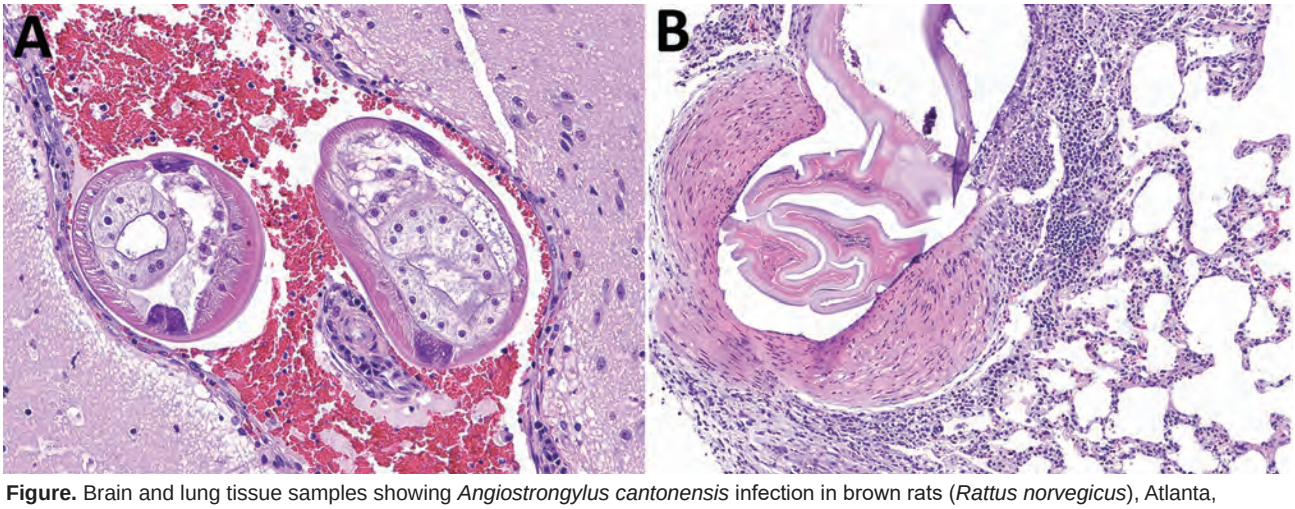

Figure. Brain and lung tissue samples showing *Angiostrongylus cantonensis* infection in brown rats (*Rattus norvegicus*), Atlanta, Georgia, USA, 2019–2022. A) Representative tissue section from the brain, stained with hematoxylin and eosin. The meninges and ventricles are multifocally and moderately expanded by abundant hemorrhage. Within the meninges and ventricles, occasional cross sections through nematodes can be seen. Nematodes were ≈250–300 μm in diameter with a thin eosinophilic cuticle, pseudocoelom, polymyarian coelomyarian musculature, lateral chords, and multinucleated intestine. Original magnification ×200 μm. B) Representative tissue section from the lung stained with hematoxylin and eosin. A large pulmonary artery contains fragments of a degenerative nematode characterized by a thin eosinophilic cuticle, pseudocoelomic space, and polymyarian coelomyarian musculature. The subtending arterial wall was sometimes necrotic and variably infiltrated by eosinophils, lymphocytes, and macrophages. The vessel also displays hypertrophy of the tunica media and occasional hypertrophy of the endothelial cells. Original magnification ×100 μm.

products using the EZNA Cycle Pure Kit (OMEGA Bio-Tek, https://www.omegabiotek.com) according to manufacturer instructions. We aligned and compared generated sequences with homologous *A. cantonensis* sequences available in GenBank. We determined genetic distances and performed phylogenetic analysis using MEGA X 10.1 (*9*) (Table).

Our molecular analysis confirmed the identity of *A. cantonensis* in 4/7 samples that had nematodes visible on histologic examination of heart, pulmonary artery, and brain tissues (Table). All 4 sequences were 100% identical to each other and to *A. cantonensis* sequences belonging to haplotype 17a, previously reported from Louisiana, USA. Among homologous sequences available in GenBank from *A. cantonensis* isolates from the United States, those belonging to haplotype 17b (Louisiana and California) were 99.5% similar, haplotype 8b (Louisiana) 98.9% similar, and haplotype 5a (Hawaii) 98.9% similar to those in haplotype 17a. Overall, compared with other *A. cantonensis* haplotypes included in the phylogenetic analysis, similarity of sequences ranged from 93.1%–99.5%, clustering in a clade with 86% bootstrap support (Appendix, https//wwwnc.cdc.gov/EID/article/29/10/23-0706-App1.pdf).

Conclusions

Discovery of autochthonous cases of *A. cantonensis* infection in definitive host rodents collected during 2019–2022 in the state of Georgia suggests that this zoonotic parasite was introduced to and has become established in a new area of the southeastern United States. Although we molecularly confirmed diagnosis in only 4/7 cases, the remaining rats had intravascular nematodes morphologically consistent with *A. cantonensis* and typical associated lesions. We could not molecularly confirm the remaining 3 cases because of insufficient sample quality and DNA degradation; thus, we could not rule out the presence of other nematode species.

Because *A. cantonensis* lungworm previously was identified in rats in neighboring states Florida and Alabama, *A. cantonensis* populations likely were in Georgia much earlier than 2019, when the first positive rat was identified in Atlanta. Furthermore, 6 suspected autochthonous human angiostrongyliasis cases were detected during 2011–2017 in Texas, Tennessee, and Alabama (*10*). Among captive wildlife, *A. cantonensis* lungworm has been reported in nonhuman primates in Florida (*11*), Louisiana (*7*,*12*), Texas (*4*), and Alabama (*13*), and a red kangaroo in Mississippi (*14*). Among free-ranging wildlife native to the southeastern United States, *A. cantonensis* infections have been identified in armadillos and an opossum (*15*).

Various native and exotic gastropod species have been shown, both naturally and experimentally, to be susceptible intermediate hosts (*3*,*5*,*11*). Although details of *A. cantonensis* invasion and spread are not fully known, identification of introduced gastropods as intermediate hosts (*11*) and Cuban tree frogs as paratenic hosts (*6*) in the southern United States suggest anthropogenic disturbance and climate-induced change in local food webs might be amplifying *A. cantonensis* transmission. Clearly, *A. cantonensis* lungworm in urban rat populations, gastropod intermediate hosts, and other paratenic hosts in the populous greater Atlanta area pose a possible threat to the health of humans and domestic, free-ranging, and captive animals.

Understanding patterns of historic, contemporary, and future expansion of the range of *A. cantonensis* lungworm in North America through surveillance, genetic analysis, and modeling is critical to mitigating risk to humans and other animals for infection by this parasitic nematode, which harbors in synanthropic wild rodent and intermediate host populations. Medical and veterinary professionals throughout the southern United States should consider *A. cantonensis* infection in differential diagnoses of aberrant central nervous system larva migrans, eosinophilic meningitis, and meningoencephalitis.

About the Author

Dr. Gottdenker is professor in the Department of Pathology at the University of Georgia College of Veterinary Medicine, Athens, GA, USA. Her research focuses on pathology and ecology of wildlife diseases, including zoonotic parasites, and the effects of anthropogenic environmental changes on disease ecology and evolution.

References

1. da Silva AJ, Morassutti AL. *Angiostrongylus* spp. (Nematoda; Metastrongyloidea) of global public health importance. Res Vet Sci. 2021;135:397–403. https://doi.org/10.1016/j.rvsc.2020.10.023
2. Wang QP, Lai DH, Zhu XQ, Chen XG, Lun ZR. Human angiostrongyliasis. Lancet Infect Dis. 2008;8:621–30. https://doi.org/10.1016/S1473-3099(08)70229-9
3. Stockdale Walden HD, Slapcinsky JD, Roff S, Mendieta Calle J, Diaz Goodwin Z, Stern J, et al. Geographic distribution of *Angiostrongylus cantonensis* in wild rats (*Rattus rattus*) and terrestrial snails in Florida, USA. PLoS One. 2017;12:e0177910. https://doi.org/10.1371/journal.pone.0177910

4. Edwards EE, Borst MM, Lewis BC, Gomez G, Flanagan JP. *Angiostrongylus cantonensis* central nervous system infection in captive callitrichids in Texas. Vet Parasitol Reg Stud Rep. 2020;19:100363. https://doi.org/10.1016/j.vprsr.2019.100363
5. Cowie RH, Ansdell V, Panosian Dunavan C, Rollins RL. Neuroangiostrongyliasis: global spread of an emerging tropical disease. Am J Trop Med Hyg. 2022;107:1166–72. https://doi.org/10.4269/ajtmh.22-0360
6. Chase EC, Ossiboff RJ, Farrell TM, Childress AL, Lykins K, Johnson SA, et al. Rat lungworm (*Angiostrongylus cantonensis*) in the invasive Cuban treefrog (*Osteopilus septentrionalis)* in central Florida, USA. J Wildl Dis. 2022;58:454–6. https://doi.org/10.7589/JWD-D-21-00140
7. Rizor J, Yanez RA, Thaiwong T, Kiupel M. *Angiostrongylus cantonensis* in a red ruffed lemur at a zoo, Louisiana, USA. Emerg Infect Dis. 2022;28:1058–60. https://doi.org/10.3201/eid2805.212287
8. Qvarnstrom Y, Xayavong M, da Silva ACA, Park SY, Whelen AC, Calimlim PS, et al. Real-time polymerase chain reaction detection of *Angiostrongylus cantonensis* DNA in cerebrospinal fluid from patients with eosinophilic meningitis. Am J Trop Med Hyg. 2016;94:176–81. https://doi.org/10.4269/ajtmh.15-0146
9. Kumar S, Stecher G, Li M, Knyaz C, Tamura K. MEGA X: molecular evolutionary genetics analysis across computing platforms. Mol Biol Evol. 2018;35:1547–9. https://doi.org/10.1093/molbev/msy096
10. Liu EW, Schwartz BS, Hysmith ND, DeVincenzo JP, Larson DT, Maves RC, et al. Rat lungworm infection associated with central nervous system disease—eight U.S. states, January 2011–January 2017. MMWR Morb Mortal Wkly Rep. 2018;67:825–8. https://doi.org/10.15585/mmwr.mm6730a4
11. Walden HDS, Slapcinsky J, Rosenberg J, Wellehan JFX. *Angiostrongylus cantonensis* (rat lungworm) in Florida, USA: current status. Parasitology. 2021;148:149–52. https://doi.org/10.1017/S0031182020001286
12. Gardiner CH, Wells S, Gutter AE, Fitzgerald L, Anderson DC, Harris RK, et al. Eosinophilic meningoencephalitis due to *Angiostrongylus cantonensis* as the cause of death in captive non-human primates. Am J Trop Med Hyg. 1990;42:70–4. https://doi.org/10.4269/ajtmh.1990.42.70
13. Kottwitz JJ, Perry KK, Rose HH, Hendrix CM. *Angiostrongylus can tonensis* infection in captive Geoffroy's tamarins (*Saguinus geoffroyi*). J Am Vet Med Assoc. 2014;245:821–7. https://doi.org/10.2460/javma.245.7.821
14. Patial S, Delcambre BA, DiGeronimo PM, Conboy G, Vatta AF, Bauer R. Verminous meningoencephalomyelitis in a red kangaroo associated with *Angiostrongylus cantonensis* infection. J Vet Diagn Invest. 2022;34:107–11. https://doi.org/10.1177/10406387211037664
15. Dalton MF, Fenton H, Cleveland CA, Elsmo EJ, Yabsley MJ. Eosinophilic meningoencephalitis associated with rat lungworm (*Angiostrongylus cantonensis*) migration in two nine-banded armadillos (*Dasypus novemcinctus*) and an opossum (*Didelphis virginiana*) in the southeastern United States. Int J Parasitol Parasites Wildl. 2017;6:131–4. https://doi.org/10.1016/j.ijppaw.2017.05.004

Address for correspondence: Guilherme G. Verocai, Texas A&M University College of Veterinary Medicine & Biomedical Sciences, Veterinary Pathobiology, 660 Raymond Stotzer Pkwy, College Station, TX 77843, USA; email: gverocai@cvm.tamu.edu

Table. Histopathologic findings of *Angiostrongylus cantonensis* nematode infection and molecular confirmation in brown rats (*Rattus norvegicus*), Atlanta, Georgia, USA, 2019–2022*

ID, age class/sex	Case submission date	Histopathologic findings	GenBank accession no.
Case 1, adult/M	2019 Feb 19	Brain: hemorrhagic and lymphohistiocytic meningoencephalitis with intralesional nematodiasis (adult nematodes, presumptive *Angiostrongylus* spp.)	OQ793715
Case 2, adult/F	2021 Feb 12	Lung: severe multifocal chronic nodular nematodiasis (adult nematodes and larvated ova, presumptive *Angiostrongylus* spp.)	OQ793716
Case 3, juvenile/ unknown	2021 Jan 20	Heart: intravascular (i.e., cardiac chamber, pulmonary artery) nematodiasis	NA
Case 4, Age unknown/unknown	2021 Aug 24	Lung: pulmonary arterial nematodiasis; pulmonary hemorrhage and edema	NA
Case 5, adult/unknown	2022 Apr 25	Heart and pulmonary artery: cardiac nematodiasis with endothelial pulmonary aortic subendothelial myxomatous change Lung: nematode cross section with similar characteristics to heart nematodes	NA
Case 6, adult/unknown	2022 Aug 09	Heart and pulmonary artery: intraventricular and intra-arterial nematodiasis Lung: moderate intraluminal, peritracheal, and pulmonary hemorrhage	OQ793717
Case 7, adult/M	2022 Oct 18	Lung: eosinophilic pulmonary arteritis with degenerate intraluminal nematodes	OQ793718

*Pre- or postmortem predation of some rats might have occurred before rats were found. Thus, representative samples of all organs might not have been available for evaluation and in some cases, sex or age class could not be determined. ID, identification; NA, not available.

FFPE Tissue Kit (QIAGEN, https://www.qiagen.com) according to manufacturer recommendations. PCR reactions targeted a 200-bp segment of the mitochondrial cytochrome oxidase subunit 1 gene (*cox1*). We performed a 25 μL reaction containing 0.25 μmol each of primers CO1ACF7 (5′-TGCCTGCTTTTGGGATTGTTAGAC-3′) and CO1ACR7 (5′-TCACTCCCGTAGGAACCGCA-3′), 1× GoTaq Green Master Mix (Promega Corporation, https://www.promega.com), and 2.5 μL of DNA template (*8*). Cycling procedure involved initial denaturation at 95°C for 2 min, then 40 cycles at 95°C for 30 s, 50°C for 30 s, 72°C for 90 s, and a final extension at 72°C for 5 min. We used nuclease-free water as a negative control and DNA of *Dirofilaria immitis* as a positive control. We purified PCR

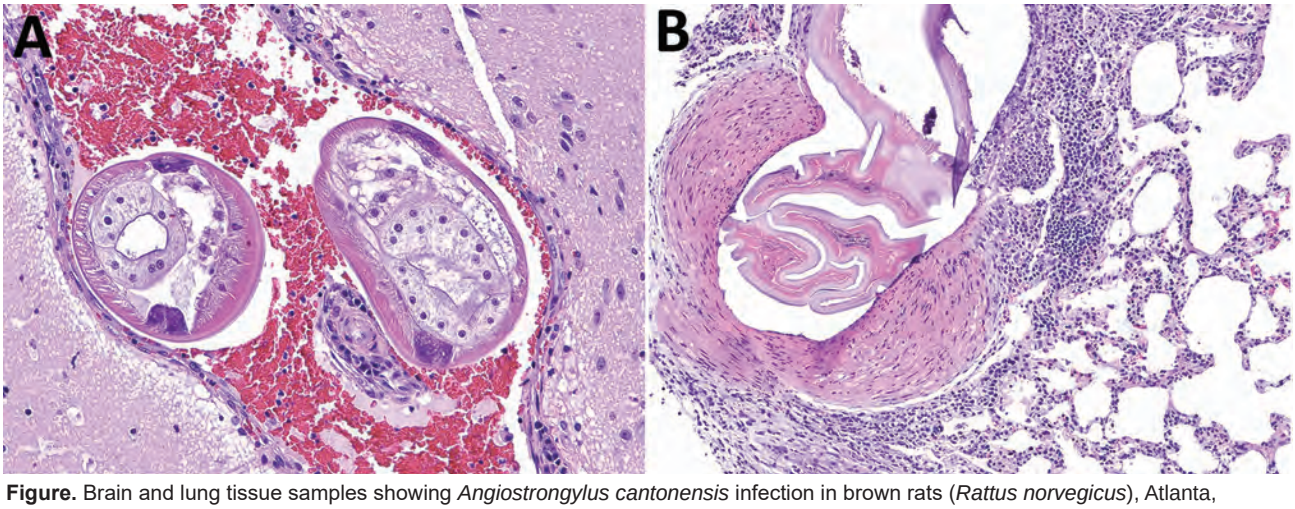

Figure. Brain and lung tissue samples showing *Angiostrongylus cantonensis* infection in brown rats (*Rattus norvegicus*), Atlanta, Georgia, USA, 2019–2022. A) Representative tissue section from the brain, stained with hematoxylin and eosin. The meninges and ventricles are multifocally and moderately expanded by abundant hemorrhage. Within the meninges and ventricles, occasional cross sections through nematodes can be seen. Nematodes were ≈250–300 μm in diameter with a thin eosinophilic cuticle, pseudocoelom, polymyarian coelomyarian musculature, lateral chords, and multinucleated intestine. Original magnification ×200 μm. B) Representative tissue section from the lung stained with hematoxylin and eosin. A large pulmonary artery contains fragments of a degenerative nematode characterized by a thin eosinophilic cuticle, pseudocoelomic space, and polymyarian coelomyarian musculature. The subtending arterial wall was sometimes necrotic and variably infiltrated by eosinophils, lymphocytes, and macrophages. The vessel also displays hypertrophy of the tunica media and occasional hypertrophy of the endothelial cells. Original magnification ×100 μm.

products using the EZNA Cycle Pure Kit (OMEGA Bio-Tek, https://www.omegabiotek.com) according to manufacturer instructions. We aligned and compared generated sequences with homologous *A. cantonensis* sequences available in GenBank. We determined genetic distances and performed phylogenetic analysis using MEGA X 10.1 (*9*) (Table).

Our molecular analysis confirmed the identity of *A. cantonensis* in 4/7 samples that had nematodes visible on histologic examination of heart, pulmonary artery, and brain tissues (Table). All 4 sequences were 100% identical to each other and to *A. cantonensis* sequences belonging to haplotype 17a, previously reported from Louisiana, USA. Among homologous sequences available in GenBank from *A. cantonensis* isolates from the United States, those belonging to haplotype 17b (Louisiana and California) were 99.5% similar, haplotype 8b (Louisiana) 98.9% similar, and haplotype 5a (Hawaii) 98.9% similar to those in haplotype 17a. Overall, compared with other *A. cantonensis* haplotypes included in the phylogenetic analysis, similarity of sequences ranged from 93.1%–99.5%, clustering in a clade with 86% bootstrap support (Appendix, https//wwwnc.cdc.gov/EID/article/29/10/23-0706-App1.pdf).

Conclusions

Discovery of autochthonous cases of *A. cantonensis* in definitive host rodents collected during 2019–2022 in the state of Georgia, suggests that the zoonotic parasite was introduced to and has become established in a new area of the southeastern United States. Although we molecularly confirmed diagnosis in only 4/7 cases, the remaining rats had intravascular nematodes morphologically consistent with *A. cantonensis* and typical associated lesions. We could not molecularly confirm the remaining 3 cases because of insufficient sample quality and DNA degradation; thus, we could not rule out the presence of other nematode species.

Because *A. cantonensis* previously was identified in rats in neighboring states Florida and Alabama, *A. cantonensis* populations likely were in Georgia much earlier than 2019, when the first positive rat was identified in Atlanta. Furthermore, 6 suspected autochthonous human angiostrongyliasis cases were detected during 2011–2017 in Texas, Tennessee, and Alabama (*10*). Among captive wildlife, *A. cantonensis* has been reported in nonhuman primates in Florida (*11*), Louisiana (*7*,*12*), Texas (*4*), and Alabama (*13*), and a red kangaroo in Mississippi (*14*). Among free-ranging wildlife native to the southeastern United States, *A. cantonensis* infections have been identified in armadillos and an opossum (*15*).

Various native and exotic gastropod species have been shown, both naturally and experimentally, to be susceptible intermediate hosts (*3*,*5*,*11*). Although details of *A. cantonensis* invasion and spread are not fully known, identification of introduced gastropods as intermediate hosts (*11*) and Cuban tree frogs as paratenic hosts (*6*) in the southern United States suggest anthropogenic disturbance and climate-induced change in local food webs might be amplifying *A. cantonensis* transmission. Clearly, *A. cantonensis* in urban rat populations, gastropod intermediate hosts, and other paratenic hosts in the populous greater-Atlanta area pose a possible threat to the health of humans and domestic, free-ranging, and captive animals.

Understanding patterns of historic, contemporary, and future expansion of the range of *A. cantonensis* in North America through surveillance, genetic analysis, and modeling. Understanding those patterns is critical to mitigate risk to humans and other animals for infection by the parasitic nematode, which harbors in synanthropic wild rodent and intermediate host populations. Medical and veterinary professionals throughout the southern United States should consider *A. cantonensis* in differential diagnoses of aberrant central nervous system larva migrans, eosinophilic meningitis, and meningoencephalitis.

About the Author

Dr. Gottdenker is an associate professor in the Department of Pathology at the University of Georgia College of Veterinary Medicine, Athens, GA, USA. Her research focuses on pathology and ecology of wildlife diseases, including zoonotic parasites, and the effects of anthropogenic environmental changes on disease ecology and evolution.

References

1. da Silva AJ, Morassutti AL. *Angiostrongylus* spp. (Nematoda; Metastrongyloidea) of global public health importance. Res Vet Sci. 2021;135:397–403. https://doi.org/10.1016/j.rvsc.2020.10.023
2. Wang QP, Lai DH, Zhu XQ, Chen XG, Lun ZR. Human angiostrongyliasis. Lancet Infect Dis. 2008;8:621–30. https://doi.org/10.1016/S1473-3099(08)70229-9
3. Stockdale Walden HD, Slapcinsky JD, Roff S, Mendieta Calle J, Diaz Goodwin Z, Stern J, et al. Geographic distribution of *Angiostrongylus cantonensis* in wild rats (*Rattus rattus*) and terrestrial snails in Florida, USA. PLoS One. 2017;12:e0177910. https://doi.org/10.1371/journal.pone.0177910

4. Edwards EE, Borst MM, Lewis BC, Gomez G, Flanagan JP. *Angiostrongylus cantonensis* central nervous system infection in captive callitrichids in Texas. Vet Parasitol Reg Stud Rep. 2020;19:100363. https://doi.org/10.1016/j.vprsr.2019.100363
5. Cowie RH, Ansdell V, Panosian Dunavan C, Rollins RL. Neuroangiostrongyliasis: global spread of an emerging tropical disease. Am J Trop Med Hyg. 2022;107:1166–72. https://doi.org/10.4269/ajtmh.22-0360
6. Chase EC, Ossiboff RJ, Farrell TM, Childress AL, Lykins K, Johnson SA, et al. Rat lungworm (*Angiostrongylus cantonensis*) in the invasive Cuban treefrog (*Osteopilus septentrionalis)* in central Florida, USA. J Wildl Dis. 2022;58:454–6. https://doi.org/10.7589/JWD-D-21-00140
7. Rizor J, Yanez RA, Thaiwong T, Kiupel M. *Angiostrongylus cantonensis* in a red ruffed lemur at a zoo, Louisiana, USA. Emerg Infect Dis. 2022;28:1058–60. https://doi.org/10.3201/eid2805.212287
8. Qvarnstrom Y, Xayavong M, da Silva ACA, Park SY, Whelen AC, Calimlim PS, et al. Real-time polymerase chain reaction detection of *Angiostrongylus cantonensis* DNA in cerebrospinal fluid from patients with eosinophilic meningitis. Am J Trop Med Hyg. 2016;94:176–81. https://doi.org/10.4269/ajtmh.15-0146
9. Kumar S, Stecher G, Li M, Knyaz C, Tamura K. MEGA X: molecular evolutionary genetics analysis across computing platforms. Mol Biol Evol. 2018;35:1547–9. https://doi.org/10.1093/molbev/msy096
10. Liu EW, Schwartz BS, Hysmith ND, DeVincenzo JP, Larson DT, Maves RC, et al. Rat lungworm infection associated with central nervous system disease—eight U.S. states, January 2011–January 2017. MMWR Morb Mortal Wkly Rep. 2018;67:825–8. https://doi.org/10.15585/mmwr.mm6730a4
11. Walden HDS, Slapcinsky J, Rosenberg J, Wellehan JFX. *Angiostrongylus cantonensis* (rat lungworm) in Florida, USA: current status. Parasitology. 2021;148:149–52. https://doi.org/10.1017/S0031182020001286
12. Gardiner CH, Wells S, Gutter AE, Fitzgerald L, Anderson DC, Harris RK, et al. Eosinophilic meningoencephalitis due to *Angiostrongylus cantonensis* as the cause of death in captive non-human primates. Am J Trop Med Hyg. 1990;42:70–4. https://doi.org/10.4269/ajtmh.1990.42.70
13. Kottwitz JJ, Perry KK, Rose HH, Hendrix CM. *Angiostrongylus can tonensis* infection in captive Geoffroy's tamarins (*Saguinus geoffroyi*). J Am Vet Med Assoc. 2014;245:821–7. https://doi.org/10.2460/javma.245.7.821
14. Patial S, Delcambre BA, DiGeronimo PM, Conboy G, Vatta AF, Bauer R. Verminous meningoencephalomyelitis in a red kangaroo associated with *Angiostrongylus cantonensis* infection. J Vet Diagn Invest. 2022;34:107–11. https://doi.org/10.1177/10406387211037664
15. Dalton MF, Fenton H, Cleveland CA, Elsmo EJ, Yabsley MJ. Eosinophilic meningoencephalitis associated with rat lungworm (*Angiostrongylus cantonensis*) migration in two nine-banded armadillos (*Dasypus novemcinctus*) and an opossum (*Didelphis virginiana*) in the southeastern United States. Int J Parasitol Parasites Wildl. 2017;6:131–4. https://doi.org/10.1016/j.ijppaw.2017.05.004

Address for correspondence: Guilherme G. Verocai, Texas A&M University College of Veterinary Medicine & Biomedical Sciences, Veterinary Pathobiology, 660 Raymond Stotzer Pkwy, College Station, TX 77843, USA; email: gverocai@cvm.tamu.edu

Bacillus subtilis Bacteremia from Gastrointestinal Perforation after Natto Ingestion, Japan

Takehiro Hashimoto, Takaaki Yahiro, Sakirul Khan, Kazunori Kimitsuki, Kazufumi Hiramatsu, Akira Nishizono

Author affiliations: Oita University Hospital, Oita, Japan (T. Hashimoto, K. Hiramatsu); Oita University Faculty of Medicine, Oita (T. Hashimoto, T. Yahiro, S. Khan, K. Kimitsuki, A. Nishizono); Research Center for Global and Local Infectious Diseases, Oita (K. Hiramatsu, A. Nishizono)

DOI: https://doi.org/10.3201/eid2910.230084

We report a case of *Bacillus subtilis* variant *natto* bacteremia from a gastrointestinal perforation in a patient who ingested natto. Genotypic methods showed the bacteria in a blood sample and the ingested natto were the same strains. Older or immunocompromised patients could be at risk for bacteremia from ingesting natto.

Bacillus subtilis is a gram-positive, rod-shaped, spore-forming bacterium with low pathogenicity (*1*). *B. subtilis* isolated from clinical specimens is sometimes considered a contaminant (*2*). However, a few cases of bacteremia caused by *B. subtilis* have been reported in Japan (*3*–*6*). We report a case of *B. subtilis* variant *natto* bacteremia and peritonitis caused by ingestion of natto, a traditional fermented food in Japan that is prepared by adding *B. subtilis* var. *natto* culture to soybeans and fermenting them.

A 65-year-old man with metastatic colorectal cancer was admitted to Oita University Hospital (Oita, Japan) with fever and perianal pain. Approximately 2 months before admission, he began chemotherapy with bevacizumab and modified oxaliplatin plus leucovorin plus 5-fluorouracilm (FOLFOX6). Six days before admission, on day 4 after the third course of chemotherapy, he experienced perianal pain. He had a history of diabetes mellitus and a custom of eating natto.

The patient's body temperature was 37.6°C, blood pressure was 132/84 mm Hg, and heart rate was 70 beats/min. A physical examination revealed lower abdominal pain. Laboratory tests revealed an elevated leukocyte count (15,150 cells/μL), elevated C-reactive protein level (20.2 mg/dL), and elevated procalcitonin level (0.55 ng/mL). Contrast-enhanced abdominal computed tomography showed free air in the perisigmoid colon, an intraabdominal abscess, and slight ascites. Peritonitis caused by sigmoid colon perforation was diagnosed, and a transverse colostomy and drainage were performed. After blood and pus cultures were collected, a course of intravenous meropenem (0.5 g every 8 h) was initiated.

On day 3, matrix-assisted laser desorption/ionization time-of-flight (MALDI-TOF) mass spectrometry (Bruker Daltonics, https://www.bruker.com) of the blood culture revealed *B. subtilis* (MALDI-TOF score 2.224), and the pus culture revealed polymicrobial bacteria, including *B. subtilis*. We performed antimicrobial resistance testing on a dry plate (Eiken Chemical Co., https://www.eiken.co.jp) by using the broth microdilution method and then analyzed images by using a Koden IA40MIC-i (Koden, https://koden.jp). MICs were as follows: cefazolin, <0.25 μg/mL; cefotiam, 0.5 μg/mL; meropenem, <0.25 μg/mL; clindamycin, 0.5 μg/mL; levofloxacin <0.25 μg/mL; minocycline, <0.25 μg/mL; and vancomycin, <0.5 μg/mL. Meropenem was administered for a total of 10 days. On day 36, additional computed tomography–guided percutaneous drainage was performed, and on day 66, the patient was discharged from the hospital after rehabilitation.

We assessed whether blood and pus culture isolates and the isolate from natto the patient consumed (brand A) were the same strain, by using pulsed-field gel electrophoresis (PFGE), as previously described (*7*). To verify *B. subtilis* var. *natto*, we tested 2 brands (brands B and C) besides brand A that the patient reported consuming. PFGE revealed that the isolates detected from the blood and pus cultures were the same as the cultures of natto brand A that the patient consumed. Moreover, those isolates were the same as isolates from natto brand C (Figure), suggesting that the blood and pus culture isolates were *B. subtilis* var. *natto*.

Other than *B. subtilis* var. *natto, B. subtilis* has multiple other subspecies: *B. subtilis* subsp. *subtilis*, *B. subtilis* subsp. *spizizenii*, *B. subtilis* subsp. *inaquosrum*, and *B. subtilis* subsp. *stercoris*. Distinguishing between those species by 16S rRNA gene sequencing and MALDI-TOF mass spectrometry can be difficult (*8*). The most common known portal of entry for *B. subtilis* bacteria is the gastrointestinal tract, but often the site of entry is unknown, and bacteremia that has a gastrointestinal tract source is presumed to be related to natto ingestion (*3*–*6*). However, *B. subtilis* var. *natto* was identified in only 2 prior cases, 1 that analyzed the draft whole-genome of each *B. subtilis* strain using next-generation sequencing (*6*) and 1 that used the biotin gene and the biotin requirement test (*5*). In our case, PFGE analysis revealed that the patient's isolate was *B. subtilis* var. *natto* that matched the natto brand he consumed.

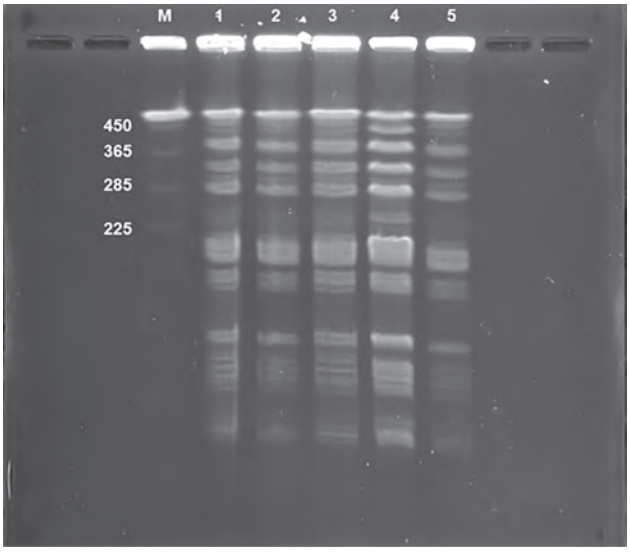

Figure. Pulsed-field gel electrophoresis patterns of restricted chromosomal DNA from *Bacillus subtilis* variant *natto* isolated from a case of bacteremia from gastrointestinal perforation after natto ingestion, Japan. *B. subtilis* strains were digested in SfiI enzyme. Lane M, CHEF DNA size marker (Bio-Rad, https://www.bio-rad.com) of *Saccharomyces cerevisiae*; lane 1, sample from blood; lane 2, sample from pus; lane 3, sample from natto brand A; lane 4, sample from natto brand B; lane 5, sample from natto brand C. Numbers at left indicate kilobases.

Although *B. subtilis* bacteremia has been reported only in Japan thus far, the popularity of Japanese cuisine is increasing worldwide (*9*). Therefore, clinicians outside Japan should also be aware of *B. subtilis* bacteremia caused by natto consumption.

PFGE analysis revealed that the natto of brands A and B contained different bacterial strains. Many brands of natto are sold in Japan. Each brand uses different soybean cultivars, processing conditions (soaking, steaming, and fermentation), and *B. subtilis* var. *natto* strains (*10*). Therefore, a history of natto consumption alone might not be associated with the cause of *B. subtilis* bacteremia because eating natto is not uncommon among the population of Japan.

In conclusion, we report a case of *B. subtilis* bacteremia and secondary peritonitis resulting from gastrointestinal perforation in a patient who ingested natto. Our case and others in the literature indicate that older or immunocompromised patients who consume natto are at risk for serious infection from natto (*4*,*6*). Clinicians should advise patients in these risk groups to avoid eating natto or food products containing *B. subtilis* bacteria.

About the Author

Dr. Hashimoto is a physician at the Infection Control Center of Oita University Hospital. His main research interest is in microbiology.

References

1. Oggioni MR, Pozzi G, Valensin PE, Galieni P, Bigazzi C. Recurrent septicemia in an immunocompromised patient due to probiotic strains of *Bacillus subtilis*. J Clin Microbiol. 1998;36:325–6. https://doi.org/10.1128/JCM.36.1.325-326.1998
2. Weber DJ, Saviteer SM, Rutala WA, Thomann CA. Clinical significance of *Bacillus* species isolated from blood cultures. South Med J. 1989;82:705–9. https://doi.org/10.1097/00007611-198906000-00008
3. Hashimoto T, Hayakawa K, Mezaki K, Kutsuna S, Takeshita N, Yamamoto K, et al. Bacteremia due to *Bacillus subtilis*: a case report and clinical evaluation of 10 cases [in Japanese]. Kansenshogaku Zasshi. 2017;91:151–4. https://doi.org/10.11150/kansenshogakuzasshi.91.151
4. Aoyagi R, Okita K, Uda K, Ikegawa K, Yuza Y, Horikoshi Y. Natto intake is a risk factor of *Bacillus subtilis* bacteremia among children undergoing chemotherapy for childhood cancer: a case-control study. J Infect Chemother. 2023;29:329–32. https://doi.org/10.1016/j.jiac.2022.12.010
5. Tanaka I, Kutsuna S, Ohkusu M, Kato T, Miyashita M, Moriya A, et al. *Bacillus subtilis* variant natto bacteremia of gastrointestinal origin, Japan. Emerg Infect Dis. 2022;28:1718–9. https://doi.org/10.3201/eid2808.211567
6. Kato A, Yoshifuji A, Komori K, Aoki K, Taniyama D, Komatsu M, et al. A case of *Bacillus subtilis* var. natto bacteremia caused by ingestion of natto during COVID-19 treatment in a maintenance hemodialysis patient with multiple myeloma. J Infect Chemother. 2022;28:1212–5. https://doi.org/10.1016/j.jiac.2022.05.006
7. Marten P, Smalla K, Berg G. Genotypic and phenotypic differentiation of an antifungal biocontrol strain belonging to *Bacillus subtilis*. J Appl Microbiol. 2000;89:463–71. https://doi.org/10.1046/j.1365-2672.2000.01136.x
8. Rooney AP, Price NP, Ehrhardt C, Swezey JL, Bannan JD. Phylogeny and molecular taxonomy of the *Bacillus subtilis* species complex and description of *Bacillus subtilis* subsp. *inaquosorum* subsp. nov. Int J Syst Evol Microbiol. 2009;59:2429–36. https://doi.org/10.1099/ijs.0.009126-0
9. Watari T, Tachibana T, Okada A, Nishikawa K, Otsuki K, Nagai N, et al. A review of food poisoning caused by local food in Japan. J Gen Fam Med. 2021;22:15–23. https://doi.org/10.1002/jgf2.384
10. Escamilla DM, Rosso ML, Holshouser DL, Chen P, Zhang B. Improvement of soybean cultivars for natto production through the selection of seed morphological and physiological characteristics and seed compositions: a review. Plant Breed. 2019;138:131–9. https://doi.org/10.1111/pbr.12678

Address for correspondence: Takehiro Hashimoto, Infection Control Center, Oita University Hospital, 1-1 Idaigaoka, Hasama-machi, Yufu, Oita 879-5593, Japan; email: hashimo2013@oita-u.ac.jp

Borrelia bavariensis in Questing *Ixodes ricinus* Ticks, United Kingdom

Grace Plahe, Jessica L. Hall, David Johnson, Lucy Gilbert, Richard J. Birtles

Author affiliations: University of Salford, Salford, UK (G. Plahe, R.J. Birtles); University of Glasgow, Glasgow, Scotland, UK (J.L. Hall, L. Gilbert), University of Manchester, Manchester, UK (D. Johnson)

DOI: http://doi.org/10.3201/eid2910.230907

We detected *Borrelia bavariensis* in *Ixodes ricinus* ticks collected near 2 towns in the United Kingdom. Human *B. bavariensis* infections have not been reported previously in the country, underscoring the value of tick surveillance to warn of emerging human disease. *B. bavariensis* should be considered in patients with suspected neuroborreliosis.

Borrelia bavariensis is one of several genospecies within the *B. burgdorferi* sensu lato complex to be associated with Lyme disease (*1*). *B. bavariensis* is widely distributed across Europe and Asia (*1*), although surveys of questing ticks in Europe indicate that *B. bavariensis* occurs at markedly lower prevalences than do other members of the *B. burgdorferi* s.l. complex (*2*). Of note, *B. bavariensis* appears to be overrepresented among *B. burgdorferi* s.l. clinical isolates in Europe (*3*), which has led to suggestions that it is more virulent than other members of the complex. Its potential enhanced pathogenicity, coupled with its specific association with neuroborreliosis (*3*), a profound manifestation of Lyme disease, has made *B. bavariensis* of particular medical concern.

During May–August 2022, we conducted questing tick surveys at 130 sites in and around 13 towns in the United Kingdom (Figure). We surveyed 10 sites around each town by conducting 15 blanket drag transects, 10 m × 1 m, per site. We identified all ticks collected morphologically as *Ixodes ricinus*, extracted DNA from each nymph and then incorporated each DNA extract separately as template in a real-time PCR to detect the presence of *B. burgdorferi* s.l. DNA (*4*). We processed 1 blank sample with every 5 nymphs to test for cross-contamination between samples; none of these blanks yielded a PCR product. In total, we found 91/1,311 nymphs (6.7%) to be infected with *B. burgdorferi* s.l. (Table). The positive samples were characterized by incorporating the DNA extracts into a conventional PCR that targeted the 5S/23S rDNA intergenic spacer region (*5*); the nucleotide base sequences were obtained by Sanger sequencing of both DNA strands. We used Geneious Prime software (https://www.geneious.com) to quality-check, collate, and analyze the sequence data. Of the 91 infected ticks, we successfully identified genospecies for 72. We encountered 5 genospecies: *B. afzelii, B. garinii, B. valaisiana, B. burgdorferi* sensu stricto, and *B. bavariensis* (Table). Given the high 5S/23S rDNA intergenic spacer region sequence similarity between strains of *B. garinii* and *B. bavariensis*, we incorporated the 4 DNA extracts suspected to be derived from *B.*

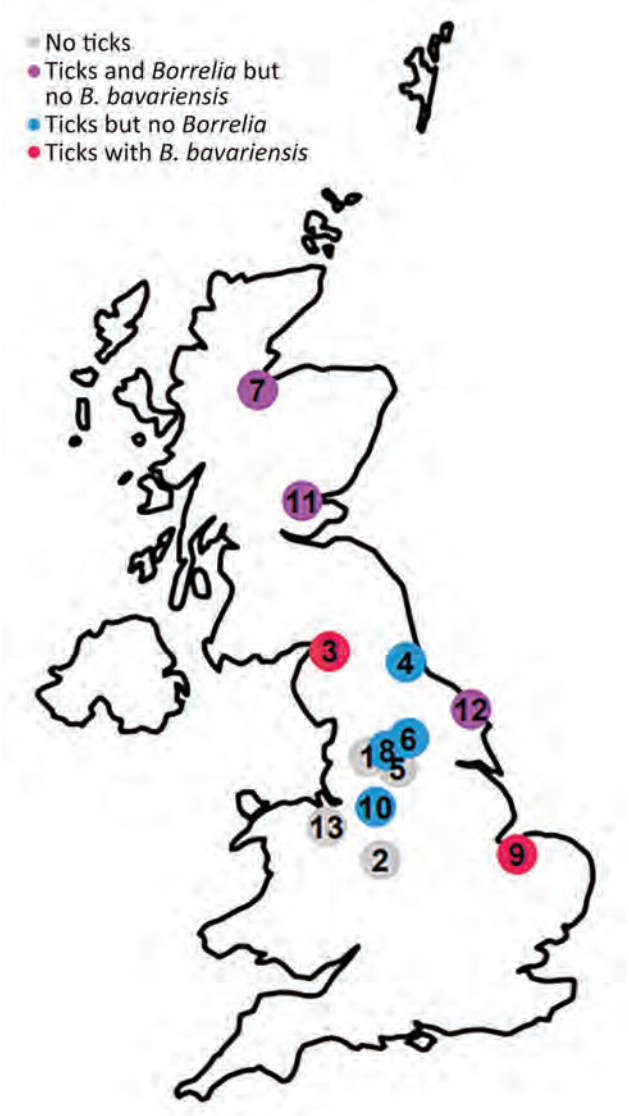

Figure. Relative locations of 13 towns where questing tick surveys were conducted in the United Kingdom to test for *Borrelia burgdorferi* sensu lato. The colors represent presence and absence of *Ixodes ricinus* ticks and their *Borrelia* infection status. The numbers correspond to the locations listed in the Table.

Table. Prevalence of *Borrelia burgdorferi* sensu lato in *Ixodes ricinus* tick nymphs sampled in 13 towns, United Kingdom*

Location	*I. ricinus* nymphs collected	*B. burgdorferi* s.l., no. (%)	*Borrelia* genospecies, no. (%), n = 91					
			B. afzelii	*B. bavariensis*	*B. burgdorferi s.s.*	*B. garinii*	*B. valaisiana*	Not identified
1 Burnley	0	0	0	0	0	0	0	0
2 Cannock	0	0	0	0	0	0	0	0
3 Carlisle	196	10 (5.1)	4 (40)	3 (30.0)	0	0	2 (20.0)	1 (10.0)
4 Durham	2	0	0	0	0	0	0	0
5 Halifax	0	0	0	0	0	0	0	0
6 Harrogate	40	0	0	0	0	0	0	0
7 Inverness	472	47 (10.0)	18 (38.3)	0	14 (29.8)	5 (10.6)	1 (2.1)	9 (19.1)
8 Keighley	7	0	0	0	0	0	0	0
9 Kings Lynn	59	1 (1.7)	0	1 (100.0)	0	0	0	0
10 Macclesfield	1	0	0	0	0	0	0	0
11 Perth	369	24 (6.5)	9 (37.5)	0	1 (4.2)	4 (16.7)	2 (8.3)	8 (33.3)
12 Scarborough	206	9 (4.4)	1 (11.1)	0	0	5 (55.6)	2 (22.2)	1 (11.1)
13 Wrexham	0	0	0	0	0	0	0	0
Total (%)	1,352	91 (6.7)	32 (35.1)	4 (4.4)	15 (16.5)	14 (15.4)	7 (7.7)	19 (20.9)

*Colors correspond to those used in the Figure. Prevalences for genospecies are in relation to the total infected ticks found in each town.

bavariensis into a seminested PCR targeting an *ospA* fragment (*6*) and sequenced products of this reaction as described above. All 4 yielded unambiguous sequence data that were indistinguishable from one another. This sequence was identical to a 734bp *ospA* fragment of PBi, the type strain of *B. bavariensis* and <95% similar to *ospA* of representatives of other *Borrelia* genospecies (Genbank accession no. for the *ospA* sequence we obtained is OR208793).

Our findings confirm the presence of *B. bavariensis* in questing *I. ricinus* nymphs in the United Kingdom. *B. bavariensis*–infected ticks were encountered at 2/130 sites surveyed, 1 near Kings Lynn and 1 near Carlisle, ≈325 km apart, which suggested a broad distribution. Encountering *B. bavariensis* is not entirely unexpected, given the pathogen's wide distribution in temperate regions of the northern hemisphere and its adaptation to woodland rodents and hedgehogs (*7*), all of which are common across the United Kingdom. That earlier surveys in the United Kingdom have not encountered the species may reflect its relatively low prevalence in ticks and the patchiness of its distribution reported in continental Europe (*2*). In addition, methods used for delineating *Borrelia* genospecies may have lacked sensitivity. A previous study highlighted problems differentiating between *B. bavariensis* and *B. garinii* based on comparative analysis of 5S–23S rRNA intergenic spacer region sequences; that approach is perhaps the most widely adopted across Europe and beyond (*8*).

Given the low number of *B. bavariensis* ticks encountered in the United Kingdom so far, drawing robust conclusions about the ecology of the genospecies is premature. Of interest, at the Carlisle site where we encountered *B. bavariensis*, 6/82 ticks tested from that site were infected with *B. burgdorferi* s.l. and 3 (50%) of those infected ticks carried *B. bavariensis*. *B. bavariensis* was not encountered in 113 ticks tested from the 3 other sites around Carlisle at which ticks were found. Those observations suggest that, even on a local scale, the occurrence of *B. bavariensis* is patchy, but enzootic hot spots may exist.

B. bavariensis is an addition to the list of zoonotic pathogens including *Anaplasma phagocytophilum*, *B. miyamotoi*, *Rickettsia helvetica*, and *Spiroplasma ixodetis* that are known to exist in UK ticks (*9*) but have yet to be reported in confirmed autochthonous cases in patients in the country. The recent confirmation of locally acquired encephalitis caused by tick-borne encephalitis virus (*10*) exemplifies the value of tick surveillance as an early warning of emerging human infections. Medical practitioners managing patients with suspected neuroborreliosis in the United Kingdom should now consider *B. bavariensis* as a potential infecting pathogen.

Acknowledgments

We thank Isobel Jones, Hannah Ravenswater, Nick Broer, Yue Sun, and Abigail Coole for help with fieldwork. We thank landowners and land managers across the United Kingdom for granting us access to sites used in our survey. We thank Gabriele Margos for advice on *ospA* PCR.

This work is an output from the project Maximising ecosystem services in urban environments (MEaSURE), funded by The Natural Environment Research Council UK (reference NE/W003120/1).

Authors' contributions: G.P.: data collection, data analysis, data interpretation, writing; J.H.: data collection, data analysis, data interpretation, writing; D.J.: conceptualization, funding acquisition, study design; L.G.: funding acquisition, literature search, study design, data collection, writing; R.B.: funding acquisition, literature search, study design, data collection, data analysis, data interpretation, writing.

About the Author

Ms. Plahe is a microbiology researcher at the University of Salford. Her primary research interest is in pathogen ecology, mainly those that are tick-transmitted or inhabit soil.

References

1. Margos G, Wilske B, Sing A, Hizo-Teufel C, Cao WC, Chu C, et al. *Borrelia bavariensis* sp. nov. is widely distributed in Europe and Asia. Int J Syst Evol Microbiol. 2013;63:4284–8. https://doi.org/10.1099/ijs.0.052001-0
2. Strnad M, Hönig V, Růžek D, Grubhoffer L, Rego ROM. Europe-wide meta-analysis of *Borrelia burgdorferi* sensu lato prevalence in questing *Ixodes ricinus* ticks. Appl Environ Microbiol. 2017;83:e00609-17. https://doi.org/10.1128/AEM.00609-17
3. Coipan EC, Jahfari S, Fonville M, Oei GA, Spanjaard L, Takumi K, et al. Imbalanced presence of *Borrelia burgdorferi* s.l. multilocus sequence types in clinical manifestations of Lyme borreliosis. Infect Genet Evol. 2016;42:66–76. https://doi.org/10.1016/j.meegid.2016.04.019
4. Courtney JW, Kostelnik LM, Zeidner NS, Massung RF. Multiplex real-time PCR for detection of *anaplasma phagocytophilum* and *Borrelia burgdorferi*. J Clin Microbiol. 2004;42:3164–8. https://doi.org/10.1128/JCM.42.7.3164-3168.2004
5. Heylen D, Tijsse E, Fonville M, Matthysen E, Sprong H. Transmission dynamics of *Borrelia burgdorferi* s.l. in a bird tick community. Environ Microbiol. 2013;15:663–73. https://doi.org/10.1111/1462-2920.12059
6. Michel H, Wilske B, Hettche G, Göttner G, Heimerl C, Reischl U, et al. An ospA-polymerase chain reaction/restriction fragment length polymorphism-based method for sensitive detection and reliable differentiation of all European *Borrelia burgdorferi* sensu lato species and OspA types. Med Microbiol Immunol (Berl). 2004;193:219–26. https://doi.org/10.1007/s00430-003-0196-8
7. Jahfari S, Ruyts SC, Frazer-Mendelewska E, Jaarsma R, Verheyen K, Sprong H. Melting pot of tick-borne zoonoses: the European hedgehog contributes to the maintenance of various tick-borne diseases in natural cycles urban and suburban areas. Parasit Vectors. 2017;10:134. https://doi.org/10.1186/s13071-017-2065-0
8. Medlock JM, Vaux AGC, Gandy S, Cull B, McGinley L, Gillingham E, et al. Spatial and temporal heterogeneity of the density of *Borrelia burgdorferi*-infected *Ixodes ricinus* ticks across a landscape: a 5-year study in southern England. Med Vet Entomol. 2022;36:356–70. https://doi.org/10.1111/mve.12574
9. Olsthoorn F, Sprong H, Fonville M, Rocchi M, Medlock J, Gilbert L, et al. Occurrence of tick-borne pathogens in questing *Ixodes ricinus* ticks from Wester Ross, Northwest Scotland. Parasit Vectors. 2021;14:430. https://doi.org/10.1186/s13071-021-04946-5
10. Mahase E. UK confirms two cases of tickborne encephalitis acquired within the country. BMJ. 2023;381: p799. https://doi.org/10.1136/bmj.p799

Address for correspondence: Richard Birtles, G47 Peel Building, School of Science, Engineering and Environment, University of Salford, The Crescent, Manchester, M5 4WT, UK; email: r.j.birtles@salford.ac.uk

Emergence of Novel Type C Botulism Strain in Household Outbreak, Japan

Rika Maeda, Misato Mori, Seiya Harada, Ichiro Izu, Takaaki Hirano, Yukie Inoue, Shunsuke Yahiro, Hiromi Koyama

Author affiliations: Kumamoto Prefectural Institute of Public Health and Environmental Science, Uto, Japan (R. Maeda, M. Mori, S. Harada, I. Izu, T. Hirano, Y. Inoue, S. Yahiro); Northern Kumamoto Administrative Headquarters Kamoto Area Development Bureau, Yamaga, Japan (H. Koyama)

DOI: https://doi.org/10.3201/eid2910.230433

In 2021, an outbreak of food poisoning caused by *Clostridium botulinum* type C occurred in Kumamoto, Japan. Analysis of the isolated strain revealed that it possessed the *bont/C* gene and was slightly different from the reference *bont/C* gene. The risk for human infection with this new toxin type may be low.

Botulism is a neuroparalytic disease caused by the botulinum toxin, which is produced by *Clostridium botulinum*. *C. botulinum* is physiologically divided into groups I–IV, and botulinum neurotoxins (BoNT) are classified into 7 types, BoNT/A–G. Human botulism is caused primarily by toxin types A, B, and E, and cases of human infection with *C. botulinum* group III, which produces toxin types C and D, are rare. Only 5 foodborne botulism outbreaks caused by *C. botulinum* group III (4 outbreaks caused by type C and 1 outbreak caused by type D) have been reported to date (*1*), and in Japan, only 1 infant botulism case caused by type C has been reported (*2*). *C. botulinum* group III is primarily known as an animal infection, and many of its toxin types have been reported as mosaic types (primarily in birds with toxin type CD and cattle with toxin type DC).

In 2021, foodborne botulism occurred in Kumamoto, Japan. A meal eaten in a domestic residence was the assumed cause, and 4 patients were affected. Botulinum toxin and *C. botulinum* were detected in 3 of the 4 specimens. A commercially prepared chicken dish was suspected to be the cause, but because no food was remaining, we were unable to conduct tests on it. We neutralized the toxin present in the specimens with type C botulinum antitoxin serum, and the isolated strain was found to carry the *bont/C* gene using PCR targeting the *bont* genes (*3*). Next-generation sequencing data revealed full-length coding regions of the *bont*

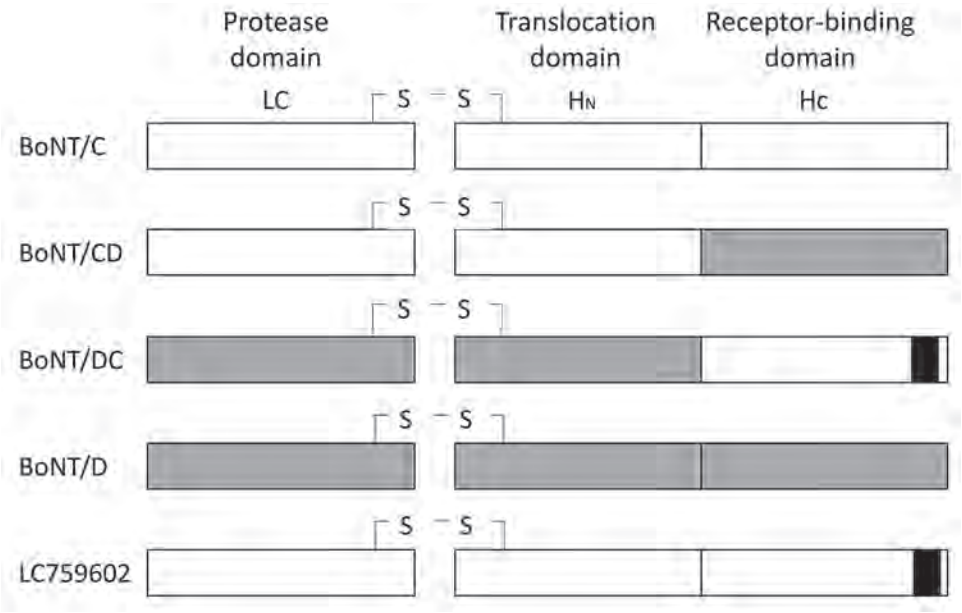

Figure. Schematic diagrams of each functional domain between BoNT (C, CD, DC, D, and LC759602) in study of novel type C botulism strain in household outbreak, Japan. Gray shaded areas indicate the partial sequence of the reference bont/D gene, white areas indicate the partial sequence of the cont/C gene, and black areas indicate the partial sequence of the reference bont/DC gene. BoNT, botulism neurotoxin.

gene of the isolated strains (GenBank accession no. LC759602). The next-generation sequencing method was as follows: after treating *C. botulinum* with 20 mg/mL lysozyme in 20 mM Tris-HCl, 2 mM EDTA, and 1% Triton X-100 (pH 8.0), we extracted DNA using a QIAamp DNA Mini Kit (QIAGEN, https://www.qiagen.com). We prepared genome-sequencing libraries using the QIAseq FX DNA Library Kit (QIAGEN) and sequenced the samples on the Illumina iSeq 100 (https://www.illumina.com). We analyzed sequencing data using CLC Genomics Workbench 22.0.2 (QIAGEN). The obtained contig was assembled from reads of 59× coverage and 29 kbp in size. In comparison with other known *bont* genes, the *bont* gene of the strain sequenced in this study had the highest amino acid sequence similarity with the *bont/C* gene (90%) but was partially different from the reference *bont/C* gene (Table). Detailed analysis revealed that the *bont* gene (LC759602) had the *bont/C* gene or the *bont/CD* gene in the protease domain (LC) and the translocation domain (H_N), as well as the *bont/DC* gene in the receptor-binding domain (H_C) (Table; Figure). The *bont* gene (LC759602) has not been previously reported, and we propose its designation as a new subtype of *C. botulinum* toxin.

The H_C domain is involved in neurotoxin binding to specific receptors in peripheral nerve terminals. The *bont* gene (LC759602) possesses the *bont/DC* gene in the H_C domain, suggesting that human susceptibility to this gene might differ from that of the reference BoNT/C toxin. Unlike other BoNTs, BoNT/C interacts only with gangliosides, and no protein receptor for this toxin has been identified (*4*). However, BoNT/DC has been reported to interact with gangliosides and protein receptors (synaptotagmin I and II) (*5*).

The *bont* gene (LC759602) was determined to be BoNT/C using PCR, which can easily distinguish between types C, D, CD, and DC of *C. botulinum* group III (*6*). It should be noted that, because not all type C strains were subjected to sequencing, the presence of the *bont* gene (LC759602) as type C, as determined by typing PCR, might already exist in other samples. Further investigation is needed to determine the proportion of *C. botulinum* carrying the *bont* gene reported in this study. The risk for human infection with this new toxin type should also be investigated in

Table. Amino acid percentage similarity between BoNTs (C, CD, DC, D, and LC759602) in study of novel type C botulism strain in household outbreak, Japan*

	LC759602			
BoNT serotype (accession no.)	BoNT gene	Protease domain	Translocation domain	Receptor-binding domain
BoNT/C(BAA14235)	89.79	97.73	93.57	78.01
BoNT/CD(BAA08418)	79.31	97.73	98.33	40.55
BoNT/DC(ABP48747)	72.87	48.05	74.45	98.57
BoNT/D(EES90380)	56.48	47.83	73.72	47.74

*BoNT, botulism neurotoxin.

future research. However, given that human infections with a similar toxin type, *C. botulinum* group III, have rarely occurred, this new toxin type might pose little threat to human health.

About the Author

Dr. Maeda is a researcher at the Kumamoto Prefectural Institute of Public Health and Environmental Science. She specializes in research on bacteria that cause disease in humans.

References

1. Rasetti-Escargueil C, Lemichez E. Michel, Popoff MR. Public health risk associated with botulism as foodborne zoonoses. Toxins (Basel). 2019;12:17.
2. Oguma K, Yokota K, Hayashi S, Takeshi K, Kumagai M, Itoh N, et al. Infant botulism due to *Clostridium botulinum* type C toxin. Lancet. 1990;336:1449–50. https://doi.org/10.1016/0140-6736(90)93157-K
3. Takeshi K, Fujinaga Y, Inoue K, Nakajima H, Oguma K, Ueno T, et al. Simple method for detection of *Clostridium botulinum* type A to F neurotoxin genes by polymerase chain reaction. Microbiol Immunol. 1996;40:5–11. https://doi.org/10.1111/j.1348-0421.1996.tb03310.x
4. Strotmeier J, Gu S, Jutzi S, Mahrhold S, Zhou J, Pich A, et al. The biological activity of botulinum neurotoxin type C is dependent upon novel types of ganglioside binding sites. Mol Microbiol. 2011;81:143–56. https://doi.org/10.1111/j.1365-2958.2011.07682.x
5. Peng L, Berntsson RP, Tepp WH, Pitkin RM, Johnson EA, Stenmark P, et al. Botulinum neurotoxin D-C uses synaptotagmin I and II as receptors, and human synaptotagmin II is not an effective receptor for type B, D-C and G toxins. J Cell Sci. 2012;125:3233–42. https://doi.org/10.1242/jcs.103564
6. Nakamura K, Kohda T, Umeda K, Yamamoto H, Mukamoto M, Kozaki S. Characterization of the D/C mosaic neurotoxin produced by *Clostridium botulinum* associated with bovine botulism in Japan. Vet Microbiol. 2010;140:147–54. https://doi.org/10.1016/j.vetmic.2009.07.023

Address for correspondence: Shunsuke Yahiro, 1240-1, Kurisaki, Uto, Kumamoto 869-0425, Japan; email: yahiro-s@pref.kumamoto.lg.jp

Plasmodium knowlesi Infection in Traveler Returning to Canada from the Philippines, 2023

Calvin Ka-Fung Lo, Katherine Plewes, Sakuntla Sharma, Alicia Low, LingHui D. Su, Sara Belga, Ferdinand V. Salazar, Jan Hajek, Muhammad Morshed, Catherine A. Hogan

Author affiliations: University of British Columbia, Vancouver, British Columbia, Canada (C. Ka-Fung Lo, K. Plewes, S. Belga, J. Hajek, M. Morshed, C.A. Hogan); Mahidol–Oxford Tropical Medicine Research Unit, Mahidol University, Bangkok, Thailand (K. Plewes); Centre for Tropical Medicine and Global Health, Nuffield Department of Medicine, University of Oxford, Oxford, UK (K. Plewes); British Columbia Centre for Disease Control, Vancouver (S. Sharma, A. Low, L.D. Su, M. Morshed, C.A. Hogan); Research Institute of Tropical Medicine, Muntinlupa, the Philippines (F.V. Salazar)

DOI: http://doi.org/10.3201/eid2910.230809

A 55-year-old man sought treatment for an uncomplicated febrile illness after returning to Canada from the Philippines. A suspected diagnosis of *Plasmodium knowlesi* infection was confirmed by PCR, and treatment with atovaquone/proguanil brought successful recovery. We review the evolving epidemiology of *P. knowlesi* malaria in the Philippines, specifically within Palawan Island.

In February 2023, a 55-year-old man sought care at the emergency department of Vancouver General Hospital, Vancouver, British Columbia, Canada, for daily fevers, headache, and abdominal pain 5 days after returning from a 3-week trip to the Philippines. He stayed mostly in Manila but spent 4 days on Palawan Island in the western Philippines 4 days before his return to Canada; he had not taken malaria chemoprophylaxis. Bloodwork was notable for platelet nadir of 48 × 10^9/L (reference range 150–450 × 10^9/L), alanine transaminase of 329 U/L (reference range 10–55 U/L), and alkaline phosphatase of 177 U/L (reference range 30–135 U/L). Results of abdominal computed tomography were unremarkable and of a single-target *Plasmodium falciparum* histidine-rich protein 2 rapid diagnostic test were negative. Peripheral blood thin smear demonstrated variable intraerythrocytic parasite morphology, including band-like forms suggestive of *P. malariae* (<0.1% parasitemia) (Figure, panels A–C). Loop-mediated isothermal amplification testing was

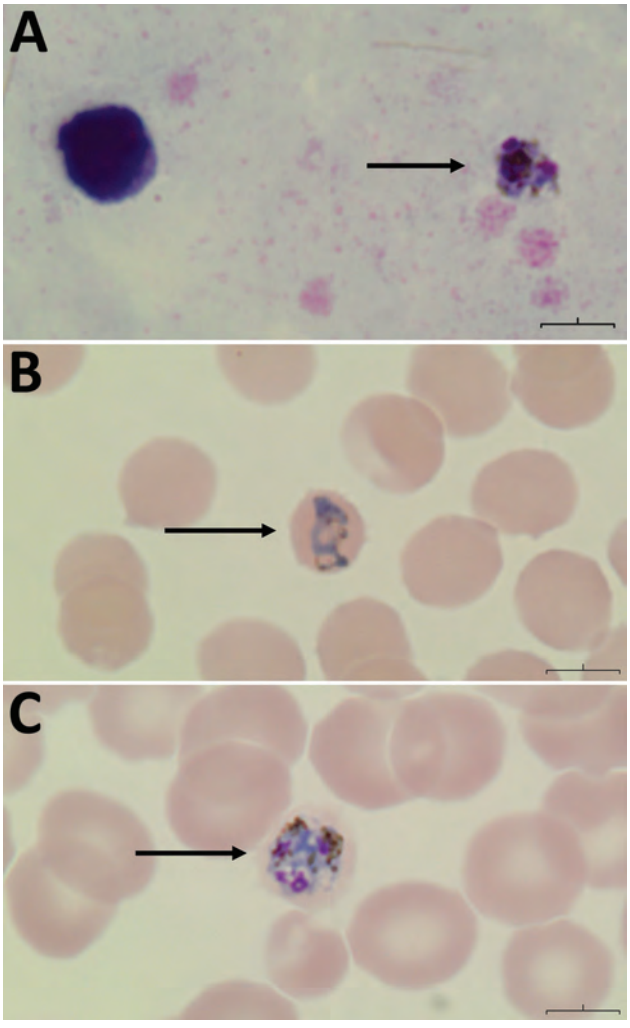

Figure. Peripheral thick and thin blood smears of a man in British Columbia, Canada, with suspected *Plasmodium knowlesi* infection after travel to the Phillippines. A) Thick smear showing *P. knowlesi* gametocyte.. B) Thin smear showing band form within a normal-sized, fimbriated erythrocyte with vacuoles present, similar to *P. malariae*. C) Thin smear showing *P. knowlesi* schizont form with presence of greenish-black pigment and lack of rosette formation. Original magnification x100 for all smears.

positive for *Plasmodium* spp. Given absence of criteria for severe malaria, he was discharged with a 3-day course of atovaquone/proguanil (250 mg/100 mg, 4×/d).

We suspected a diagnosis of *P. knowlesi*, given the patient's travel history and blood smear morphology, and subsequently confirmed the infection via species-specific laboratory-developed PCR. Amplicon sequencing on a 118-bp sequence also confirmed *P. knowlesi* identification. The patient was afebrile at follow-up 4 days after drug therapy, with resolution of thrombocytopenia and symptoms.

P. knowlesi malaria cases within the Philippines have been concentrated in Cebu Province and, as in this case, Palawan Island (Appendix Figure, http://wwwnc.cdc.gov/EID/article/29/10/23-0809-App1.pdf) (*1*–*4*). Although *P. knowlesi* is primarily a simian malaria infecting nonhuman primate hosts, there has been clear transmission evidence across Southeast Asia since the large 2004 Malaysian outbreak in Sabah (*5*).

Palawan Island contains a diverse landscape of beaches, karst, and mangrove forests, including its well-known Puerto Princesa Subterranean River National Park. The island provides an ideal feeding and breeding ground for ≈500 long-tailed macaques (*Macaca fascicularis*), the only monkey species naturally found in the Philippines and natural host reservoirs for *P. knowlesi* (*6*). Given the close proximity of the island's diverse habitats to human settlements and recreation areas, constant contact occurs between forest mosquito vectors, macaque hosts, and, potentially, human hosts (*6*). The first 5 confirmed local cases within Palawan were documented in 2005 (*1*); since 2008, only 2 *P. knowlesi* malaria cases have been documented in North America, both in travelers with implicated exposure from Palawan (Table) (*2*,*7*). According to the Philippines Research Institute of Tropical Medicine, >30 *P. knowlesi* cases have been documented, <5 in tourists traveling to Palawan (Philippines Research Institute of Tropical Medicine, pers. comm., email, 2023 Mar 1). However, the true burden is likely underestimated, given the lack of routine molecular testing for species confirmation in the Philippines. Because early ring-form trophozoites of *P. knowlesi* can resemble *P. falciparum* and developing band-like trophozoites can resemble *P. malariae*

Table. Summary of published *Plasmodium knowlesi* cases in North America imported from the Philippines*

Patient age, y	Patient sex	Year	Geographic location presented	Region of Philippines traveled	Diagnosis	Treatment
50	F	2008 (*2*)	New York, NY, USA	Palawan	PCR failed to identify species; confirmed by 1,055-bp PCR product sequencing	Atovaquone/ proguanil and primaquine
NA	NA	2018 (*7*)	NA	NA	PCR	Atovaquone/ proguanil
55	M	2023 (this case)	Vancouver, British Columbia, Canada	Palawan	PCR; confirmed by 118-bp PCR sequencing	Atovaquone/ proguanil

*NA, not available.

(*1*), molecular species confirmation is a highlighted need in areas at risk for *P. knowlesi*.

The 24-hour *P. knowlesi* erythrocytic cycle is shortest among *Plasmodium* spp., which may contribute to rapid development of high parasitemia (*5*), although this case showed ultra-low parasitemia. The World Health Organization (WHO) recommends that uncomplicated *P. knowlesi* malaria infections acquired in *P. vivax* chloroquine-susceptible regions be treated with an oral artemisinin-combination therapy or chloroquine; cases acquired in *P. vivax* chloroquine-resistant regions should be treated with locally available artemisinin-combination therapy (*8*). Despite limited data regarding antimalarial resistance among *P. knowlesi* parasites, this strategy ensures adequate treatment of undiagnosed mixed infections and simplification of uncomplicated malaria treatment. Intravenous artesunate remains first-line treatment for severe *P. knowlesi* malaria. As in this case, atovaquone/proguanil is also considered reasonable empiric treatment.

The Philippines successfully established 0 indigenous cases of malaria across 78 of 81 provinces in 2019; ≈97% of indigenous cases were *P. falciparum* or *P. vivax*. Recent serologic work showed that 1.1% of personsin Palawan tested positive for *P. knowlesi*–specific PkSERA3ag1 antibody (*9*). Current control strategies for human-species malaria (e.g., insecticide-treated nets, indoor spraying) have limited impact on monkey reservoirs and on forest-dwelling *P. knowlesi* vectors, given limited evidence of indoor biting (*9*,*10*). Palawan and Sabah surveillance data identified that most biting by *Anopheles balabacensis* mosquitoes occurred during 6–10 PM, when many rural residents are still outdoors. Although Palawan reports more sporadic cases than does Malaysia, increased encroachment into deforested areas and close proximity (<100 km) to endemic Sabah raises concern of *P. knowlesi* becoming a predominant species in future years. Ongoing investigations into mosquito behavior implicated with cross-species transmission will help inform appropriate control strategies for *P. knowlesi* and other simian species (*9*).

In summary, *P. knowlesi* malaria should be considered in persons with febrile illness who have traveled to the Philippines (especially Cebu Province and Palawan Island). Because of overlapping microscopy features with *P. falciparum* and *P. malariae*, molecular confirmation is required to enable early diagnosis and appropriate treatment. Despite gains in control of *P. falciparum* and *P. vivax* infection in Southeast Asia, the zoonotic nature of *P. knowlesi* and rise in cases highlight the need for tailored prevention and control strategies.

Acknowledgments

We thank the parasitology staff and microbiologists of the British Columbia Centre of Disease and Control Public Health Laboratory for their contribution toward testing and workup of patient specimen and John Tyson for confirmatory sequencing. We also thank the Philippines Research Institute of Tropical Medicine for providing their expert opinion regarding local *P. knowlesi* epidemiologic trends.

About the Author

Dr. Lo is a medical microbiology resident physician at the University of British Columbia. His research interests include tropical infectious diseases, parasitology, and *Clostridioides difficile* infection prevention.

References

1. Luchavez J, Espino F, Curameng P, Espina R, Bell D, Chiodini P, et al. Human infections with *Plasmodium knowlesi*, the Philippines. Emerg Infect Dis. 2008;14:811–3. https://doi.org/10.3201/eid1405.071407
2. Centers for Disease Control and Prevention (CDC). Simian malaria in a U.S. traveler—New York, 2008. MMWR Morb Mortal Wkly Rep. 2009;58:229–32.
3. De Canale E, Sgarabotto D, Marini G, Menegotto N, Masiero S, Akkouche W, et al. *Plasmodium knowlesi* malaria in a traveller returning from the Philippines to Italy, 2016. New Microbiol. 2017;40:291–4.
4. Takaya S, Kutsuna S, Suzuki T, Komaki-Yasuda K, Kano S, Ohmagari N. Case report: *Plasmodium knowlesi* infection with rhabdomyolysis in a Japanese traveler to Palawan, the Philippines. Am J Trop Med Hyg. 2018;99:967–9. https://doi.org/10.4269/ajtmh.18-0348
5. Singh B, Daneshvar C. Human infections and detection of *Plasmodium knowlesi*. Clin Microbiol Rev. 2013;26:165–84. https://doi.org/10.1128/CMR.00079-12
6. Gamalo LE, Dimalibot J, Kadir KA, Singh B, Paller VG. *Plasmodium knowlesi* and other malaria parasites in long-tailed macaques from the Philippines. Malar J. 2019;18:147. https://doi.org/10.1186/s12936-019-2780-4
7. Mace KE, Lucchi NW, Tan KR. Malaria Surveillance - United States, 2018. MMWR Surveill Summ. 2022;71(No. SS-8):1–35. https://doi.org/10.15585/mmwr.ss7108a1
8. World Health Organization. Guidelines for malaria. Report no.: CC BY-NC-SA 3.0 IGO. Geneva: The Organization; 2023.
9. Malijan RPB, Mechan F, Braganza JC Jr, Valle KMR, Salazar FV, Torno MM, et al. The seasonal dynamics and biting behavior of potential *Anopheles* vectors of *Plasmodium knowlesi* in Palawan, Philippines. Parasit Vectors. 2021;14:357. https://doi.org/10.1186/s13071-021-04853-9
10. Thang ND, Erhart A, Speybroeck N, Xa NX, Thanh NN, Ky PV, et al. Long-lasting insecticidal hammocks for controlling forest malaria: a community-based trial in a rural area of central Vietnam. PLoS One. 2009;4:e7369. https://doi.org/10.1371/journal.pone.0007369

Address for correspondence: Catherine A. Hogan, British Columbia Centre of Disease and Control, 655 W 12th Ave, Rm 2054, Vancouver, BC V6R 2M7, Canada; email: catherine.hogan@bccdc.ca

Reemergence of Cosmopolitan Genotype Dengue Virus Serotype 2, Southern Vietnam

Vi T. Tran,[1] Rhys P.D. Inward,[1] Bernardo Gutierrez, Nguyet M. Nguyen, Phong T. Nguyen, Isabelle Rajendiran, Tam T. Cao, Kien T.H. Duong, Moritz U.G. Kraemer, Sophie Yacoub

Author affiliations: Oxford University Clinical Research Unit, Ho Chi Minh City, Vietnam (V.T. Tran, N.M. Nguyen, K.T.H. Duong, S. Yacoub); University of Oxford, Oxford, UK (R.P.D. Inward, B. Gutierrez, M.U.G. Kraemer, S. Yacoub); Universidad San Francisco de Quito, Quito, Ecuador (B. Gutierrez); Hospital for Tropical Diseases, Ho Chi Minh City (P.T. Nguyen, T.T. Cao); Imperial College London, UK (I. Rajendiran).

DOI: https://doi.org/10.3201/eid2910.230529

We performed phylogenetic analysis on dengue virus serotype 2 Cosmopolitan genotype in Ho Chi Minh City, Vietnam. We document virus emergence, probable routes of introduction, and timeline of events. Our findings highlight the need for continuous, systematic genomic surveillance to manage outbreaks and forecast future epidemics.

Dengue virus (DENV) represents a major public health concern globally and in Vietnam, where an estimated 1.6 million cases occur each year (*1*). Clinical manifestations range from fever to severe organ dysfunction (*2*). DENV includes 4 distinct serotypes (DENV 1–4), which have evolved into distinguishable genotypes; all are transmitted primarily by *Aedes aegypti* mosquitoes (*3*). DENV is endemic in both urban and peri-urban areas of Vietnam with substantial seasonal temporal and spatial variation. Although all 4 DENV serotypes have circulated in Vietnam, DENV-1 and DENV-2 have been most prevalent over the past 20 years.

In 2022, Ho Chi Minh City, Vietnam, experienced a 3-fold increase in reported DENV cases compared with 2020 and 5-fold compared with 2021 (*4*,*5*). Possible drivers of transmission include climate factors because optimal temperatures and humidity increase vector abundance (*6*), reduced population immunity because of lower rates of transmission in previous years (*6*), and possible introduction of new serotypes or genotypes or diversification of circulating lineages (*7*). Scarcity of available data on DENV circulation by lineage in Vietnam limits testing those hypotheses. Our study explored the DENV lineages circulating in Ho Chi Minh City over the past 5 years, aiming to provide a detailed assessment of DENV dynamics in Vietnam.

We randomly selected 362 samples from dengue patients enrolled in research studies (reviewed by the ethics committee and approved by the internal review board of the hospital) at the Hospital for Tropical Diseases in Ho Chi Minh City during 2017–2022. Of those patients, 303 (83.7%) tested positive for dengue using quantitative reverse transcription PCR. DENV-2 was predominant (72.3%); DENV-1 accounted for 23.1% and DENV-4 for 4.6% of positive samples. From those samples, we sequenced 45 DENV-2 viral envelope (E) genes. We amplified E genes using PCR, and after PCR product purification, we conducted Sanger sequencing on samples with nucleic acid concentrations >10 ng/μL. We supplemented the new sequences with a background dataset of DENV-2 genome and E-gene sequences from southern and southeast Asia (Appendix 1, https://wwwnc.cdc.gov/EID/article/29/10/23-0529-App1.pdf).

We constructed maximum-likelihood trees for all DENV-2 genotypes, as well as a time-scaled tree in which we estimated ancestral node locations and conducted root-to-tip regression analyses. Our results showed DENV-2 replaced DENV-1 as the predominant serotype in 2019, and multiple DENV-2 genotypes were cocirculating (Appendix 1 Figure 1). Seventeen sequences belonged to Asia I genotype, which has been established in the region since 2006; another 28 sequences were identified as sporadically detected Cosmopolitan genotype. Cosmopolitan genotype virus strain has displayed signs of reemergence, with indicators of ≥3 distinct recent introductions of clades A, B, and C into southern Vietnam (Appendix 1 Figure 2). Cosmopolitan phylogeny (Figure), constructed similarly to the broader DENV-2 tree, shows most (27/28) sequences from this region clustered within these 3 clades; clades A and B share ancestry with sequences from Indonesia and clade C shares ancestry with sequences from Cambodia.

The clades were detected across several provinces in southern Vietnam, including all 3 clades in Ho Chi Minh City. Clade A circulated in provinces north and east of Ho Chi Minh City; clades B and C were found in provinces north and west of the city (Appendix 1 Figure 3). Estimated time to the most recent common ancestor suggests that clade A has been in circulation the longest, followed by clades B and C (Appendix 1 Figure 4). These findings indicate

[1]These authors contributed equally to the article.

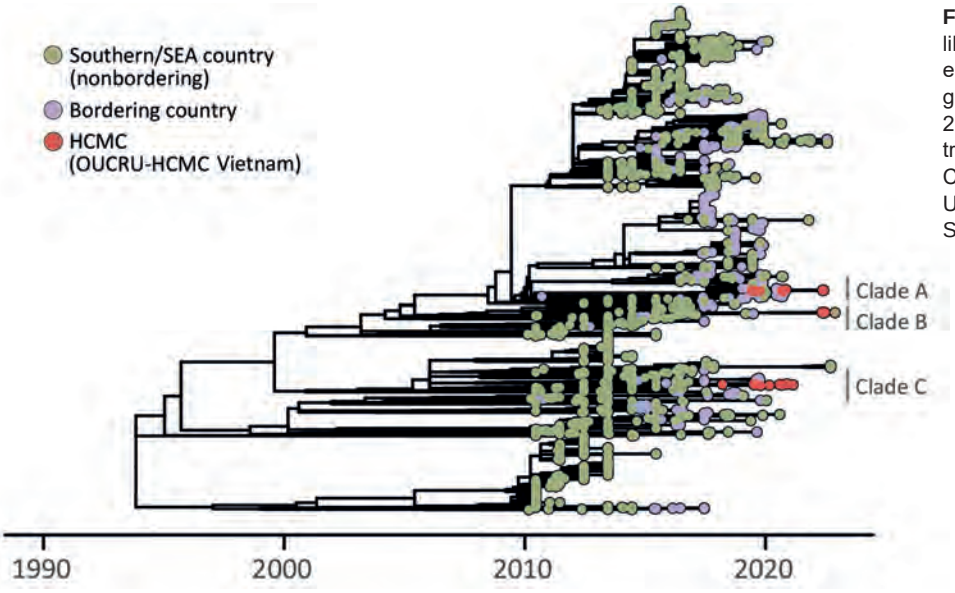

Figure. Time-scaled maximum-likelihood phylogenic tree showing emergence of the Cosmopolitan genotype of dengue virus serotype 2 in Vietnam. Clades A–C refer to transmission lineages. HCMC, Ho Chi Minh City; OUCRU, Oxford University Clinical Research Unit; SEA, southeast Asia

continuous introductions of the Cosmopolitan genotype into southern Vietnam over multiple years. Clades A and C have persisted locally for at least half a decade, with approximately 2 years between the earliest most recent common ancestor and the earliest sampling date, suggesting undetected Cosmopolitan genotype might have been cryptically transmitted during multiple dengue seasons.

Dynamics of DENV prevalence and spread within Vietnam might have been influenced by successive seedings of the Cosmopolitan genotype, thereby increasing likelihood of establishment and sustained transmission (*8*,*9*). Although the Cosmopolitan genotype has circulated in neighboring countries, likely since the late 1990s (Appendix 1 Figures 5, 6), it had not been reported in Vietnam until recently. Mechanisms underlying a specific genotype reemerging after new introductions and subsequent establishment warrant further investigation. Large-scale dengue surveillance in hyperendemic settings like Vietnam is a formidable challenge because it relies on syndromic surveillance and awareness of heterogeneous epidemiologic trends, and limited resources are available to support viral genomic sequencing to identify circulating strains. To refine our understanding of transmission pathways for specific lineages of DENV, improving surveillance using strategies that reduce sampling bias is critical (*10*). We emphasize the importance of continuous, systematic virus sequencing in urban centers in Vietnam and across southeast Asia to swiftly identify novel viral lineages. These strategies, paired with clinical and socioeconomic data, will support preventive measures and outbreak forecasting.

Acknowledgments

We thank the researchers who provided sequences to GISAID (https://www.gisaid.org) that we used for this research. A list of sequences is provided in Appendix 2 (https://wwwnc.cdc.gov/EID/article/29/10/23-0529-App2.xlsx).

R.P.D.I. and M.U.G.K acknowledge funding from the European Union Horizon 2020 project MOOD (874850). M.U.G.K. and B.G. acknowledge funding from the Oxford Martin School Pandemic Genomics program. M.U.G.K. acknowledges funding from the Wellcome Trust, a Branco Weiss Fellowship, The Rockefeller Foundation, and Google.org. V.T.T., K.T.H.D., N.M.N. and S.Y. acknowledge funding from the Wellcome Trust (106680).

Contributions: R.P.D.I., V.T.T., S.Y., B.G.G., and M.U.G.K. developed the idea and planned the research. V.T.T. collected samples and performed sequencing. R.P.D.I., B.G., and I.R. developed the bioinformatic pipeline; R.P.D.I. conducting the analyses. R.P.D.I., V.T.T., S.Y., B.G., and M.U.G.K. wrote the first draft of the manuscript. K.T.H.D. contributed to the sequencing procedure for samples and initial data cleaning. N.M.N. contributed to areas related to clinical knowledge and patient recruitment. P.N.T. and T.C.T. contributed to management and oversight of conducting the study in the hospital. All authors interpreted the data, contributed to writing, and approved the manuscript.

About the Author

Vi Thuy Tran is a senior research assistant working in the dengue research group at Oxford University Clinical Research Unit, Ho Chi Minh City, Vietnam. Her primary research interest focuses on the investigating evolution of dengue virus and its transmission dynamic.

References

1. Cattarino L, Rodriguez-Barraquer I, Imai N, Cummings DAT, Ferguson NM. Mapping global variation in dengue transmission intensity. Sci Transl Med. 2020;12:eaax4144. PubMed https://doi.org/10.1126/scitranslmed.aax4144
2. Yacoub S, Wills B. Dengue: an update for clinicians working in non-endemic areas. Clin Med (Lond). 2015;15:82–5. https://doi.org/10.7861/clinmedicine.15-1-82
3. Nguyen-Tien T, Lundkvist Å, Lindahl J. Urban transmission of mosquito-borne flaviviruses—a review of the risk for humans in Vietnam. Infect Ecol Epidemiol. 2019;9:1660129. PubMed https://doi.org/10.1080/20008686.2019.1660129
4. Ho Chi Minh City Center for Disease Control. Ho Chi Minh City: warning about the risk of epidemic dengue fever is complicated [in Vietnamese]. [cited 2022 Apr 22] https://hcdc.vn/tphcm-canh-bao-nguy-co-dich-benh-sot-xuat-huyet-dien-bien-phuc-tap-4ac4d90b7e3c5ef9feaf468a4073b101.html
5. Ho Chi Minh City Center for Disease Control. Epidemic situation dengue, hand, foot and mouth updated to week 50 (as of 11/12/2022) [in Vietnamese]. [cited 2022 Dec 14]. https://hcdc.vn/tinh-hinh-dich-benh-sot-xuat-huyet-tay-chan-mieng-cap-nhat-den-tuan-50-tinh-den-ngay-11122022-8dfd9a4597e0425a7f0fc2d3ed204188.html
6. Rabaa MA, Simmons CP, Fox A, Le MQ, Nguyen TTT, Le HY, et al. Dengue virus in sub-tropical northern and central Viet Nam: population immunity and climate shape patterns of viral invasion and maintenance. PLoS Negl Trop Dis. 2013;7:e2581. https://doi.org/10.1371/journal.pntd.0002581
7. Zhang C, Mammen MP Jr, Chinnawirotpisan P, Klungthong C, Rodpradit P, Monkongdee P, et al. Clade replacements in dengue virus serotypes 1 and 3 are associated with changing serotype prevalence. J Virol. 2005;79:15123–30. https://doi.org/10.1128/JVI.79.24.15123-15130.2005
8. Sasmono RT, Kalalo LP, Trismiasih S, Denis D, Yohan B, Hayati RF, et al. Multiple introductions of dengue virus strains contribute to dengue outbreaks in East Kalimantan, Indonesia, in 2015–2016. Virol J. 2019;16:93. https://doi.org/10.1186/s12985-019-1202-0
9. Tian H, Sun Z, Faria NR, Yang J, Cazelles B, Huang S, et al. Increasing airline travel may facilitate co-circulation of multiple dengue virus serotypes in Asia. PLoS Negl Trop Dis. 2017;11:e0005694. https://doi.org/10.1371/journal.pntd.0005694
10. ZElliott P, Whitaker M, Tang D, Eales O, Steyn N, Bodinier B, et al. Design and implementation of a national SARS-CoV-2 monitoring program in England: REACT-1 study. Am J Public Health. 2023;113:545–54. https://doi.org/10.2105/AJPH.2023.307230

Address for correspondence: Vi T Tran, Oxford University Clinical Research Unit, Vietnam, Dengue Research Group, 764 Vo Van Kiet, Ward 1, District 5 Ho Chi Minh City 700000, Vietnam; email: vitt@oucru.org; Rhys PD Inward, University of Oxford, Broad St, Oxford OX1 3AZ, UK; email: rhys.inward@biology.ox.ac.uk

etymologia revisited

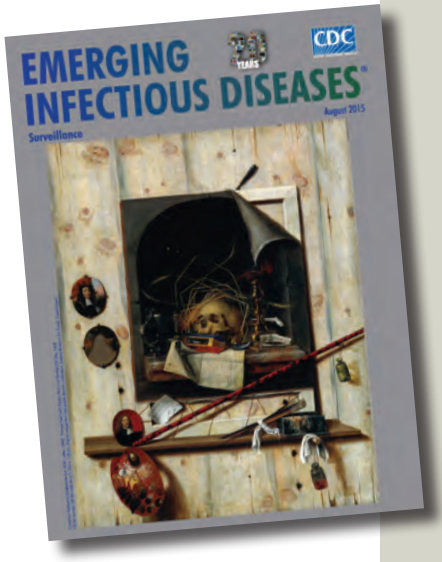

Originally published in August 2015

Escherichia coli

[esh″ə-rik′e-ə co′lī]

A gram-negative, facultatively anaerobic rod, *Escherichia coli* was named for Theodor Escherich, a German-Austrian pediatrician. Escherich isolated a variety of bacteria from infant fecal samples by using his own anaerobic culture methods and Hans Christian Gram's new staining technique. Escherich originally named the common colon bacillus *Bacterium coli commune*. Castellani and Chalmers proposed the name *E. coli* in 1919, but it was not officially recognized until 1958.

References:

1. Oberbauer BA. Theodor Escherich—Leben und Werk. Munich: Futuramed-Verlag; 1992.
2. Shulman ST, Friedmann HC, Sims RH. Theodor Escherich: the first pediatric infectious diseases physician? Clin Infect Dis. 2007;45:1025–9

https://wwwnc.cdc.gov/eid/article/21/8/et-2108_article

Parasites: The Inside Story

Scott L. Gardner, Judy Diamond, Gabor R. Rácz; Princeton University Press, Princeton, New Jersey, USA, 2022; ISBN-10: 0691206872; ISBN-13: 978-0691206875; Pages: 224; Price: US $29.95 (hardcover)

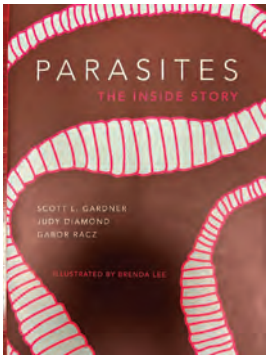

Parasites: The Inside Story shows how parasites coexisted and spread around the world through host migration, particularly through humans, and researches their origin and evolution. The book describes how the choice of host has affected the successful survival of some parasites and avoidance of extinction. The authors show how parasites influence and manipulate their intermediate host, which makes them more visible and easier prey for the next host, causing the host to "look foolish." The authors use novel and entertaining approaches to explore their subject, such as describing how the Israelite Jonah spent 3 days in the belly of a whale and what parasites he might have encountered during that 3-day stay.

Another entertaining approach was participation in the parasite Olympics, where parasites earned medals according to their success and survival by choosing and adjusting to their hosts. *Ascaris lumbricoides* is a gold medal winner as one of the most durable internal parasites of humans. However, the book overlooked *Strongyloides stercoralis*, which can cause hyperinfection syndrome in immunocompromised hosts and is considered an emerging infectious disease and deserves an honorary Olympic medal. Babesiosis is another notable emerging parasitic disease that was overlooked.

I appreciated the novel and appealing way in which the authors show how parasites affect other species and human lives, while also incorporating their nonharmful roles, as in the case of mutualism and commensalism. I loved the immense and vivid imagery used to describe the breathtaking basin of the Congo River but was saddened that many persons living along the river might not continue to see that beautiful scenery because of river blindness caused by *Onchocerca volvulus*. The stories, connections to real persons, and references to at least 3 movies and 1 television series indicate the detailed efforts involved in writing this book.

The book has a high level of scientific detail as it dives into history, ecology, evolution, and future outlooks. The authors discuss how climate change is affecting parasite existence. An example is the migration of triatomine kissing bugs to the southern half of the United States, which might increase the risk for *Trypanosoma cruzi* transmission, causing Chagas disease (to which the book attributes Charles Darwin's death, from an infection he acquired during a trip to South America). The authors also elaborate on international scientific collaboration during epidemiologic investigations, such as the collaboration between researchers from the United States and Mongolia during a hantavirus infection outbreak in New Mexico. Readers will learn about parasite eradication campaigns, some of which did not turn out well, as was the case for the *Schistosoma mansoni* eradication campaign in Egypt that resulted in populationwide infections with hepatitis C virus.

The book has 29 color photos, making the stories only more vibrant, and helps in understanding parasite life cycles and in making diagnoses. This book will appeal to readers interested in emerging infectious diseases, nonparasitologists, scientists, and clinicians and is an admirable expedition into the amazing world of parasites.

Rezhan H. Hussein

Author affiliation: Penn State College of Medicine, Hershey, Pennsylvania, USA

DOI: https://doi.org/10.3201/eid2910.230235

Address for correspondence: Rezhan H. Hussein, Division of Infectious Diseases and Epidemiology, Department of Medicine, Penn State Milton Hershey Medical Center, Penn State College of Medicine, 500 University Dr, MC H036, Hershey, PA 17033, USA; email: rhussein@pennstatehealth.psu.edu

Edvard Munch (1863–1944), *Inheritance* (detail), 1897–1899. Oil on canvas, 55.5 in × 47.25 in/141 cm × 120 cm. Munch Museum, Oslo, Norway. Photo credit: Erich Lessing. Digital image from Art Resource, New York, New York, USA.

"Living People Who Breathe and Feel and Suffer and Love"

Byron Breedlove

Since its initial appearance in Europe during the 1400s, syphilis has been a scourge across all levels of society, and it remains one of the most common sexually transmitted infections around the world. The Centers for Disease Control and Prevention (CDC) reports that after the rate of primary and secondary syphilis in the United States dipped to historic lows in 2000 and 2001, the rate has increased almost every year since then; the annual increase for 2020–2021 was 29%. The World Health Or ganization estimated that, globally in 2020, approximately 7.1 million adults, 15–49 years of age, acquired syphilis.

Rates of infections with congenital syphilis, which is syphilis transmitted to a fetus either before or during birth from an infected mother, are escalating at an even faster pace. The CDC reports that, in 2021, the US national rate of reported congenital syphilis was 78 cases per 100,000 live births, an increase of 31% from 60 cases per 100,000 live births in 2020. The World Health Organization reports: "Congenital syphilis is the second leading cause of preventable stillbirth globally, preceded only by malaria."

A pair of articles from this issue of Emerging Infectious Diseases provide more data about those soaring rates. MacKenzie, McEvoy, and Ford document the resurgence of sexually transmitted and congenital syphilis across many high-income countries and describe prevention efforts. Staneva, Hobbs, and Dobbs report that, in Mississippi, congenital syphilis rates have exploded in recent years, increasing 1,000% from 2016 to 2021.

Congenital syphilis can be prevented if a mother is adequately treated for syphilis at least one month before delivery. Early detection is also critical because infants can be treated with penicillin during their first days of life. If untreated, congenital syphilis may cause death for neonates or a range of devastating birth defects and neurologic deficits in infected infants. This month's cover image, *Inheritance*, by Norwegian artist Edvard Munch, bears witness to some of those effects.

Munch completed this painting in the late 1890s after visiting Hôpital Saint-Louis, one of three

Author affiliation: Centers for Disease Control and Prevention, Atlanta, Georgia, USA

DOI: https://10.3201/doi.org/eid2910.AC2910

hospitals in Paris that accepted patients with syphilis. There, he encountered a grieving young woman and her infected child. Several years earlier Munch had written, "No longer shall I paint interiors with men reading and women knitting. I will paint living people who breathe and feel and suffer and love." In *Inheritance*, and several other paintings, he made good on that declaration. The Munch Museum in Oslo, Norway, where this painting is housed, notes that Munch used a similar palette of red, green, black, and white in several paintings, including this one, that dealt with illness, death, and suffering.

The young mother, herself a victim of syphilis, sitting alone on a narrow wooden bench in a drab waiting room, daubs at her lips with a white handkerchief as her left arm dangles limply. Her flushed face, red from grief and very likely from a syphilitic rash, contrasts with her dark hat and jacket. Art historian Shelley Wood Cordulack notes, "the bright red plume on the mother's hat accentuates the acuteness of both disease and emotional trauma." The patterns in her skirt represent falling leaves, a symbol of death, which, as Cordulack writes, Munch also incorporated into a dress his sister is wearing in an 1892 portrait and again in his 1893 painting *Death in the Sickroom*.

The unswaddled newborn lying on a shimmering gossamer blanket that surrounds him like an ectoplasmic apparition is sprawled across his mother's lap. Munch takes pains to show how the pale, lethargic infant has been ravaged by congenital syphilis. The child's torso is covered with red pustules, his thin arms are folded into triangles, he is jaundiced, and his blank eyes peer from a malformed head.

Physician Antonio Perciaccante and researcher Alessia Coralli wrote, "The work shocked society because Munch had depicted a person with a sexually transmitted disease, a taboo of that time." They also pointed out, "The portrait's title is very interesting. It's a reminder that, in the 1890s, syphilis in neonates was assumed to be an hereditary disease." How syphilis was transmitted to infants, they add, was a subject of vigorous debate: "the hereditists supported the transmission by paternal sperm, whereas the contagionists stated that the infection was propagated by maternal way."

In 1905, approximately 7 years after Munch finished *Inheritance*, a discovery settled that debate. German scientists Fritz Schaudinn and Erich Hoffmann identified the causative organism of syphilis as the bacterium *Treponema pallidum*, and the term "congenital syphilis" entered the medical lexicon. Breakthroughs and refinements in diagnostic methods followed, and in 1943, the year before Munch died, penicillin was found to be an effective treatment for syphilis.

By the end of the 20th Century, public health aspirations to eliminate syphilis seemed within reach. CDC's 1999 National Plan to Eliminate Syphilis from the United States expresses that optimism: "As we approach the end of the 20th century, the United States is faced with a unique opportunity to eliminate syphilis within its borders. Syphilis is easy to detect and cure, given adequate access to and utilization of care. Nationally, it is at the lowest rate ever recorded and it is confined to a very limited number of geographic areas."

Public health funding to support surveillance, testing, and treatment for sexually transmitted infections, including syphilis, has not been prioritized or sustained. Consequently, somber scenes such as the one Munch immortalized more than 125 years ago still occur in waiting rooms and clinics across the United States and parts of the world.

Bibliography

1. Centers for Disease Control and Prevention. The national plan to eliminate syphilis from the United States [cited 2023 Aug 15]. https://www.cdc.gov/stopsyphilis/plan.pdf
2. Centers for Disease Control and Prevention. National overview of STDs, 2021 [cited 2023 Aug 15]. https://www.cdc.gov/std/statistics/2021/overview.htm#:~:text=Since%20reaching%20a%20historic%20low,and%20in%20all%20age%20groups
3. Chen C. Syphilis is resurging in the U.S., a sign of public health's funding crisis. [cited 2023 Aug 10]. https://www.npr.org/sections/health-shots/2021/11/01/1050568646/syphilis-std-public-health-funding
4. Cordulack SW. Edvard Munch and the physiology of symbolism. Madison (NJ): Fairleigh Dickinson University Press; 2002. p. 91–2.
5. Eggum A. Edvard Munch: paintings, sketches, and studies. New York: C.N. Potter; 1984. p. 10.
6. MacKenzie H, McEvoy SP, Ford TJ. Managing risk for congenital syphilis, Perth, Western Australia, Australia. Emerg Infect Dis. 2023;29:2093–2101. https://doi.org/10.3201/eid2910.230432
7. Perciaccante A, Coralli A. The history of congenital syphilis behind *The Inheritance* by Edvard Munch. JAMA Dermatol. 2018;154:280. https://doi.org/10.1001/jamadermatol.2017.5834
8. Schaudinn FR, Hoffmann E. Preliminary report on the occurrence of spirochaetes in syphilitic disease products and in papillomas. Works from the Imperial Health Office [in German]. Berlin: Imperial Health Office; 1905. p. 527–34.
9. Staneva M, Hobbs C, Dobbs T. Spike in congenital syphilis, Mississippi, USA, 2016–2022. Emerg Infect Dis. 2023:29:1965–72. https://doi.org/10.3201/eid2910.230421
10. Tampa M, Sarbu I, Matei C, Benea V, Georgescu SR. Brief history of syphilis. J Med Life. 2014;7:4–10.
11. World Health Organization. Mother-to-child transmission of syphilis [cited 2023 Aug 15]. https://www.who.int/teams/global-hiv-hepatitis-and-stis-programmes/stis/prevention/mother-to-child-transmission-of-syphilis

Address for correspondence: Byron Breedlove, EID Journal, Centers for Disease Control and Prevention, 1600 Clifton Rd NE, Mailstop H16-2, Atlanta, GA 30329-4027, USA; email: wbb1@cdc.gov

EMERGING INFECTIOUS DISEASES®

Upcoming Issue

Respiratory Infections

- Group A Streptococcus Primary Peritonitis in Children, New Zealand
- Severe *Rickettsia typhi* Infections, Costa Rica
- Congenital Mpox Syndrome (Clade I) in Stillborn Fetus after Placental Infection and Intrauterine Transmission, Democratic Republic of the Congo, 2008
- *Campylobacter fetus* Invasive Infections and Risks for Death, France, 2000–2021
- Human Salmonellosis Linked to *Salmonella Typhimurium* Epidemic in Wild Songbirds, United States, 2020–2021
- Global Phylogeography and Genomic Epidemiology of Carbapenem-Resistant $bla_{OXA-232}$–Carrying *Klebsiella pneumoniae* ST15 Lineage
- Monkeypox Virus in Wastewater Samples from Santiago Metropolitan Region, Chile
- Genotypic Evolution of *Klebsiella pneumoniae* Sequence Type 512 during Ceftazidime/Avibactam, Meropenem/Vaborbactam, and Cefiderocol Treatment, Italy
- SARS-CoV-2 Reinfection Risk in Persons Living with HIV, Chicago, Illinois, USA, 2020–2022
- Micro–Global Positioning System for Identification of Nightly Opportunities for Marburg Virus Spillover to Humans by Egyptian Rosette Bats
- Surveillance Using Genomic Sequencing to Identify Antigenic Site Mutations of Respiratory Syncytial Virus, Arizona, USA
- New SARS-CoV-2 Omicron Variant with Spike Protein Mutation Y451H, Kilifi, Kenya, March–May 2023
- Domestically Acquired NDM-1–Producing *Pseudomonas aeruginosa*, Southern California, USA, 2023

Complete list of articles in the November issue at https://wwwnc.cdc.gov/eid/#issue-304

Earning CME Credit

To obtain credit, you should first read the journal article. After reading the article, you should be able to answer the following, related, multiple-choice questions. To complete the questions (with a minimum 75% passing score) and earn continuing medical education (CME) credit, please go to http://www.medscape.org/journal/eid. Credit cannot be obtained for tests completed on paper, although you may use the worksheet below to keep a record of your answers.

You must be a registered user on http://www.medscape.org. If you are not registered on http://www.medscape.org, please click on the "Register" link on the right hand side of the website.

Only one answer is correct for each question. Once you successfully answer all post-test questions, you will be able to view and/or print your certificate. For questions regarding this activity, contact the accredited provider, CME@medscape.net. For technical assistance, contact CME@medscape.net. American Medical Association's Physician's Recognition Award (AMA PRA) credits are accepted in the US as evidence of participation in CME activities. For further information on this award, please go to https://www.ama-assn.org. The AMA has determined that physicians not licensed in the US who participate in this CME activity are eligible for AMA PRA Category 1 Credits™. Through agreements that the AMA has made with agencies in some countries, AMA PRA credit may be acceptable as evidence of participation in CME activities. If you are not licensed in the US, please complete the questions online, print the AMA PRA CME credit certificate, and present it to your national medical association for review.

Article Title

Serotype Distribution and Disease Severity in Adults Hospitalized with *Streptococcus pneumoniae* Infection, Bristol and Bath, UK, 2006–2022

CME Questions

1. Which one of the following statements regarding general trends in cases of pneumococcal disease in the United Kingdom through 2006-17?

A. PCV7 serotype disease remained stable among children
B. PCV7 serotype disease remained stable among adults
C. There was an overall increase in non-PCV13 serotypes in all groups
D. The overall incidence of invasive pneumococcal disease (IPD) among older adults declined substantially from 2010 to 2016

2. What does the current study demonstrate regarding trends in hospitalization for pneumococcal disease in England from 2019 to 2022?

A. A marked decrease in pneumococcal cases during 2020 was followed by a gradual increase in cases during 2022
B. Pneumococcal disease rates remained stable during the COVID-19 pandemic because testing was more common
C. The incidence of pneumococcal disease declined steadily from 2019 to 2022
D. Pneumococcal disease rates increased during 2022, but remained well below prepandemic levels

3. Which one of the following statements best describes trends in the incidence of different pneumococcal serotypes in the current study?

A. PCV7 serotypes decreased substantially from 2006 to 2022, but PCV13-7 serotypes less so
B. PCV7 and PCV13-7 serotypes both decreased substantially to a similar degree between 2006 and 2022
C. PCV13-7 serotype incidence decreased from 2006 to 2022, but PCV7 serotypes remained the same
D. Incidence rates of both PCV7 and PCV13-7 serotypes remained stable between 2006 and 2022

4. What were the most common pneumococcal serotypes in the current study recorded after the emergence of SARS-CoV-2?

A. 1, 2, 3, 5, 6B, 8
B. 18C, 19A, 20, 22F, 23F, 33F
C. 6B, 7F, 9A, 11A, 23F, 33F
D. 3, 8, 9N, 19F, 19A, 22F

5. Which one of the following temporal trends was noted in the clinical outcomes of pneumococcal infection over time in the current study?

A. The age of patients admitted with IPD declined over time
B. Disease severity of IPD declined over time
C. ICU admissions declined steadily over time
D. Inpatient mortality increased over time

Earning CME Credit

To obtain credit, you should first read the journal article. After reading the article, you should be able to answer the following, related, multiple-choice questions. To complete the questions (with a minimum 75% passing score) and earn continuing medical education (CME) credit, please go to http://www.medscape.org/journal/eid. Credit cannot be obtained for tests completed on paper, although you may use the worksheet below to keep a record of your answers.

You must be a registered user on http://www.medscape.org. If you are not registered on http://www.medscape.org, please click on the "Register" link on the right hand side of the website.

Only one answer is correct for each question. Once you successfully answer all post-test questions, you will be able to view and/or print your certificate. For questions regarding this activity, contact the accredited provider, CME@medscape.net. For technical assistance, contact CME@medscape.net. American Medical Association's Physician's Recognition Award (AMA PRA) credits are accepted in the US as evidence of participation in CME activities. For further information on this award, please go to https://www.ama-assn.org. The AMA has determined that physicians not licensed in the US who participate in this CME activity are eligible for AMA PRA Category 1 Credits™. Through agreements that the AMA has made with agencies in some countries, AMA PRA credit may be acceptable as evidence of participation in CME activities. If you are not licensed in the US, please complete the questions online, print the AMA PRA CME credit certificate, and present it to your national medical association for review.

Article Title

Spike in Congenital Syphilis, Mississippi, USA, 2016–2022

CME Questions

1. According to the results of the current study, which one of the following was characteristic of infants with congenital syphilis (CS) hospitalized between 2016 and 2022 in Mississippi?

A. About half were receiving Medicaid
B. About one third were African American
C. About three quarters came from urban counties
D. More than 90% received their diagnosis at hospitalization for delivery

2. What was the rate of increase for infants hospitalized with CS from 2016 to 2022 in the current study?

A. 25%
B. 100%
C. 200%
D. 1000%

3. Which one of the following variables was most significantly associated with a higher risk for CS in the current study?

A. Maternal substance use
B. Having Medicaid insurance
C. Being African American
D. Living in an urban county

4. All of the following clinical outcomes were significantly associated with CS in the current study EXCEPT:

A. Stillbirth
B. Premature delivery
C. Respiratory distress
D. Low birth weight